

General Disclaimer

One or more of the Following Statements may affect this Document

- This document has been reproduced from the best copy furnished by the organizational source. It is being released in the interest of making available as much information as possible.
- This document may contain data, which exceeds the sheet parameters. It was furnished in this condition by the organizational source and is the best copy available.
- This document may contain tone-on-tone or color graphs, charts and/or pictures, which have been reproduced in black and white.
- This document is paginated as submitted by the original source.
- Portions of this document are not fully legible due to the historical nature of some of the material. However, it is the best reproduction available from the original submission.

DOE/NASA/0032-16
NASA CR-167935
MTI Report No. 80ASE142DR1

Automotive Stirling Engine Mod I Design Review Report

Volume I

(NASA-CR-167935) AUTOMOTIVE STIRLING ENGINE
MOD I DESIGN REVIEW, VOLUME 1 Final Report
(Mechanical Technology, Inc.) 654 p
HC A99/MF A01

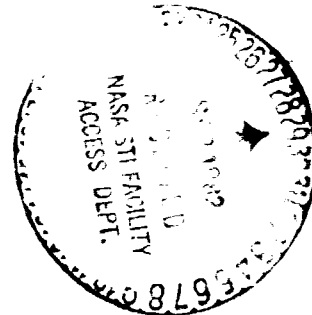
N82-34311

CSCI 13F

Unclas
G3/85 35307

Mechanical Technology Incorporated

August 1982



Prepared for
NATIONAL AERONAUTICS AND SPACE ADMINISTRATION
Lewis Research Center
Under Contract DEN 3-32

for
U.S. DEPARTMENT OF ENERGY
Conservation and Renewable Energy
Office of Vehicle and Engine R&D

DOE/NASA/0032-16
NASA CR-167935
MTI Report No. 80ASE142DR1

Automotive Stirling Engine Mod I Design Review Report

Volume I

Mechanical Technology Incorporated
968 Albany-Shaker Road
Latham, New York 12110

August 1982

Prepared for
National Aeronautics and Space Administration
Lewis Research Center
Cleveland, Ohio 44135
Under Contract DEN 3-32

for
U.S. DEPARTMENT OF ENERGY
Conservation and Renewable Energy
Office of Vehicle and Engine R&D
Washington, D.C. 20545
Under Interagency Agreement DE-AI01-77CS51040

TABLE OF CONTENTS

FOR

VOLUME I

	<u>Page</u>
A. MATERIAL PRESENTED AT THE DESIGN REVIEW MEETING	
A.1 Preface.....	I-1
A.2 Agenda for the May 22-23, 1980 Meeting.....	I-5
A.3 Introduction.....	I-11
A.4 Executive Summary.....	I-51
A.5 Risk Assessment.....	I-75
A.6 Safety Analysis of ASE Mod I.....	
A.7 Design Criteria and Materials Properties for the ASE Mod I and Reference Engines.....	I-87
A.8 Combustion Air Blower Development.....	I-99
A.9 Mod I Engine Starter Motor.....	I-119
A.10 Conclusions and Recommendations.....	I-127
B. TECHNICAL INFORMATION DELIVERED PRIOR TO THE MEETING	
B.1 Table of Contents.....	I-131
B.2 Stirling Engine System.....	I-135
B.3 Basic Stirling Engine.....	I-155
B.4 External Heat System.....	I-231
B.5 Hot Engine System.....	I-355
B.6 Cold Engine System.....	I-427
B.7 Engine Drive System.....	I-499
B.8 Ricardo Consulting Engineerings - Engine Drive System...	I-507

A.1 - PREFACE

Paragraph E.4.2.1.1 "Engine Design review" of Contract DEN3-32 states:

"The Contractor shall present an Engine Design Review of the preliminary design to NASA. NASA approval shall be required prior to initiating detail design and hardware procurement. Detail design of some components or parts required to evaluate the preliminary design and procurement of critical long-lead hardware may be initiated under special circumstances with NASA approval. Information to be presented at the design review shall include layout drawings, materials, fabrication techniques, and the results of performance, stress and thermal analyses. Material presented during the Design Review Meeting as well as discussions, conclusions and recommendations shall be summarized in a Design Review Report."

This report constitutes the required Design Review Report. It is a compilation of all of the unrestricted (non-protectable) information presented/discussed at the May 22-23, 1980 ASE Mod I Design Review held at NASA-LeRC. This Design Review Meeting was an update to the preliminary ASE Mod I Design Assessment Meeting held at NASA-LeRC on January 16-17, 1980. As the result of the January review, NASA authorized MTI to proceed with the procurement/fabrication of certain long lead time parts.

On June 12, 1980, NASA-LeRC approved the design of the ASE Mod I Engine System (NASA/MTI 080-41) as presented at the May review. This letter directed MTI "...to proceed with the procurement of ASE Mod I engine controls, auxiliaries, and accessories," which along with the previous approvals, constituted approval to proceed with the ASE Mod I design according to the approved schedules and work plan. The approval was given subject to the understanding, open issues, and action items reproduced on the following two pages.

On the basis of the Design Review and the subsequent approval received from NASA-LeRC, effort on the ASE Mod I fabrication/procurement is underway.

PRECEDING PAGE BLANK NOT FILMED

EXCERPTS FROM NASA-LeRC LETTER: NASA/MTI 080-41

Understandings

1. MTI will coordinate follow-up meetings among MTI, USS, and NASA to continue review of NASA's experience in finite element analysis and low cycle fatigue analysis. These meetings should be in the U.S.
2. Data supporting the selection of an air excess ratio objective of 1.1 will be provided to NASA at the June 1980 External Heat System Task Team Meeting in Malmo, Sweden.
3. Detailed review of component and engine system test data and analyses will be conducted through the respective task teams.

Open Issues

1. MTI will review the logic used in arriving at the hydrogen loss specification for 7500 miles. It appears that the heater tubes alone are allowed to lose 20 to 30% of the hydrogen bottle capacity. What losses were considered for seals, connections, etc.? Shouldn't the criteria be presented in terms of engine control and performance?
2. MTI will investigate the lateral tolerance build-up effects on misalignment of the cylinder liners in the engine block and the resulting eccentric load on the O-rings and piston rings. The tolerance of hole locations as well as squareness and concentricity should be considered.

Recommendations

1. NASA is still concerned with potential problems with dynamic structural resonance of the ASE Mod I engine and believes modal surveys of the ASE Mod I hardware are warranted. It is recommended that MTI coordinate activities in this area to utilize NASA in-house expertise in structural resonance.
2. Reconsideration of normal air conditioning condenser location and normal passenger compartment heater sizing is recommended for the ASE Mod I vehicle. NASA's concern is that a Stirling vehicle with too many nonconventional features may have a negative public impact during demonstrations.
3. Further investigation by the Controls Task Team of the adequacy of the 50 millisecond computational cycle time of the ASE Mod I engine electronics is recommended.
4. Measurement of the pressure drop of the air supply system --components and total system-- is recommended.
5. Reassessment of the 150°F (65.6°C) maximum air blower bearing temperature is recommended.

6. Individual measurement of accessory and auxiliary power consumptions prior to installation on the ASE Mod I engine is recommended.

Action Items

1. MTI shall provide NASA the following pumping Leningrader seal information:
 - Projected life expectancy.
 - H_2 leakage rates experienced to date and/or expected leakage rates for the ASE Mod I application.
 - Data or estimates of power dissipation as a function of engine speed.

Due October 16, 1980 (Seals Task Force Meeting).

2. MTI shall recommend to NASA methods to conveniently recover the 8% loss in ASE Mod I maximum power, if the ASE Mod I vehicle proves to be too sluggish. Due August 28, 1980.
3. MTI shall submit for NASA approval the specifications for the Air/Fuel Control and the Power Control. This will ensure that all parties (Task Teams, Designers, etc.) are working towards the same objectives. Due September 25, 1980 (Controls Task Team Meeting).
4. MTI shall provide NASA an outline and schedule for analyzing interactions between the temperature control and the air blower control systems. Due September 25, 1980 (Controls Task Team Meeting).
5. MTI shall provide NASA a revised hydrogen loss specification (see Open Issue #1). Due September 30, 1980.

A.2 Agenda for the May 22-23, 1980 Meeting

MOD I DESIGN REVIEW

A G E N D A

THURSDAY, MAY 22, 1980

8:30	OPENING REMARKS	NASA
8:40	INTRODUCTION	NOEL NIGHTINGALE
8:50	EXECUTIVE SUMMARY	STEN HOLGERSSON
9:50	MOD I BASIC STIRLING ENGINE UPDATE	BENGT-OVE MOODYSSON
11:05	MOD I STIRLING ENGINE SYSTEM	
11:05	● CONTROL AND AUXILIARY OVERVIEW	STEN-HAKAN ALMSTROM
11:20	● AUXILIARIES	LARS HENRIKSSON
12:05	LUNCH	
1:05	● AUXILIARIES (CONTINUED)	GEORGE RIECKE
1:20	● ACCESSORIES	ART DYBOWSKI
1:30	● AIR/FUEL CONTROL SYSTEM	LARS HENRIKSSON
1:45	● POWER CONTROL SYSTEM	STEN-HAKAN ALMSTROM
2:45	● CONTROL SYSTEM	STEN-HAKAN ALMSTROM
3:15	● ELECTRONICS	SIXTEN LEWENHAUPT
4:15	VEHICLE INTEGRATION	JOHN VIGNEAULT ART DYBOWSKI
4:45	COOLING SYSTEM	STEN HOLGERSSON
5:15	VEHICLE MILEAGE PROJECTIONS	STEVE ARNOLD
5:35	FAILURE MODE ANALYSIS	STEN HOLGERSSON
5:45	ADJOURN	

*3:00 PM TECHNICAL SPLINTER MEETING ON "DYNAMIC RESONANCE
OF MOD I TIE BOLTS"

MOD I DESIGN REVIEW

A G E N D A

FRIDAY, MAY 23, 1980

8:00	RISK ASSESSMENT	MACK DOWDY
9:45	CONCLUSIONS AND RECOMMENDATIONS	NOEL NIGHTINGALE
10:00	NASA CRITIQUE	
10:45	OPEN DISCUSSION	

*1:00 P.M. TECHNICAL SPLINTER MEETING ON "LOW CYCLE FATIGUE
AND FINITE ELEMENT ANALYSIS ON HEATER HEADS"

ORIGINAL PAGE IS
OF POOR QUALITY

AUTOMOTIVE STIRLING ENGINE DEVELOPMENT PROGRAM

MOD I STIRLING ENGINE SYSTEM

DESIGN REVIEW

MAY 22, 1980

INTRODUCTION

PRECEDING PAGE BLANK NOT FILMED

MECHANICAL TECHNOLOGY INCORPORATED
968 ALBANY-SHAKER ROAD
LATHAM, NEW YORK 12110

ORIGINAL PAGE IS
OF POOR QUALITY

MOD I DESIGN REVIEW
MAY 22, 1980
INTRODUCTION

DESIGN REVIEW OBJECTIVES

- TO UPDATE MOD I BASIC STIRLING ENGINE DESIGN.
- TO REVIEW DETAIL DESIGN OF MOD I STIRLING ENGINE SYSTEM:
 - CONTROL SYSTEM
 - AUXILIARIES
 - VEHICLE INTEGRATION
- TO SEEK NASA APPROVAL OF MOD I STIRLING ENGINE SYSTEM DESIGN.
- TO SEEK NASA APPROVAL TO COMMENCE PROCUREMENT OF STIRLING ENGINE SYSTEM HARDWARE FOR MOD I PROGRAM.
- TO UPDATE AND EVALUATE THE RISK ASSESSMENT OF MOD I ENGINE DESIGN.

MOD I DESIGN REVIEW
MAY 22, 1980
INTRODUCTION

ORIGINAL PAGE IS
OF POOR QUALITY

MOD I ENGINE OBJECTIVES

- DESIGN, FABRICATE, TEST AND DEVELOP A STIRLING ENGINE FOR AUTOMOTIVE APPLICATION.
- USE P-40 AND P-75 TECHNOLOGY AS BASIS FOR IMPROVEMENT.
- IMPROVE POWER DENSITY.
- IMPROVE OVERALL ENGINE PERFORMANCE.

AUTOMOTIVE STIRLING ENGINE DEVELOPMENT PROGRAM

Program Milestones

Fiscal Year

1979	1980	1981	1982	1983	1984
	▼ ASE Mod I Design Freeze		▼ ASE Mod I Dyno Test		
		Dyno Characterization	▼ ASE Mod I Upgraded		
		ASE Mod I EPA Vehicle Test	▼		
		ASE Mod II Dyno Test	▼		
		ASE Mod II EPA Vehicle Test	▼		

MOD I DESIGN REVIEW
MAY 22, 1980
INTRODUCTION

MOD I ENGINE SCHEDULE

ORDER LONG-LEAD HARDWARE
IN DRIVE SYSTEM

BASIC ENGINE DESIGN ASSESSMENT

ORDER LONG-LEAD HARDWARE IN
BASIC ENGINE

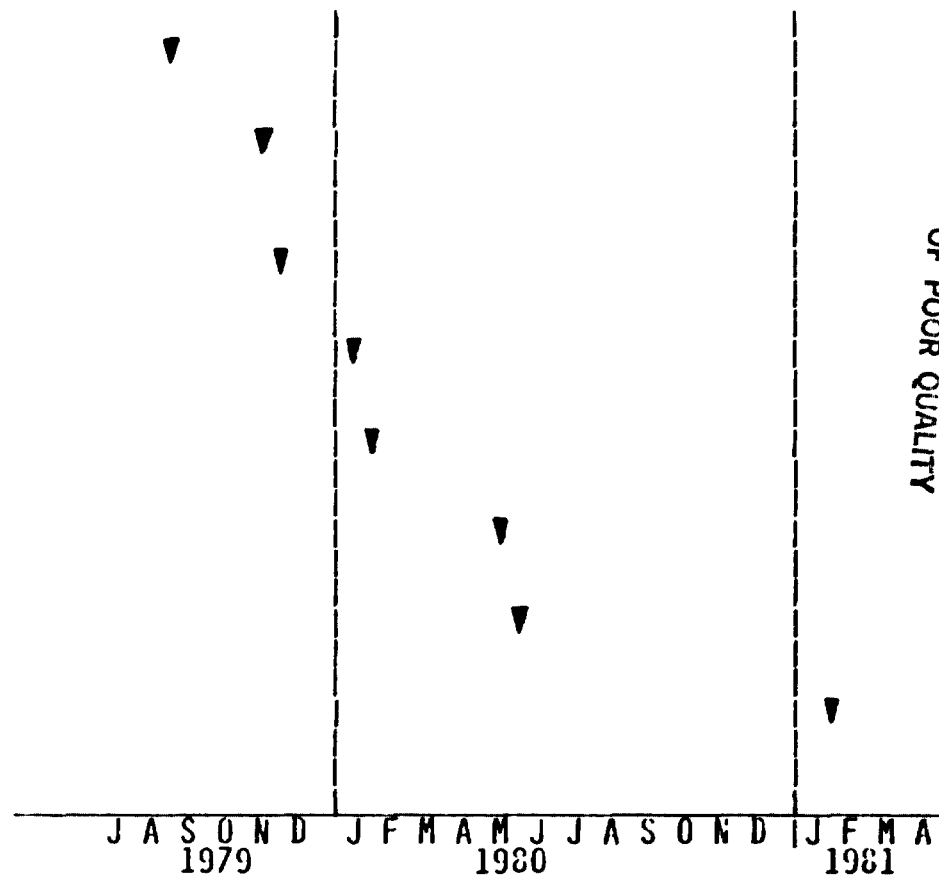
DESIGN REVIEW BASIC ENGINE

ORDER BASIC ENGINE HARDWARE

DESIGN REVIEW STIRLING SYSTEM

ORDER STIRLING SYSTEM HARDWARE

TEST FIRST MOD I ENGINE



ORIGINAL PAGE IS
OF POOR QUALITY

ORIGINAL PAGE IS
OF POOR QUALITY
AUTOMOTIVE STIRLING ENGINE DEVELOPMENT PROGRAM

MOD I STIRLING ENGINE SYSTEM
DESIGN REVIEW
MAY 22, 1980

EXECUTIVE SUMMARY

PRECEDING PAGE BLANK NOT FILMED

MECHANICAL TECHNOLOGY INCORPORATED
968 ALBANY-SHAKER ROAD
LATHAM, NEW YORK 12110

MOD I DESIGN REVIEW
MAY 22, 1980
EXECUTIVE SUMMARY

ORIGINAL PAGE IS
OF POOR QUALITY

- UPDATING OF BASIC STIRLING ENGINE PRESENTED IN JANUARY 1980:
 - NEW PISTON DOME DESIGN
 - CGR COMBUSTOR WITHOUT BY-PASS VALVE
 - ASSEMBLY SEQUENCE - TOLERANCE STACK-UP
- CONCENTRATION ON THE OTHER PARTS OF THE STIRLING ENGINE SYSTEM:
 - AUXILIARIES
 - AIR/FUEL CONTROL
 - POWER CONTROL
 - ELECTRONIC CONTROL

INSTALLATION IN VEHICLE

PACKAGING AND VEHICLE MODIFICATIONS

COOLING SYSTEM

MOD I DESIGN REVIEW
MAY 22, 1980
EXECUTIVE SUMMARY

ORIGINAL PAGE IS
OF POOR QUALITY

MOD I DESIGN OBJECTIVES

- FROM EXISTING BASELINE ENGINE TECHNOLOGY (P-40 AND P-75)
DEVELOP AN ENGINE FOR AUTOMOTIVE APPLICATION
 - IMPROVED POWER TO WEIGHT RATIO
 - IMPROVED POWER TO VOLUME RATIO
 - DESIGN FOR PART LOAD OPERATION
 - IMPROVED MATCHING OF AUXILIARIES
 - SIMPLIFIED ASSEMBLY AND IMPROVED MAINTENANCE

MOD I DESIGN REVIEW
MAY 22, 1980
EXECUTIVE SUMMARY

LOGIC OF DESIGN AND APPROACH

- BASELINE TECHNOLOGY
 - U-4 CONFIGURATION
 - INVOLUTE HEATER
 - CANISTER REGENERATORS
- POWER/WEIGHT RATIO
 - NEW MECHANICAL DESIGN IN ORDER TO USE ALUMINUM
- OPTIMIZED FOR PART POWER OPERATION
 - REDUCED REGENERATOR CROSS SECTIONAL AREA
- MATCHING OF AUXILIARIES
 - DEVELOP NEW BLOWER
 - DEVELOP VARIABLE DRIVE
- SIMPLIFIED ASSEMBLY
 - INTEGRATION OF CONTROL SYSTEM PARTS AND SUBASSEMBLIES

BASIC STIRLING ENGINE

MOD I DESIGN REVIEW
MAY 22, 1980
EXECUTIVE SUMMARY

BASIC MOD I STIRLING ENGINE

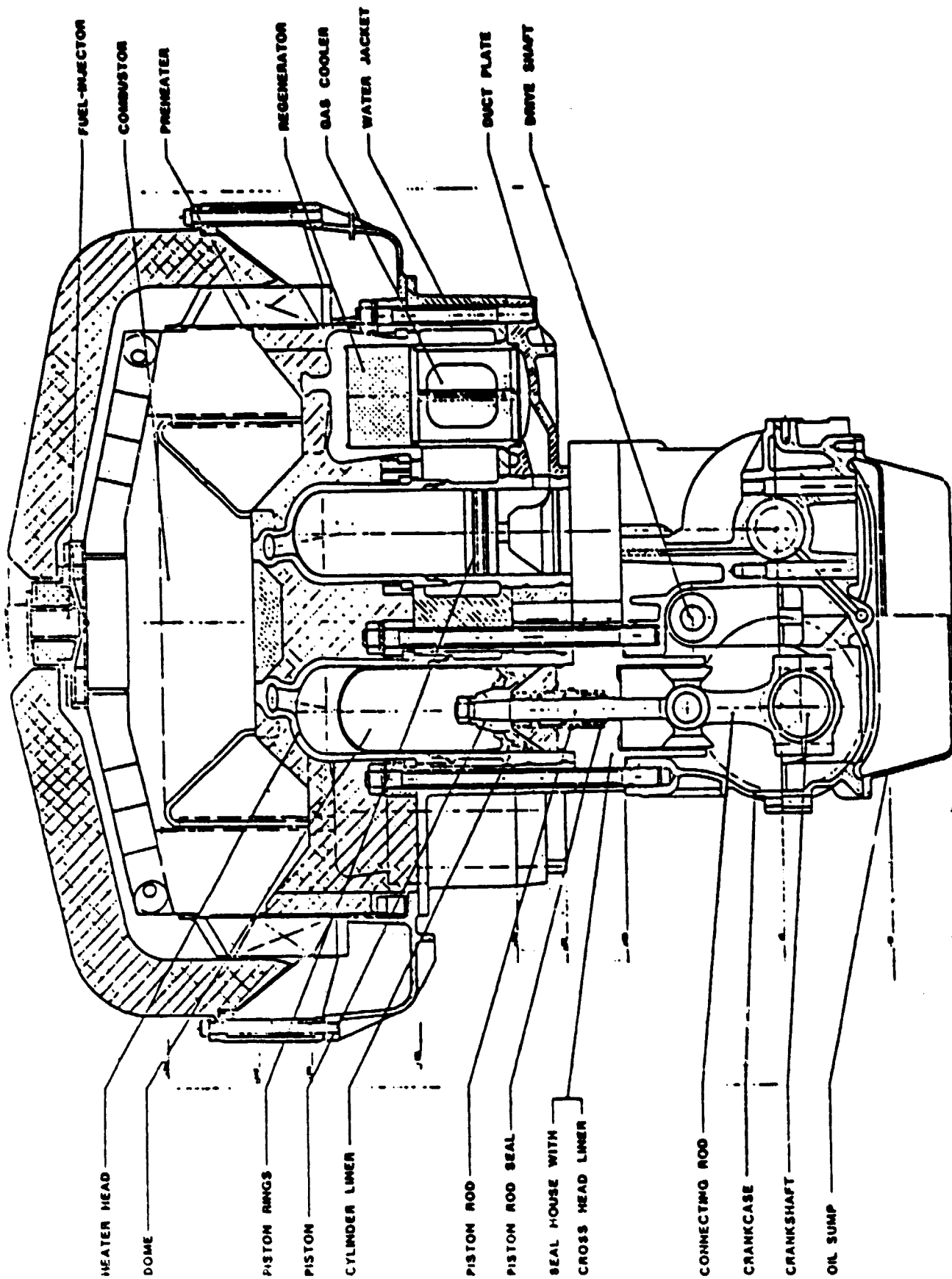
- EXTERNAL HEAT SYSTEM
 - COMBUSTOR
 - PREHEATER WITH HOUSING

- HOT ENGINE SYSTEM
 - HEATER HEAD
 - REGENERATORS (4)
 - COOLERS (4)

- COLD ENGINE SYSTEM
 - CYLINDER BLOCK (INCLUDING DUCT PLATE)
 - PISTON, PISTON ROD ASSEMBLY
 - PISTON ROD SEALS

- ENGINE DRIVE SYSTEM
 - CRANKCASE ASSEMBLY
 - MAIN POWER TAKE-OFF
 - AUXILIARY DRIVES

ORIGINAL PAGE IS
OF POOR QUALITY



Basic Mod I Stirling Engine

MOD I DESIGN REVIEW
MAY 22, 1980
EXECUTIVE SUMMARY

ORIGINAL PAGE IS
OF POOR QUALITY

SOLUTION TO P-40 FAILURE MODES

<u>P-40 PROBLEM AREAS</u>	<u>MOD I DESIGN SOLUTION</u>	<u>STATUS</u>
CHECK VALVES (FAILURES)	DESIGNED SPECIFICALLY FOR STIRLING CYCLE	SUCCESSFULLY TEST > 600 HRS
PISTON DOME (BUCKLING)	0.5 MM THICKER WALL STRONGER MATERIAL	ANALYTICALLY VALIDATED
PISTON ROD SEAL (OIL LEAKAGE)	PUMPING LENINGRADER	SUCCESSFUL ENGINE AND RIG TESTS >40000 HRS
PISTON RINGS (MALFUNCTION)	<ul style="list-style-type: none">● TEMPERATURE LOWERED BY INCREASED DOME HEIGHT● WET CYLINDER LINERS	
HEATER HEAD BOLT (FAILURES)	NECKED DOWN LONG TIE BOLTS	FATIGUE TESTS PERFORMED ON SUBASSEMBLY MODEL
REGENERATOR HOUSING (DISTORTION)	SYMMETRICAL PRESSURE VESSELS; LOOSE FLANGES WITH RETAINER RINGS	
HEATER HEAD MANIFOLDS (CRACKS)	ELLIPTICAL MANIFOLD; CROSS SECTION STRESSES REDUCED BY 2.8	ANALYTICALLY VALIDATED
CYLINDER O-RINGS (LEAKAGE)	O-RINGS MOVED TO COOLER REGION	

MOD I DESIGN REVIEW
MAY 22, 1980
EXECUTIVE SUMMARY

PROCUREMENT SITUATION BEGINNING OF MAY

HEAT GENERATING SYSTEM

- MANUFACTURING STARTED IN APRIL
- DELIVERY BY MID-SEPTEMBER

AIR INLET MANIFOLD

- 4-5 WEEKS TO CAST - KARL SCHMIDT
- DELIVERY BY MID-SEPTEMBER

HEATER

- PATTERNS ARE BEING MADE
- DELIVERY BY END OF AUGUST

REGENERATORS

- DELIVERY BY MID-AUGUST

GAS COOLERS

- NOT CRITICAL TIME PATH ITEM
- DELIVERY BY END OF AUGUST

NOTE

ALL DELIVERY TIMES ARE GIVEN WITH THE ASSUMPTION
THAT THE TWO WEEK LOCKOUT IN SWEDEN WILL NOT
IMPACT THE DELIVERY. SOME DATES COULD MOVE BY
2 WEEKS DUE TO LOCKOUT.

PROCUREMENT SITUATION (CONTINUED)

COLD CONNECTING DUCT

- SKF DOING CASTINGS
- KROMMEKANO AB, MALMO, WILL DO MACHINING
- DELIVERY BY KROMMEKANO BEGINNING OF JUNE

WATER JACKET

- KROMMEKANO AB, MALMO, DOING MACHINING
- AREA AROUND TIE-BOLT HOLES WAS CHECKED FOR MATERIAL THICKNESS AND PASSED
- FIRST PART FINISHED

DOME

- FFV WELDING DOMES TO BASE
- INCO 718 IS A BACK-UP MATERIAL
- DELIVERY BY MID-JUNE

PISTON

- BEING PACED BY DOME WELDING RESULTS
- DELIVERY BY END OF MAY

NOTE

ALL DELIVERY TIMES ARE GIVEN WITH THE ASSUMPTION THAT THE TWO WEEK LOCKOUT IN SWEDEN WILL NOT IMPACT THE DELIVERY. SOME DATES COULD MOVE BY 2 WEEKS DUE TO LOCKOUT.

MOD I DESIGN REVIEW
MAY 22, 1980
EXECUTIVE SUMMARY

ORIGINAL PAGE IS
OF POOR QUALITY.

PROCUREMENT SITUATION (CONTINUED)

PISTON ROD

- FORGINGS BEING MACHINED
- DELIVERY BY END OF MAY

SEALS

- DELIVERY BY END OF MAY

LOWER END UNIT

- RICARDO IS SHIPPING FIRST UNIT WEEK OF MAY 12
- INSPECTION SHOWED ALL PARTS TO BE IN EXCELLENT CONDITION

NOTE

ALL DELIVERY TIMES ARE GIVEN WITH THE ASSUMPTION THAT THE TWO WEEK LOCKOUT IN SWEDEN WILL NOT IMPACT THE DELIVERY. SOME DATES COULD MOVE BY 2 WEEKS DUE TO LOCKOUT.

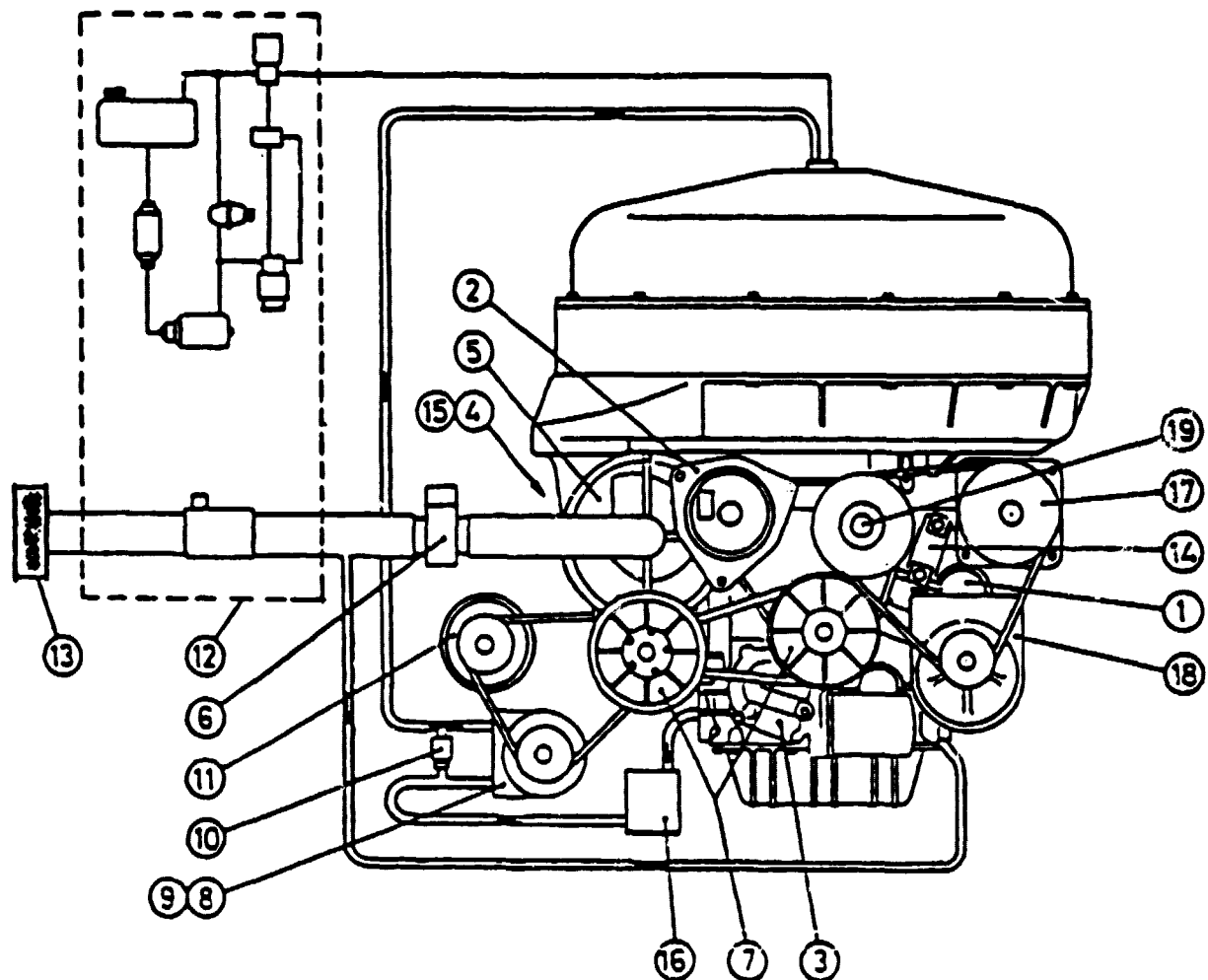
ORIGINAL PAGE IS
OF POOR QUALITY

STIRLING ENGINE SYSTEM

- AUXILIARIES
- CONTROL SYSTEMS

PRECEDING PAGE BLANK NOT FILMED

ORIGINAL PAGE 13
OF POOR QUALITY



- | | |
|------------------------------|-----------------------------------|
| 1. Starter motor | 11. Electric blower motor |
| 2. Alternator | 12. Air-fuel system |
| 3. Lubrication oil pump | 13. Air filter |
| 4. Water pump | 14. Hydrogen compressor |
| 5. Combustion air blowr | 15. After cooling pump |
| 6. Air throttle | 16. Crank case ventilation system |
| 7. Variable ratio belt drive | 17. Air-conditioning compressor |
| 8. Atomizer air compressor | 18. Power steering pump |
| 9. Servo oil pump | 19. Radiator fan shaft |
| 10. Relief valve | |

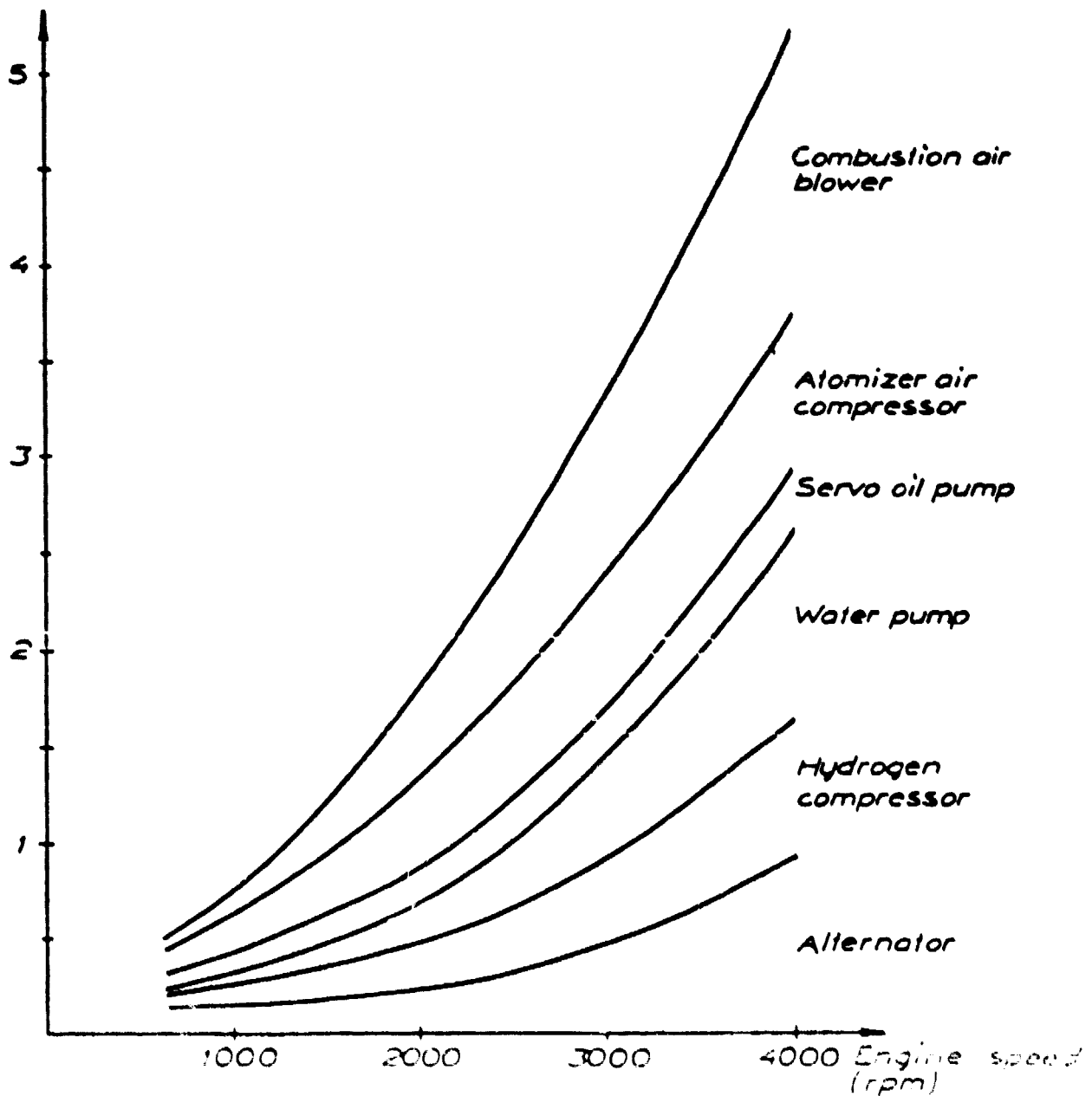
Fig. Auxiliaries and Accessories of ASE Mod I

ASE MOD I

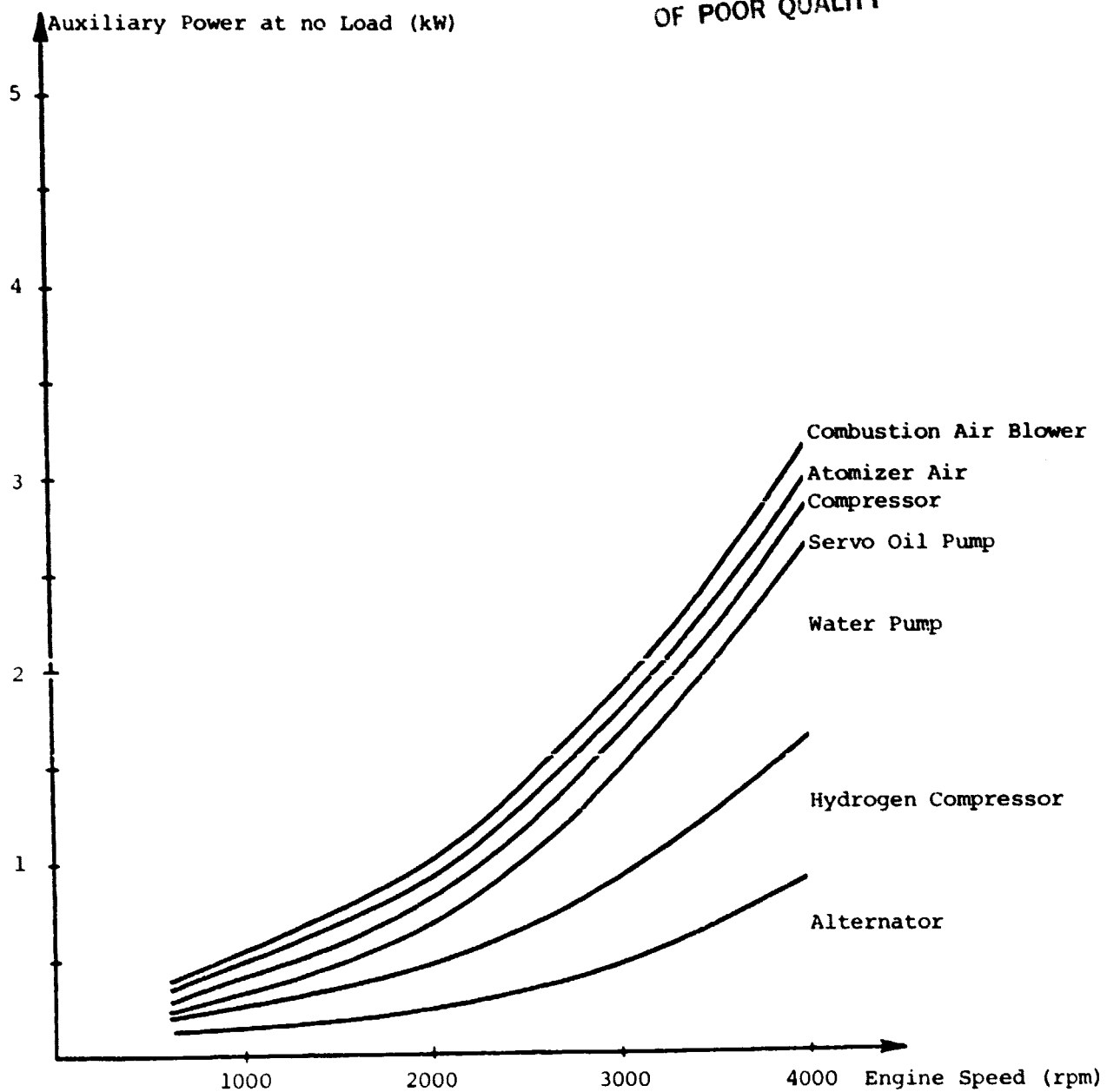
ORIGINAL PAGE IS
OF POOR QUALITY

TOTAL AUXILIARY POWER DEMAND AT FULL LOAD (No accessories)

Auxiliary power at full load (kw)

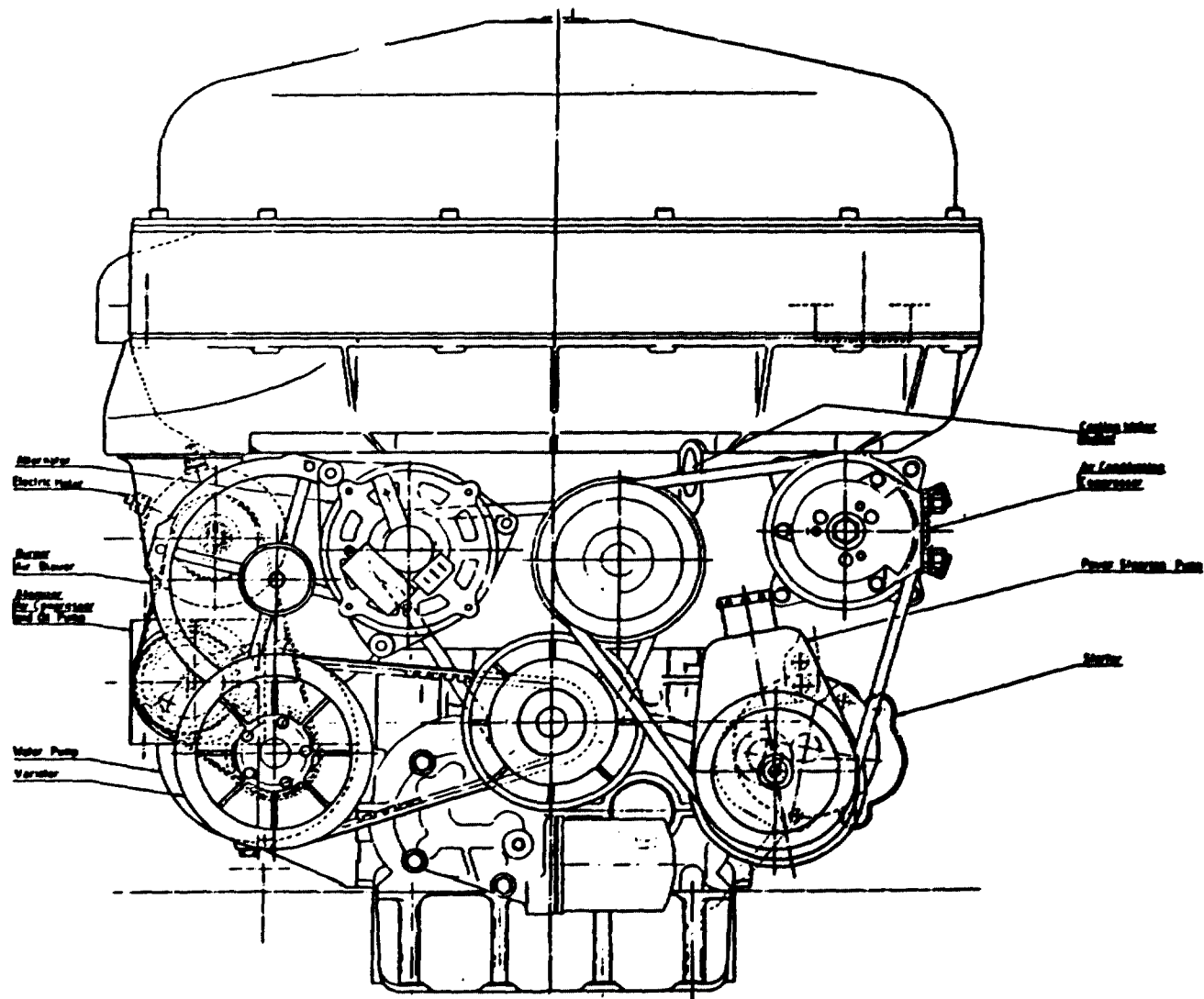


ORIGINAL PAGE IS
OF POOR QUALITY



Total Auxiliary Power Demand at Full Load
(no accessories)

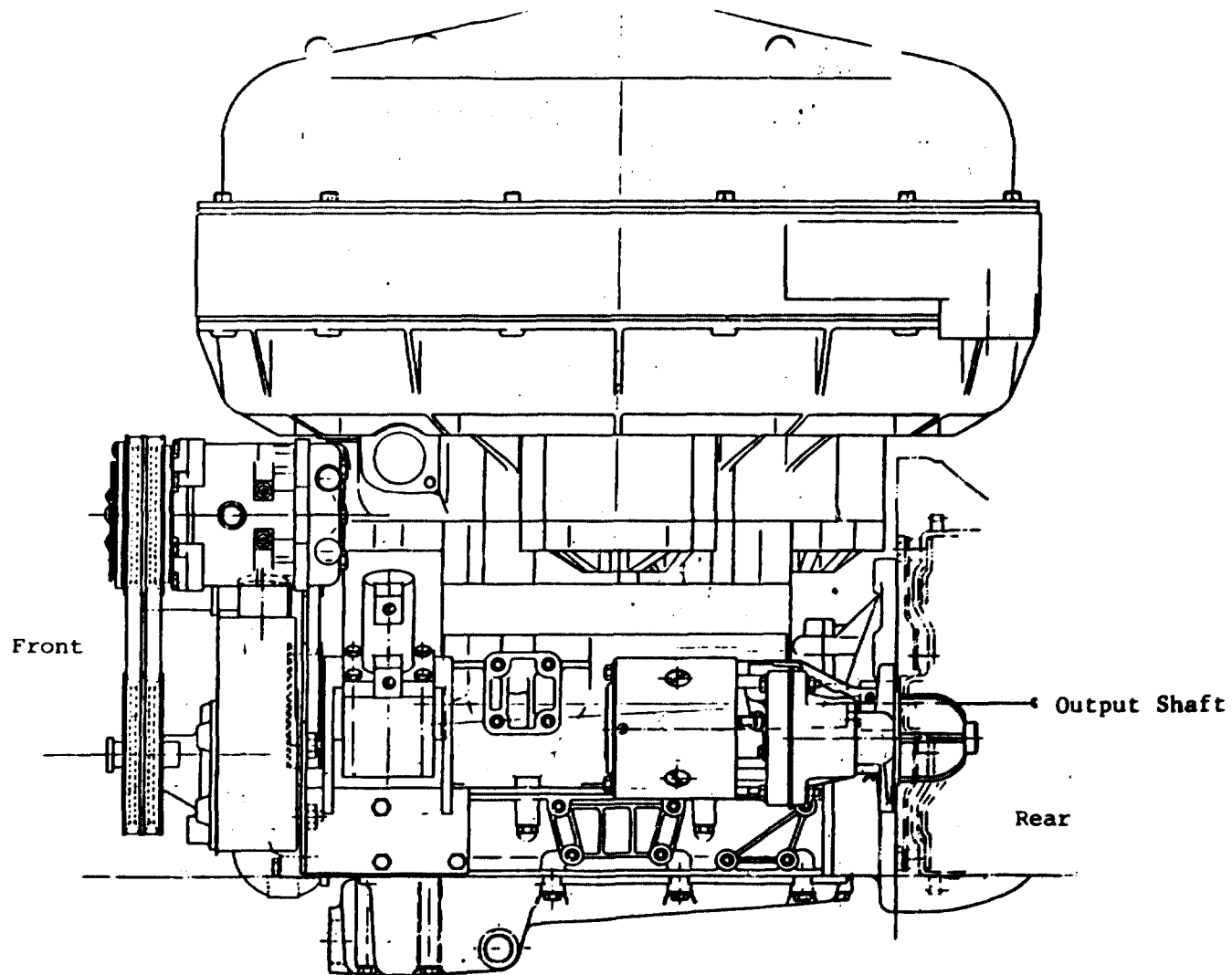
Left
Side



Right
Side

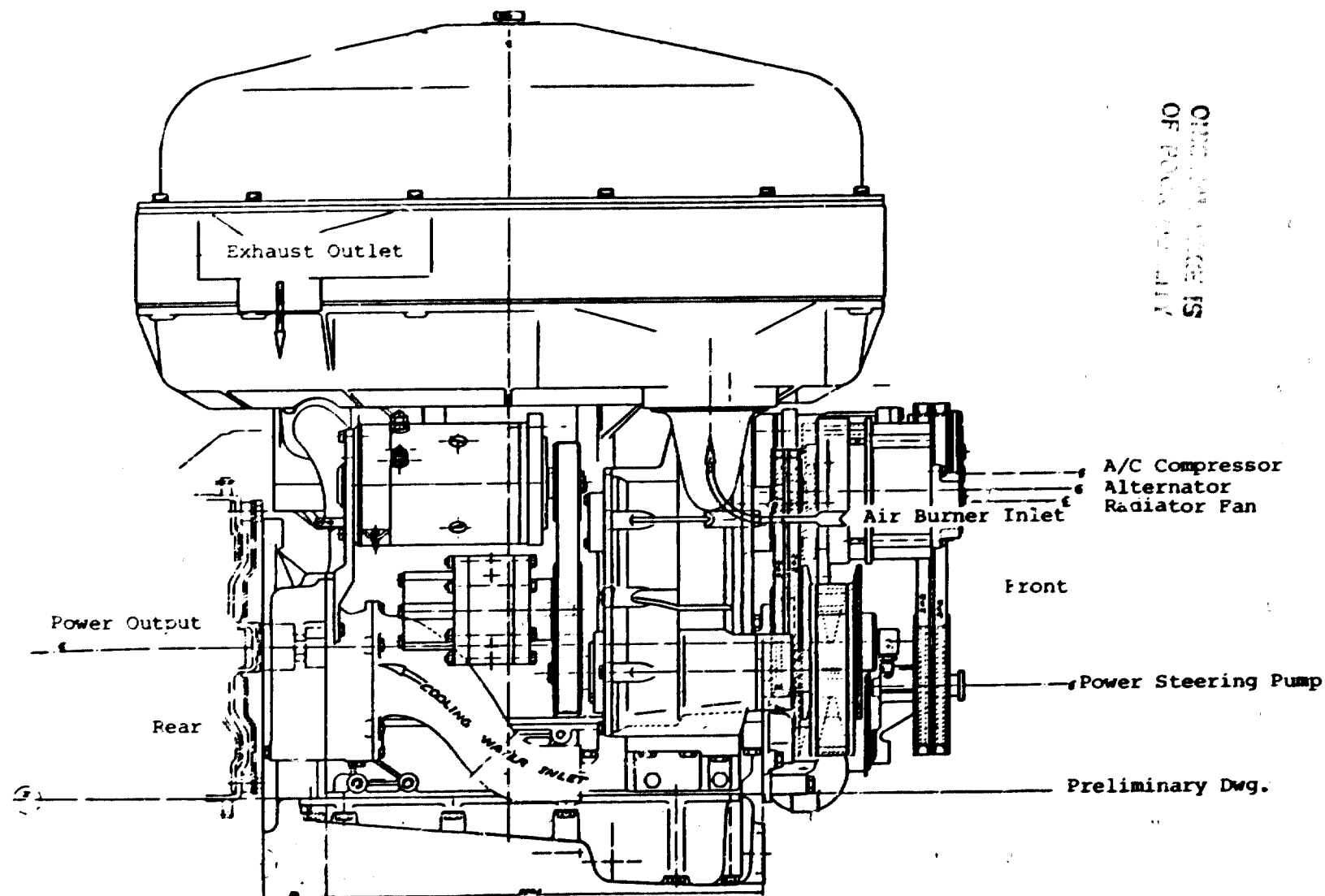
ORIGINAL PAGE IS
OF POOR QUALITY

Stirling Engine System ASE Mod I (Front End View)



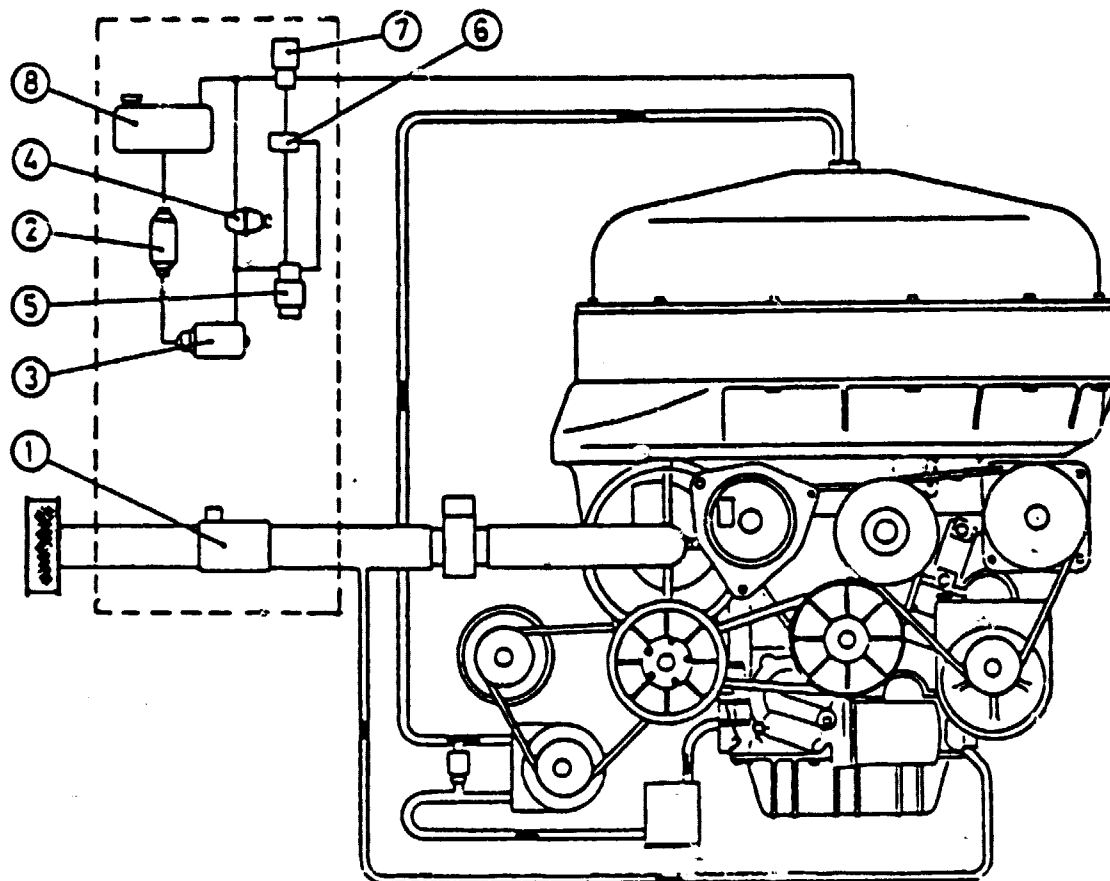
Stirling Engine System ASE Mod I (Lefthand Side View)

ORIGINAL PAGE IS
OF POOR QUALITY



Stirling Engine System ASE Mod I (Right-hand Side View)

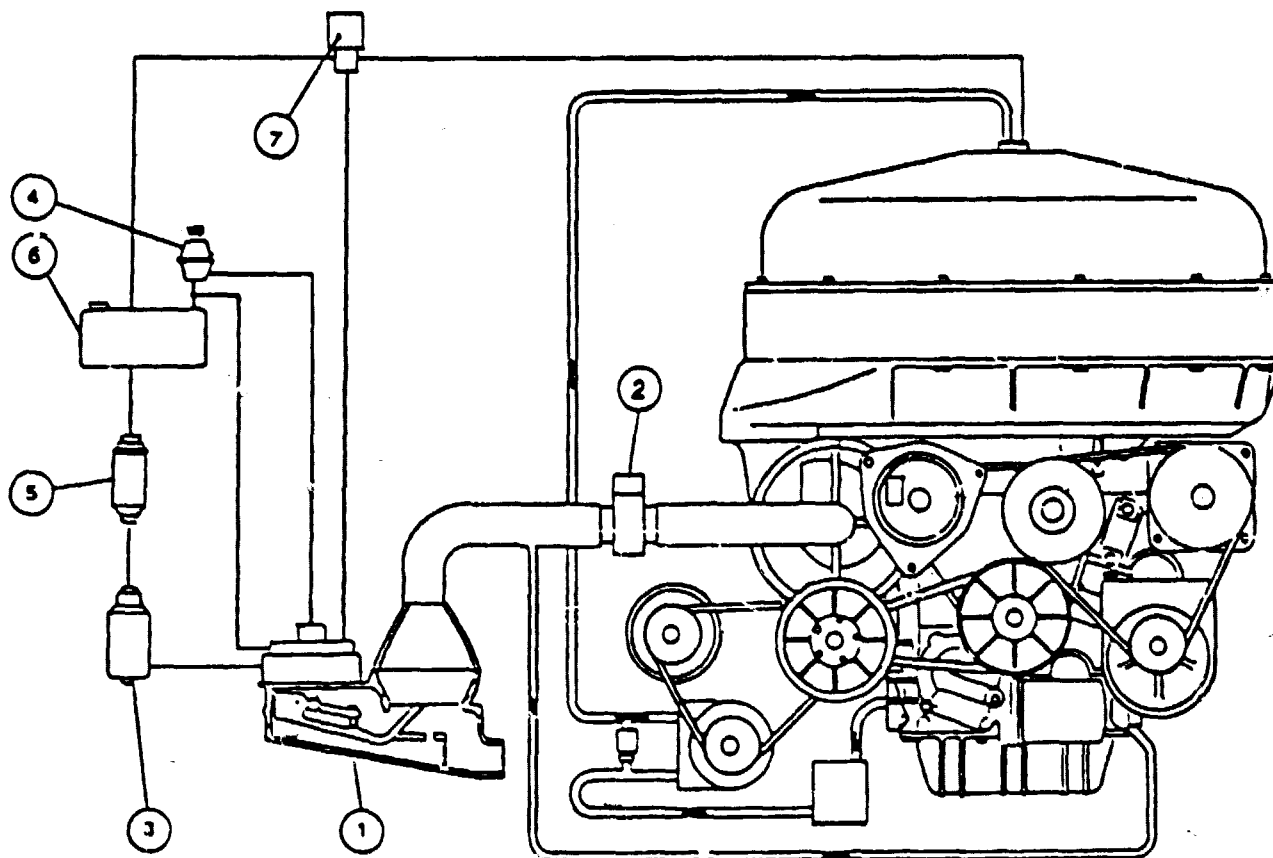
ORIGINAL PAGE IS
OF POOR QUALITY



1. Airflow meter
2. Fuel filter
3. Fuel supply pump
4. Fuel pressure regulator
5. Fuel metering pump
6. Fuel equalizer valve
7. Fuel valve
8. Fuel tank

Air-Fuel System Diagram

ORIGINAL PAGE IS
OF POOR QUALITY

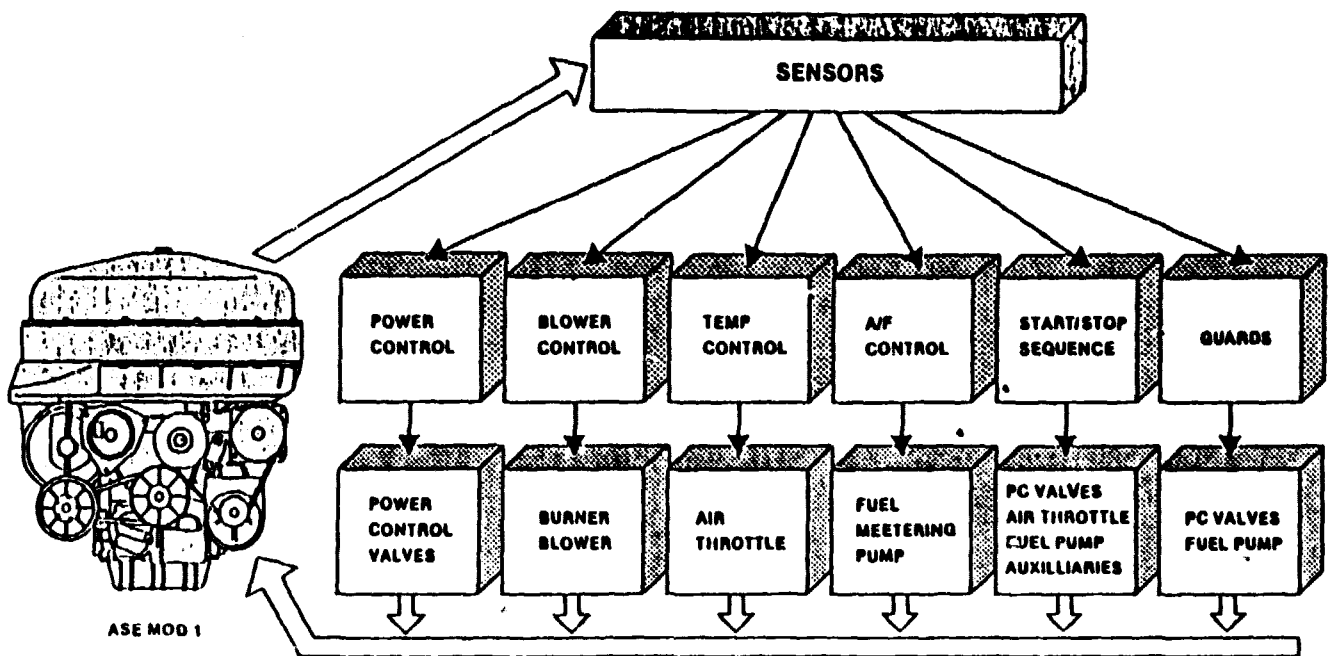


1. Bosch K-Jetronic
2. Air Throttle
3. Fuel Pump
4. Pressure Relief Valve
5. Fuel Filter
6. Fuel Tank
7. Fuel Valve

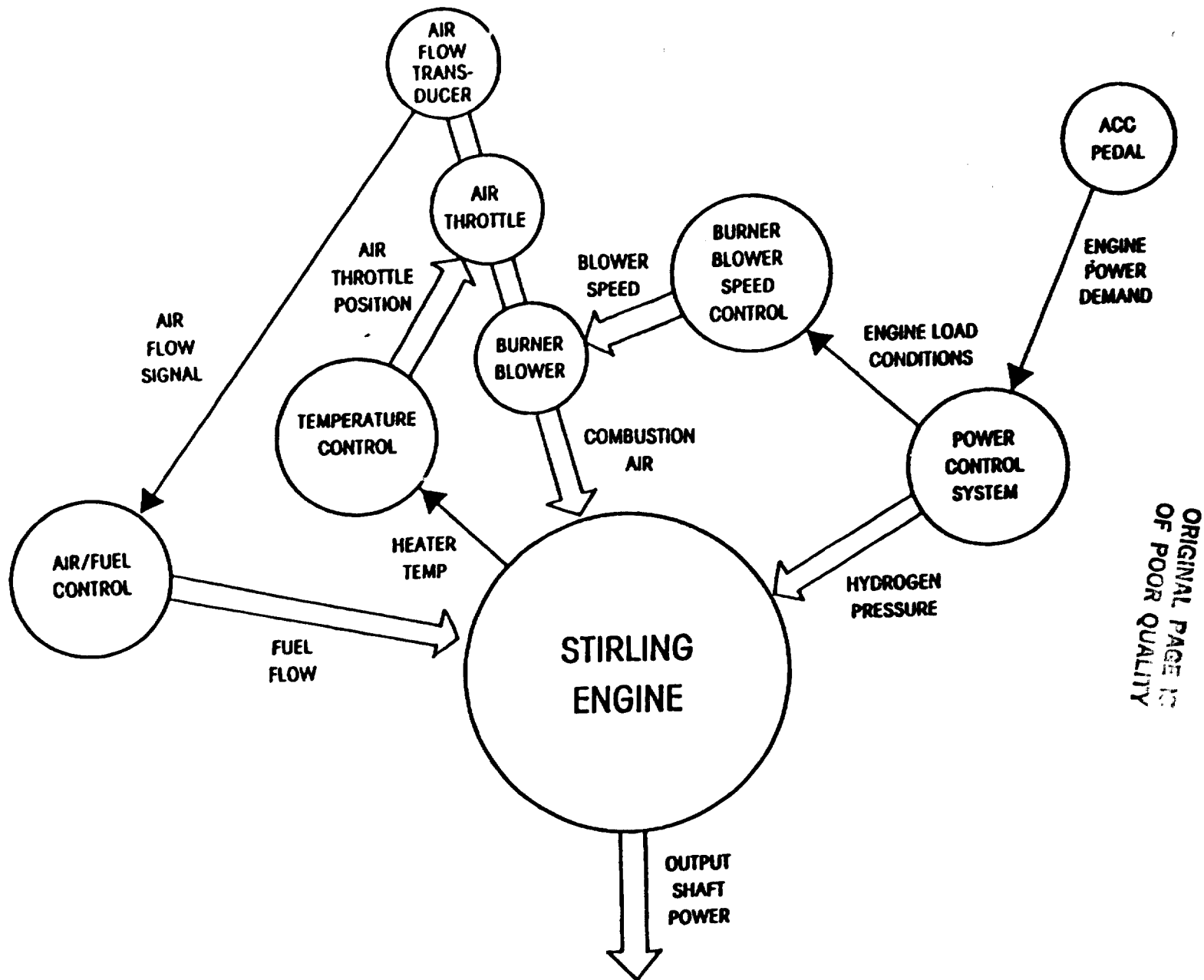
Bosch K-Jetronic Air/Fuel System Diagram as Back-up

ORIGINAL PAGE IS
OF POOR QUALITY

**ASE MOD 1
CONTROL BLOCKS**



ASE Mod I Control Systems



ASE Mod I Control System Interactions

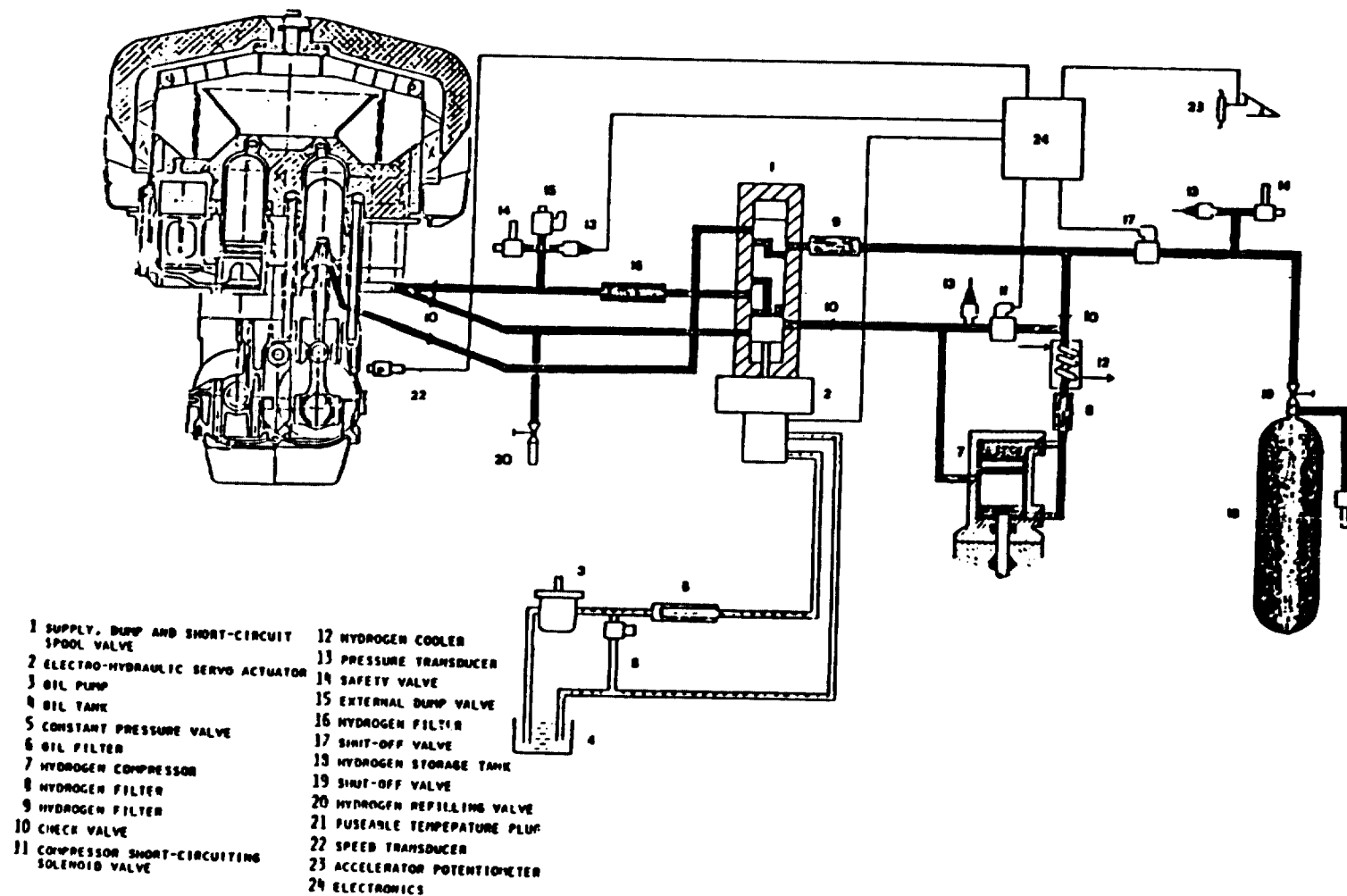
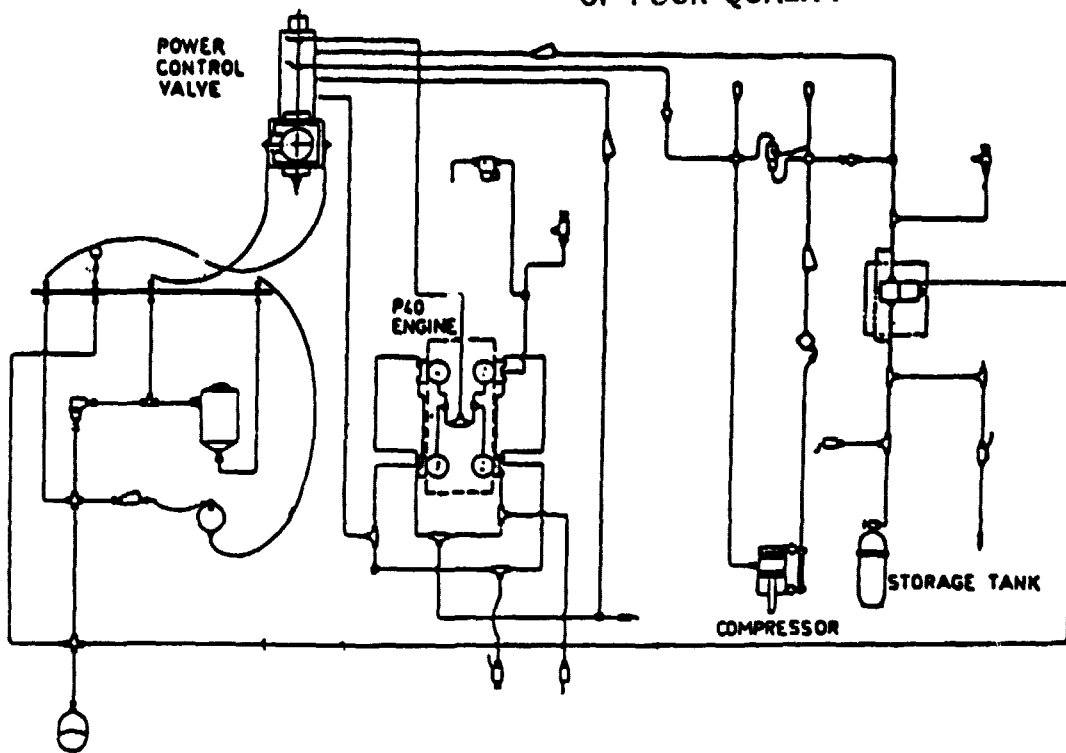


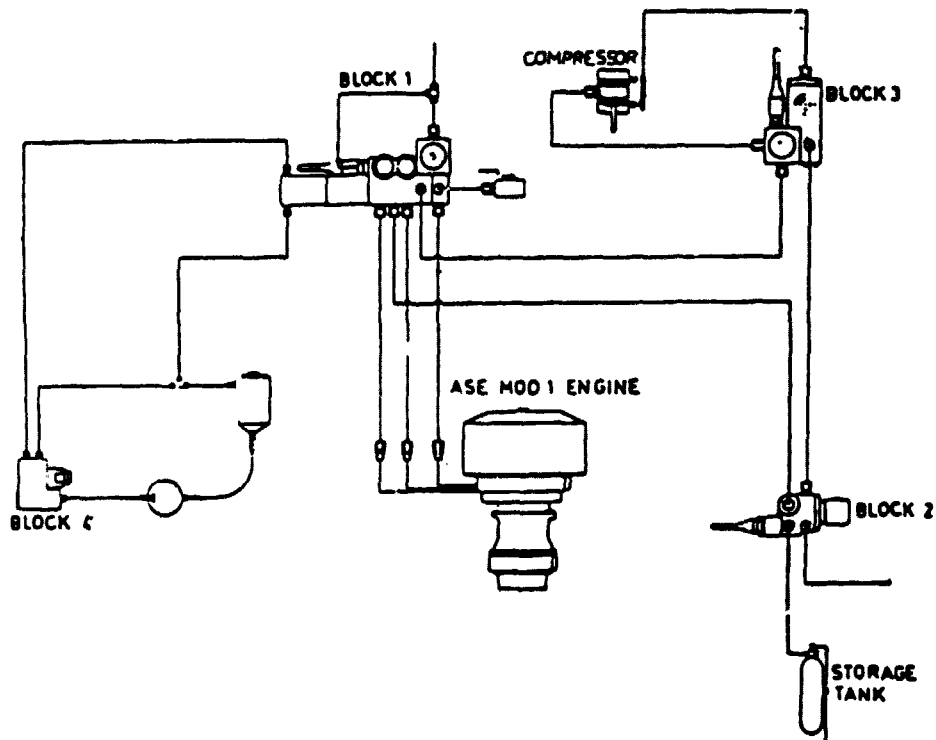
Figure 8.4:24 Block Scheme of the ASE Mod I Power Control System

ORIGINAL PAGE IS
OF POOR QUALITY

ORIGINAL PAGE IS
OF POOR QUALITY

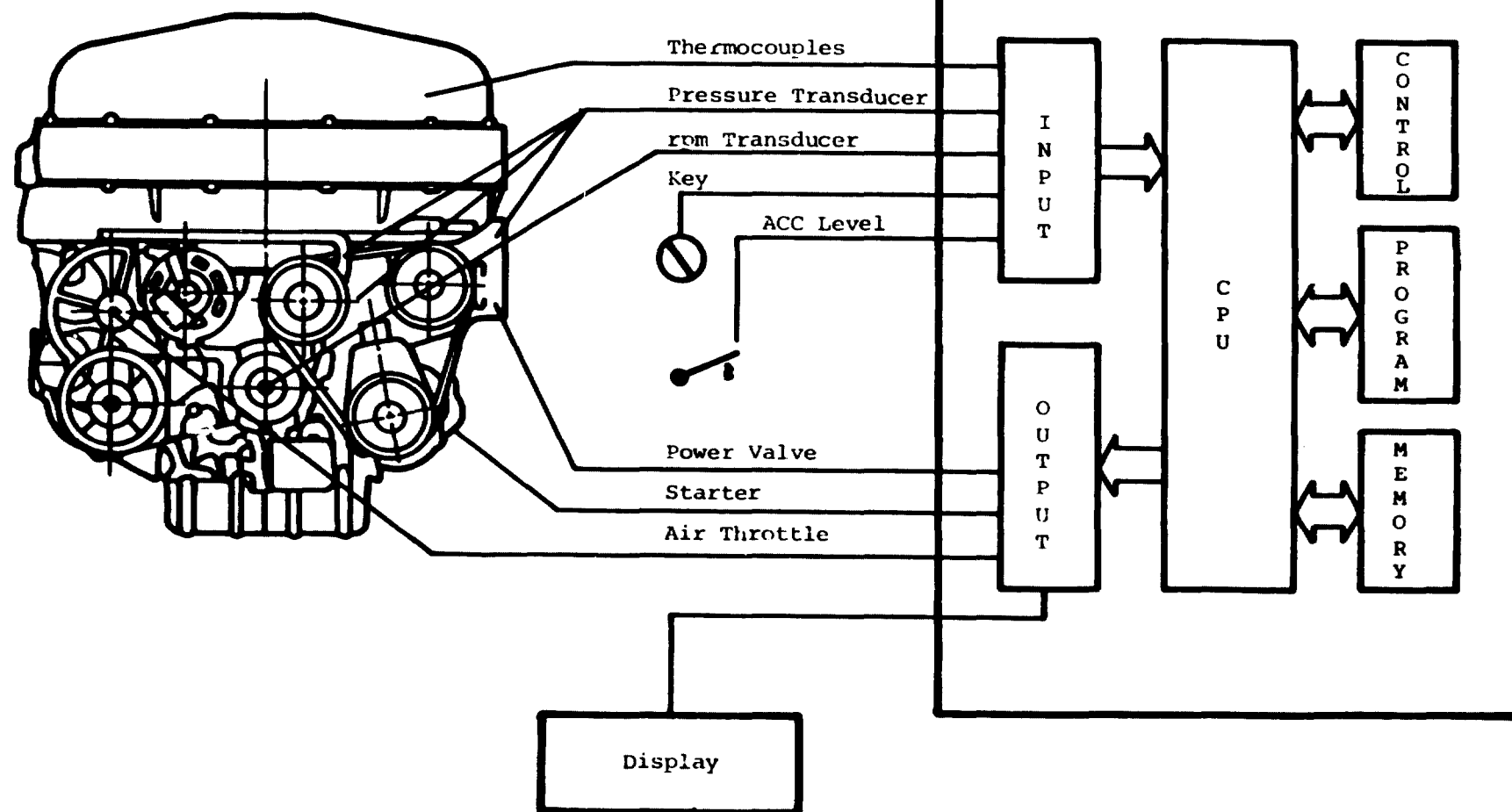


Tubing Arrangement of One P-40 Power Control System

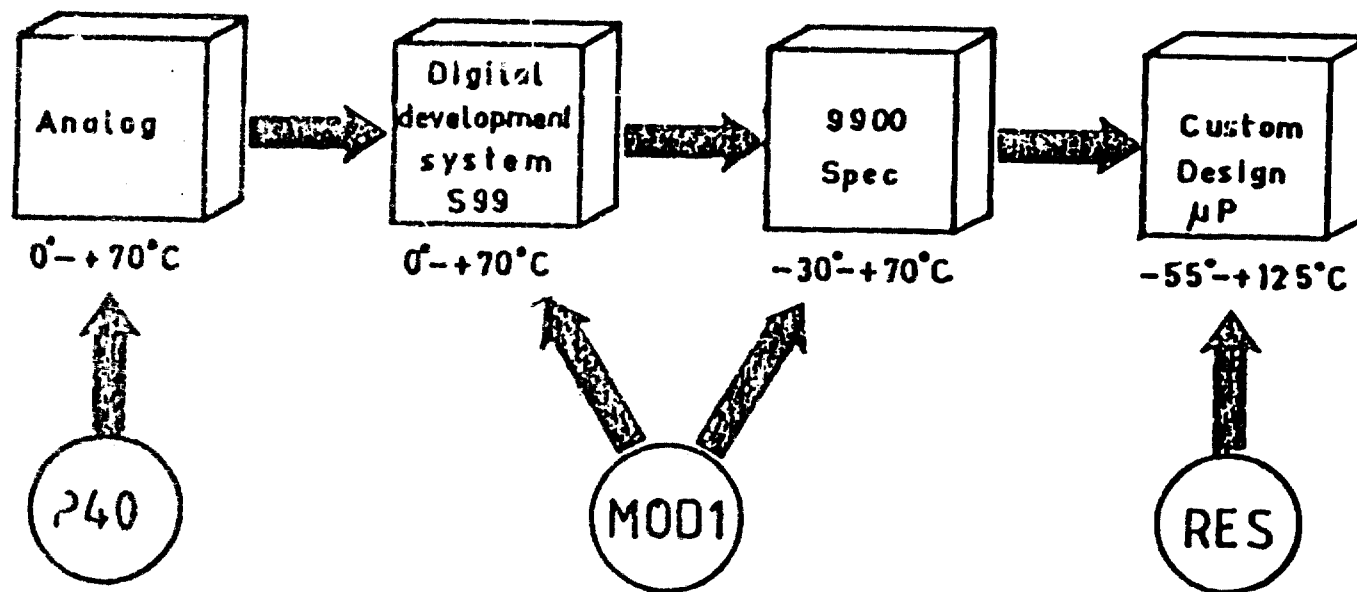


Tubing Arrangement of the ASE Mod I Power Control System

Engine Electronic



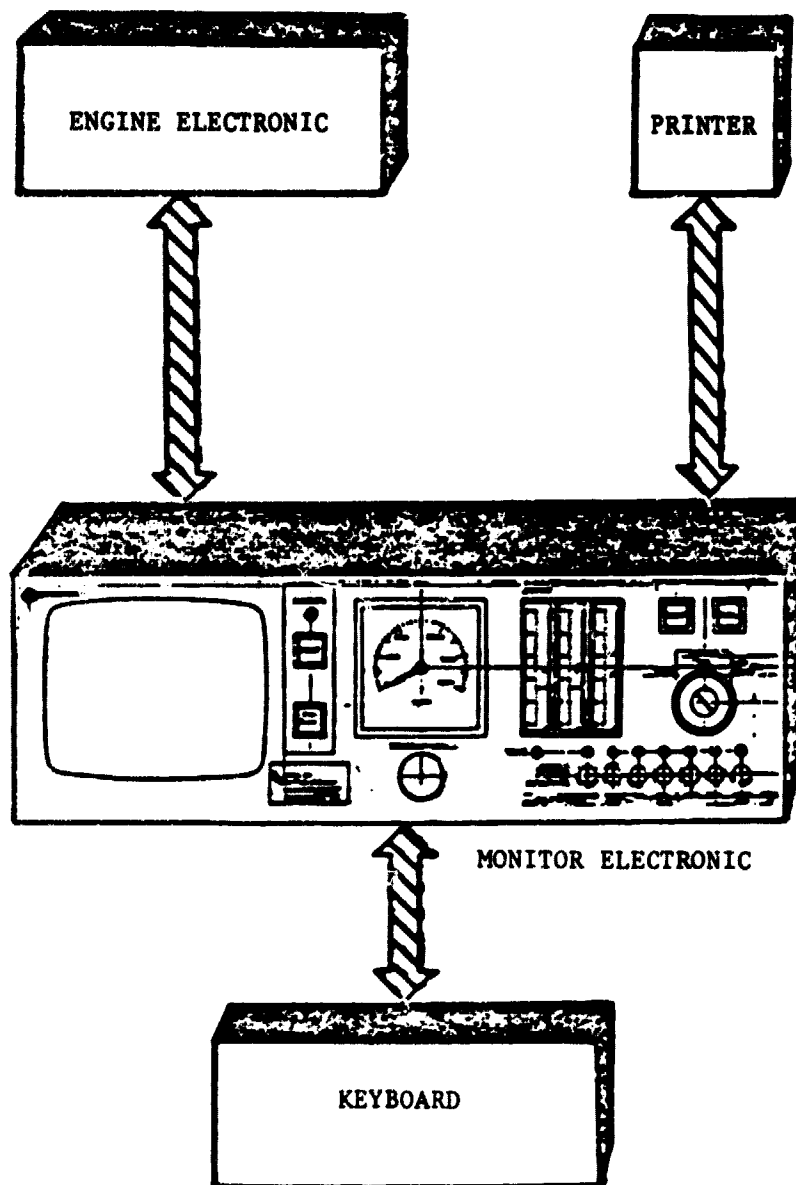
Electronic Control Block Diagram



ORIGINAL PRODUCT
OF POOR QUALITY

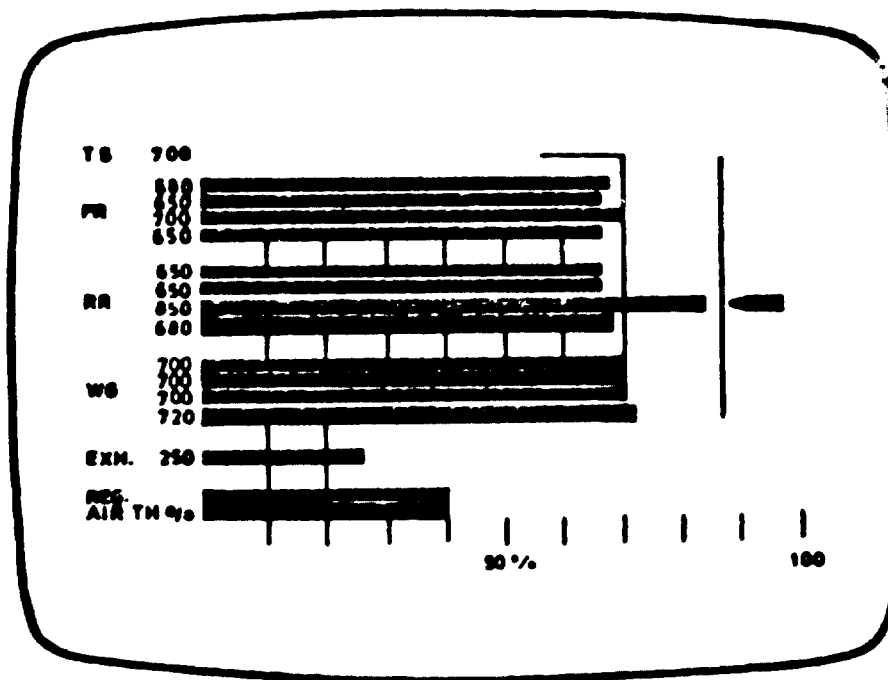
Stirling Electronic Development

ORIGINAL PAGE IS
OF POOR QUALITY



Mod I Prototype Electronic Test System

VIDEO SCREEN



DISPLAY 1

ORIGINAL PAGE IS
OF POOR QUALITY

SES PERFORMANCE

PRECEDING PAGE BLANK NOT FILMED

MOD I DESIGN REVIEW
MAY 22, 1980
EXECUTIVE SUMMARY

ORIGINAL PAGE IS
OF POOR QUALITY

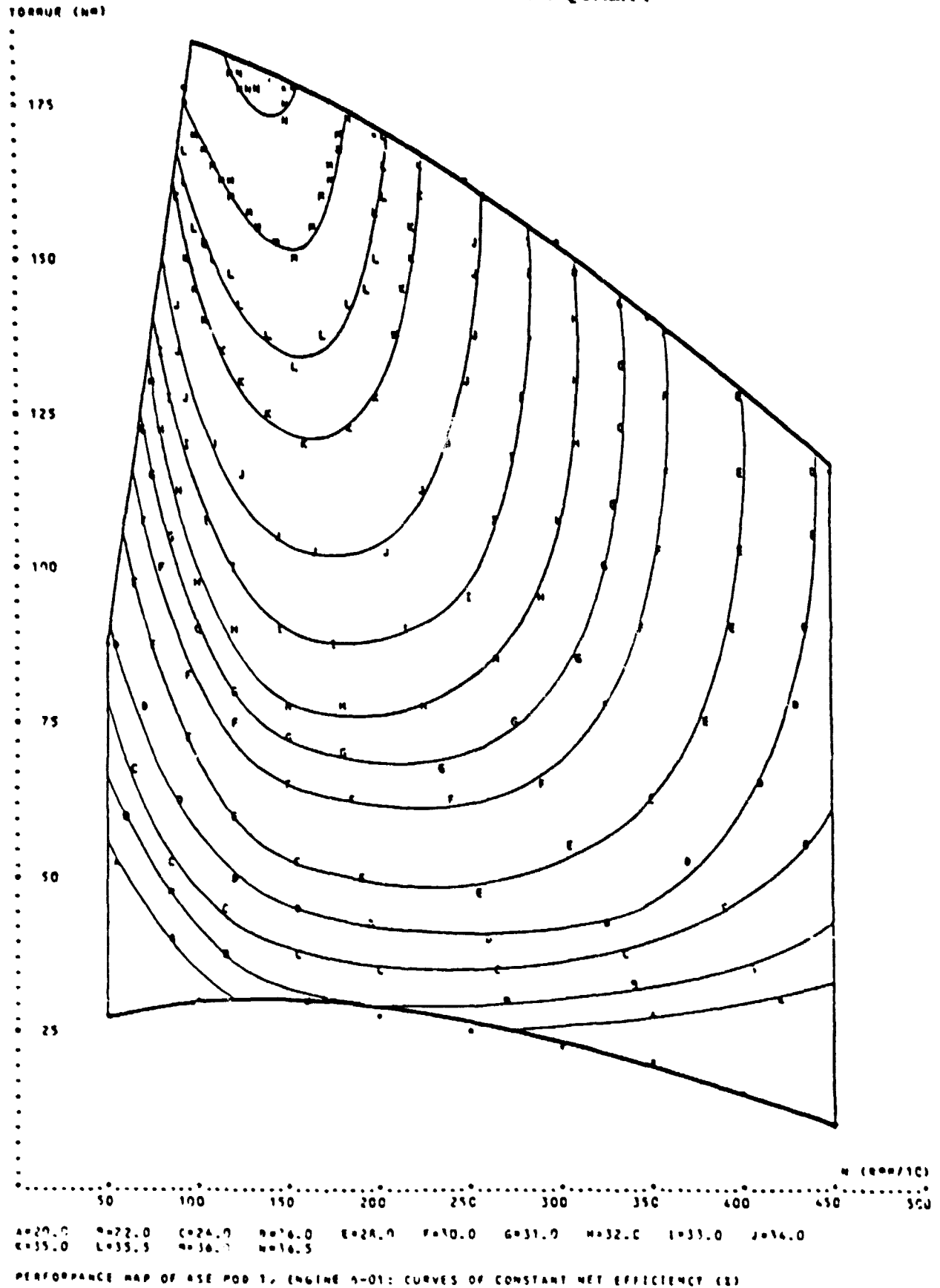
ENGINE PERFORMANCE PREDICTIONS

POINT/PARAMETER	POWER (kW)	EFFICIENCY (%)	PRESSURE (MPa)	SPEED (RPM)
MAX POWER	53.6*	28.1	15	4000
MAX EFFICIENCY	24.6	36.7	15	1300
PART LOAD POINT (AOP FOR FUEL FLOW)	10.7	28.8	5	2000

*DIFFERENCE AS COMPARED TO JANUARY, 1980

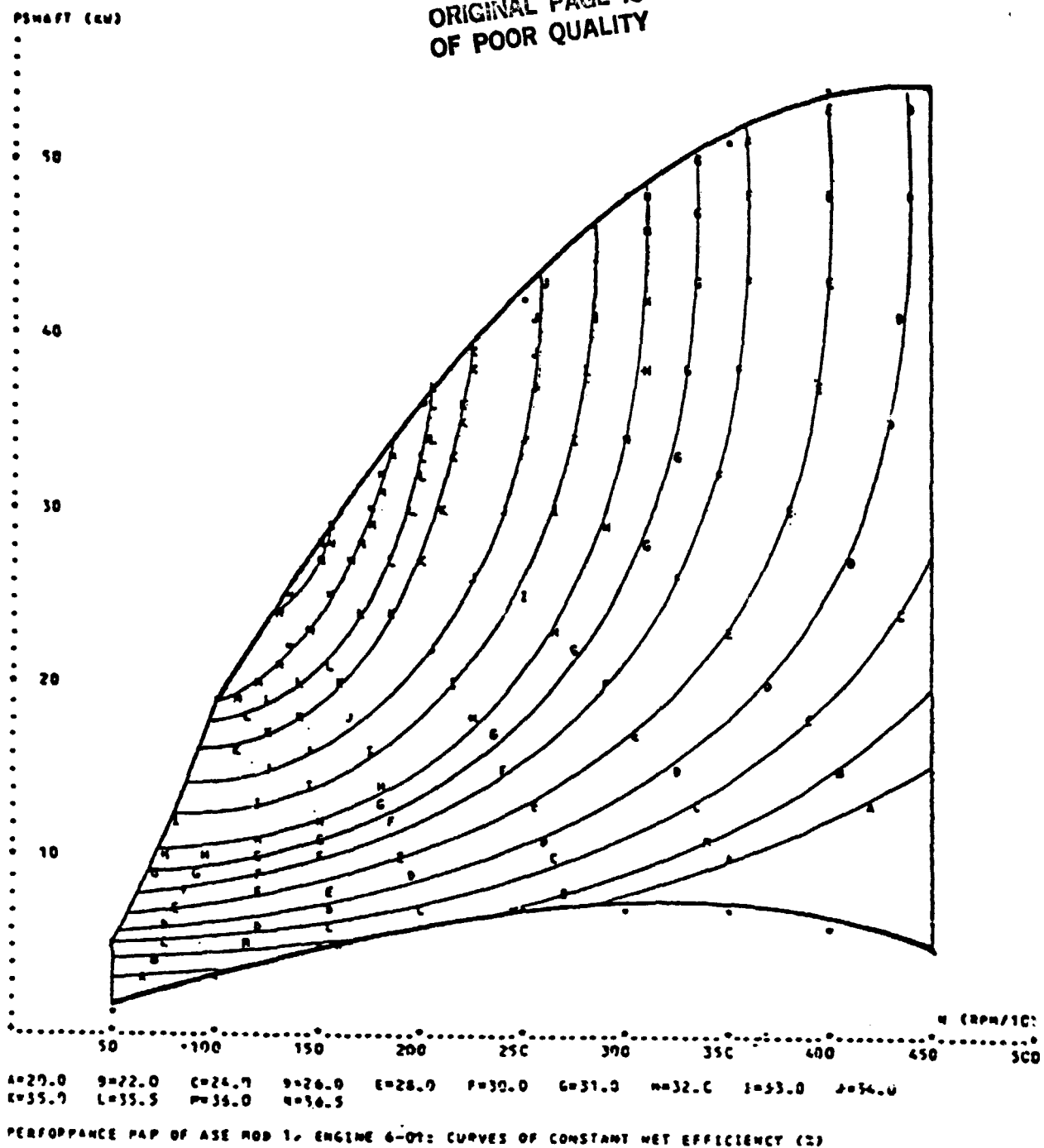
<u>JANUARY 1980</u>	58.0 kW
UPDATING OF AUXILIARY POWER	- 1.7 kW
- INCREASED ALTERNATOR SPEED	
- INCREASED COMBUSTOR PRESSURE DROP (BLOWER POWER)	
BASIC ENGINE FINALIZATION	- 2.7 kW
- INCREASED PRESSURE DROP FACTOR IN HEATER (AFTER MODEL FLOW TEST)	
- INCREASED CCD DEAD VOLUME	
- INCREASED DEAD VOLUME IN REGENERATOR MANIFOLD	
<u>MAY 1980</u>	53.6

ORIGINAL PAGE IS
OF POOR QUALITY



Performance map with net shaft torque versus speed.

ORIGINAL PAGE IS
OF POOR QUALITY



Performance map with net shaft power versus speed.

MOD I DESIGN REVIEW
MAY 22, 1980
EXECUTIVE SUMMARY

ORIGINAL PAGE IS
OF POOR QUALITY

WEIGHT/POWER SUMMARY

		<u>P-40</u>	<u>MOD I</u>
WEIGHT*	KG	329	266
	LB	724	587
POWER	KW	40.0	53.6
	HP	54.0	72.4
WEIGHT/POWER (LB/HP)		13.4	8.1

*DRY WEIGHT INCLUDING AUXILIARIES, WITHOUT ACCESSORIES

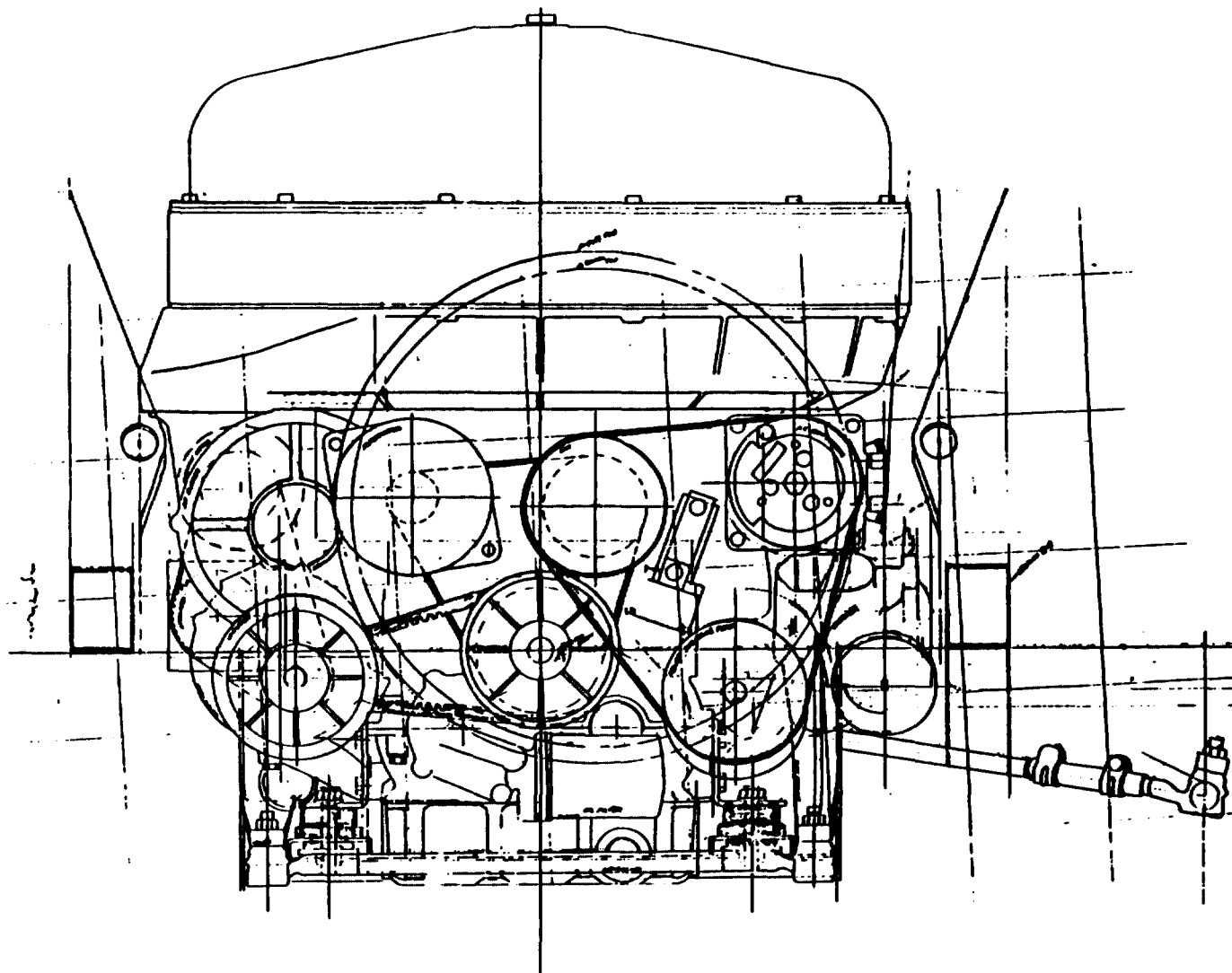
MOD I DESIGN REVIEW
MAY 22, 1980
EXECUTIVE SUMMARY

ORIGINAL PAGE IS
OF POOR QUALITY

INSTALLATION IN VEHICLE

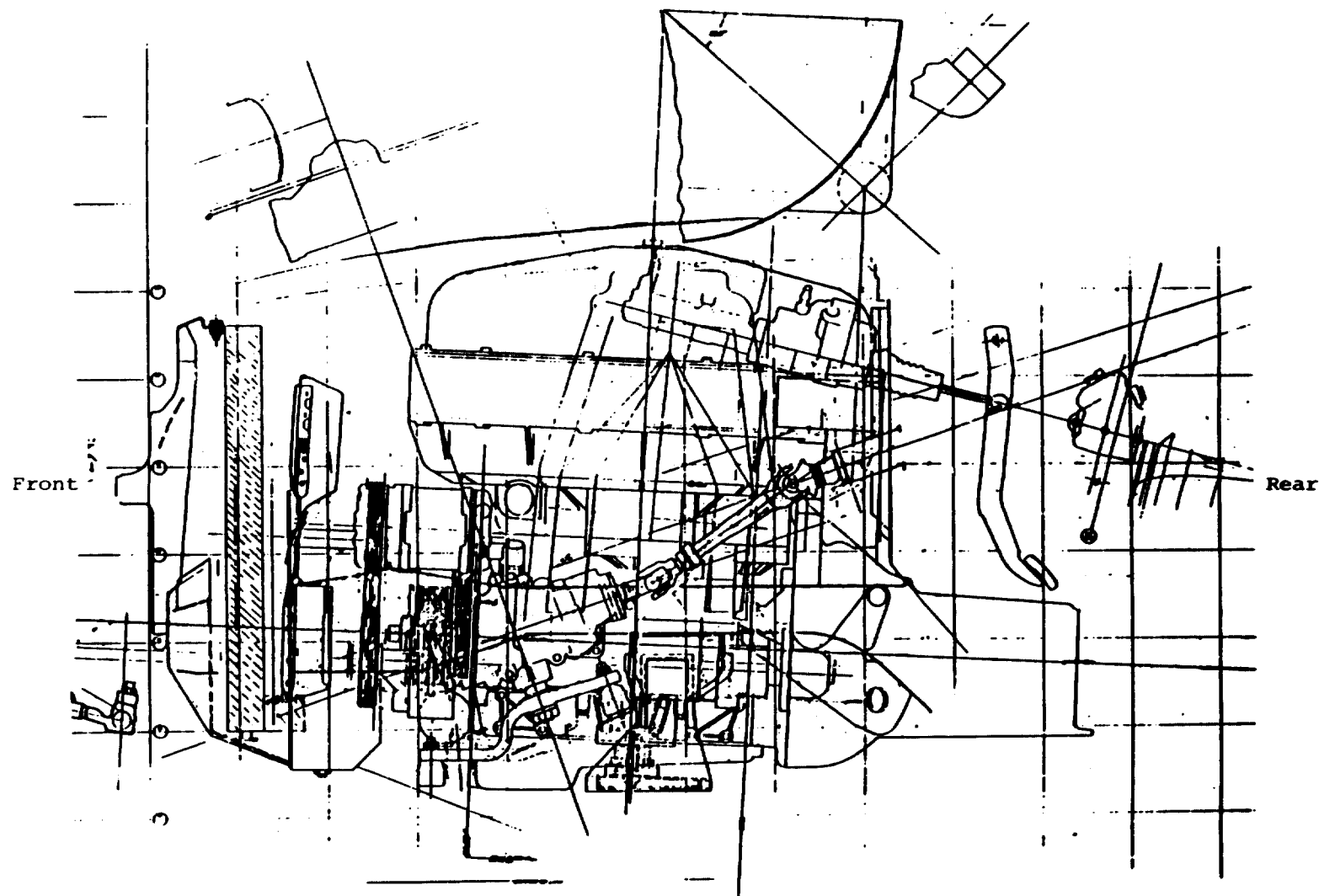
- PACKAGE INTO SPIRIT WITH MODIFIED FRONT SUSPENSION
- COOLING SYSTEM DESIGN IS ADEQUATE
- 12V BATTERY SYSTEM

ORIGINAL PAGE IS
OF POOR QUALITY



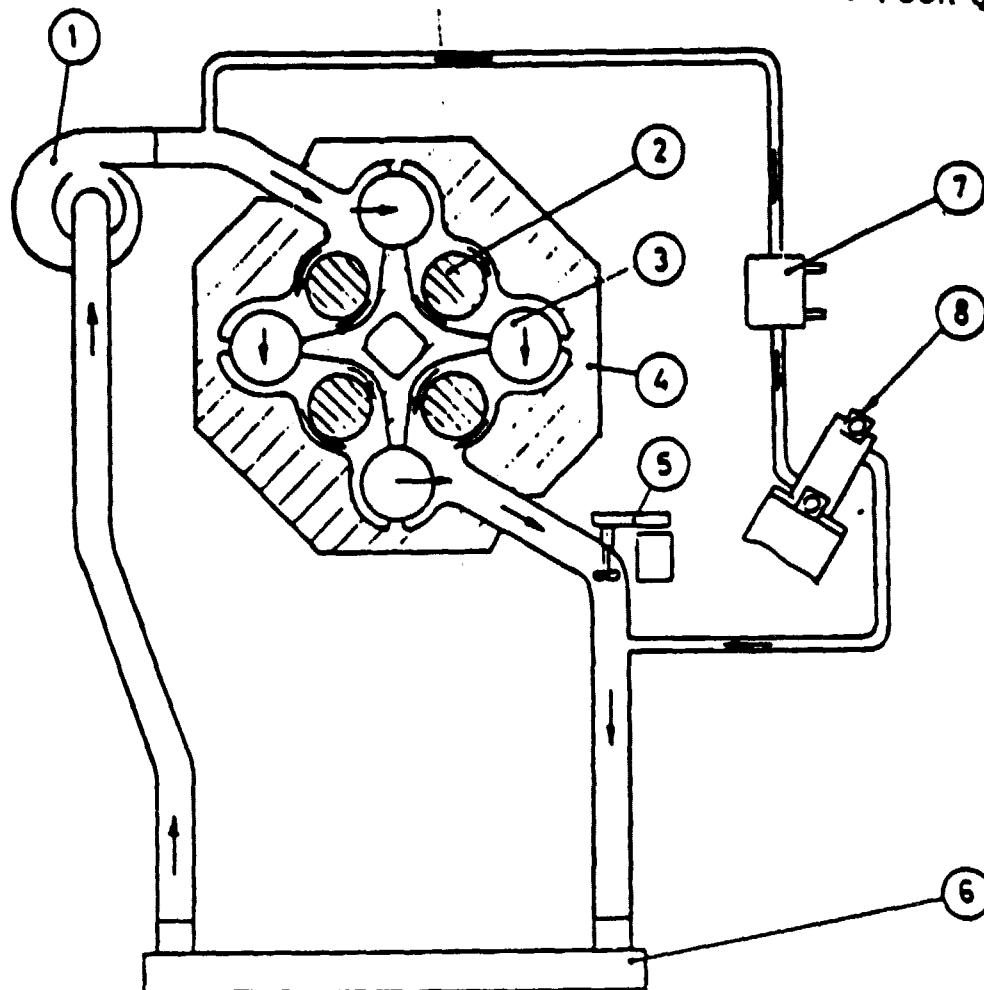
Engine Installation in Vehicle Showing Accessories (Front View)

ORIGINAL PAGE IS
OF POOR QUALITY



Engine Installation in Vehicle Showing Accessories (Right-hand Side View)

ORIGINAL PAGE IS
OF POOR QUALITY



1. Water pump
2. Cylinder
3. Gas cooler
4. Water jacket
5. After cooling pump
6. Radiator
7. Hydrogen cooler
8. Hydrogen compressor

ASE Mod 1 Cooling Circuit Diagram

MOD I DESIGN REVIEW
MAY 22, 1980
EXECUTIVE SUMMARY

ORIGINAL PAGE IS
OF POOR QUALITY

VEHICLE PERFORMANCE PREDICTIONS

<u>MILEAGE (MPG)</u>	<u>I.C. ENGINE</u>	<u>P-40</u>	<u>MOD I</u>	<u>% IMPROVEMENT</u>
EPA COMBINED CYCLE				
(WITH A/C)	-	20.8	26.7**	28**
(WITHOUT A/C)	22.2		27.1**	22**

<u>ACCELERATION (SEC)</u>	<u>I.C. ENGINE</u>	<u>P-40</u>	<u>MOD I</u>
0-60 MPH 1979 SPIRIT	19.1	38	-
1981 SPIRIT	15.9*	-	22

EMISSIONS (G/MILE)

BASED ON LATEST CGR COMBUSTOR TEST DATA:

NO_x < 0.3

HC < 0.1

CO < 0.7

*1981 SPIRIT HAS 151 CU. IN. ENGINE WHEREAS 1979 SPIRIT
HAD 121 CU. IN. ENGINE

**DATA UPDATED AFTER 5/22/80 MEETING.

AUTOMOTIVE STIRLING ENGINE DEVELOPMENT PROGRAM

NASA/DOE CONTRACT NO. DEN3-32

MAY 23, 1980

RISK ASSESSMENT

MECHANICAL TECHNOLOGY INCORPORATED
968 ALBANY-SHAKER ROAD
LATHAM, NEW YORK 12110

ORIGINAL PAGE IS
OF POOR QUALITY

RISK ASSESSMENT OBJECTIVE

DETERMINE THE PROBABILITY OF ACHIEVING THE PROGRAM OBJECTIVES WITHIN THE GUIDELINES OF:

- CURRENT STATE OF THE TECHNOLOGY.
- WORK PLAN, TIME FRAME, AND BUDGET AS NEGOTIATED WITH NASA.

ORIGINAL PAGE IS
OF POOR QUALITY

KEY PROGRAM OBJECTIVES AND GOALS

	<u>BASELINE P-40 SPIRIT</u>	<u>RESD/MOD 11</u>
ENGINE EFFICIENCY	24%	35%
VEHICLE FUEL ECONOMY	21 MPG	35 MPG
ENGINE SPECIFIC WEIGHT	13.4 LB/HP	<6 LB/HP
RELIABILITY		3500 HRS LIFE

EXHAUST EMISSIONS

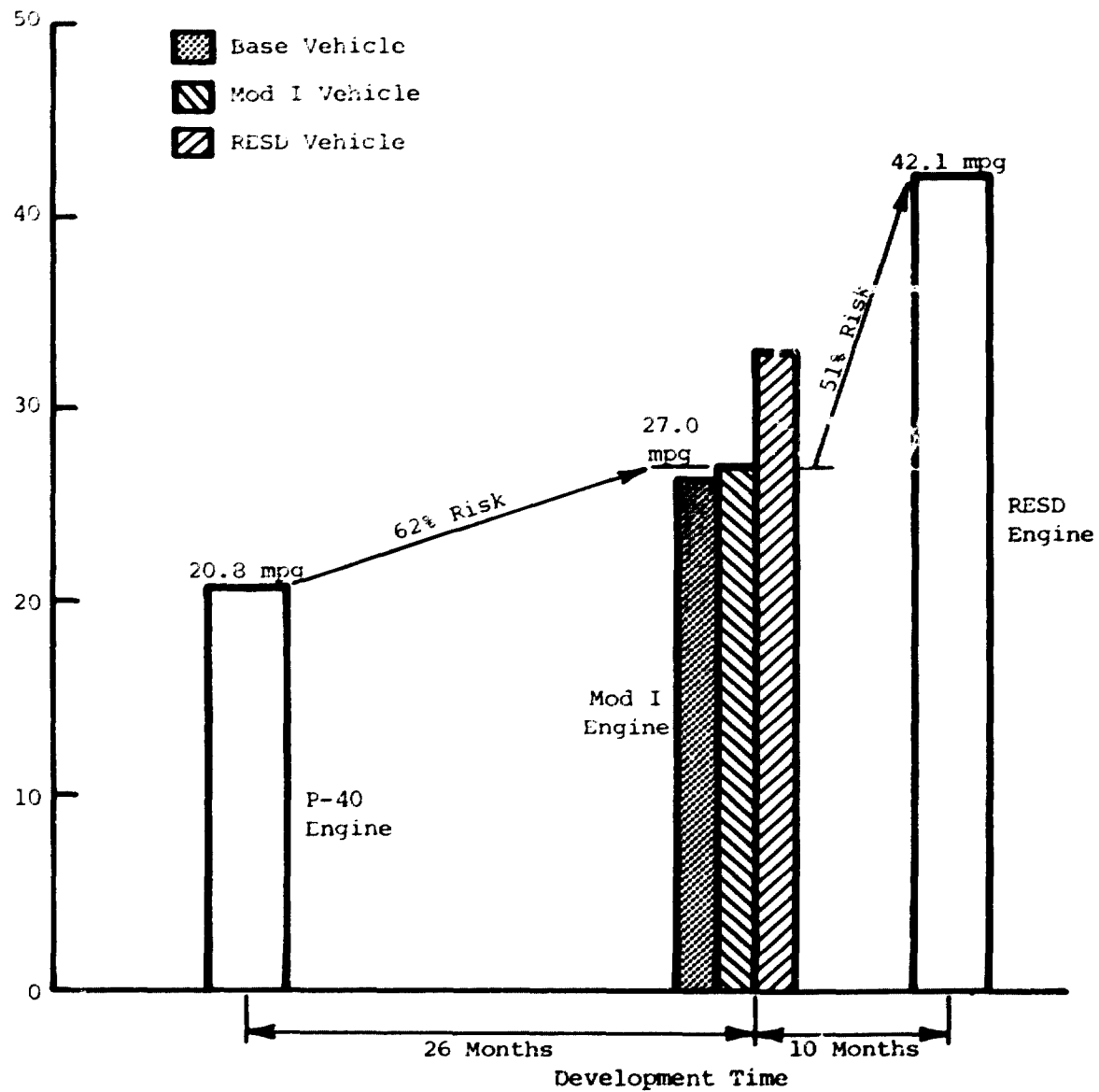
1985 LEGISLATED STANDARDS

3.4 g/mi CO
0.41 g/mi HC
0.4 g/mi NO_x
0.2 g/mi PARTICULATES

ENGINE AND VEHICLE CHARACTERISTICS

ENGINE	VEHICLE	ENGINE EFFICIENCY (AOP) (%)	ENGINE SPECIFIC WEIGHT (LB/HP)	VEHICLE FUEL ECONOMY (MPG)	VEHICLE (0-60 MPH) ACCELERATION TIME (SEC)
P-40	1979 SPIRIT	23	13.4	20.8	38
MOD I	1981 SPIRIT	30	7.3	27.1	22
RES-D	1984 GM "X" BODY	38	4.6	42.1	15

ORIGINAL FACTORY
OF POOR QUALITY



Fuel Economy Results

ORIGINAL PAGE IS
OF POOR QUALITY

MOD 1 COMPARISON WITH P-40

ENGINE PERFORMANCE IMPROVEMENTS

PART POWER DESIGN	12.0
IMPROVED COMBUSTOR/PREHEATER DESIGN	9.5
CGR	4.5
AUXILIARY MATCHING	7.0
TOTAL	33.0

VEHICLE PERFORMANCE IMPROVEMENTS

VEHICLE EFFECTS	0.2
ENGINE EFFICIENCY EFFECTS	6.1
TOTAL	6.3 MPG

ORIGINAL PRICE
OF POOR QUALITY

ENGINE WEIGHT REDUCTION

ALUMINUM MATERIAL	55 LBS
COMBUSTION BLOWER	29 LBS
RADIATOR FAN AND CLUTCH	68 LBS
CONTROLS	11 LBS

RESD COMPARISON WITH MOD 1

ENGINE PERFORMANCE IMPROVEMENTS

IMPROVED PREHEATER AND INSULATION	6.5
820°C CYCLE TEMP. w/ENGINE OPTIMIZED	4.5
DRIVE	7.0
SEAL AND PISTON RING FRICTION	3.0
TOTAL	<u>21.0%</u>

VEHICLE PERFORMANCE IMPROVEMENTS

VEHICLE EFFECTS	6.8
ENGINE EFFICIENCY EFFECTS	8.2
TOTAL	<u>15.0</u> MPG

ENGINE WEIGHT REDUCTION

COMPACT DRIVE	51 LBS
INTEGRATED COLD SYSTEM	20 LBS
HIGH TEMP. EFFECT ON HEATER HEAD	31 LBS
AIR-COOLED THIN INSULATION w/THIN SHEET PREHEATER	20 LBS
AUXILIARIES, ACCESSORIES AND CONTROLS	40 LBS

ORIGINAL PAGE IS
OF POOR QUALITY

MOD I DESIGN FACTORS AFFECTING RISK ASSESSMENT

PERFORMANCE

PART POWER DESIGN

- EXCELLENT CODE CORRELATION WITHIN EXPERIENCE
- MOD I REGENERATOR DESIGN OUTSIDE EXPERIENCE W/SCALED VOLUMES.

CGR COMBUSTION SYSTEM

- TEST RIG DATA INDICATES IMPROVEMENT IN PERFORMANCE
- FURTHER FULL SCALE ENGINE TESTING UNDER TRANSIENT CONDITIONS REQUIRED
- P-40 OPEL TESTS TO PROVIDE PRELIMINARY INDICATION OF PERFORMANCE.

AUXILIARIES MATCHING

- ACTUAL TEST DATA NEEDED.

DRIVE SYSTEM

- BASED ON P-40/P-75 EXPERIENCE.

ORIGINAL PAGE IS
OF POOR QUALITY

MOD I DESIGN FACTORS AFFECTING RISK ASSESSMENT (CONTINUED)

MECHANICAL DESIGN

INVOLUTE HEATER HEAD W/4 REGENERATOR HOUSINGS

- NEW DESIGN AXISYMMETRIC VESSELS W/LONGER MANIFOLD CONFIGURATION,
- MAY REPRESENT DIFFICULT MANUFACTURING PROCESS.
- COLD TESTS MUST BE PERFORMED TO INSURE INTEGRITY.
- CRACKS DEVELOPED IN ANNULAR REGENERATOR COLD TEST.

ALUMINUM CRANKCASE HOUSING AND WATER JACKET

- INITIAL USE OF ALUMINUM.
- FULL SCALED DRIVE SYSTEM TESTS PLANNED.
- NEW MECHANICAL APPROACH TO ASSEMBLY AND ALIGNMENT OF PISTON/CYLINDER/ SEAL/CROSSHEAD SYSTEM.

TIE BOLT CLAMPED CONSTRUCTION

- P-40 DESIGN USES BOLTED ASSEMBLIES.

MOD I DESIGN FACTORS AFFECTING RISK ASSESSMENT (CONTINUED)

MECHANICAL DESIGN (CONTINUED)

SEAL CONFIGURATION

- PUMPING LENINGRADER.
- P-40/P-75 EXPERIENCE.
- HIGH TEMPERATURE P-40 HAS 900 HOURS WITH H₂.

COMBUSTION SYSTEM CONFIGURATION

- NEW MECHANICAL CONFIGURATION
- FULL SCALED TESTS PLANNED.

CONTROL SYSTEM

- NEW CHECK VALVE DESIGN W/SIGNIFICANT TEST RIG PROOF TEST.
- HYDROGEN COMPRESSOR REDESIGN.
- SUBSTITUTE MICROPROCESSOR FOR ANALOG.

RESID FACTORS AFFECTING RISK ASSESSMENT

PERFORMANCE

ENGINE OPTIMIZATION

- INITIAL ATTEMPTS TO ALLOW CODE TO OPTIMIZE ENGINE AT PART POWER.

HIGH TEMP. OPERATION

- 820°C HEATER TUBE TEMPERATURE.
- COMPONENT TEST ON HI-TEMP P-40 ENGINE PLANNED.

ALUMINUM COOLER

- MANUFACTURING SUCCESS NECESSARY TO ACHIEVE PERFORMANCE EQUAL TO SS COOLER CONFIGURATION.

PREHEATER

- FOLDED THIN SHEET REPRESENTS INITIAL ATTEMPT AT THIS CONFIGURATION.

REGENERATOR

- SIGNIFICANT DEPARTURE FROM EXPERIENCE.
- MOD I ENGINE REPRESENTS PARTIAL EXPERIENCE.

RESD FACTORS AFFECTING RISK ASSESSMENT (CONTINUED)

MECHANICAL DESIGN

EXTERNAL HEAT SYSTEM

- COMPACTNESS ATTAINED BY REDESIGN OF REGENERATOR/COOLER ASSEMBLY
- DIFFERENT AIR INTAKE CONFIGURATION.
- REDUCED INSULATION AND REDUCED COMBUSTION VOLUME.

ALTERNATE MATERIALS

- INITIAL ATTEMPT TO UTILIZE LOWER COST NON-STRATEGIC ALLOYS.
- MAJOR MATERIALS EFFORT IN COMPONENT PROGRAM.

REGENERATOR/COOLER

- INTEGRAL HOUSING.
- PRESSURE BALANCED HEIGHT COMPACTNESS ACHIEVED BY LOCATING PISTON ROD SEAL FURTHER WITHIN PISTON DOME.
- LIMITED EXPERIENCE.

RESID FACTORS AFFECTING RISK ASSESSMENT (CONTINUED)

MECHANICAL DESIGN (CONTINUED)

SEAL CONFIGURATION

- INTEGRAL COLD DUCT/SEAL HOUSING.
- LOWER ENGINE HEIGHT.
- REMOVED CAP SEAL.

DRIVE SYSTEM

- LOWER FRICTION DESIGN.

FRONT WHEEL DRIVE INSTALLATION

- INITIAL DEMONSTRATION.
- MOD I FWD ENGINEERING VEHICLE IN PROGRAM.

ORIGINAL PAGE
OF POOR QUALITY

OTHER FACTORS AFFECTING RISK ASSESSMENT

- MOD I ENGINE TEST EXPERIENCE HAS MINIMUM IMPACT ON MOD II DESIGN DUE TO TIMING.
- MOD II DEVELOPMENT TIME IS SHORT - 10 MONTHS TIME FROM FIRST ENGINE TEST TO VEHICLE DELIVERY TO EPA. EQUIVALENT TIME FOR MOD I IS 26 MONTHS.
- TOTAL NUMBER OF DEVELOPMENT ENGINES IN PROGRAM IS LOW: 4 MOD I DEVELOPMENT ENGINES AND 2 MOD II DEVELOPMENT ENGINES.
- FUNDING LIMITS INVOLVEMENT OF U.S. COMPONENT MANUFACTURERS IN PROGRAM - BENEFITS OF SPECIALIZED EXPERTISE IS MINIMUM.

MOD I RISK ASSESSMENT

PERFORMANCE FACTORS	EFFECT ON MOD I SUCCESS		MOD I OVERALL RISK	COMMENTS
	P-40	COMPONENT DEVELOPMENT		
PART POWER DESIGN	L	L	H	NO EXPERIMENTAL VERIFICATION OF PREDICTED PERFORMANCE ~ 35% OF NEEDED IMPROVEMENT.
IMPROVED COMBUSTOR SYSTEM	L	H	L	FULL SCALE TEST RIG OPERATION OF CGR COMBUSTION SYSTEM IN PROGRAM.
CGR	L	H	L	
AUXILIARY MATCH	L	H	M	MOST PERFORMANCE CURVES WILL BE GENERATED IN PROGRAM.
VEHICLE SIMULATION	H	H	L	CONTINUED SIMULATION AND COMPARISON WITH PREDICTIONS FROM DYNAMOMETER TESTS.

I-65

ORIGINAL PAGE 13
OF POON 000000

MOD I RISK ASSESSMENT (CONTINUED)

MECHANICAL DESIGN FACTORS	EFFECT ON MOD I SUCCESS P-40 COMPONENT DEVELOPMENT	MOD I OVERALL RISK	COMMENTS	
HEATER/REGENERATOR/ CYLINDER	L	M	H	COLD TESTS TO BE PERFORMED. NEW DESIGN CONFIGURATION.
ALUMINUM HOUSING AND BLOCK	L	M	M	NEW MECHANICAL APPROACH.
TIE BOLT CONSTRU- TION	L	M	H	NEW MECHANICAL DESIGN APPROACH.
ROD SEAL CONFIGU- RATION	H	H	L	LARGE RIG TEST PROGRAM AND IN-VEHICLE TESTING.
COMBUSTION (CGR) CONFIGURATION	L	H	L	LARGE RIG TEST PROGRAM.
CONTROL SYSTEM	M	M	L	COMPONENT TESTING ONLY - BACKUP WITH P-40 SYSTEM

99-1

ORIGINAL PART IS
OF POOR QUALITY

MOD I RISK ASSESSMENT

FACTORS	RELATIVE CONTRIBUTION 0-100 SCALE	RISK 0-1 SCALE	SUBTOTAL	TOTALS	SUB-WEIGHTED RISK
PERFORMANCE FACTORS REPRESENT 40% OF RISK					
PART POWER	35	(H) .8	28.0		
COMBUSTOR	41	(L) .4	16.4		
AUXILIARY	14	(M) .6	8.4		
OTHER	10	(L) .2	2.0	54.8	21.9
MECHANICAL DESIGN FACTORS REPRESENT 60% OF RISK					
HEATER/REG/COOLER	35	(H) .9	31.5		
ALUMINUM HOUSING	10	(M) .6	6.0		
TIE BOLT CONSTRUCTION	25	(H) .8	20.0		
ROD SEAL CONFIGURATION	15	(L) .4	6.0		
COMBUSTION CONFIGURATION	10	(L) .2	2.0		
CONTROL SYSTEM	5	(L) .2	1.0	66.5	39.9

WEIGHTED RISK: 62%

ORIGINAL
OF POOR QUALITY

MOD I RESULTS

- A 62% RISK IS ASSOCIATED WITH THE MOD I ENGINE PROGRAM ACHIEVING ITS PROJECTED PERFORMANCE (27.0 MPG).
- MOD I ENGINE PROGRAM REPRESENTS APPROXIMATELY 50% OF THE REQUIRED ENGINE EFFICIENCY INCREASE FROM BASELINE P-40 TO MEET RESD PROJECTED PERFORMANCE (42.1 MPG).
- MOD I ENGINE PROGRAM REPRESENTS 45% OF REQUIRED MPG IMPROVEMENT FROM BASELINE P-40 SPIRIT TO MEET PROGRAM OBJECTIVES (35 MPG).
- MOD I ENGINE PROGRAM REPRESENTS DEMONSTRATION OF THE MAJOR MECHANICAL DESIGN APPROACHES REQUIRED TO MEET PROGRAM ENGINE WEIGHT GOALS (<6 LB/HP). APPROXIMATELY 50% OF THE WEIGHT REDUCTION IS ACCOMPLISHED IN MOD I.
- THE 30% IMPROVEMENT IN MPG OF THE MOD I VEHICLE OVER THE P-40 SPIRIT IS ALL ENGINE-RELATED.

RES D RISK ASSESSMENT

PERFORMANCE FACTORS	EFFECT ON RES D SUCCESS		RES D OVERALL RISK	COMMENTS
	MOD I	COMPONENT DEVELOPMENT		
IMPROVED PREHEATER AND INSULATION	L	M	L	ANALYSIS WELL KNOWN-COMPONENT TESTS PLANNED.
820°C CYCLE TEMP ENGINE OPTIMIZATION	M	H	M	REPRESENTS APPROXIMATELY 1 MPG BENEFIT - LIMITED MAX POWER.
DRIVE	H	L	M	PREDICTIONS WILL BE VERIFIED ON MOD I.
ALUMINUM COOLER	L	H	M	SS COOLERS ARE BACKUP IF PERFORMANCE PENALTY REALIZED.
SEALS AND PISTON RING FRICTION	L	H	L	TEST RIG VERIFICATION AND ENGINE EXPERIENCE - LOW MPG EFFECT.
VEHICLE EFFECTS	H	H	L	VEHICLE CHOSEN IS WELL DOCUMENTED - MOD I VEHICLE EXPERIENCE.

ORIGINAL PAGE IS
OF POOR QUALITY

RESD RISK ASSESSMENT (CONTINUED)

MECHANICAL DESIGN FACTORS	EFFECT ON RESD SUCCESS		RESD OVERALL RISK	COMMENTS
	MOD I	COMPONENT DEVELOPMENT		
HEATER SYSTEM w/NEW HEATER/CYL/REGEN	H	H	M	NEW MECHANICAL CONFIGURATION - PREVIOUSLY (MOD I) EXECUTED DESIGN.
ALTERNATIVE MATERIALS	L	H	M	LARGE COMPONENT DEVELOPMENT PROGRAM - BACKUP w/KNOWN MATERIALS AT HIGHER COST.
REGENERATOR/COOLER	L	L	M	NEW MECHANICAL DESIGN - PROOF TEST.
SEAL HOUSING AND SEAL	M	M	H	PERFORM COLD TEST OF SEAL OPERATION - SEAL LOCATED IN DOME UNDER HIGH TEMPERATURE CONDITIONS IN ENGINE.
ENGINE BLOCK	L	L	M	PROOF TEST PROGRAM.
DRIVE SYSTEM	M	L	L	MOD I DESIGN ENGINE AND RIG TESTED.
FWD INSTALLATION	H	H	L	MOD I ENGINE IN X-BODY FOR ENGINEERING TESTS.

ORIGINAL PAGE IS
OF POOR QUALITY

RESID RISK ASSESSMENT

FACTORS	RELATIVE CONTRIBUTION 0-100 SCALE	RISK 0-1 SCALE	SUBTOTAL	TOTALS	SUB-WEIGHTED RISK
PERFORMANCE FACTORS REPRESENT 30% OF RISK					
PREHEATER	17	(L) .4	6.8		
820°C CYCLE	12	(M) .6	7.2		
DRIVE	18	(M) .6	10.8		
SEAL AND PISTON RING	8	(L) .4	3.2		
VEHICLE	45	(L) .2	9.0	37.0	11.1
MECHANICAL DESIGN FACTORS REPRESENT 70% OF RISK					
HEATER SYSTEM	25	(M) .6	15.0		
ALTERNATE MATERIALS	15	(M) .5	7.5		
REGENERATOR/COOLER	15	(M) .5	7.5		
SEAL HOUSING AND SEAL	25	(H) .9	22.5		
ENGINE BLOCK	10	(M) .5	5.0		
DRIVE SYSTEM	5	(L) .2	1.0		
FWD INSTALLATION	5	(L) .2	1.0	59.5	41.7

WEIGHTED RISK: 53%

ORIGINAL PAGE IS
OF POOR QUALITY

RESD RESULTS

- A 53% RISK IS ASSOCIATED WITH THE RESD ENGINE PROGRAM ACHIEVING ITS PROJECTED PERFORMANCE (42.1 MPG).
- RESD PROGRAM REPRESENTS APPROXIMATELY 50% OF THE REQUIRED ENGINE EFFICIENCY INCREASE FROM BASELINE P-40 TO MEET RESD PROJECTED PERFORMANCE (42.1 MPG).
- RESD PROGRAM REPRESENTS 55% OF REQUIRED MPG IMPROVEMENT FROM BASELINE P-40 SPIRIT TO MEET PROGRAM OBJECTIVES (35 MPG).
- THE 55% IMPROVEMENT IN MPG OF RESD VEHICLE OVER THE MOD I VEHICLE RESULTS FROM 6.8 MPG VEHICLE-RELATED IMPROVEMENT (45%) AND 8.3 MPG ENGINE-RELATED IMPROVEMENT (55%).
- RESD PROGRAM REPRESENTS DEMONSTRATION OF THE ENGINE SPECIFIC WEIGHT GOALS OF PROGRAM (<6 LB/HP).

ORIGINAL PAGE IS
OF POOR QUALITY

CONCLUSIONS FROM RISK ASSESSMENT

- A 67% IMPROVEMENT IN VEHICLE MPG IS REQUIRED OVER BASELINE P-40 SPIRIT TO MEET PROGRAM OBJECTIVES (35 MPG).
- APPROXIMATELY 50% OF REQUIRED MPG IMPROVEMENT IS DERIVED FROM MOD I PROGRAM WHICH IS ASSESSED AT A 65% RISK.
- ALL MOD I MPG IMPROVEMENT IS ENGINE-RELATED AND, THEREFORE, ACCOUNTING FOR TIME FRAME AVAILABLE AND NUMBER OF DEVELOPMENT ENGINES IN PROGRAM, THE RISK IS JUDGED ACCEPTABLE AND CONSISTENT.
- AN ADDITIONAL 55% IMPROVEMENT IN MPG OVER THE MOD I IS DERIVED FROM THE RESD PROGRAM WHICH IS ASSESSED AT A 55% RISK. THE PROJECTED RESD FUEL ECONOMY (42.1 MPG) EXCEEDS PROGRAM OBJECTIVES (35 MPG).
- MPG IMPROVEMENTS IN RESD PROGRAM ARE 45% VEHICLE-RELATED AND 55% ENGINE-RELATED.
- THE WEIGHT REDUCTION OF 300 LBS FROM THE BASELINE WITH A CORRESPONDING 33 HP INCREASE REPRESENTS A MAJOR FACTOR IN THE RISK ASSESSMENT.
- MTI CONCLUDES THAT THE RISK SPLIT AND LEVEL ARE ACCEPTABLE.

ORIGINAL PAGE IS
OF POOR QUALITY

A.6 Safety Analysis of ASE Mod I

PRECEDING PAGE BLANK NOT FILMED

FFV Industriprodukter AB

Test/Handel ISO/Göran Rvdman <i>Göran Rvdman</i>	Date 1980-05-09	Reg nr ISO-80:09
Location Jönköping	Mettagare/Delegering []	
Agenda Safety analysis of ASE Mod 1.	Roland Emanuelsson, USS	

Abstract

A preliminary safety analysis has been performed for the Automotive Stirling Engine Mod 1 as it was designed in April 1980. The method used is Failure Mode & Effect Analysis with special emphasis on potential safety hazards. The analysis shows that there are many different potential safety hazards but also that most of them are minimized by different guards or other preventive actions.

Purpose

The main purpose of this safety analysis is to discover and evaluate possible safety related failures connected with ASE Mod 1 in order to facilitate preventive actions and to be a basis for estimation of the overall design status.

Method

Failure Mode and Effect Analysis has been used as a method for systemizing the work. This method consists of the following steps:

1. Divide the design into subsystems/components.
2. For each subsystem/component find out possible failure modes on component level. Possible causes are also described. In this analysis only those components and failures have been examined that are safety related and that are not self-evident.
3. Investigate what the consequences would be on the subsystem or component level (including secondary failures) and how the engine as a system will be affected.
4. Investigate potential safety related risks provided the engine is used in a passenger car.
5. Note any additional information that makes the judgement of the risks easier.

Result

The result is shown in form of a table on the following pages.

ORIGINAL PAGE IS
OF POOR QUALITY

SUBSYSTEM COMPONENT	FUNCTION	FAILURE MODE	POSSIBLE CAUSES	LOCAL EFFECT	SYSTEM EFFECT	POTENTIAL SAFETY HAZARD	COMMENTS
DRIVE UNIT							
Heater head	Contain hot hydrogen gas under pressure	Fracture cracks	Manufacturing error	Large H ₂ leakage to combustion. Possible damage to preheater due to raised combustion gas temperature. Fracture parts if any will be withheld by heater insulation. A pressure peak might damage the heater walls.	Loss of H ₂ pressure. Fuel will be shut off (high tube temp.). Engine will stop.	Sudden loss of power.	Pressure tests performed after manufacture. At start the combustor will be ventilated for three seconds.
Cylinder liner	Work space for pistons Contain hydrogen gas under pressure	Bolts loose or broken	Assembly error Material failure	H ₂ leakage to water channels. Deformation of heater head if remaining bolts break.	Possible large interior damage to heater head and drive mechanism. Engine stops abruptly.	Possible burst of cooling water hoses. Sudden stop of engine. Some breaking.	Hydrodynamic transmission
Drive mechanism	Move hydrogen gas between the cylinders. Transfer net power to gear-box.	Seizes	Manufacturing error Insufficient lubrication	Drive mechanism stops more or less suddenly.	Fuel will be shut off (high tube temp.). Engine stops abruptly.	Sudden stop of engine. Some breaking.	Hydrodynamic transmission
Piston rod seal, seal house	Prevent hydrogen gas from entering crank-case.	Leakage	Worn out seal Manufacturing error	H ₂ will enter crank-case.	No immediate effect. In the long run loss of power.	Explosion possible in crank-case in case of ignition eg. from overheated bearings.	Some leakage is normal during running. Low oil pressure indicated by warning lamp. Crank-case ventilated by atomizer air.

ORIGINAL PAGE IS
OF POOR QUALITY

SUBSYSTEM COMPONENT	FUNCTION	FAILURE MODE	POSSIBLE CAUSES	LOCAL EFFECT	SYSTEM EFFECT	POTENTIAL SAFETY HAZARD	COMMENTS
AIR-FUEL CONTROL SYSTEM	Distribute the correct air-fuel mixture to combustor.	Air-fuel mixture too rich	Corrosion or contaminants in fuel control valve	Combustion prolonged. High temperature in preheater.	High IIC emissions. Engine (fuel) will be shut off by preheater overtemperature guard.		
OUTER HEATER SYSTEM							
Injector	Spread out fuel in the combustor.	Bolts missing	Assembly or service error	Injector might fall out if there is a pressure peak in the combustor. This might occur if there is residual fuel in the combustor at start that has not been vaporized during ventilation.	Total loss of power	Burning fuel might be spread over the engine as long as blower is running.	2 bolts fuel lines will probably keep injector in position.
		Unsymmetrical fuel distribution	Contaminants in injector	Unsymmetrical flame. Lower mean gas temperature. Combustion prolonged in some directions might lead to high temperature in part of preheater.	Engine less efficient. Lower max. power.	Open fire if heat does not hit preheater overtemperature guard.	High temperature above preheater at two places will shut off fuel.
Combustor	Contain burning air-fuel mixture.	Cracks in inner wall	Material failure Erosion	Minor disturbance to flame due to air entering combustor through crack.	Might increase exhaust emissions.		
		Cracks in outer wall	Manufacturing error Pressure peak in combustor	Burner air will leak out. Air-fuel mix will be too rich.	High IIC emissions. Engine (fuel) will be shut off by preheater overtemperature guard.		
Ignitor	Ignite air-fuel mixture.	Bad Ignition		Fuel will be collected in combustor and preheater. After start: risk for high temperature and damages in preheater.	Difficult to start engine. After start: first high IIC emissions then no effect.	Small risk for unprotected fire in preheater if several start failures.	Max. a few seconds before fuel is shut off.

ORIGINAL PAGE IS
OF POOR QUALITY

SUBSYSTEM COMPONENT	FUNCTION	FAILURE MODE	POSSIBLE CAUSES	LOCAL EFFECT	SYSTEM EFFECT	POTENTIAL SAFETY HAZARD	COMMENTS
TEMPERATURE REGULATION	Preheater	Cracks	Corrosion Erosion Welding error Exceeded temperature limit	Air passes directly to exhaust side. Air-fuel mixture in the combustor will be richer. Unburned fuel turns on fire in the preheater in an accelerating manner.	No immediate	Open fire	High temperature above preheater at two places will shut off fuel.
		Clogged	Sulphur in fuel	Less efficient heat transfer. Rising pressure drop.	Lower efficiency. Higher exhaust gas temperature. Lower max power.		Throttle position indicated by gauge.
	Heater tubes	Fracture	Manufacturing failure Erosion from high combustion temperature	See "DRIVE UNIT: Heater head" If it occurs directly after engine stop a hydrogen gas explosion is possible which could deform top of engine.	Heater damaged		4 thermocouples Less probable at stop because of lower pressure.
	Thermocouples	Measure heater	Short-circuited	If one: tube temperature will be set lower. If more than one: electronics will shut off fuel.	Engine less efficient Lower max power Loss of power		
		Bruken	Manufacturing error Handling	If one: tube temperature will be set lower. If more than one: electronics will shut off fuel.	Engine less efficient Lower max power Loss of power		

ORIGINAL PAGE IS
OF POOR QUALITY

SUBSYSTEM COMPONENT	FUNCTION	FAILURE MODE	POSSIBLE CAUSES	LOCAL EFFECT	SYSTEM EFFECT	POTENTIAL SAFETY HAZARD	COMMENTS
POWER CONTROL SYSTEM	Hydrogen storage tank	Pressure too high	Inadvertant filling from outer source	Safety valve will open and release excess of H ₂ .	H ₂ will leak outside engine compartment.		
		Heating of tank	Fire in engine compartment	Safety valve will open and release excess of H ₂ or fusible temperature plug will discharge the tank.	H ₂ will leak outside engine compartment or complete loss of H ₂ and the engine shuts down.	A fire will be supported by discharged H ₂ .	
		Structural failure	Manufacturing error Corrosion	Tank might rupture. H ₂ leaks out.	Complete loss of H ₂ . Engine shuts down.	Minor fragments might be scattered inside engine compartment.	Every tank pressure tested.
	Control valve	Control the supply and dump of gas to and short-circuit of the Stirling cycle	Piston sticks in supply position Corrosion contaminants Mechanical failure	Cycle mean pressure increases. Fuel system will follow unless "ignition" key is switched off.	Engine power increases. By "Neutral" gear fuel will be shut off by overspeed guard.	Vehicle will accelerate unless breaks are applied or gear is shifted to "Neutral". If ignition is switched off, acceleration will continue for a few seconds.	Piston works normally full strokes. Signal from electronics supervised regarding acceptable level. Manual shut off facilities exist.
Electro-hydraulic servo actuator incl. oil system	Move control valve	No oil pressure	Pump failure Contaminated filter Pressure valve failure	Control valve will go to dump and by-pass position.	Engine will stop.	Sudden loss of power.	ORIGINAL PAGE IS OF POOR QUALITY
		No electrical signal	Wire broken Electronics failure	Control valve will go to dump and by-pass position.	Engine will stop.	Sudden loss of power.	
Compressor short circuiting solenoid valve	Short circuit sides of compressor	Does not close	Valve failure	No dump function. Engine power controlled by more or less short-circuiting Stirling cycle.	Bad fuel economy. Impossible to restart engine unless external dump valve is released. If so loss of hydrogen.		



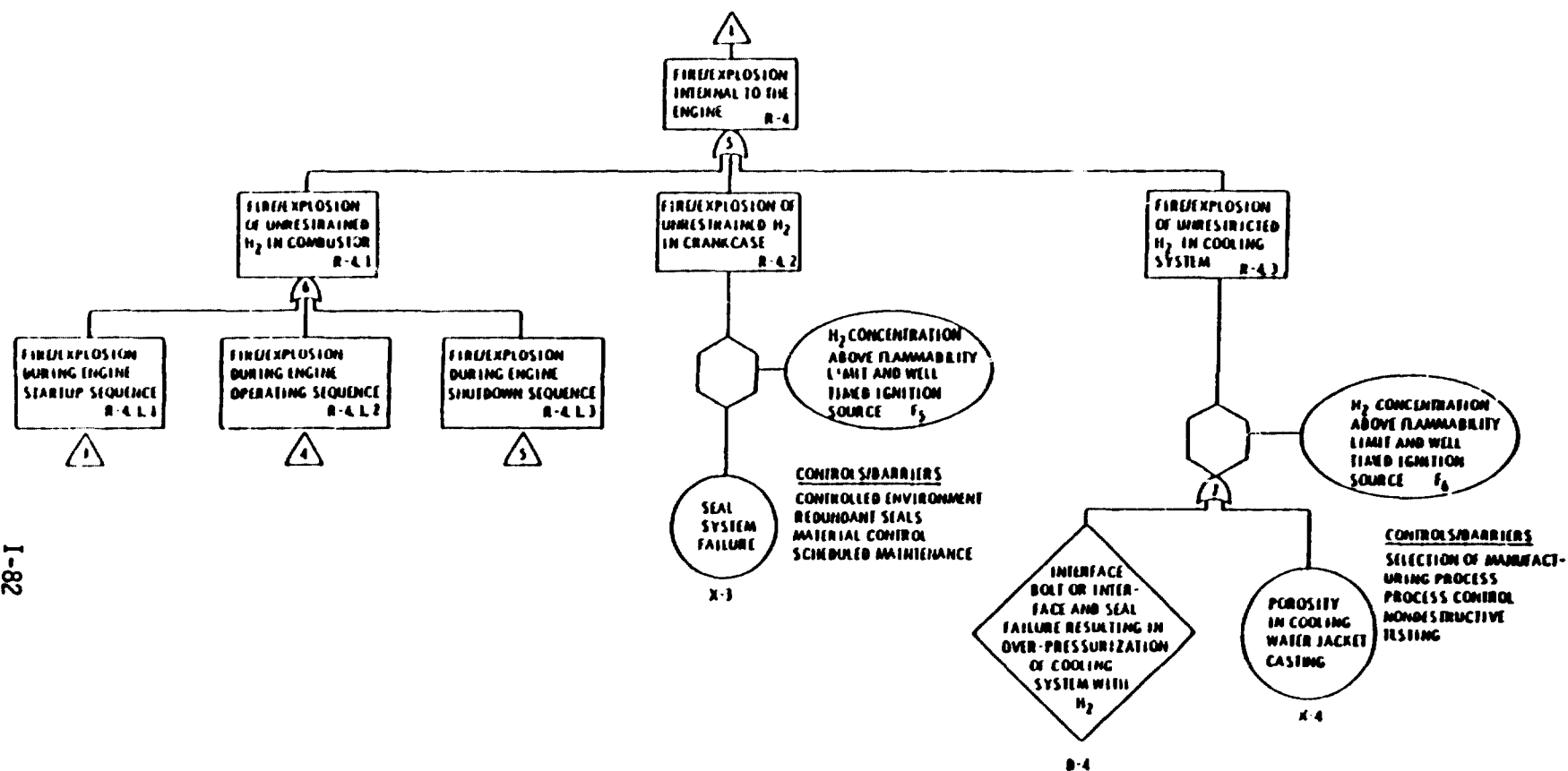


Figure 6. Fault Tree Logic Display (con't)

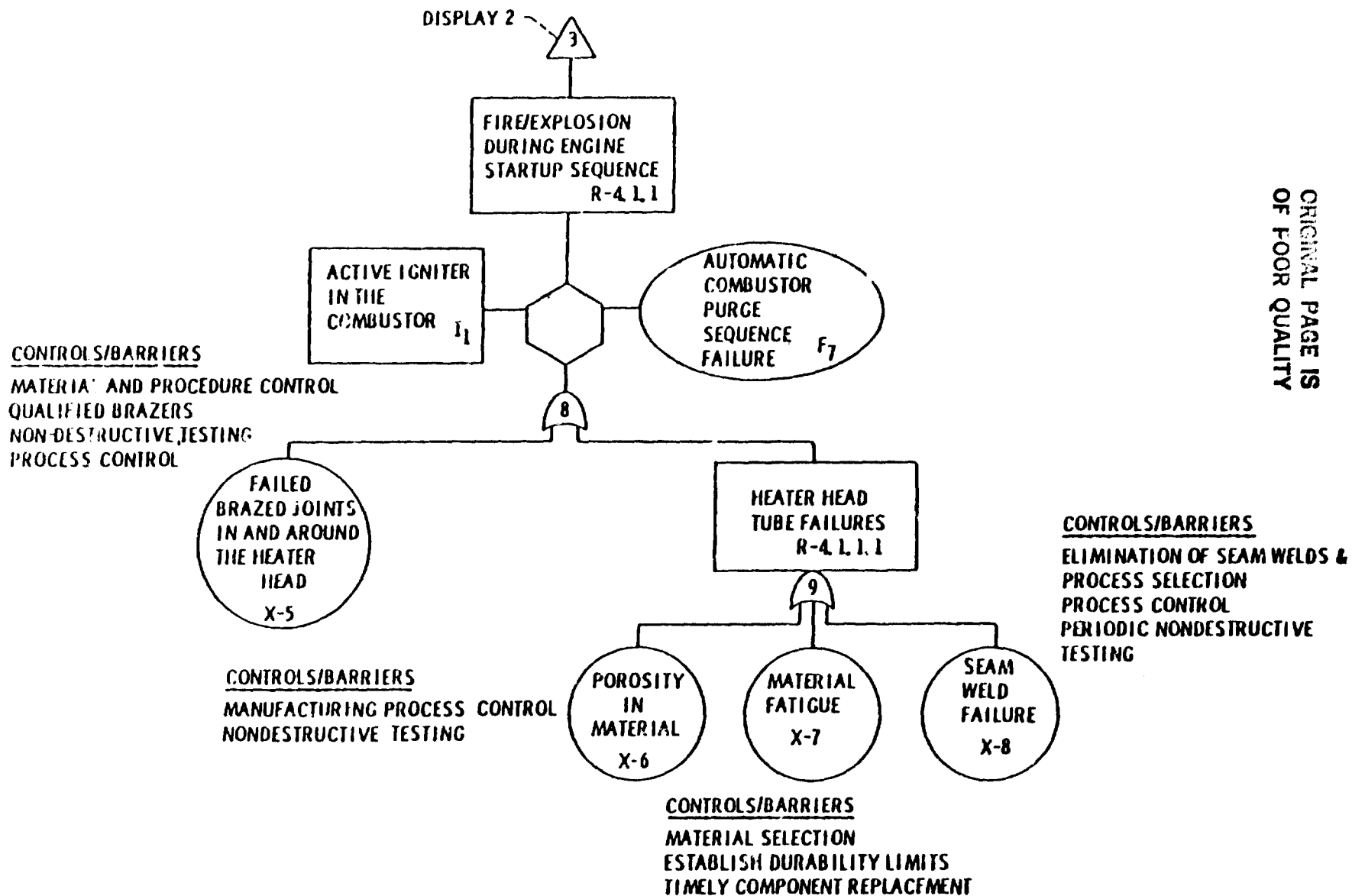
ORIGINAL PAGE IS
OF POOR QUALITY

Figure 6. Fault Tree Logic Display (con't)

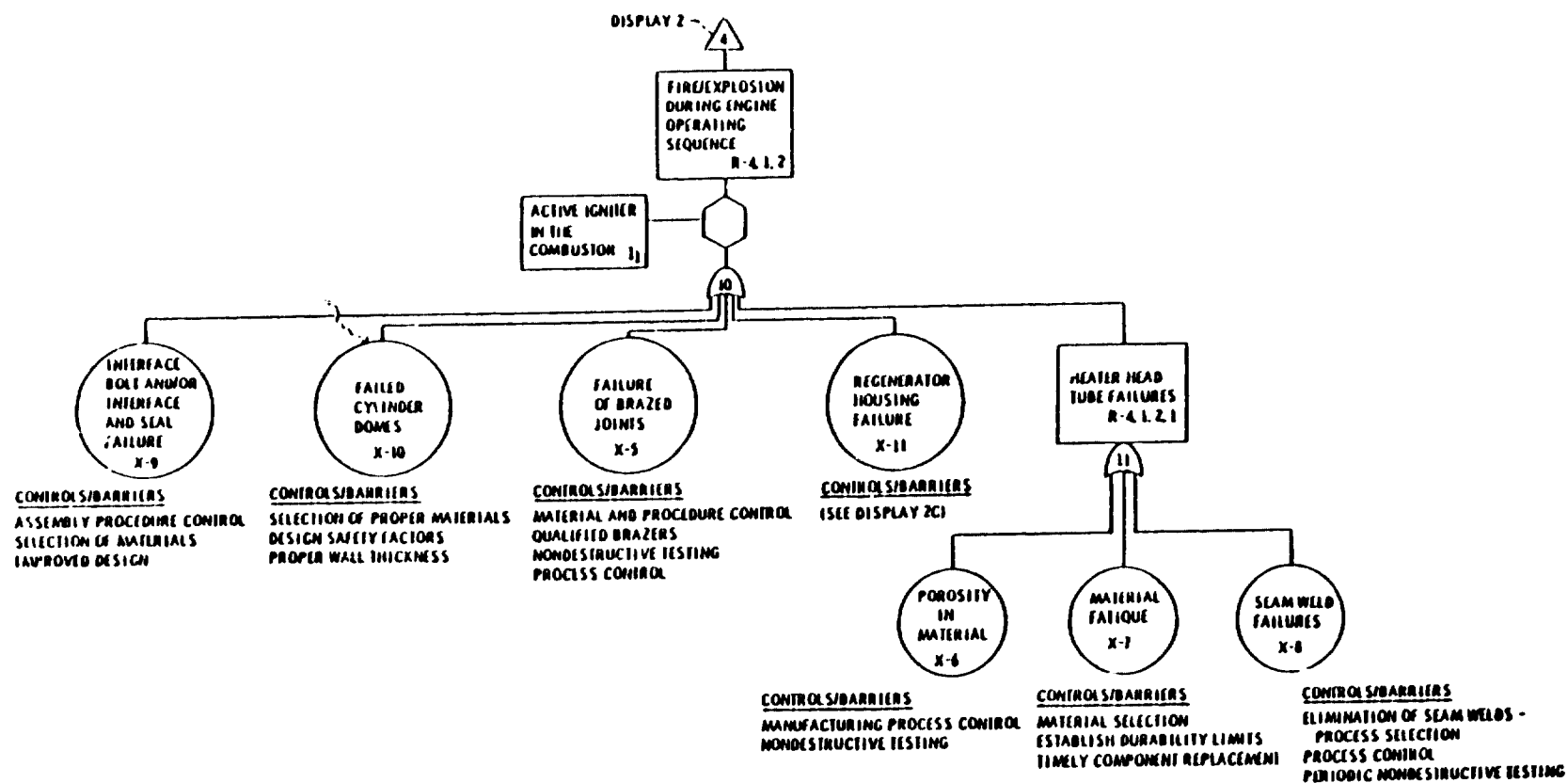


Figure 6. Fault Tree Logic Display (con't)

IIB/RPC 4/1/80

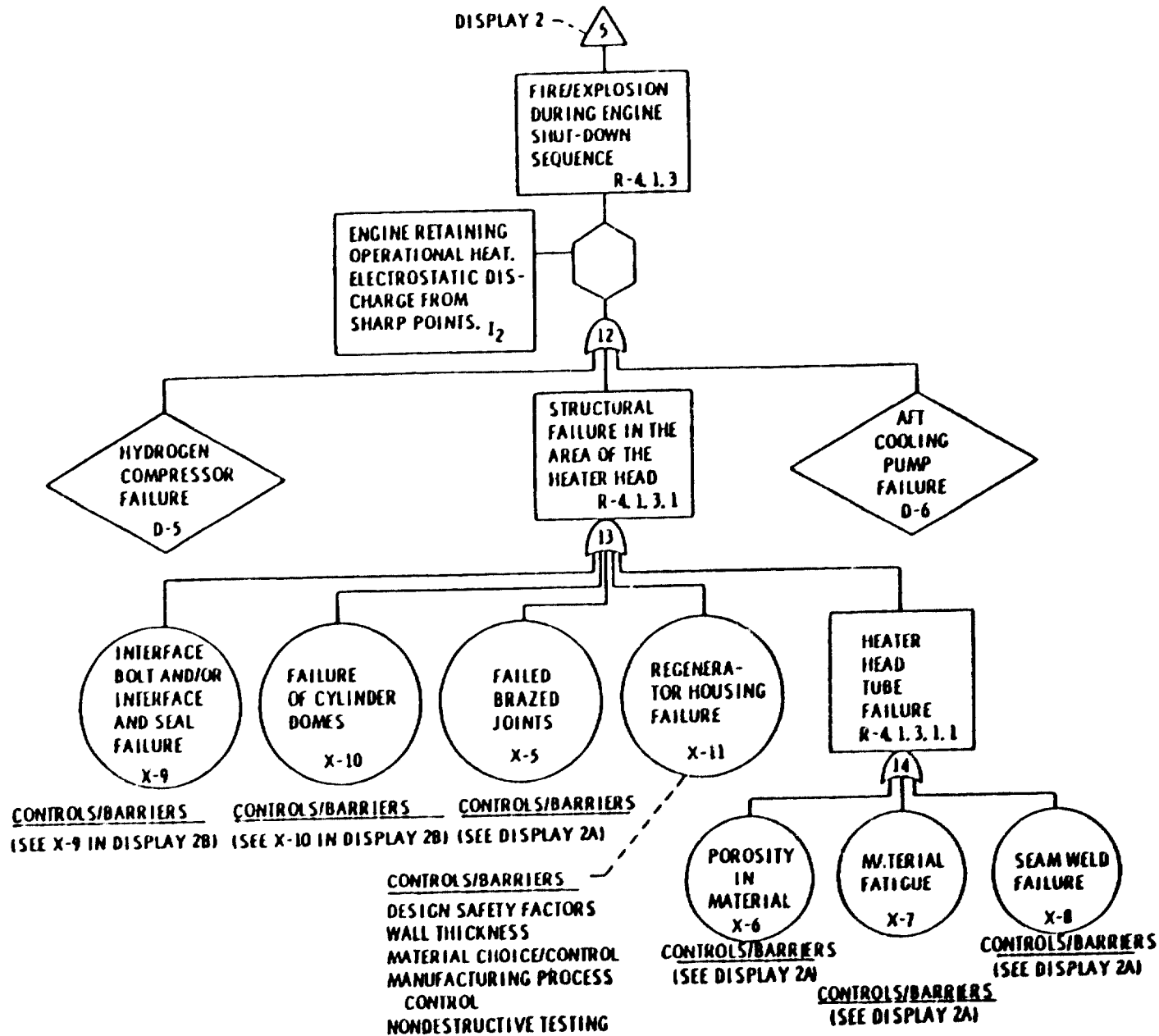


Figure 6. Fault Tree Logic Display (con't)

ORIGINAL FIGURE IS
OF POOR QUALITY

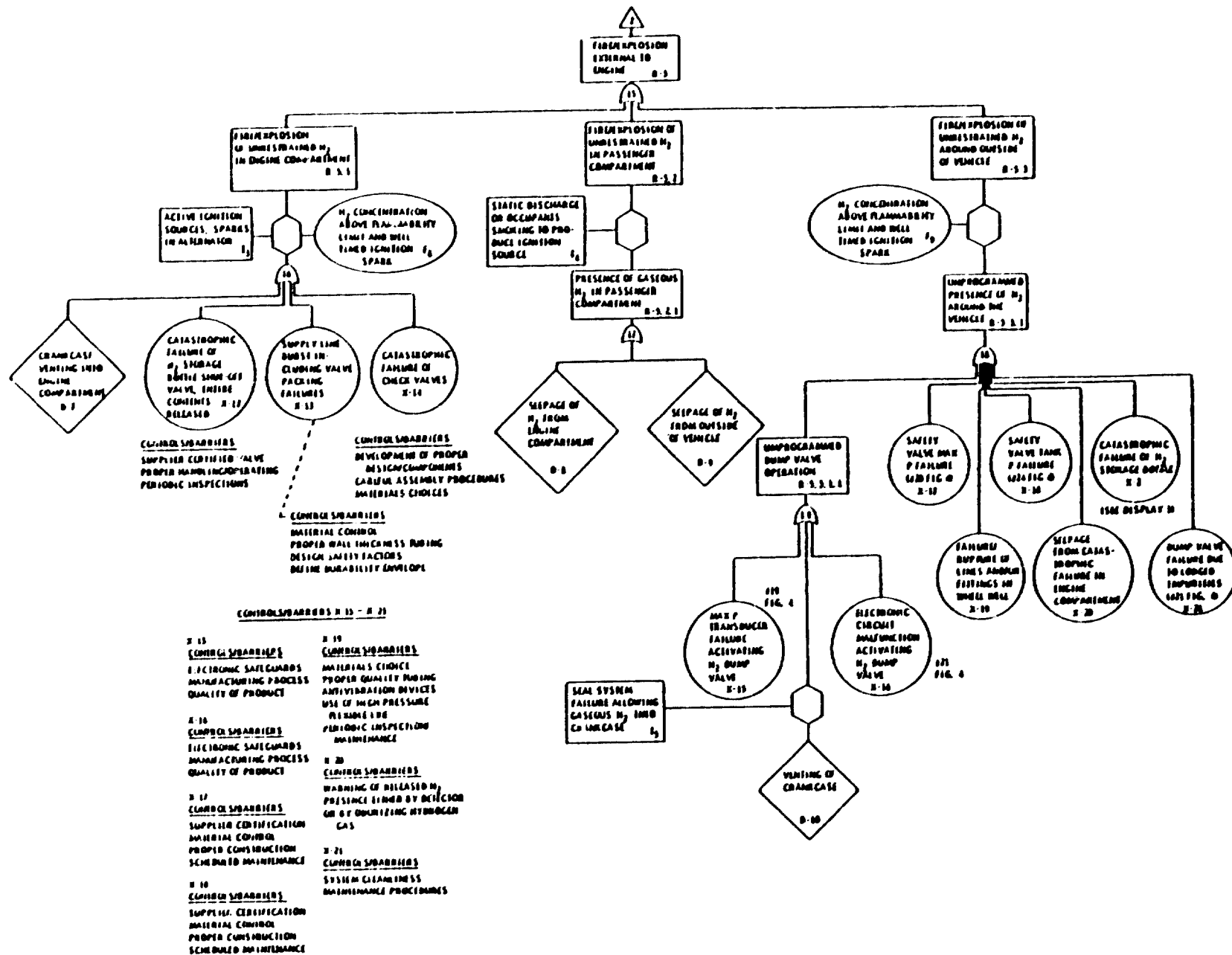
ORIGINAL PAGE IS
OF POOR QUALITY

Figure 6. Fault Tree Logic Display (con't)

AUTOMOTIVE STIRLING ENGINE DEVELOPMENT PROGRAM

NASA/DOE CONTRACT No. DEN3-32

DESIGN CRITERIA AND MATERIALS PROPERTIES FOR THE
ASE MOD I AND REFERENCE ENGINES

MECHANICAL TECHNOLOGY INCORPORATED
968 ALBANY-SHAKER ROAD
LATHAM, NEW YORK 12110

DESIGN CRITERIA AND MATERIALS PROPERTIES FOR THE
MOD I AND REFERENCE ENGINES

The strength criterion has been established for each of the components of the MOD I and Reference engines experiencing significant stresses during engine operation. In several cases the strength criterion is in terms of more than one testing condition. For example, the cylinder heads and regenerator housings have associated with them a criterion for yield strength, creep strength and fatigue strength. The heater tubes have a criterion for hydrogen loss rate as well as strength criteria.

Table 1 lists the components of the MOD I and Reference engines with their associated strength criteria. The stress levels calculated for the MOD I engine are also indicated. Aside from the heater tubes the expected stress levels for the Reference engine have not been established. Attached is a copy of the general description of the several types of strength criteria. This document was presented by United Stirling at the most recent materials and design task force meetings.

Selection of materials for the Reference and MOD II engines will require testing of the several candidate materials. The type of tests to be performed is dictated by the factors which we presently understand as being important to the endurance and function of the component. Table 2 lists the candidate materials for the components of the Reference and MOD II engines along with the testing which will be performed for the sake of qualifying these materials. Where appropriate, testing will also be performed on materials for the MOD I to verify material properties.

TABLE 1
DESIGN CRITERIA FOR THE MOD I ENGINE

<u>COMPONENT</u>	<u>STRENGTH CRITERIA APPLIED</u>	<u>COMMENTS</u>
1. Heater Tubes	1.1 creep strength based on a creep relaxed hoop strength, an equivalent pressure calculated from the 55% Urban 45% Highway Driving Cycle, and a safety factor of 1.5	1.1 Maximum creep relaxed hoop stress is 2.25 times pressure. The equivalent pressure calculated for the 55% Urban-45% Highway Driving Cycle is around 7.5 MPa for most materials.
	1.2 fatigue strength based on a Haigh diagram representing creep-fatigue interaction.	1.2 Haigh Diagrams for N-155 at 1500°F show that the effects of the cyclic stresses on tube life are negligible.
	1.3 The heater tubes must not allow a loss of hydrogen greater than 25 grams in 7500 miles of the 55% Urban-45% Highway Driving Cycle	
2. Cylinder Heads and Regenerator Housings	2.1 Creep strength; the von Mises effective stress averaged through the wall for 15MPa pressure shall be less than the 4000 Hr creep rupture strength of the material divided by 1.5	2.1 The maximum temperature experienced by the MOD I cylinder and regenerator housings is 700°C. The highest value of wall averaged stress is 119 MPa for the regenerator housing and 99 MPa for the cylinder head in the hot region.
	2.2 Yield strength: The average effective stress through the wall for 20 MPa and no thermal stresses will be less than the yield strength divided by 1.5	The values of stress at several points in the cylinder head/regenerator housings and for the relevant load cases are given in the MOD I report.
	The average effective stress through the wall for a pressure of 20 MPa and with thermal stresses shall be less than the yield strength Fatigue Strength: All regions will resist fatigue with a safety factor of 1.5* along the load line in the Haigh Diagram representing creep-fatigue or yield fatigue interaction.	

* A proposed factor of 2.0 is under review for Mod II.

TABLE 1 (Cont'd)

DESIGN CRITERIA FOR THE MOD I ENGINE

<u>COMPONENT</u>	<u>STRENGTH CRITERIA APPLIED</u>	<u>COMMENTS</u>
3. Coolers	Buckling: The cooler tubes will resist elastic buckling with a safety factor of 2.5. The cooler as a whole should resist plastic buckling with a safety factor of 1.5	<p>The tubes are made of AISI 321 which has a 0.2 yield strength of 210 MPa and a fatigue limit of 190 MPa (at RT)</p> <p>The housing and support are constructed with AISI 319 which has a yield strength of 220 MPa and a fatigue limit of 185 MPa.</p>
4. Cold Connecting Duct Plate	Yield Strength: The duct plate will resist yielding with a safety factor of 2.	
5. Piston Rods	The piston rods must have a safety factor of 1.5 against yielding and 2.0 against fatigue failure	
6. Piston Dome	The dome must resist elastic and plastic buckling with a safety factor of 2.5.	<p>The adoption of the plastic buckling criterion with a safety factor of 2.5 minimizes the occurrence of dome buckling. This criteria is fulfilled with NIMONIC 80A or Inconel 718 and dome thickness of 2.3mm.</p>

TABLE 2

MATERIALS TESTING FOR THE MOD II ENGINE

Heater Tubes:	1. Hydrogen Permeability (NASA)
Sandvik 253 MA	2. Pressurized Tube Creep Testing (Sandvik)
Sanicro 31H	3. Creep Testing in Hydrogen (NASA-IITRI)
Sanicro 32	4. Hydrogen Aging Studies (NASA)
12RN72	5. Fatigue Testing (MTI)
Incoloy 901	6. Study of Effect of Brazing Cycle on Creep Properties (Sandvik)
Inconel X-750	7. Brazeability Studies (MTI)
Inconel 625	
XN-520	
Cylinder Heads 1	1. Hydrogen Permeability (NASA)
Regenerator Housings	2. Creep Testing in Air and Hydrogen (NASA-IITRI)
XF-818	3. Fatigue Testing (MTI)
CRM-6D	4. Hydrogen Aging Studies (NASA)
SAF-11	5. Cyclic Hydraulic Fluid Fatigue Test (USS)
Piston Domes:	1. Creep Testing in H ₂ (NASA-IITRI)
Inconel 718	2. Proof Testing of Fabricated Domes with Pressurized Fluid (USS)
Nimonic 80A	3. Aging studies in Argon and Hydrogen (NASA)

PROPOSED DESIGN CRITERIA
=====

DISCUSSION MATERIAL FOR TASK FORCE MEETING IN ENGINE DESIGN APRIL 15-17, 1980
.....

1. CREEP

IN CREEP ANALYSIS THE REFERENCE STRESS TECHNIQUE IS THE MOST PROMISING METHOD WHEN CORRELATING DIFFERENT CREEP DEFORMATIONS TO UNI-AXIAL CREEP DATA. A DRAWBACK IS THE EFFORT TO CALCULATE THE REFERENCE STRESS IN ANYTHING BUT ACADEMIC PROBLEMS. APPROXIMATELY THE REFERENCE STRESS CAN BE REPLACED BY THE LARGEST RELAXED CREEP STRESS.

PURE PRIMARY BENDING STRESSES AS ON THE TOP OF THE REGENERATOR HOUSING (MANIFOLD EXCLUDED) WILL RELAX TO ABOUT 70 PER CENT OF THE MAXIMUM ELASTIC STRESS. HOWEVER THE PEAK STRESSES IN THE MANIFOLDS AND THEIR CONNECTIONS TO THE HOUSINGS REQUIRE A FINITE ELEMENT CREEP ANALYSIS FOR THE DETERMINATION OF THE RELAXED STRESS STATE.

THE COMPUTED EFFECTIVE CREEP STRESS WILL BE USED IN THE DESIGN CRITERIA FOR THE HOUSINGS AND MANIFOLDS. AS A CONSEQUENCE THE RELAXED STRESS (MOOP) ON THE OUTSIDE OF THE TUBES WILL BE USED FOR THE TUBES ($2.25 \cdot P$ FOR 3/4.5 TUBING).

THE PEAK STRESSES WILL BE PRESENT INITIALLY BEFORE THE TOTAL RELAXATION HAS TAKEN PLACE. THUS THESE STRESSES WILL BE CONSIDERED WITH RESPECT TO HIGH CYCLE FATIGUE.

$$\sigma_s (P_{eq}) \leq \frac{\sigma_{cr}}{1.5}$$

WHERE

σ_s = RELAXED SECONDARY CREEP STRESS

σ_{cr} = CREEP RUPTURE STRESS, 3500 HOURS, ACTUAL TEMPERATURE
IN THE POINT

P_{eq} = EQUIVALENT MEAN PRESSURE COMPUTED WITH RESPECT TO LINEAR
DAMAGE THEORY (COMBINED CITY-HIGHWAY CYCLE)

COMBINED CREEP AND HIGH CYCLE FATIGUE DIAGRAMS FOR HIGH TEMPERATURE ALLOYS INDICATE THAT THE MEAN PRESSURE CAN BE USED RATHER THAN THE MAXIMUM ONE FOR SUCH MODERATE PRESSURE AMPLITUDES AS IN THE GAS CYCLE ($P-MAX/P-MEAN=1/3$).

DRIVING CYCLE SIMULATIONS FOR THE REFERENCE ENGINE IN AN X-CAR WITH FRONT WHEEL DRIVE GIVES A MEAN PRESSURE DISTRIBUTION AS SHOWN IN FIG. 1. FOR TUBE MATERIALS THIS GIVES AN APPROXIMATE EQUIVALENT MEAN PRESSURE OF 50 PER CENT, I.E. 7.5 MPa.

ORIGINAL PAGE IS
OF POOR QUALITY

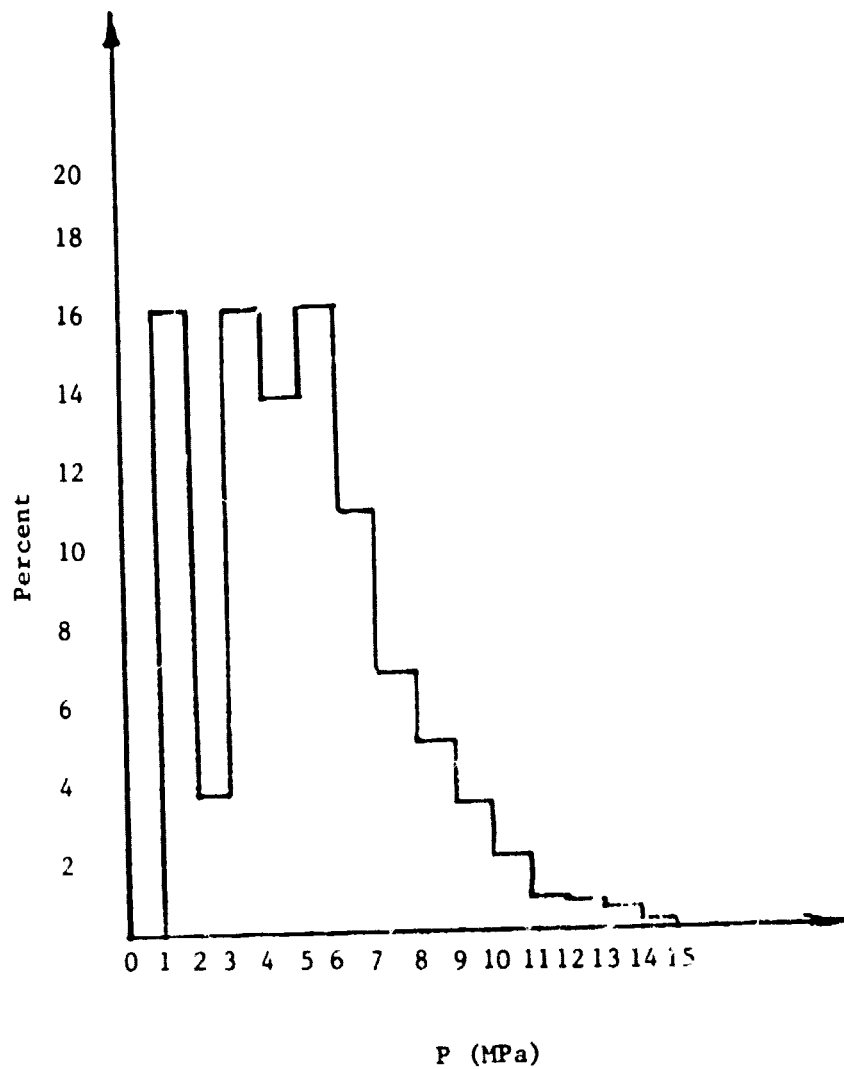


FIG. 1. THE MEAN PRESSURE DISTRIBUTION FOR REFERENCE ENGINE.

ORIGINAL PAGE IS
OF POOR QUALITY

2. YIELDING

THE STRESSES ARE SEPARATED IN PRIMARY, SECONDARY AND PEAK STRESSES. THE PRIMARY STRESSES CONSISTS OF MEMBRANE AND BENDING STRESSES CAUSED BY THE PRESSURE LOAD BUT EXCLUDE PEAK STRESSES AT DISCONTINUITIES. THE SECONDARY STRESSES ARE CAUSED BY THERMAL LOADS EXCLUDING PEAK STRESSES.

PRIMARY MEMBRANE STRESSES: $\sigma_e (p\text{-max}) \leq \frac{\sigma_y}{1.5}$

PRIMARY STRESSES: $\sigma_e (p\text{-max}) \leq \sigma_y$

PRIMARY AND SECONDARY STRESSES: $\sigma_e (p\text{-max}) \leq \sigma_y$

WHERE

σ_e = V. MISES EFFECTIVE STRESS

σ_y = YIELD STRESS (0.2 PER CENT)

P-MAX = MAXIMUM CYCLE PRESSURE 20 MPA

PEAK STRESSES ARE ANALYZED WITH RESPECT TO FATIGUE.

3. BUCKLING.

PLASTIC BUCKLING: $P\text{-MAX} < P\text{-CRITICAL} / 2.5$

WHERE $P\text{-MAX} = 20$ MPA.

PLASTIC BUCKLING IS CONTROLLED BY THE YIELDING CONDITION, I.E. A SAFETY FACTOR OF 1.5.

ORIGINAL PAGE IS
OF PCOR QUALITY

4.0 FATIGUE

4.1. GENERAL

IN TRI-AXIAL STRESS STATES CAUSED BY BOTH MECHANICAL AND THERMAL LOADS THE PRINCIPAL STRESSES AT THE SURFACE ARE USED IN COMBINATION WITH THE MISES YIELD CRITERION TO GET EQUIVALENT MEAN AND ALTERNATING STRESS COMPONENTS.

4.2. HIGH CYCLE FATIGUE

THE HIGH CYCLE FATIGUE IS CAUSED BY THE CYCLIC PRESSURE BETWEEN 10 AND 20 MPa. THIS LOAD CAN ACT IN COMBINATION WITH A STATIC THERMAL LOAD.

SURFACE CONDITIONS, TECHNOLOGICAL AND VOLUME DEPENDENCE AS WELL AS NOTCH SENSITIVITY IS TAKEN INTO CONSIDERATION. IN SUCH A REDUCED DIAGRAM (E.G. HAIGH) A SAFETY FACTOR OF 2 IS REQUIRED. THIS FACTOR IS IMPLEMENTED AS THE RATIO BETWEEN THE TWO DISTANCES OB AND OA IN FIG. 2. THE POINT A REPRESENTS THE COMPUTED STRESS LEVEL.

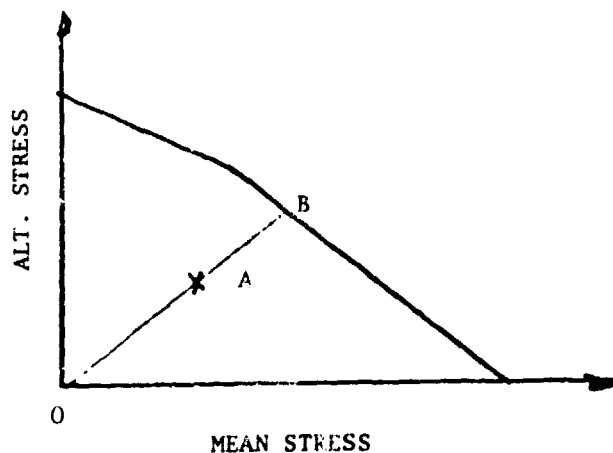


FIG. 2. A HAIGH DIAGRAM. THE POINT A REPRESENTS THE COMPUTED STRESS LEVEL.

4.2. LOW CYCLE FATIGUE.

ORIGINAL PAGE IS
OF POOR QUALITY

THE LOW CYCLE FATIGUE IS CAUSED BY THE VARIATIONS OF THE MEAN PRESSURE OF THE GAS CYCLE. THIS VARIATION FOR THE REFERENCE ENGINE IN AN X-CAR IS SHOWN IN FIG. 3 FOR THE CITY AND HIGHWAY CYCLES SEPARATELY. BESIDES THERMAL TRANSIENTS IN THE HOT REGION CAN CAUSE LOW CYCLE FATIGUE.

CYCLE COUNTING AND CUMULATIVE DAMAGE THEORY WILL BE USED. IF ADEQUATE LOW CYCLE FATIGUE DATA ARE NOT AVAILABLE AN APPROXIMATIVE TREATMENT AS COFFIN-MANSON'S LAW CAN BE USED.

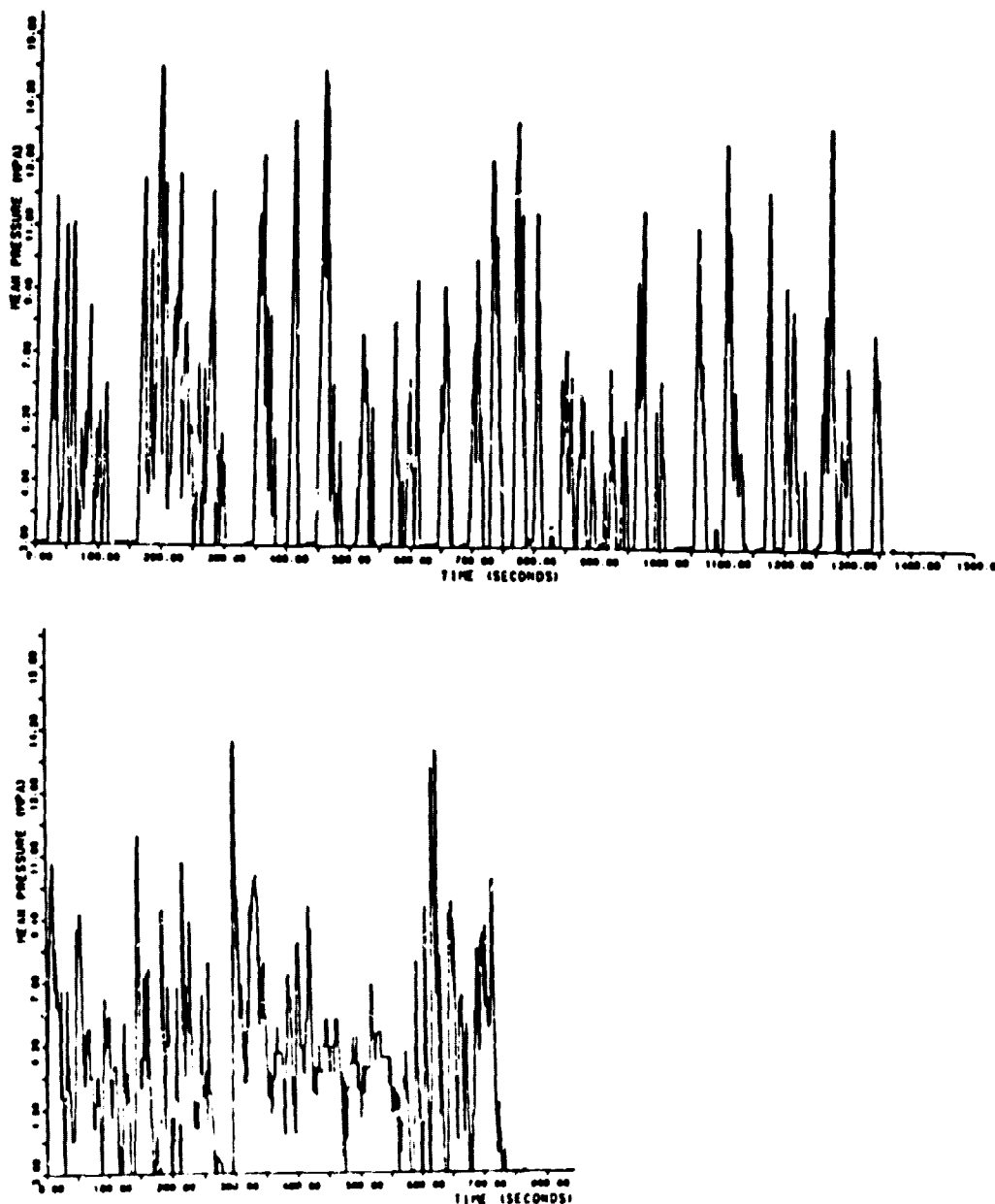


FIG. 3. THE MEAN PRESSURE VARIATION FOR REFERENCE ENGINE IN AN X-CAR. ABOVE. THE CITY CYCLE
BELOW. THE HIGHWAY CYCLE

ORIGINAL PAGE IS
OF POOR QUALITY

5. BOLT DESIGN

THE BOLT ARRANGEMENTS ARE DESIGNED IN ACCORDANCE WITH VDI 2230 (VEREIN DEUTSCHER INGENIEURE: SYSTEMATIC CALCULATION OF HIGH DUTY BOLTED JOINTS). THE MOST IMPORTANT POINTS ARE:

A. THE BOLT LOAD CONTRIBUTION $F_{SA} \leq 0.1 \sigma_y A_s$

WHERE σ_y = BOLT YIELD STRESS

A_s = BOLT CROSS SECTIONAL AREA

B. THE BOLT STRESS AMPLITUDE $\sigma_a < 64 \text{ MPA (M4-M8)}$

$\sigma_a < 54 \text{ MPA (M10-M16)}$

02

A.8 Combustion Air Blower Development

PRECEDING PAGE BLANK NOT FILMED

COMBUSTION AIR BLOWER DEVELOPMENT

- BENEFITS OF DEVELOPMENT
- SPECIFICATION
- PARAMETRIC STUDY
- EXPERIMENTAL AND PROPOSED PRODUCTION DESIGN
- EXPERIMENTAL SETUP
- DATA TO DATE
 - 1ST BUILD - EFFICIENCY
 - POWER REQUIREMENT
 - IMPELLER/HOUSING CLEARANCE SENSITIVITY
 - REDUCED VOLUME VOLUTE HOUSING
- TESTS TO BE COMPLETED

MOD I COMBUSTION AIR BLOWER
BENEFIT OF DEVELOPMENT

P-40 AUXILIARIES PARASITIC LOSSES

AUXILIARIES

LOSSES (@ 15MPA & 4000 RPM)

	Kw	%
COMBUSTION AIR BLOWER	3.2	43%
ALTERNATOR	2.2	57%
LUB OIL PUMP	.45	
WATER PUMP	.65	
OIL SERVE PUMP	.27	
ATOMIZING AIR COMPRESSOR	.55	
FUEL PUMP	<u>.15</u>	
TOTAL	7.47	100%

ORIGINAL PAGE IS
OF FOUR QUALITY

CONCLUSIONS

- COMBUSTION AIR BLOWER 43% OF AUXILIARIES PARASITIC LOSSES
- SIGNIFICANT REDUCTION IN PARASITIC LOSSES IS AVAILABLE THROUGH DEVELOPMENT OF A SMALL, EFFICIENT BLOWER
- ESTIMATED AVAILABLE POWER REDUCTION - 2Kw @ MAX POWER OR 30% OF PARASITIC LOSSES

COMBUSTION AIR BLOWER SPECIFICATION

GEOMETRY:	MAXIMUM DIAMETER	- 200MM (7.87 IN.)
	ROTATION	- CLOCKWISE LOOKING INTO BLOWER INLET
	USS/MTI INTERFACE	- BACK SURFACE OF IMPELLER HOUSING
PERFORMANCE:	SPEED	- TO BE DETERMINED BY PARAMETRIC STUDY
	EFFICIENCY	- 65-70% AT LOWEST AIRFLOW POSSIBLE, WITHOUT AN EXCESSIVE COMPROMISE OF MAX FLOW EFFICIENCY REQUIRED FOR ENGINE ACCELERATION
	AIRFLOW CAPACITY	- 5.3 GRAMS/SEC MIN (START/IDLE) 79 GRAMS/SEC MAX, INCLUDES 4 GRAMS/SEC MARGIN FOR LEAKAGE
	PRESSURE DROP	- 2 ALTERNATIVE COMBUSTION SYSTEMS (FOLLOWING FIGURE) 1) <u>CGR SYSTEM WITH VALVE</u> BLOWER MUST PROVIDE FULL RANGE OF FLOW WITH STABLE OPERATION, AND WITH CGR VALVE FAILED, STABLE OPERATION BUT NOT FULL RANGE OF FLOW. 2) <u>CGR STRAIGHT VANE SYSTEM</u> BLOWER MUST PROVIDE FULL RANGE OF FLOW WITH STABLE OPERATION.
	NOISE	- LOW NOISE LEVEL (APPROXIMATELY 78 DBA GOAL) WITH INLET MUFFLER INSTALLED.
	ENVIRONMENT	- MAXIMUM INLET TEMP. 40°C (104°F)

BEARING/ROTOR
ANALYSIS:

LIFE -3000 HOURS

OPERATION -%TIME

5%

MAX

30%

83%

50%

67%

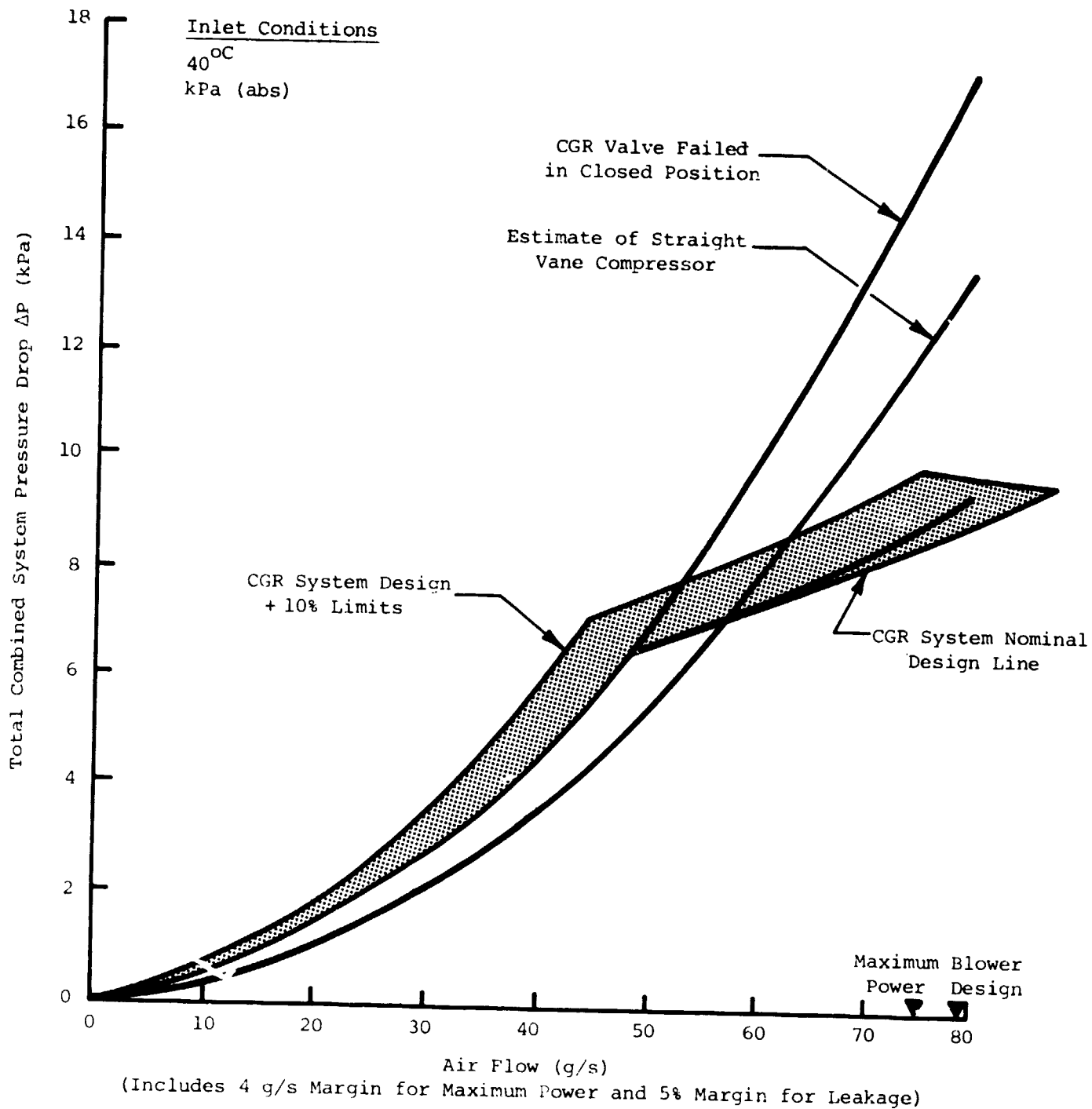
15%

44%

BELT FORCE:
$$- \left(\frac{32 \text{ KG} + \text{BLOWER FORCE}}{2} \right) \leq 50 \text{ KG MAX}$$

ORIGINAL PAGE IS
OF POOR QUALITY

ORIGINAL PAGE IS
OF POOR QUALITY



Combustion Air Blower Design Requirement

MOD I COMBUSTION AIR BLOWER PARAMETRIC STUDY

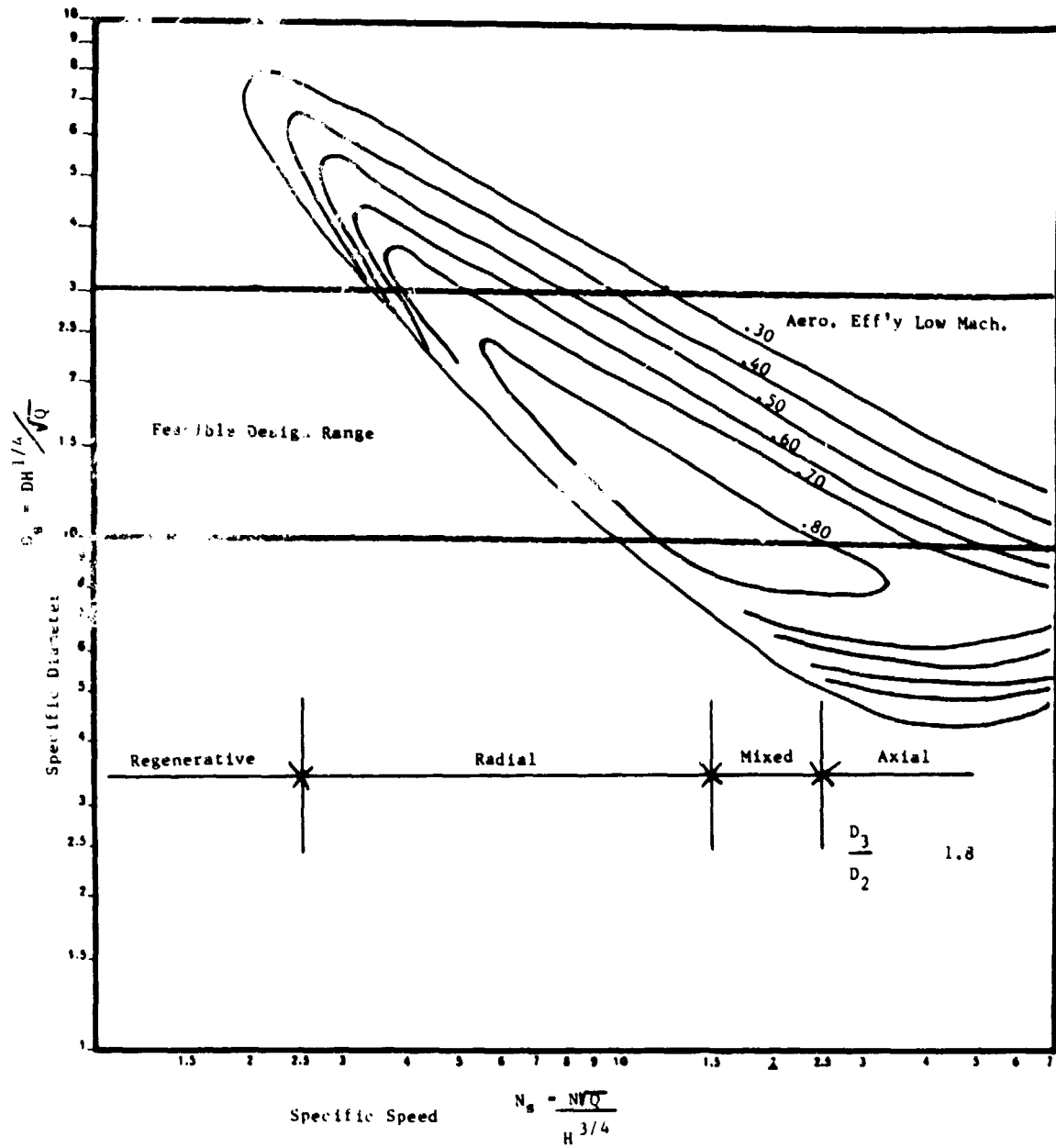
OBJECTIVE

- DEFINE TYPE OF BLOWER FOR APPLICATION
- DEFINE OPTIMUM BLOWER GEOMETRY
- DEFINE BLOWER SPEED

PARAMETERS INVESTIGATED

- BLOWER GEOMETRY
 - REGENERATIVE
 - CENTRIFUGAL
 - AXIAL OR MIXED
- OPTIMUM BLOWER PERFORMANCE
 - BLOWER SPEED
 - 3 DIMENSIONAL VANES
 - BACKWARD LEANING VANES
 - VANED DIFFUSER
 - IMPELLER DIAMETER
- CRITICAL SPEED
- BEARING LIFE - EVALUATE BEARINGS FOR:
 - FATIGUE
 - LUBRICANT STARVATION & LIFE
 - CAGE FAILURE

ORIGINAL PAGE IS
OF POOR QUALITY



Mod I Combustion Air Blower (Feasible Design Range)

MOD I COMBUSTION AIR BLOWER

PARAMETRIC STUDY

BLOWER GEOMETRY

GEOMETRY

ADVANTAGES

DISADVANTAGES

REGENERATIVE

- HIGH PRESSURE CAPABILITY
- LOW SPEED
- NO SURGE FLOW RESTRICTION

SIZE
WEIGHT
INEFFICIENT

AXIAL

- STEEPLY RISING PRESSURE CHARACTERISTICS
- SMALL DIAMETER

- POOR SURGE MARGIN
- INEFFICIENT
- SIZE FOR IMPROVED EFFICIENCY (LONG DIFFUSOR)
- ULTRA HIGH SPEED

CENTRIFUGAL

- GOOD SURGE MARGIN
- COMPACT SIZE
- GOOD EFFICIENCY

- HIGH SPEED

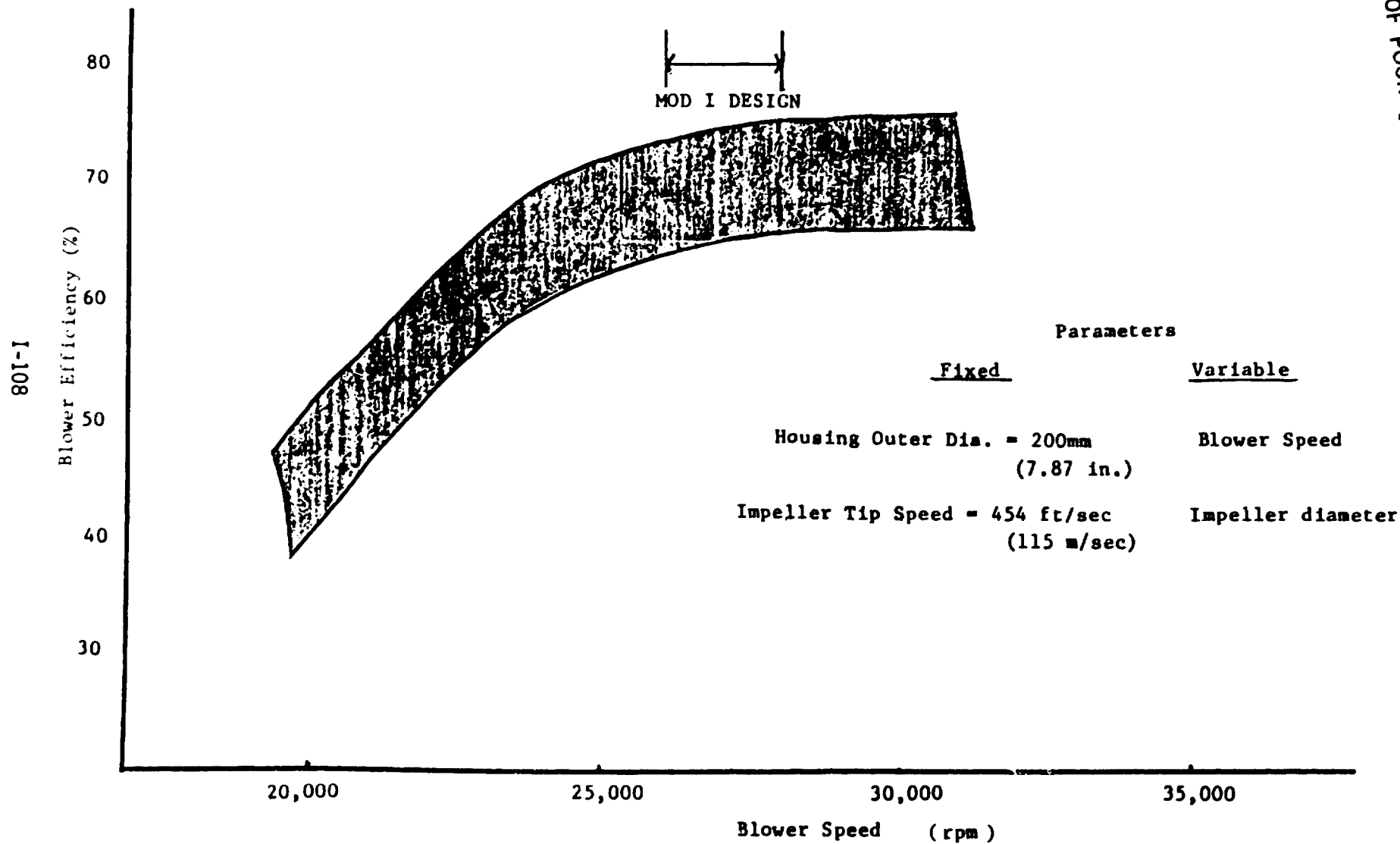
- STRAIGHT BLADES
- BACKWARD LEANING BLADES
- 3 DIMENSIONAL BLADES
- DIFFUSER VANES

- 65-75% EFFICIENCY
- <1% CHANGE IN EFFICIENCY @ LOW PRESSURE RATIO
- <1% CHANGE IN EFFICIENCY
- 2% CHANGE IN EFFICIENCY

- PRODUCTION & DEVELOPMENT COST
- PRODUCTION & DEVELOPMENT COST
- PRODUCTION & DEVELOPMENT COST
- EFFICIENCY IMPROVEMENT GOOD FOR ONLY A NARROW RANGE OF FLOW

ORIGINAL PAGE IS
OF POOR QUALITY

MOD I COMBUSTION AIR BLOWER PARAMETRIC STUDY

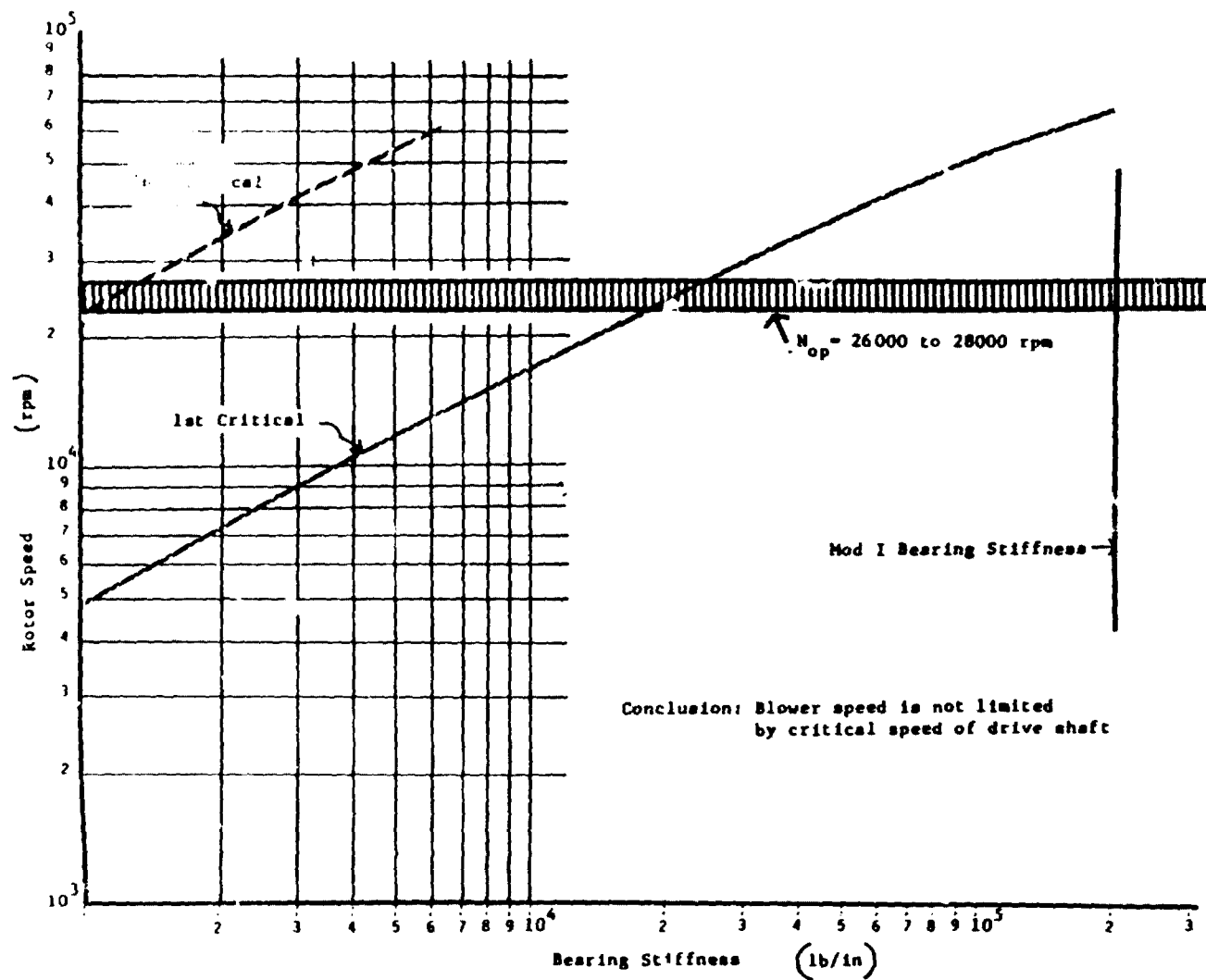


ORIGINAL FILED IN
OF POOR QUALITY

MOD I COMBUSTION AIR BLOWER
PARAMETRIC STUDY
CONCLUSIONS OF BLOWER GEOMETRY STUDY

- CENTRIFUGAL BLOWER BEST FOR AUTOMOTIVE APPLICATION
- LEAST COMPLICATED GEOMETRY MOST COST EFFECTIVE
- OPTIMUM SPEED FOR SIZE 26,000 - 28,000 RPM

ORIGINAL PAGE IS
OF POOR QUALITY



Mod I Stirling Blower Critical Speed Map

ORIGINAL PAGE IS
OF POOR QUALITY

MOD I COMBUSTION AIR BLOWER
BEARING LIFE STUDY
CONCLUSIONS

FATIGUE

- BEARINGS HAVE MORE THAN ADEQUATE LIFE WITH NORMAL CONDITIONS OF LUBRICATION AT 28,000 RPM
- BLOWER SPEED IS NOT LIMITED BY BEARING FATIGUE

LUBRICANT STARVATION AND LIFE

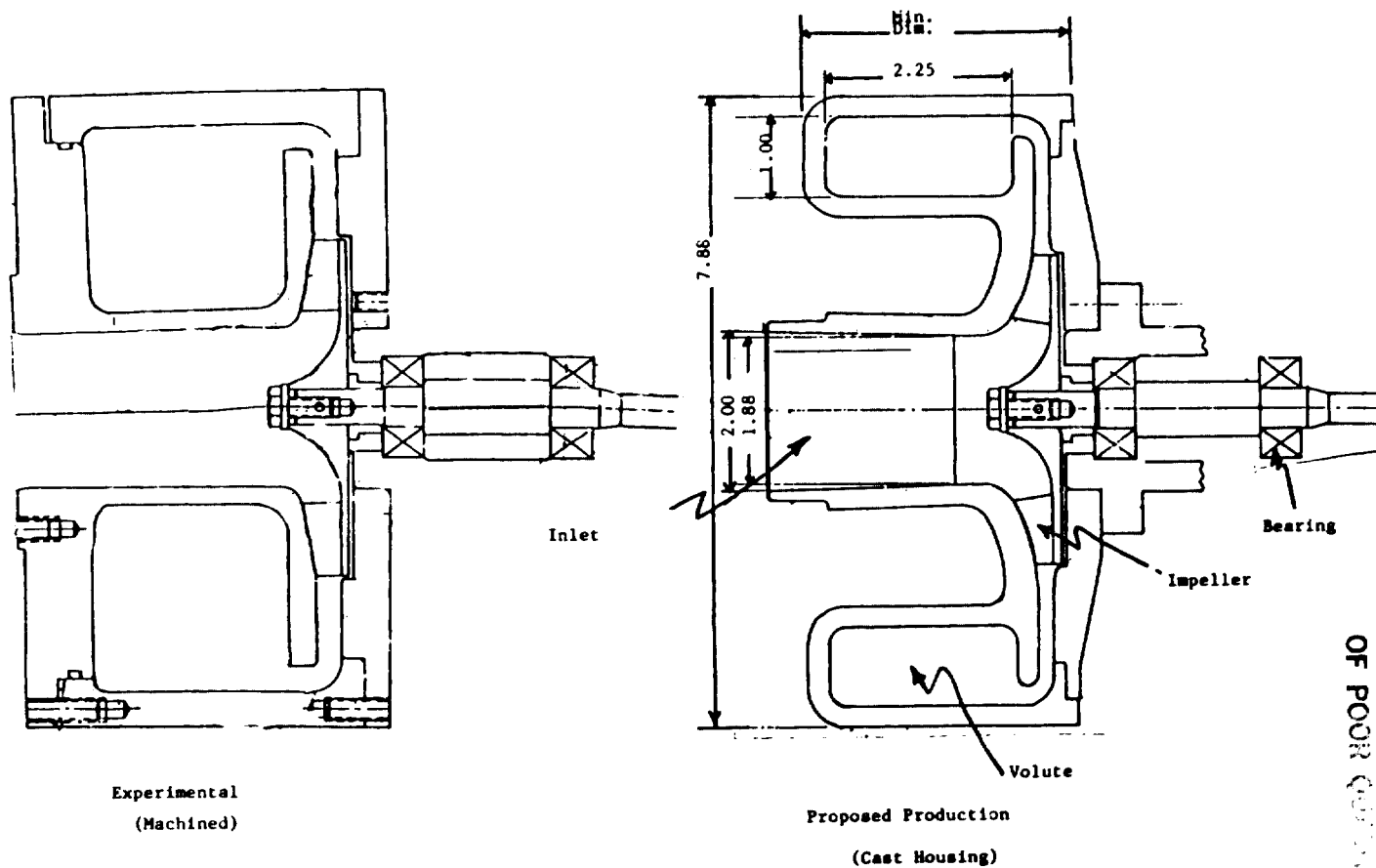
- NORMAL LUBRICATION CAN BE MAINTAINED AT BEARING ENVIRONMENTAL TEMPERATURE OF 150°F OR LESS
- 2100 HRS GREASE LIFE REQUIRES 1 REPLACEMENT DURING LIFE OF BLOWER
- BLOWER SPEED LIMITED BY GREASE LIFE

CAGE FAILURE

- SELECTED A BARDON 201 SST X 1 BEARING WITH PHENOLIC AND ALUMINUM CAGES FOR IMPROVED CAGE LIFE

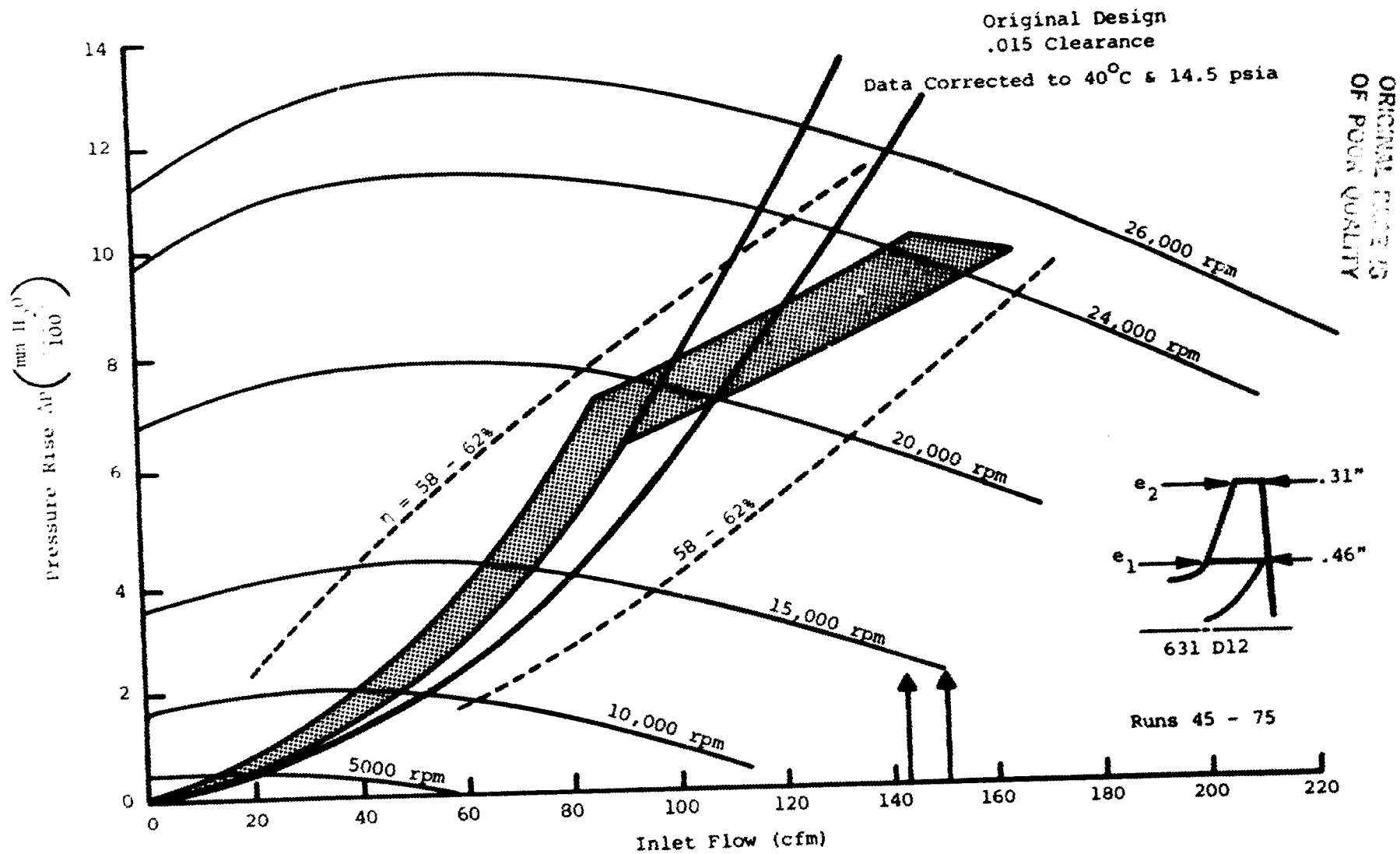
RECOMMENDATIONS

- USE EXXON ANDOK "C" OR TEXACO MULTIFAK - ALL PURPOSE GREASE
- THE ENVIRONMENTAL TEMPERATURE OF THE BEARINGS SHOULD BE MONITORED IN TESTS



ORIGINAL DESIGN
OF POOR QUALITY

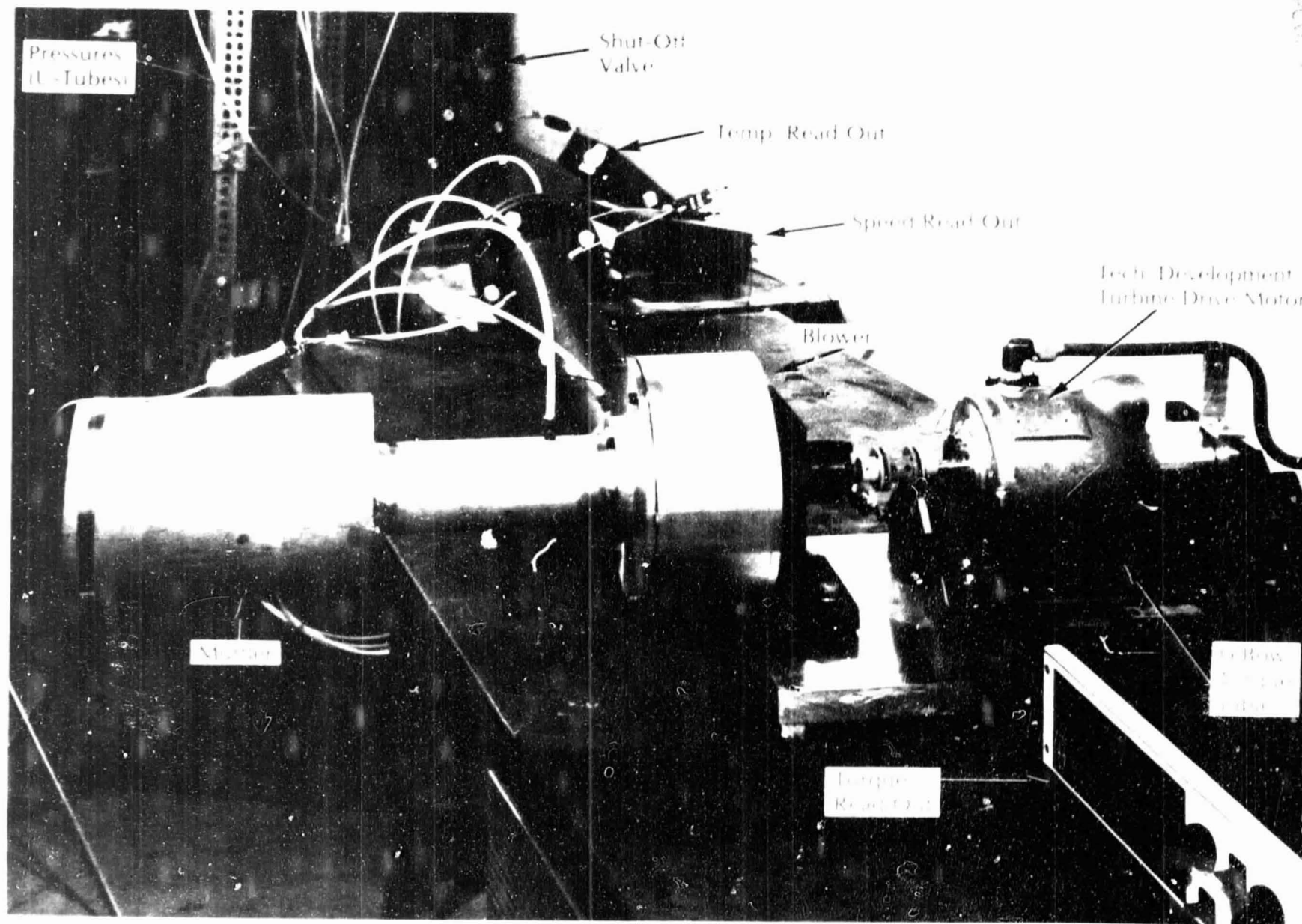
Mod I Combustion Blower Air Blower Designs

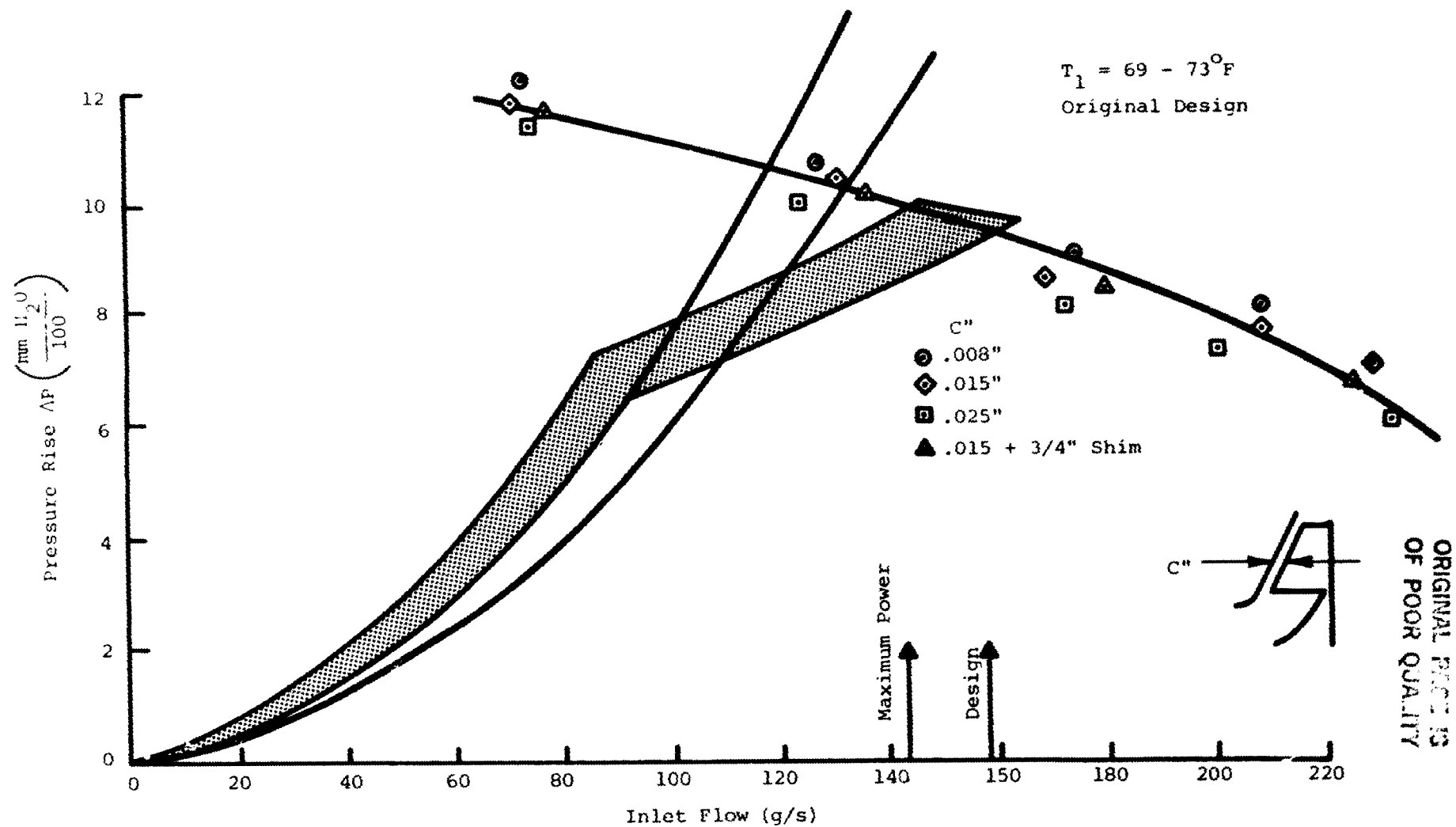


Mod I Combustion Air Blower Test Results, Efficiency

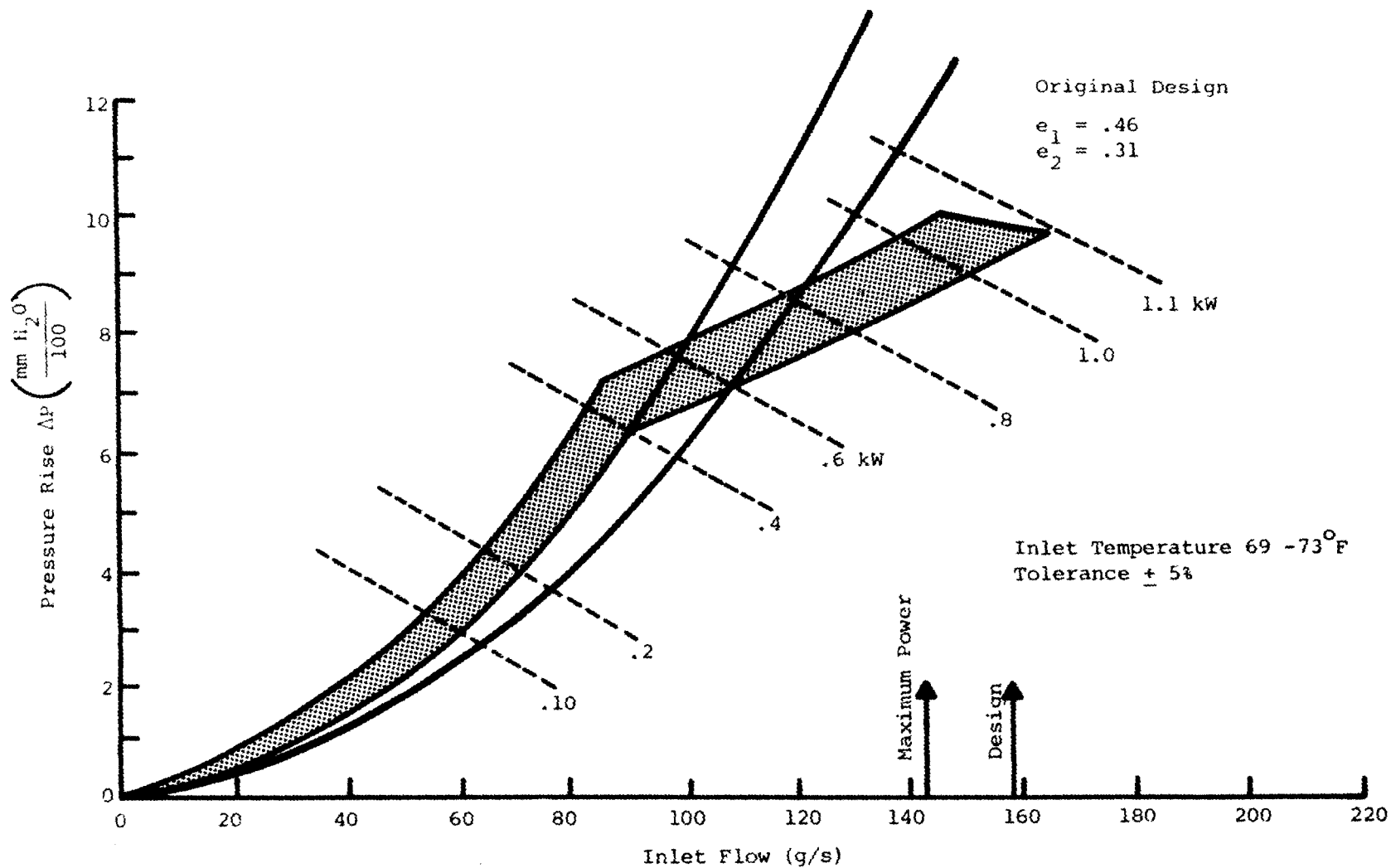
MODI Combustion Air Blower Experimental Test Rig

ORIGIN
OF POWER





Mod I Combustion Air Blower Test Results
Effect of Vane Clearance and Volute Volume at 24,000 rpm



Mod I Combustion Air Blower Test Results, Build 1 Power Demand

ORIGINAL PAGE IS
OF POOR QUALITY

MOD I COMBUSTION AIR BLOWER
TESTS TO BE COMPLETED

<u>TEST</u>	<u>PURPOSE</u>
MODIFIED IMPELLER HEIGHT (.100 IN REDUCTION)	IMPROVE EFFICIENCY
INCREASED DIFFUSER RATIO	IMPROVED EFFICIENCY
SIMULATED CAST VOLUTE HOUSING	VERIFY PRODUCTION DESIGN
REDUCED VOLUME SIMULATED CAST HOUSING	REDUCE BLOWER SIZE
NOISE TESTS	QUANTIFY NOISE
ELIMINATE RADIUS AT HOUSING/BACKING PLATE INTERFACE	REDUCE PRODUCTION COST

A.9 Mod I Engine Starter Development

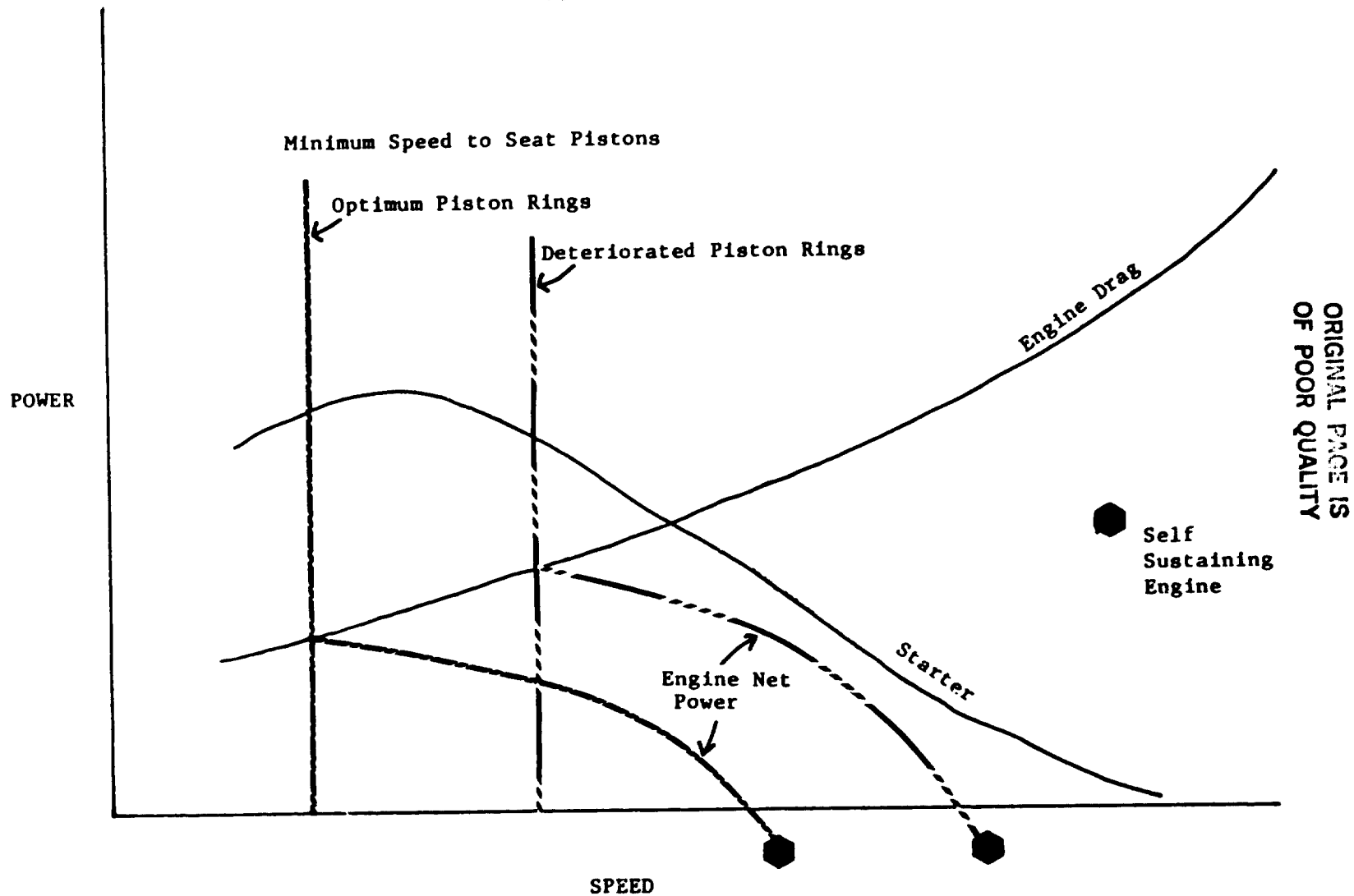
PRECEDING PAGE BLANK NOT FILMED

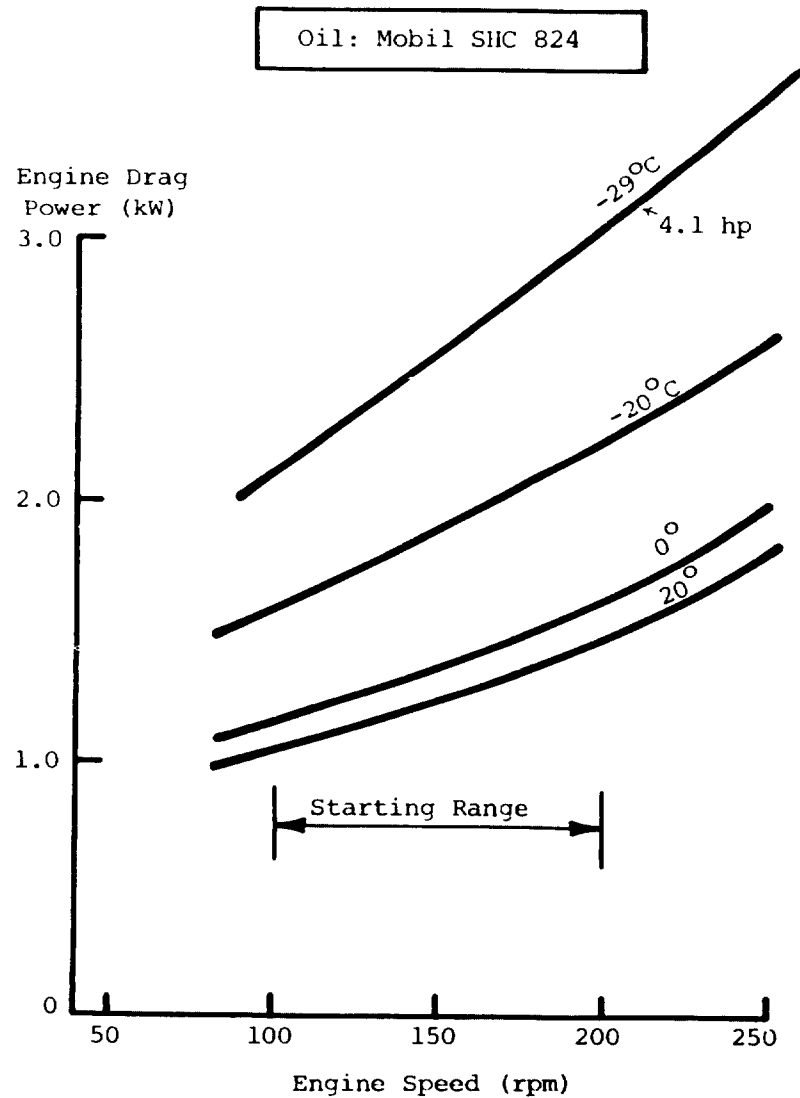
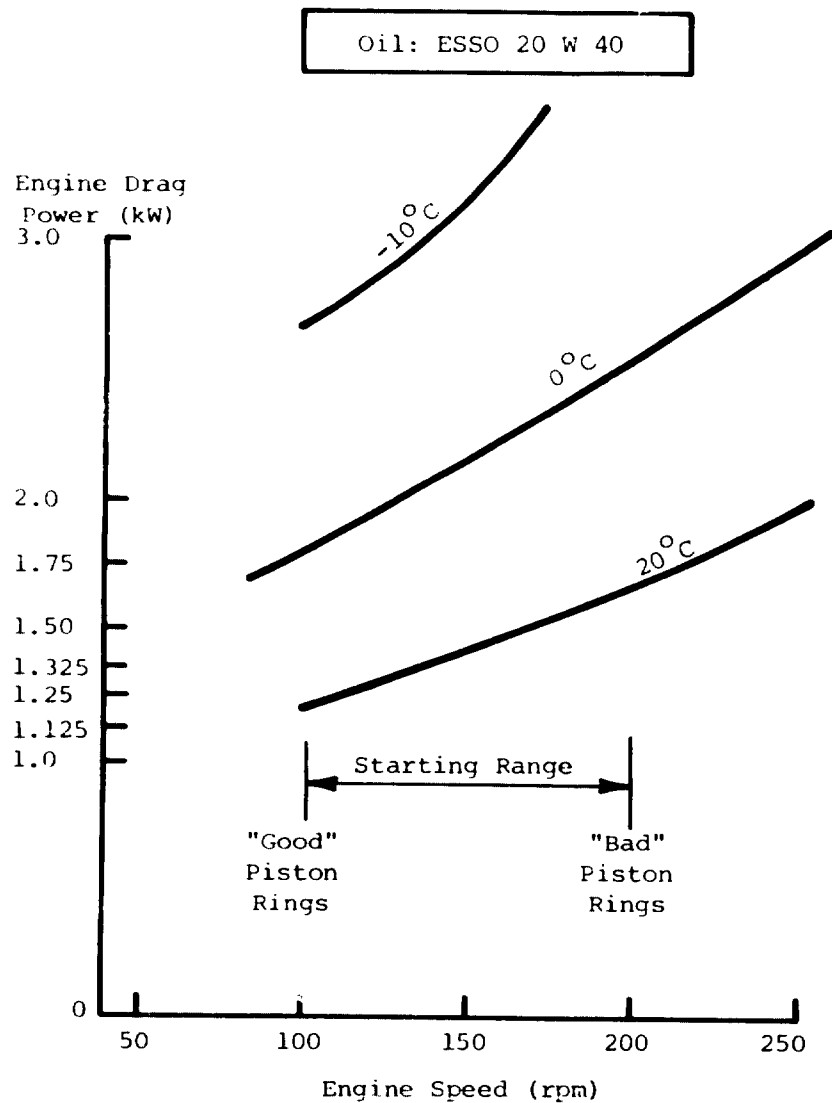
MOD I ENGINE STARTER MOTOR

- STARTER CHARACTERISTICS
- REQUIREMENTS
- COMPARISON OF P-40 EXPERIENCE TO MOD I
- MOD I STARTING WITH MOBIL LOW VISCOSITY OILS
- CONCLUSIONS/RECOMMENDATIONS

ORIGINAL PAGE IS
OF POOR QUALITY

STARTING POWER CHARACTERISTICS

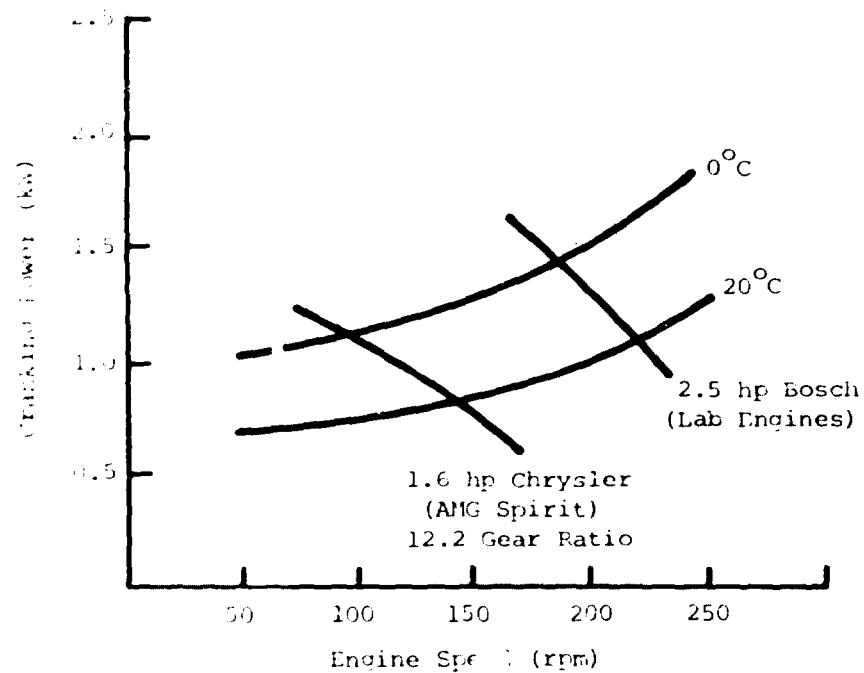




Mod I Starter Requirements
-29°C Starting Temperature, Automotive Standard

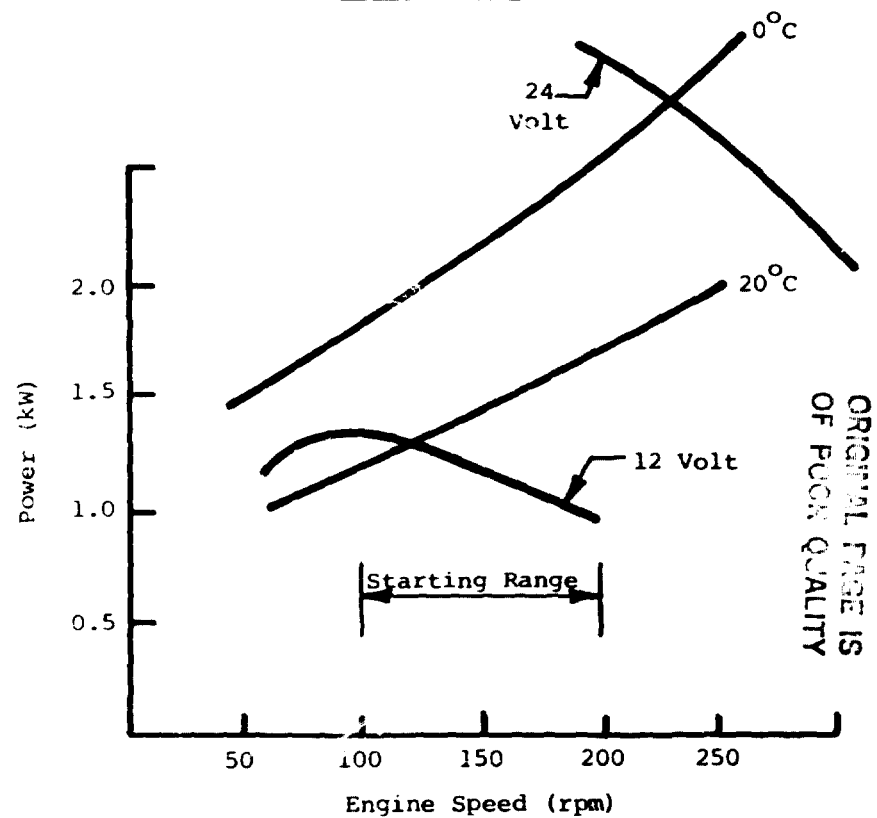
ORIGINAL PAGE IS
OF POOR QUALITY

P-40



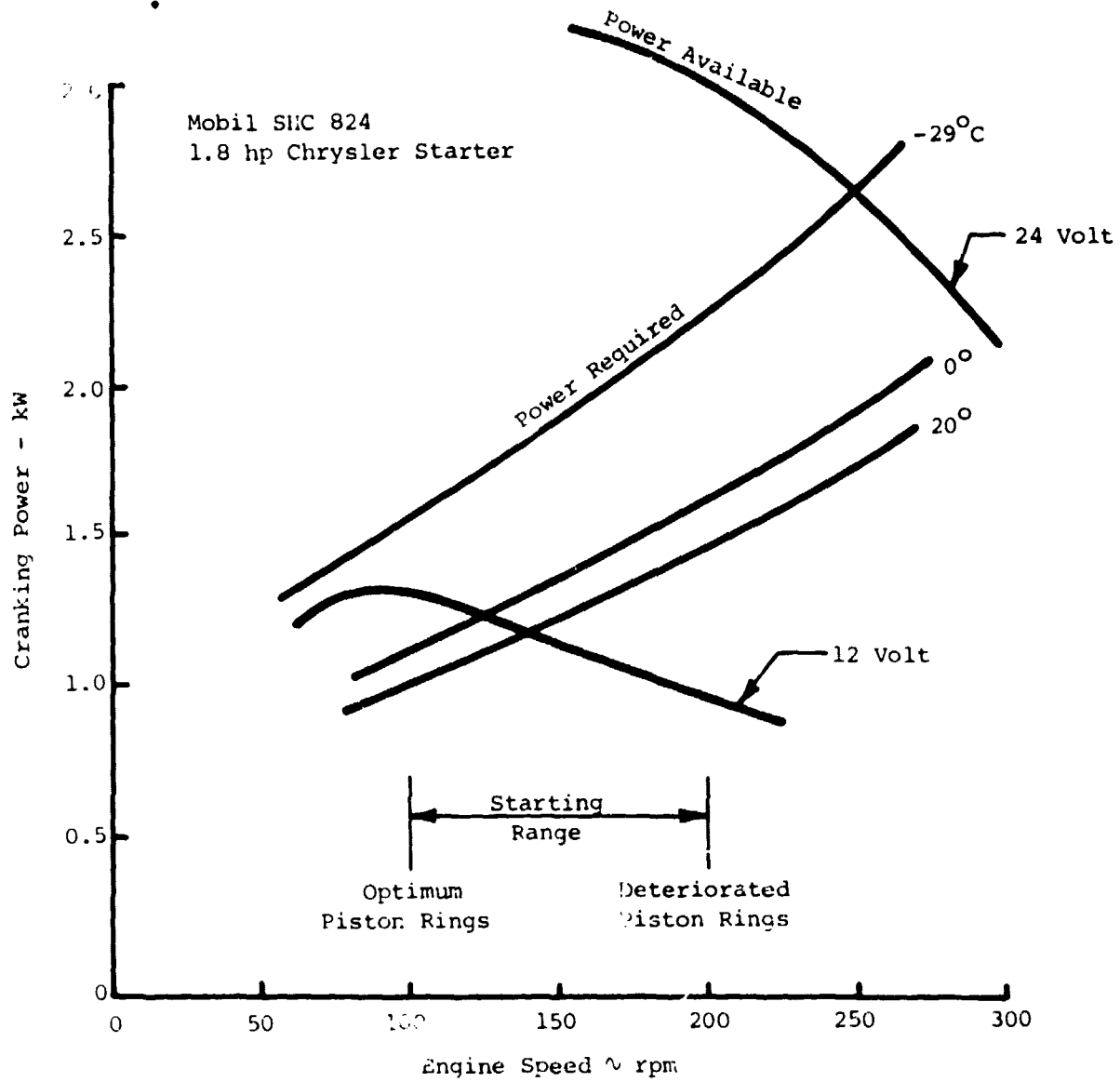
ESSO Extra 20 W 40

Mod I

ESSO Extra 20 W 40
1.8 hp Chrysler Starter

Mod I Starter - Comparison of P-40 to Mod I

OF POOR QUALITY



ASE Mod I Starting

MOD I ENGINE STARTER MOTOR

CONCLUSIONS

- (1.3 Kw) 1.8 HP - 12v STARTER WILL PROVIDE STARTING CAPABILITY COMPARABLE TO CURRENT AMG P-40 SPIRIT WITH ESSO 20 W 40 OIL
- (1.3 Kw) 1.8 HP - 12v STARTER ESTIMATED CAPABLE OF STARTING MOD I TO 0°C OR LOWER WITH MOBIL SCH - 824 OIL

RECOMMENDATIONS

- RUN VEHICLE WITH ESSO 20 W 40 IN WARM WEATHER AND CHANGE TO MOBIL SCH 824 WHEN TEMP IS LESS THAN 10°C
- FUTURE DEVELOPMENT SHOULD INCLUDE:
 - A) REDUCED POWER CHAIN LOSSES
 - B) CONTINUED DEVELOPMENT OF PISTON RINGS
 - C) DEVELOPMENT OF TEST DATA TO IMPROVE STARTER MOTOR SPECIFICATION

AUTOMOTIVE STIRLING ENGINE DEVELOPMENT PROGRAM

MODEL 1 STIRLING ENGINE SYSTEM

DESIGN REVIEW

MAY 22, 1980

ORIGINAL PAGE IS
OF POOR QUALITY

CONCLUSIONS AND RECOMMENDATIONS

PRECEDING PAGE BLANK NOT FILMED

MECHANICAL TECHNOLOGY INCORPORATED
908 ALBANY-SHAKER ROAD
LATHAM, NEW YORK 12110

MOD I DESIGN REVIEW
MAY 22, 1980
CONCLUSIONS AND RECOMMENDATIONS

CONCLUSIONS

- MOD I STIRLING ENGINE SYSTEM HAS BEEN DESIGNED WITH ADEQUATE RISK TO ENABLE DEMONSTRATION OF ITS PERFORMANCE GOALS.
- MOD I STIRLING ENGINE SYSTEM HAS BEEN DESIGNED WITH SUFFICIENT RISK TO PROVIDE HIGH PROBABILITY THAT MOD II WILL MEET PROGRAM OBJECTIVES.
- MOD I STIRLING SYSTEM HAS MECHANICAL INTEGRITY.
- MOD I CONTROL AND AUXILIARY SYSTEM DESIGNS REPRESENT SIGNIFICANT IMPROVEMENTS IN PERFORMANCE AND RELIABILITY OVER THOSE IN THE P-40 ENGINE.
- MOD I STIRLING ENGINE SYSTEM PERFORMANCE PROJECTIONS ARE ACHIEVABLE.

MOD I DESIGN REVIEW
MAY 22, 1980
CONCLUSIONS AND RECOMMENDATIONS

ORIGINAL PAGE IS
OF POOR QUALITY

RECOMMENDATIONS

- NASA APPROVE THE MOD I STIRLING ENGINE SYSTEM DESIGN.
- NASA APPROVE THE PROCUREMENT OF MOD I STIRLING ENGINE SYSTEM HARDWARE.

PRECEDING PAGE BLANK NOT FILMED

B.1 Table of Contents

TABLE OF CONTENTS OF TECHNICAL INFORMATION DELIVERED
PRIOR TO THE MEETING

- B.1 TABLE OF CONTENTS
- B.2 STIRLING ENGINE SYSTEM
 - 2.1 General Description
 - 2.2 Engine Specification
 - 2.3 Drawings are in Volume III
- B.3 BASIC STIRLING ENGINE
 - 3.1 General Description
 - 3.2 Drawings are in Volume III
 - 3.3 Calculations Update
 - 3.4 Procurement Schedule
- B.4 EXTERNAL HEAT SYSTEM
 - 4.1 General Description
 - 4.2 Drawings are in Volume III
 - 4.3 Calculations
 - 4.4 Flow Distribution Test. Air Preheater
 - 4.5 Joining Test. Air Preheater Matrix
 - 4.6 Combustion Tests
 - 4.7 Material Selection and Rationale
 - 4.8 CGR and EGR Update
 - 4.9 Calculations Update
- B.5 HOT ENGINE SYSTEM
 - 5.1 General Description
 - 5.2 Drawings are in Volume III
 - 5.3 Stress Calculations of Heater, Cylinder and Regenerator Housing and Cooler
 - 5.4 Heat Transfer for Heater Tubes
 - 5.5 Flow Distribution Tests on Cylinder, Manifold and Regenerator Housing
 - 5.6 Manufacturing Method
 - 5.7 Material Selection and Rationale
- B.6 COLD ENGINE SYSTEM
 - 6.1 General Description
 - 6.2 Drawings are in Volume III
 - 6.3 Stress Calculations of Water Jacket, Cold Connecting Duct Plate, Dome, Piston, Bolts in Warm/Cold Parts
 - 6.4 Fatigue Test of Cylinder - Water Jacket - Duct Plate
 - 6.5 Fabrication Technique and Material Selection

TABLE OF CONTENTS (Concluded)

B.7 ENGINE DRIVE SYSTEM

- 7.1 General Description
- 7.2 Drawings are in Volume III
- 7.3 Calculations

B.8 CONTROL SYSTEM AND AUXILIARIES

See Volume II for Table of Contents

B.9 VEHICLE INTEGRATION

See Volume II for Table of Contents

B.10 COST ANALYSIS OF THE STIRLING ENGINE MOD I IN A MASS PRODUCTION
QUANTITY OF 200,000 UNITS/YEAR

See Volume II for Table of Contents

PRECEDING PAGE BLANK NOT FILMED

B.2 Stirling Engine System

2. STIRLING ENGINE SYSTEM

2.1 General description

The design is based on the approved concept A of RESD (Reference Engine System Design) Conceptual Study as been reported in USSw July 4, 1979.

The RES design has then been updated and presented in September 1979.

The studies and different design/arrangement evaluations in parallel (1978) forms the original platform for present ASE Mod I design.

In addition this design has also been backed up by accumulated experiences from Baseline Engine tests and separate development activities.

Compared to RES the ASE Mod I has a closer resemblance to the Baseline Engine. The design philosophy has been to rely on experienced design criteria and to introduce changes only when necessary for a more extensive use of aluminium alloys and to use automotive design practices whenever possible for different components, mainly on the engine body.

Some known Baseline Engine weakness and drawbacks are eliminated and the specific operating conditions, more part-load, taken into account.

The design process, from optimization point of view, is briefly discussed separately (section 2.2) and major changes/improvements relative to Baseline Engine are listed in the following table (section 3:1).

These may be summarized as follows:

- a) Four instead of eight regenerator/cooler units. This means less parts and gas seals that are more simple and lighter cylinder block parts. A low, wide, external heat system with a CGR combustor (internal recirculation).
- b) Functionally improved cold engine system parts and better general arrangement with respect to taking up gas pressure loads and to maintenance. Aluminum crankcase structure. Reduced weight.
- c) Improvements on external gas system and power control devices (fewer parts), auxiliaries and vehicle integration. These items will be dealt with separately at a later SES design review.

Specific stress analysis and material selection for major components are presented in separate sections below. Various separate tests for design substantiation are also described separately for each component/subsystem.

Required auxiliaries and control data are defined in the engine specification. Preliminary SES arrangement and vehicle integration schemes

have been performed to assure installation in a Spirit. The principal SES arrangement is settled and all BSE interfaces (auxiliary drives, mounting faces etc) are defined. The installation requirements have influenced the design and will call for some vehicle modifications (see section 9.1).

2.2 Engine specification for ASE Mod 1
(Replaces USS design specification 79-0042 C)

- 2.2.1 Basic design goals
- 2.2.2 Additional design goals
- 2.2.3 Operating conditions
- 2.2.4 Standard conditions
- 2.2.5 Salient design data of different subsystems
 - 2.2.5.1 Stirling engine system
 - 2.2.5.2 External heat system
 - 2.2.5.2.1 Combustor
 - 2.2.5.2.2 Air preheater
 - 2.2.5.3 Hot engine system
 - 2.2.5.3.1 Heater
 - 2.2.5.3.2 Regenerator
 - 2.2.5.3.3 Gas cooler
 - 2.2.5.4 Cold engine system
 - 2.2.5.4.1 Cylinder block
 - 2.2.5.4.2 Piston and piston rod
 - 2.2.5.4.3 Piston rod seal
 - 2.2.5.5 Engine drive system
 - 2.2.5.5.1 Crankcase
 - 2.2.5.5.2 Crankshaft and main shaft arrangement
 - 2.2.5.5.3 Connecting rods
 - 2.2.5.5.4 Lubrication system

- 2.2.5.5.5 Auxiliary drives
- 2.2.5.6 Auxiliaries *
- 2.2.5.6.1 Cooling water pump
- 2.2.5.6.2 Combustion air blower
- 2.2.5.6.3 Atomizing air compressor
- 2.2.5.6.4 Fuel pump
- 2.2.5.6.5 Air flow meter
- 2.2.5.6.6 Air throttle actuator
- 2.2.5.6.7 Power control compressor
- 2.2.5.6.8 Power control valve actuator
- 2.2.5.6.9 Oil pump for power control valve actuator
- 2.2.5.6.10 Alternator
- 2.2.5.6.11 Starter motor
- 2.2.5.6.12 Electric motor for heating up sequence
- 2.2.5.6.13 Electronic control unit
- 2.2.5.6.14 Radiator fan
- 2.2.5.7 Accessories
- 2.2.5.7.1 Hydraulic pump for power steering and brakes
- 2.2.5.7.2 Air conditioning compressor

* Lubrication oil pump is covered in 2.2.5.5.4 Lubrication System

2.2.1 Basic design goals

Net shaft power	58 kW
Fuel economy (in AMC Spirit)	27,5 mpg
Net peak efficiency	34 %
Exhaust emissions (in AMC Spirit)	NO _x : 0,4 g/mile CO: 3.4 g/mile HC: 0.41 g/mile
Weight of SES	260 kg
Noise emissions	Lower than P40 Opel

2.2.2 Additional design goals

Installation requirements	Package in AMC Spirit after necessary vehicle modifications. No bump in hood allowed.
Design life	3500 hrs combined cycle (To be used as general guide line)
Optimization	Part load performance to be emphasized.

2.2.3 Operating conditions

a. Working medium	Hydrogen
b. Max. mean pressure	15 MPa
c. Mean heater tube temperture	720°C
d. Engine speed at max. power	4000 rpm
e. Idling speed	700 rpm in neutral, 600 rpm in drive
f. Fuel, normal	Unleaded gasoline
, optional	Diesel fuel*
g. Coolant	Water, with possibility to add suitable anti-freeze
h. Ambient temperature	0°C to +40°C
Operating attitude	Sea level to 4260 m
Relative humidity	0-100%
Engine inclination	15°, front or rear end down

*The specification of the fuel used in the development tests is shown on page 2.2:15.

2.2.4 Standard conditions

Engine performance calculations are related to the following standard conditions.

Ambient temperature	+20°C
Atmospheric pressure	760 mm of Mercury
Cooling water outlet temperature (pure water)	+50°C

2.2.5 Salient design data for different subsystems

2.2.5.1 Stirling engine system

a. Engine type	Double-acting Rinia with parallel cylinders and crank type drive mechanism
b. Number of cylinders	4
c. Bore	68 mm
d. Stroke	34 mm
e. Swept volume	123.5 cm ³ per cylinder
f. Number of regenerators	4 cannisters, located outside cylinders
g. Type of drive	2 crankshafts and 1 main shaft, coupled together.
h. Number of combustion chambers	1
i. Preheater	Recuperative, plate type
j. Heater	Involute type, 4 quadrants
k. Gas cooler	Tubular type, 4 per engine
l. Regenerators	Sintered screen, 4 per engine
m. Power Control Principle	Mean pressure control by means of engine driven hydrogen compressor.
n. Main Auxiliaries	Cooling water pump, combustion air blower, atomizing air compressor, power control compressor, oil pump for power control valve actuator, alternator, starter motor, electric motor for starting up sequence, radiator fan, lubrication oil pump.

o. Accessories

Hydraulic pump for power steering
and brakes.

A/C compressor

2.2.5.2 External heat system

The calculated fuel flow at maximum engine power is 4.5 g/s,
but the combustor and preheater shall be designed to be able
to operate with up to 5 g/s of fuel flow.

Combustion gas recirculation by means of ejectors (CGR) will be
used. Should, at a later stage, conventional exhaust gas recir-
culation be desirable to test, it will be possible to use the
same air preheater matrix.

External heat system

efficiency η_B

0.88 at full power

0.88 at "AOP" ($P_{\text{mean}} = 5 \text{ MPa}$, $n = 2000 \text{ rpm}$)

Max. allowable air leakage

5% of flow.

2.2.5.2.1 Combustor

a. Fuel atomization

Air assisted

b. Ignition

Spark plug integrated in fuel
nozzle.

c. Recirculation principle

Combustion gas recirculation
(CGR) by means of ejectors.

d. Fuel flow at max. power

4.5 g/s

e. Idle fuel flow

0.3 g/s

f. Combustion air flow at max. power

75 g/s

g. Min. combustion air flow (includ-

ing atomizing air flow)

6.5 g/s

h. Atomizing air flow to fuel nozzle

1.5 g/s

i. Atomizing air pressure

70 kPa

j. Air-fuel ratio and amount of combustion gas recirculation will be
varied over the load range.

2.2.5.2.2 Air preheater

a. Matrix geometry	Annular matrix, formed from stacked and joined stainless steel plates, stamped in involute shape to form headers and flow channels.
b. Flow pattern	Counter flow (in main part)
c. Number of plates	1200
d. Total plate area	5.78 m ²
e. Plate thickness	0.15 mm
f. Plate material	SS 142361

2.2.5.3 Hot engine system

2.2.5.3.1 Heater

a. Type	2 pass, cross flow heat exchanger. 4 quadrants, each formed by 1 cylinder head and 1 regenerator housing interconnected by heater tubes. First row: Involute bent plain tubes. Second row: Straight tubes with brazed on plate type fins.
b. Pitch radius:	First row: 85.8 mm Second row: 161 mm
c. Number of tubes	96 (4 x 24)
d. Tube dimension ID/OD	3/4.5
e. Tube length, effective	257.5 mm (one tube)
f. Material	Tubes: Multimet Cylinder head: Haynes 31 Regenerator housing: Haynes 31

2.2.5.3.2 Regenerator

- a. Type Cylinder shaped matrix, formed from stacked stainless steel gauze layers, inserted in thin ferrule.
- b. Number of regenerators 4

2.2.5.3.3 Gas cooler

- Type Tubular type, cross flow heat exchange
- Number of coolers 4

Material Tubes SS 142337
Housing and endplates SS 142343

2.2.5.4 Cold engine system

2.2.5.4.1 Cylinder block

- a. Design Aluminum water jacket, with exchangeable wet cylinder liners, and 4 separate, bolted on connecting duct plates.
- b. Water jacket Aluminum alloy casting
Material: DIN 1725 G-AlSi10Mg wa
- c. Water flow pattern 2 parallel passages, each containing two gas coolers in series.
- d. Duct plate Nodular cast iron, SS 140737

2.2.5.4.2 Piston and piston rod

a. Piston dome

Machined from bar and welded to dome base.

Material: Nimonic 80 A

b. Piston

Machined from steel bar, attached to piston rod by means of tapered friction joint and securing nut. Two piston rings are located in grooves in piston.

c. Piston rod

Designed with integral crosshead sliders. Machined from nitriding steel, SS 142940. Diameter 15 mm.

2.2.5.4.3 Piston rod seal

Pumping "Leningrader" type and "Kapseal".

Seal housing connected to minimum pressure line.

2.2.5.5 Engine drive system

Connecting rods from the four crossheads drive two parallel crankshafts, which are coupled together with one main shaft, the rear end of which will be connected to the vehicle transmission.

2.2.5.5.1 Crankcase

a. Type

Bedplate design, with main bearing caps integrated into common structure.

b. Material

Sand cast aluminum alloy DIN 1725 G-AlSi10Mg wa.

2.2.5.5.2 Crankshaft and main shaft arrangement

a. Crankshafts

Machined from steel bar. Grade B.S. En 40B. Design scantlings sufficient for S. G. iron casting

b. Crankshaft bearings	3 main bearings on each shaft. Standard split type bearing shells and separate thrust washers.
c. Shaft synchronization	Crank case designed to accept 3 alternative synchronizing mechanisms. Alt. 1 All gear. Alt. 2 Links and gears Alt. 3 Chains and gears
d. Balancing	Crankshafts and main shaft equipped with counter weights. Crankshafts rotate in opposite direction to main shaft. 1st and 2nd order unbalance from main piston and crank mechanism, and 1st order unbalance from hydrogen compressor eliminated.
2.2.5.5.3 Connecting rods	
a. Design	Formed as fork in small end
b. Material	S. G. iron casting Grade 37/2
c. Length	95 mm between bearing centers
2.2.5.5.4 Lubricating system	
Oil pump	Internal gear type. Driven off front end of one crankshaft.
Pumps capacity	60 l/min at 4000 rpm
Pressure control valve setting	400 kPa
Oil filter	Cartridge type full flow filter
Oil cooler	Provisions for fitting included
2.2.5.5.5 Auxiliary drives	
a. Front end of main shaft	Driving burner blower, atomizing air compressor, power control servo pump, radiator fan, alternator, and hydraulic pump for power steering and brakes, A/C compressor.

- b. Front end of right hand crankshaft
- c. Front end of left hand crankshaft
- d. Gear train in intercase between crankcase and transmission
- e. Principal power take off

Driving lubrication oil pump

Driving hydrogen compressor

Driving water pump

Designed to fit to Chrysler Transmission Case 3743336 and Torque Converter 4058171-P

2.2.5.6 Auxiliaries

2.2.5.6.1 Cooling water pump

- a. Design
- b. Material
- c. Drive arrangement

Centrifugal type

Impeller: Stainless steel

Housing: Aluminum alloy

Gear: Pump speed 3664 rpm at engine speed 4000 rpm

2.2.5.6.2 Combustion air blower

- a. Design
- b. Material
- c. Drive arrangement

Centrifugal type

Impeller: Aluminum alloy

Housing: Aluminum alloy

Primary drive: Variable speed belt drive
Secondary drive: High speed flat belt drive

Max. blower speed 25000-30000 rpm

During the starting up sequence, the blower is electrically driven (same motor as atomizing air compressor)

- d. Max. flow

78 g/s of air (corresponds to 4.5 g/s of fuel with 5% margin for leakage).

c. Total pressure rise at max. flow	12 kPa
f. Max. power requirement	1.5 kW
2.2.5.6.3 Atomizing air compressor	
a. Design	Dry running, vane type
b. Drive arrangement	Primary drive: Variable speed belt drive (same as burner blower) Secondary drive: Toothed belt Max. speed: 3 000 rpm During the starting up sequence, the compressor is electrically driven (same motor as combustion air blower) 1.5 g/s of air from engine idle speed to full speed. Excess air is fed back to suction line through pressure control valve.
c. Max. flow	
d. Pressure control valve setting	70 kPa
e. Max. power requirement	0.8 kW
2.2.5.6.4 Fuel pump	
a. Design	Metering pump, speed controlled
b. Drive arrangement	Electrically driven, governed by electronic control system.

2.2.5.6.5	Air flow meter Design	Air mass flow meter K-Jetronic
2.2.5.6.6	Air throttle actuator Electric motor with position feed back potentiometer	
2.2.5.6.7	Power control Design	One stage, double acting piston compressor. Water cooled.
	Bore	22 mm
	Stroke	20 mm
	Drive arrangement	Driven by crank at front end of left hand crankshaft. Short- circuited when not pumping.
	Max power consumption when short-circuited	700 W
2.2.5.6.8	Power control valve actuator Design	Hydraulic cylinder, governed by Moog 1-stage servo valve with mechanical feed-back. Integrated from single unit.
	Stroke	20 mm
	Max force	970 N at 5 MPa pressure
	Velocity	50 mm/sec

2.2.5.6.9 Oil pump for power control valve actuator

Design	Gear pump
Drive arrangement	Driven off free shaft end of atomizing air compressor.
Max flow	3 l/min
Pressure control valve setting	3 MPa
Max power requirement	0.3 kW

2.2.5.6.10 Alternator

Voltage	14 V
Amp. rating	55 A
Drive arrangement	Belt driven off front and of main shaft.
Max speed	TBD
Max power requirement	2 kW

2.2.5.6.11 Starter motor

Design	Geared type
Voltage	12 V
Power output	2 kW
Drive arrangement	Bolted to Chrysler transmission case, driving ring gear on torque converter. Geared to deliver max power at 200 engine rpm.

2.2.5.6.12 Electric motor for heating up sequence

Design	Series wound DC-motor
Voltage	12 V
Power output	780 W
Drive arrangement	Drives combustion air blower, atomizing air compressor, and oil pump for power control servo via overrunning clutch and toothed belt.

2.2.5.6.13	Electronic control unit	
	Type	Microprocessor based (TI 9 900 family)
	Functions	<ul style="list-style-type: none"> - Starting and stopping functions - Air-fuel control for constant heater tube temperature and correct air-fuel ratio - Power control valve positioning, governed by accelerator pedal position together with pressure and speed signal feed-back - Engine monitoring and safe-guarding
2.2.5.6.14	Radiator fan	
	Design	Axial flow
	Drive arrangement	Belt driven from front end of main shaft. Slipping clutch arrangement.
2.2.5.7	Accessories	
2.2.5.7.1	Hydraulic pump for power steering and brakes	
	Design	Vane type, AMC part No. 3237195
	Max. power requirement	1.5 kW
	Drive arrangement	Belt driven from radiator fan shaft
2.2.5.7.2	A/C Compressor	
	Design	Sankyo SD 507
	Max. power requirement	4 kW
	Drive arrangement	Belt driven from radiator fan shaft

2.2.5.8 Specification of diesel fuel used by USS

(Diesel fuel)

Density, 15° C	0.825	g/ml
Flashpoint (Pensky-Martens)	62	°C
Cloud point, summer	-13	°C
" " winter	-24	°C
Minimum filtering temp, summer	-15	°C
" " " winter	-27	°C
Minimum handling temp, summer	-18	°C
" " " winter	-30	°C
Viscosity 20°C	3.3	c St
Sulphur	0.4	% mass
Water and sediment	0.01	% volume
Ash	0.005	% mass
Coke number	0.05	% mass
Distillation 10% volume	200	°C
" 50% volume	240	°C
" 90% volume	290	°C
" Final boiling point	306	°C
Cetane number	55	

(Unleaded gasoline)

Density at 15° C	0.715-0.755	g/ml
Vapour pressure at 37.8° C	50-90	kPa
Distillation temp at 10% recovered	max 65	°C
at 50% recovered	max 110	°C
at 90% recovered	max 180	°C
End point	max 210	°C
Residue	max 2	% by volume
Existent gum	max 5	mg/100 ml
Water and particulate contaminants	No visible amount	
Sulphur content	max 0.05	% by weight
Research octane number	93	

Fuel values used in mileage calculations

	Heating value	Density
Diesel fuel	42.8 kJ/kg	739.3 kg/m ³
Gasoline	42.8 kJ/kg	849.5 kg/m ³

ESTIMATED MOD I COMPONENT/SYSTEM WEIGHTS IN KG

Crankcase and Bedplate Assembly	17
Crankshafts, Main Shaft and Bearings	21
Main Transmission Gears Assembly	5
Transmission Intercasing	2
Oil-pan, Pump and Filter Assembly	5
Connecting Rods	3
Piston/Dome and Rod/Crosshead Assembly	7
Crosshead Guides	8
Piston Rod Seal Assembly	4
(Cold Connecting) Duct Plate Assembly	14
Water Jacket with Cylinder Liners	14
Engine Block with Cylinder Liners	-
Regenerators and Gas Coolers	8
Heater Assembly with Retainment Parts	36
External Heat System with Burner	22
Water Pump Assembly with Drive	4
Variable Belt Drive Assembly	4
Combustion Air Blower with Motor	16
Air/Fuel System and its Auxiliaries	7
Gas Compressor, Control Blocks, Gas Bottle etc	30
Alternator and Starter	12
Electronics and its Cableage	3
Bolts, Tubes, Brackets, Pulleys, Belts etc	12
Radiator Fan with Clutch and Brackets	6
Mounting Devices (Rig or Vehicle)	6
<hr/>	
TOTAL DRY WEIGHT excl accessories	266 kg
Power Steering Pump	4.5 kg
A/C Compressor	6.6 kg

B.3 Basic Stirling Engine

FIGURE 10-10 STIRLING ENGINE

3. BASIC STIRLING ENGINE

3.1 General description

General iterations between analysis, design and assembly considerations have, once the performance objectives were determined, resulted in the main design data that are listed in a following table (Table 3:1).

Predicted engine performance is based on these data. Further input to the vehicle mileage predictions are discussed in other chapters (results in section 9:3).

Throughout the design, different ideas of how to arrange and assemble the engine have been investigated. Present design is considered to be a reliable synthesis of various requirements: good performance, realistic approaches/verified techniques, low weight and installation dimensions, easy maintenance and back-up options. Various separate tests and analysis have been performed to support this engine design effort. Critical components are easy to replace or change since they are separate and built together in subassemblies (for example cylinder-block and external heat system).

Major subassemblies are assembled in the following sequence (reference drawing No 17043):

- The engine drive system is equipped with piston rods/cross-heads and cross-head liners/seal housings. These have some horizontal clearance to the crankcase. The main bolting connection studs, attached in the crankcase, are passing through the thick flanges of the seal housings, also with generous clearances.
- Check-valves and tubings to the external gas system (not shown) are placed in position.
- Piston rod seal system elements and its top lid are mounted and centered. Piston and dome assemblies are attached to the rods.
- The cylinder block subassembly (water jacket, duct plates and wet piston liners) with inserted gas coolers is lowered onto the bottom parts. The regenerator stud-bolts are attached to the duct plates and the cylinder stud-bolts are now also passing through the assembly.

- This step simultaneously centers the piston and cross-head liners to good alignment since they are spigoted to each other. This means that the cylinder block subassembly, as also the one-piece cylinder block of Baseline Engine, determines the final positions of the cylinder center lines. Actual tolerances are allowed for in the engine drive system bearings.
- The regenerators and the loose flanges are positioned on the gas coolers and water jacket top face respectively. The heater quadrants are mounted individually. Their cylinder and regenerator housings are positioned by corresponding liners and coolers respectively, both spigoted in each duct plate. Small tolerances are compensated by heater tube flexibility. Clearances in the water jacket (water seals) allows for this.
- The split retainer rings are inserted and all nuts tightened prior to insulation of spaces between the pressure vessels.

As an alternative the heater may be assembled to the cylinder block before mounting to the drive system. Then the heater and block is kept together by the regenerator stud-bolts and nuts and then fastened to the drive system by the cylinder stud-bolts and nuts.

- Prior to insulation, the inlet air manifold structure of the external heat system is mounted on the water jacket. The preheater core with its exhaust gas manifold parts are mounted, the insulation completed, combustor and seals assembled, the top lid put on and the assembly closed by bolts threaded into the inlet air manifold flange.
- The BSE is finally equipped with power control devices and auxiliaries, connected to the test environment mounted on corresponding bed and, when required, disassembled in reversed order. It should be pointed out, that the procedure described is simplified by separating subsystems when possible. External gas system and power control is one example: they will be easily disconnected and remain mounted on the engine structure when heat exchangers and pistons/seal components are removed.

The strong interaction between BSE and power control/auxiliary design is obvious. In spite of this the following more detailed design description is focused on BSE systems.

- Main, characteristic dimensions and other design data are summarized in Table 3:1;
- Some salient design features of BSE, compared to Baseline Engine, are listed in Table 3:2;
- General component/subsystem descriptions are given below (including some development tests);
- Performance and stress analyses and material selection and rationale for the design are concentrated to separate sections, including also development tests;
- Reference is as well made to the updated engine specification, section 2.2.
- A dome clearance study is summarized in the end of this section (to exemplify design approaches to tolerance stack-up control).

Table 3:1

Main ASE Mod I dimensions and design data

Overall SES dimensions (mm)

(Note: Approximately, but close to final)

Total height (sump/preheater house)	802
Max width (front view projection)	700
Max length (excl radiator fan)	745
Height from output shaft	585

Overall BSE dimensions (mm)

Total height (sump/preheater house)	802
Max width, engine drive system	312
, ext heat system	700
Max length, engine drive system	447
, ext heat system (ø)	672

Drive mechanism, cylinders, cold parts (mm)

Cylinder distance (square side)	140
Crankshaft distance (chain standard)	138.9
Main bearing distance (per shaft)	148
Main bearing diameter	45
Big end crankpin diameter	42
Counterweight radius	69
Crank radius	17
Connecting rod length	95
Stroke	34
Bore	68
Piston rod diameter	15
Piston/dome height	171
Dome/cylinder gap height	110
" " " width (goal)	--
Piston rod seal system height	94

Heat exchangers (gas cycle)

Cooler tubes per unit	-
Inside tube diameter	-
Outside " "	-
Total length of one tube	-
Cooler housing length	93
Cooler diameter, top	81
" " , bottom	82
Regenerator length	52
" diameter	81
Reg matrix length	50
" " diameter	80
Wire diameter (gauze)	-
Filling factor (%), approx	-
Heater tubes per unit	24
Inside tube diameter	-
Outside tube diameter	-
Total length of one tube	282
Inner pitch circle radius	-
Outer " " "	-
Second row fins, width (mean)	10
" " finned length	-

External heat system (mm)

Combustion chamber height (h)	110
Combustor parts height (above h)	107
Preheater core, inner radius (approx)	234
" " , outer " "	268
Number of plates (2 x 600)	1 200
Plate height, tot	127
Plate width (pressed involute)	52
Insulation thickness	50
System height, tot	350
" diameter, max	670

Table 3:2

Some salient BSE design features as qualitatively
compared to Baseline Engine (P40)

External heat system:

- CGR combustor type (internal Comb Gas Recirculation)
- Lower combustion chamber (requires CGR)
- Lower preheater core position, better manifolds
- Good combustion gas flow pattern (low core)
- Removeable matrix (cleaning/replacement)
- The same corrugated part of matrix plates but elongated ends
- Thicker insulation, less convection/radiation loss
- Relatively low h.p. wide assembly

Heater head:

- Principally the same tube geometry (45° involute)
- Constant tube gaps (pitch) in each row
- Identical tubes (except for those with T/C)
- Two fin variants (spec tube and wide gap)
- Good inside gas flow to/from housings (wider ducts and more central inlets)
- Somewhat increased duct volumes (relative to swept volume)
- 8 instead of 12 housings (2 vs 3 variants)
- Simpler pressure vessel castings (axisymmetric flanges, less geometry-changing and porosity problems).
- Longer regenerator manifolds (possibly separate)
- Increased cylinder dome height (temp grad)
- Better gas seal (O-ring) cooling conditions
- Reduced stress levels in critical points
- Same brazing technique and procedure

Regenerator:

- 4 instead of 8 units (one per cycle)
- Scaled size, moderately reduced for part load operation
- Improved matrix cover (easier to manufacture)
- Better gas flow distribution to and through the matrix
- Otherwise conventional, established gauge type

Gas cooler:

- 4 instead of 8 units (one per cycle)
- Improved cooling water flow distribution
- Less and improved gas seals, minimal air pockets
- Better locked in place (sealed off water)
- Otherwise conventional (stainless steel) but lighter relative to size
- No separate flow-plates (integral with duct plate)

Cylinder block:

- Split in water jacket, (duct plates and wet liners)
- Light aluminium casting water jacket
- Two parallel, almost identical water passages
- Equal flow distribution/cooling of gas coolers and liners
- Eliminated de-airation problems (no air pockets)
- Less machining and volume (4 instead of 8 reg)
- Separate cylinder liners, easy to replace (wear)
- Separate duct plates (one per cycle)
(liners and duct plates can be integrated)
- Less casting surface area exposed to working gas
- All major gas O-ring to adjacent parts radially mounted
- Separate, improved check valve and tubing arrangement
(easier serviced)
- Liners kept in place by cycle pressure (integration of duct plate/liners eliminates O-rings)
- All other pieces clamped by reg/cyl studs/nuts
- Symmetrical gas load distribution (stresses)
- Less deflections and maintained liner roundness/alignment
- Two extra height tolerances to be counted for in main connection
- Overall compactness and low weight

Piston/piston rod and seal systems:

- Principally the same sliding seal system, but successively refined
- PL seal rings introduced, no membrane valve
- Seal system more tapered into piston bottom
- Minor cap-seal and supply bushing modifications

Integral piston rod/cross head (alignment and conn. rod length).

Modified piston to rod attachment.

All piston and guiding rings in bottom part, same check-valve function.

Higher dome, favourable to piston rings (friction and wear).

Redesigned dome bottom to piston assembly.

All together rather short assembly, relatively low reciprocating mass.

Provision for tests with p-connections via cylinder liners (if dome height allows it).

Seal housing flanges (two variants) contain parts of several functions, e.g. max. and min. pressure valves, gas supply, piston rod cooling, crankcase ventilation.

Engine drive system:

Aluminum structure (crankcase and bedplate).

Integral front cover with H₂-compressor mounted.

Integral rear end intercase and water pump housing and drive.

Starter mounted on gear-box cover.

Compact lubrication oil system, pump mounted in front of crankshaft.

Rearranged balance weights to allow for a central link or chain synchronization (alternatives).

Overall compactness and considerably lower weight.

Design prepared for pressure die-casting.

Differences in design philosophy and overall arrangement are extensive as briefly exemplified by the BSE cross section and assembly sequence presented above.

Approaches to Tolerance Stack-up Control

Any engine design involves tolerance considerations in various areas. For a Stirling engine, all dimensions affecting the dome-to-cylinder clearance are critical, since a small gap is functionally important. The selection of proper tolerances must be checked throughout the designs.

Since MOD I, for reasons of development flexibility, is built up from several structural parts and since it utilizes some new design principles and materials, its tolerances and clearances must be very accurately controlled. This involves design analysis, hardware follow-up and drawing revision in an iterative process.

For example, an initial study on dome clearances, as summarized below, has identified critical tolerances to be requested on detail drawings. These are discussed with the vendors. Some tolerances may be tightened with a suitable sequence of tooling operations. Early experiences may also suggest final tooling of sub-assemblies. Once realistic tolerances are verified (often much better than guaranteed by the supplier), their interaction and their total impact on dome clearance must be evaluated. Findings from separate component inspections and assembly checks will be fed back into the analysis, resulting in a semi-empirical value of the nominal dome gap.

If the involved concentricity, parallelity and angularity tolerances were on their extreme limit and, at the same time, assembled in the most unfavourable way, the 0.4 mm dome gap aimed at, would be insufficient.

Designing for such a (theoretical) worst case and also taking lateral crosshead movement, thermal growth, etc. into account would call for an unacceptably wide dome gap. Available experiences instead support the described semi-empirical approach. The result of such an iterative process is, of course, a revised set of

drawings and defined manufacturing and assembly procedures that ensure proper engine operation.

Other tolerance stack-up areas, although less intricate, are treated similarly.

**ORIGINAL PAGE IS
OF POOR QUALITY**

ASE MOD I, SOME REPRESENTATIVE CRITICAL TOLERANCE STACK-UPS

- DOME TO CYLINDER HEAD CLEARANCE
 - MACHINING TOLERANCES
 - THERMAL EXPANSION (COLD START TO OPERATING)
[THE ACCOMPANYING ILLUSTRATION EXEMPLIFIES
THE ANALYSIS (NOT YET COMPLETE)]
- PISTON TO SEAL SYSTEM CLEARANCE
 - SIMILAR TO THE ABOVE (PLUS A RADIAL COMPONENT)
- DOME GAP TO CYLINDER HEAD WALL
 - MACHINING TOLERANCES
 - THERMAL EXPANSION
 - DYNAMIC BEHAVIOR
- PISTON AND CROSSHEAD ALIGNMENT IN LINERS (FOR SEALS)
 - MACHINING TOLERANCES/CLEARANCES
 - PILOTING AND ASSEMBLY METHOD
 - DYNAMIC DEFLECTIONS (SIDE FORCES)

ORIGINAL PAGE IS
OF POOR QUALITY

ASE MOD I, SOME REPRESENTATIVE CRITICAL TOLERANCE STACK-UPS - CONT'D

- HEIGHT AND PARALLELLITY OF STACKED PARTS IN MAIN BOLTING ARRANGEMENT
 - MACHINING TOLERANCES (SEPARATE PARTS PER QUADRANT)
- LOCATION OF CYLINDER AND REGENERATOR/COOLER CENTERS
 - MACHINING TOLERANCES (IN DUCT PLATE)
 - FLEXIBILITY IN HEATER TUBES
 - CLEARANCES IN WATER JACKET (WATER SEALS)
 - CLEARANCES IN CRANKCASE/BEARINGS (PIN LENGTHS)
- RADIAL CLEARANCES BETWEEN O-RING GAS-SEALED PARTS
 - ESTABLISHED EXPERIENCE (TOLERANCES)
 - TYPE OF MOUNTING (RADIAL WITH SUPPORT RINGS)
- PLAIN BEARING AND THRUST WASHER CLEARANCES AND GEAR TEETH CLEARANCE
 - MACHINING TOLERANCES AND POLAR MOVEMENT OF SHAFTS
 - OIL FILM ANALYSIS REQUIREMENTS
 - THERMAL EXPANSION (AXIAL MAIN BEARING FLOAT)
(SHAFT CENTER DISTANCE VARIATION)

Check of the Machining Tolerances Influence of the Radial Clearance between Dome and Cylinder "S".

(See figures on the following pages)

S is of great influence on a number of functions: thermal stress in the cylinder-walls, the temperature on piston rings, permitted start up time, temperature on the seals between hot and cold parts, heat loss to the cooling water, are some of the most important.

A nominal clearance of 0.4 mm in cold condition is chosen as a starting value for MOD I, based on experiences from earlier engines.

The clearances have to allow for some run-out and misalignment due to unavoidable deviation in machining size on static and reciprocating parts.

Tolerances of influence are shown in fig 1 and fig 2. If limit values are added to the most unfavourable case, it is obvious that a clearance close to zero can be reached. The statistic probability of this case is, however, very low, and by choice of the most suitable machining procedure on the different parts an almost perfect centricity and parallelity can be reached on most surfaces.

If the cylinder top is kept in a run-out of max 0.2 mm relative to the bores A and B, and the dome top in a max run-out of 0.1 mm relative to the piston foot and the crosshead, one can be rather confident. This case gives a max clearance of 0.55 on one side and 0.25 mm on the opposite side of the piston.

Theoretically, this alone allows for a 460° C higher temperature on the dome top, compared with the cylinder wall under starting up.

This temperature, however, must be reduced since there is a lateral movement on the piston top, caused by the side forces on the crosshead, see fig 3. This movement is largest under the first shaft revolutions, before the lube-oil film is built up and then reduced

to a lower value that depends on oil viscosity, side forces, deformation and difference in thermal expansion on crosshead and guide.

Another factor that may reduce clearances is any unsymmetrical temperature-distribution around the circumference of dome and cylinder top.

The true answer to all these questions has to be based on running experiences.

ORIGINAL PAGE 18
OF POOR QUALITY

CRITICAL TOLERANCE STACK-UP

List of Figures

<u>Page</u>	<u>Figure</u>	<u>Showing:</u>
B-17	1	Critical tolerances, static parts
B-18	2	Critical tolerances, moving parts
B-19	3	Expected stack-up, design goal*
B-20	4	<u>Max.</u> dome gap reduction, static parts
B-21	5	<u>Max.</u> dome gap reduction, piston liner
B-22	6	<u>Max.</u> dome gap reduction, moving parts
B-23	7	<u>Max.</u> dome gap reduction, total (cold)
B-24	8	Tolerance effects on dome gap, including temperature considerations
B-25	9	Dome-top/cylinder head clearance, including temperature considerations

* Minimal dome gap (nominal 0.4 mm) with interchangeable (spare) parts

Functioning engine with max. (or min.) stack-up of tolerances and other relevant parameters

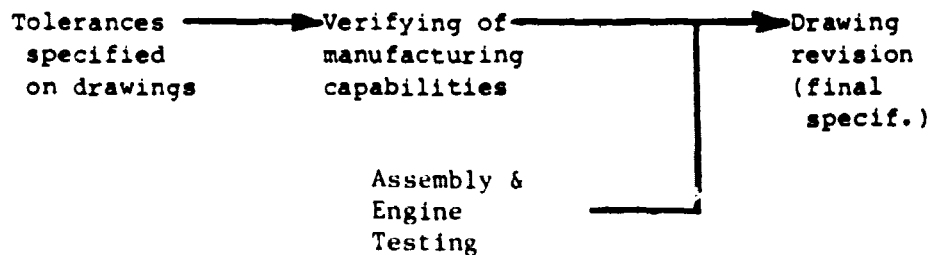


Figure 1

ORIGINAL PAGE IS
OF POOR QUALITY

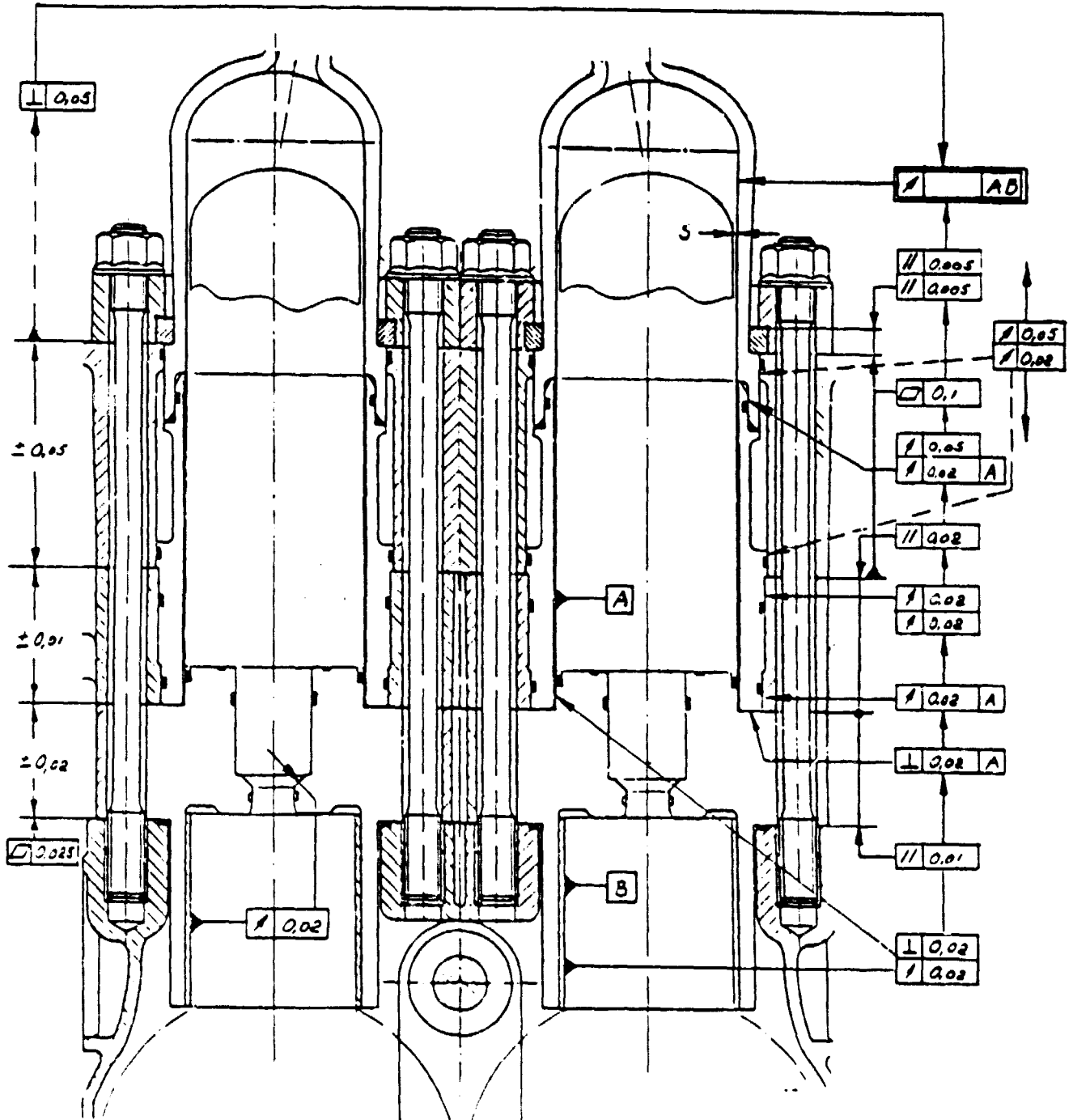
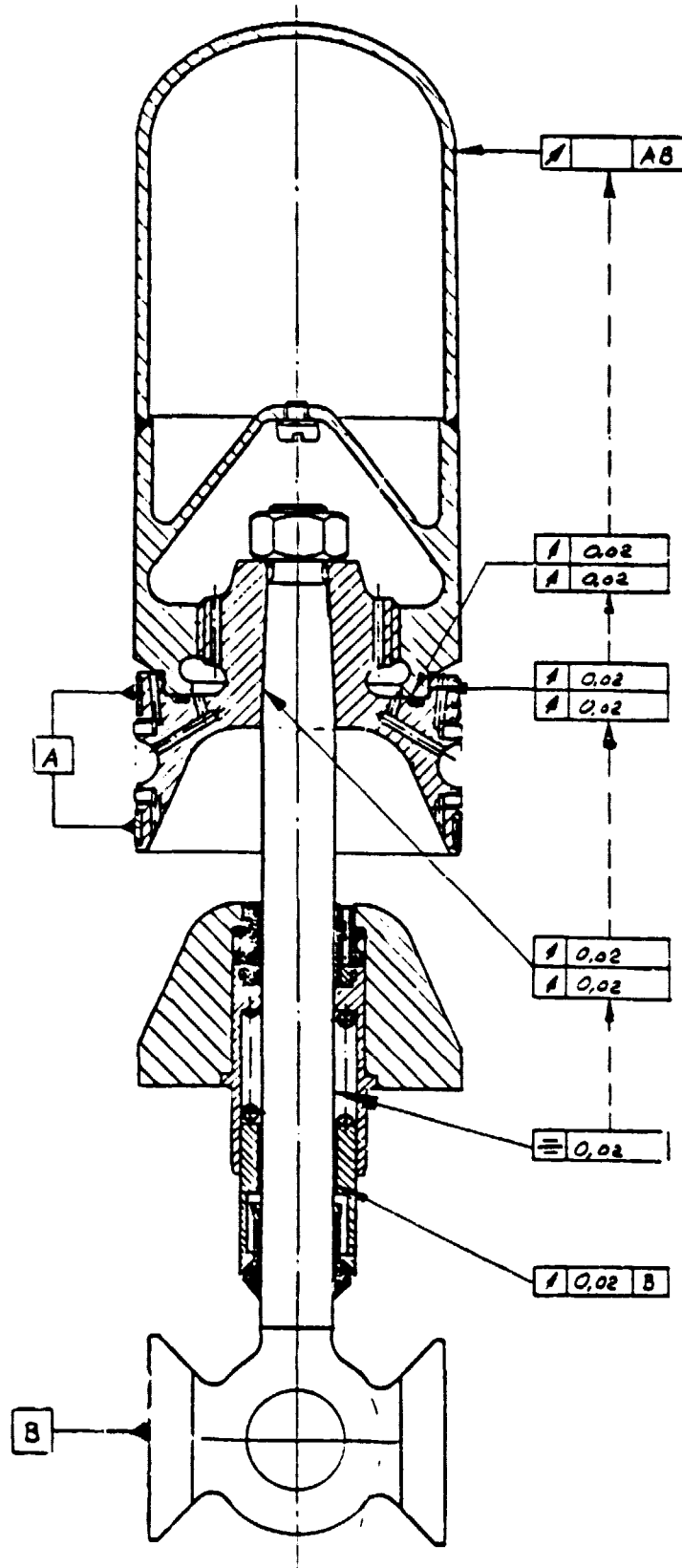
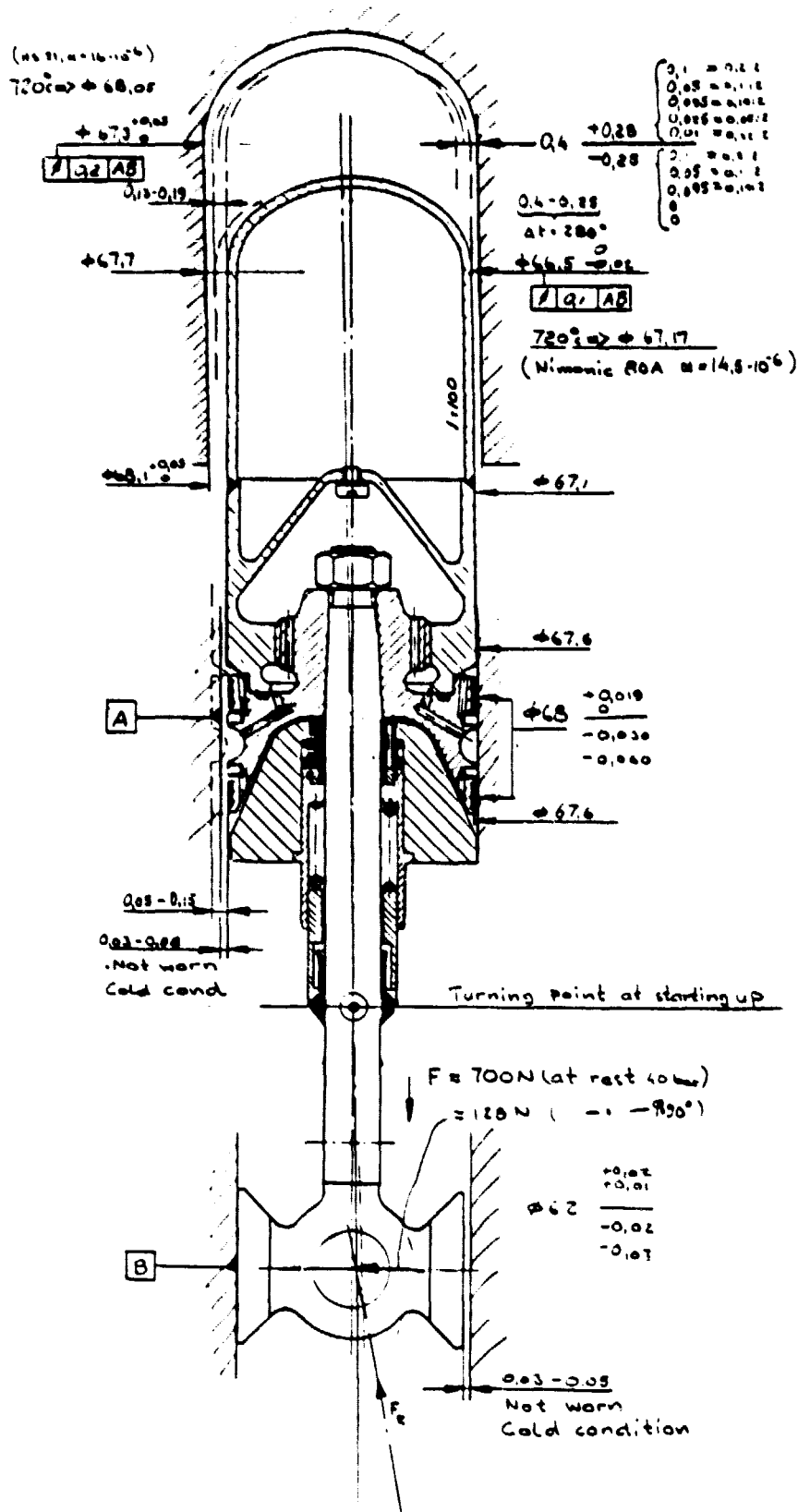


Figure 2

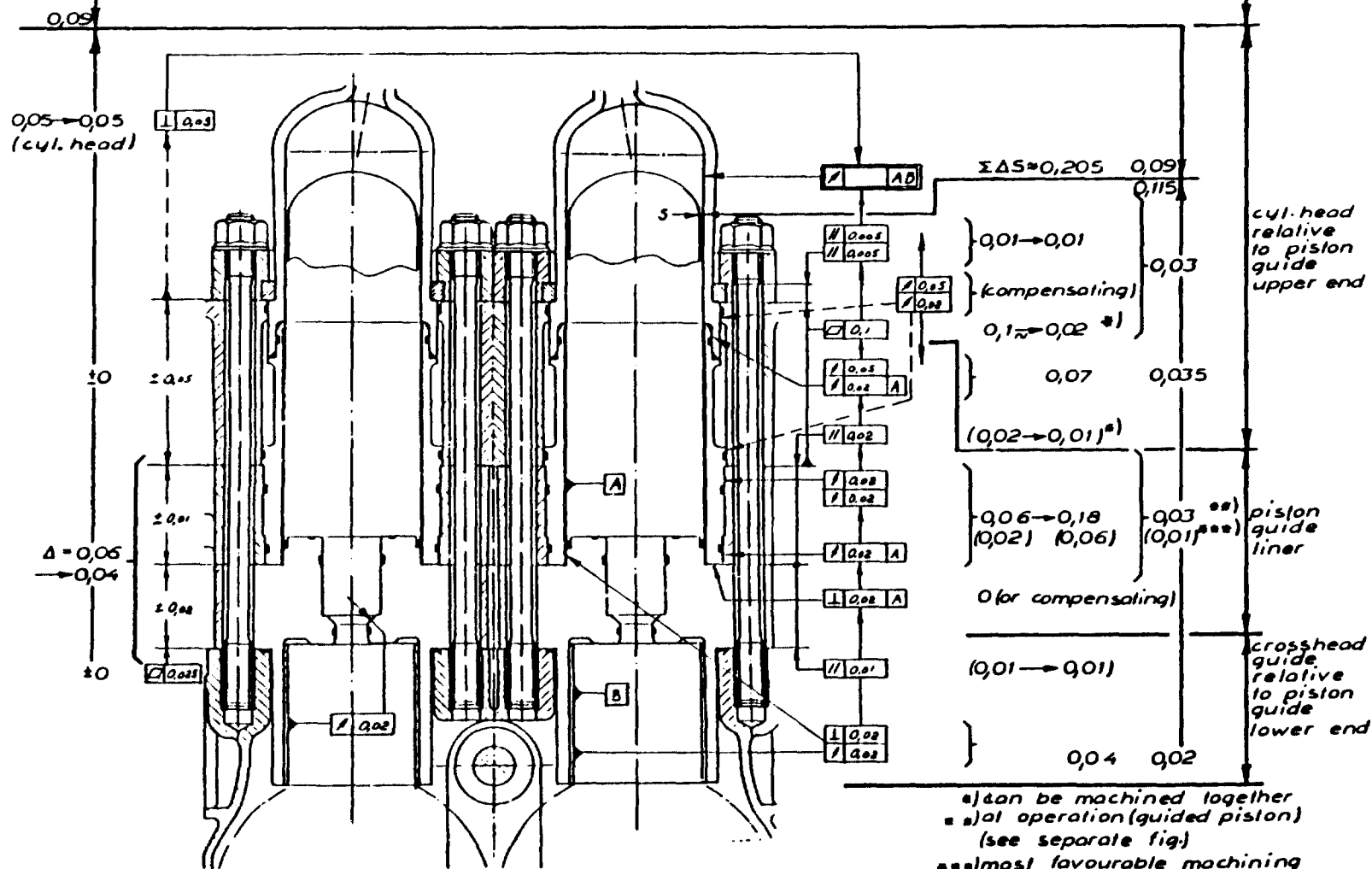


ORIGINAL PAGE IS
OF POOR QUALITY

Figure 3



Max. estimated dome gap
effect from machining
tolerances of stable parts --



ORIGINAL PAGE IS
OF POOR QUALITY

- a) can be machined together
- b) 1st operation (guided piston)
(see separate fig)
- c) most favourable machining sequence

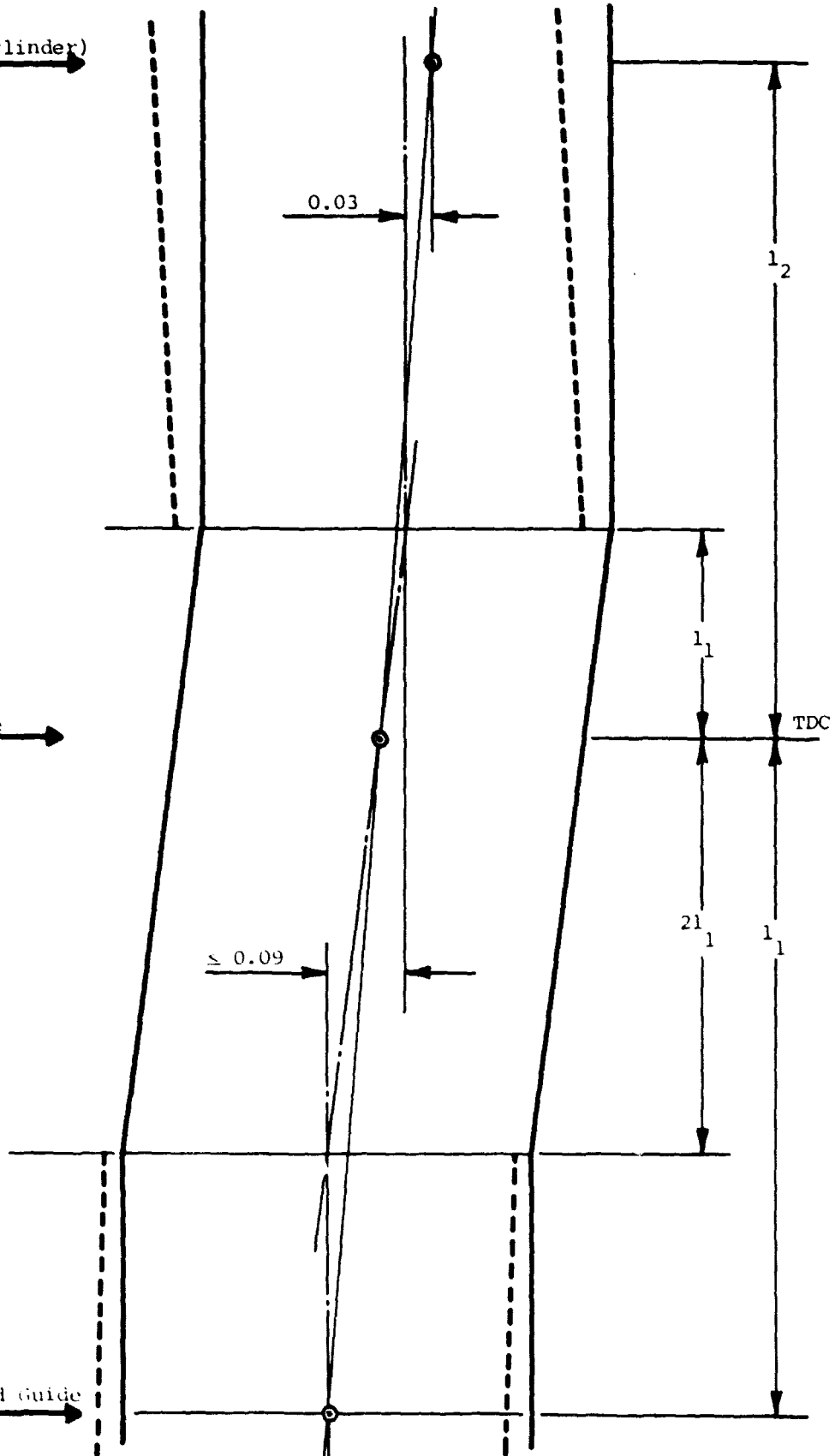
ORIGINAL FACE IS
OF POOR QUALITY

Figure 5

Dome Top (Cylinder) →

Piston Guide →

Crosshead Guide →

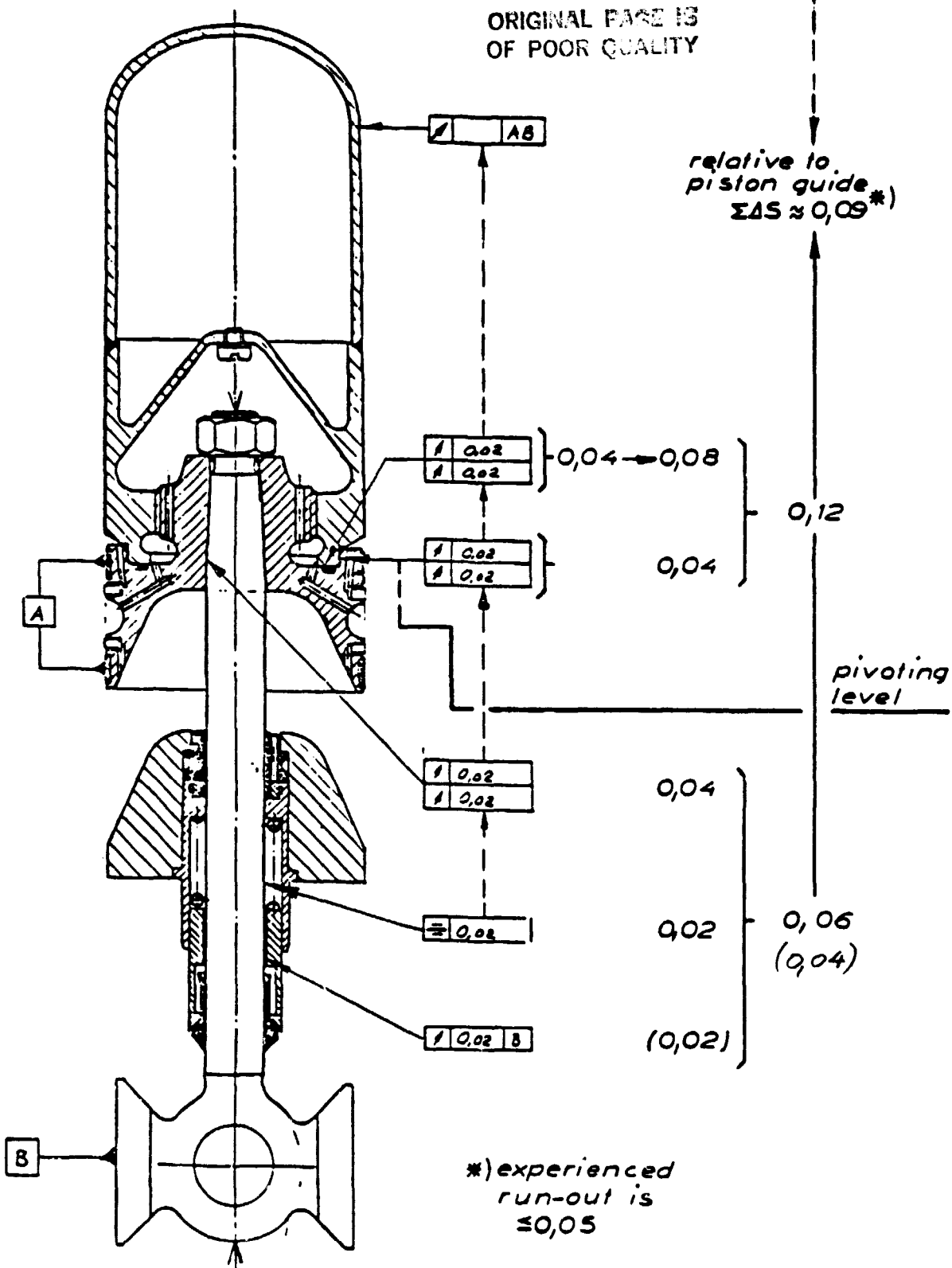


Max. estimated dome gap
effect from machining
tolerances of moving parts

Figure 6

Figure 6

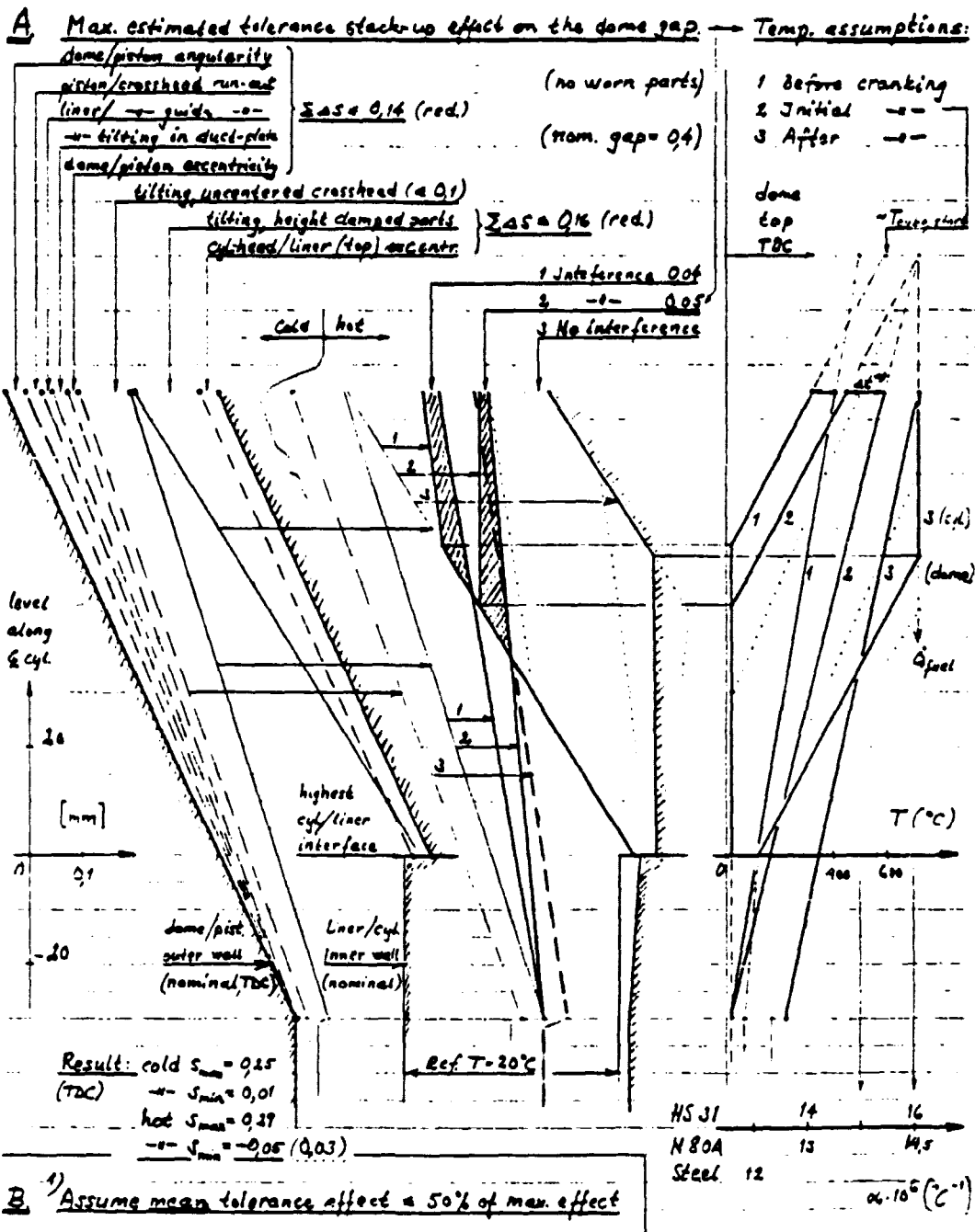
ORIGINAL FACE IS
OF POOR QUALITY



ORIGINAL PAGE IS
OF POOR QUALITY



Figure 8



B 1) Assume mean tolerance affect a 50% of max. effect

→ Max. $\Sigma \Delta S = 0.14 + 0.16 = 0.3 \rightarrow 0.15$ which allows piston guiding ring wear $\Delta \phi \approx 0.1$ for $S_{min} > 0$ if

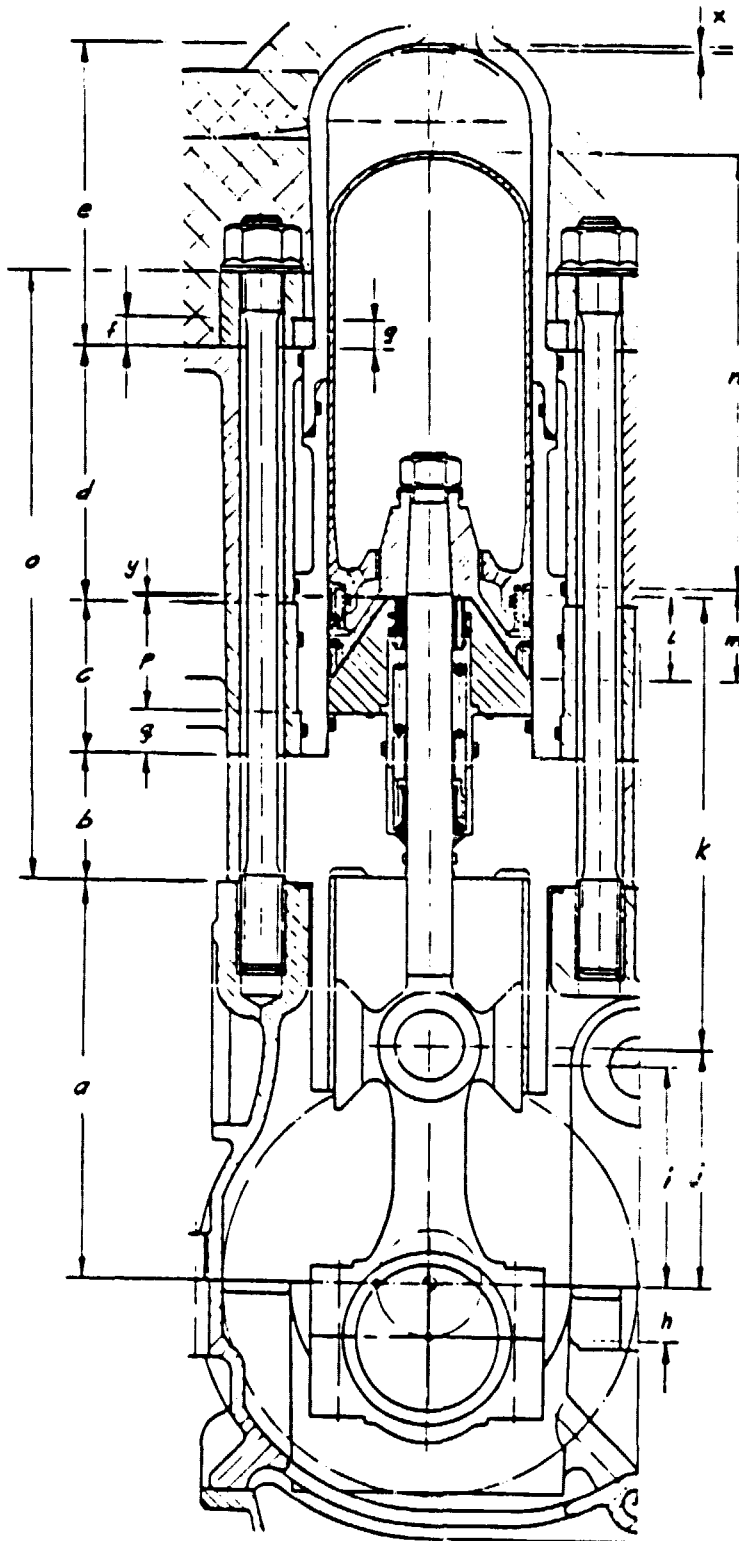
$$T_{max} - T_{avg} = 150^{\circ}\text{C}$$

2) Or increase nom. dome gap with 0.15 which gives $S_{max} = 0.3 \rightarrow 0.45$ (hot before wear)

C Alt. 1) is recommended in comb with hard ware follow-up and engine tests.

ASE Mod I Dome Gaps
(the dome in its TDC position)

8004 10/ASP



	tol.	δ/t	$\delta/-20^{\circ}\text{C}$	α
a	$\pm 0,05$	$0,22/_{-0,10}^{+0,10}$	0,12	$24 \cdot 10^{-6}$
b	$\pm 0,02$	$0,07/_{-0,05}^{+0,05}$	0,04	$24 \cdot 10^{-6}$
c	$\pm 0,01$	$0,01/_{-0,01}^{+0,01}$	0,02	$11 \cdot 10^{-6}$
d	$\pm 0,05$	$0,1/_{-0,05}^{+0,05}$	0,08	$24 \cdot 10^{-6}$
e	$\pm 0,1$	$0,53/_{-0,45}^{+0,45}$	0,06	$13 \cdot 10^{-6}$
f	$\pm 0,1$	—	—	—
g	$\pm 0,05$	—	—	—
h	$\pm 0,025$	$0,03/_{-0,02}^{+0,02}$	0,007	$11 \cdot 10^{-6}$
i	$\pm 0,03$	$0,12/_{-0,07}^{+0,07}$	0,07	$24 \cdot 10^{-6}$
j	$\pm 0,03$	$0,07/_{-0,04}^{+0,04}$	0,04	$11 \cdot 10^{-6}$
k	$\pm 0,1$	$0,15/_{-0,08}^{+0,08}$	0,06	$11 \cdot 10^{-6}$
l	$\pm 0,05$	—	—	—
m	$\pm 0,05$	—	—	—
n	$\pm 0,05$	$0,17/_{-0,15}^{+0,15}$	0,07	$13 \cdot 10^{-6}$
o	—	$0,15/_{-0,07}^{+0,07}$	0,09	$11 \cdot 10^{-6}$
p	$\pm 0,1$	$0,02/_{-0,01}^{+0,01}$	0,01	$24 \cdot 10^{-6}$
q	$\pm 0,1$	$0,04/_{-0,02}^{+0,02}$	0,04	$24 \cdot 10^{-6}$
x	nominal = 1			
y	nominal = 0,5			

Tol. space dome - cyl top:

Added tol. space solid parts:

$$a+b+c+d+e+g+e = \pm 0,38/-0,18$$

Added tol. space moving parts:

$$h+i+j+k+l+m+n = \pm 0,31$$

Min. clearance regarding cold start at -20°C : 0,4 mm

Min. clearance at working temp:

$$1,0 - 0,31 - 0,31 - 0,18 - 0,18 - 0,18 - 0,18 - 0,18 = 0,5$$

Max. clearance with max.

$$\text{tolerances} = 1,0 + 0,38 + 0,31 = 1,7$$

Tolerances and Temp. Exp. - Mod I

Gas Tightness Control (emphasized approaches*)

1. Component qualification:

- a) Seal housing
- b) External gas system
- c) Duct plate/(cylinder liner)
- d) (Piston dome)
- e) Gas cooler
- f) Heater section

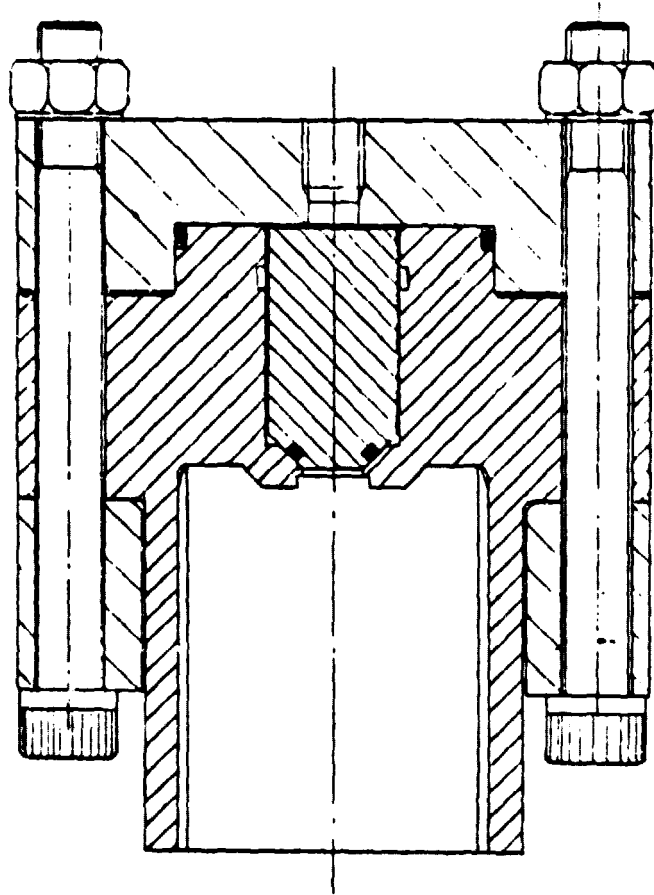
2. Subassembly checks:

- a) Seal housing/ext. gas system
(duct plate/cylinder liner)
- b) Cylinder block/gas cooler
- c) Cylinder block/heater head
- d) Cylinder block/lower parts (alt. ass'y)
(Seal system/piston rod - crankcase vent.)
 - Ext. gas system - mating faces
 - Cyl. liner, bottom part - mating faces or locking screw
 - Cyl. liner, above ccd - mating faces or special groove
 - Gas cooler, above ccd - mating faces or special groove
 - Cyl. liner, upper part - coolant circuit
 - Gas cooler, upper part - coolant circuit
 - Power control comp. - mating faces

*Initial hardware experiences will indicate the real needs (steps may be added or omitted).

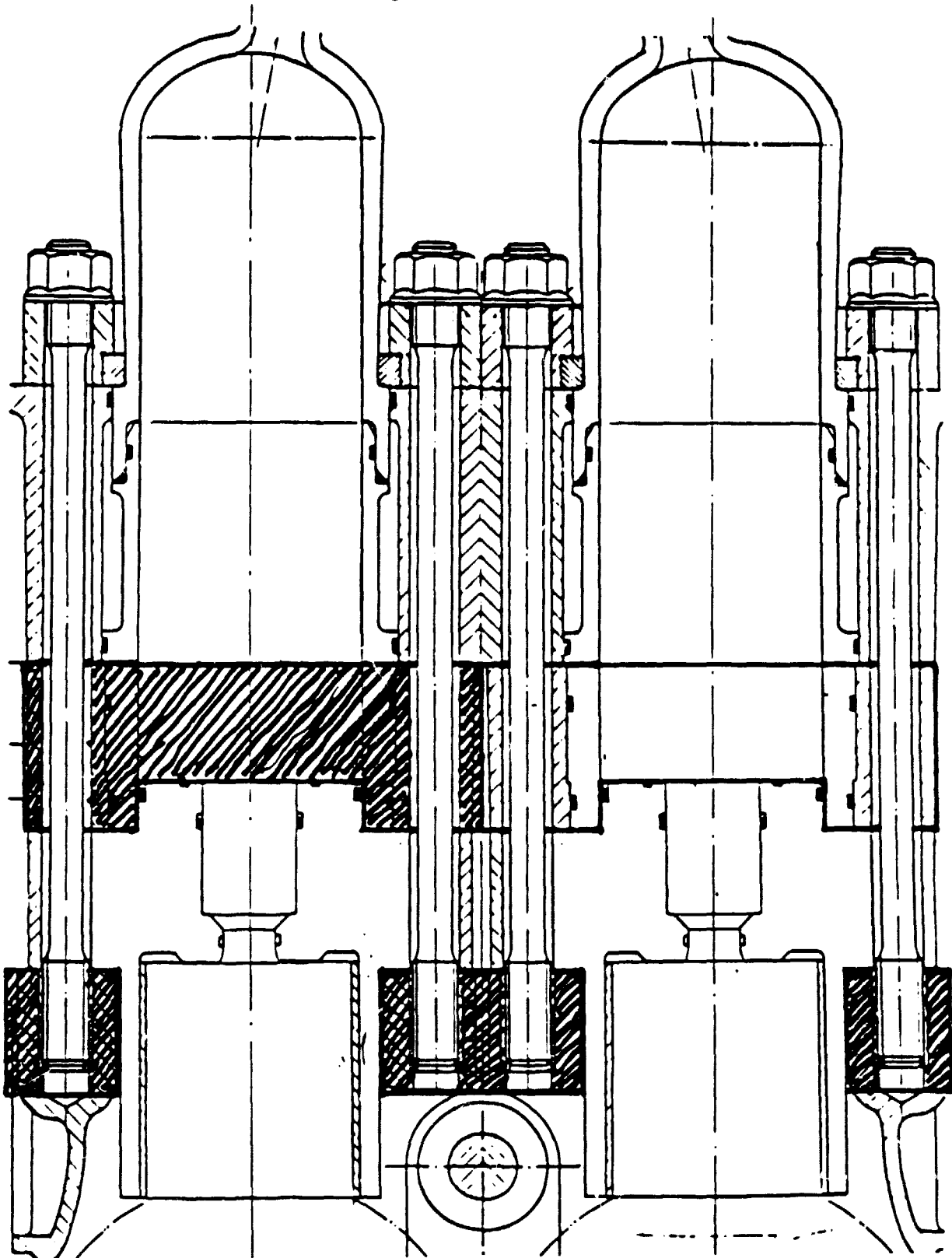
Figure 1a

ORIGINAL PAGE IS
OF POOR QUALITY



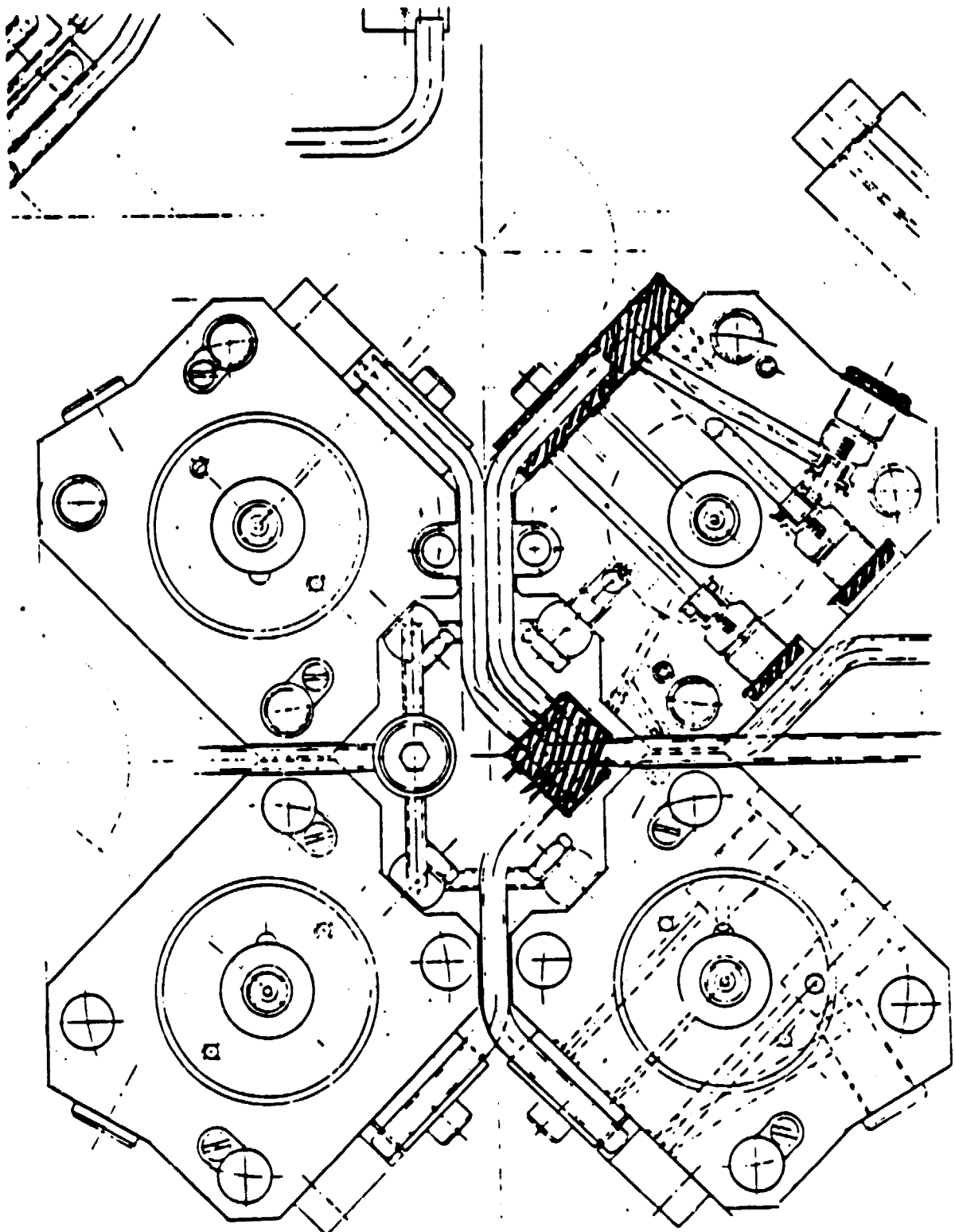
ORIGINAL PAGE IS
OF POOR QUALITY

Figure 1b (1)



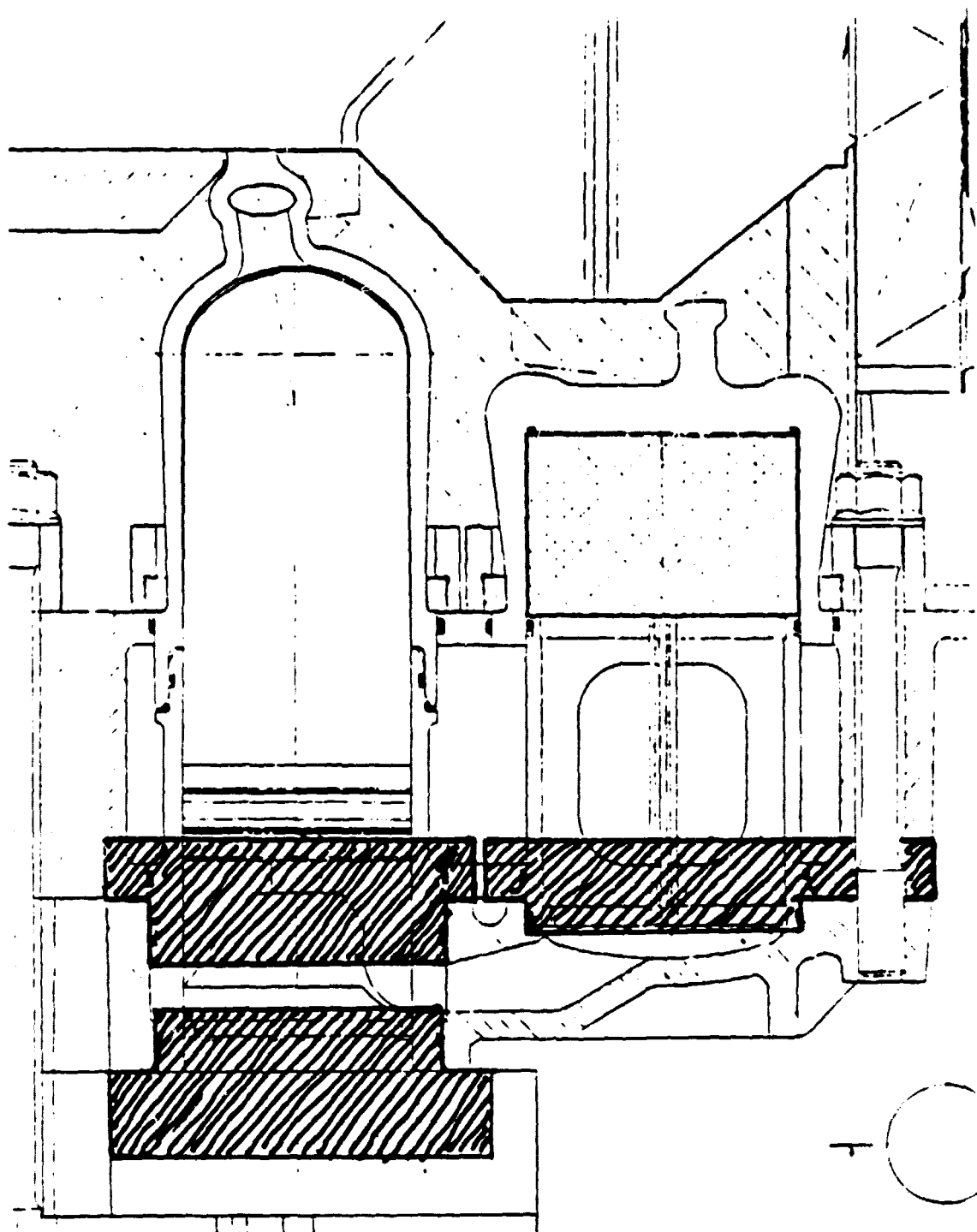
ORIGINAL PAGE IS
OF POOR QUALITY

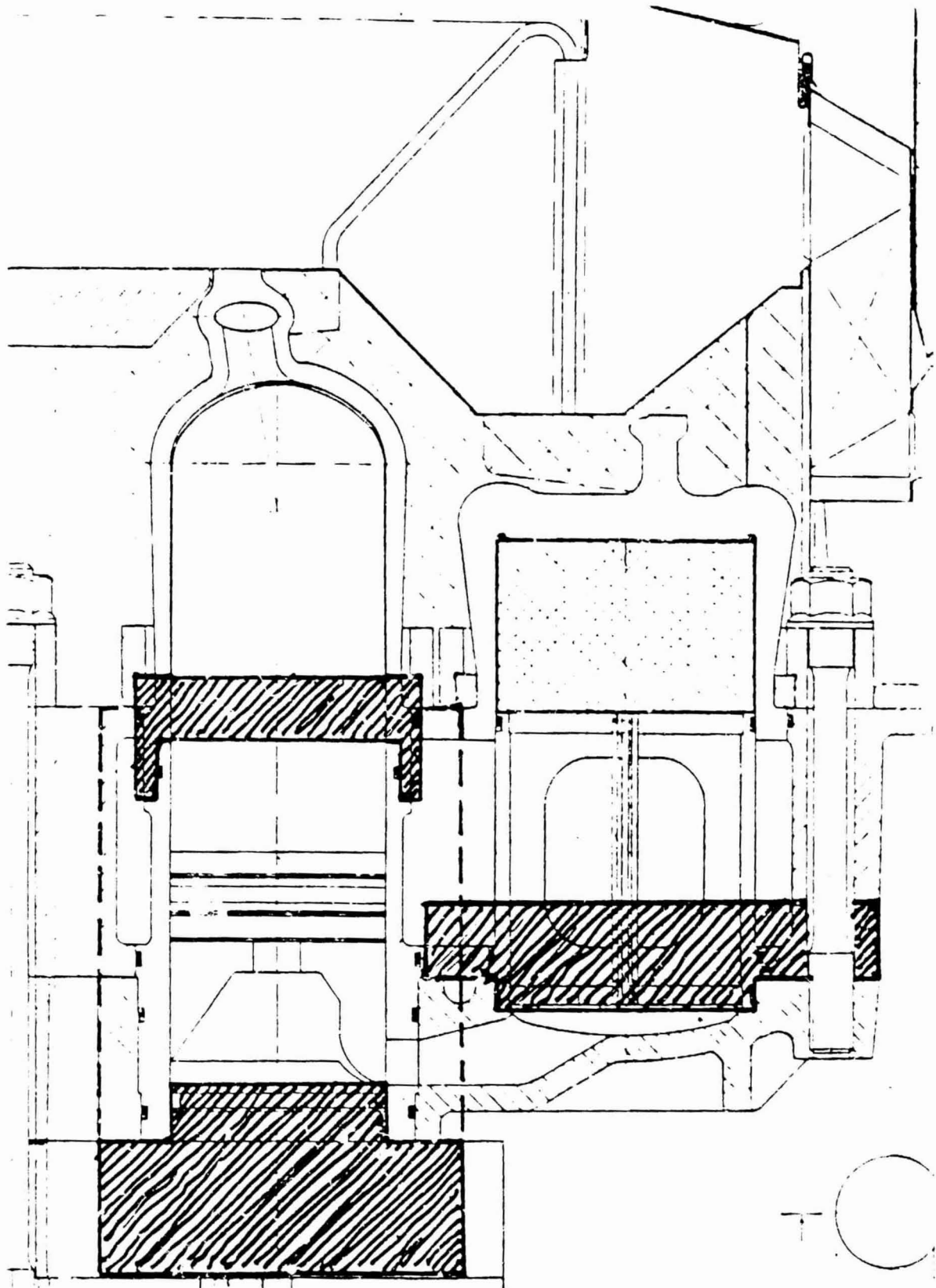
Figure 1b (2)



ORIGINAL PAGE IS
OF POOR QUALITY

Figure 1c (1)





ORIGINAL FILE IS
OF POOR QUALITY

Figure 1d

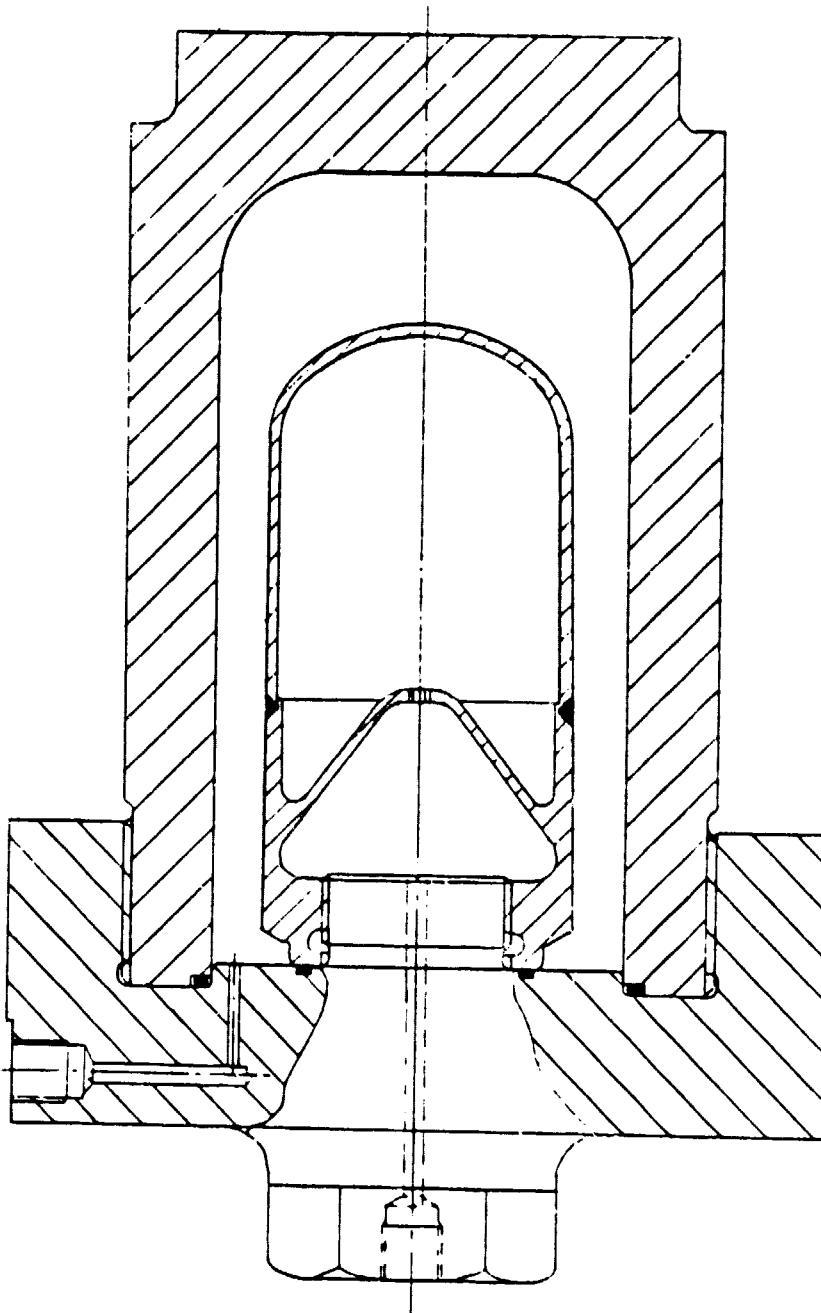


Figure 1e

ORIGINAL PAGE IS
OF POOR QUALITY

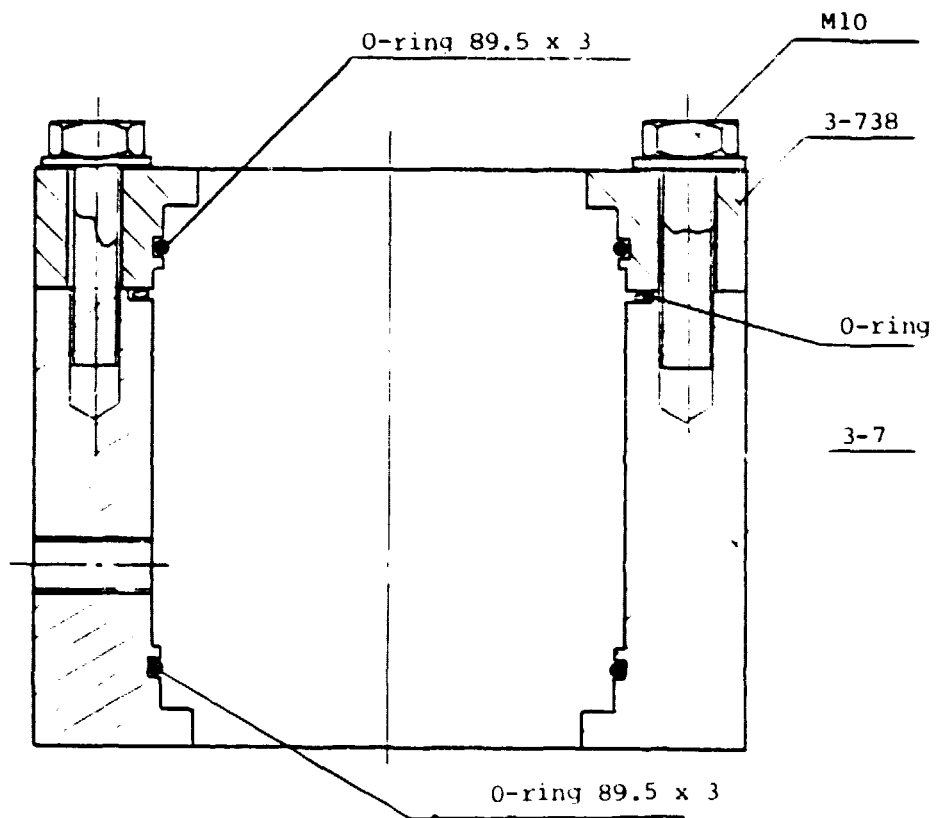
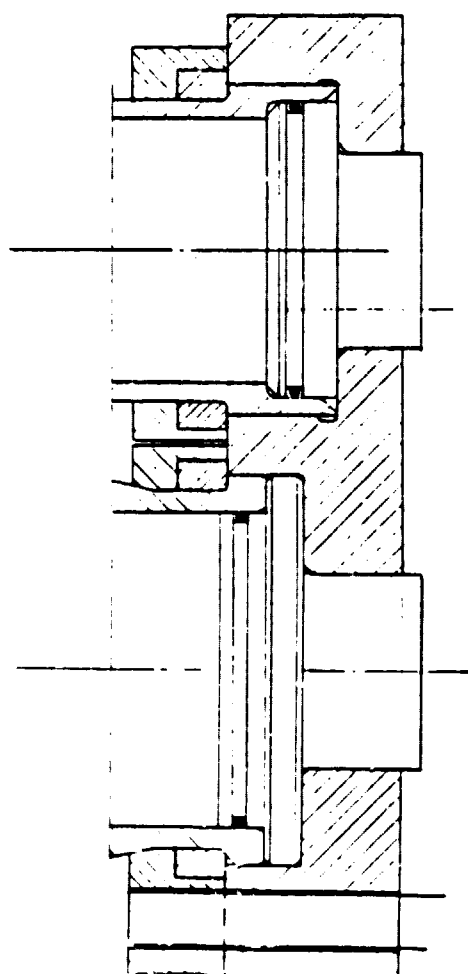
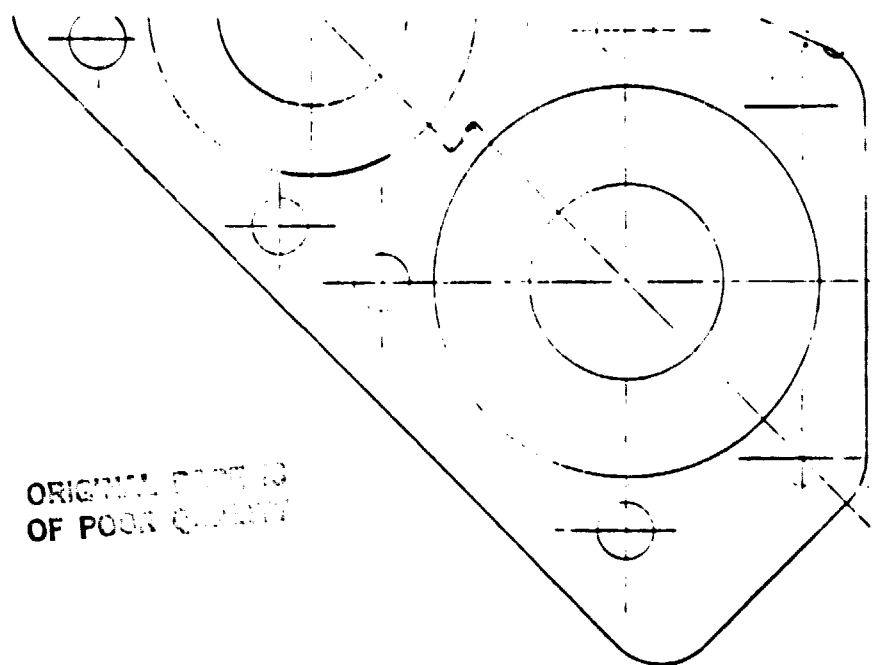
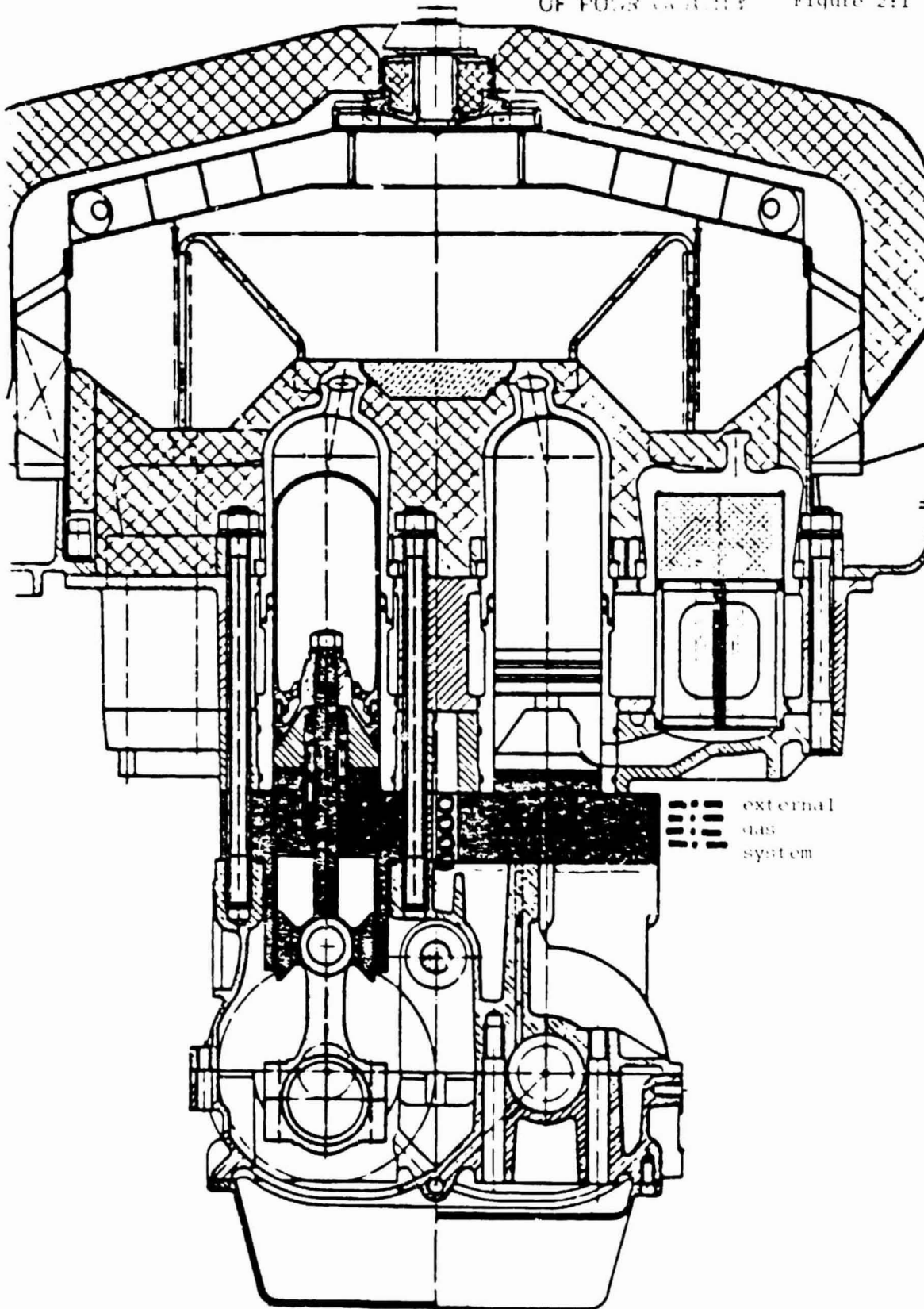


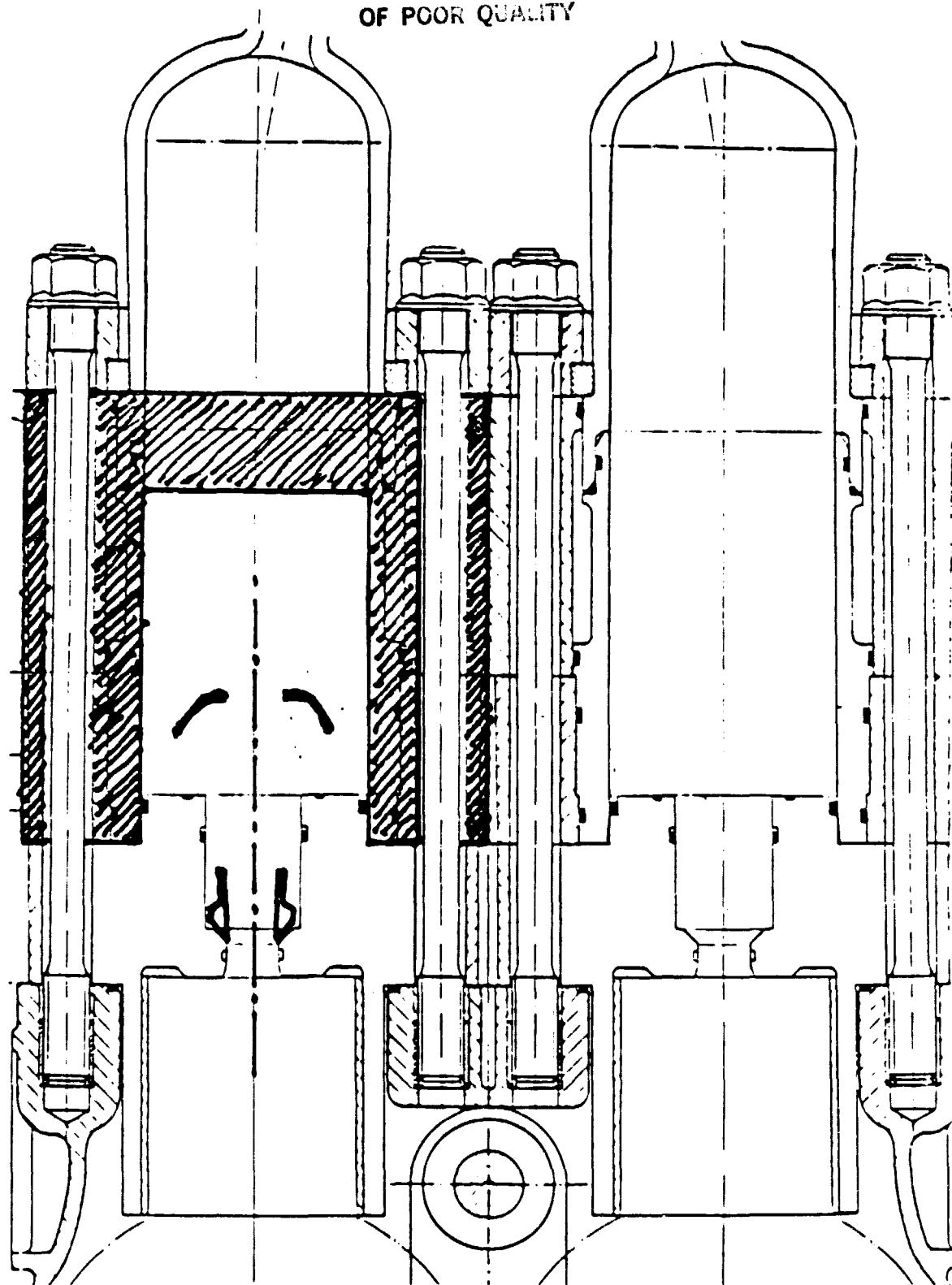
Figure 1f





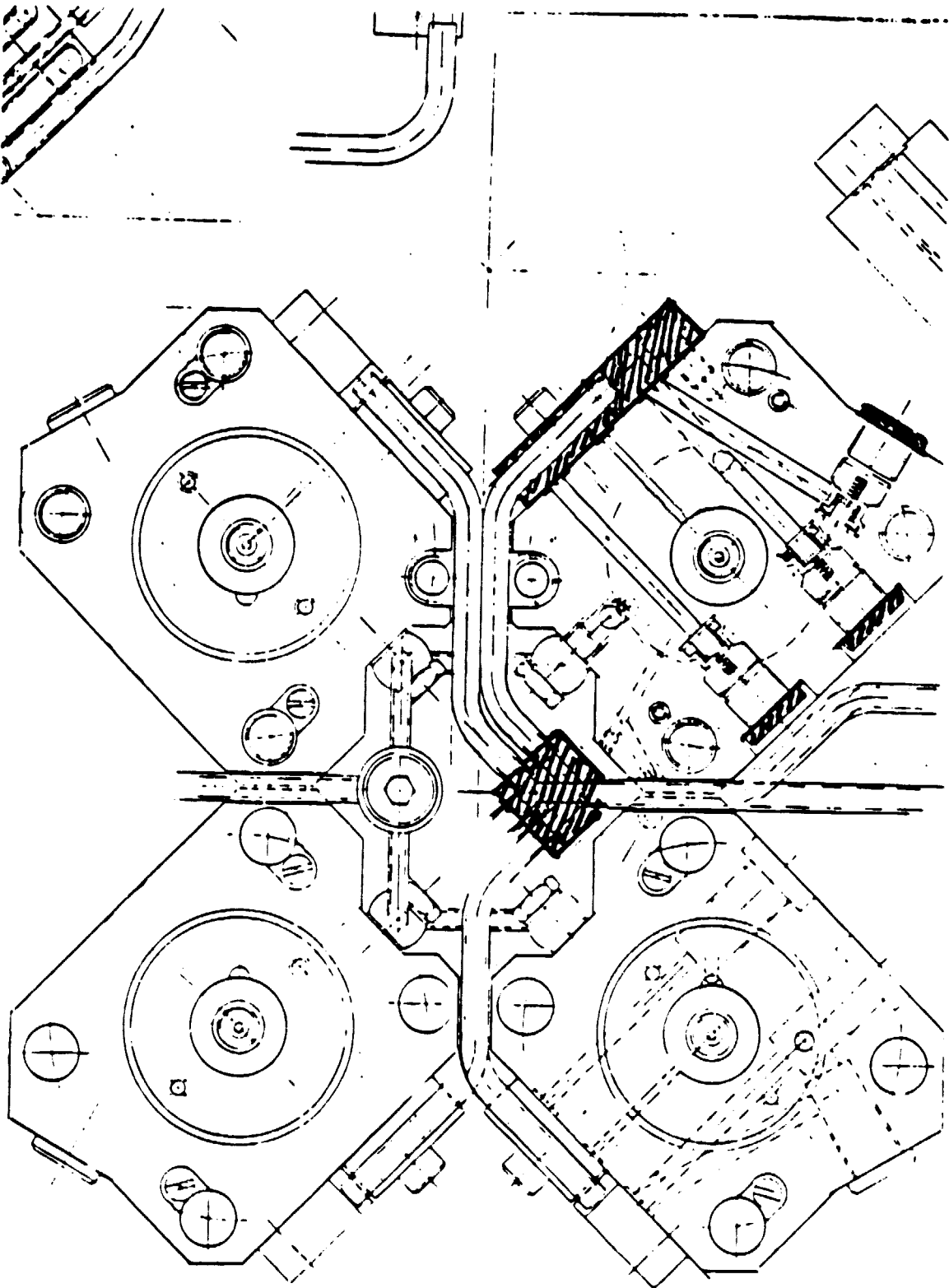
ORIGINAL PAGE IS
OF POOR QUALITY

Figure 2a (1)



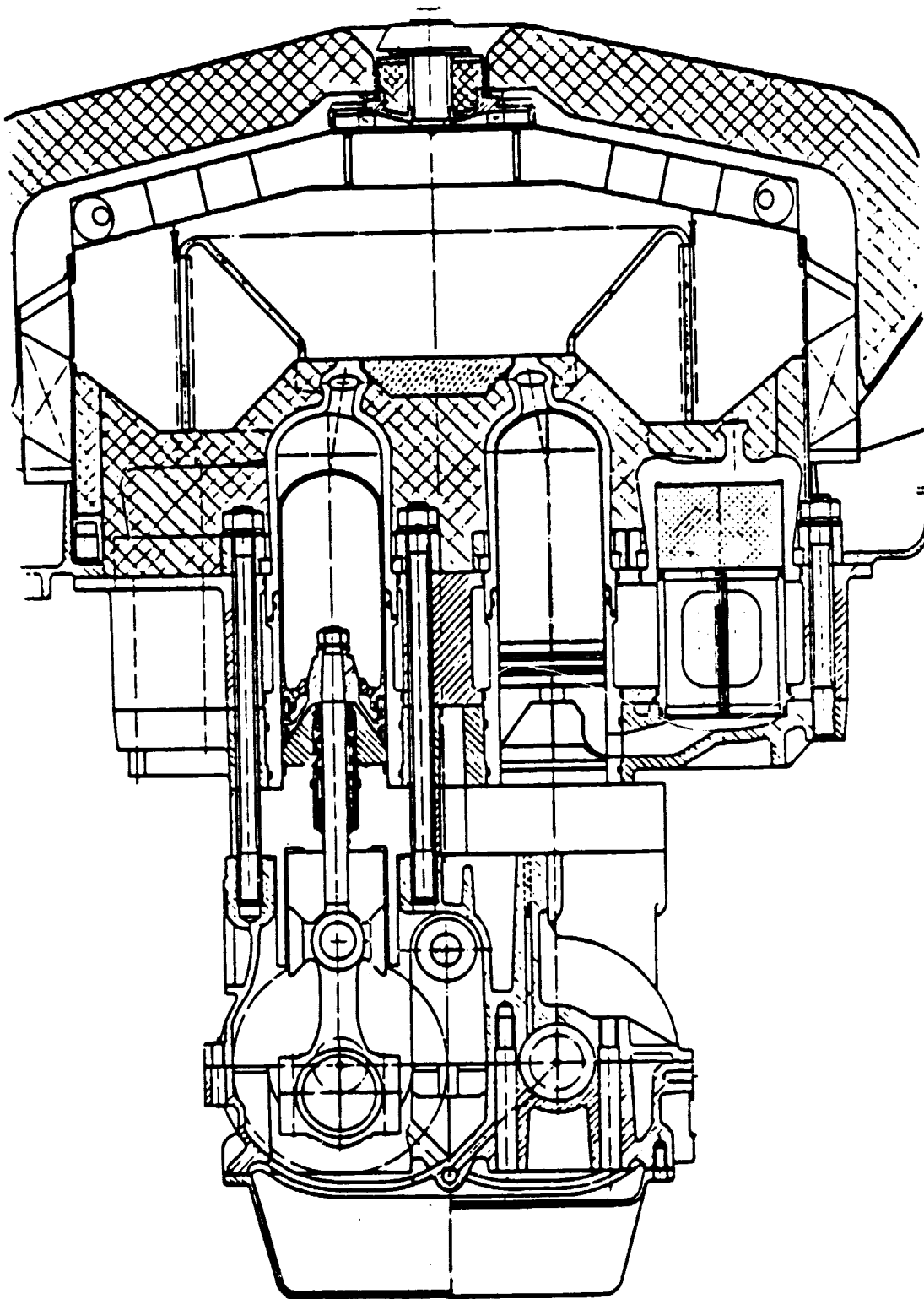
ORIGINAL PAGE IS
OF POOR QUALITY

Figure 2a (2)



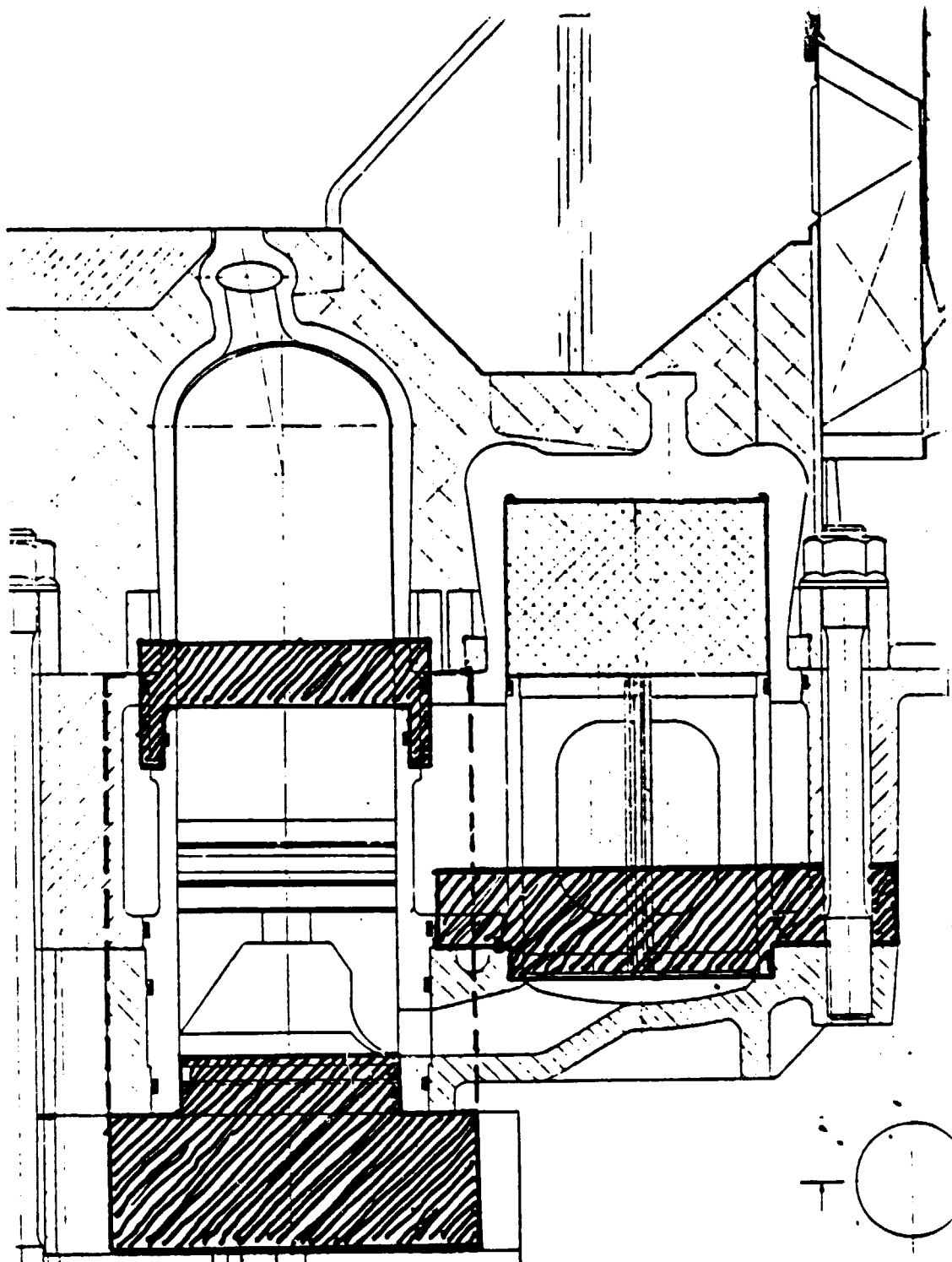
ORIGINAL FILED IN
OF POOR QUALITY

Figure 2:2



ORIGINAL PAGE IS
OF POOR QUALITY

Figure 2b (1)



ORIGINAL PARTS
OF POOR QUALITY

Figure 2b (2)

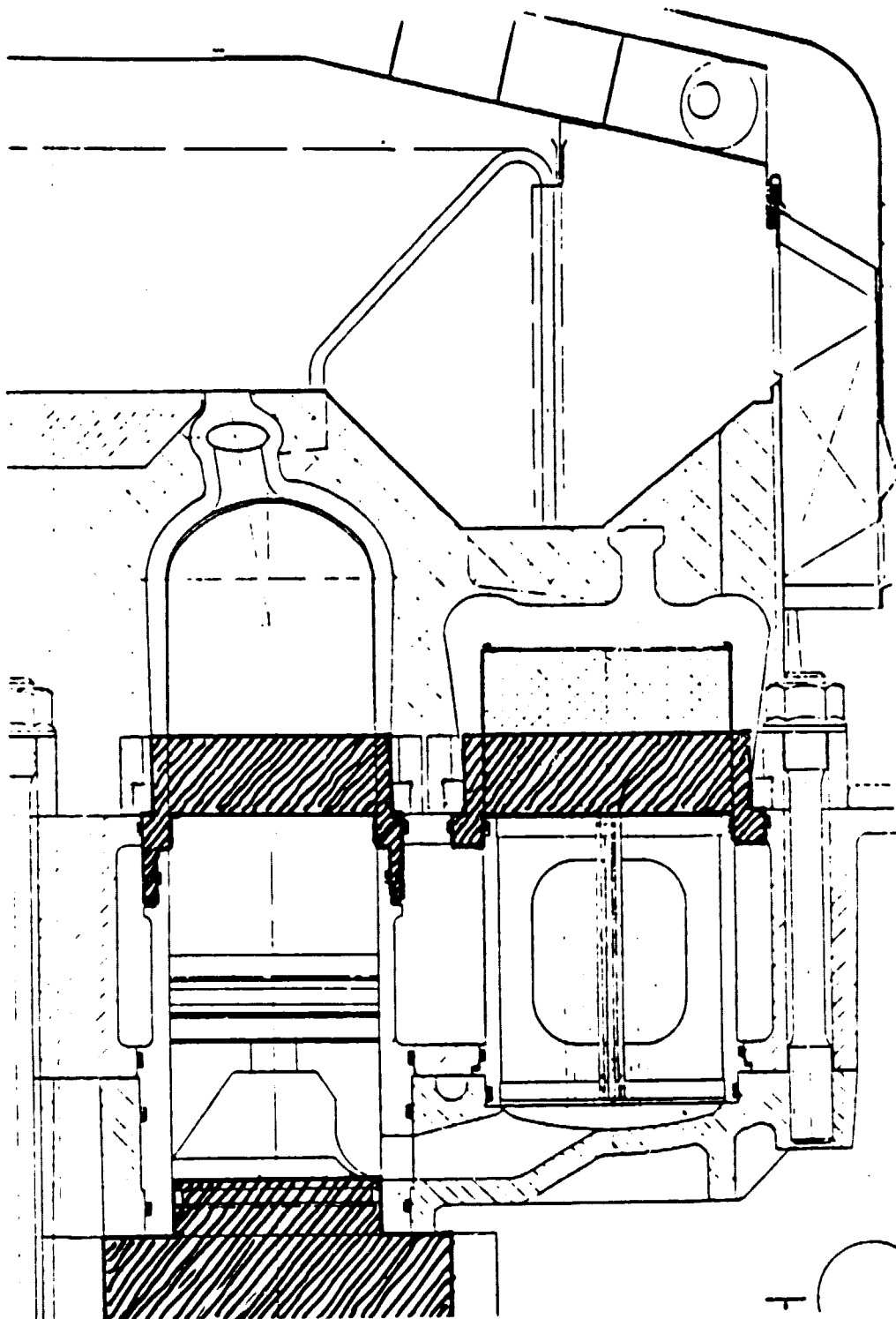
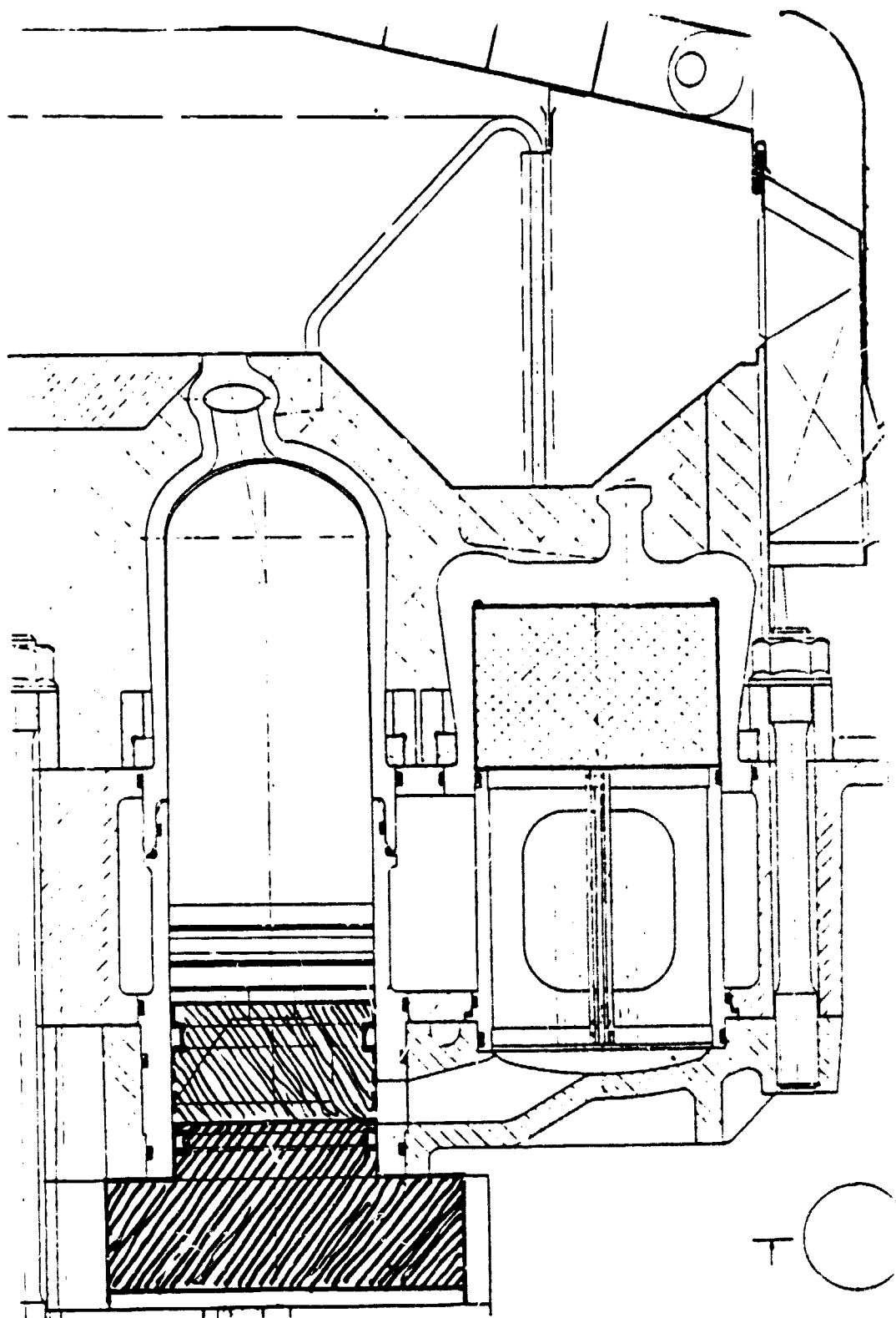
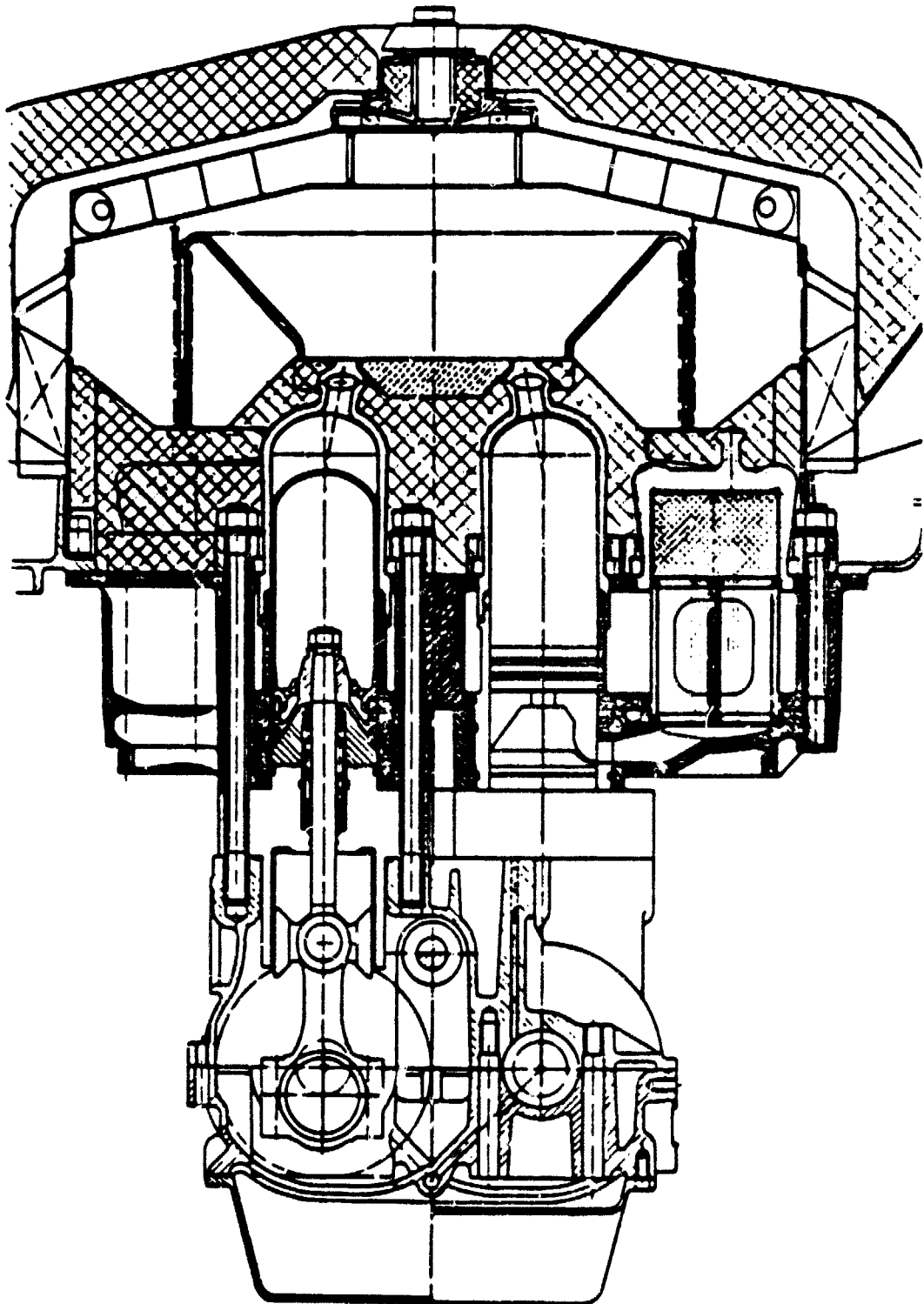


Figure 2c

ORIGINAL PAGE IS
OF POOR QUALITY



CROSS SECTION
OF PUMP QUALITY



ORIGINAL DESIGN
OF POOR QUALITY

Figure 2d

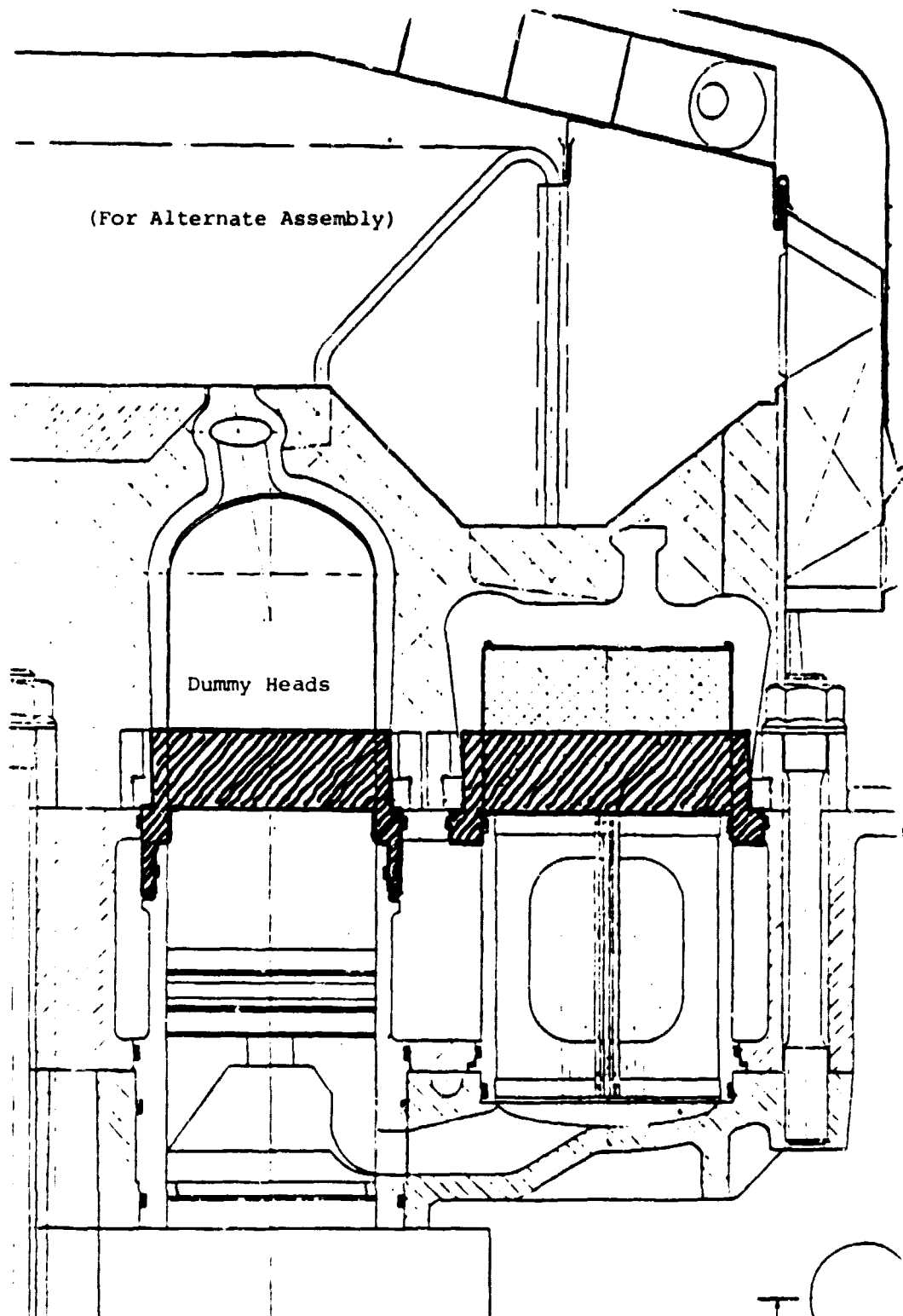
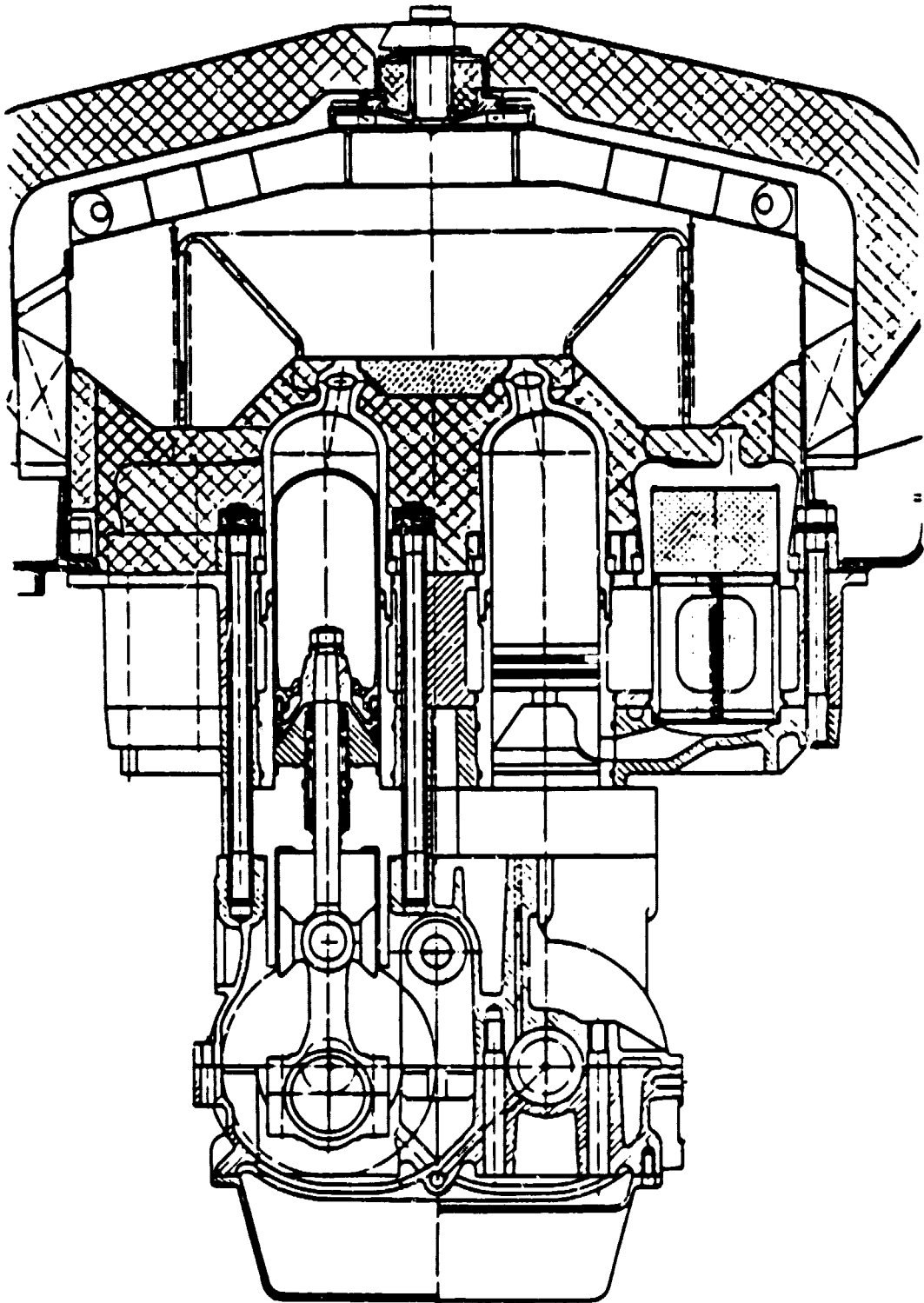


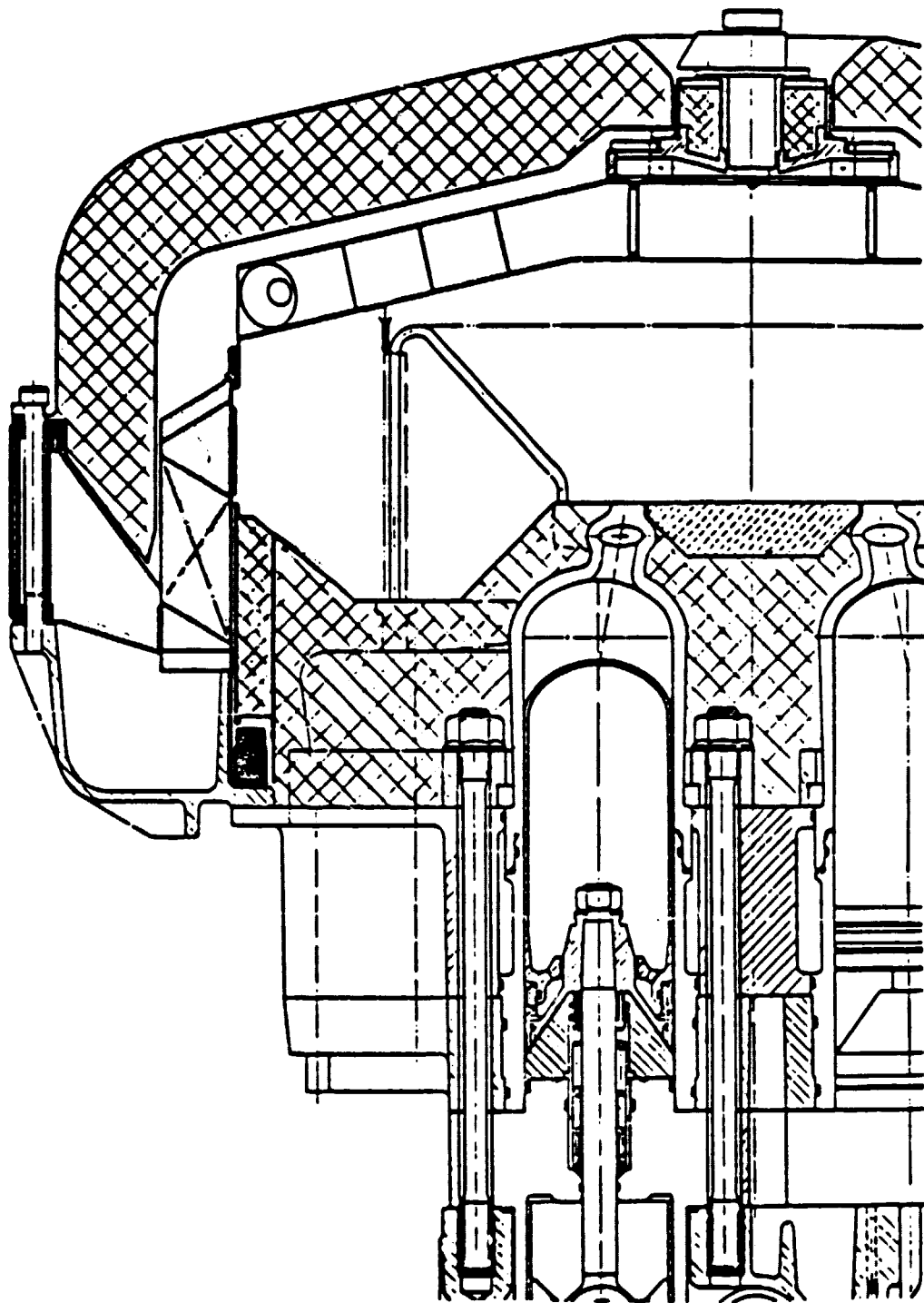
Figure 2:4

ORIGINAL PAGE IS
OF POOR QUALITY



ORIGINAL PAGE IS
OF POOR QUALITY

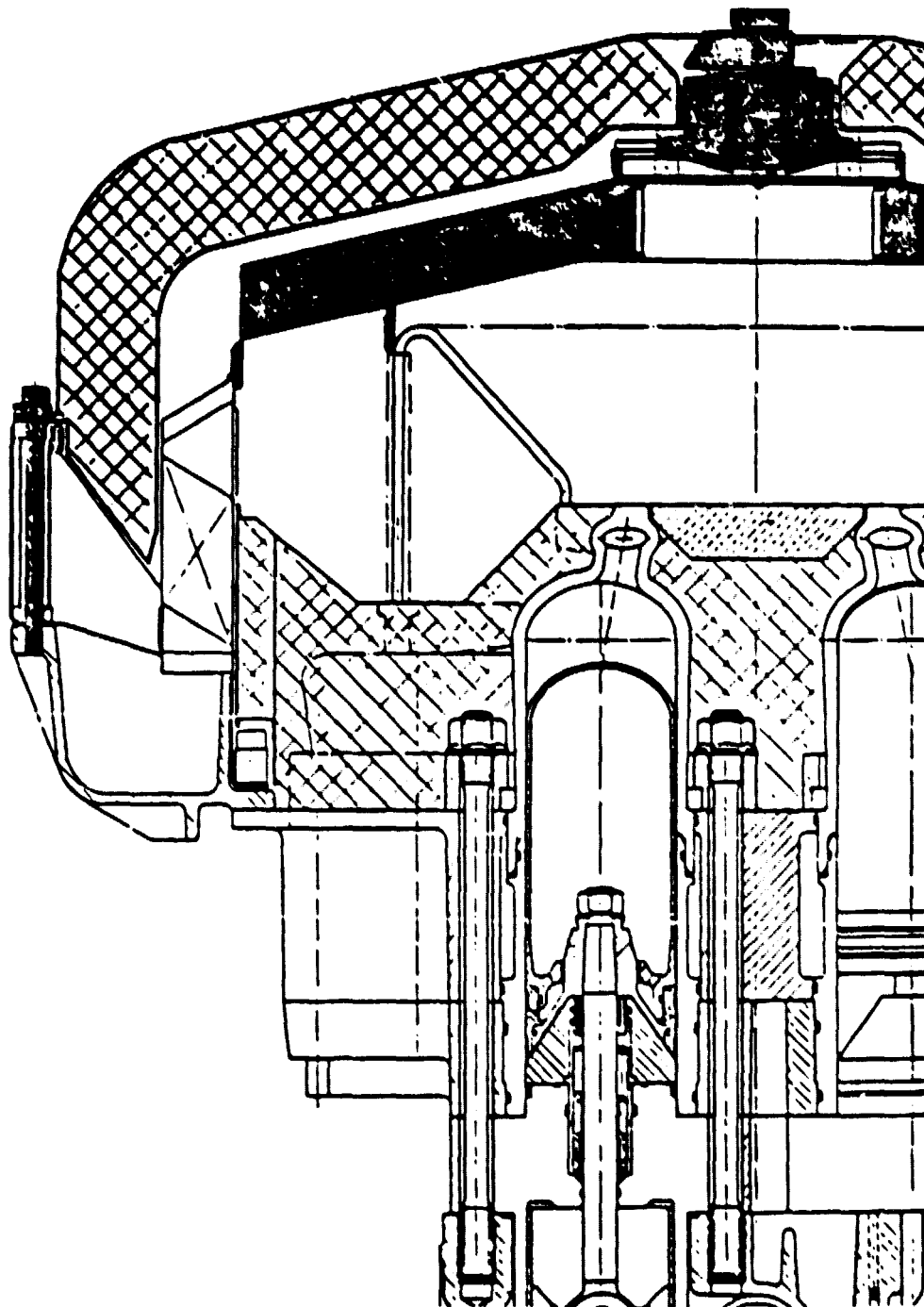
Figure 2:5



2-3

OF POOR QUALITY

Figure 2:6



ORIGINAL PAGE IS
OF POOR QUALITY

Figure 3 (1)

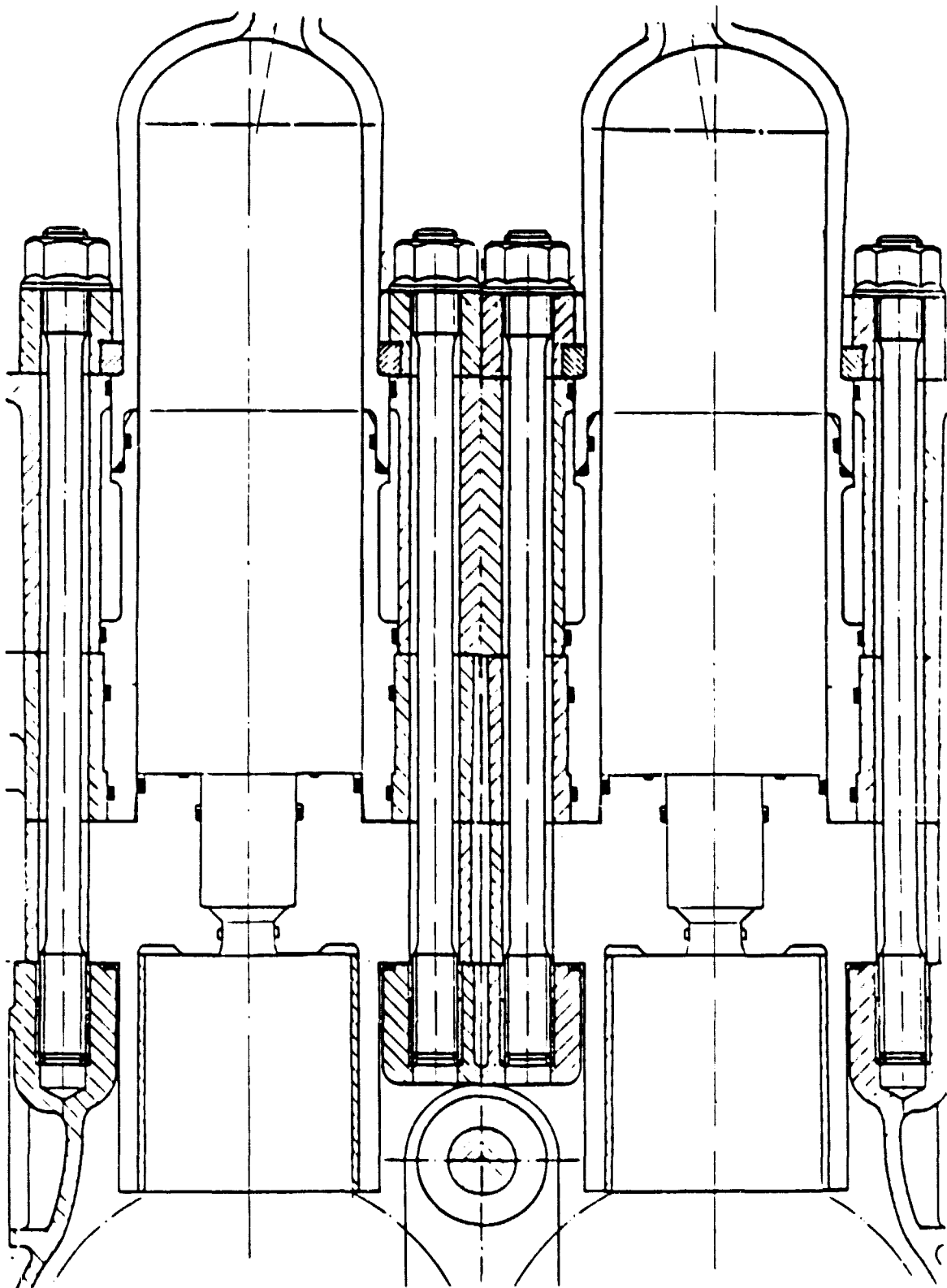
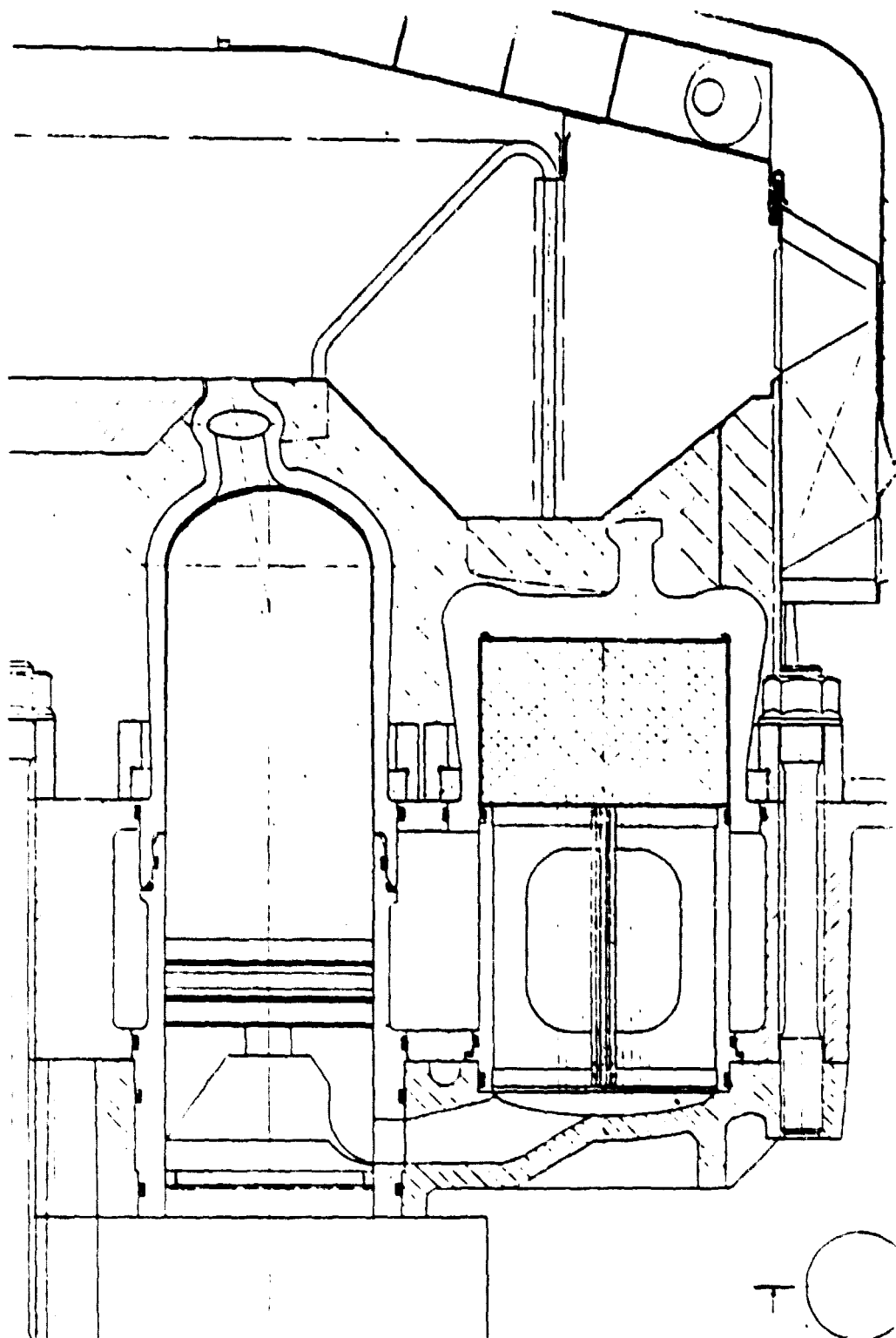


Figure 3 (2)

ORIGINAL PAGE IS
OF POOR QUALITY



3.3 Calculations Update

3.3.1 Stirling Cycle Design Process

A programmatic final objectives flow chart of MOD I is shown in fig 3.3:1. The size of the MOD I engine is determined by the power level requirement of the MOD II engine. The main difference between MOD I and MOD II is that MOD II has a heater temperature of 820°C compared to the 720°C for MOD I. Full speed of 4 000 RPM and full mean pressure of 15 MPa is the same for the two engines. As MOD II shall have a maximum shaft power of 65 kW, the estimated demand in indicated power has to be about 85 kW which corresponds to 14 kW mechanical friction and 6 kW for the auxiliaries. Decreasing the heater temperature from 820°C to 720°C will decrease the indicated power from 85 kW to about 75 kW and thus 75 kW indicated max power was the value that was used when the size of the MOD I engine was determined.

Throughout all the Stirling cycle calculations a coolant top tank temperature of 50°C has been used.

Using the same thermodynamic design philosophy as has been used on P40 and P75 and taking into account that MOD I should have better part load performance than P40, it was now possible with aid of the Stirling cycle computer program to determine the swept volume and the dimensions of the heat exchangers. The design process is shown in the flow charts of the figures 3.3:2-3.

3.3.2 The Drive

After iterations the swept volume was finalized to 124 cc with bore 68 mm and stroke 34 mm.

The bore stroke ratio of 2, which is larger than 1.4 on P40, was chosen for three reasons. Firstly, it would reduce the height of the engine which we knew was critical in an automotive engine. Secondly,

earlier investigations had shown that the minimum size of the crankcase taking into consideration the size of the counter-weights on the crankshaft and the bolting pattern for the cylinder bolts would be obtained for a bore-stroke ratio of about 2. Thirdly, an increased bore-stroke ratio will decrease the piston speed, which has a positive influence on the endurance of the piston rings and the seals.

ORIGINAL PAGE IS
OF POOR QUALITY

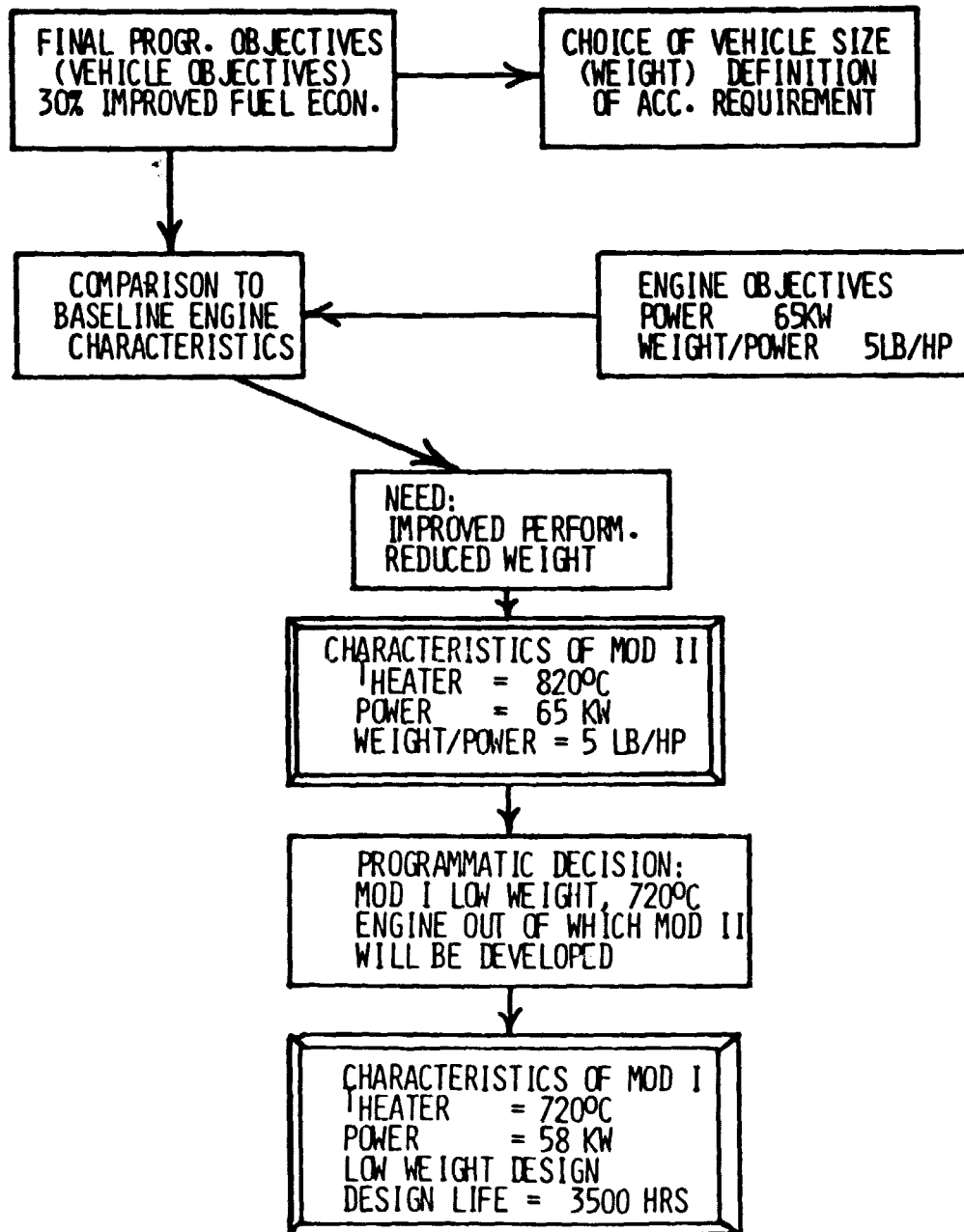


Fig 3.3:1 Final Objectives Programmatic Flow Chart of MOD I.

ORIGINAL PAGE IS
OF POOR QUALITY

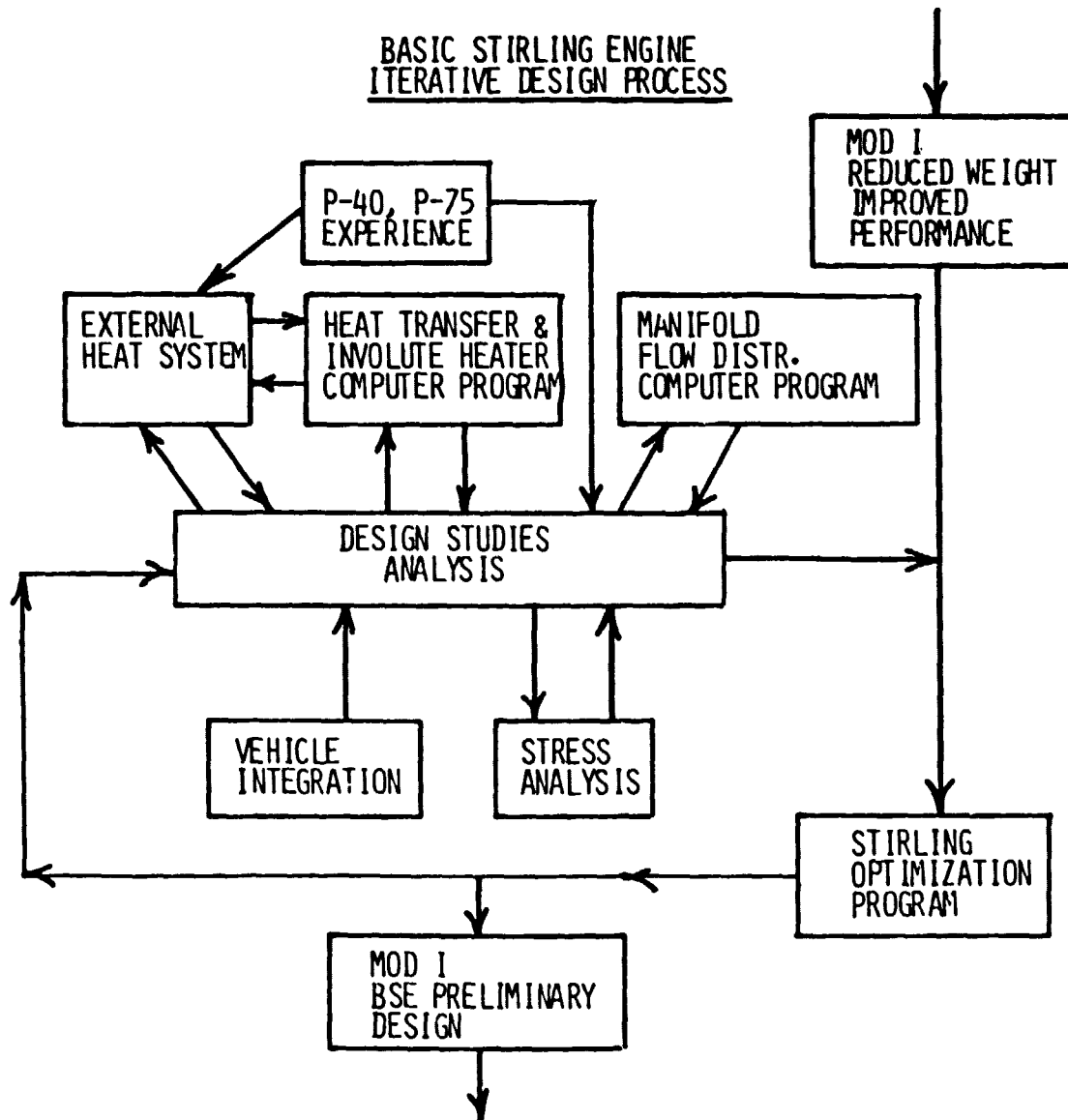


Fig 3.3:2 Iterative Design Process. Flow Chart of the Basic Stirling Engine.

STIRLING ENGINE SYSTEM
ITERATIVE DESIGN PROCESS

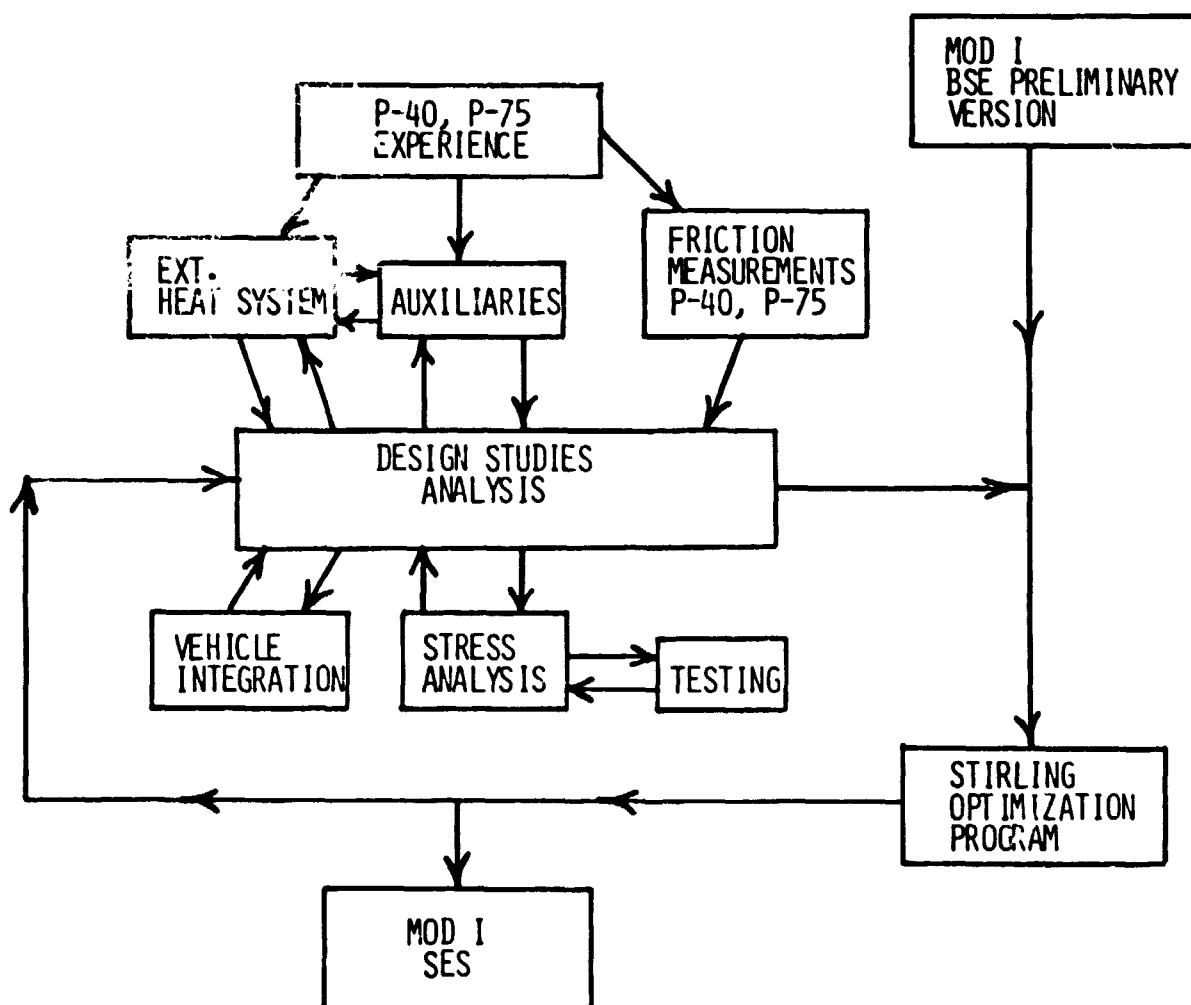


Fig 3.3:3 Iterative Design Process. Flow Chart of the Stirling Engine System.

3.3.3

Heater

It was decided to use the same type of tubes as on the P40 engine and the Stirling cycle analysis showed that the required number of tubes should be between 22 and 28 per cylinder. The gap between the tubes was chosen to 1 mm which, based on P40 experience, would give good heat-load balance between first and second tube-row.

the outer tube diameter is 4.5 mm and with the gap of 1 mm it is now possible to calculate the inner radius of the heater-cage to

$$R_i = 4 \times n \times (4.5 + 1) / (2 \times \pi)$$

where n is the number of tubes per cylinder. From the involute geometry the ratio between outer radius R_o and inner radius R_i shall be 1.92. In the fig 3.3:4 the heater cage radius is given as a function of the number of heater tubes.

The distance from the center of the engine to the center of the cylinder is determined by the distance between the crankshafts (140 mm) and is $70 \times \sqrt{2} = 99$ mm. The distance from the center of the engine and the center of the regenerator is 152 mm. The criteria for choosing the number of tubes is that the inner heater-cage radius should be as close to 99 mm as possible and the outer heater-cage radius should be as close to 152 mm as possible in order to have the manifolds to go down in the center of cylinder and the regenerator. The best compromise was found to be 24 tubes giving an inner radius of 84 mm and an outer radius of 161 mm. This gives an offset of 15 mm on the cylinder and 9 mm on the regenerator.

With 24 tubes the MOD I engine will have approximately the same heat load as P40 and as the number 24 can be even divided by 3, we can use the same type of fins as on P40 where one fin is common for three tubes. The outer radius of 161 mm also fits very well to the preheater inner radius when the preheater is lowered outside the regenerators. The length of the tubes can for geometrical reasons

not be less than about 280 mm, but can be larger if the straight parts above the cylinder and the regenerator are increased. The analysis shows that the lowest length should be chosen.

3.3.4 Regenerator

The MOD I engine has only one regenerator per cylinder compared with two for the P40 engine which means that the diameter of the regenerator is comparatively large on MOD I. If the regenerator cross-sectional area on P40 is scaled up with the swept volume it should give a regenerator diameter on MOD I of 91 mm. This diameter is considered to be too large relative to the length of the regenerator, which is 40 mm on P40, because of the stresses occurring in the regenerator housing. As the Mod I engine is going to be used as an automotive engine where the full speed efficiency is of less interest, it was decided that the regenerator diameter of MOD I should not be larger than 80 mm. This will cause some extra flow losses at full speed, but it will also increase the part load efficiency if the regenerator length at the same time is increased. The regenerator length was determined to 50 mm which is a good compromise between part load efficiency and full speed power. We are also convinced that the stress problem can be solved with the diameter of 80 mm and the length of 50 mm.

All the P75 engines and the P40 engine have a filling factor of the regenerator in the range of @40% and in order to obtain high predictability on the Mod I engine, it was decided not to go outside of this range.

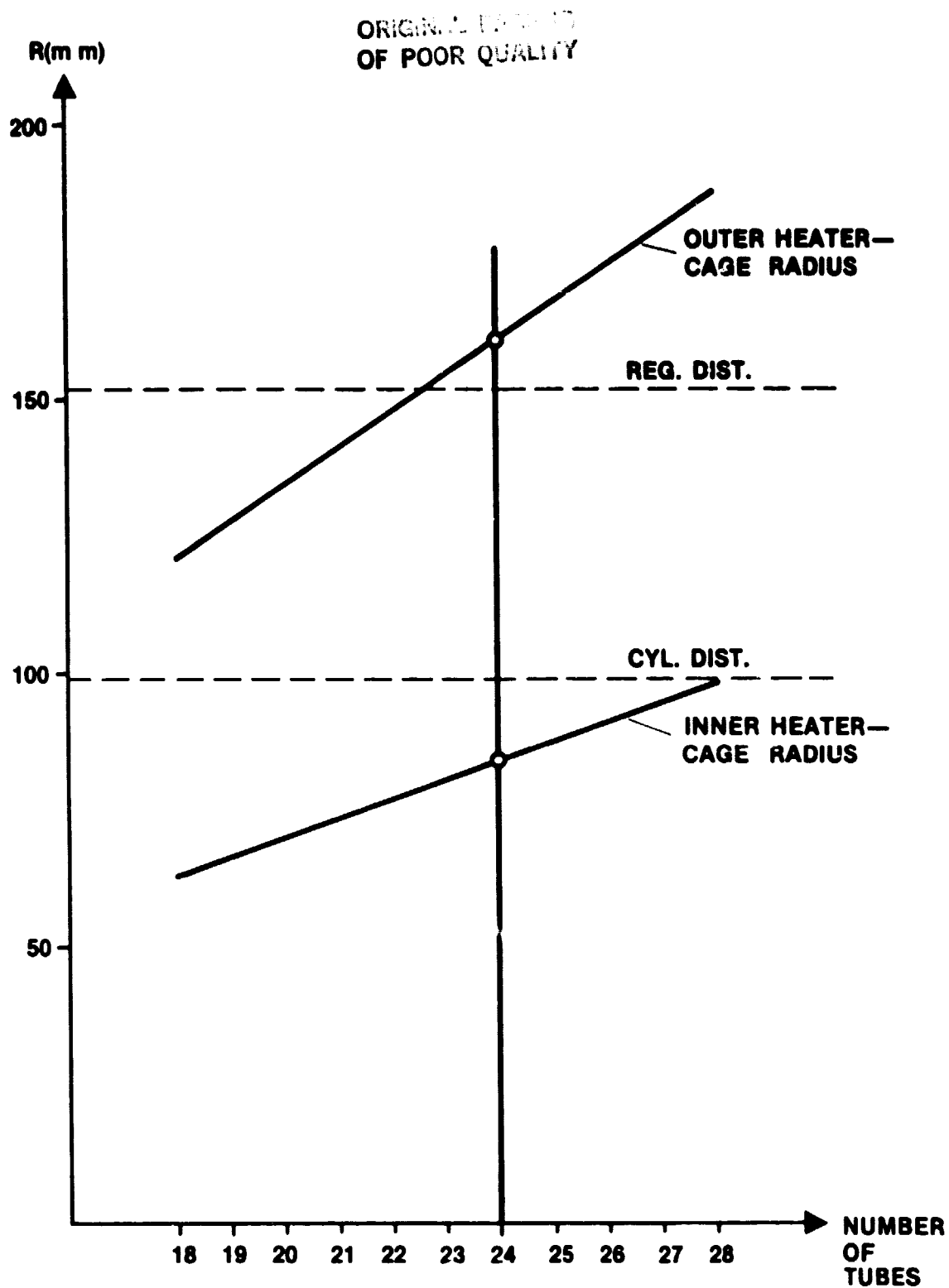


Fig 3.3:4 Heater Cage Radius as a Function of Number of Tubes.

3.3.5

Cooler

Based on experience from P40 and P75 it was decided to use similar cooler tubes. The performance calculations have been performed for stainless steel coolers. The number of tubes can be varied in a rather wide range according to the Stirling cycle program. The actual number of tubes are determined by the heat transfer on the water side which puts a requirement on the gaps between the tubes.

The length of tubes is strongly coupled to the height of the water block. This height is determined by the piston stroke and the position of the O-ring between the cylinder housing and the piston liner. The length used in the performance calculation has been 93 mm.

3.3.6

Geometrical Data

Geometrical data for the engine are given on the pages B.3-59-61.

A comparison between P40, MOD I and reference engine (Sept 1979) is given on page B.3-61. The cross sectional area and dead volumes per swept volume are normalized to P40 values. The cross sectional area may be considered as a measure of the flow resistance of the regenerators. As can be seen the engines are very much alike considering the heater. As pointed out earlier, the regenerator has been modified with respect to its slenderness ratio (diameter to length ratio). The regenerator cross sectional area for MOD I was reduced and its length increased (keeping the regenerator mass essentially unchanged) thereby increasing the part load efficiency. For reference engine the relative decrease is carried further as a result of the optimization. Since MOD I shall rely on proven technology (P40 and P75) and have a lower risk level than reference engine the reduction of the regenerator cross sectional area has been limited.

The decrease of the cooler cross sectional area is a consequence of the smaller regenerator.

Considering the dead volumes Mod I and P40 are very alike. Reference engine has smaller dead volumes causing a larger compression ratio.

$P_{\text{mas}}/P_{\text{min}}$ at full load

<u>P40</u>	<u>Mod I</u>	<u>Reference Engine</u>
1.69	1.68	1.79

MOD I STIRLING CYCLE GEOMETRY

Drive Mechanism, Cylinders

Piston diameter	68	mm
Piston rod diameter	15	"
Displacer dome height	120	"
Crank Radius	17	"
Stroke	34	"
Connecting Rod Length	95	"
Swept Volume	123.5	cm ³

Connecting Duct Cylinder-Cooler

Volume	44	cm ³
Cross section area (narrowest passage)	3.50	cm ²

Cooler

Units per cycle	1
Effective length of one tube	81.6 mm

Connecting Duct Cooler-Regenerator

Volume	3.0 cm ³
Length	0.5 mm

Regenerator (Gauze Type)

Units per cycle	1
Diameter	80 mm
Length	50 "
Weight per engine	3.4 kg

Connecting Duct Regenerator-Heater

Volume	21.5 cm ³
--------	----------------------

Heater

Tubes per cycle	24
Inside tube diameter	3 mm
Outside tube diameter	4.5 "
Effective length of one tube	257.5 "

Connecting Duct Heater-Cylinder

Volume 17 cm³

Cylinder

Clearance volume exp space 3.6 cm³

Clearance volume comp space 3.4 cm³

COMPARISON BETWEEN P40, MOD I AND REFERENCE ENGINE (SEPT 79)

CROSS SECTIONAL AREA PER SWEPT VOLUME NORMALIZED TO P40

	P40	MOD I	REF ENG
Cooler	1	0.88	0.85
Regenerator	1	0.76	0.58
Heater	1	1.02	1.03

DEAD VOLUMES PER SWEPT VOLUME NORMALIZED TO P40

	P40	MOD I	REF ENG
Cooler	1	1.00	0.74
Regenerator	1	0.95	0.82
Heater	1	1.08	0.95

COMPRESSION RATIO

	P40	MOD I	REF ENG
p_{\max} / p_{\min} at full load	1.69	1.68	1.79

3.3.7 Mechanical Friction

The mechanical friction for the MOD I engine has been estimated based on experimental tests on P40 and P75. Maximum friction power, which includes the oil pump, is 14 kW. The linear shape of the curves is based on experiments and has not yet been fully understood as an analytical model would predict a more quadratic increase with speed, see fig 3.3:5. There are some limitations in the performed motoring tests. The drive unit with dummy cylinders has only been tested up to 3 000 RPM on the P40 engine because of limitations of the equipment used to drive the drive unit. An extrapolation of the curves up to 4 000 RPM can be justified because the shaft power from a running engine is in good agreement with the calculated values also at full speed using extrapolated values for the friction power.

3.3.8 Auxiliaries

Concerning the auxiliaries power consumption curves used in the calculations: see section 8.3

3.3.9 External Heat System Efficiency

The external heat system efficiency curve used in the calculations is shown in section 4.9.

3.3.10 Performance

Indicated power, net power and subsystem efficiencies, are given in detail for four different load points on pages I-219 to I-222.

Performance maps as isotherm diagrams are given on pages I-223 to I-224.

ORIGINAL PAGE IS
OF POOR QUALITY

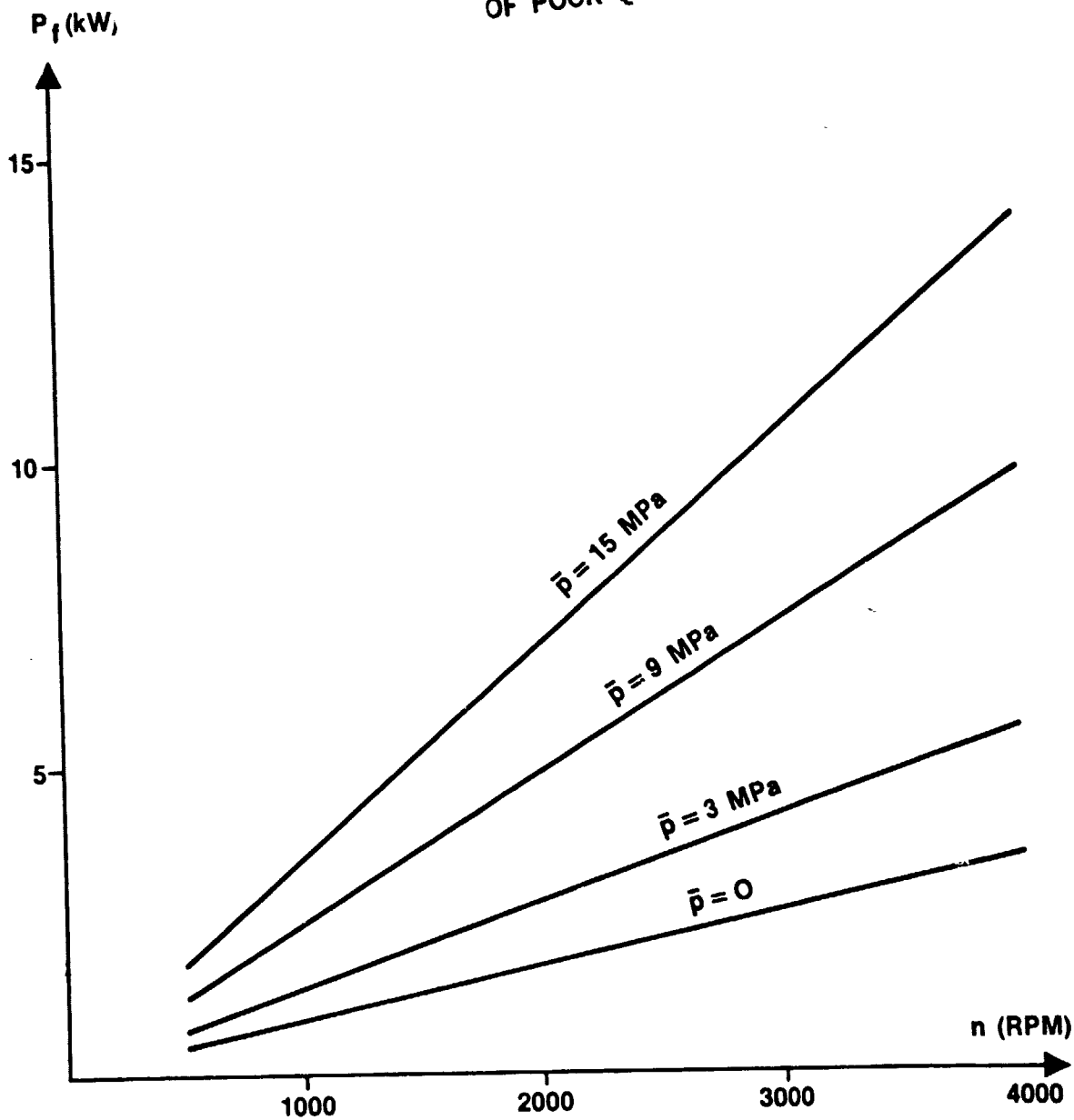


Fig. 3.3:5 Mechanical Friction versus Rotational Speed, Mean Pressure as Parameter (H_2 Working Gas)

MOD I PERFORMANCE (CALC SEQ NO 6-03)

FULL LOAD POINT

p = 15 MPa

n = 4 000 rpm

INDICATED POWER	73.1 kW
FRICTION	14.0 kW
AUXILIARIES	5.4 kW
NET POWER	53.6 kW
EXT HEATING EFFICIENCY	88.2 %
NET EFFICIENCY	28.1 %

PART LOAD POINT

p = 5 MPa

n = 2 000 rpm

INDICATED POWER	15.3 kW
FRICTION	3.5 kW
AUXILIARIES	1.1 kW
NET POWER	10.7 kW
EXT HEATING EFFICIENCY	88.1 %
NET EFFICIENCY	28.8 %

MAX EFFICIENCY POINT

p = 15 MPa

n = 1 300 rpm

INDICATED POWER	30.2 kW
FRICTION	4.6 kW
AUXILIARIES	1.0 kW
NET POWER	24.6 kW
EXT HEATING EFFICIENCY	90.0 %
NET EFFICIENCY	36.7 %

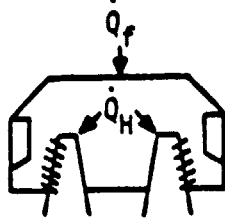
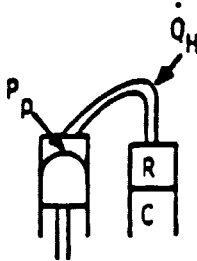
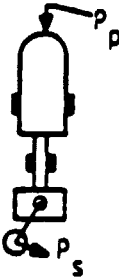
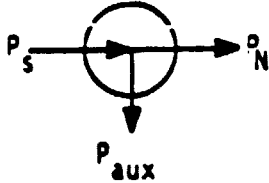
LOW LOAD POINT

p = 5 MPa

n = 1 000 rpm

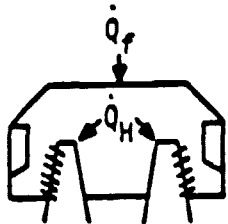
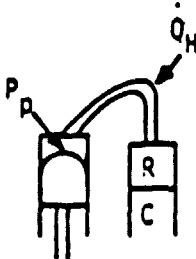
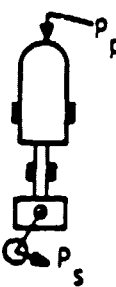
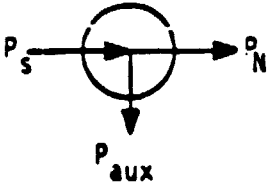
INDICATED POWER	8.2 kW
FRICTION	1.8 kW
AUXILIARIES	0.7 kW
NET POWER	5.8 kW
EXT HEATING EFFICIENCY	84.6 %
NET EFFICIENCY	26.3 %

ORIGINAL PAGE IS
OF POOR QUALITY

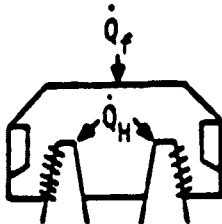
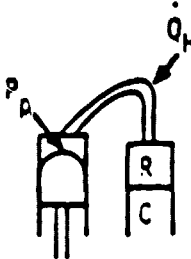
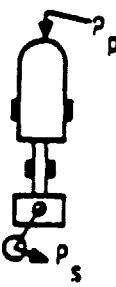
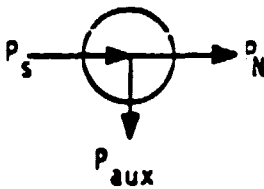
SUBSYSTEM	BOUNDARIES	EFFICIENCY	DEFINITION
EXTERNAL HEAT SYSTEM		88.2%	$\frac{\dot{Q}_{\text{HEATER}}}{\dot{Q}_{\text{FUEL}}}$
ENGINE		43.4%	$\frac{P_{\text{PISTON}}}{\dot{Q}_{\text{HEATER}}}$
DRIVE and SEALS		80.8%	$\frac{P_{\text{SHAFT}}}{P_{\text{PISTON}}}$
AUXILIARIES and CONTROLS		90.9%	$\frac{P_{\text{NET}}}{P_{\text{SHAFT}}}$
		28.1%	$\frac{P_{\text{NET}}}{\dot{Q}_{\text{FUEL}}}$

Subsystem Efficiencies at Full Load ($p = 15 \text{ MPa}$, 4 000 rpm).

ORIGINAL PAGE IS
OF POOR QUALITY

SUBSYSTEM	BOUNDARIES	EFFICIENCY	DEFINITION
EXTERNAL HEAT SYSTEM		90.0%	$\frac{\dot{Q}_{\text{HEATER}}}{\dot{Q}_{\text{FUEL}}}$
ENGINE		50.1%	$\frac{P_{\text{PISTON}}}{\dot{Q}_{\text{HEATER}}}$
DRIVE and SEALS		84.9%	$\frac{P_{\text{SHAFT}}}{P_{\text{PISTON}}}$
AUXILIARIES and CONTROLS		95.9%	$\frac{P_{\text{NET}}}{P_{\text{SHAFT}}}$
		36.7%	$\frac{P_{\text{NET}}}{\dot{Q}_{\text{FUEL}}}$

Subsystem Efficiencies at Maximum Efficiency ($p = 15 \text{ MPa}$, 1 300 rpm).

SUBSYSTEM	BOUNDARIES	EFFICIENCY	DEFINITION
EXTERNAL HEAT SYSTEM		84.6%	$\frac{\dot{Q}_{\text{HEATER}}}{\dot{Q}_{\text{FUEL}}}$
ENGINE		44.1%	$\frac{P_{\text{PISTON}}}{\dot{Q}_{\text{HEATER}}}$
DRIVE and SEALS		78.0%	$\frac{P_{\text{SHAFT}}}{P_{\text{PISTON}}}$
AUXILIARIES and CONTROLS		90.4%	$\frac{P_{\text{NET}}}{P_{\text{SHAFT}}}$
		26.3%	$\frac{P_{\text{NET}}}{\dot{Q}_{\text{FUEL}}}$

Subsystem Efficiencies at Low Load ($p = 5 \text{ MPa}$, 1 000 rpm).

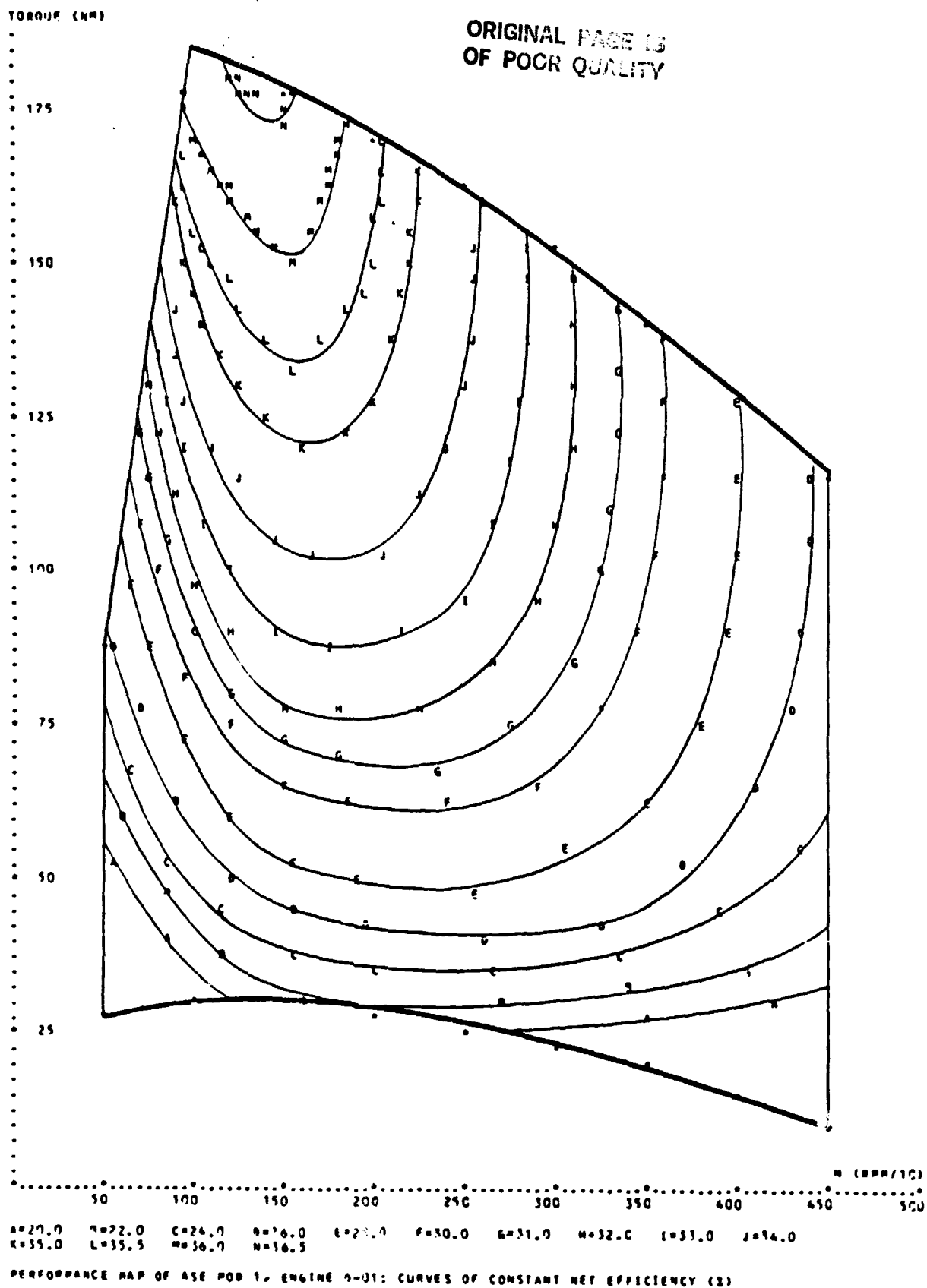


Fig 3.3:6 Performance map with net shaft torque versus speed.

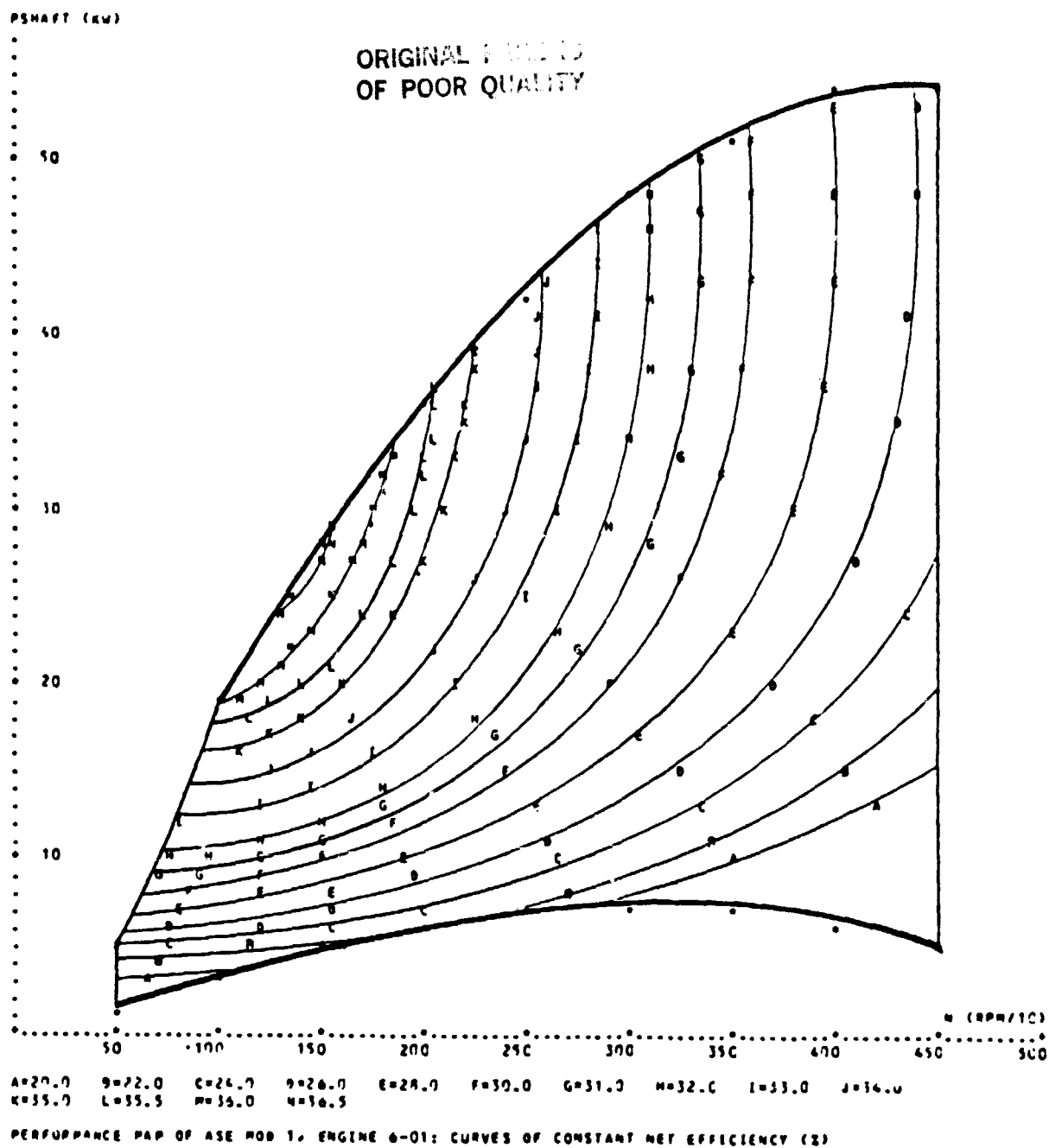


Fig 3.3:7 Performance map with net shaft power versus speed.

The Heat Flows in MOD I

- \dot{Q}_f = Heat from the fuel
- \dot{Q}_{ex} = Heat losses in heat generating system
- \dot{Q}_E = Heat to the heaterhead
- \dot{Q}_{cb} = Heat losses in cylinders and regenerators
- \dot{Q}_C = Rejected heat in the cycle coolers
- P_i = Indicated power

A = Full load. $p = 15$ MPa, $n = 4\ 000$ rpm

B = Part load. $p = 5$ MPa, $n = 2\ 000$ rpm

C = Max efficiency load. $p = 15$ MPa, $n = 1\ 300$ rpm

D = Low load. $p = 5$ MPa, $n = 1\ 000$ RPM

All values in kW.

	A	B	C	D
\dot{Q}_f	191.0	37.2	67.0	22.1
\dot{Q}_{ex}	22.5	4.4	6.7	3.4
\dot{Q}_e	168.5	32.8	60.3	18.7
\dot{Q}_{cb}	3.0	3.2	3.1	3.2
\dot{Q}_C	95.4	17.5	30.1	10.5
P_i	73.1	15.3	30.2	8.2

3.3.11

A Comment on the Engine Full Load Power

The initially projected full load point (4 000 rpm, 15 MPa) net shaft power of the ASE MOD I engine was 58 kW.

The 4.4 kW lower calculated power level of 53.6 kW is due to the following changes:

1. The preliminary values of the auxiliaries power consumption have been updated to reflect the latest findings. Change: +1.72 kW.
2. The geometrical computer input for the Stirling cycle has been updated in accordance with the final drawings. The changes responsible for most of the power drop are the increase of the cold connecting duct volume by 4 cm^3 , a correction of the pressure drop factor in the heater with connecting ducts, an increase of the duct volume between regenerator and heater by 2.5 cm^3 and some other minor adjustments to match the drawings.

3.4

Procurement schedule

The procurement schedule shows milestones of the manufacturing of parts of basic Stirling engine.

Separate legends show: Complete detail drawings, start manufacture/procurement. (The required date of purchase order acceptance by MTI).

Delivery to USS (from manufacturer) and System Assembly engine.

Figures assigned to the legends indicate number of components ordered.



ASE MOD I

3.4 PROCUREMENT SCHEDULE

1979				1980								1981												
S	O	N	D	J	F	M	A	M	J	J	A	S	O	N	D	J	F	M	A	M	J	J	A	S

EXTERNAL HEAT SYSTEM

Preheater matrix

Tools for manufacture preheater matrix

Preheater housing

Preheater matrix/housing

Heat generating system

HOT ENGINE SYSTEM

Cylinder/regenerator housing

Heater tubes

Fin section

Fixture

Thermocouple equipment

Complete heater

Regenerator

Adapter for regenerator

Gas cooler

Adapter for gas cooler

Assemble External heat/Hot engine system on engine


▲ Complete detail drawings ▽ Deliver to USS
 ▲ Start manufacture/procure ▼ Assemble on engine

ORIGINAL PAGE IS
OF POOR QUALITY



ASE MCD I

3.4 PROCUREMENT SCHEDULE

 ASE MCD I	1979												1980												1981													
	S	O	N	D	J	F	M	A	M	J	J	A	S	O	N	D	J	F	M	A	M	J	J	A	S	O	N	D	J	F	M	A	M	J	J	A	S	
3.4 PROCUREMENT SCHEDULE																																						
COLD ENGINE SYSTEM																																						
Water manifold castings			▲▲12			▽																																
Water manifold machining			△				▲3		▽				▲5		▲4		▽																					
Cold connecting duct plate, castings			▲▲48			▽																																
Cold connecting duct plate, machining			△				▲12		▽				▲20		▲16		▽																					
Net line							▲20		▽				▲20		▽																							
Tools for leak test of cylinder block							△		▲1		▽																											
Piston dome			▲10						▽				▲20		▽		▲10		▽																			
Tools for testing dome							△		▲1		▽																											
Piston rod			▲10					▽				▲20		▽		▲10		▽																				
Piston			▲10					▽				▲20		▽		▲10		▽																				
Seals							▲10		▽			▲20		▽		▲10		▽																				
Seal housing							▲10		▽			▲20		▽		▲10		▽																				
Assemble Cold engine system on engine												▽			▽			▽	▽	▽	▽	▽	▽															
ENGINE DRIVE SYSTEM																																						
Ricardo deliver drive unit												▽	▽				▽	▽	▽	▽	▽	▽																
△ Complete detail drawings ▽ Deliver to USS ▲ Start manufacture/procure ▼ Assemble on engine																																						

1-229

ORIGINAL PAGE IS
OF POOR QUALITY

B.4 External Heat System

PRECEDING PAGE BLANK NOT FILMED

4. EXTERNAL HEAT SYSTEM

4.1 General description

4.1.1 Combustion gas recirculation system CGR. Update

Combustion gas recirculation system CGR is favoured over exhaust gas recirculation (EGR). The advantage of the CGR-system over the EGR-system is the increased efficiency of the external heat exchanger system. Calculations performed for MOD I show in mileage of about 0.8 mile/gallon in the CVS-cycle.

The CGR-system consists of 10 channels divided from each other by straight shaped partition walls. In front of each channel a metal ejector is located through which the preheated air flows. The lowest pressure after the ejector is below that of the combustion gas after the heater causing part of the combustion gas to mix and flow with the preheated air into the combustor.

4.1.2 Fuel injection

See drawing.

Fuel atomized air. The usual system with a central fuel nozzle and an atomizer air flow of 1.6 (g/s) all over the load.

4.1.3 Air preheater, recuperative

See drawing.

The preheater matrix is located in such a position that the combustion gas inlet is straight opposite the second heater tube row. The exhaust gas is collected in a manifold just below the matrix and from there it is diverted from the engine by means of two exhaust pipes, one on each of the engine.

The fresh air from the blower is directed into a ~~casted~~ manifold before it enters the preheater matrix. In this way and since the ejectors are located to the air outlet, the air will be evenly distributed over the entire preheater matrix. The preheater is of counter flow type and the matrix can be removed from the preheater housing at special occasions as for cleaning if clogged by exhaust products or reparation.

The insulation inside the preheater matrix is made up of aluminium-silica formed in such a way that they surround all of the heater parts and are easily installed.

The outer insulation between the channel for preheated air and cover is made up of aluminium-silica wool formed and packed before the inner cover-plate is sealed off.

4.3 Calculations

4.3.1 Demands on the external heat system

The main demand on the external heat system is to deliver heat to the Stirling cycle. The interface between the cycle and the external heat system is in the Stirling heater (see below). The efficiency of the system, i.e. how much of the available energy of fuel is transferred to the cycle, is called η_B . This efficiency is the first link in a chain of efficiencies that all together will give the overall efficiency η_e which is closely related to mileage in an automotive applications.

The external heat system has another influence on mileage besides η_B and that is its demand for shaft power for burner air blower, atomizer air compressor and fuel pump.

In the ASR program a demand for very clean exhaust gases are added to the objectives and this has a very decisive influence on the performance of the external heat system.

4.3.1.1 Demands on the external heat system efficiency (η_B)

In the process of designing the Mod I engine the overall engine performance objectives have been broken down into objectives for the different subsystems. The objective for the external heat system efficiency has been settled to $\eta_B \approx 85\%$. This value is a mean value for the CVS-cycle. The blower power demand has been restricted by maximizing the pressure loss of the system.

4.3.1.2 Demands on exhaust emissions

The emission objectives correspond to the original 1976 CVS emission legislations i.e.:

$$\text{NO}_x \leq 0,40 \text{ g/mile}$$

$$\text{CO} \leq 3,4 \text{ g/mile}$$

$$\text{HC} \leq 0,41 \text{ g/mile}$$

In order to meet these objectives special arrangements must be performed to reduce NO_x -emissions. It is a well known fact that the NO_x -formation

rate is very temperature dependent. This means that one way of reducing NO_x is to decrease the temperature of the flame. An established way of reducing the flame temperature is to increase the mass flow of the gases involved in the combustion process. The heat from the fuel is thus absorbed by a bigger mass and the temperature will be reduced. Exhaust Gas Recirculation (EGR) is one way of increasing the mass flow through the combustor. Alternative ways are increased air excess or water injection. For MOD I gas recirculation is the best alternative.

Gas recirculation could be achieved in two ways. One way is to mix the air and the exhaust gases prior to the blower. The additional mass flow then passes the entire external heat system. This method is from now on called the EGR-system. An alternative way of gas recirculation is to reduce the recirculation circuit to involve only the combustor and the heater. This system will be called the CGR-system (Combustion Gas Recirculation.)

4.3.2 Components of the external heat system

The components of the external heat system and their function can be described by following the burner air flow through the system. The flow path is also illustrated in fig. 4.3:1 (pg. I-258).

The burner air is sucked through the air filter and the air fuel control by the blower. If the EGR-system is used the exhaust pipe is connected to the blower inlet down stream the air fuel control. The burner air is then brought into the intake manifold of the external heat system. The manifold is designed to deliver a circumferencely even distributed flow to the preheater. In the preheater the temperature of the burner air is increased by the heat transferred from the combustion gas. The preheated air enters the swirler region of the combustor where the fuel is injected. If the CGR-system is used the preheated air is mixed with combustion gases prior to the combustor. By burning of the fuel heat is released in the combustor and the gas temperature is increased to its maximum level. From the combustor the flue gas passes the heater head and heat is transferred to the Stirling cycle through the walls of the heater head. By absorption of heat in the heater the combustion gas temperature is drastically lowered. From this spot, i.e. immediately down stream the heater head, some combustion gas is brought to and mixed with the preheated air entering the combustor in the CGR-system. After the passage of the heater the combustion gas flow leaves the external heat system through the preheater and the exhaust manifold. The temperature is reduced in the preheater as heat is transferred to the incoming combustor air. The exhaust gases leave the engine through the exhaust pipes which are connected to the exhaust manifold.

4.3.2.1 The preheater

The MOD I preheater is a plate type counter flow heat exchanger. The plates consist of a corrugated part in which the true counter flow exists, the rest of the plates are forming cross-headers. The distance between the plates are defined by the corrugation and by small dimples in the cross-head sections. These plates are welded together in a cylindrical structure, where the gap between the plates are kept constant by bending the plates in an involute shape, fig. 4.3:2 (pg. I-259).

In the mathematical model of the preheater the plates are transformed into rectangles consisting of three rectangles representing the two cross-headers and the corrugated part. As the model is numerical each rectangle is divided into a certain number of elements, fig. 4.3:3 (pg. I-260).

The heat balance for each element is then calculated analytically.

In each element the heat content of the combustion gas is reduced by convective heat transfer to the plate. The heat is then transferred to the air side of the plate by conduction and convectively absorbed by the air.

The convective heat transfer is described by

$$Nu = C \cdot Re^M \cdot Pr^N \cdot (\eta / \eta_w)^K \quad (1)$$

where C, M, N and K are empirically established constants and η is the dynamic viscosity of the fluid.

The conduction through the plate element is described by

$$Q = \Delta T \cdot k \cdot \frac{A}{L} \quad (2)$$

where Q is the heat flow and k, the conductivity of the material. ΔT is the temperature difference across the plate, L the thickness and A the area of the element.

A temperature difference is also established along the length of the plate element which means that heat flows in the same direction as the combustion gas. This heat flow along the plates is small but has a significant influence on the performance of the preheater at lower loads. This "internal heat leak" is treated mathematically by the same type of expression as (2).

The situation is even more complicated by the fact that a temperature difference is established radially in the preheater. This means that the conductive heat transfer in the plate element is three dimensional. In order to be able to calculate the radial heat flux of the elements the insulation around the preheater has to be incorporated in the model. The different heat flows are shown in fig. 4.3:3 (pg. I-260).

The cross head sections are not true counter flow heat exchanger depending on the flow pattern. However in the model they are treated as such. No empirical data for the convective heat transfer are available for the cross heads but an approximative calculation is made based on data from tests on corrugated plates with bead angle of 5° . The error due to these approximations are hard to estimate.

Two different preheater models are used in the calculation of the external heat system. The one that is used to calculate the thermal performance of the preheater does not include the contribution from the cross heads due to the uncertain approximations in the model. This means that the calculated data are a bit pessimistic. However the cross heads are included when the pressure drop of the preheater is calculated.

The pressure drop in each element is a function of the geometry of the gap, the temperature of the gas and the mass flow. The influence on the different parameters can be expressed by

$$f = c \cdot Re^m \left(\eta / \eta_w \right)^k \quad (3)$$

where: f = friction factor

c, m, k = empirical constants

The pressure drop calculated with this model is a bit too high as the cross heads are treated as a corrugated parts (bead angle 5°).

4.3.2.2 The combustor

There are several ways that the combustor and the combustion process can be treated analytically. In the MOD I program some reaction rate calculations for NO_x formation have been performed in order to decide the amount of CGR/EGR. However most efforts have been laid on developing a heat balance model for the combustor volume.

In the combustor model the flame temperature is estimated to start an iterative loop. Heat is lost in the combustor volume by radiation and convective heat transfer to the walls. The heat flow through the flame tube is neglected as most of it is absorbed by the incoming combustion air and thus brought back into the combustor volume. In the model this means that the temperature of the fluid entering the combustor is not increased when passing the flame tube. This also means that the only heat flow from the volume that has a negative influence on η_p is the flow through the ceramic stone to the cooled block fig. 4.3:4 (pg.II-408).

The losses from the flame is calculated based on the estimated start value. A new flame temperature can then be calculated. This procedure is repeated until the iteration converge.

The pressure drop of the combustor is closely related to the design of the swirler region and is calculated by semi-empirical expressions. In the CGR case the pressure drop across the ejector nozzles is very well defined.

4.3.2.3 The heater

The heater consists of two tube rows. In the first row the tubes are bare and bent in an involute shape in order to maintain constant gap between the tubes when going from one radius to another. In the second row the tubes are straight and furnished with large plate type fins.

The heat transfer to the tubes are calculated differently depending on the row. The heat transfer to the first row is calculated analytically. By assuming constant wall temperature (T_w) the reduction in combustion gas temperature (ΔT) when passing a small area of the tube surface (ΔA) can be expressed by:

$$\Delta T = (T - T_w) \cdot \frac{\Delta A \cdot \alpha}{\dot{m} \cdot C_p} \quad (4)$$

where α is the convective heat transfer number \dot{m} is the mass flow

C_p is the specific heat valve of the gas

T is the mean gas temperature

(4) can be transformed into

$$\frac{\Delta T}{T - T_w} = \Delta A \cdot \frac{\alpha}{\dot{m} \cdot C_p} \quad (5)$$

By integration over the tube area the following expression will be achieved:

$$\ln \frac{T_1 - T_w}{T_2 - T_w} = A \cdot \frac{\alpha}{\dot{m} \cdot C_p} \quad (6)$$

By introducing dimensionless numbers (6) is transformed to

$$\ln \frac{T_1 - T_w}{T_2 - T_w} = \frac{Nu}{Pr \cdot Re} \cdot \frac{A}{S} \quad (7)$$

where T_1 is the combustion gas temperature before the first row
 T_2 is the combustion gas temperature after the first row
 S is the gap between the tubes.

The right side of (7) is recognized as A for the first row. The relation between Nu and Re has been settled empirically.

As was mentioned above the heat transfer model of the first row is not adequate for the second row. The reason for this is that the fins can not be considered as isothermal. The model used is based on finite difference technique where the fin is divided into a number of rectangular elements. As the gas flow between the closely spaced fins is laminar, Nu can be considered constant.

For a given heater design A for the two rows can be expressed a function of the mass flow.

$$A = f(\dot{m}) \quad (8)$$

The pressure drop of the first tube row is calculated assuming turbulent flow by expressions like

$$P = Eu \cdot \frac{\rho C^2}{2}$$

where Eu is number of Euler

Eu is a function of Re . The $f(Re)$ is established empirically

ρ is density

C is velocity of the fluid

The pressure drop of the second tube row is calculated by assuming laminar flow.

4.3.2.4 Insulations

In order to reduce undesired heat flows in the external heat system layer of insulative material is used at strategic points in the system. The way these insulative layer is treated mathematically varies with their location in the system. However the following general model is applicable for all cases.

Heat is transferred to and from the insulative layer by

A. Convection where the heat flow is given by

$$Q_{\text{conv}} = \alpha \cdot (T_{\text{gas}} - T_{\text{wall}}) \cdot A \quad (9)$$

Where α is the convective heat transfer number and A the area of the layer.

B. Radiation where the heat flow is given by

$$Q_{\text{rad}} = \frac{1}{2} \alpha_f (1 + \alpha_w) [\epsilon_f \cdot T_f^4 - \alpha_f T_w^4] \cdot A \cdot F \quad (10)$$

where σ is Boltzman's number α_w is the absorptivity of the surface (gas) of the lower temperature

ϵ_f is the emissivity of the surface (gas) of the higher temperature

α_f is the absorptivity of the surface (gas) of the higher temperature

A = Area

F = Shape factor (view factor)

T_f = The higher temperature

T_w = The lower temperature

The absorptivity α_f can be expressed by

$$\alpha_f = \epsilon_f \left(\frac{T_f}{T_w} \right)^{1,5} \quad (11)$$

C. Conduction where the heat flow is given by

$$Q_{\text{cond}} = \Delta T \cdot k \cdot \frac{A}{L} \quad (12)$$

where ΔT = The temperature gap in the solid in contact with the insulation.

k = Conductivity

A = Area

L = Thickness

The heat transfer within the insulation is also of conductive nature and are expressed by (12).

4.3.3 The external heat system model

In order to describe the structure of the mathematical model used for the Mod I external heat system a nomenclature has to be settled.

4.3.3.1 Temperatures, see fig. 4.3:5.

T_{AMB} = The ambient temperature

T_{A1} = The temperature of the air leaving the air/fuel control

T_{A2} = The temperature of the air prior to the blower

T_{A3} = The temperature of the air after the blower

T_{A4} = The temperature of the air after the preheater

T_{A5} = The temperature of the air up-stream the CGR inlet

T_{A6} = The temperature of the air prior to the combustor

T_{AA} = The temperature of the atomizer air

T_{C1} = The temperature of the combustion gas in the combustor

T_{C2} = The temperature of the combustion gas after the first tube row of the heater

T_{C3} = The temperature of the combustion gas before the second tube row of the heater

T_{C4} = The temperature of the combustion gas after the second tube row of the heater

T_{C5} = The temperature of the combustion gas before the preheater

T_{C6} = The temperature of the combustion gas after the preheater
(exhaust gas)

T_{BL} = The temperature of engine block

T_{WG} = The temperature of the working gas

T_{TUBE} = The heater tube temperature

4.3.3.2 Heat flows, see fig. 4.3: 5.

<u>Symbol</u>	<u>Heat flow from - to</u>
\dot{Q}_{10}	Combustion gas before the heater - engine block
\dot{Q}_{11}	Combustion gas before the heater - cylinders
\dot{Q}_{20}	Combustion gas between tube rows - engine block
\dot{Q}_{21}	Combustion gas between tube rows - cylinders and regenerators
\dot{Q}_{30}	Combustion gas after the heater - engine block
\dot{Q}_{31}	Combustion gas after the heater - cylinders and regenerators
\dot{Q}_{40}	Preheated air - surroundings through the fuel nozzle
\dot{Q}_{50}	Preheated air - surroundings through the housing
\dot{Q}_{60}	Preheater matrix - surroundings
\dot{Q}_{61}	Combustion gas after the heater - preheater matrix

4.3.3.3 Pressure levels

P_{AMB} = The ambient pressure

P_{A2} = The pressure prior to the blower

P_{A3} = The pressure after the blower

- $P_{A3.5}$ = The pressure after the intake manifold
- P_{A4} = The pressure after the preheater
- P_{A0} = The pressure prior to the combustor
- P_{C1} = The pressure in the combustion volume
- P_{C4} = The pressure after the heater
- P_{C0} = The pressure before the exhaust manifold

4.3.3.4 Calculation logic, CGR system

Step

1. The calculation is started by giving T_{C4} the value of T_{TUBE} . This is done to define a start value for the big iteration loop.
2. \dot{Q}_{30} and \dot{Q}_{31} can now be calculated as the temperature difference across the insulation layer is defined as $T_{C4} - T_{RI}$ and $T_{C4} - T_{WG}$ respectively.
3. At this point \dot{Q}_{61} is initially given estimated value. T_{C5} is calculated by reducing the heat content of the combustion gas after the heater (T_{C4}) by \dot{Q}_{30} , \dot{Q}_{31} and \dot{Q}_{61} .
4. The input requirements from the preheater program are now fulfilled and values for T_{C6} , T_{A4} and \dot{Q}_{61} are calculated. If the difference between the old and the new temperature values is greater than $0,05^{\circ}\text{C}$ a new calculation in the preheater program is made.
5. At this point the heat balance of the preheater is settled for the given value of T_{C4} .
6. As T_{A4} , T_{C5} and % CGR is given T_{A5} can be calculated.
7. Next to be calculated are \dot{Q}_{40} and \dot{Q}_{50} and this can be done as T_{A5} and T_{AMB} are known.

8. T_{A6} are calculated by reducing the heat content corresponding to T_{C5} by \dot{Q}_{40} and \dot{Q}_{50} .
9. In the combustor an initial value of T_{C1} is estimated and the heat flows through the ceramic stone, \dot{Q}_{10} and \dot{Q}_{11} , are settled for this value of T_{C1} . As this calculation was based on an estimated T_{C1} a new calculation based on T_{A6} , \dot{Q}_{10} , \dot{Q}_{11} and input values (\dot{m}_{fuel} , \dot{m}_{air} , \dot{m}_{aa} , T_{AA} and % CGR) is performed. This calculation is repeated until T_{C1} converge.
10. Knowing the mass flow and the geometrical data of the heater the Λ for the first tube row can be calculated. The Λ calculation is followed by a T_{C2} calculation.
11. The heat flow through the insulating material between the tube rows (\dot{Q}_{20} and \dot{Q}_{21}) are calculated from T_{C2} , T_{BL} and T_{WG} .
12. Next to be calculated are T_{C3} and this can be done as \dot{Q}_{21} , \dot{Q}_{20} and T_{C2} are known.
13. The combustion gas temperature is decreased further by the passage of the second tube row. The temperature after the heater T_{C4} is calculated the same way as T_{C2} .
14. This is the end of the big loop. If the difference between the new and the old T_{C4} is greater than $0,05^{\circ}\text{C}$, the old T_{C4} is replaced by the new T_{C4} and the loop starts from the beginning again.
15. η_B can now be calculated by the following expression:

$$\eta_B = \frac{\dot{m}_{tot} (h_{C1} - h_{C2} + h_{C3} - h_{C4}) + \dot{Q}_{11} + \dot{Q}_{21} + \dot{Q}_{31}}{\dot{m}_{fuel} \cdot H_{u,fuel}}$$

where \dot{m}_{tot} = The total mass flow through the heater

h_{Ci} = The entahlpy of the gas at the point where the

gas temperature is T_{ci}

\dot{m}_{fuel} = The fuel mass flow

Hu_{fuel} = The calorific heat value of the fuel

4.3.3.5 Pressure drop calculations

The pressure drop of the external heat system is calculated when the heat balance of the system is settled. This means that all temperature are quantified.

Pressure drop

$P_{A3} - P_{A3.5}$

$P_{A3.5} - P_{A4}$

$P_{A4} - P_{A6}$

$P_{A6} - P_{C1}$

$P_{C1} - P_{C4}$

$P_{C4} - P_{C6}$

$P_{C6} - P_{AMB}$

Calculation principle

Intake manifold. Estimated value

Pressure drop across the preheater matrix
see 4.3.2.1 expression (3)

Ejector nozzle pressure drop.
Turbulent pressure drop. $Eu = 1$

Swirler pressure drop. Semi-empirical
expressions

Heater pressure drop. First row turbulent
 $Eu = f(Re)$. Second row laminar

Preheater pressure drop combustion gas
side. See 4.3.2.1 expression (3)

Exhaust manifold and exhaust pipe.
Estimated value

4.3.4 MOD I design specification for the external heat system

Fuel mass flow = 0.3 - 4.5 g/s (gasoline)

Burner air flow = 7,5 - 75 g/s

Total pressure drop < 6 KPa with CGR

" < 14 KPa with EGR

Atomizer air flow < 1,5 g/s

External heat system efficiency (η_B) > 0,85 (mean value based on the CVS cycle)

The external heat system shall be optimized for the CGR case.

4.3.5 ~~Input~~ data for the external heat system heat balance program

In order to use the heat balance program (see section 4.3.3) some calculated input data are required. The data are based on the lay-out of the external heat system.

4.3.5.1 The heater

Number of tubes = 96

Front row

No surface enlargement

Active tube length = 150 mm

Distance between tube centres = 5.50 mm

Rear row

Surface enlargement: Plate fins

Active tube length = 107.5 mm

Distance between tube centres = 10.54 mm

Fin length = 10 mm

Fin thickness = 0.6 mm

Distance between fins = 0.7 mm

Based on this data for the two rows have been calculated.

$$\Delta \text{ Front row} = K_1 / \dot{m}^n$$

$$\Delta \text{ Rear row} = K_2 / \dot{m}^m + K_3$$

4.3.5.2 The combustor

The input needed from the combustion system is the % CGR and the pressure drop over the load range. Based on NO_x formation rate calculations and experiences from the Mod I combustor development program a CGR system has been chosen. This system is characterized by the % CGR and pressure drop curve given in fig. 4.3:6.

4.3.5.3 The insulation

The thickness of the insulation layer can not be chosen arbitrarily as the available space is limited. In the lay-out work of the external heat system insulation layer thicknesses at different places have been proposed. These data has been used in the heat balance calculations. Insulation data are shown in table 4.3:1.

4.3.5.4 Preheater plates

In order to reduce the number of variables the P40 preheater plate was chosen for Mod I. This plate has a proven design as far as internal flow pattern, heat transfer and pressure drop are concerned. This means that the only free parameter in the preheater calculation is the number of plates.

4.3.5.5 Calculation of η_B

The mean value of the external heat system efficiency (η_B) is specified to $\eta_B = 0,85$ over the CVS-cycle. As calculating η_B for every time step of the cycle would require too much computer time the CVS-cycle is approximated by seven stationary load points. This points are shown in table 4.3:2 below.

Fuel flow (g/s)	Residence time (s)
0,4	339
0,6	196
0,8	343
1,0	214
1,5	198
2,1	60
2,7	22

Table 4.3:2

The external heat system efficiency is calculated for these seven points and the mean value is given by

$$\bar{\eta}_B = \frac{\sum_{j=1}^7 \dot{m}_{fj} \cdot (time)_j \cdot \eta_{Bj}}{\sum_{j=1}^7 \dot{m}_{fj} \cdot (time)_j}$$

4.3.6 Preheater calculations

In order to explore the theoretical limits of the efficiency of the external heat system the first calculation was made assuming a temperature efficiency on the air side of 100%. This means that the preheated air T_{A4} has reached the temperature of the incoming combustion gas (T_{C4}). The radial and the axial conductive heat flows in the preheater are given the value of zero. The results from the calculation are presented in table 4.3:3 and fig. 4.3: 7. As can be seen from the curve in fig. 4.3:7, the efficiency is very drastically reduced at lower loads. This is explained by the fact that the losses to the surroundings and the engine block are almost independent of load. Thus the relative losses are increased with decreasing load. Another reason for the declination is the influence of the atomizer air. This mass flow is very small (1,5 g/s) but at lower loads it causes a significant difference in mass flow between the combustion gas side and the air side of the preheater. This unbalance increases the exhaust gas losses and thus decreases the efficiency.

4.3.6.1 Number of plates

As the number of plates is the only free variable of the preheater, calculations were performed with different numbers. The heat losses that were calculated for the "ideal" preheater were also used at these calculations. The results from calculations with six different sets of plates are presented in table 4.3:3. The pressure drops at maximum load are also shown. The efficiency is decreasing with the number of plates at lower loads (≤ 1 g/s) due to conduction losses. At higher loads the effect of increasing preheater area dominates and the efficiency goes up with increased plate number. However the mean value of the efficiency have a maximum around 1100 plates.

In order to fulfil the pressure drop specification of the external heat system the pressure drop across the preheater has been maximized to

1500 Pa. As can be seen from table 4.3:3 the pressure drop is increasing with decreasing number of plates. From the pressure drop point of view the number of plates should exceed 1200. This means that the most suitable number of plates is 1200.

4.3.6.2 Calculated performance

As the calculations presented above were based on some approximate assumptions a more accurate calculation were performed with the chosen preheater. The number of load points were increased and the heat losses were calculated. The total pressure drop of the preheater, combustor and heater was calculated for all load points. The results are shown in fig. 4.3:8.

The average external heat system efficiency became 86.09 % fig. 4.3:7, which means that the objectives would be exceeded with 1% with the chosen preheater according to the used model.

4.3.7 EGR or CGR?

Two alternative gas recirculation systems have been developed for Mod I, the CGR system and the EGR system. The final choice shall be based on results from the Mod I combustor development program and the influence on engine performance of the different systems. Thus the efficiency and the pressure drop of the external heat system have been calculated for the EGR system and the CGR system. The performance of a system with no gas recirculation has also been studied.

4.3.7.1 Input data

The 1200 plate preheater presented in section 4.3.6 was optimized for the CGR case. In order to make a fair comparison between the EGR system and CGR system calculations were made with the 1200 plate preheater and a 1420 plate preheater. The latter is the biggest preheater that is feasible with the given geometrical restrictions. The preheater plate is the same in both cases (P40 plate).

The CGR/EGR characteristics and the air excess used in the calculations are shown in fig. 4.3:9.

4.3.7.2 Preheater calculations

The external heat system efficiency and the pressure drop across the two preheaters were calculated for the two recirculation systems. The "no recirculation" system was calculated with the 1200 plate preheater. The results are shown in fig. 4.3:10 and table 4.3:4 and 4.3:5.

As can be seen from table 4.3:4 the smaller preheater is best at lower loads and the bigger preheater is best at higher loads independent of recirculation system. However the cross-over load is 1,5 g/s for the CGR system and 1,0 g/s for the EGR-system.

The efficiency of the EGR system is about 2% units lower than CGR system efficiency at a mean load point of the CVS cycle. The efficiency difference between the CGR system and the "no recirculation system" is very small ~0,1 % units.

The preheater pressure drop is presented for two loads in table 4.3:4. The pressure drop difference at the lower load is explained by the higher mass flow in the EGR case. At the higher load the % EGR and % CGR are

zero see fig. 4.3:4, which means that the preheater mass flow is the same in both cases. It is worth noticing the small gain in pressure drop with the bigger preheater.

In the previous section it was concluded that the 1200 plate preheater was the most suitable for the CGR system. In order to determine the optimal preheater for the EGR system CVS cycle simulation calculations were performed with the two preheaters. In the CVS cycle simulations the entire vehicle is integrated in the model. In the calculations the external heat system pressure drop is given the same value in both cases. This is a minor approximation as the difference in preheater pressure drop is very small and the preheater pressure drop represents just a small part of the total pressure drop of the external heat system.

The results are given as relative mileage values for the different parts of the CVS cycle. Table 4.3:6. There is practically no difference in mileage between the two systems. At the Metro part of the CVS-cycle the small preheater has a small advantage over the big one but the situation is the opposite in the Highway part. In the combined cycle they give the same results. However the small preheater is the best choice as it reduces the mass of the system and, owing to this, the cold start penalty (CSP).

4.3.7.3 CGR and EGR mileage

In order to quantify the difference in vehicle performance with the two alternative gas recirculation systems a CVS-simulation calculation was performed. The latest engine data and some results from the combustor development program were used as input data. The results are presented in table 4.3.7. For comparison the performance of a system with no gas recirculation was also calculated. As can be seen from the results a gain in mileage of ~ 0.8 miles/gallon can be achieved with the CGR-system compared with the EGR-system. Another interesting point is that the difference between the CGR-system and the system with no gas recirculation is so small, ~ 0.1 miles/gallon.

TABLE 4.3:1

Insulation data for the heat flows in entire heat system.

Heat flow (Q) number	Heat transfer area (m^2)	Thickness of Insulation (mm)	Insulation material
10	$5.45 \cdot 10^{-3}$	80	Mackechnie H.T.2 (160 kg/m ³)
11	$2.08 \cdot 10^{-2}$	20	" "
20	$4.48 \cdot 10^{-2}$	60	" "
21	$1.29 \cdot 10^{-2}$	20	" "
30	$4.80 \cdot 10^{-2}$	60	" "
31	$2.36 \cdot 10^{-2}$	20	" "
50	$4.57 \cdot 10^{-1}$	50	" "
60	$1.564 \cdot 10^{-1}$	35-0	" "
61	$1.33 \cdot 10^{-1}$	0-50	" "
40	$1.65 \cdot 10^{-3}$	70	steel

External heat system

Insulation data

Heat flow number	Heat transmission area (m ²)	Insulation - thickness (mm)	Insulation type	λ x) W/mh
\dot{Q}_{10}	$5.45 \cdot 10^{-3}$	80	Mackechnic HT 2 160 kg/m ³	0.202
\dot{Q}_{11}	$2.08 \cdot 10^{-2}$	20	"	0.279
\dot{Q}_{20}	$4.48 \cdot 10^{-2}$	60	"	0.139
\dot{Q}_{21}	$1.29 \cdot 10^{-2}$	20	"	0.279
\dot{Q}_{30}	$4.80 \cdot 10^{-2}$	60	"	0.1
\dot{Q}_{31}	$2.36 \cdot 10^{-2}$	20	"	0.2
\dot{Q}_{50}	$4.57 \cdot 10^{-1}$	50	"	0.086
\dot{Q}_{60}	$1.564 \cdot 10^{-1}$	35-0	"	0.113
\dot{Q}_{61}	$1.33 \cdot 10^{-1}$	0-50	"	0.139
\dot{Q}_{40}	$1.65 \cdot 10^{-3}$	70	Steel	17.0

x) The different λ values correspond to different temperatures.

The heat flow numbers are referring to fig. 4.3.5 in the design assessment report. The insulation has a wool like structure and is confined between walls of sheet metal.

2. The emission data discussed at the task team meeting ($\text{NO}_x \sim 0.2$ g/mile, $\text{CO} \sim 1.0$ g/mile and $\text{HC} \sim 0.1$ g/mile) are calculated values based on emission measurements in the AP 80 scale combustor rig. The big reduction in NO_x emissions compared to the values achieved with the P40 Opel is explained by some reduction in EINO_x and the mileage increase expected from the Mod 1 - Spirit.

3. The design of the CGR-combustor for the reference engine has not yet been backed up by tests. Therefore it is not advisable to reduce the mixing channel height for the Mod 1 combustor at this stage. If however the channel height could be reduced the freed volume should preferably be used in the combustor or as insulation volume rather than to lower the engine.

TABLE 4.3:3

ORIGINAL PAGE IS
OF POOR QUALITY η_B with different number of preheater plates and CGR.

Fuel flow (g/s)	Time at point (sec)	η_B ideal prehea- ter	η_B 1500 plates	η_B 1400 plates	η_B 1300 plates	η_B 1200 plates	η_B 1100 plates	η_B 1000 plates
0.4	339	84.0	77.53	77.83	78.12	78.42	78.71	79.00
0.6	196	87.9	82.46	82.66	82.86	83.04	83.21	83.37
0.8	343	89.7	84.76	84.88	85.01	85.11	85.20	85.27
1.0	214	90.8	86.14	86.22	86.28	86.32	86.34	86.34
1.5	198	92.4	87.75	87.73	87.69	87.63	87.54	87.41
2.1	60	93.2	88.46	88.37	88.26	88.13	87.95	87.74
2.7	22	93.6	88.62	88.48	88.32	88.13	87.90	87.62
Averaged η_B		90.29	85.27	85.35	85.41	85.45	85.47	85.47
Δp_{\max} (Pa)	$\dot{m}_f = 4.5\text{g/s}$		1185	1282	1397	1533	1699	1906

ORIGINAL PAGE IS
OF POOR QUALITY

TABLE 4.3:4

η_B versus fuel flow for two different preheaters with EGR, CGR and no EGR/CGR.

Fuel flow g/s	η_B with preheater for CGR 1200 plates			η_B with max. preheater 1420 plates	
	NO EGR/CGR	EGR	CGR	EGR	CGR
0,2	69.32	66.23	68.81	65.44	68.33
0.4	79.98	77.86	79.72	77.33	79.21
0.6	84.07	81.88	83.90	81.62	83.53
0.8	86.17	83.77	86.05	83.71	85.81
1.0	87.44	84.81	87.34	84.90	87.20
1.5	88.89	85.66	88.82	86.02	88.86
2.0	89.50	85.79	89.40	86.30	89.56
2.5	89.59	86.20	89.42	86.78	89.58
3.0	89.51	86.54	89.32	87.14	89.66
3.5	89.36	87.11	89.17	87.71	89.58
4.0	89.16	87.66	88.99	88.21	89.44
4.5	88.86	88.05	88.77	88.60	89.27
5.0	88.53	88.53	88.53	89.07	89.07

TABLE 4.3:5

ORIGINAL PAGE IS
OF POOR QUALITY

Pressure drops in Pa for preheaters

Fuel flow	1200 plates		1420 plates	
	CGR and no gasrecirculation	EGR	CGR and no gasrecirculation	EGR
0,8 g/s	266	391	223	329
5,0 g/s	1680	1680	1389	1389

TABLE 4.3:6

Relatively mileage values

Number of preheater plates cycle	1200	1420
Metro	1	0.9985
Highway	1	1.0023
Metro/Highway	1	0.9997

TABLE 4.3:7

Miles per gallon with different systems. The cold start penalty is excluded.

Cycle	No gas recirculation	EGR	CGR
Metro	25.47	24.74	25.36
Highway	35.86	34.63	35.71
Metro & Highway	29.29	28.39	29.16

ORIGINAL PAGE IS
OF POOR QUALITY

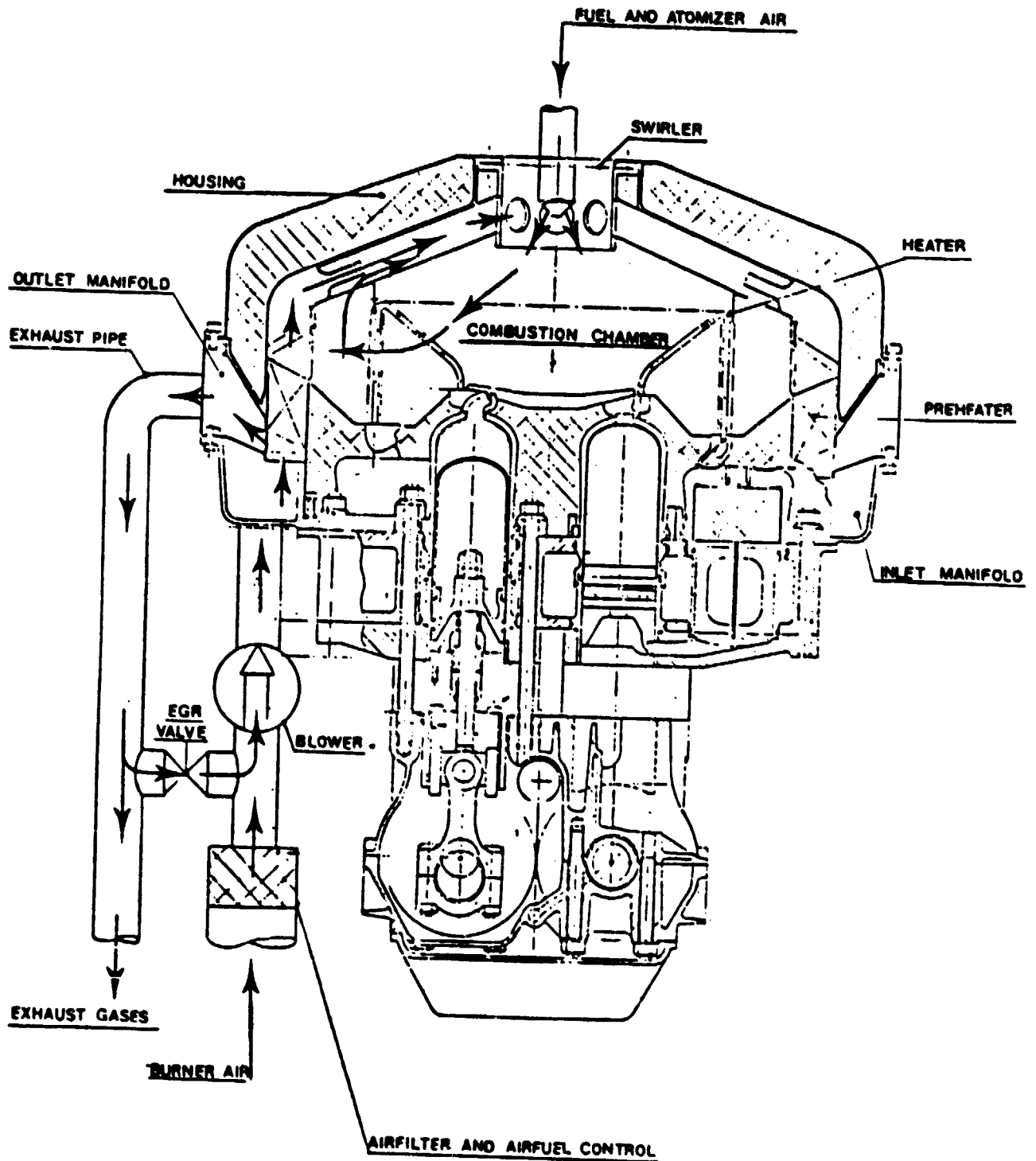


Figure 4.3 : 1

ORIGINAL PAGE IS
OF POOR QUALITY

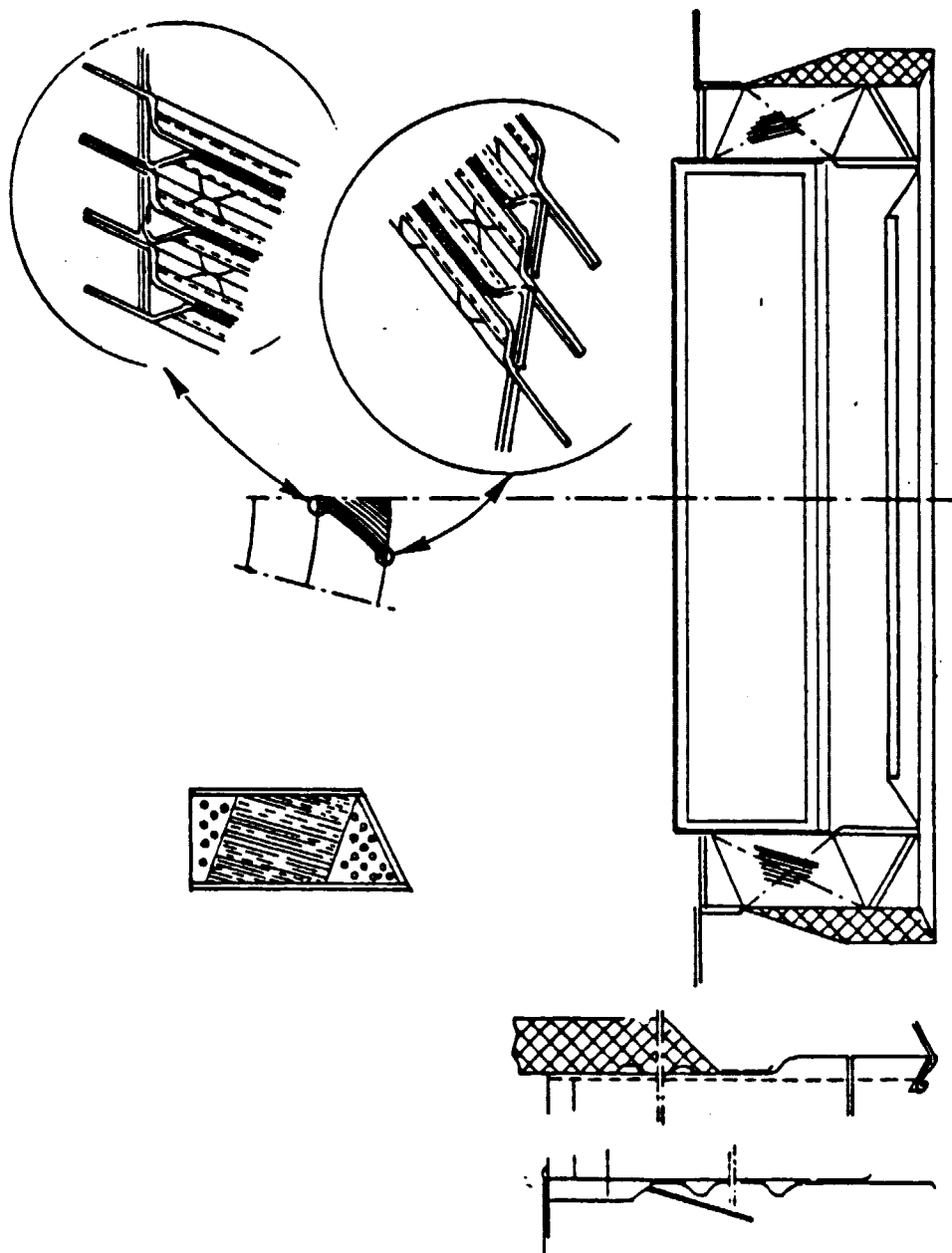
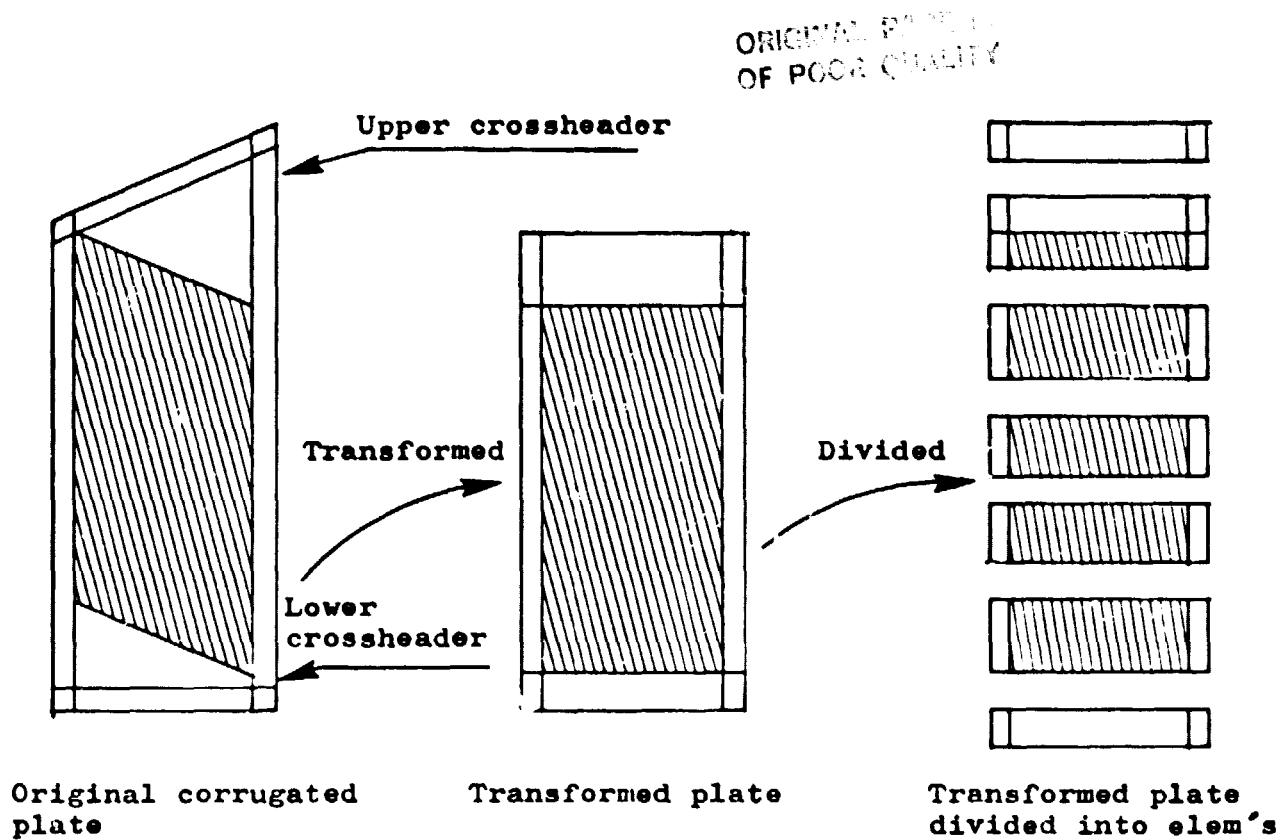


Figure 4.3:2 Preheater and preheater plates.



Heatflux directions on plate element

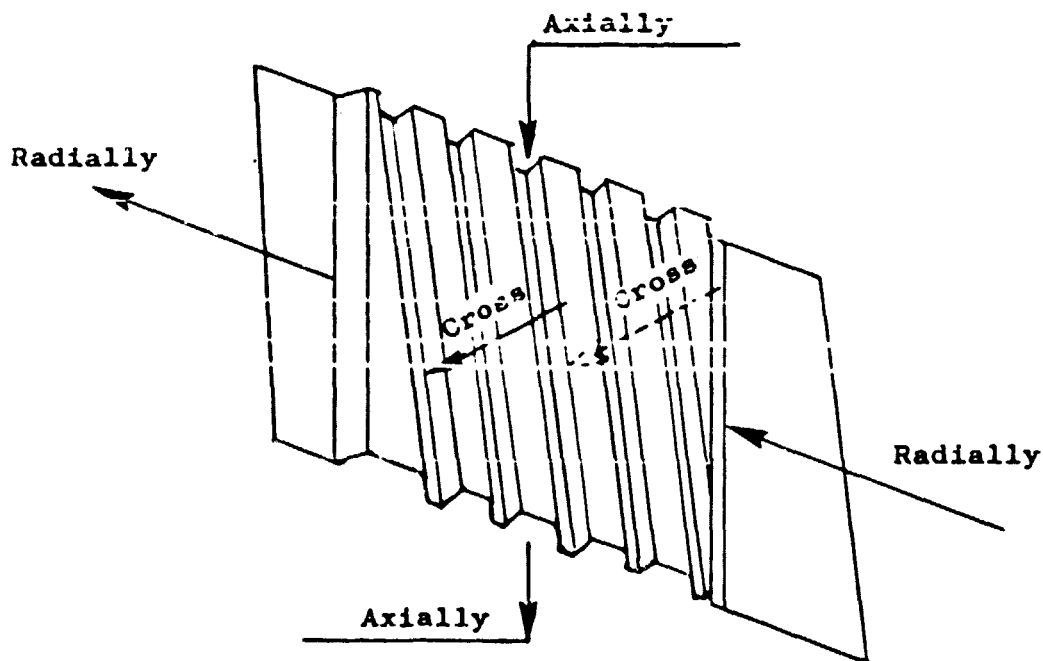


Figure 4.3:3 Preheater Plate.

ORIGINAL DESIGN
OF POOR QUALITY

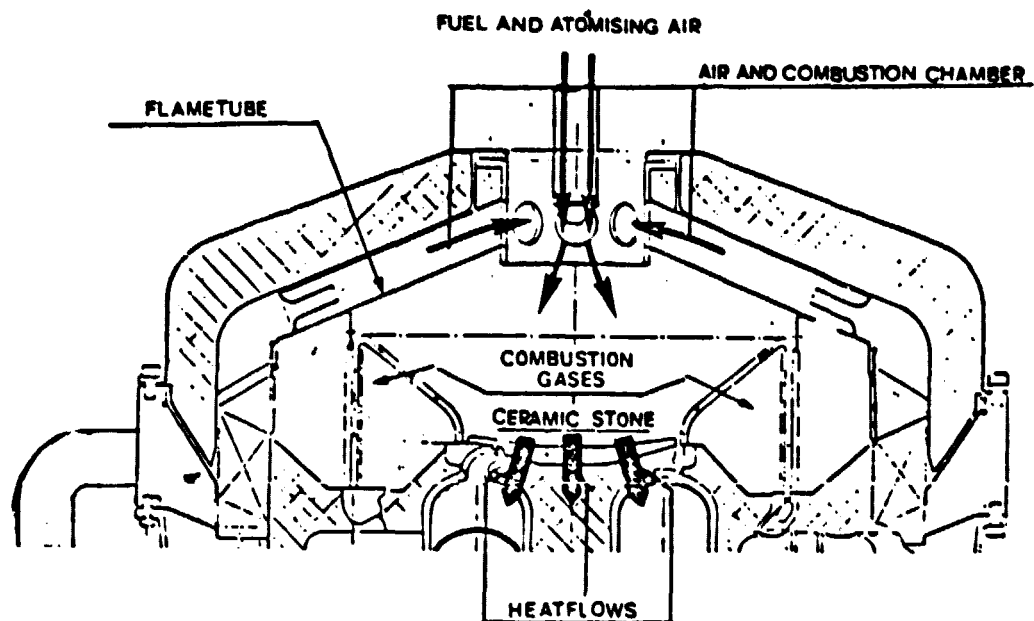


Figure 4.3 : 4 Combustion Chamber

Figure 4.3 : 5 Temperatures and Heat Flows in the
Model for the External Heat System

Figure 4.3 : 6 % OGR and Pressure Drop vs Air Flow

were removed from this report because they contained
Patentable Information

ORIGINAL L.
OF POOR QUALITY

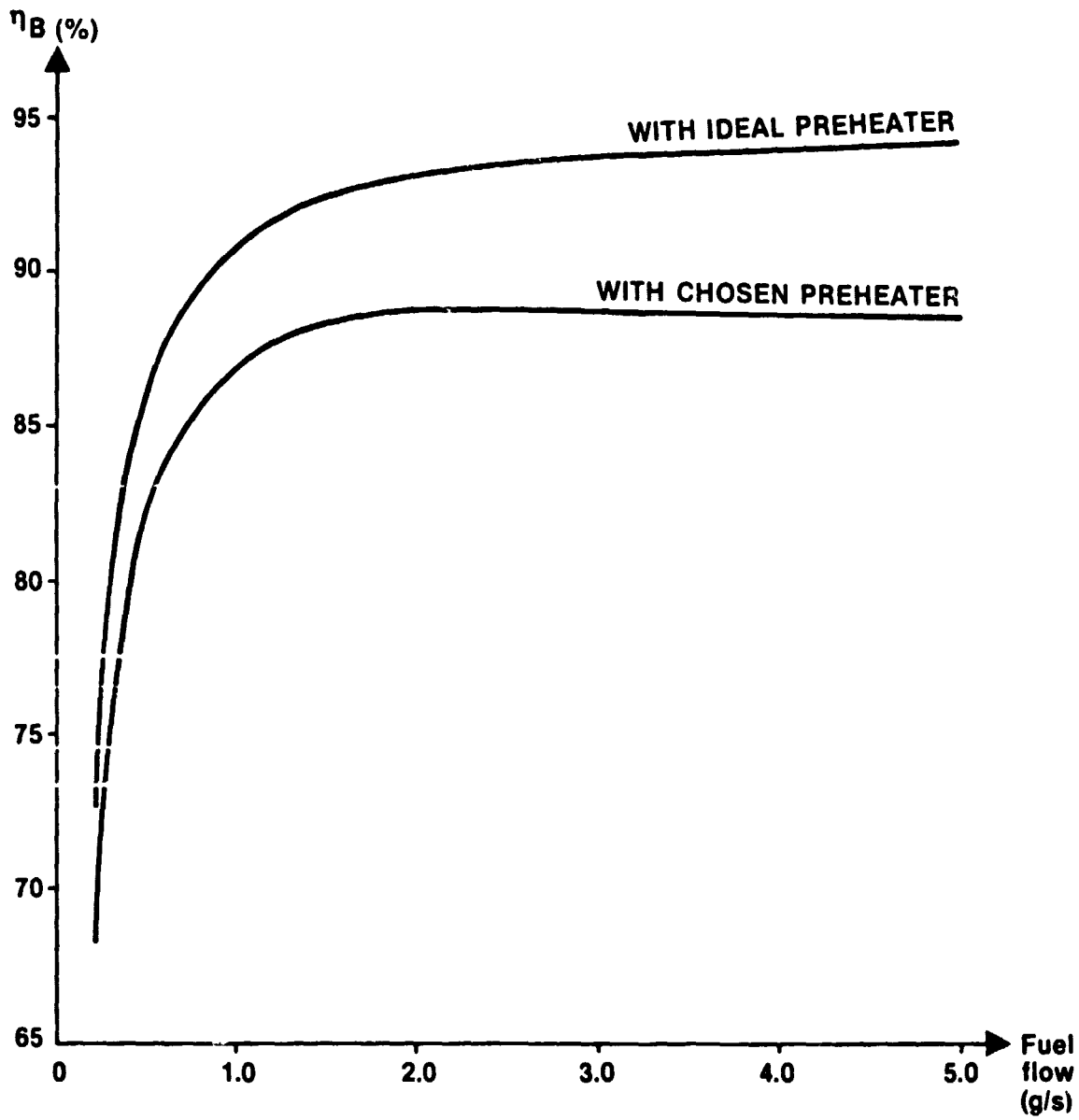


FIG 4.3:7 CALCULATED EFFICIENCY [η_B] FOR EXTERNAL HEATSYSTEM

ORIGINAL PAGE IS
OF POOR QUALITY

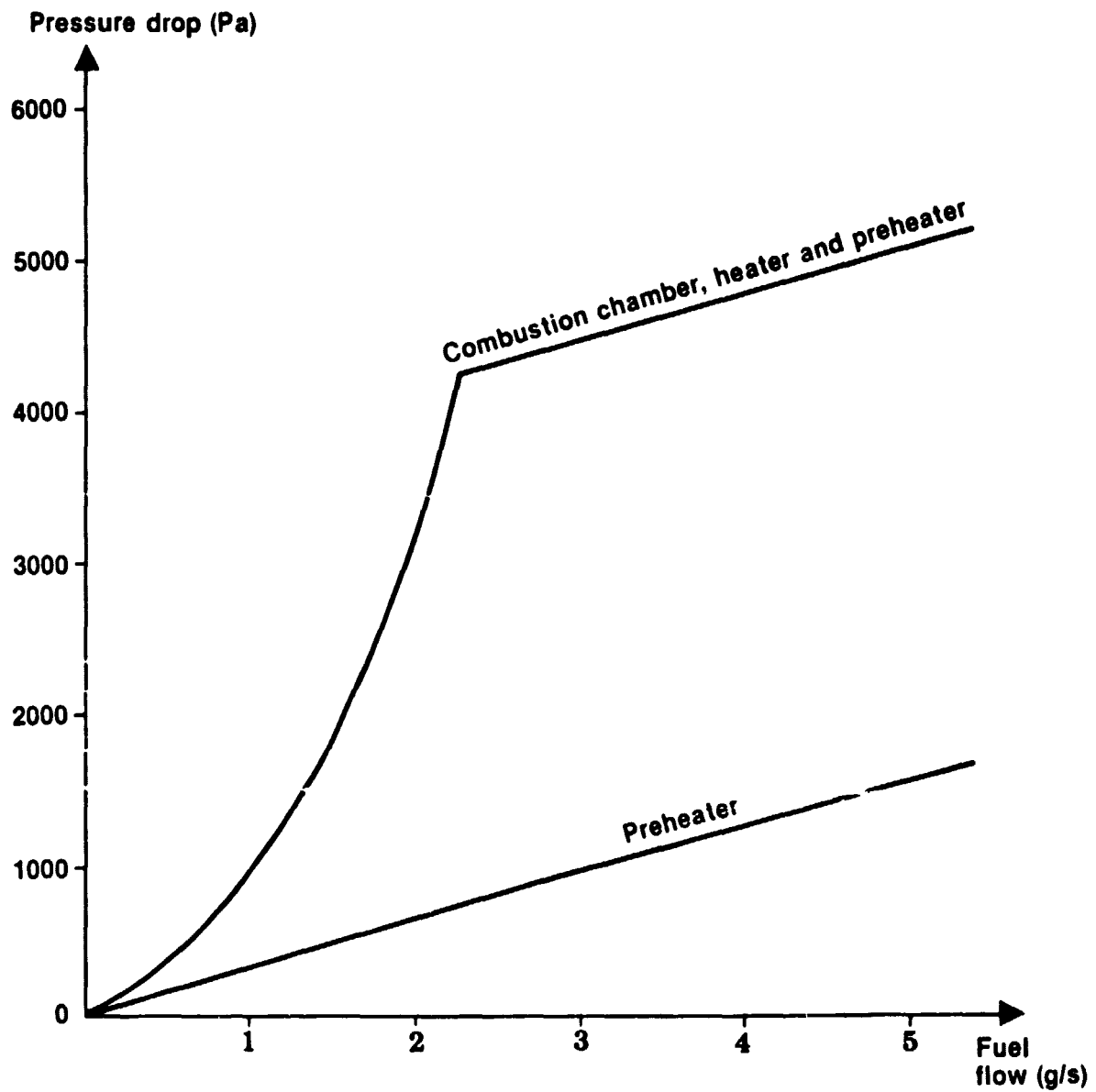


FIG 4.3:8 CALCULATED PRESSURE DROP FOR EXTERNAL HEAT SYSTEM

ORIGINAL PAGE 13
OF POOR QUALITY

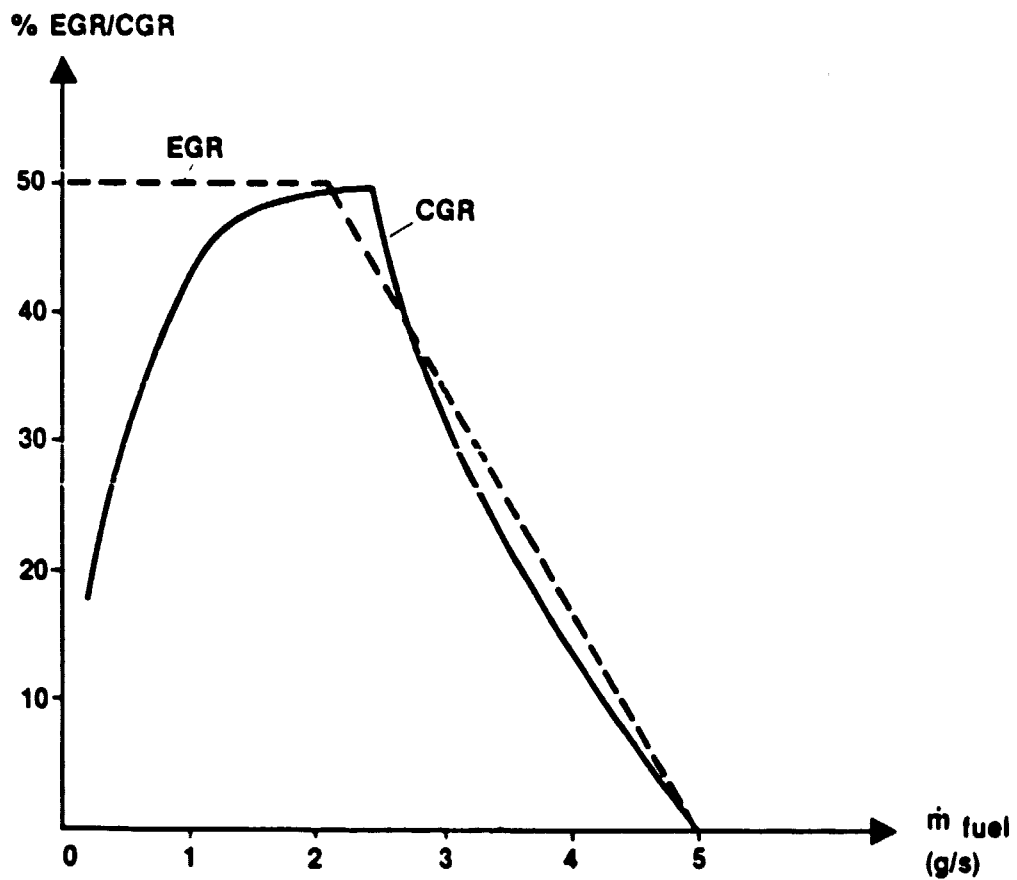
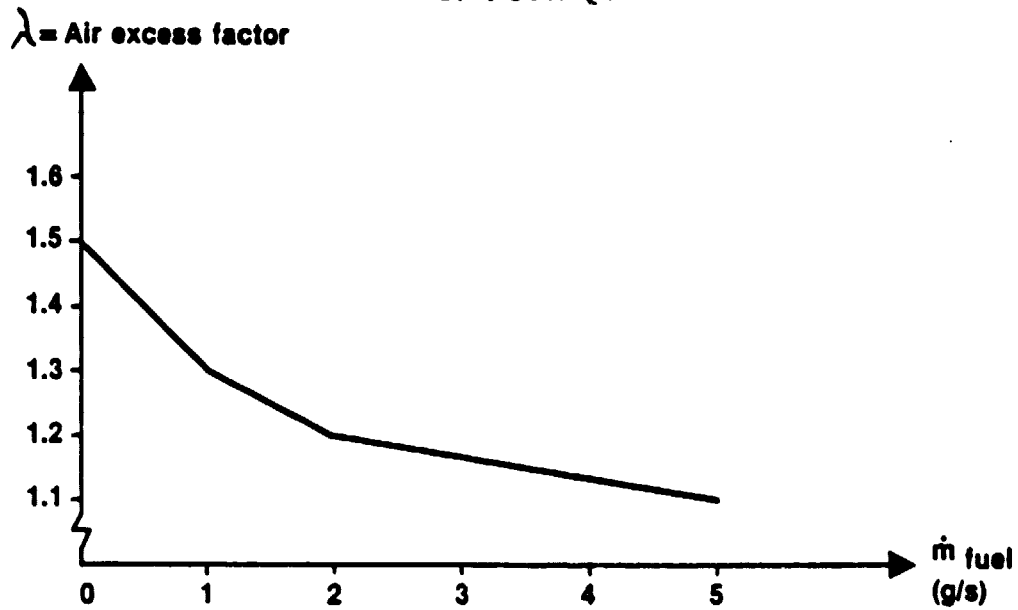


FIG 4.3:9 AIR EXCESS FACTOR AND % EGR/CGR VERSUS FUEL FLOW

ORIGINAL DESIGN
OF POOR QUALITY

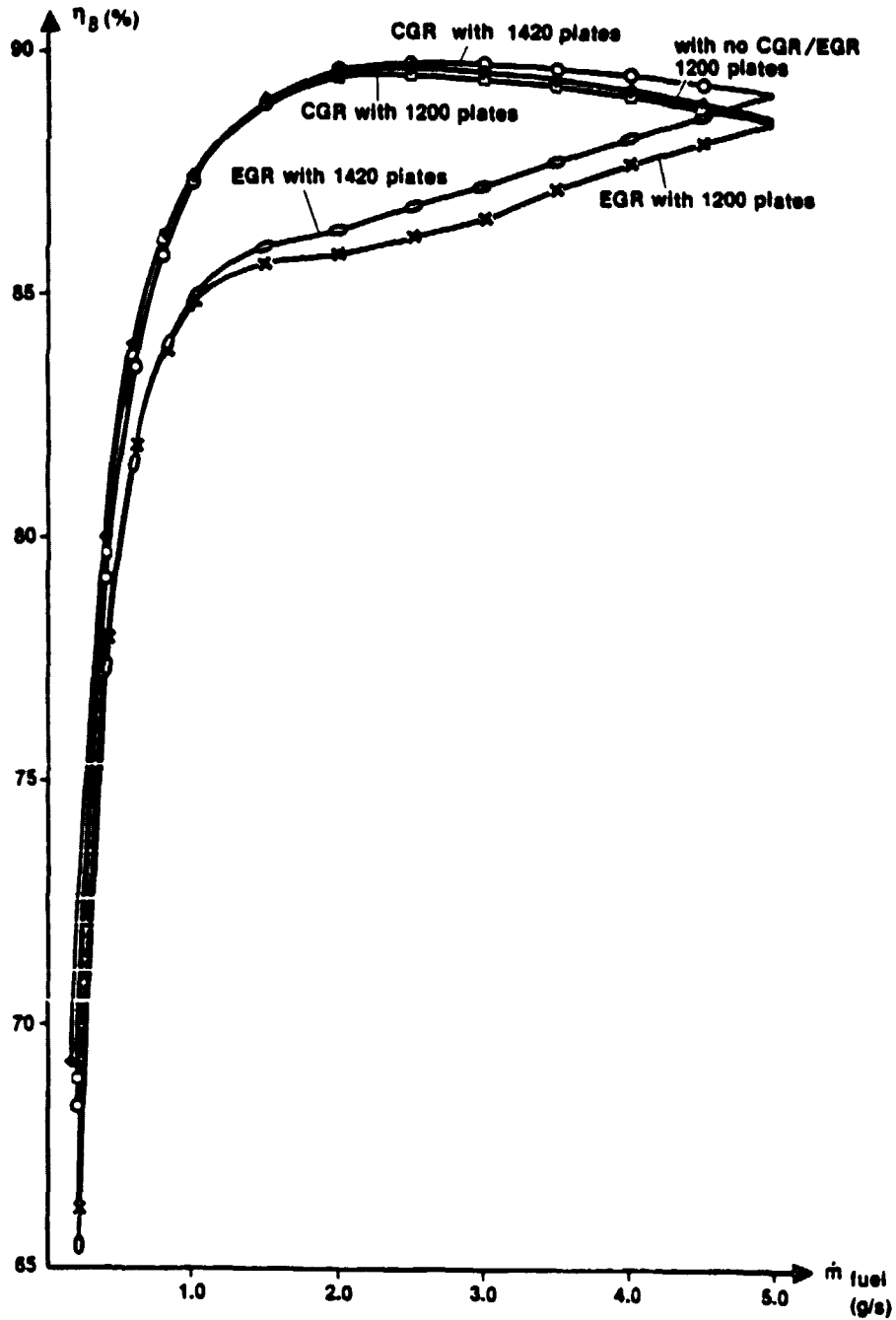


Figure 4.3:10

Calculated Efficiency $[\eta_B]$ of External Heat System with Two Different Preheaters for EGR, CGR and no Gas Recirculation

4.4 Flow distribution test. Air preheater.

Flow distribution in preheat π matrix is shown in drawing 1-73570.

The air preheater is an important component due to efficiency for the Stirling engine. The preheater matrix has been optimized due to height, width, pressure drop and temperature efficiency. In this calculations we have considered an equal mass flow distribution on air side and exhaust gas side in each element of the matrix.

The locations of the exhaust gas and air inlet pipes have a major effect on the flow distribution and thereby the efficiency for the preheater.

The test rig is designed and manufactured around a preheater matrix with dimensions according to MOD I external heat system.

The dimensions of the heat exchanger plates have the same size as P-40 engine preheater.

The matrix is located in a housing with O-ring-seals in the four corners.

The air inlet (1) and exhaust gas outlets (2) can be located independent of each other in different positions around the preheater matrix.

Above the preheater matrix on the air outlet side there will be a ring with 10 holes and with the same dimensions as the ejector nozzles, which gives part of the combustor pressure drop.

1. The fresh air from the blower is directed into the manifold, and air is distributed through the preheater matrix. The massflow is measured at the top of the matrix (air side) and after the ejector nozzle.
2. Air is sucked through the preheater matrix and the exhaust gas channel and the massflow of air is measured at the gas inlet side (hot side).

These measurements will be made at different circumferential locations at the out- and inlets and the shape and size of the channels will be adjusted till an even distribution is reached. The experientially formed channel will then be used on the engine.

4.4.1

Test results (Comp./Sub-system Dev. Ext. Heat System)

The External Heat System Drawing 0-S-1317 shows the air preheater with one air inlet duct and two exhaust gas outlets.

The exhaust ducts will have a span of approx. 90° . This arrangement will give an acceptable installation of the engine in the vehicle. The air inlet will be arranged according to the locations of the blower fan.

The flow distribution test showed a rather even distribution on the air side as well as on the combustion gas side within the preheater matrix. The maximum deviation is shown to be; (max flow/min flow)
air side 1.25 exhaust side 1.16 See fig. 4.4:1.

At hot conditions the deviation in mass-flow will decrease due to higher pressure drop between air inlet - air outlet preheater matrix as well as on the exhaust gas side.

Experience on P40 engines shows that the efficiency is not adversely affected by the above mentioned values.

Relative Flow Variation through Preheater
 Airflow 100 g/s Temperature = 24°C

ORIGINAL PAGE 13
 OF POOR QUALITY

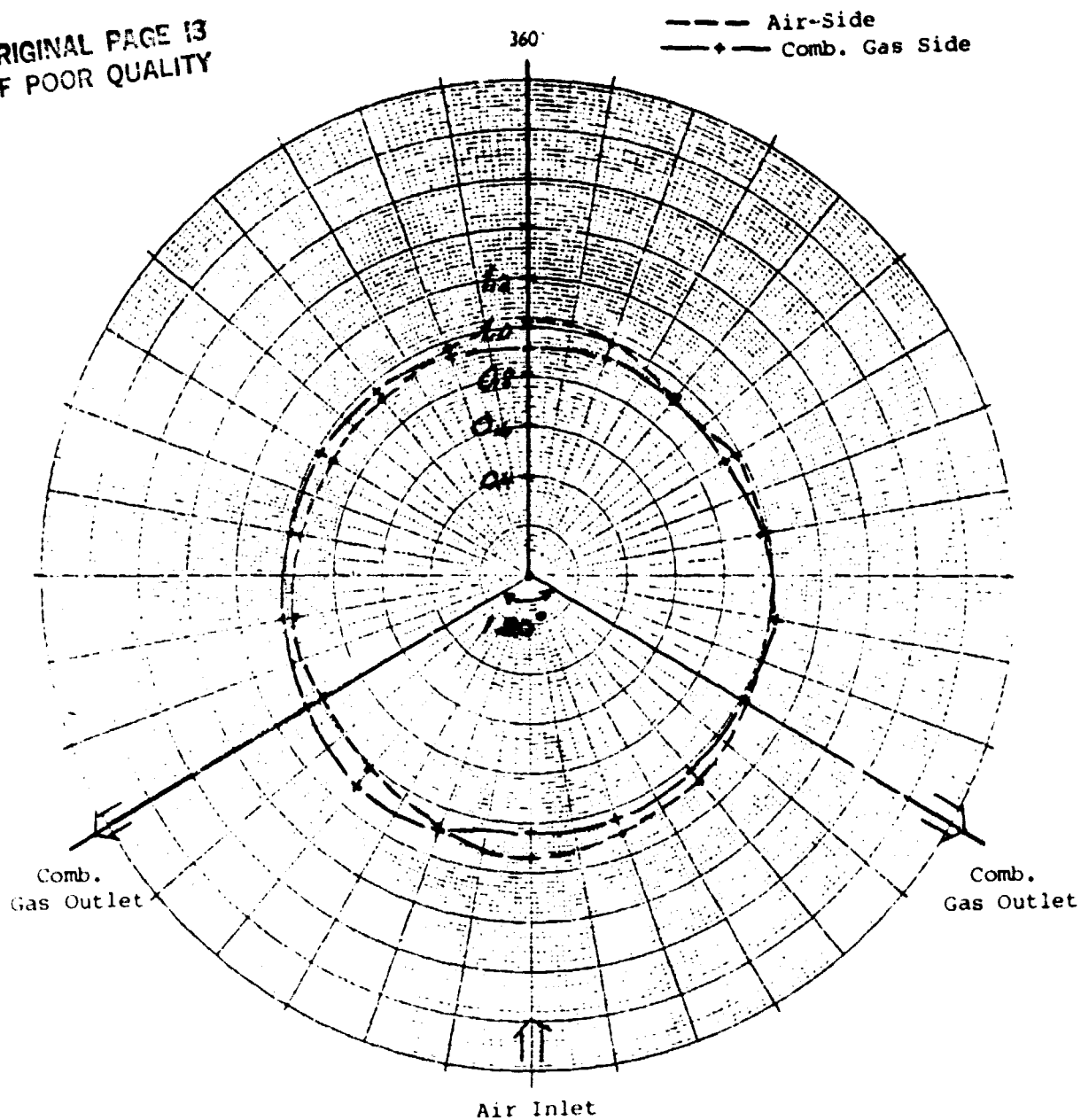


Figure 4.4:1 Relative Flow Variation in Preheater

4.5 Joining test. Air preheater matrix.

In the present design of the preheater the housing is welded to the mating flanges and preheaterhousing. In each corner an extra weld is applied to seal against overflow between the heatexchangers different flow passages. These welds constitute some problems with regard to endurance, since the material dimensions during temperature variations tends to set up stresses in these areas leading to fatigue.

To avoid problems of that kind, a design study was performed resulting in a proposal in which most of or all of the individual preheater plates will be brazed onto or in some way connected to the heatexchanger.

The plate will be prepared for brazing, stacked in a fixture and ground.

The preheater core will be brazed in a separate fixture which results in a stressrelieved unit to be integrated with the preheater housing previous to applying the insulation material.

4.6 Joining test. Air preheater matrix. Update

Completed tests have shown that the method to braze a preheater matrix has failed. The leakage from air side to exhaust gas side was too high, about 18% of full flow. The leakage was located to the corners of the matrix in the hot and cold ends.

According to the above mentioned results and P40 experience the seal elements will now be welded to the matrix.

The amount of weld-materials have decreased due to slight changes in design. See drawing No. 1-17054 in section 4.2.

4.6 Combustion tests

4.6.1 Redesign of the HT P40 involute air-combustor

It was concluded from the tests with the involute CGR-combustor within the HT P40 program that the angle between the radius and the centerline of the mixing channels was too large. Theoretically the flow should leave the channels at an angle of 30° to the radius but due to the velocity profile in the channel the angle became much larger. Thus the swirl generated was too strong and the pressure drop across the combustor chamber unnecessarily high which lowered the % CGR. (See report 79-0011C).

The new design was accomplished by making minor modification of the guide vanes on the original combustor in order to decrease the inlet angle, fig. 4.6:1. As a result of the modifications the % CGR increased by 10-15% units, see fig 4.6:2. As a consequence of the increased % CGR the NO_x emission was reduced, see fig 4.6:3. The combustor pressuredrop was not effected, fig 4.6:4. However, the flow pattern in the combustor was influenced by the reduced swirl intensity in the way that the angle of the central cone (fig 4.6:5) was decreased. As this has a bad influence on the axial temperature distribution the combustor height should be increased in some way.

4.6.2 Long term test

During the long term test most attention was paid to the flame tube and the atomizer. The combustor rig was dismounted four times during the test and pictures were taken on the flame tube, atomizer and rig heater head. Emissions were checked at three occasions. The test were performed at stationary load points within the range 0,9 - 3,15 g/s of fuel. The relative duration at the different loads is shown in fig. 4.6:6.

4.6.2.1 Flame tube

The flame tube is defined as the combustor surface that faces the flame. It consists of the flat ejector channel bottom which is made from thick (3 mm) sheetmetal. Fig. 4.6:1. This surface is cooled by the combustor air-CGR mixture in the channels. Very little scaling and no geometrical changes due to thermal expansion were noticed.

At the conical and the cylindrical parts (fig. 4.6:1) the scaling was more pronounced especially at the weld between the cone and cylinder ~~were~~ holes were observed after 1000 h. The cooling of these parts is attained by convective heat transfer to the CGR-flow and radiation.

4.6.2.2 Fuel nozzle

The fuel nozzle is combined with the ignitor fig. 4.6:7. Compressed air of 0.7 bar is used for fuel atomization. Some air is also used as shroud air to keep the ignitor clean. During the previous tests on involute ejector combustors fuel nozzle clogging was a big problem. The problem was caused by the intensive swirl and the large combustor inlet area. The redesign of the inlet angle decreased the nozzle built up to some extent. The present situation is that there is still a tendency of clogging but the rate of build up is low. Furthermore, the clogging does not seem to affect the combustion properties as far as emissions are concerned.

4.6.2.3 Rig heater head

The rig heater has the same geometrical shape as the engine heater. The main difference is that the rig heater is cooled by air flowing in one direction while the engine heater is cooled by H_2 or He with altering direction of flow. This difference reduces the ~~valve~~ of long term tests on rig heaters. However, the coloring of the first row gives a good hint of the temperature distribution on the heater. Scaling of the tube material has taken place at the lower part of the first row, indicating higher temperature. The direction of cooling air was from the first row to the second row.

4.6.3 Emissions

Emissions were measured at 0 hour, 536 hours, and 1009 hours. No significant variation due to accumulated hours could be noticed. In fig. 4.6:8 NO_x -emissions are shown as a function of load (fuel flow) at the three test occasions. The variations that were noticed were explained by differences in air inlet temperature and air fuel/ratio.

4.6.4 Tests on the second generation CGR-valve on the HT P40 involute CGR-combustor

4.6.4.1 Background

The main disadvantage with the CGR-system is that the pressure drop across the ejector jets tends to be very high at higher loads. In fig. 4.6:9 the pressure drop across the combustor (including the jets) and the heater on the HT P40 combustor rig is plotted against mass flow of air. The full load pressure drop of the HT P40 and MOD I is also shown in fig. 4.6:9.

The MOD I pressure drop is achieved by an extrapolation from the HT P40 curve. As can be seen from the figure the pressure drop of the HT P40 could be accepted but the MOD I pressure drop is too high and would affect engine performance and mileage.

One way of reducing the pressure drop is to by-pass some combustion air directly into the combustor without passing the ejector jets fig. 4.6:10.

The first by-pass valves were developed in the HT P40 program. The primary reason for by-pass valves in that program was not to lower the pressure drop at high loads but to reduce % CGR during start up (see report 79-0009 C). The HT P40 valves had on/off characteristics and gave very poor combustion when operated. These properties are acceptable during start up but not at steady state operation. As a consequence a new by-pass system had to be developed in the MOD I program.

4.6.4.2 By-pass valve design

It was concluded from the experiences from the HT P40 by-pass system that it is essential that the by-passed combustion air is very well mixed with the fuel.

The new valve was designed as a radial swirler with drilled holes fig. 4.6:11. The throttling was achieved by a concentric ring in which holes were drilled in the same pattern as on the swirler. By turning this ring the open area could be continuously varied. The surface between the swirler and the ring was conical in order to minimize the leakages due to thermal expansion.

4.6.4.3 Freeburning tests

The by-pass valve was mounted on top of the HT P40 involute CGR combustor in the freeburning rig. Freeburning tests were performed in order to visually study the influence on the combustion processes of the valve. The lean ignition limits was also settled for the combustor with the valve open and closed.

It was found that the operation of the valve had very little influence on temperature distribution and flame stability when the dummy heater head was attached. However, without the dummy heater the flame stability was acceptable with the valve open but very bad with the valve closed.

Ignition tests were performed with diesel oil and gasoline. The ignitor and the fuel nozzle were one part design (fig. 4.6:7) and the spark was generated in a capacitive device at a frequency of ~ 3 Hz. The results from the ignition tests is presented in fig. 4.6:12-13. It is worth noticing the big difference between open and closed valve with diesel fuel. However, the ability to ignite the two fuels is good with by-pass valve closed.

4.6.4.4 Combustor rig tests

Combustor rig tests were performed in order to test the valve at high temperatures. During the tests emissions and combustor pressure drop were recorded.

4.6.4.4.1 Tests at steady state

Initial combustor rig tests were performed with A: by pass-valve open and B: by pass-valve closed. The influence on the pressure drop of the combustor is shown in fig. 4.6:14. As can be seen from the curves the pressure drop is reduced by a factor $\sim 2,2$ with by-pass valve open and this indicating an area increase of $\sim 50\%$. However, the nominal area increase is $\sim 86\%$, which means that only $\sim 60\%$ of the by-pass valve area is effective.

The % CGR is also reduced when the by-pass valve is open fig. 4.6:15 and as a consequence the NO_x emissions is increased fig. 4.6:16. The other emissions (CO and HC) were not effected.

Tests were also performed with the valve partly opened in order to find out if the throttling of the valve would cause any irregularities in the combustor performance. The valve setting was defined by the combustor pressure drop. Results from two loads are shown in fig. 4.6:17-18. As can be seen no major irregularities occur. The EICO varies within reasonable limits. EI NO_x are increased continuously with decreasing % CGR.

4.6.4.4.2 Transient tests

The first transient test was performed at constant load with very fast valve operation. The valve was opened and closed by a double acting pneumatic piston. The compressed air passed through an electrically operated valve which was governed by a time relay. The valve was scheduled to stay open for ~4,3 seconds and then momentarily closed. The duration at closed mode was also ~4,3 seconds and then the valve was momentarily opened and the sequence was repeated, fig. 4.6:19. The objective of this test was to find out if very rapid valve operations would cause instability of the flame and flame outs. Emissions were also recorded.

The test was interrupted after ~22 000 cycles (~48 h of operation). No flame outs occurred during this test. The cycling of the valve had very small influence on CO and HC emissions while NO_x-emissions varied dramatically as expected, see fig. 4.6:20.

The second transient test was performed at varying load with heater head cooling constant (this means varying heater tube temperature). The valve was governed and operated by the combustor air pressure after the blower. The valve control consisted of a spring loaded membrane ($\varnothing = 170$ mm) pneumatically connected on one side to the air inlet and on the other side mechanically to the valve. The spring was preloaded to a force corresponding to a total pressure drop of 600 mm WG. The effect on the combustor pressure drop over the load range is shown in fig. 4.6:21. The shadowed area of the curve is illustrating the hysteresis of the valve control. This effect is caused by stick slip behaviour of the valve.

The load was governed by a timer connected to the burner air flow control. The schedule for the test cycle is shown in fig. 4.6:22. This cycle was repeated for 75 hours and after that time no degeneration of the valve or the valve operating system was noticed.

4.6.4.4.3 Mechanical problems

The tests with the valve have shown that a by-pass system of this design is an effective method of reducing the combustor pressure drop. The influence on flame stability of valve operation is small. However, some mechanical problems were experienced during the test:

1. The valve started to leak after a few hours of operation.
This leakage was caused by distortion due to stress relaxation in the valve material. The valve was ground and the leakage problem did not occur again.
2. The force to operate the valve was very high due to high friction in the sliding surfaces. This friction also caused the stick slip behaviour discussed above.

In the design of the next generation of by-pass valves measures have been taken to eliminate the remaining problems.

4.6.5 Development of a conventional combustion system for the MOD I engine

4.6.5.1 Summary

Three combustor heights have been tested with three different swirlers. No significant difference between the swirlers has been found, neither when looking on emissions, nor testing the temperature distribution. The 30° swirler, however, has the lowest pressure drop, and seem to be a good alternative to the conventional 45° swirler.

Diesel fuel and gasoline gave approximately the same emissions. Methanol emissions are considerably lower.

4.6.5.2 Objective

The objective of this part of the program is to develop a combustor with low pressure drop and good temperature distribution capability for the Mod I engine, based on the experiences from the HT P-40. The emissions with diesel fuel, gasoline and methanol are studied.

In order to find an optimal design, three alternative swirlers with different swirl angles and pressure drops are examined. Tests in a combustor rig on a given combustor show the influence of emissions, pressure drop, flame stability and idling conditions. The temperature distribution with three swirlers and three different combustor heights is studied in the free burning rig.

4.6.5.3 Test object

The MOD I combustor is an upscaled HT P40 combustor. To fit the combustor rig, which is designed for the AP 80 combustor, the tested MOD I combustor is unnecessarily big, see fig. 4.6:23. However, the combustor properties studied in the rig are not too sensitive to the rig size.

4.6.5.4 Combustion rig test

The combustor rig, see fig. 4.6:24, will give the same burning conditions as the engine. A 12-hole 90° atomizer is used in all tests. Burning air temperature is 700°C .

The combustor is tested with three alternative swirlers with swirl angle 30° , 45° and 60° , see fig 4.6:25-27.

The 60° swirler is the best one when looking at NO_x-emissions without EGR, see fig 4.6:28. Previous experiences indicate that the required amount of EGR will be around 35%, and a test with 35% EGR, see fig. 4.6:29 does not indicate any special variations in emissions between the swirlers.

The pressure drop across the combustor and the heater cage obtains its greatest value with the 60° swirler (32,4 cm² cross section area) and a lower value with the 45° swirler (43,5 cm²) and 30° swirler (45,6 cm²), see fig. 4.6:30.

EGR is a very efficient way to lower NO_x-emissions. The tested MOD I combustor is reduced from EI NO_x = 15,5 g/kg without EGR to EI NO_x = 2 g/kg at 55% EGR with a fuel flow of 2,5 g/s, see fig. 4.6:31.

A reduced air excess will reduce the NO_x-emissions, see fig. 4.6:32, but the CO-emissions will increase.

It is unacceptable to have an air excess below $\lambda = 1,15-1,20$ because of problems to keep λ constant at transients.

Burning gasoline compared to diesel fuel at 35% EGR in the MOD I combustor will not increase the influence of the emissions, see fig. 4.6:33. Burning methanol without EGR will only give 25% of NO_x emissions compared to diesel fuel, and at 35% EGR it will give about 50% of NO_x-emissions at the same fuel flow. Methanol has only half the calorific heating value compared to gasoline and diesel fuel, which means lower flame temperature. An increase of the atomizer air pressure from 0,7 to 1,0 bar lowered the CO-emissions at high load, see fig 4.6:34-36.

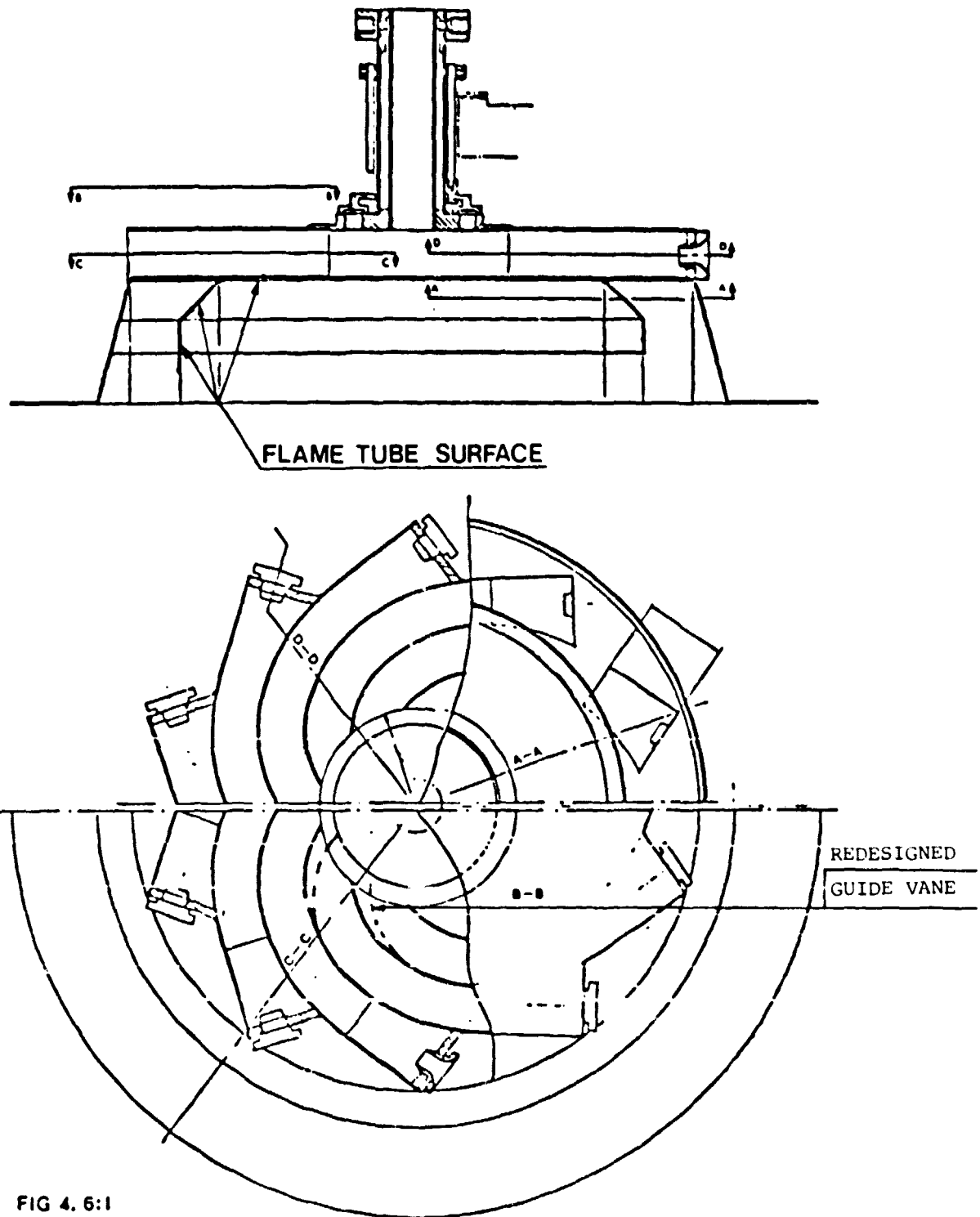
4.6.5.5 Free burning rig test

The ignition test, see fig. 4.6:37, shows that the ignitor-atomizer with a capacitance ignition system, see fig 4.6:38, gave the best ignition qualities. The conventional spark plug close to the outlet (Ø 80) was acceptable.

The temperature distribution is tested in the free burning rig with a dummy heater made of perforated sheet metal. Three different combustor heights were tested, see Fig. 4.6:39.

The high (70 mm) combustor was somewhat better than the others.
No significant difference in temperature distribution between the
three tested swirlers was found. The test result will be discussed
more in detail in a later report.

ORIGINAL PAGE IS
OF POOR QUALITY



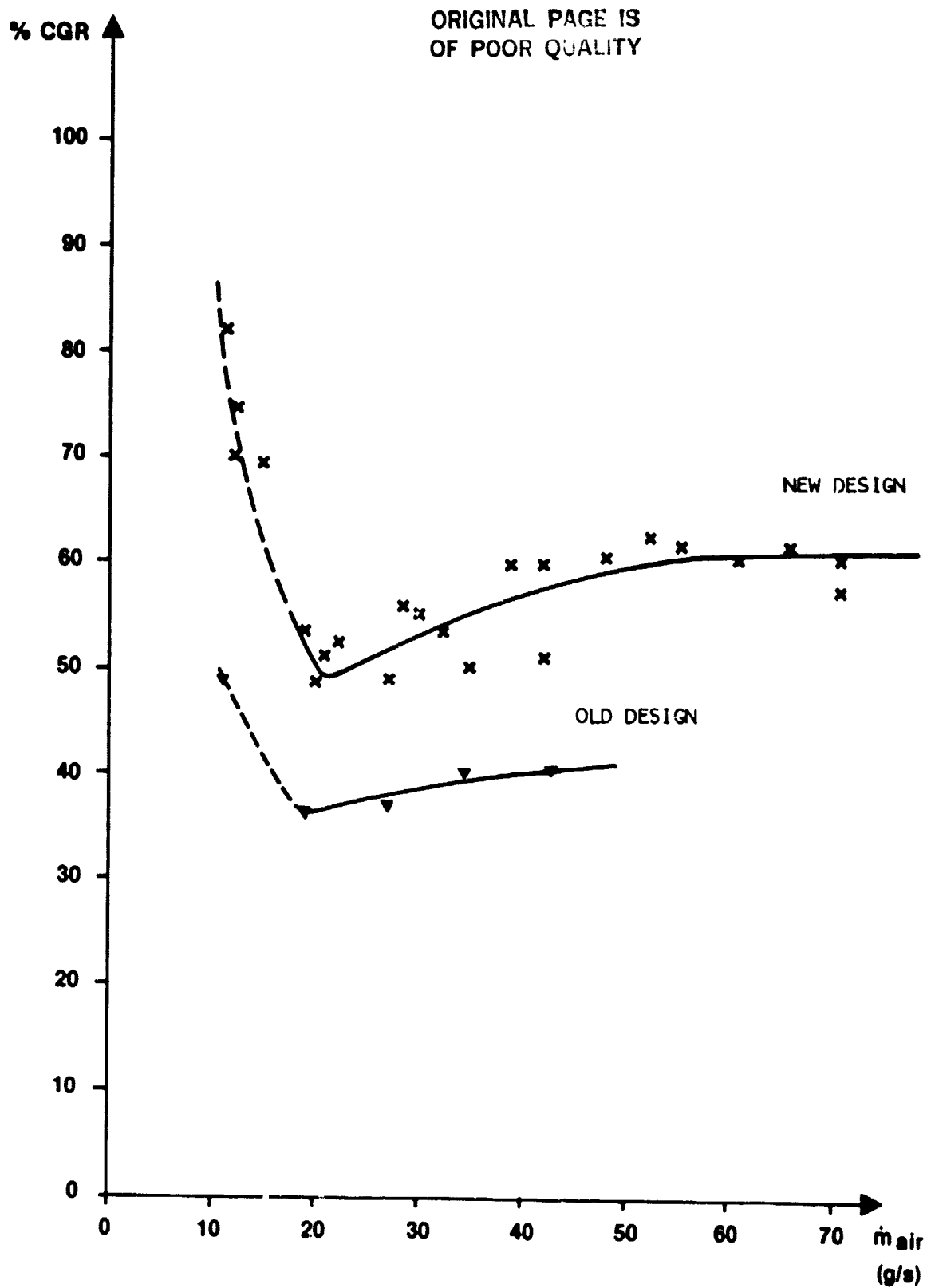


FIG 4.6:2 % CGR VERSUS BURNER AIR FLOW

ORIGINAL PAGE 13
OF POOR QUALITY.

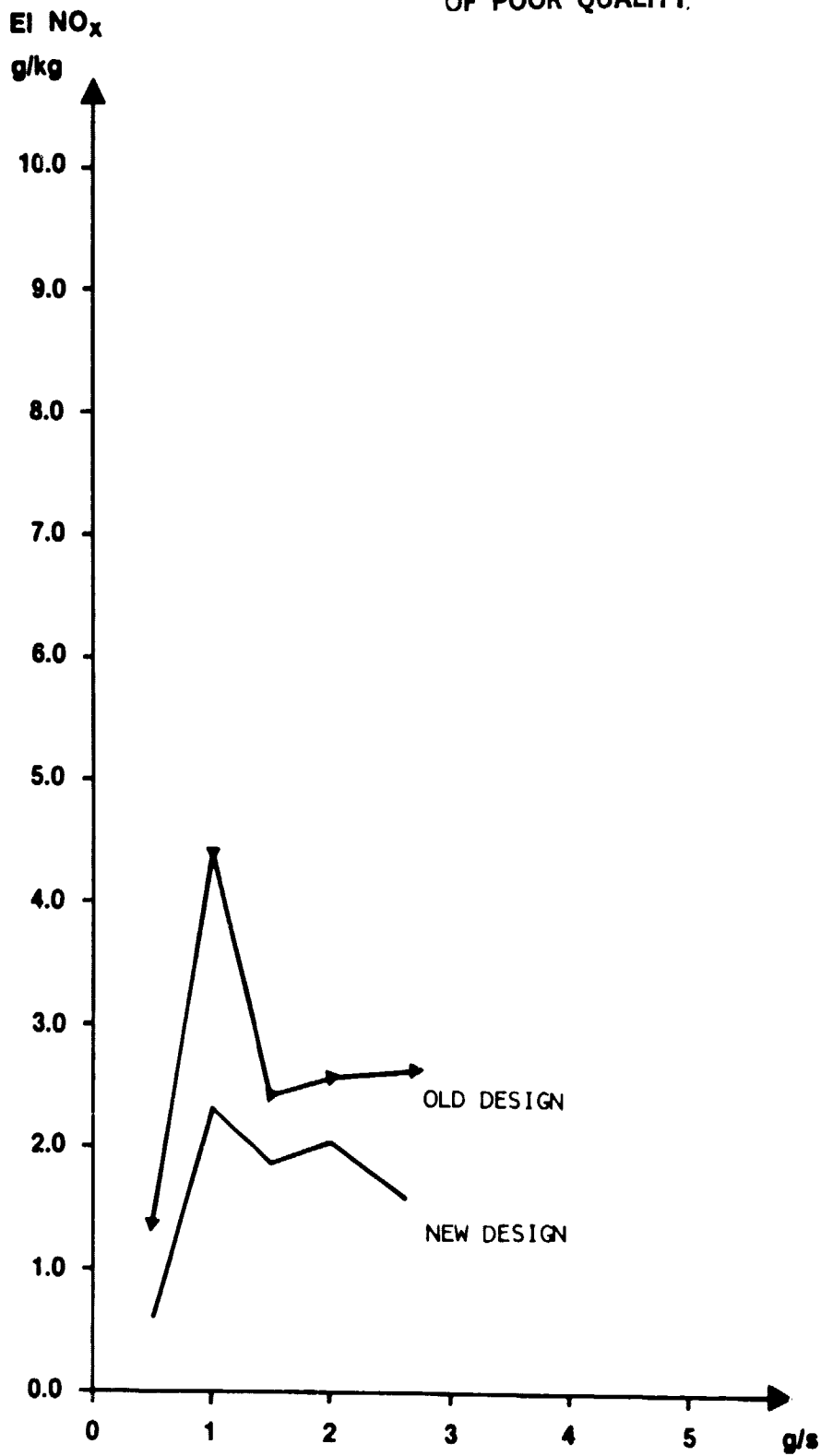


FIG 4.6:3 EI NO_x VERSUS FUEL FLOW

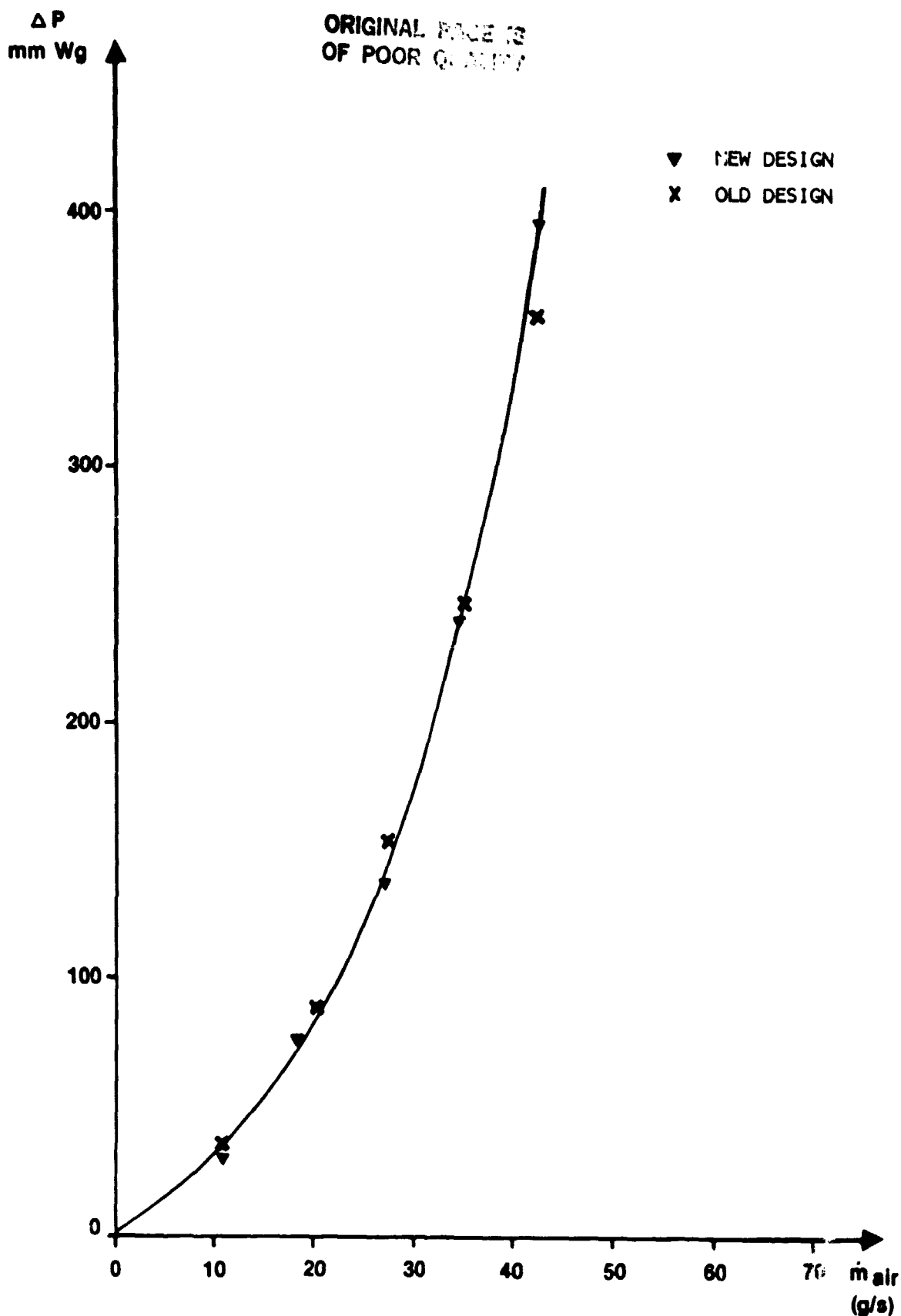


FIG 4.6:4 COMBUSTOR AND HEATER PRESSURE DROP AND HEATER PRESSURE DROP
VERSUS BURNER AIR FLOW

ORIGINAL FILE IS
OF POOR QUALITY

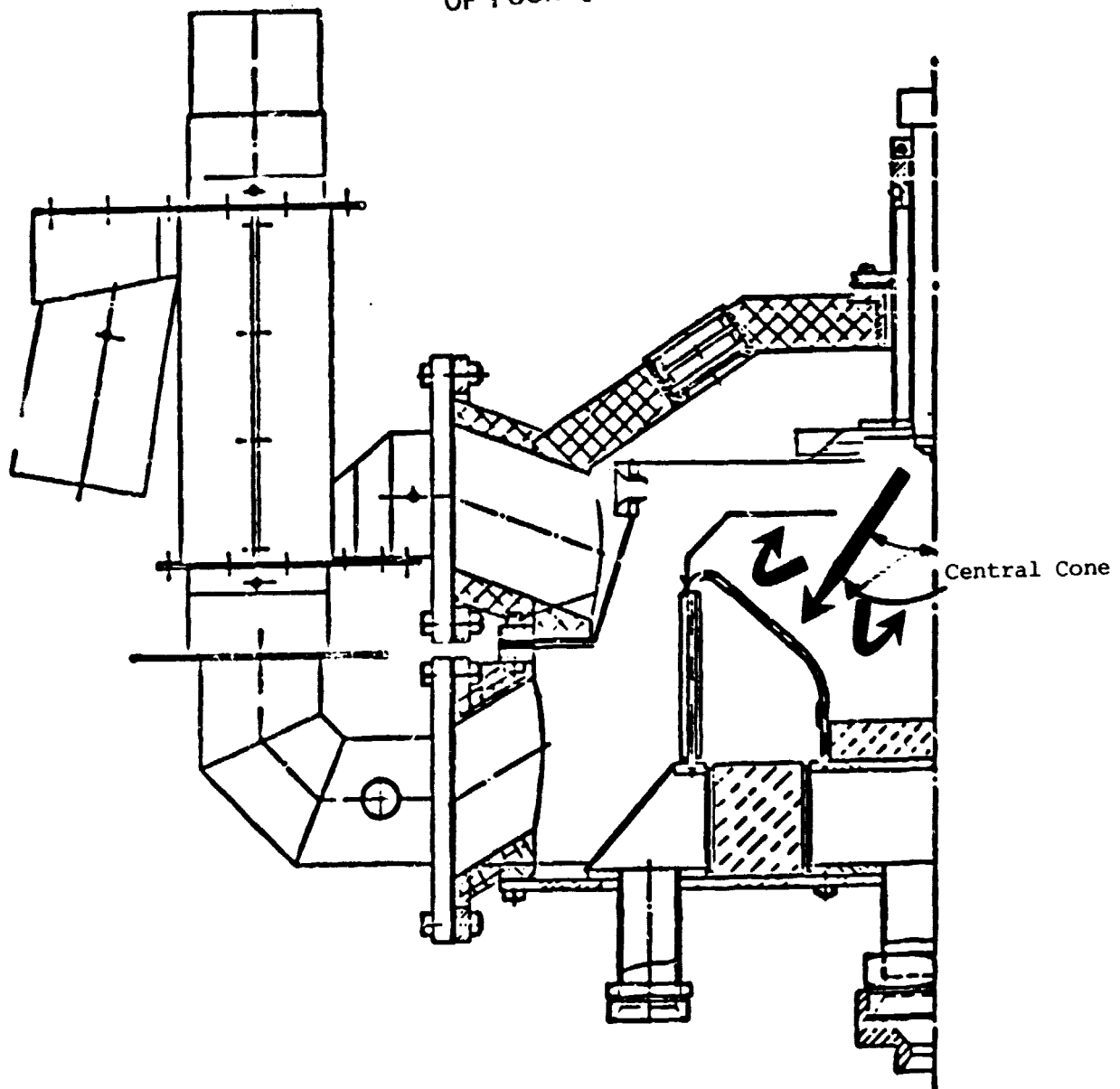


Fig. 4.6:5 Flow Pattern in the Combustor

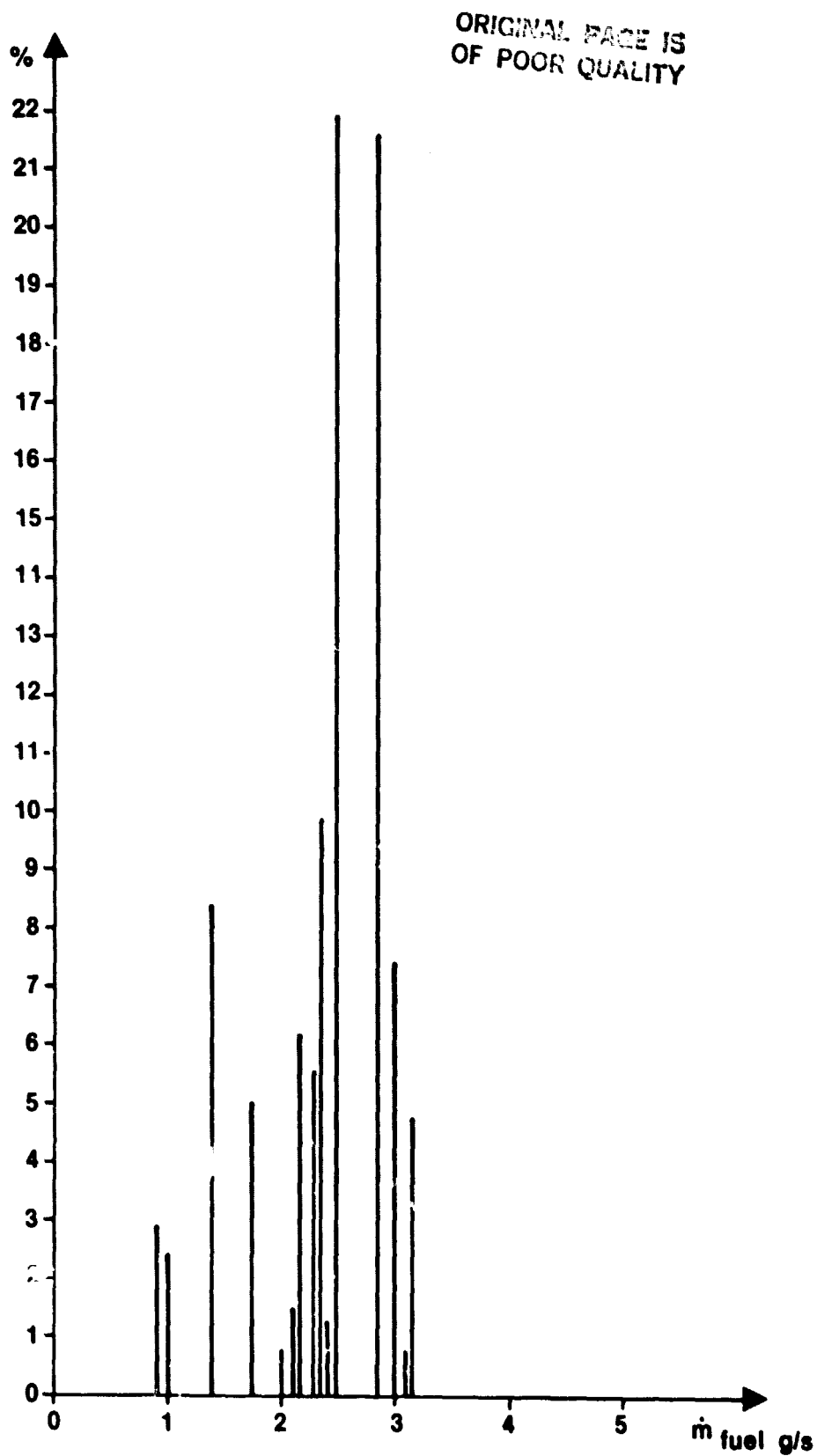


FIG 4.6:6 RELATIVE DURATION AT DIFFERENT LOADS DURING THE
LONG TERM TEST

ORIGINAL PAGE IS
OF POOR QUALITY

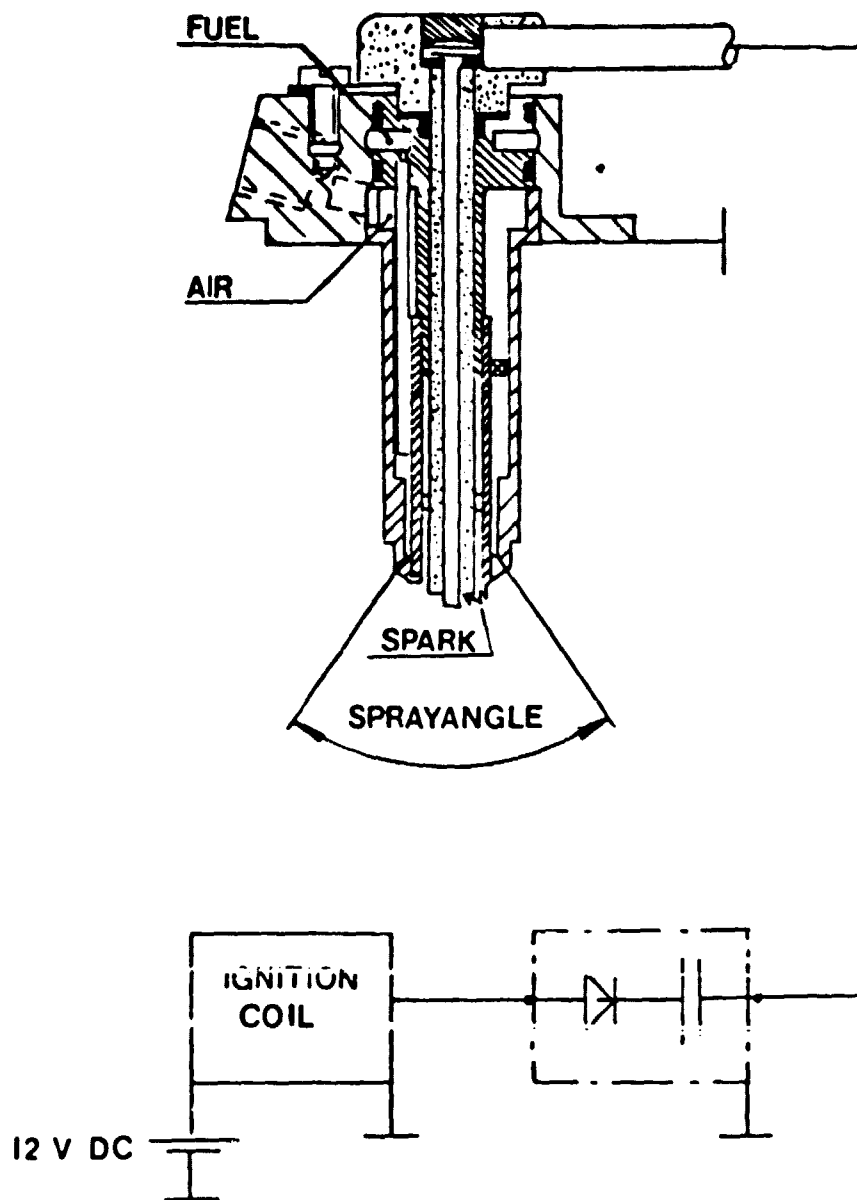


FIG 4. 6:7 ATOMIZER/IGNITOR

ORIGINAL PAGE IS
OF POOR QUALITY

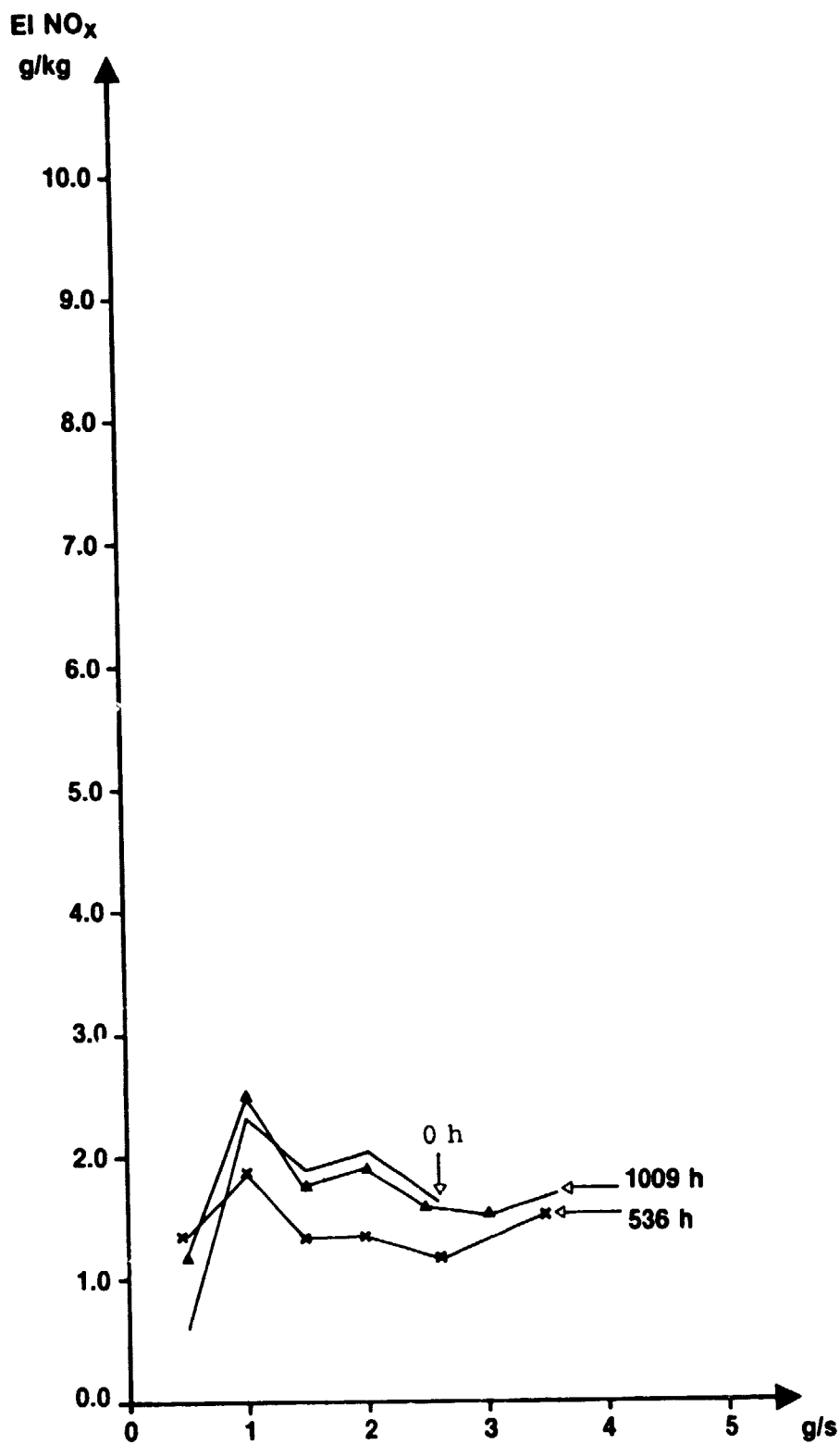


FIG 4.6:8 EI NO_x VERSUS FUEL FLOW AT THREE OCCASIONS DURING THE
LONG TERM TEST

ORIGINAL PAGE IS
OF POOR QUALITY

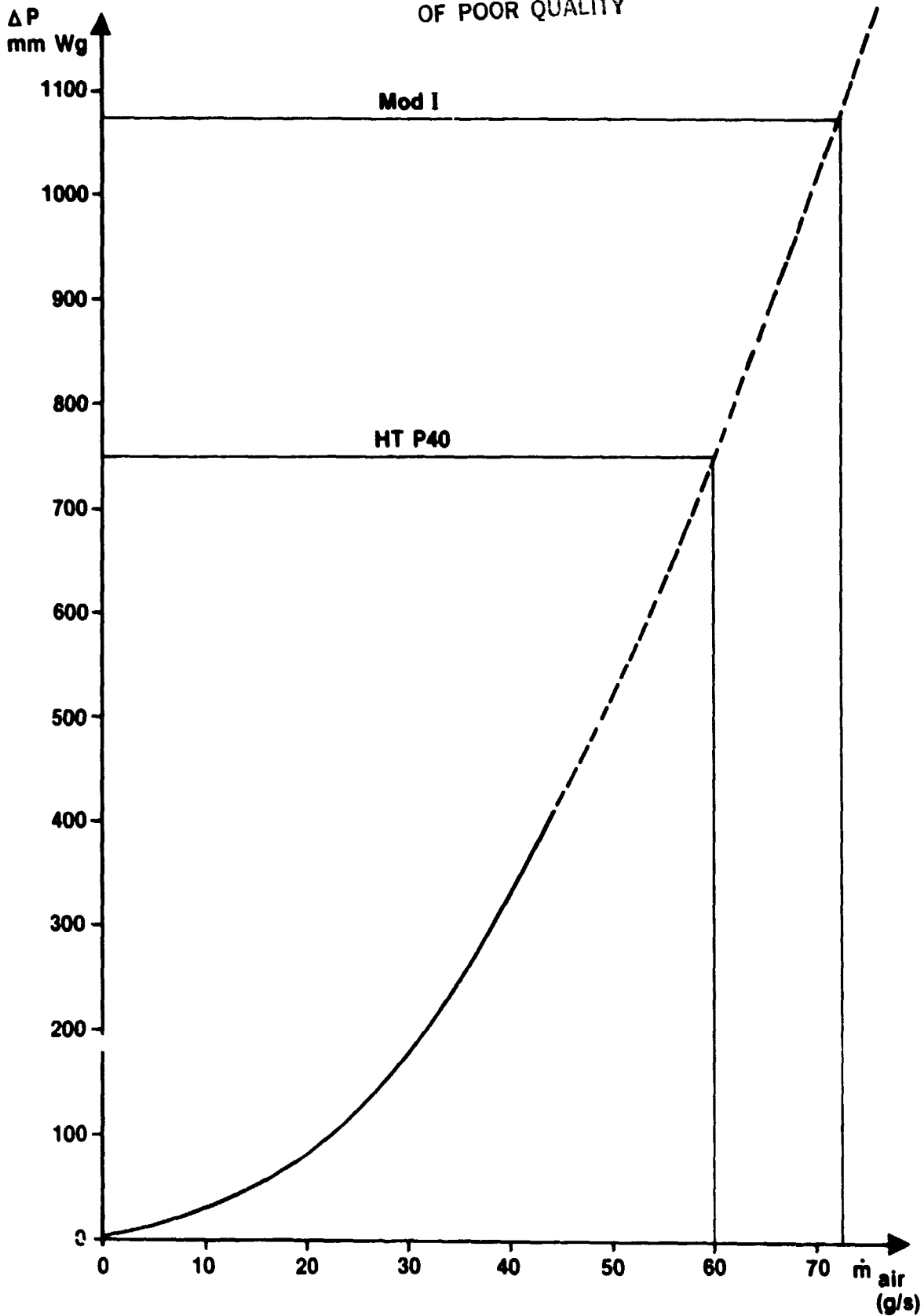


FIG 4.6:9 PRESSURE DROP ACROSS THE COMBUSTOR VERSUS BURNER AIR FLOW

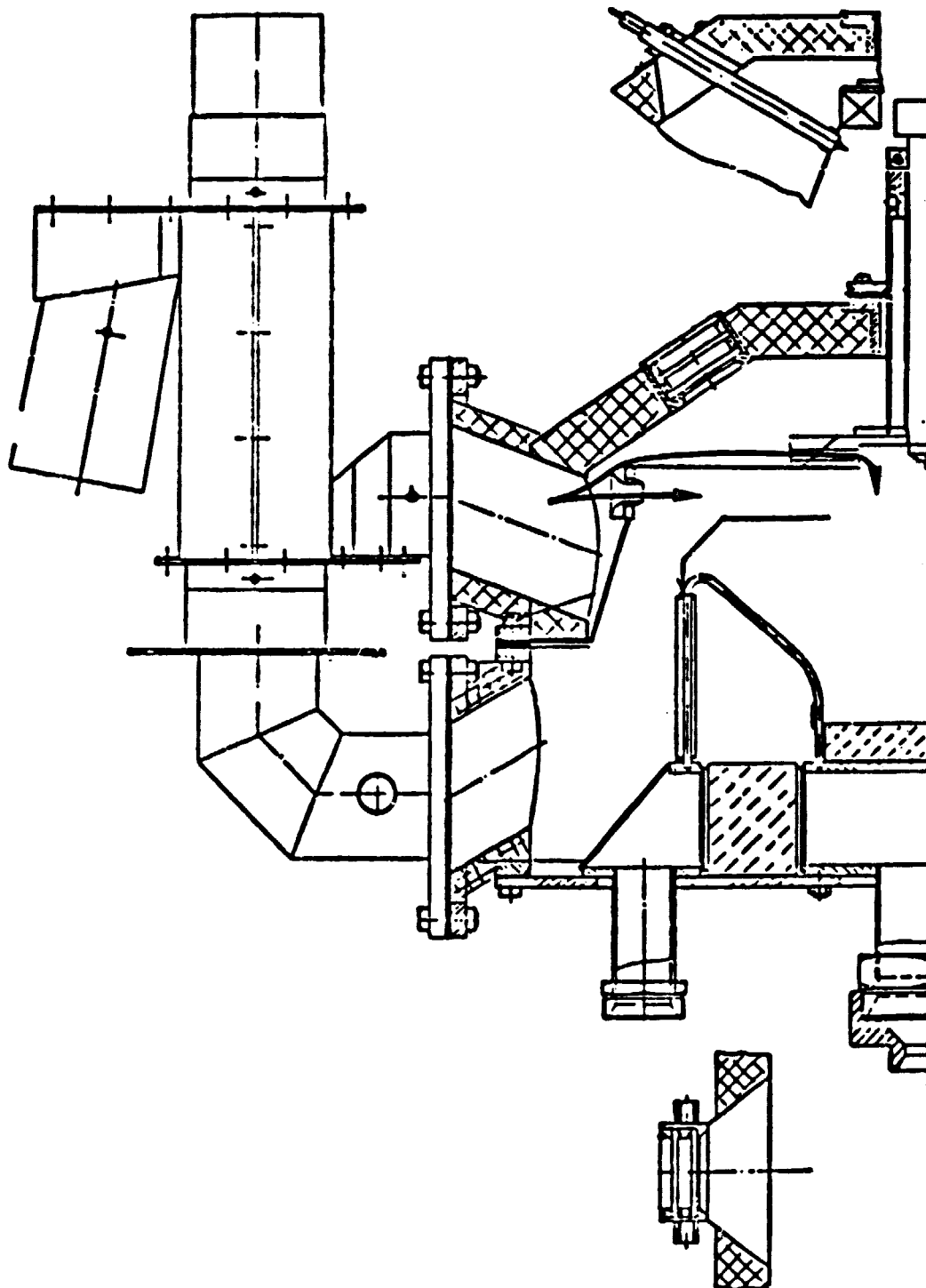


Fig. 4.6:10 Bypass System

ORIGINAL PAGE IS
OF POOR QUALITY

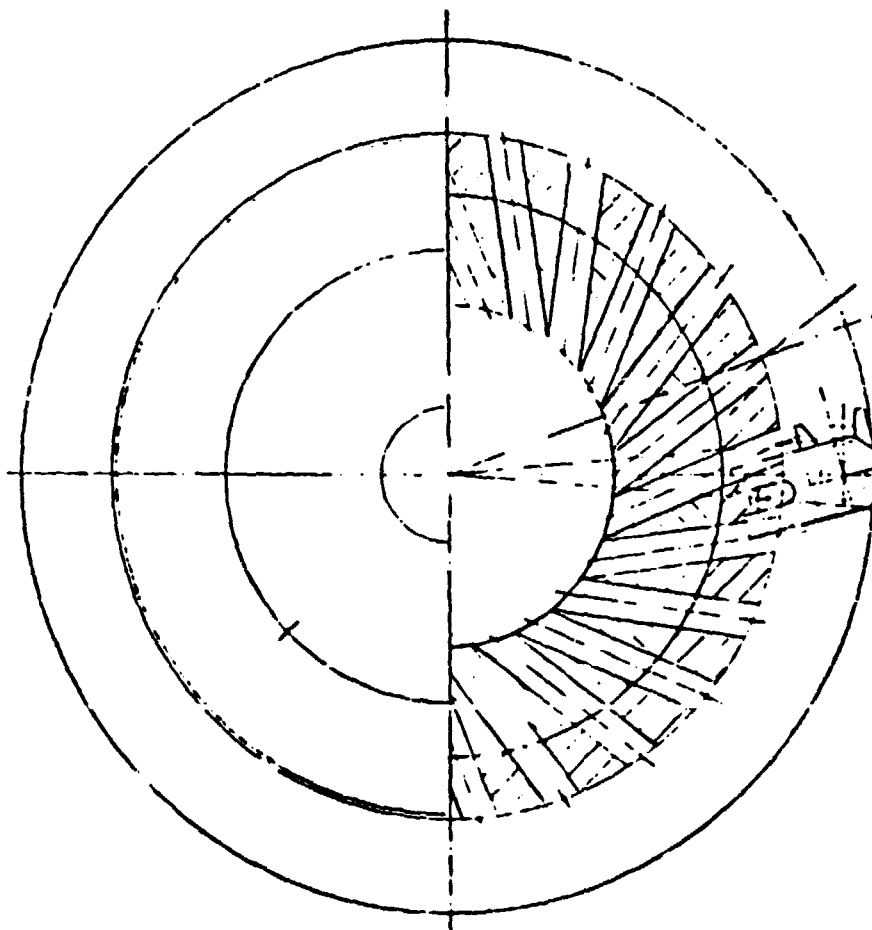
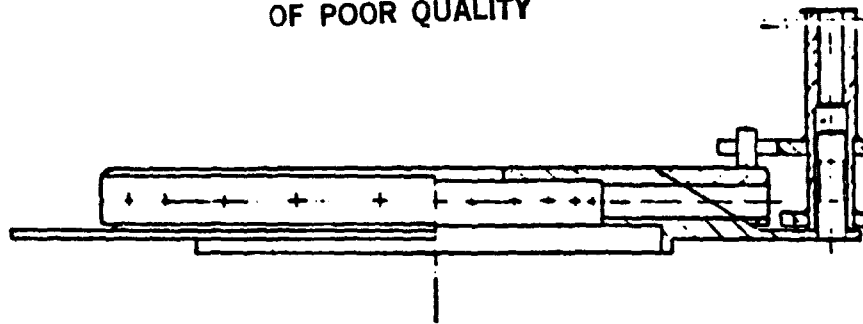


FIG 4.6:11 BY PASS VALVE

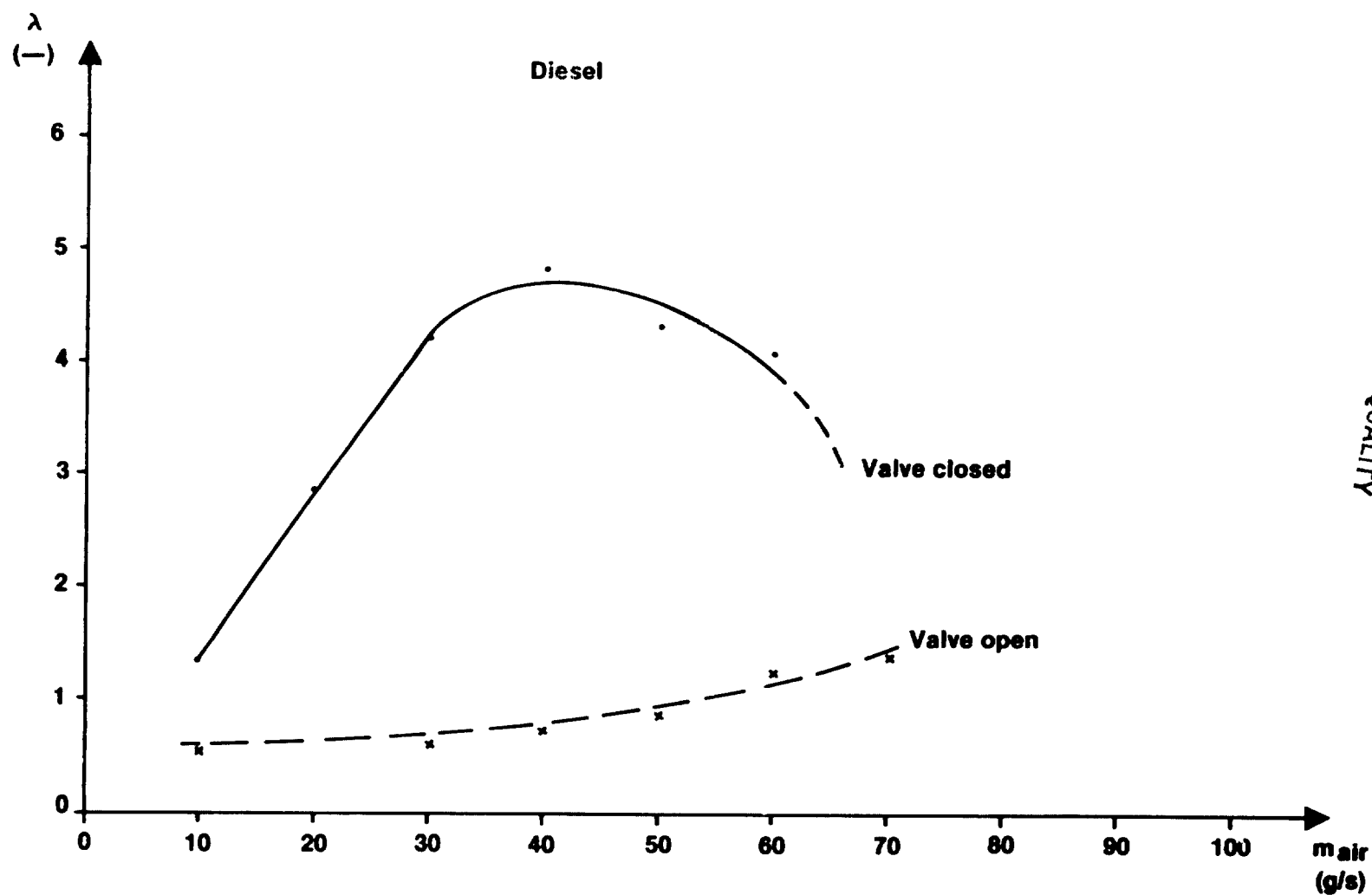


FIG 4.6:12 IGNITEABILITY AT FREE BURNING TESTS
IGNITION OCCURS BELOW THE CURVES

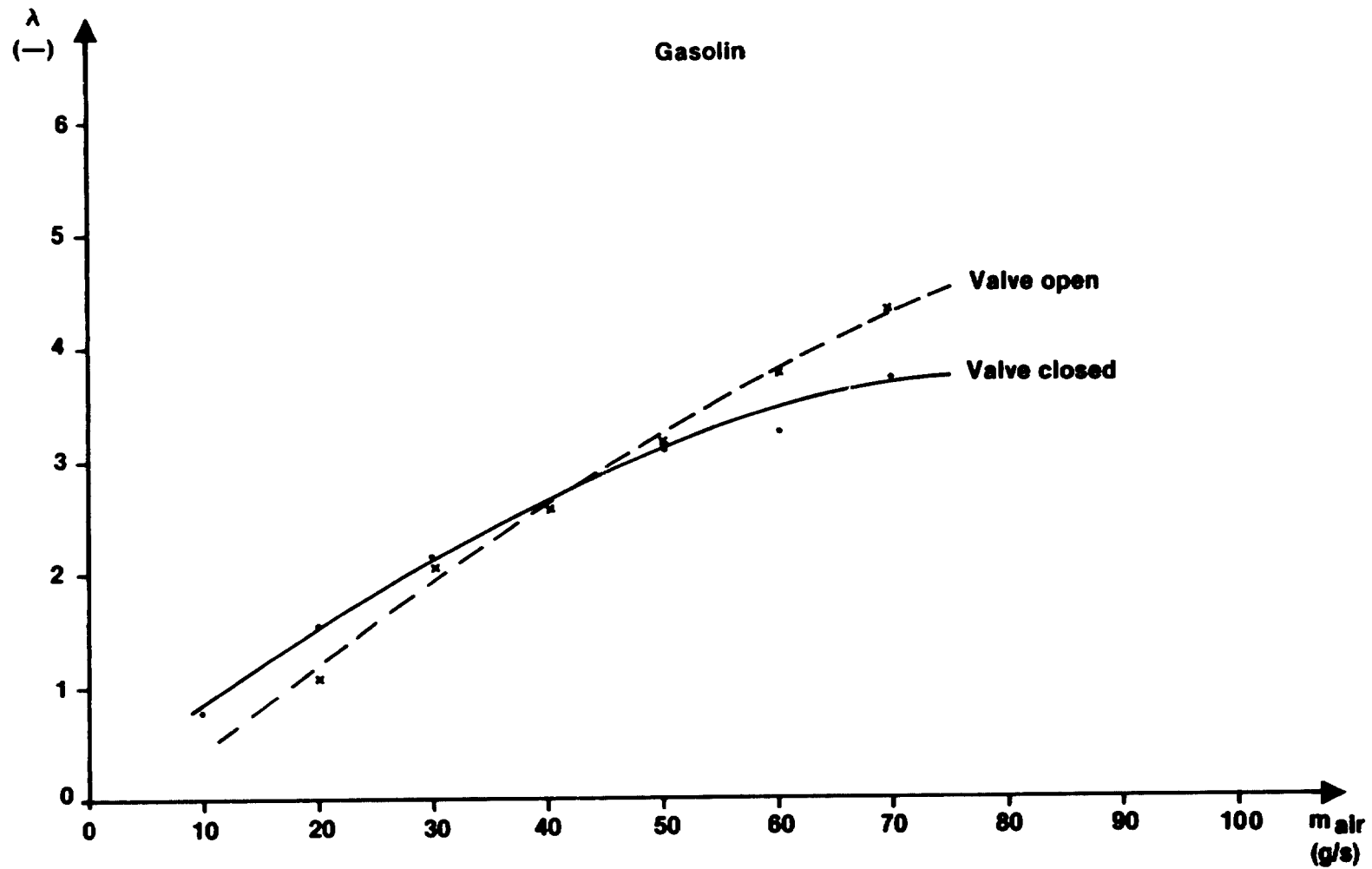


FIG 4.6:13 IGNITEABILITY AT FREE BURNING TEST
IGNITION OCCURS BELOW THE CURVES

ORIGINAL PAGE IS
OF POOR QUALITY

ORIGINAL PAGE IS
OF POOR QUALITY

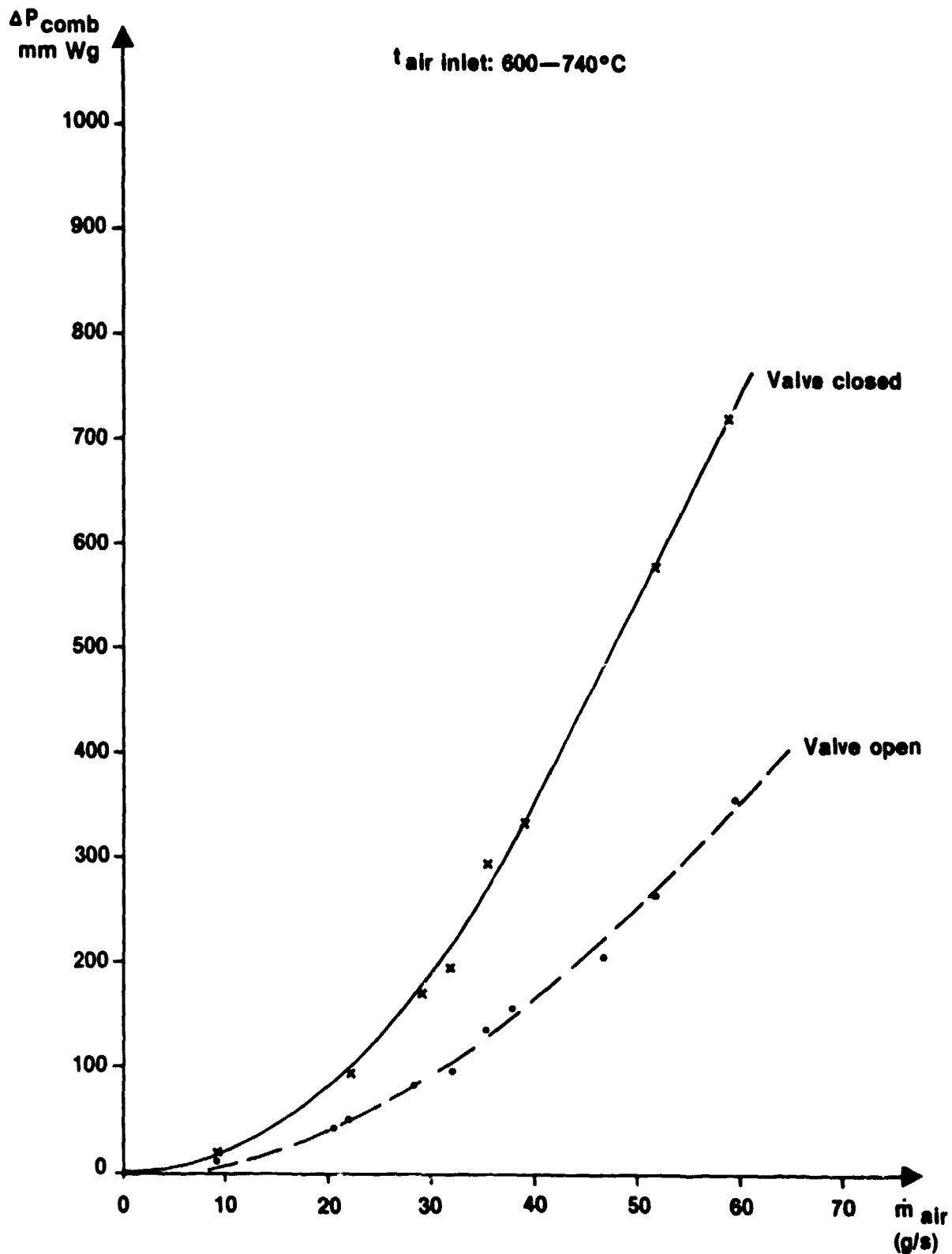


FIG 4.6:14 PRESSUREDROP ACROSS THE COMBUSTOR AND HEATER
VERSUS BURNER AIR FLOW

ORIGINAL PAGE IS
OF POOR QUALITY

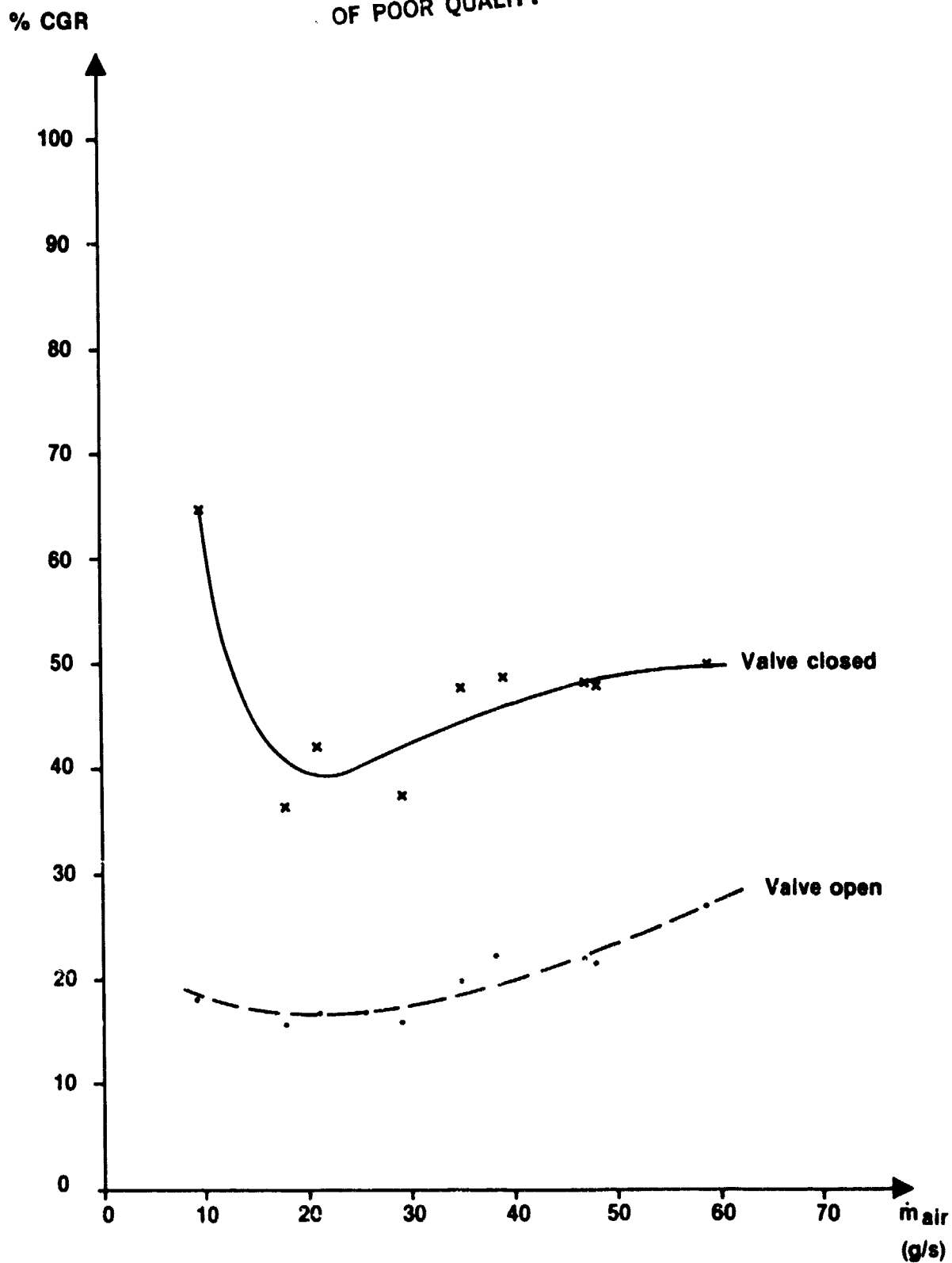


FIG 4.6:15 % CGR VERSUS BURNER AIR FLOW.
THE CGR FLOW IS RELATED TO THE FLOW
THROUGH THE EJECTOR JETS

ORIGINAL PAGE IS
OF POOR QUALITY

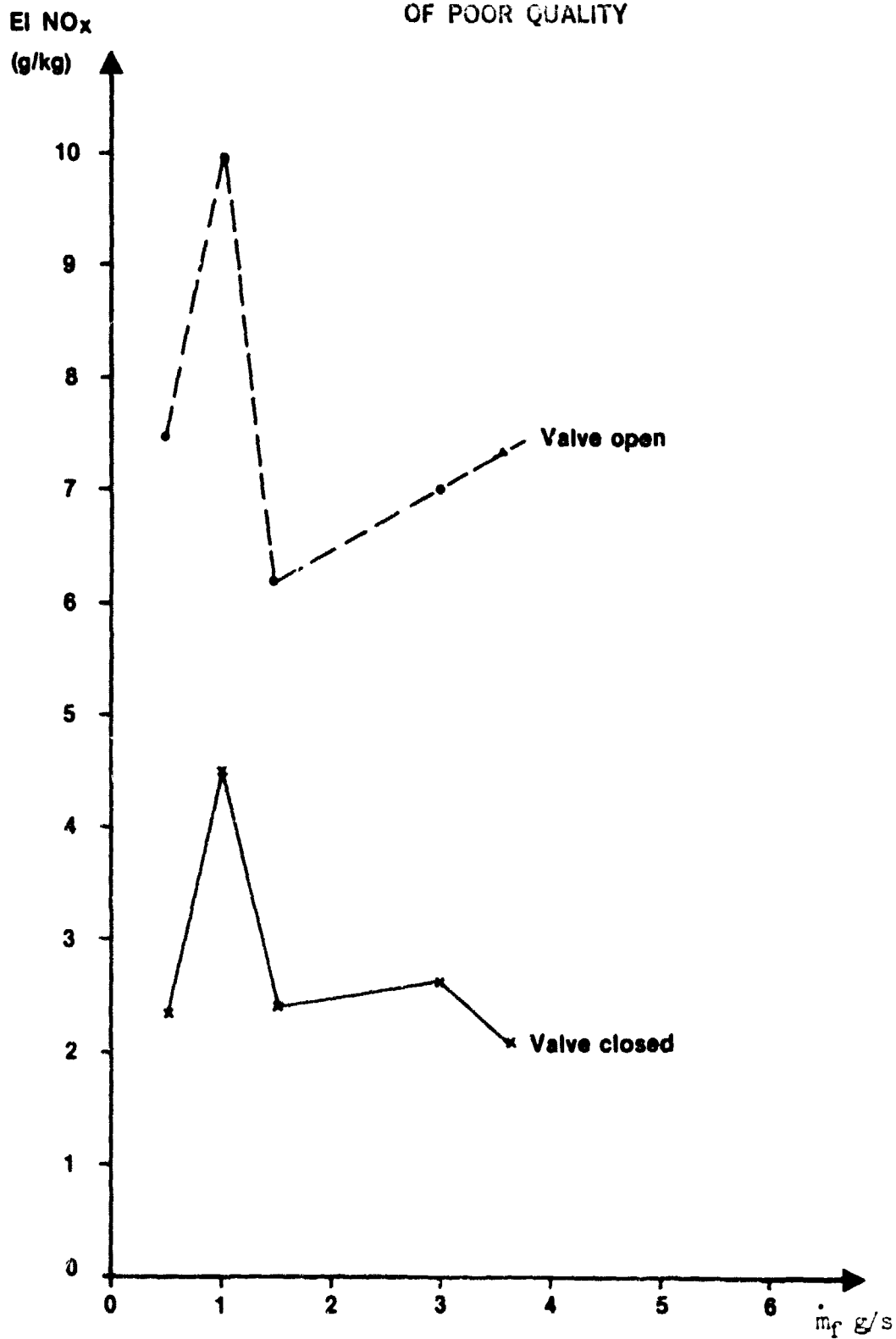


FIG 4.6:16 EI NO_x VERSUS FUEL FLOW

ORIGINAL PAGE IS
OF POOR QUALITY

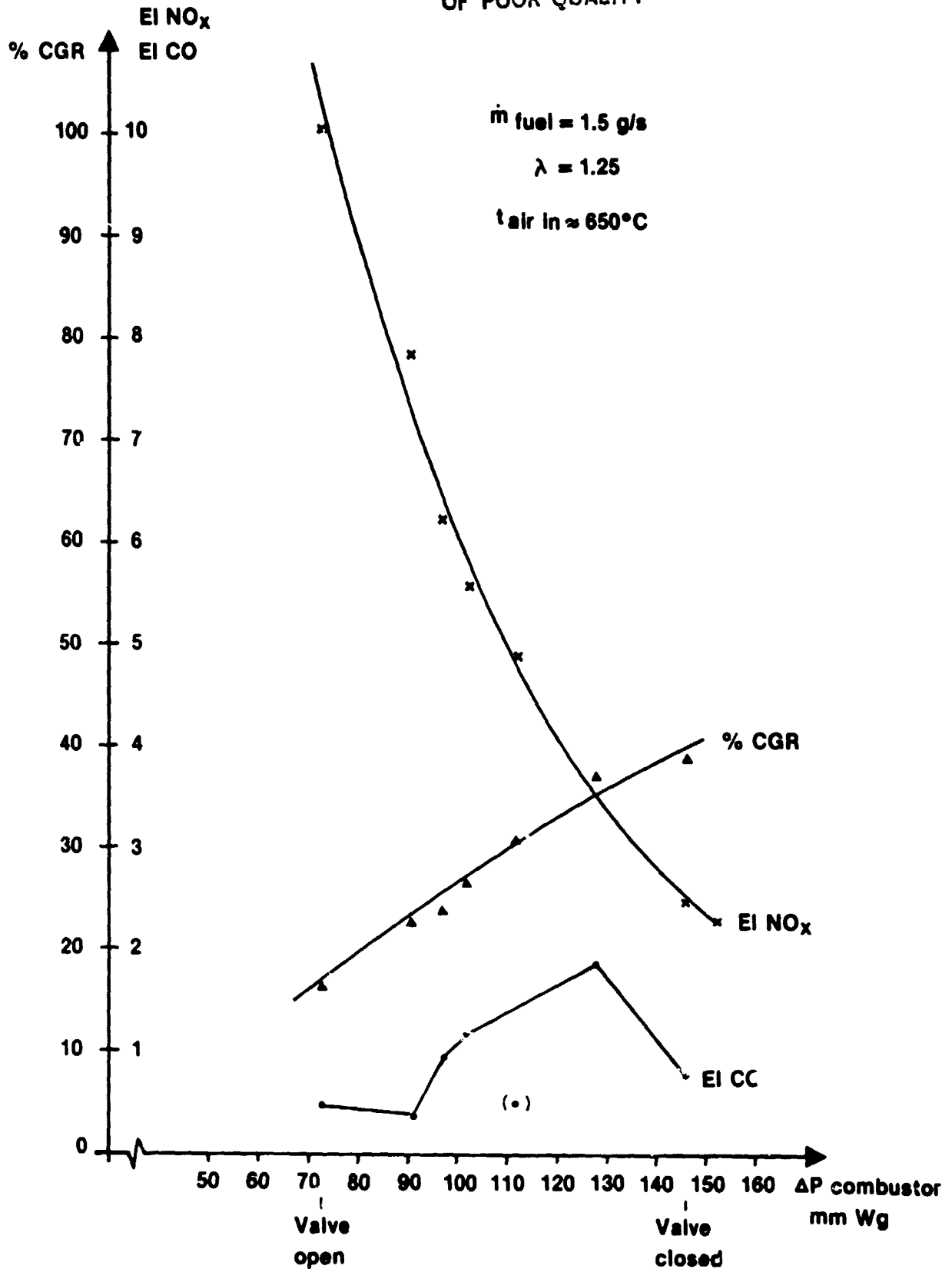


FIG 4.6:17 % CGR, EI NO_x AND EI CO VERSUS COMBUSTOR
AND HEATER PRESSUREDROP

ORIGINAL PAGE IS
OF POOR QUALITY

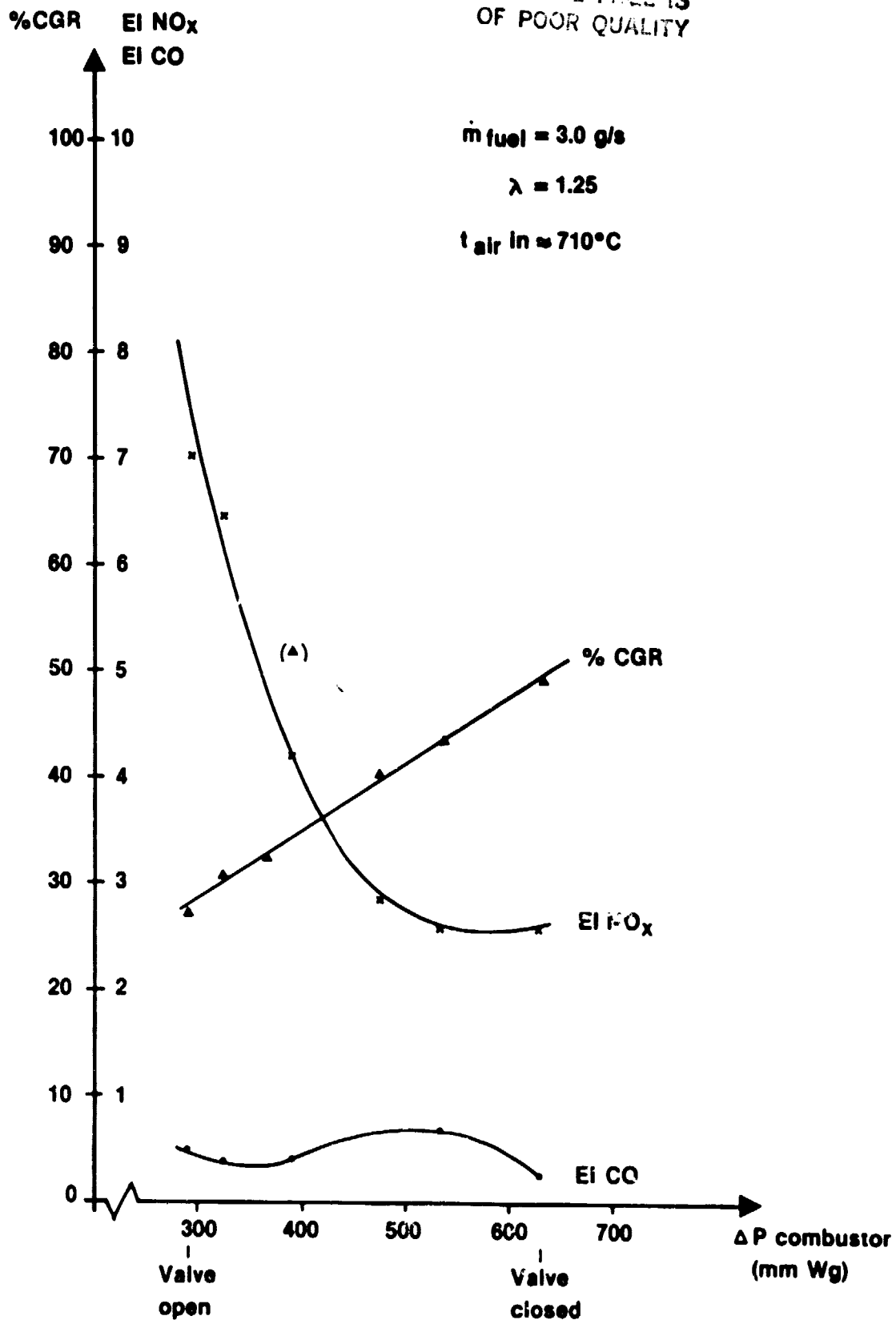


FIG 4.6:18 %CGR, EI NO_x AND EI CO VERSUS COMBUSTOR
AND HEATER PRESSURE DROP

ORIGINAL PAGE IS
OF POOR QUALITY

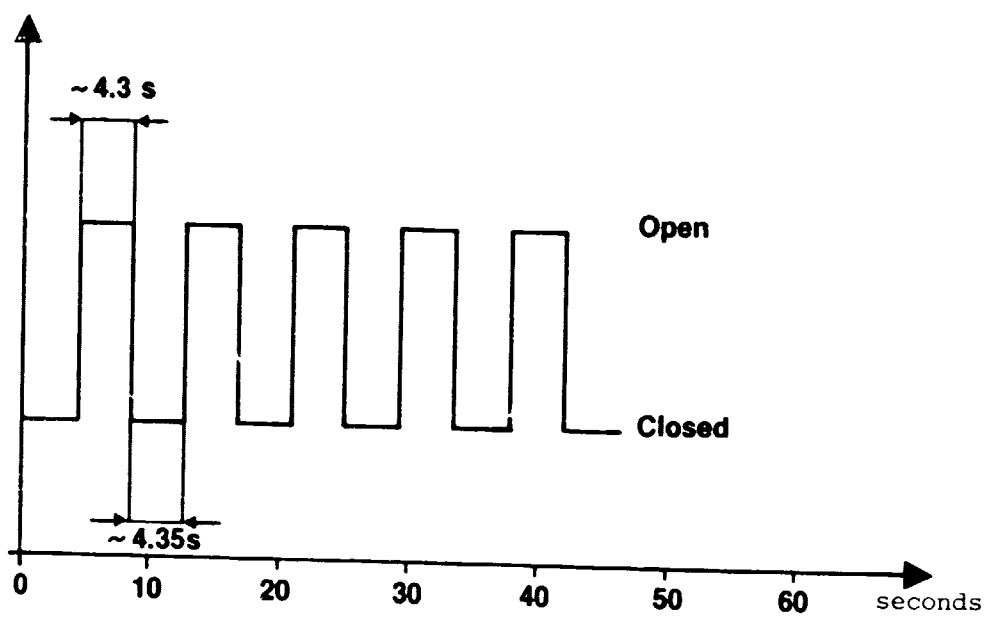


Fig. 4.6:19 Valve Operating Sequence

ORIGINAL PHOTO IS
OF POOR QUALITY

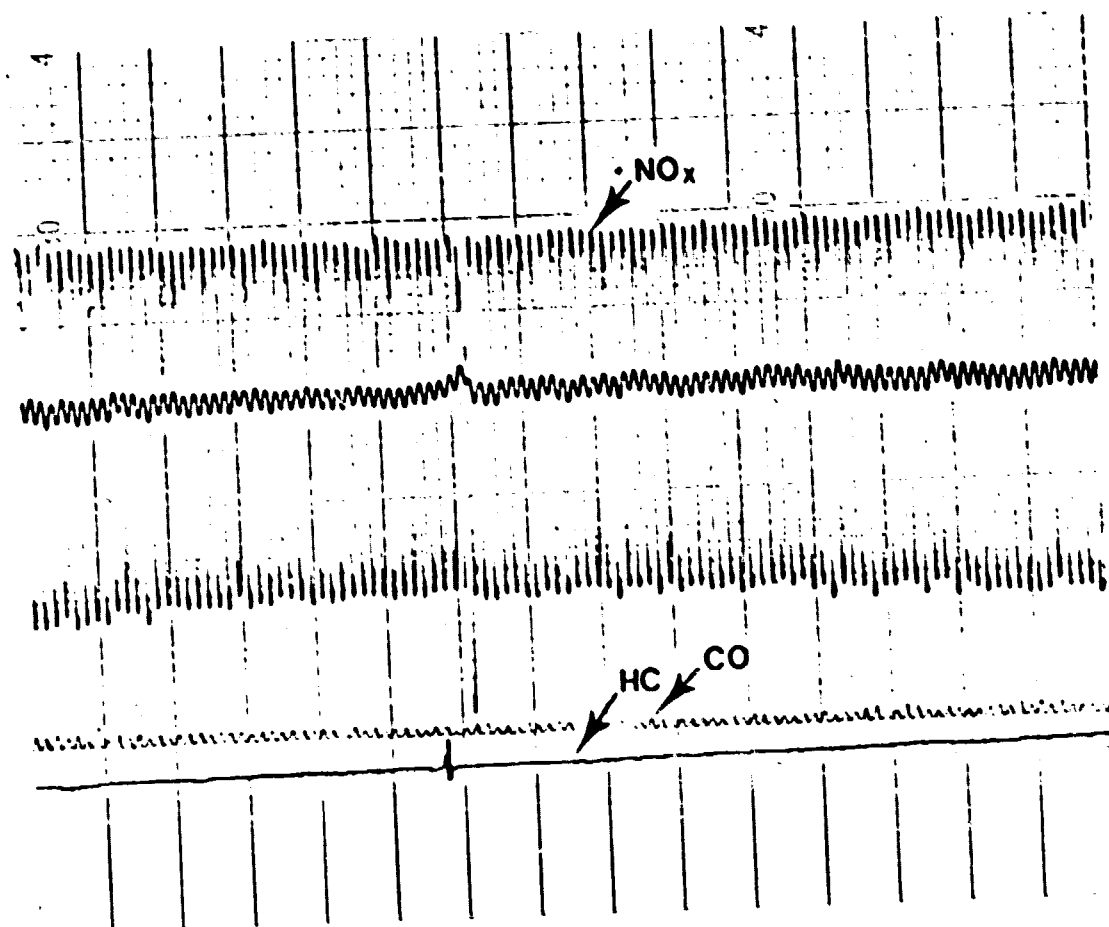


FIG 4.6:20 VARIATION OF EMISSIONS DURING
THE VALVE TEST

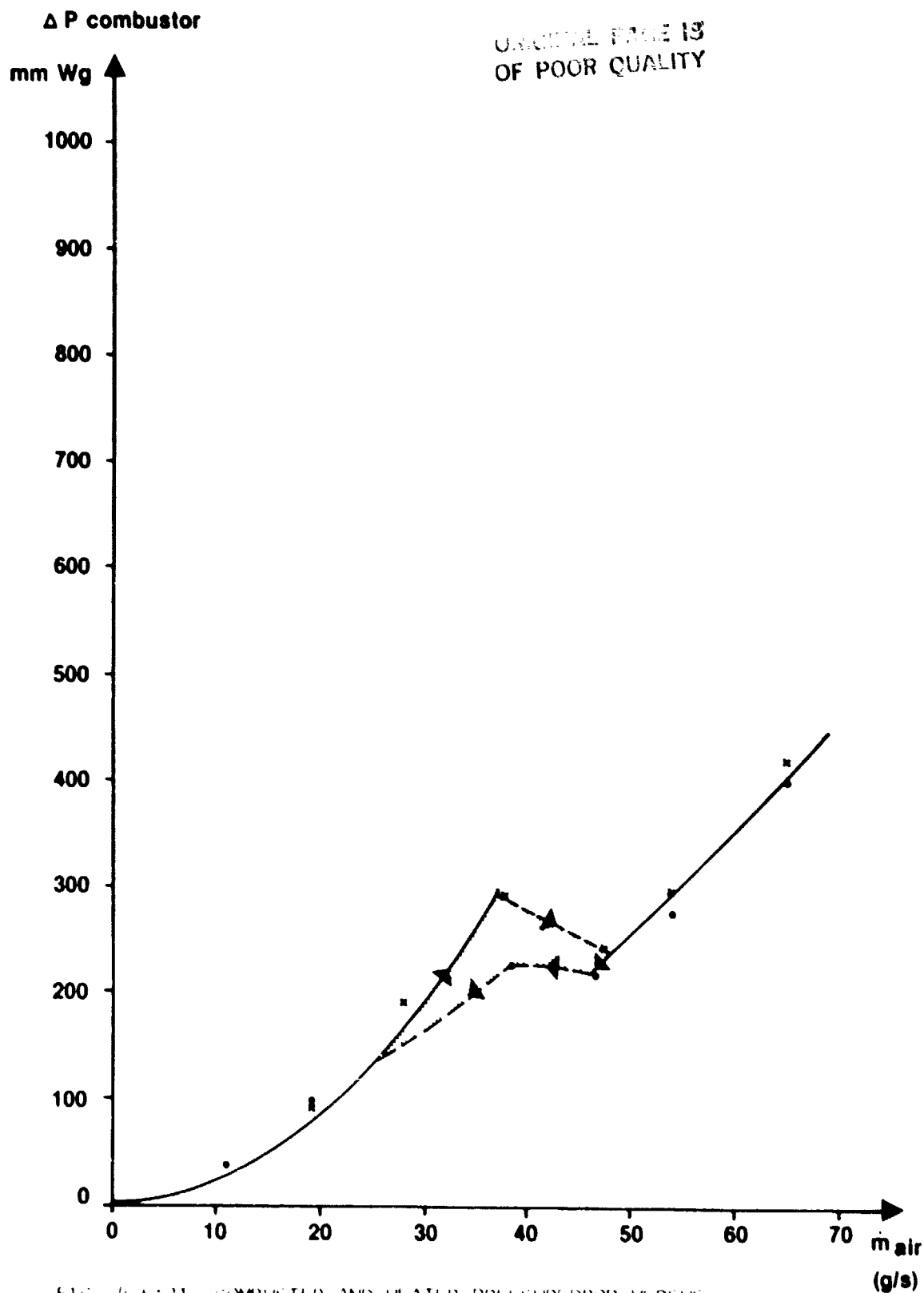


FIG 4.6.21 COMBUSTOR AND HEATER PRESSURE DROP VERSUS
BURNER AIR FLOW WITH AUTOMATIC BYPASS CONTROL

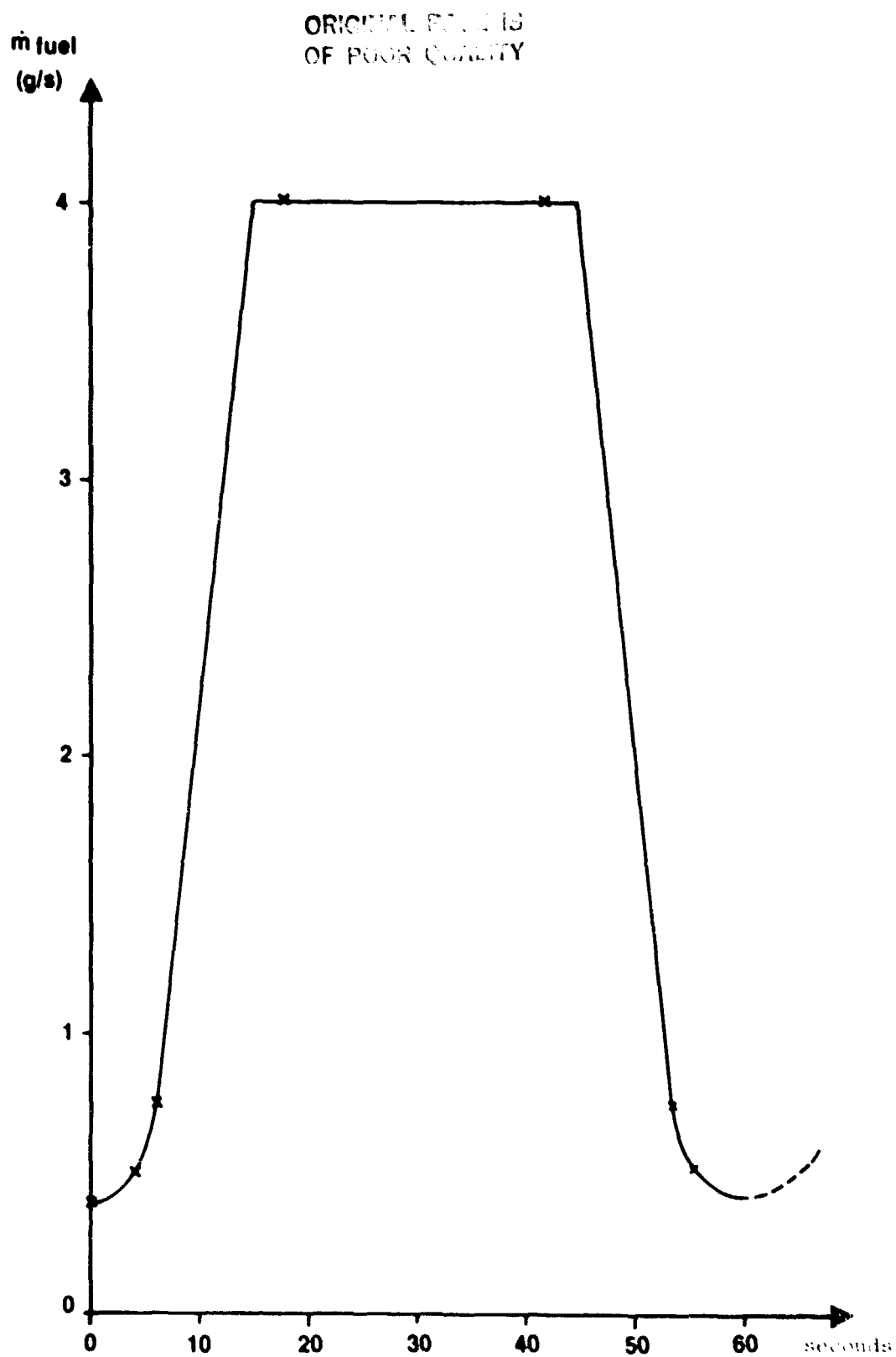


FIG 4.6:22 LOAD VARIATION SCHEDULE DURING THE TRANSIENT TEST

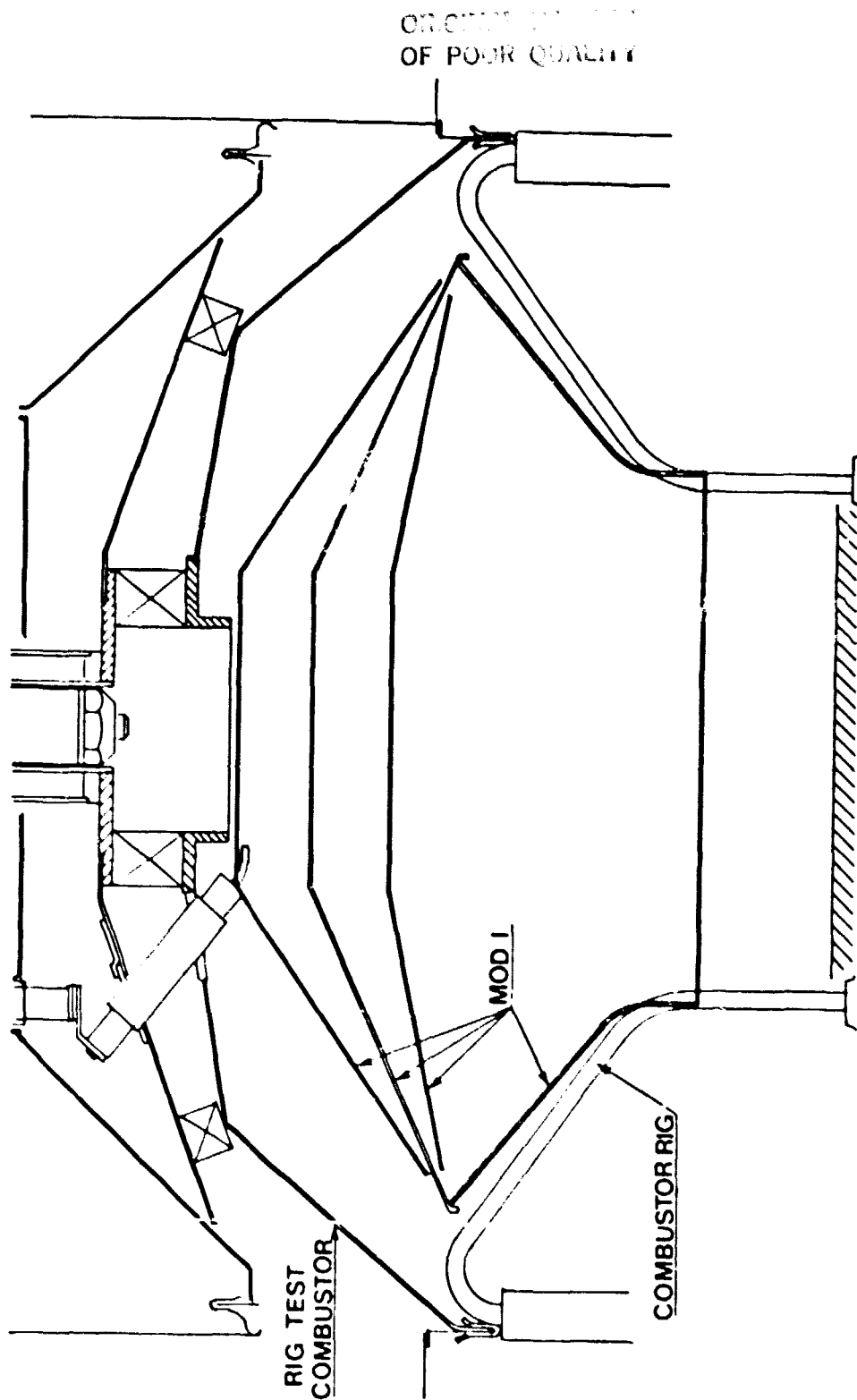


FIG 4. 6:23 THE MOD 1 COMBUSTORS AND DUMMY HEATER COMPARED WITH THE AP 80 COMBUSTOR RIG

ORIGINAL DRAWING IS
OF POOR QUALITY

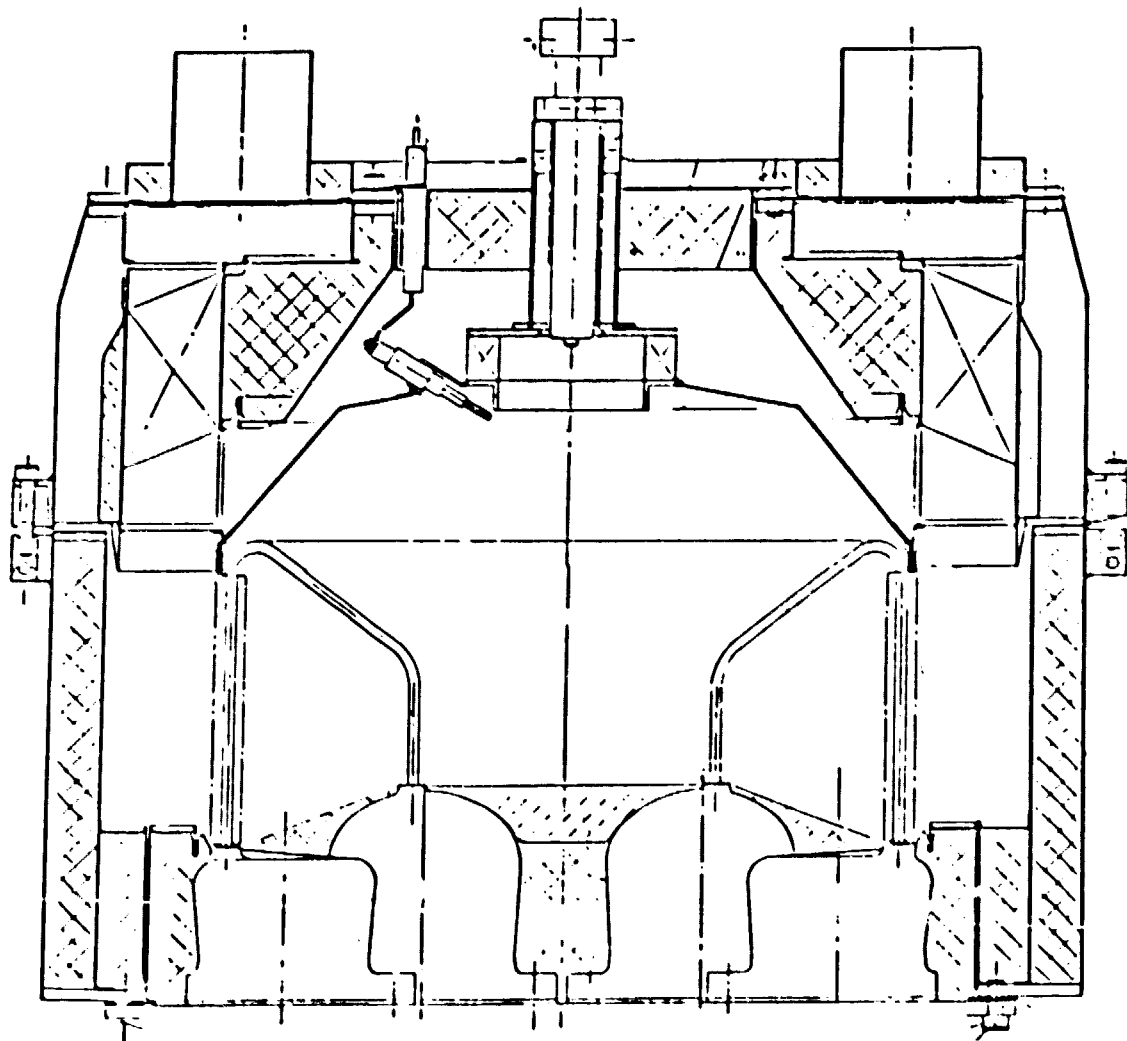
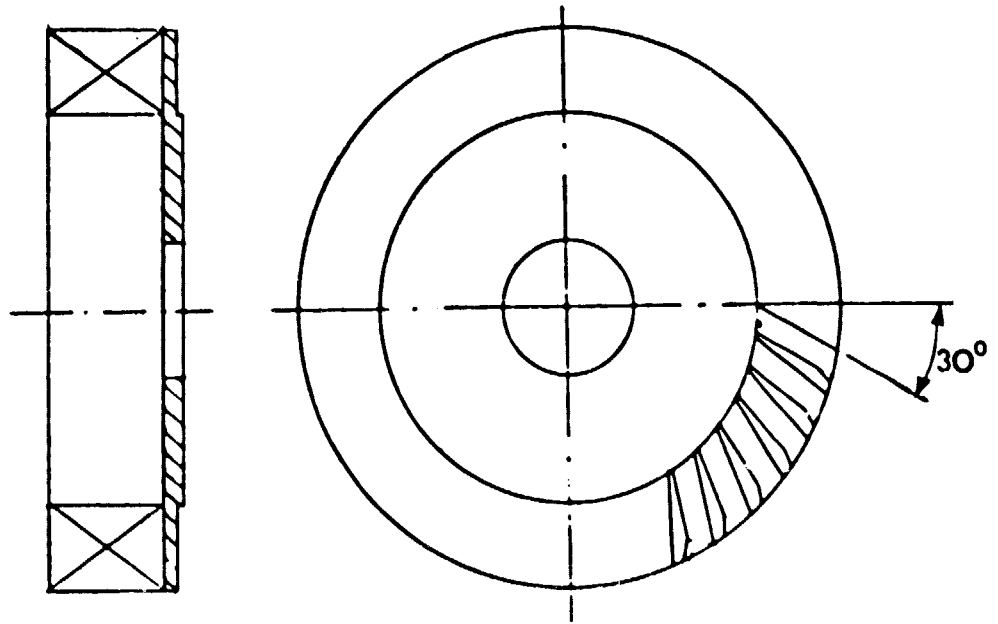


FIG 4.6:24 COMBUSTOR RIG ASE MOD 2

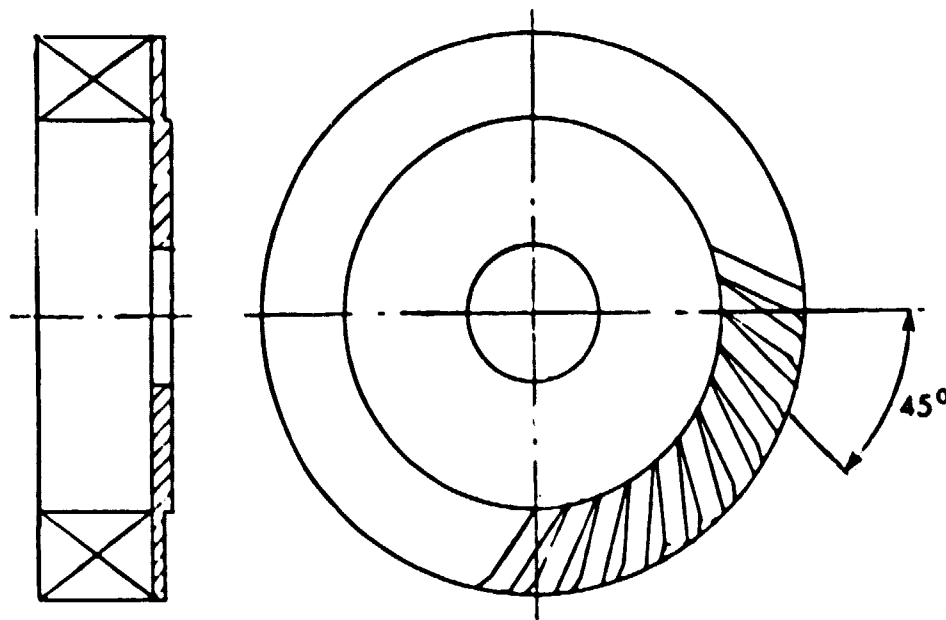
OF THE



SWIRLER OUTLET AREA - 45.6 cm^2

FIG 4.6:25 SWIRLER 30°

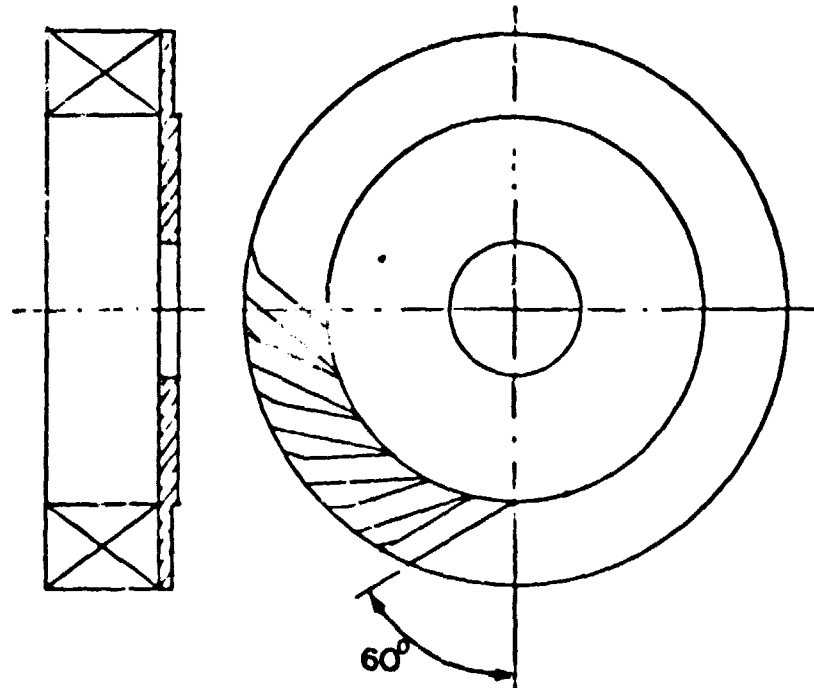
ONCE THE QUALITY
OF POOR QUALITY



SWIRLER OUTLET AREA = 43.5cm^2

FIG 4.6:26 SWIRLER 45°

ORIGINAL DESIGN
OF POOR QUALITY



SWIRLER OUTLET AREA = 32.4 cm^2

FIG 4.6:27 SWIRLER 60°

ORIGINAL IMAGE IS
OF POOR QUALITY

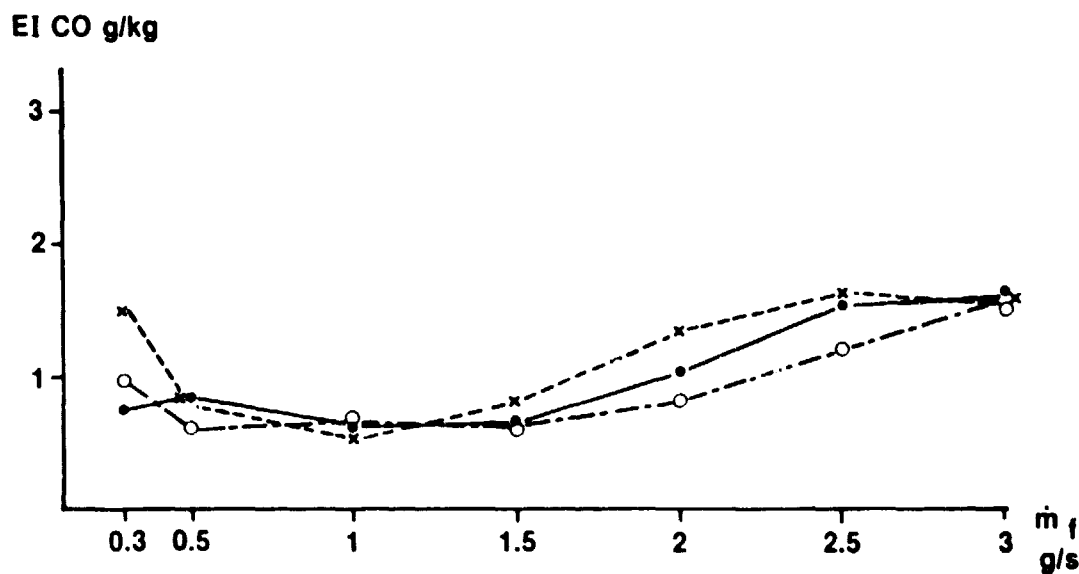
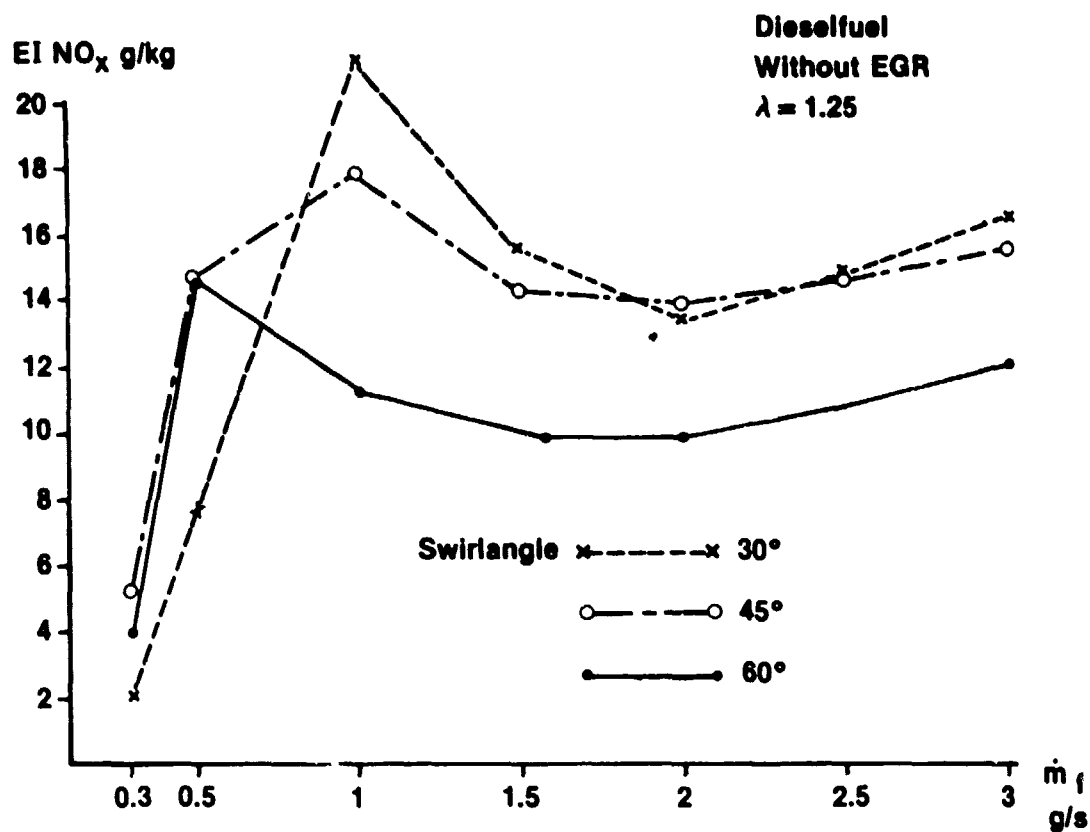


FIG 4.6:28 EMISSION INDEX NO_x AND CO VERSUS FUEL FLOW WITH
3 SWIRLERS. SWIRLANGE 30°, 45°, 60°

ORIGINAL PAGE IS
OF POOR QUALITY

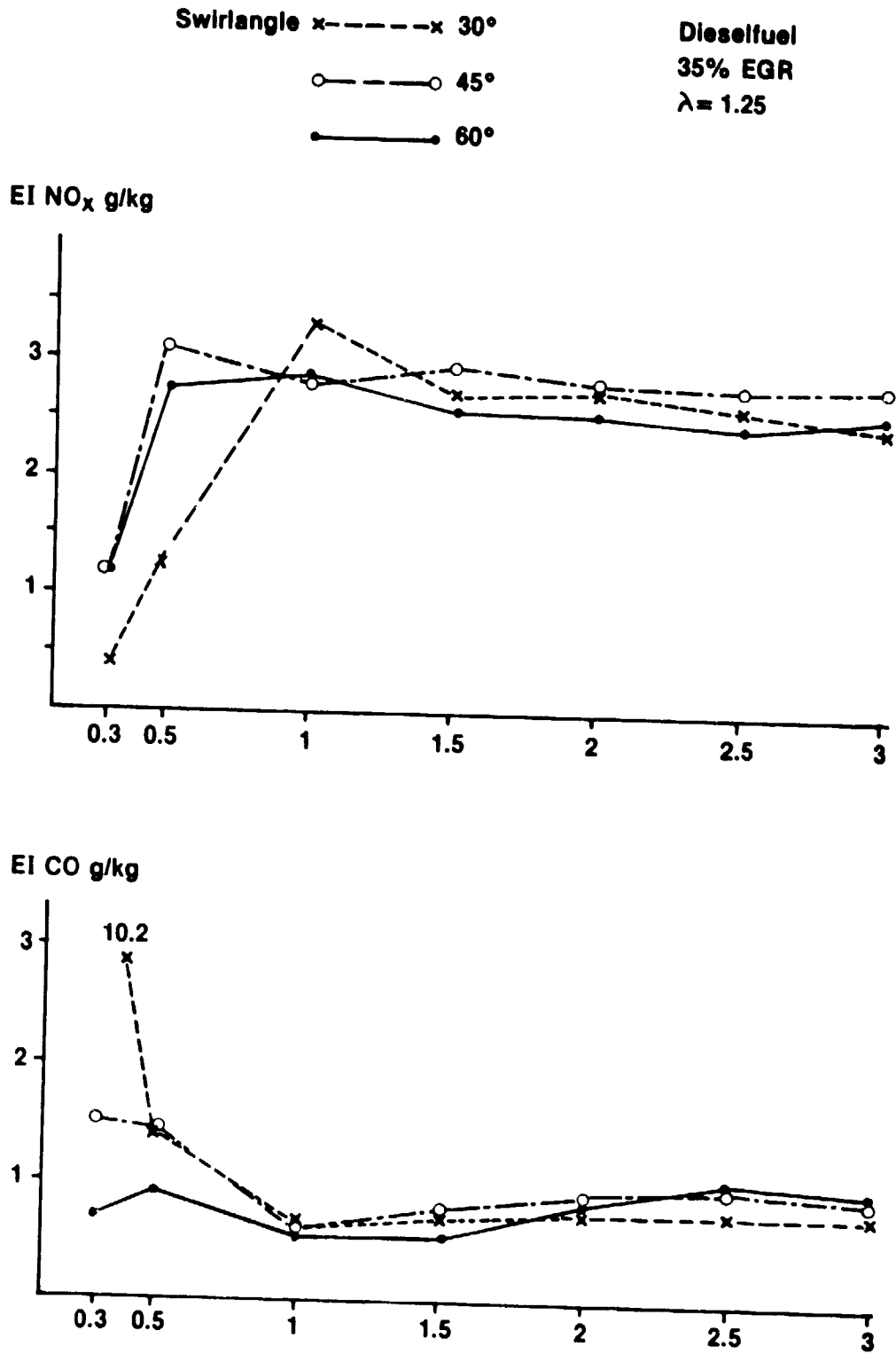


FIG 4.6:29 EMISSION INDEX NO_x AND CO VERSUS FUEL FLOW WITH 3 SWIRLERS.
 SWIRL ANGLE 30°, 45°, 60°

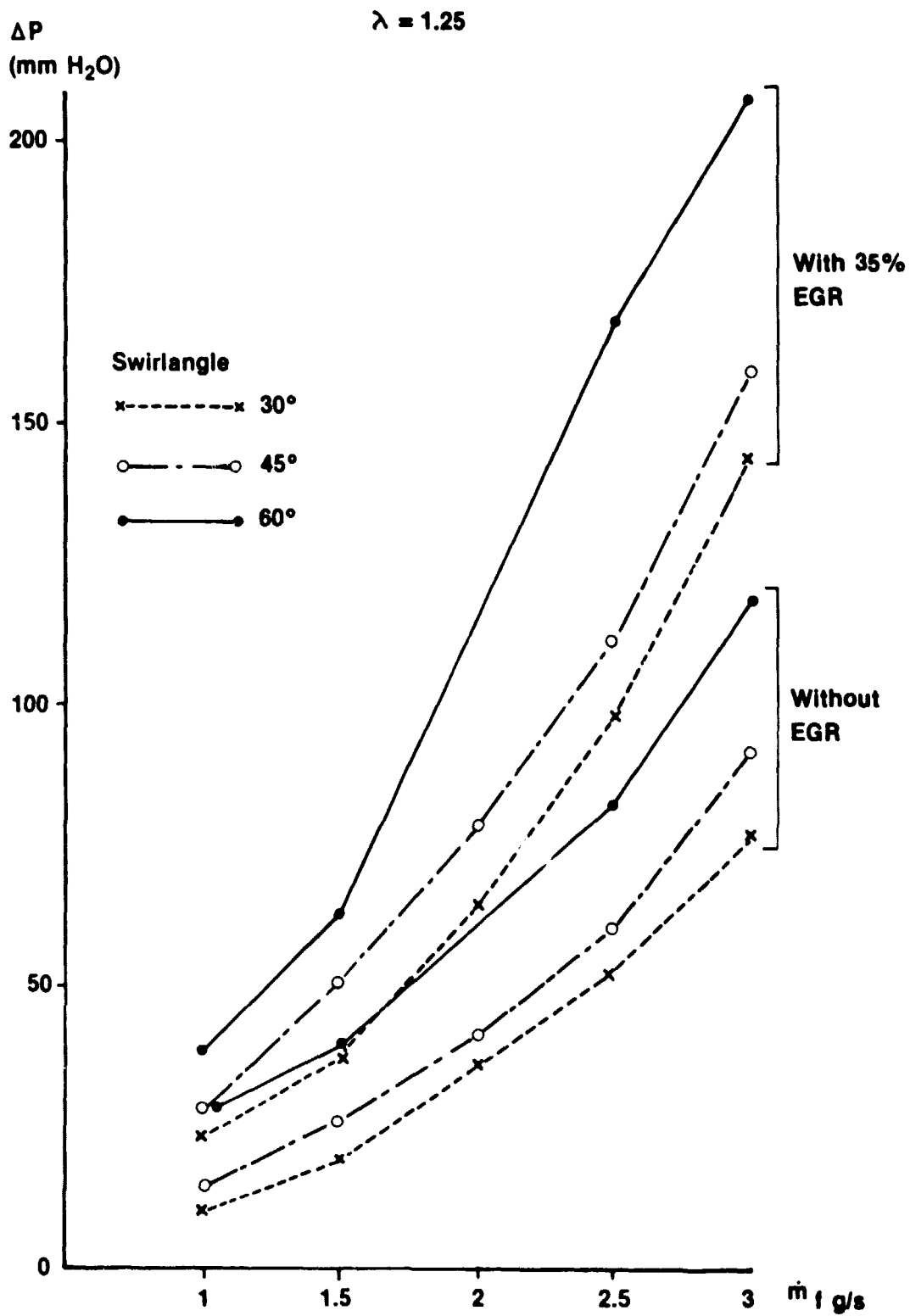


FIG 4.6:30 PRESSURE DROP ACROSS COMBUSTOR AND HEATER CAGE VERSUS FUEL FLOW. SWIRL ANGLE 30°, 45°, 60°. WITH AND WITHOUT EGR

ORIGINAL INTENT
OF POOR QUALITY

Gasoline

$\lambda = 1.25$

Swirlangle 45°

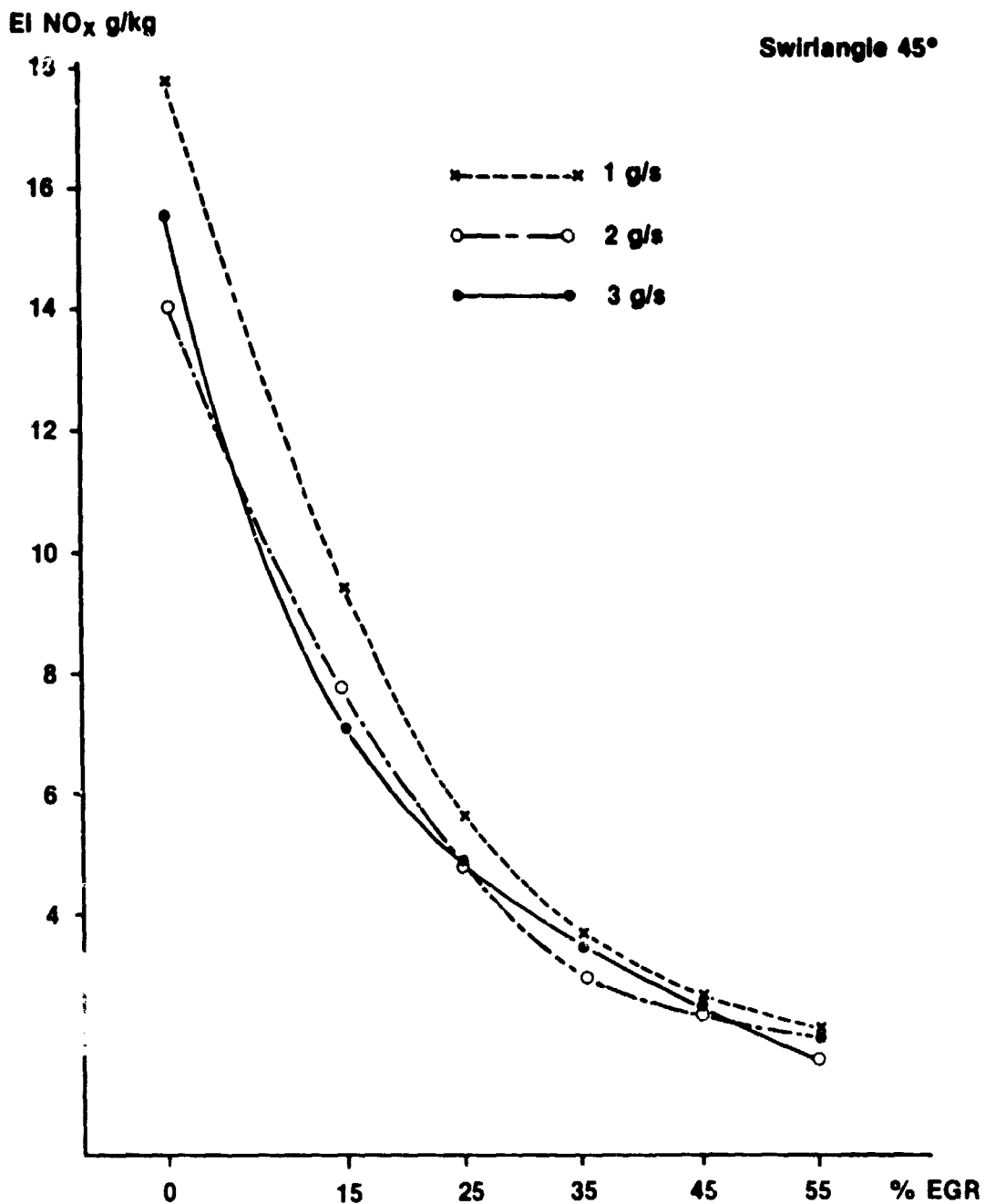
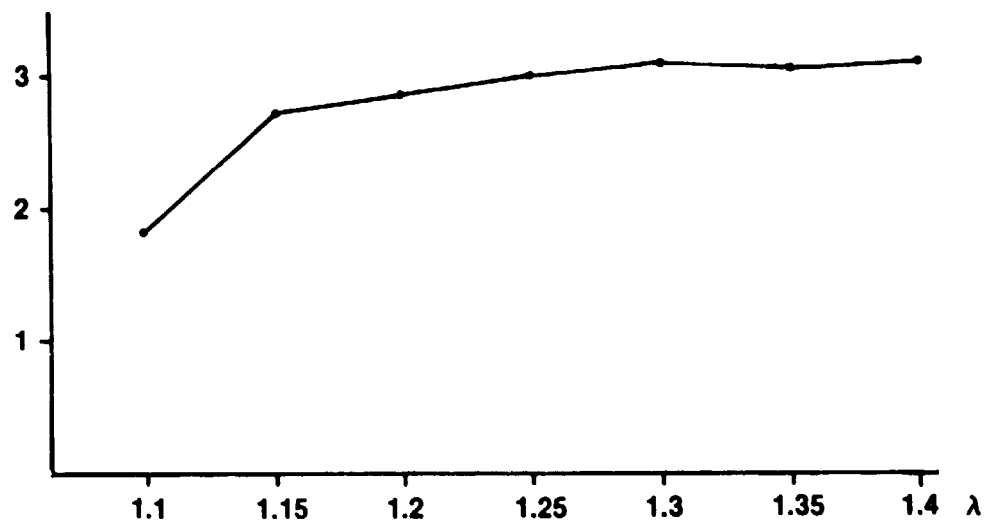


FIG 4.6.31 EMISSION INDEX NO_x VERSUS EGR.
FUEL FLOW 1, 2, 3 g/s

ORIGINAL QUALITY
OF FUEL QUALITY

$\lambda = 1.25$

EI NO_x g/kg



EI CO g/kg

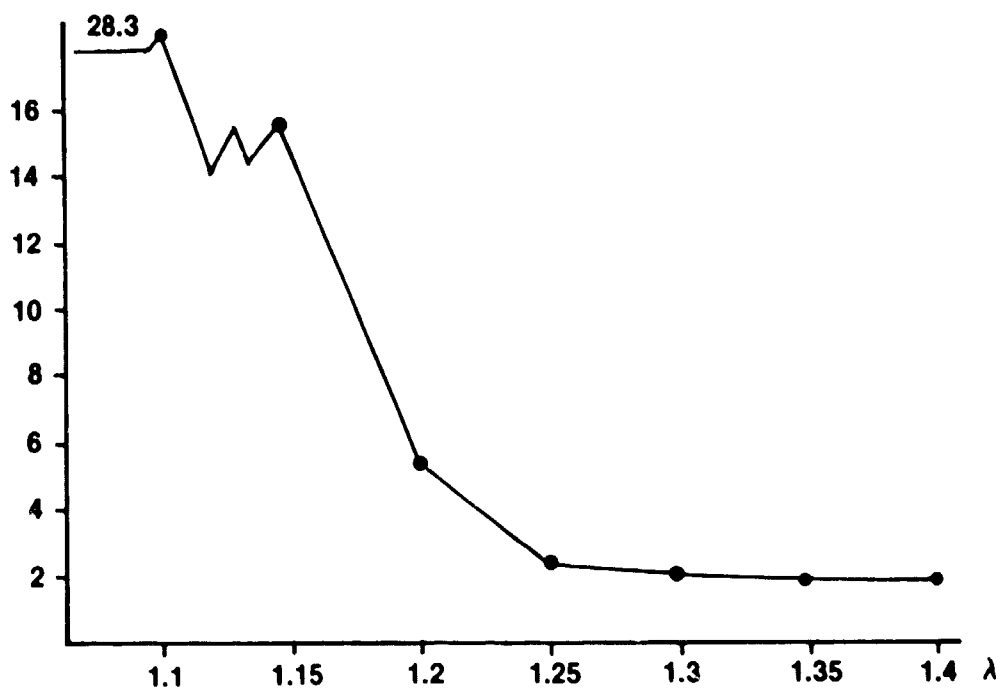


FIG 4.6:32 EMISSION INDEX VERSUS AIR EXCESS WITH 35 % EGR
FUEL FLOW 2,5 g/s
SWIRL ANGLE 45°

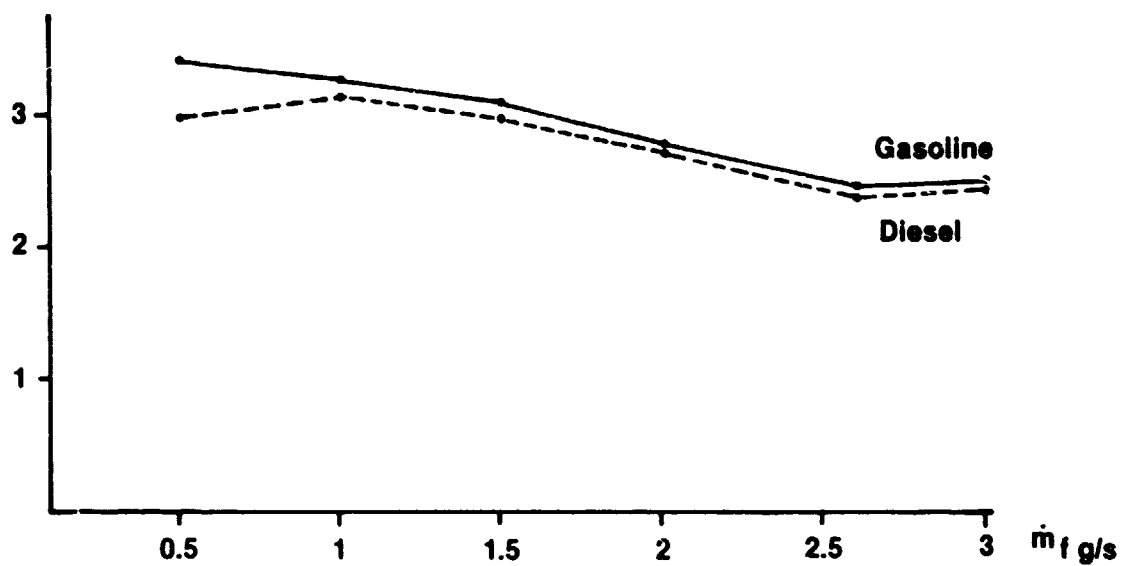
ORIGINAL IMAGE IS
OF POOR QUALITY

$\lambda = 1.25$

35% EGR

Swirlangle 45°

EI NO_x g/kg



EI CO g/kg

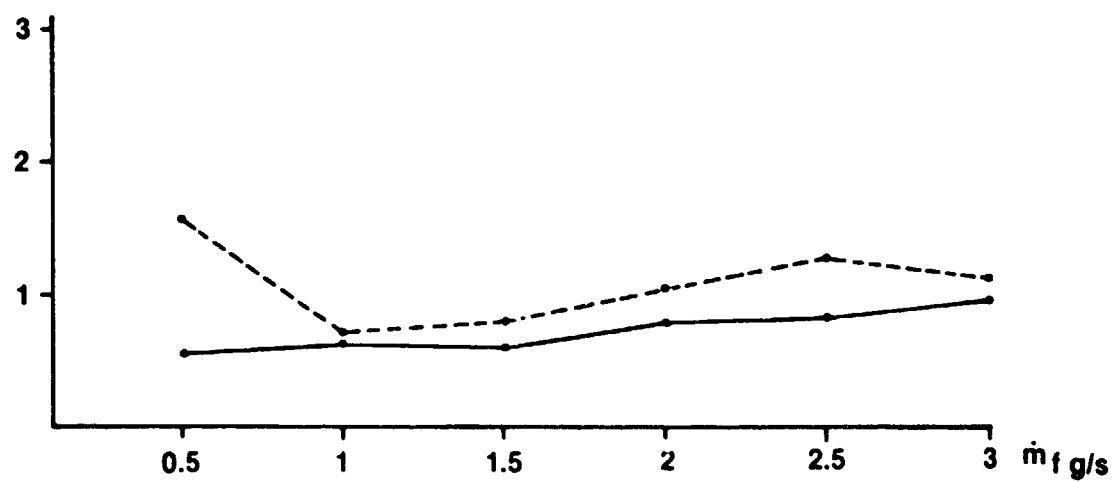


FIG 4.6:33 EMISSION INDEX NO_x AND CO VERSUS FUEL FLOW WITH
GASOLINE AND DIESELFUEL

ORIGINAL PAGE IS
OF POOR QUALITY

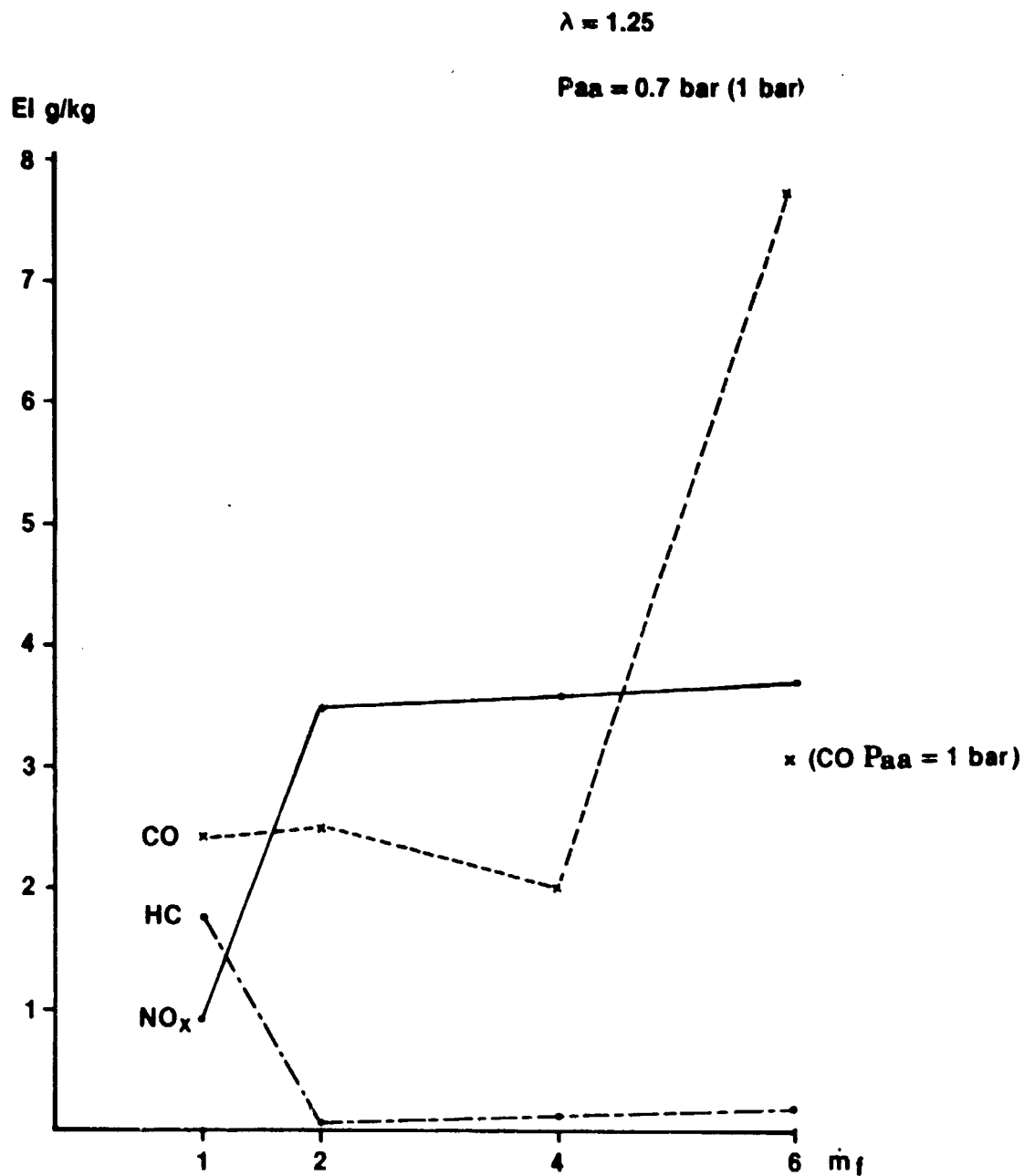


FIG 4.6:34 EMISSION INDEX VERSUS FUEL FLOW
SWIRL ANGLE 45°
METHANOL

OF POOR QUALITY

$$\lambda = 1.25$$

$$m_f = 4 \text{ g/s}$$

$$P_{aa} = 0.7 \text{ bar (1 bar)}$$

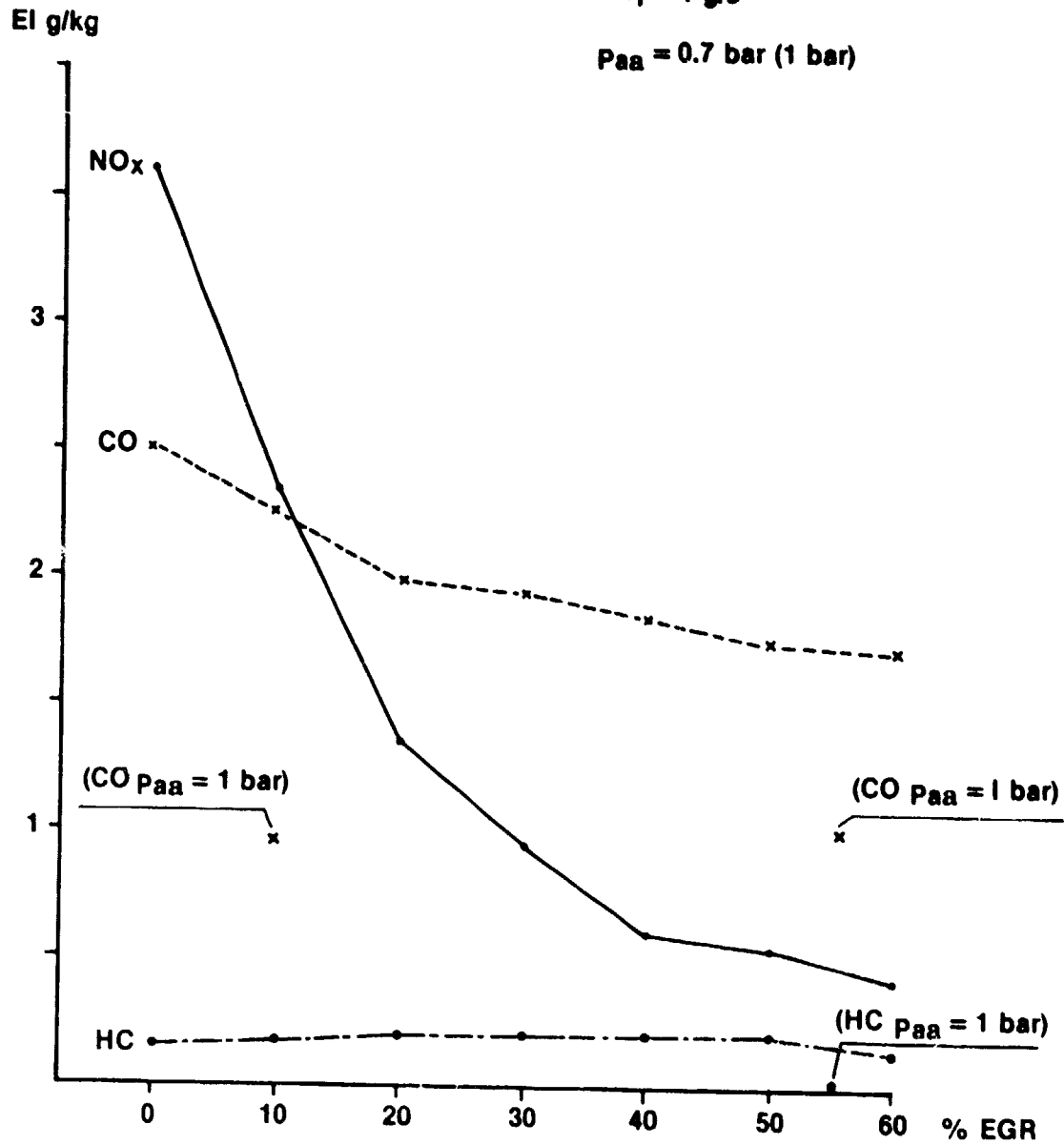


FIG 4.6:35 EMISSION INDEX VERSUS EGR.
METHANOL

$P_{aa} = 0.7 \text{ bar}$

$\dot{m}_f = 4 \text{ g/s}$

ORIGINAL PAGE IS
OF POOR QUALITY

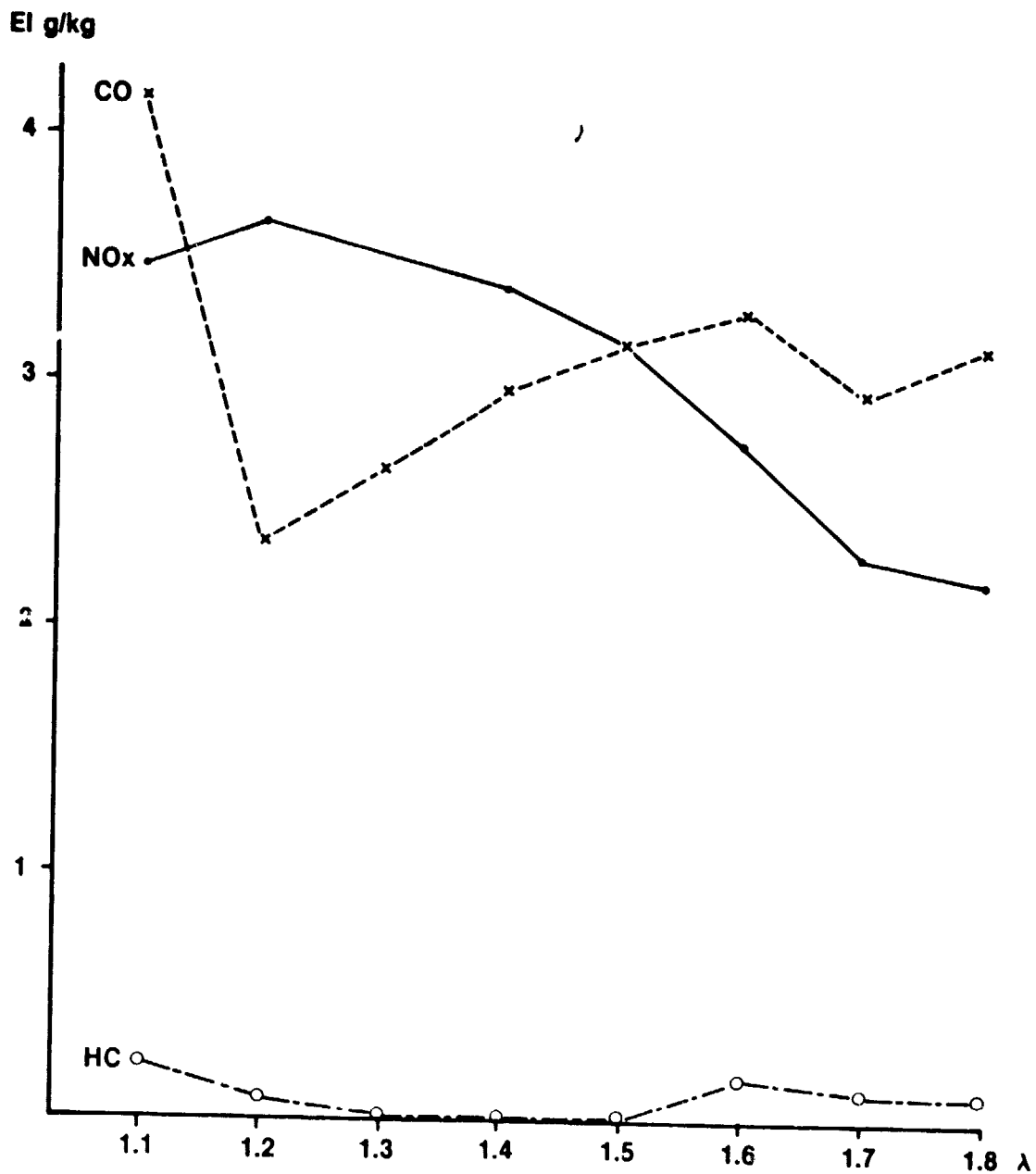


FIG 4.6:36 EMISSION INDEX VERSUS AIR EXCESS
METHANOL

ORIGINAL PAGE IS
OF POOR QUALITY

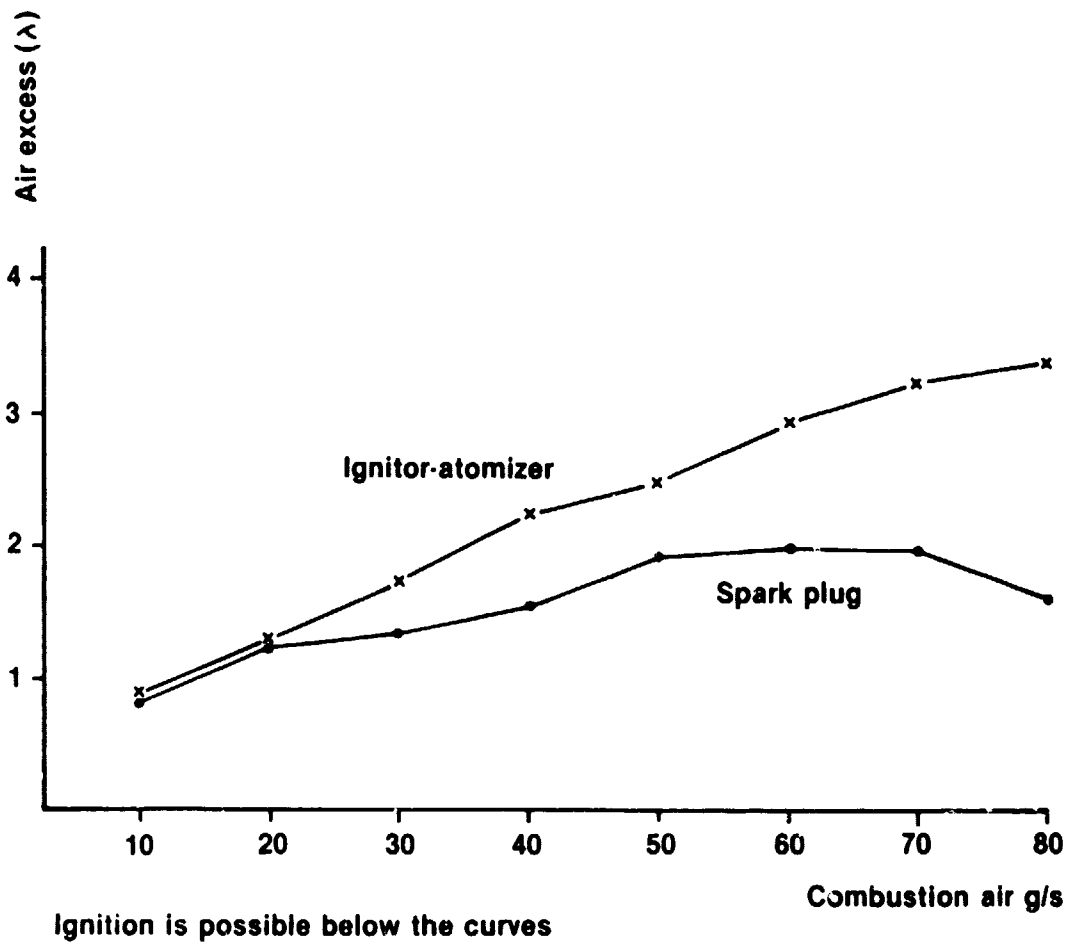
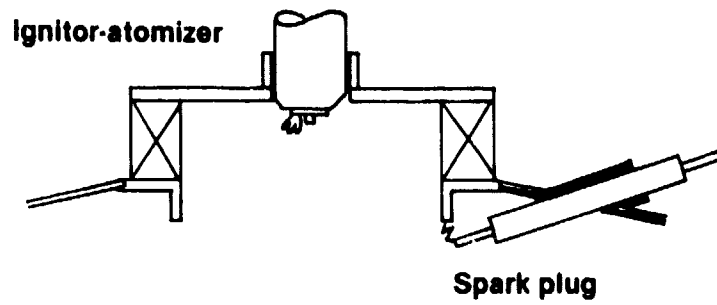


FIG 4.6:37 IGNITIONTEST
SWIRL ANGLE 45
FREE BURNING RIG
GASOLINE

CAUSE
OF POOR QUALITY

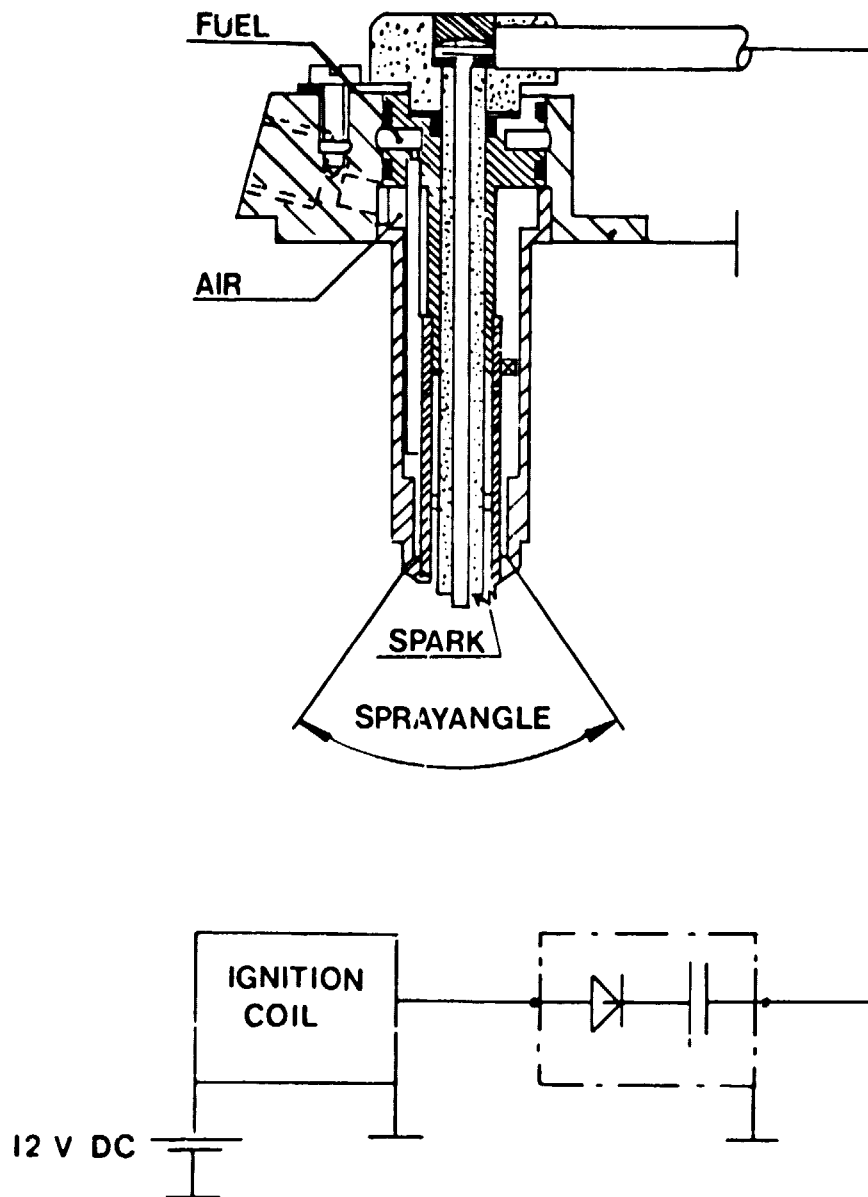


FIG 4.6:38 ATOMIZER / IGNITOR

OF POOR

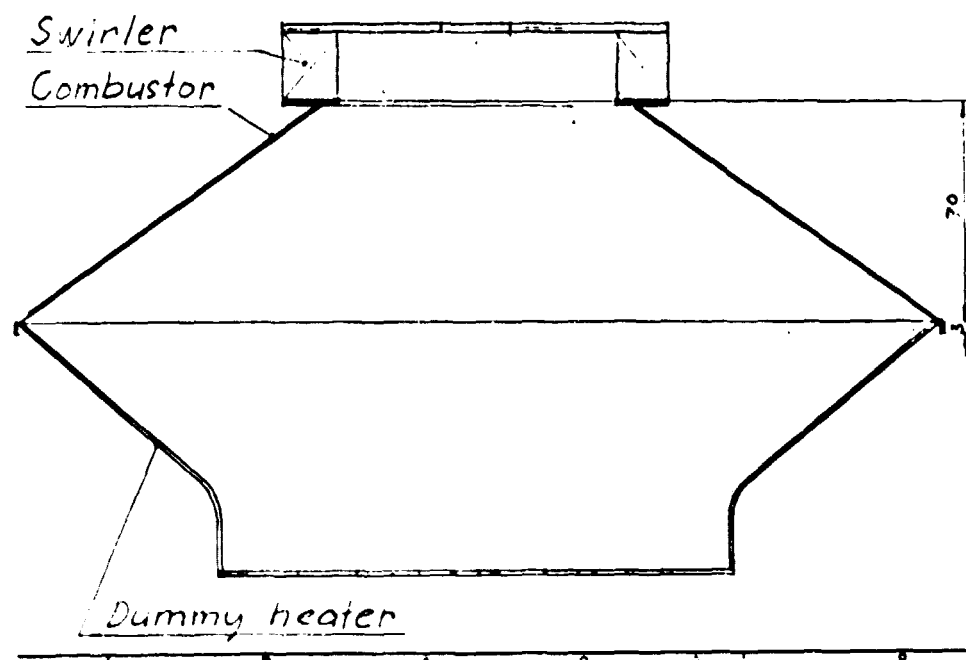
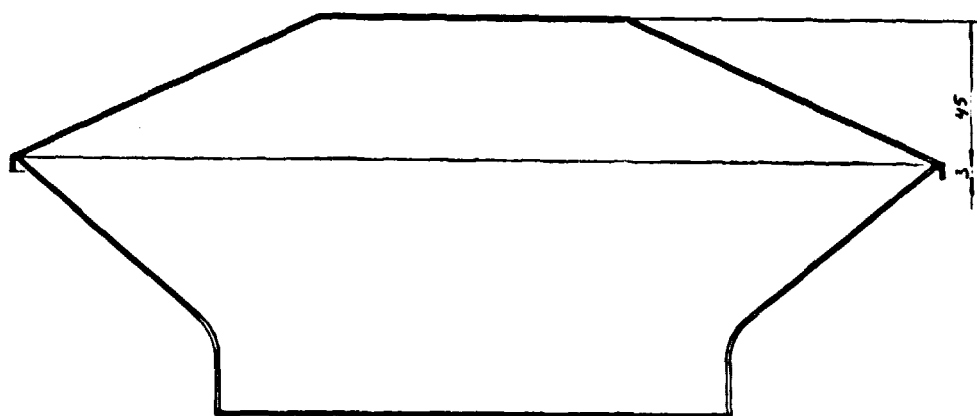
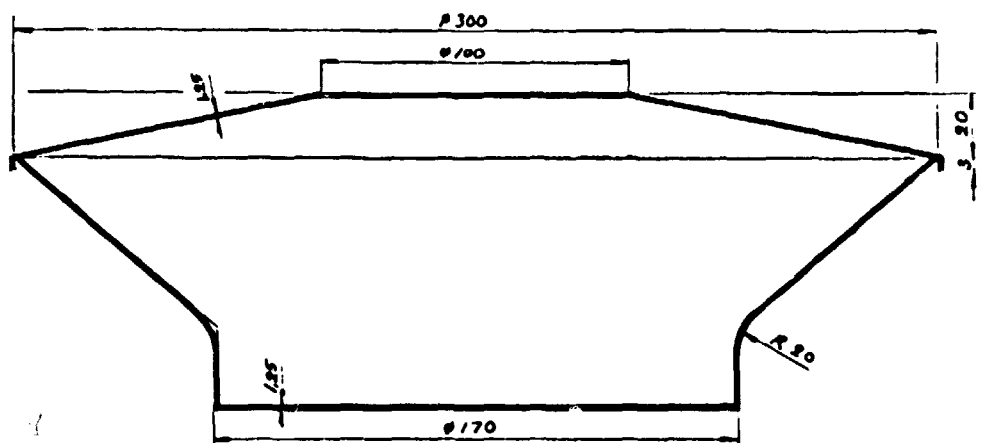


FIG 4.6:39 FREEBURNING COMBUSTOR RIG

4.7 Material selection and rationale

The major components are (see fig. 4.7:1):

Housing

Air preheater

CGR-system

Connecting duct

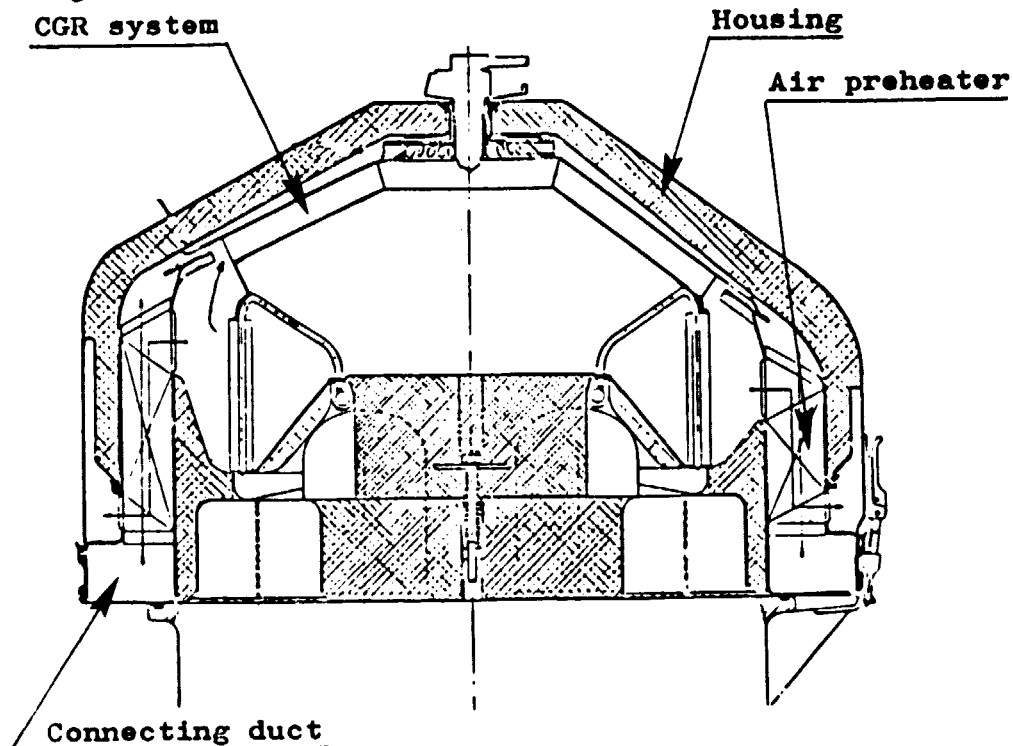


Fig. 4.7:1

Major components in the external heat system.

4.7.1 Housing

The inside of the house is in contact with preheated air of temperature up to about 700°C. The chosen alloy AISI 310S (SIS 2361) is a common combustion chamber material containing 25% Cr and 20% Ni. It has very good oxidation resistance and good high temperature strength, formability and weldability. The sheet thickness is 0,3 mm (0,012").

As insulation an alumina silica fiber material with the trade name Triton Kaowool has been chosen. The material has been used with good results in previous engine generations.

The outer shell will be manufactured in 0,4 - 0,7 mm (0,016-0,025") thick austenitic stainless steel AISI 304 (SIS 2333) or similar quality.

4.7.2 Air preheater

The incoming air to the combustor is preheated by means of the outgoing combustion gases (see fig. 4.7:2). The temperature of the combustion gases is about 800°C, as it enters the air preheater and about 230°C at the preheater's exit. In the exhaust gas outlet there is a risk (especially at starts) that the exhaust gas will condensate. If the fuel then contains sulphur, sulphuric acid will form in the condensate.

The air preheater is manufactured from 1200 0,15 mm (0,006") thick corrugated sheets, which are welded together. Since a combination of high temperature oxidation resistance, good formability, good weldability, resistance to low temperature corrosion and a low sensitivity to intergranular corrosion after welding is needed, it is difficult to choose the optimum alloy without extensive component testing. The material AISI 310 S (SIS 2361) is therefore chosen, since it has been used for air preheaters in earlier design with rather good results.

4.7.3 CGR-system

The recirculation in the CGR-system is achieved by means of ejectors in the inlet air flow-path. Part of the combustion gases are sucked back and mixed with the incoming air before entering the combustor, see fig. 4.7:2.

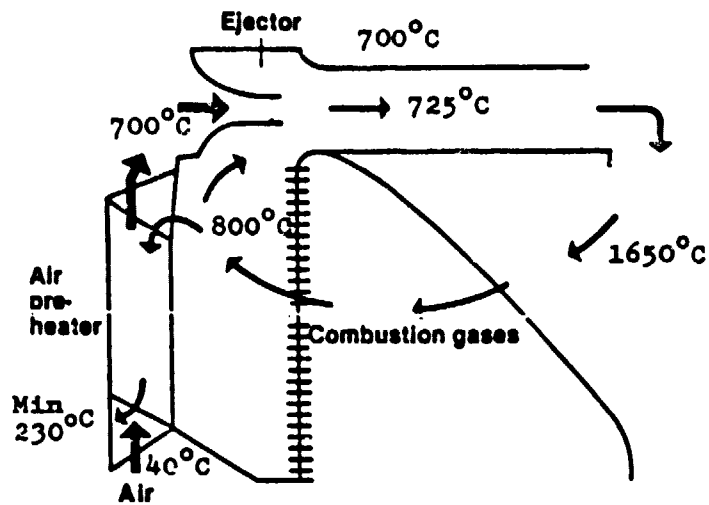


Fig. 4.7:2. Principal sketch and gas temperatures.

The mixture of air and recirculating combustion gases are guided into the center of the combustor, through 'mixing tubes'. These are built in involute shape in order to cover the whole combustor can and not leave any uncooled sections in between (see fig. 4.7:3).

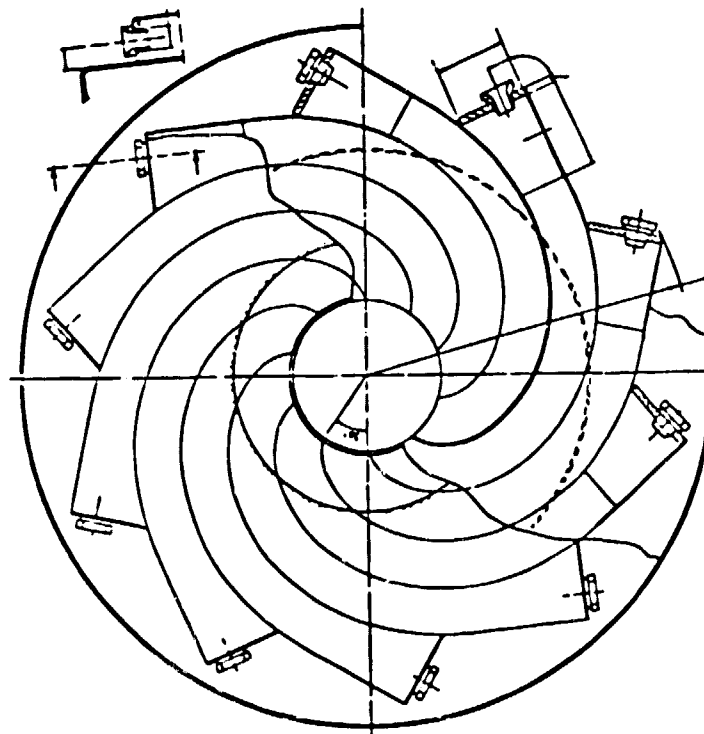


Fig. 4.7:3. In volute 'mixing tubes' in the CGR-system.

Another advantage is that this design makes the CGR-channels rather sturdy and insensitive to buckling.

The highest material temperature will occur in the center of the combustor lid, which is radiated by the flames and will be in the range of 1000 to 1100°C.

For this application a common combustor material, Nimonic 75, with excellent high temperature oxidation resistance, good high temperature strength and weldability has been selected. It has been used for combustor cans in previous engines with good result.

4.7.4 Air inlet casing

The air inlet casing shall hold the air preheater and the housing in place and also distribute the incoming air from the blower to the air preheater. Aluminum casting has been chosen as the material, but the exact composition of the aluminum is not yet determined. It will most probably be a silica copper alloy (AlSi8Cu3), which is easy to cast in a sandmold.

MOD I combustor development work

The combustor development work for the MOD I engine has followed two main paths: Development of the conventional combustor with EGR and development of the CGR-system.

The EGR system

The conventional combustor with EGR has been further developed. In the previous design (used on the Opel and the Spirit) the EGR flow was controlled by a two step EGR valve fig 4.8:1. One step was temperature controlled by a bimetal spring and the second step was controlled by the load and the temperature via a solenoid. The disadvantage with such a system was the step by step changes in mass flow to the combustor. This could cause flame out. Another disadvantage with the system was that the EGR flow was unnecessarily high at low loads. See fig 4.8:2. The solution for these problems is a continuously variable EGR valve which is capable of keeping the % EGR constant through the load range. Such a valve has been designed and tested. In order to reduce the blower power demands, tests have been performed with different swirlers to find a design that reduces the combustor pressure loss. Tests with alternative fuels such as methanol and diesel oil have also been performed with the EGR system. The objective of these tests was to chart future problem areas in utilizing the multifuel capability of the Stirling engine.

The new EGR valve (fig 4.8:3) is governed by the total pressure built up from the blower in a way that the open valve area is increased with increased pressure. The movement of the valve plate is attained by the force from the pressure working at a membrane. The valve stroke is controlled by an adjustable spring.

Results from the tests show that the valve works satisfactory. There is still a minor decrease in % EGR with load, fig 4.8:4, but that can probably be eliminated by changing the spring characteristic. The main problem during the work was clogging of the surfaces within the valve. The effect of this clogging was that the valve got stuck. In the latest design these problems are eliminated.

The combustor pressure drop was reduced about 10% by changing the swirlangle from 45° to 30°, fig 4.8:5. The influence on emissions was slight. EICO went up and EINO_x went down below idle load thus indicating some deterioration in the fuel air mixing, fig 4.8:6.

At the tests with different fuels it was evident that diesel oil and gasoline are very close as far as emissions are concerned, fig 4.8:7. Methanol emissions were very low (fig 4.8:8). This is specially true for NO_x. Emissions of CO were initially higher than the corresponding diesel and gasoline emissions, but were reduced by increasing the atomizer air flow.

The CGR system

The development work on the CGR system has been concentrated to reducing the combustor pressure drop, without increasing the NO_x emissions (decreasing the CGR) or deteriorate the flame stability or the temperature distribution. The combustor pressure drop is dominated by the pressure drop of the ejector jets. The choice of jets is dictated by the demands for CGR in combination with the momentum exchange efficiency and the pressure losses on the swirler, the combustor and the heater. A mathematical model of the CGR system has been developed and the influence of various parameters on the performance of the CGR-circuit is fairly well understood. Verification tests have been performed in the Fluid Dynamics Laboratory (test equipment is shown in fig 4.8:9). Good agreement between calculated and measured values was found, fig 4.8:10. The model is not capable of predicting performance of other ejectors than the straight tubular type. In order to improve flame tube cooling different types of rectangular cross section channels (fig 4.8:11-12) have been tested in a special test rig, fig 4.8:13. From these tests four different geometries were selected for further tests at burning conditions (fig 4.8:14-17). Free burning tests and combustor rig tests showed that all four combustors manufactured had about the same pressure drop and temperature distribution, but one combustor gave considerably more CGR and thus lower NO_x emissions, fig 4.8:18. This combustor had straight guide vanes which formed narrowing mixing channels.

The other combustors had involute shaped guide vanes forming mixing channels with constant width. The very high CGR-circuit efficiency of the straight guide vanes combustor could be used either to get very low emissions but with the disadvantage of a by pass valve to reduce the pressure drop at high loads or to lower the pressure drop by increasing the jet diameter and allow NO_x emissions to increase somewhat. It has been stated that full load combustor pressure drop of about 800 mmW is acceptable from the viewpoint of the blower. According to calculations this could be achieved by using a jet diameter of 11.25 mm (fig 4.8:19). This means that the by pass valve is unnecessary, if the NO_x emissions are acceptable. Recent combustor rig tests have clearly verified that NO_x emissions are well below the limits set up by emission objectives ($\text{EINO}_x \leq 3.77 \text{ g/kg}$) utilizing ejector jets that give a combustor pressure drop of about 800 mmW at full load, 4.8:20-21. Different types of by pass valves have been designed and tested. Long term tests have been performed with a rotating valve with a conical sliding surface (fig 4.8:22). This valve suffered initially from leakage due to thermal distortion. After regrinding the problem disappeared. However, the friction forces on the sliding surface caused a stick-slip behaviour when the valve was rotated, fig 4.8:23. This problem was reduced by making the sliding surface two dimensional, fig 4.8:24.

Conclusions

The two competing combustion systems have been analytically evaluated and it has been found that the CGR-system gives about 0.8 MPG better mileage than the EGR system according to the models used. Based on the performance calculations and the experiences from the rig tests the CGR system must be considered as the prime alternative for the MOD I engine.

[illegible]

I-326

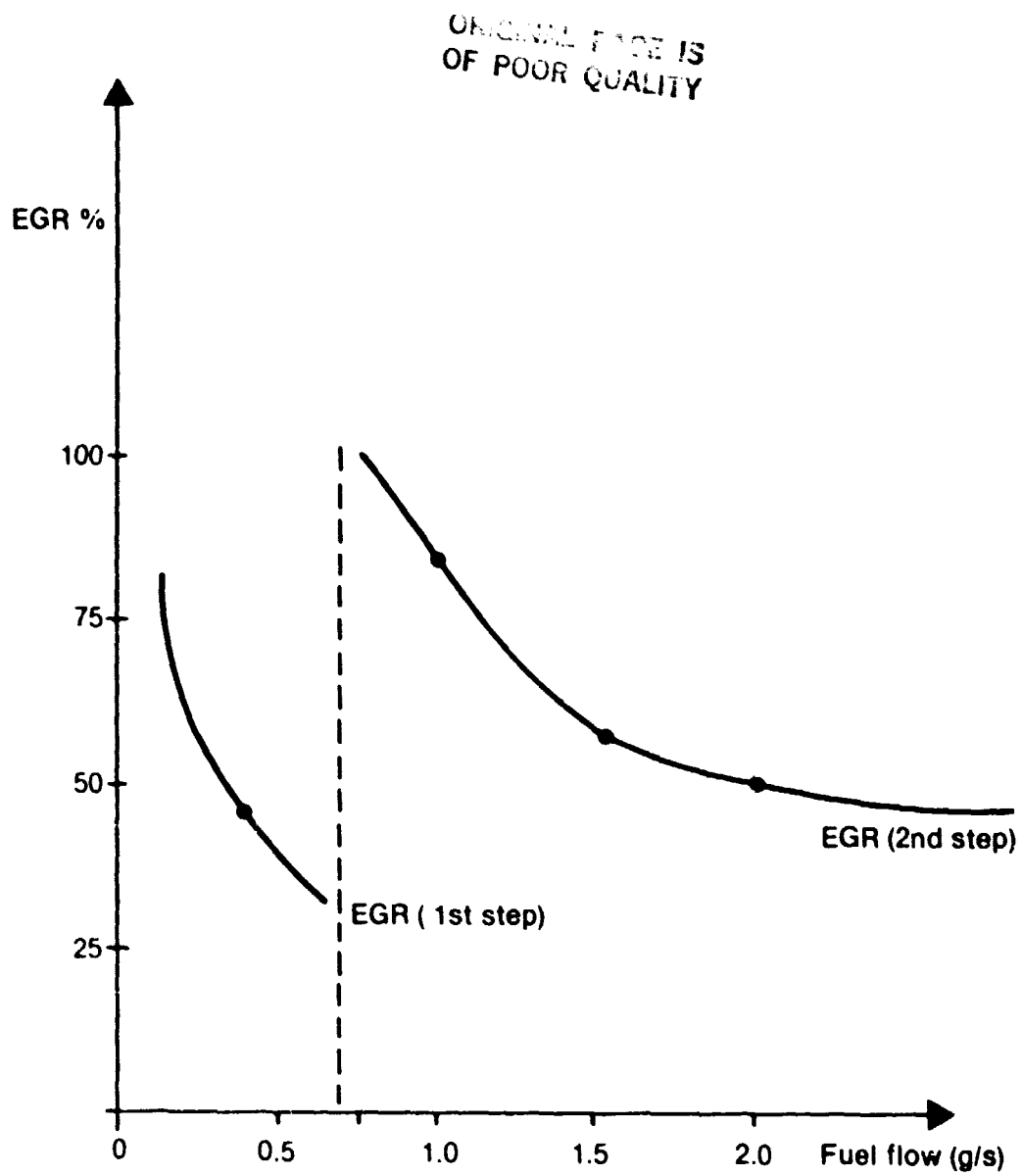


Fig. 4.8:2
Exhaust gas recirculation
(EGR) versus fuel flow

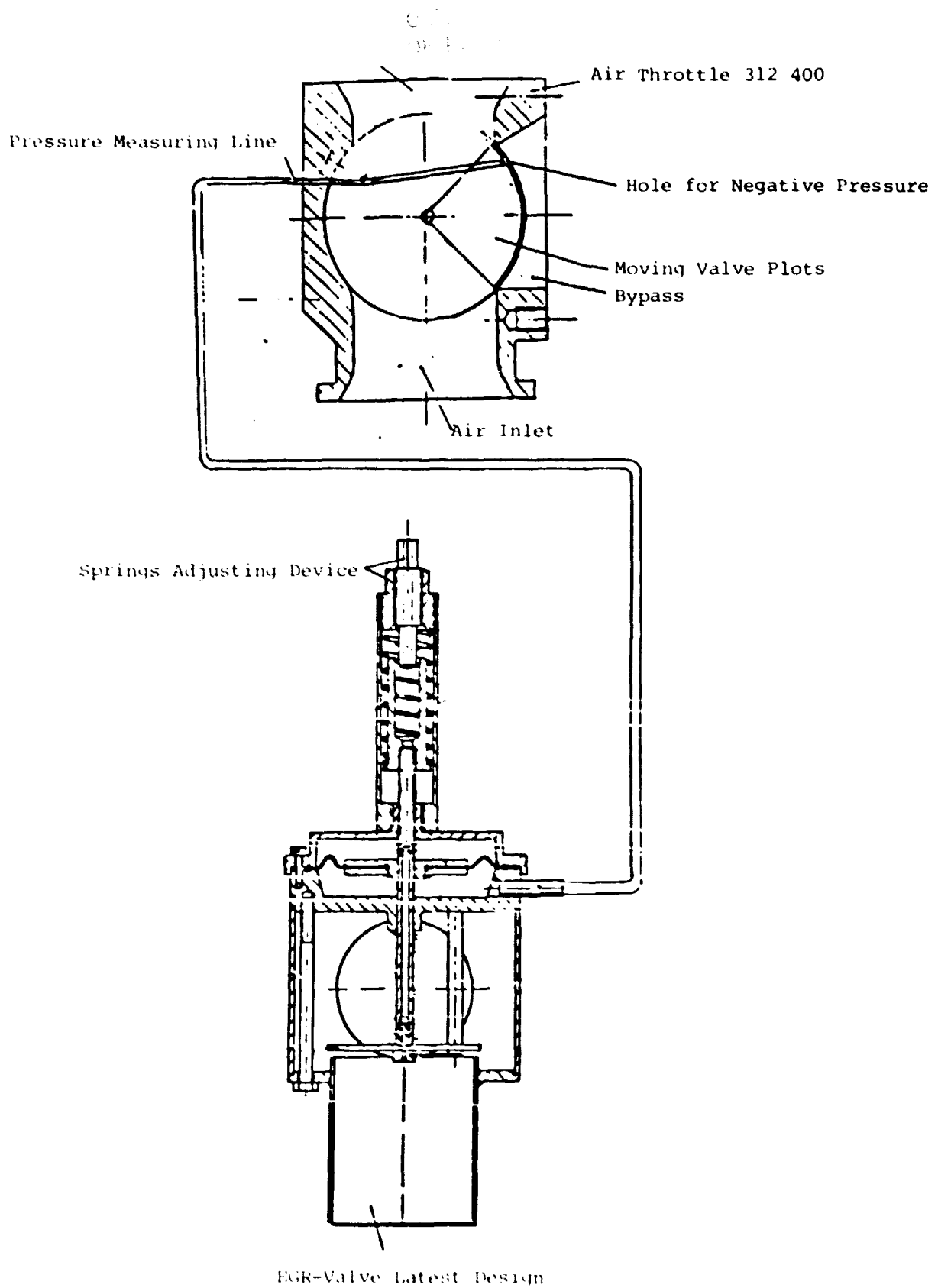


Figure 4.8:3

ORIGINAL PHOTO
OF POOR QUALITY

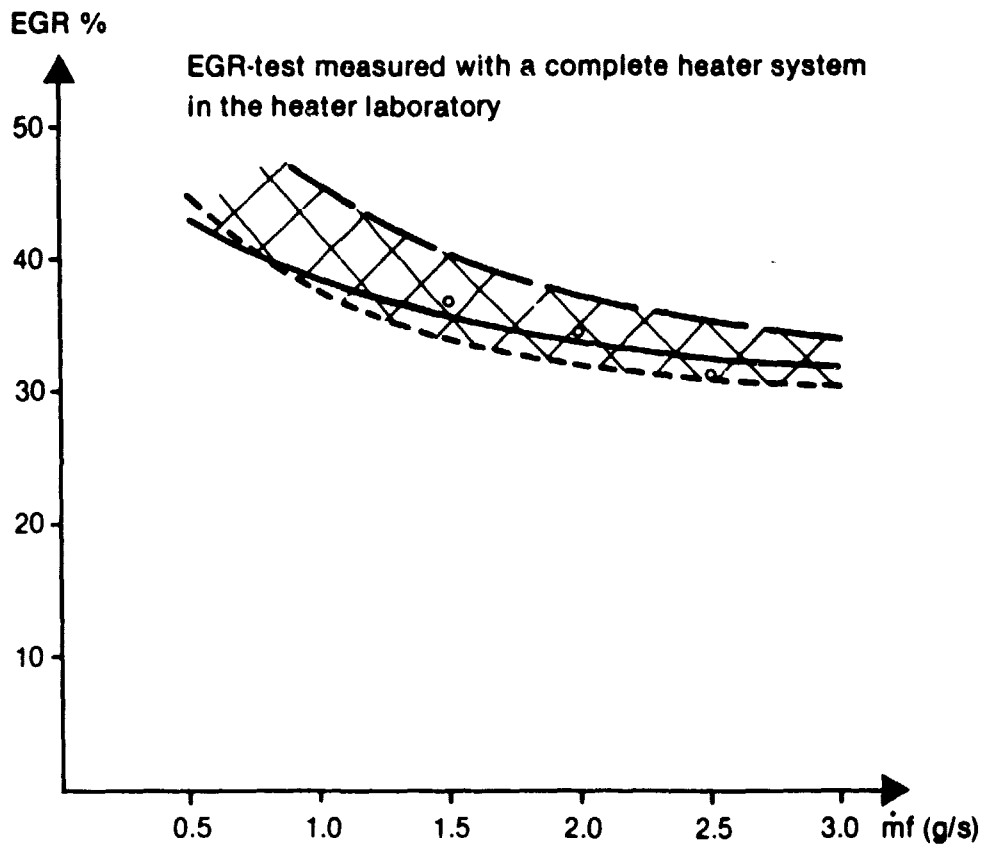


Fig. 4.8:4
EGR-percent versus fuel flow
for EGR-valve

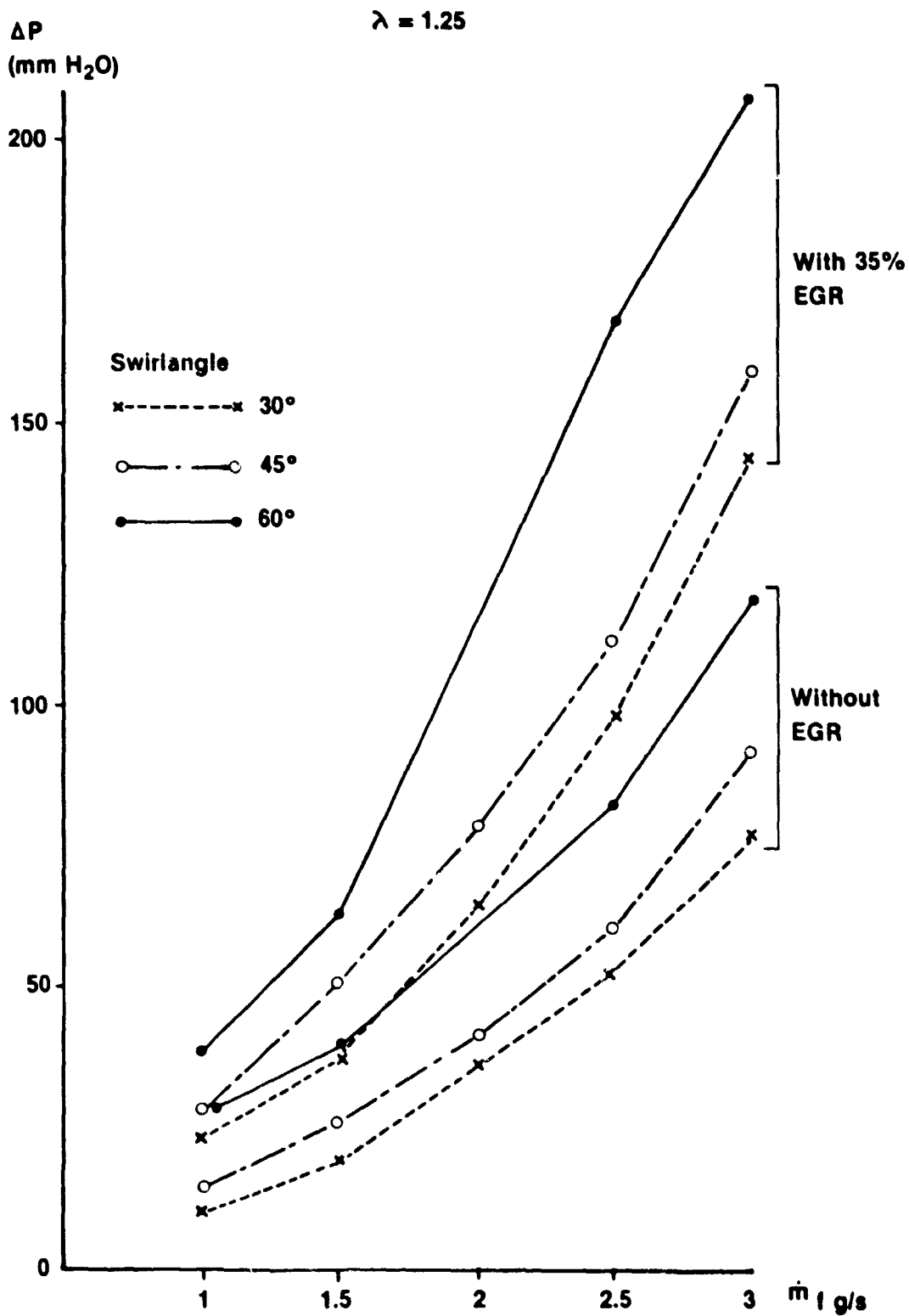


FIG 4.8.5 PRESSUREDROD ACROSS COMBUSTOR AND HEATER CAGE VERSUS FUEL FLOW. SWIRL ANGLE 30°, 45°, 60°. WITH AND WITHOUT EGR

OF FUEL ECONOMY

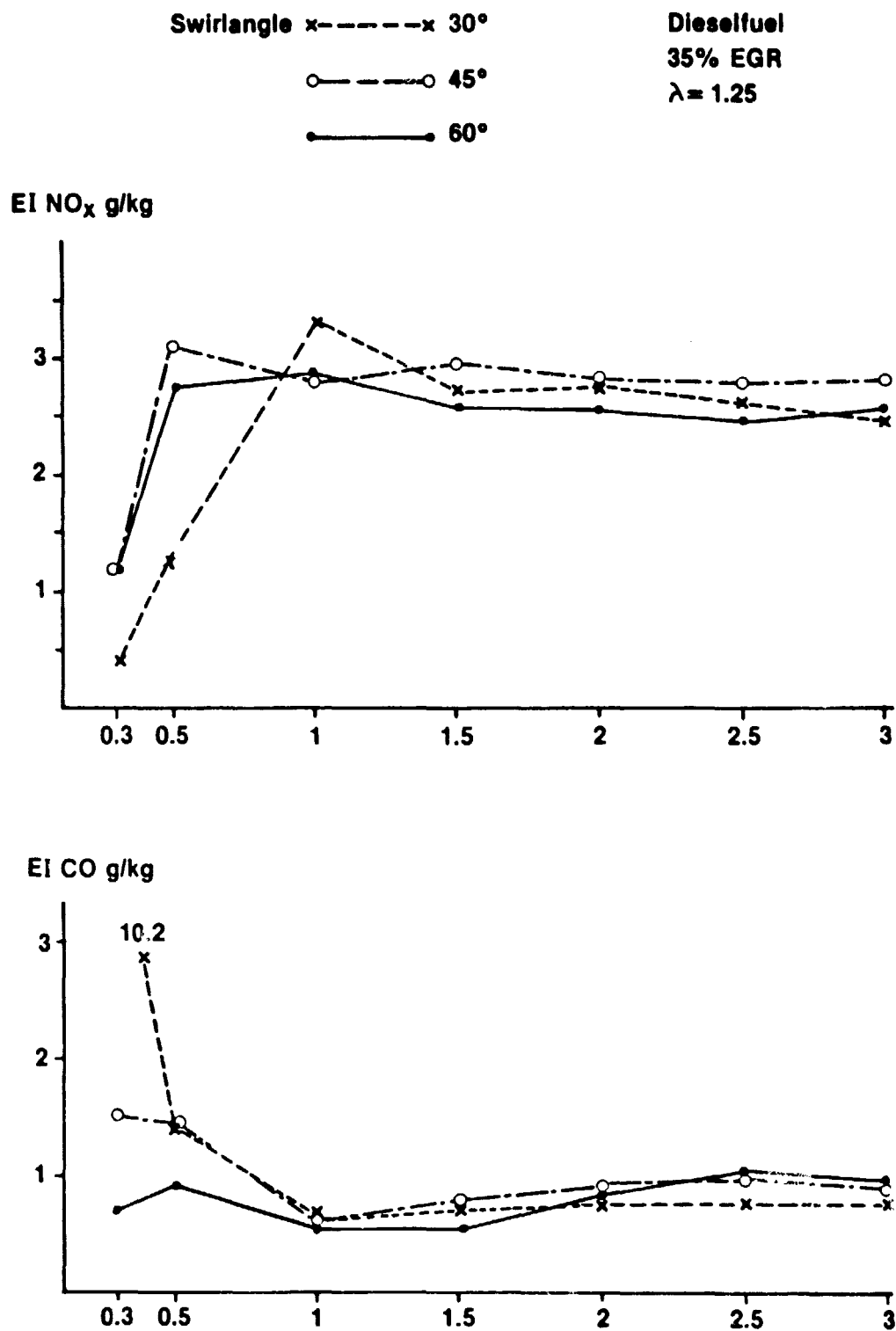


FIG 4.8:6 EMISSION INDEX NO_x AND CO VERSUS FUEL FLOW WITH 3 SWIRLERS.
 SWIRLANGE 30°, 45°, 60°

ORIGINAL PAGE IS
OF POOR QUALITY

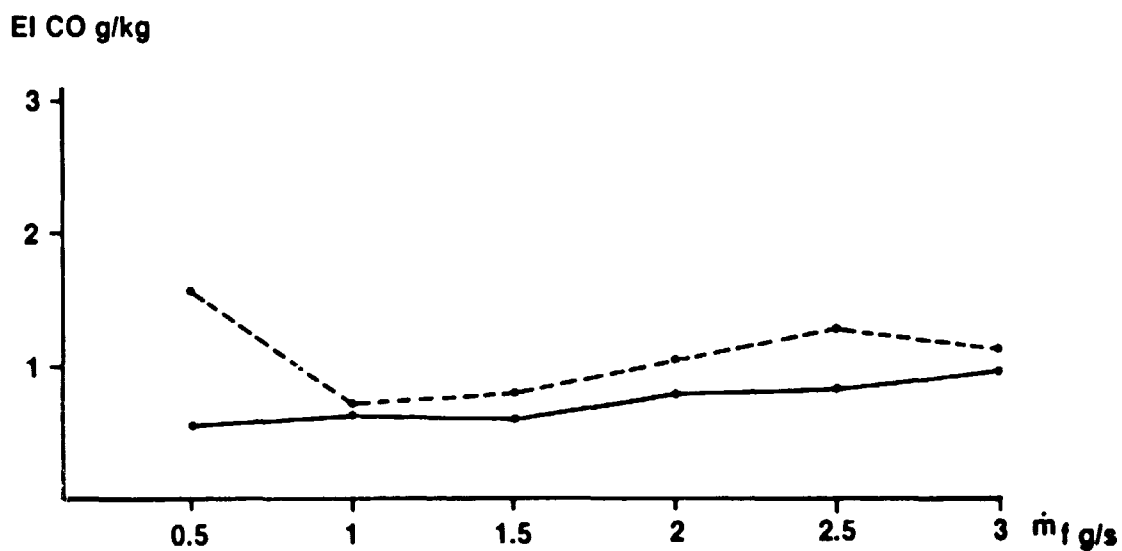
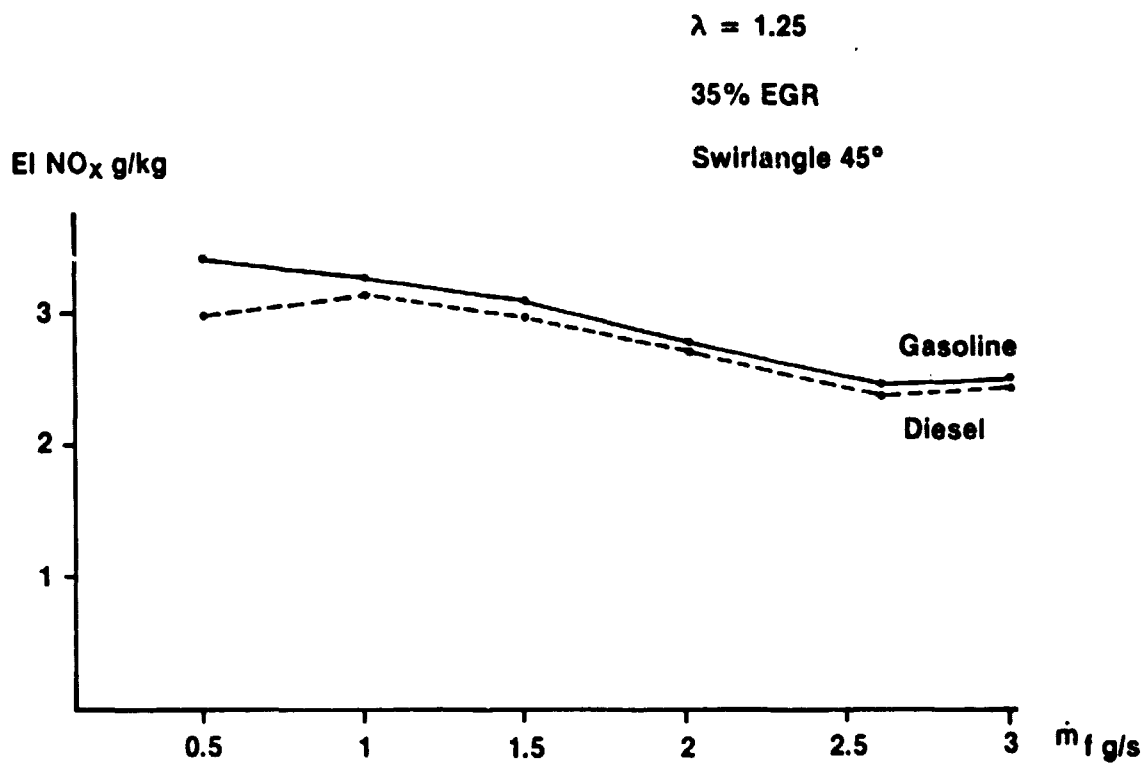


FIG 4.8:7 EMISSION INDEX NO_x AND CO VERSUS FUEL FLOW WITH
GASOLINE AND DIESELFUEL

ORIGINAL SERIES
OF PUBLICATIONS

$$\lambda = 1.25$$

$$m_f = 4 \text{ g/s}$$

$$p_{aa} = 0.7 \text{ bar (1 bar)}$$

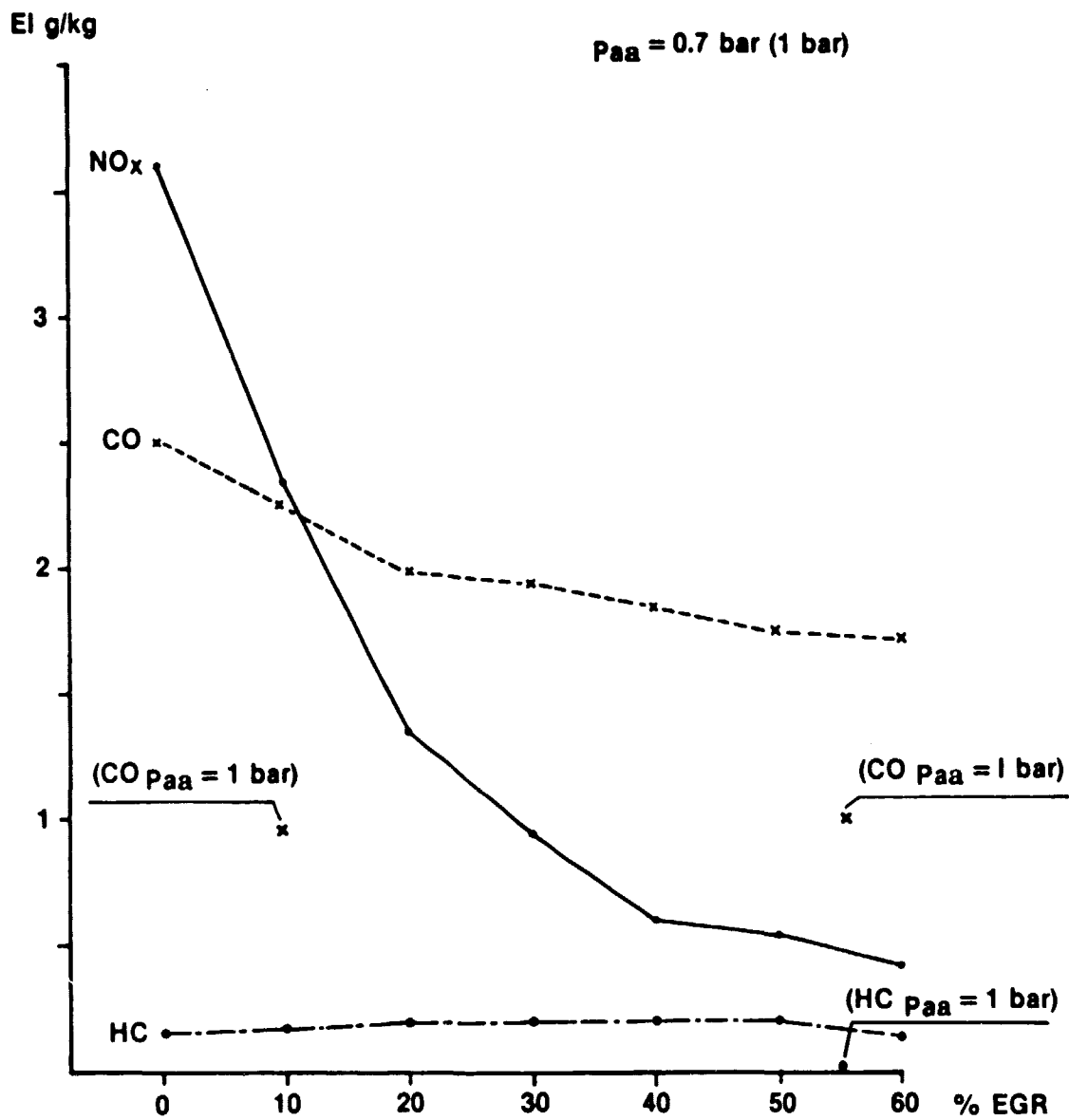


FIG 4.8:8 EMISSION INDEX VERSUS EGR.
METHANOL

Ejector Test Equipment

Exchangeable Inlet to Mixing
Tube Smooth and Sharp Edged

Exchangeable Nozzle $\phi d = 16, 12, 8$ and 6

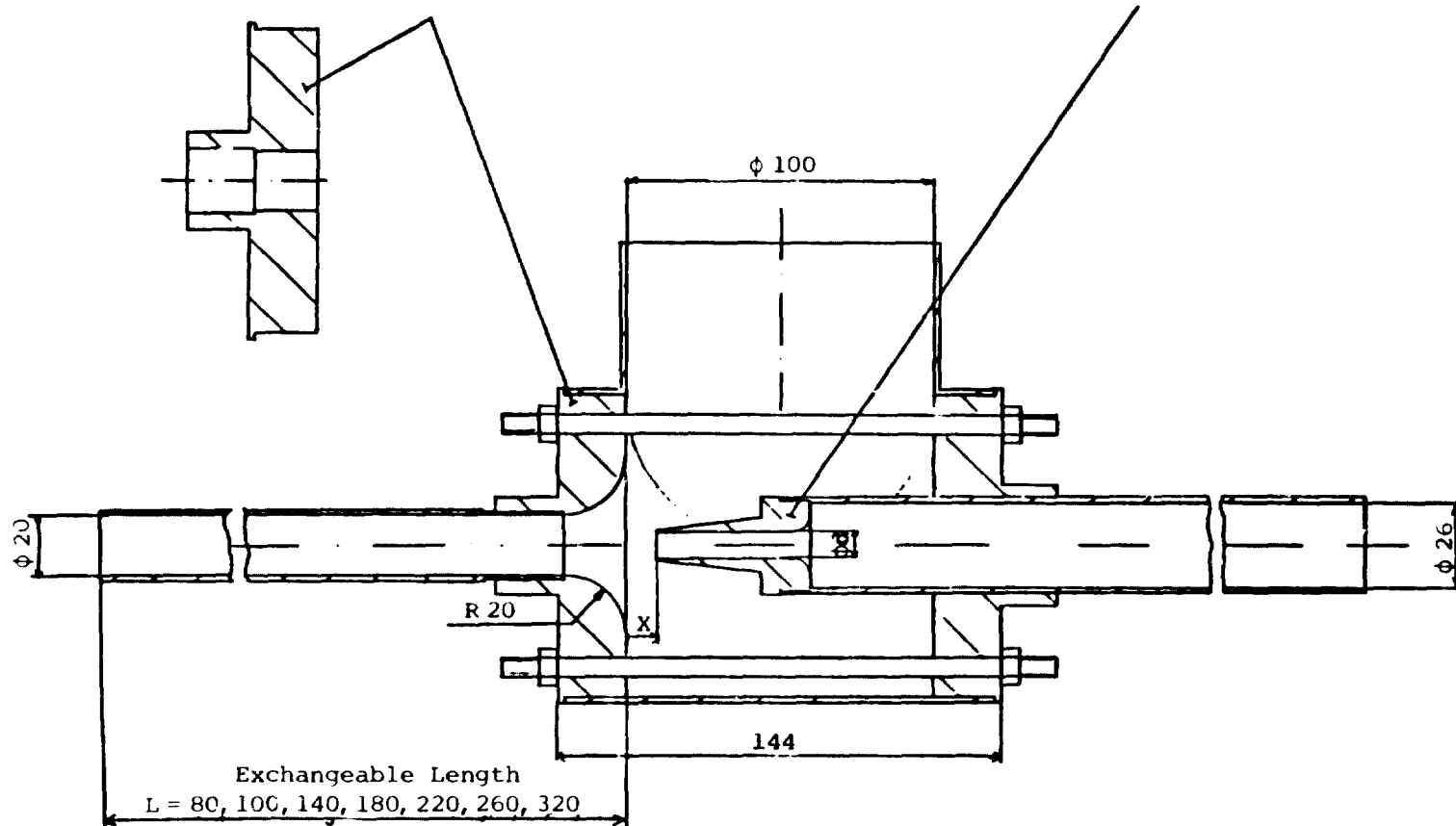


Figure 4.8:9 Ejector Test Equipment Scale 1:2
(Enclosure 1 - USSW Report 79-0126C)

ORIGINAL PAGE IS
OF POOR QUALITY

Measured values

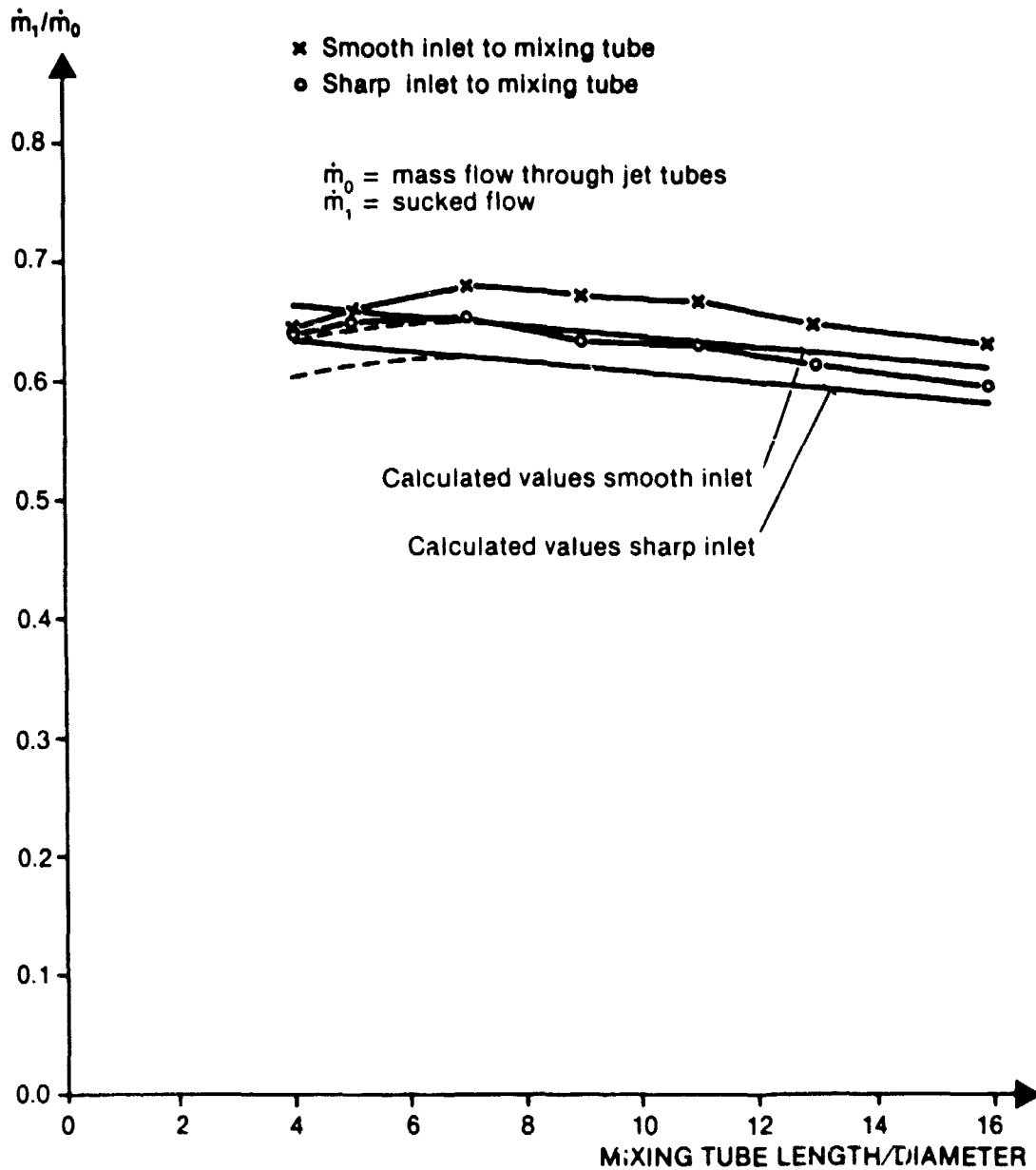


Fig. 4.8:10
Comparison of calculated and measured
values
Jet tube diameter = 12 mm

ORIGINAL FIGURE
OF FOUR CHANNELS

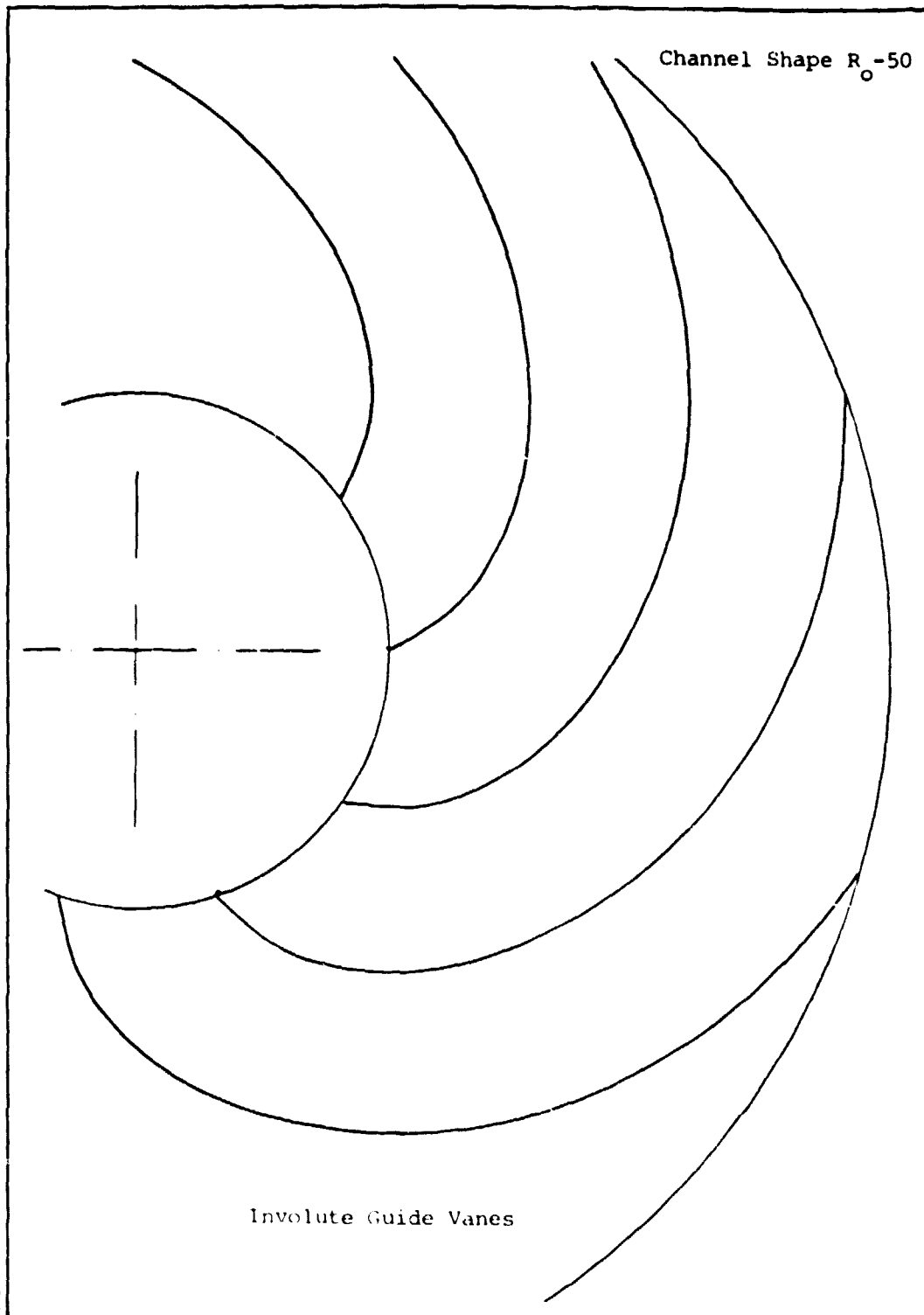
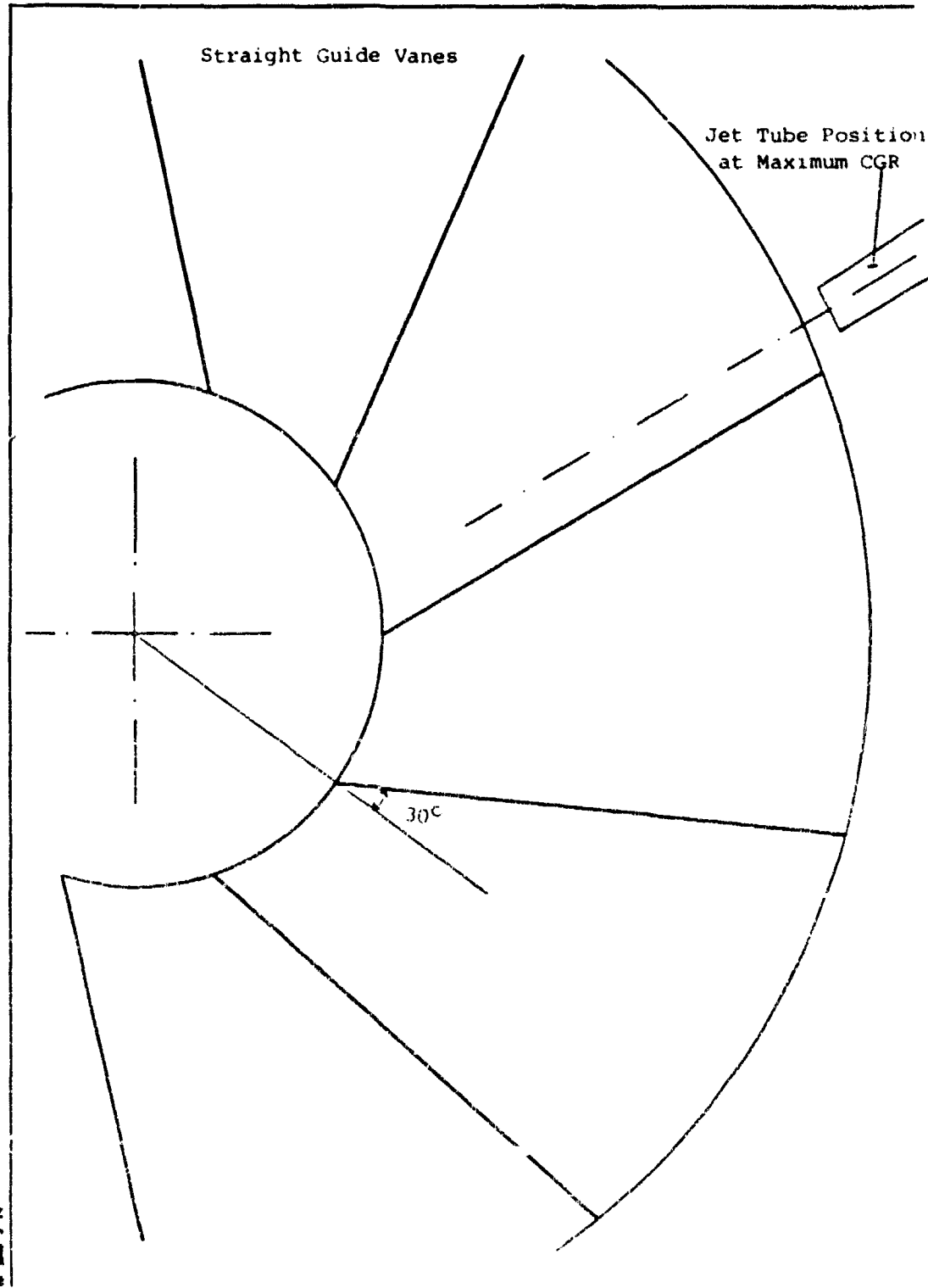


Figure 4.8:11



Straight Guide Vanes

Figure 4.8:12

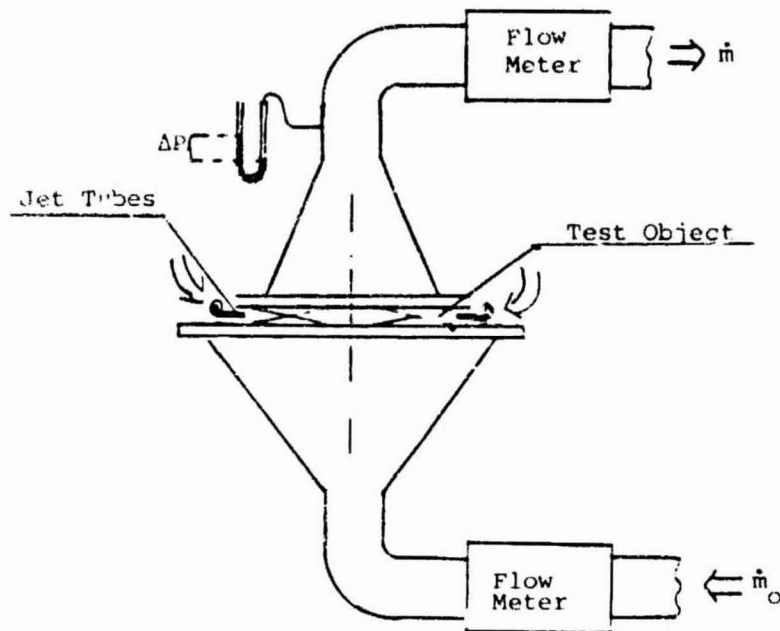


Fig. 4.8.13a Combustor Rig Schematic

The combustor test rig, Fig. 4.8.13b, has 10 jet tubes with the diameter ϕ 10 mm. The inlet of the combustor is ϕ 100. The height of the tested channels was 25 mm. The jet tubes were mounted at the center of the channel height.



Figure 4.8:13b Combustor Test Rig

ORIGINAL PAGE IS
OF POOR QUALITY

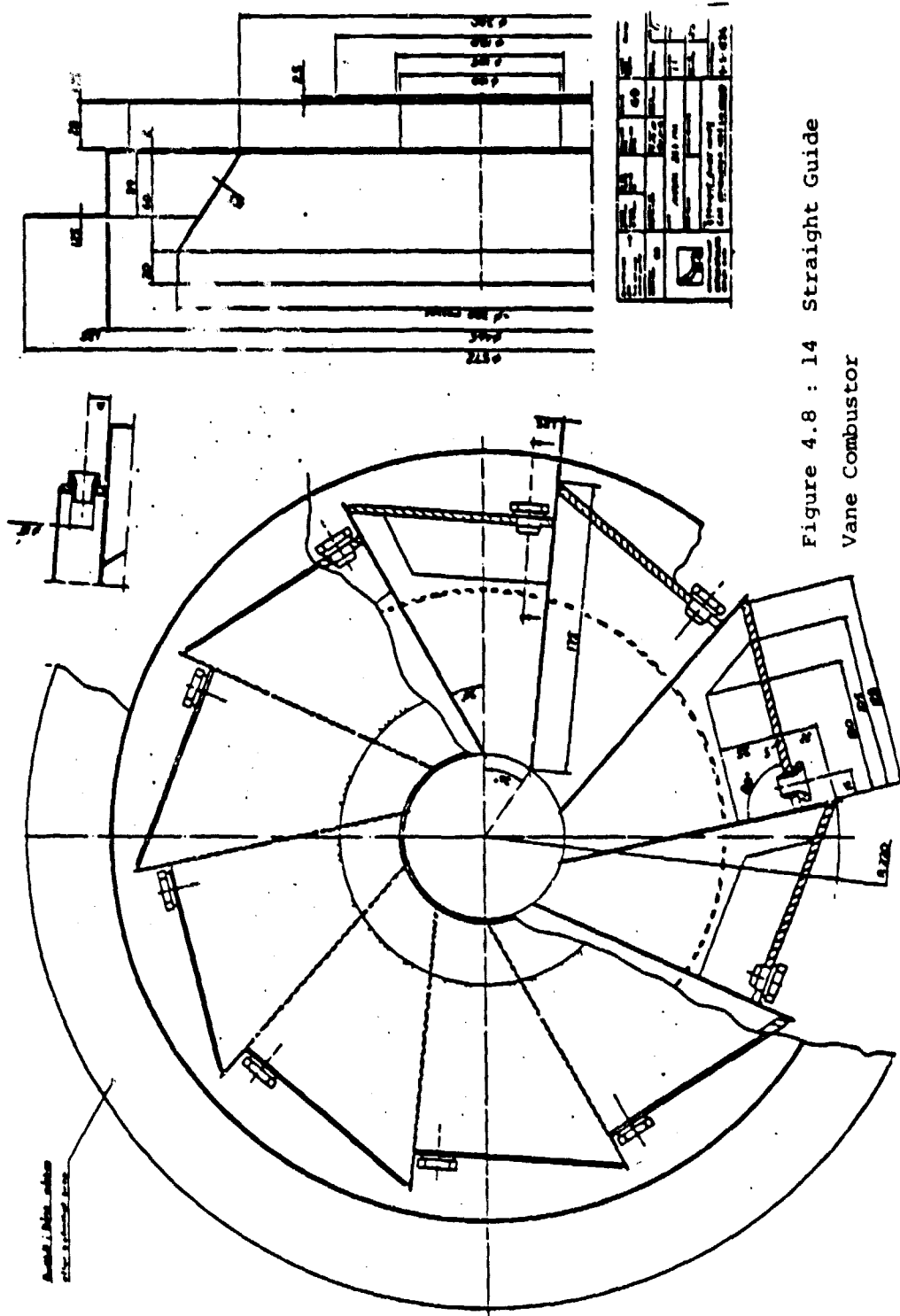
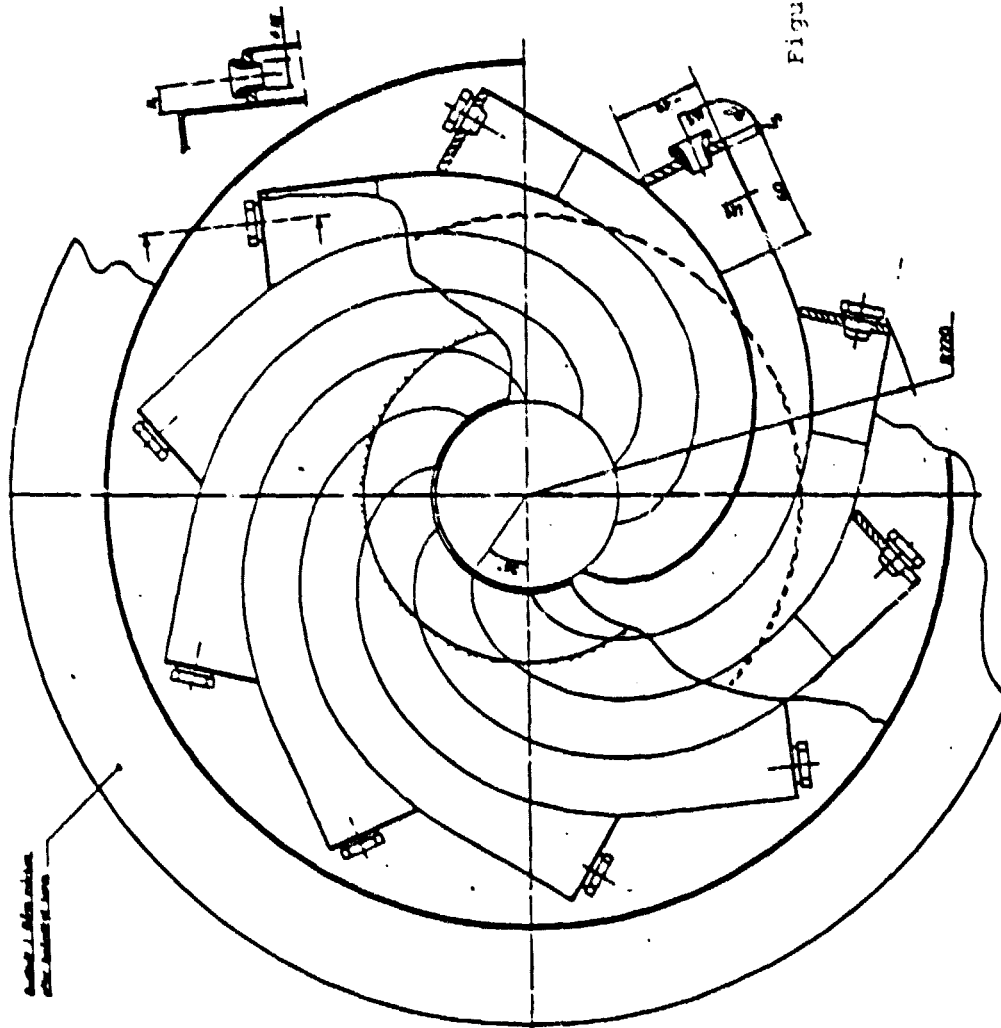


Figure 4.8 : 14 Straight Guide
Vane Combustor

1. The first step in the process of identifying a problem is to recognize that a problem exists. This is often done by comparing current performance with a desired state or goal. If there is a significant difference, a problem is identified.



Figure 4.8 : 16 Involute CGR Combustor



ORIGINAL FROM IS
OF POOR QUALITY

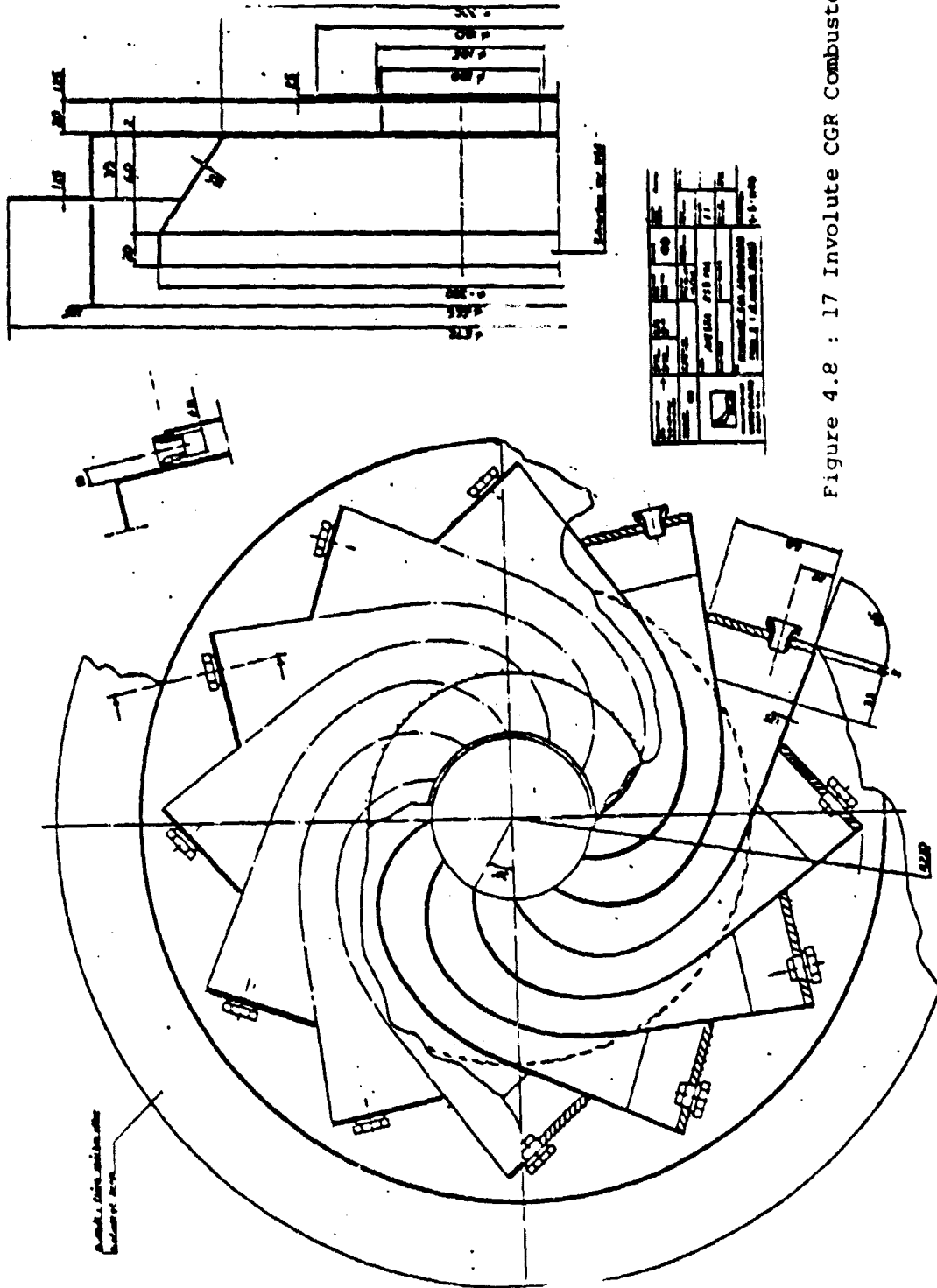


Figure 4.8 : 17 Involute CGR Combustor

ORIGINAL PAGE IS
OF POOR QUALITY

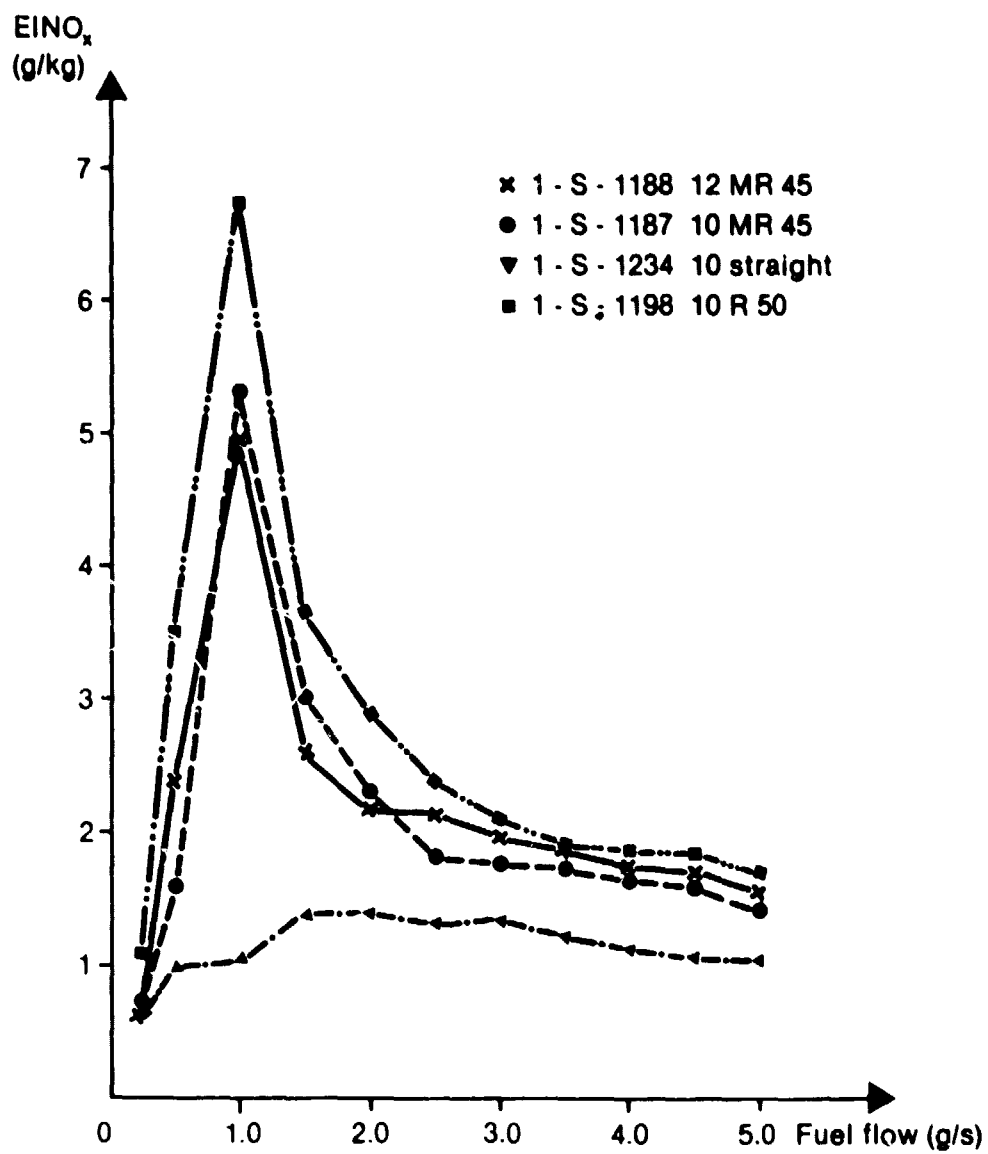


Fig. 4.8:18
 $EINO_x$ versus fuel flow
Four different combustors

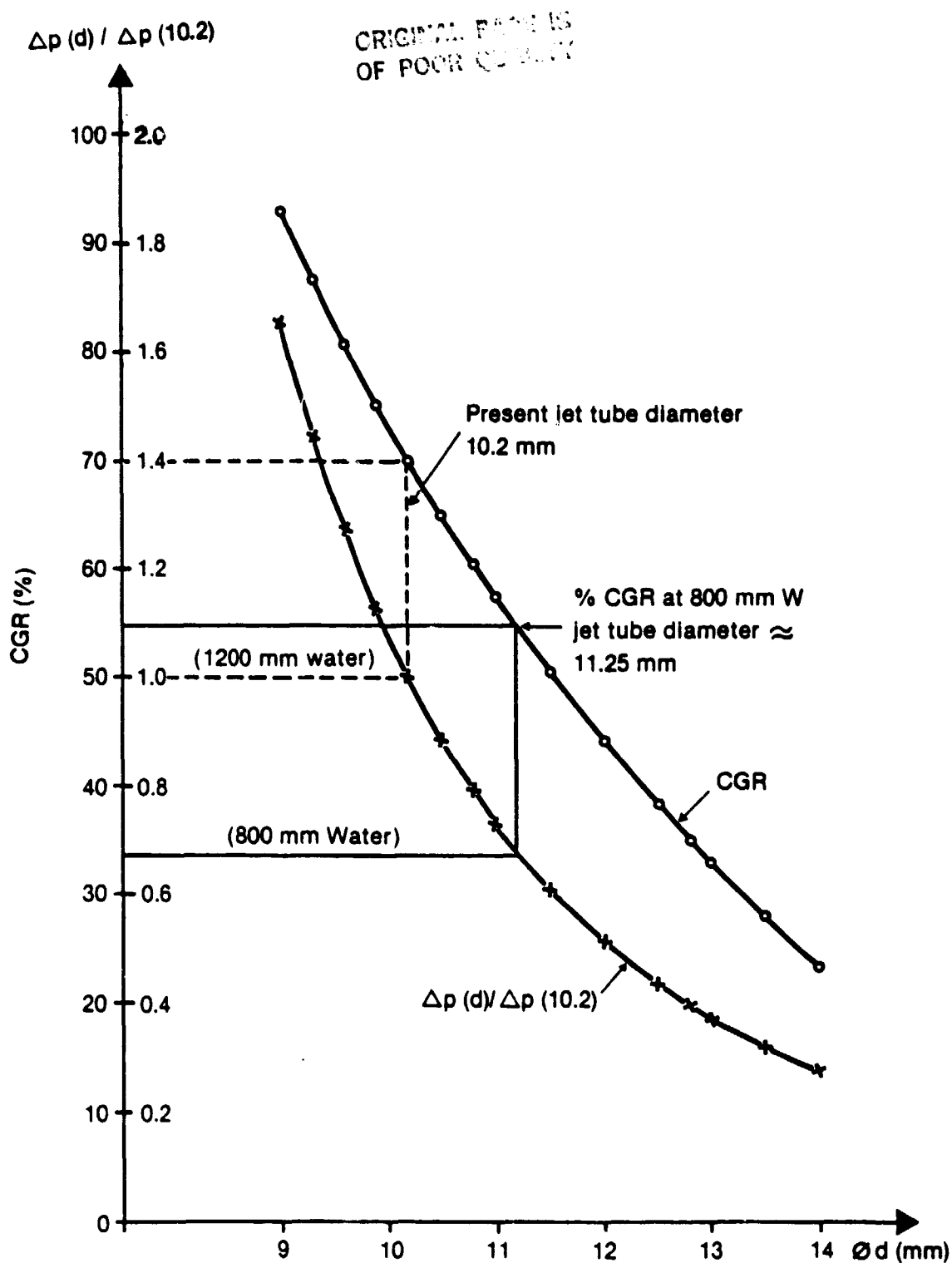


Fig. 4.8:19
CGR and pressure drop versus
jet diameter

ORIGINAL OF POOR QUALITY

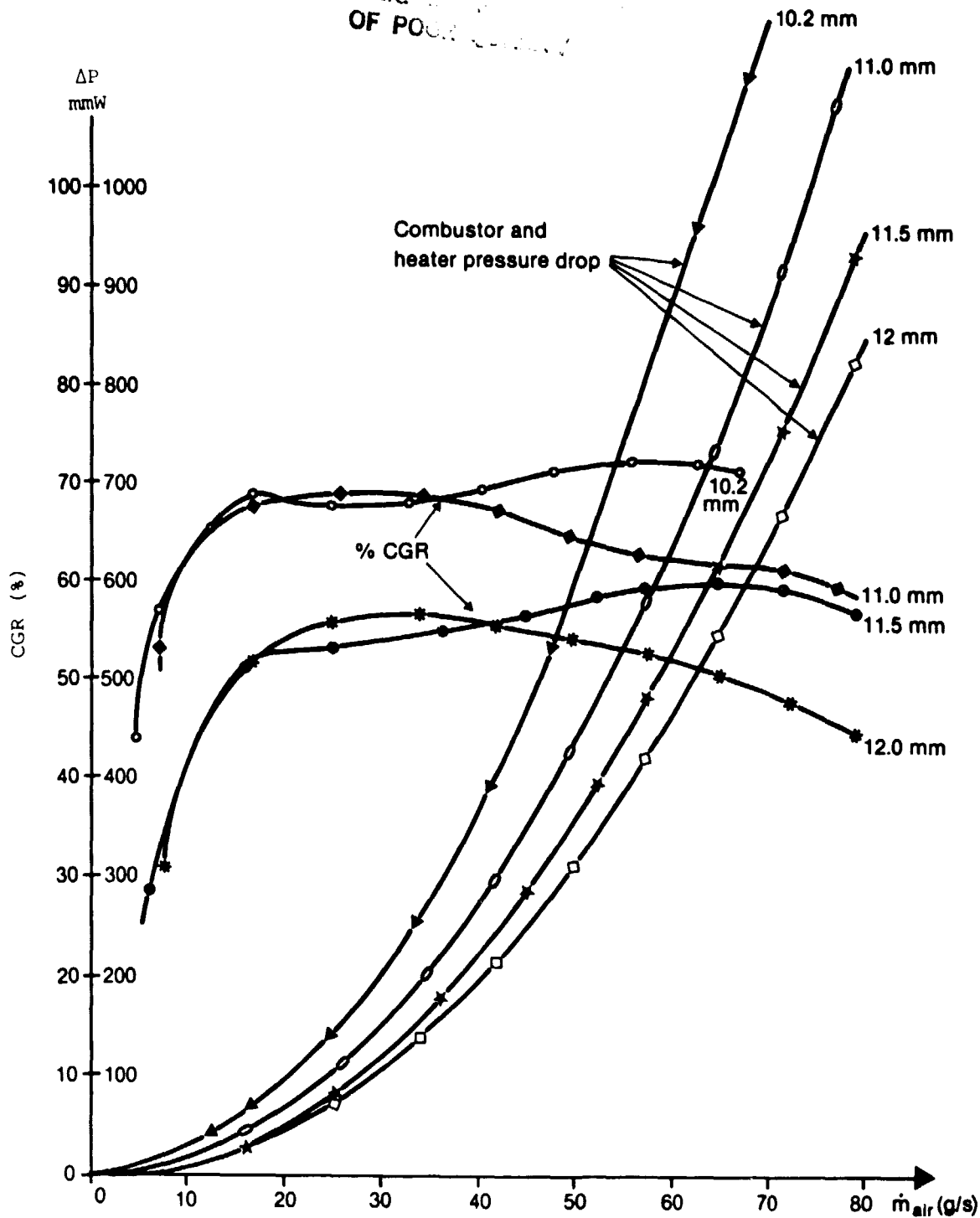


Fig. 4.8:20 Effect of Ejector Jet Diameter on % CGR and ΔP for Straight Guide Vanes

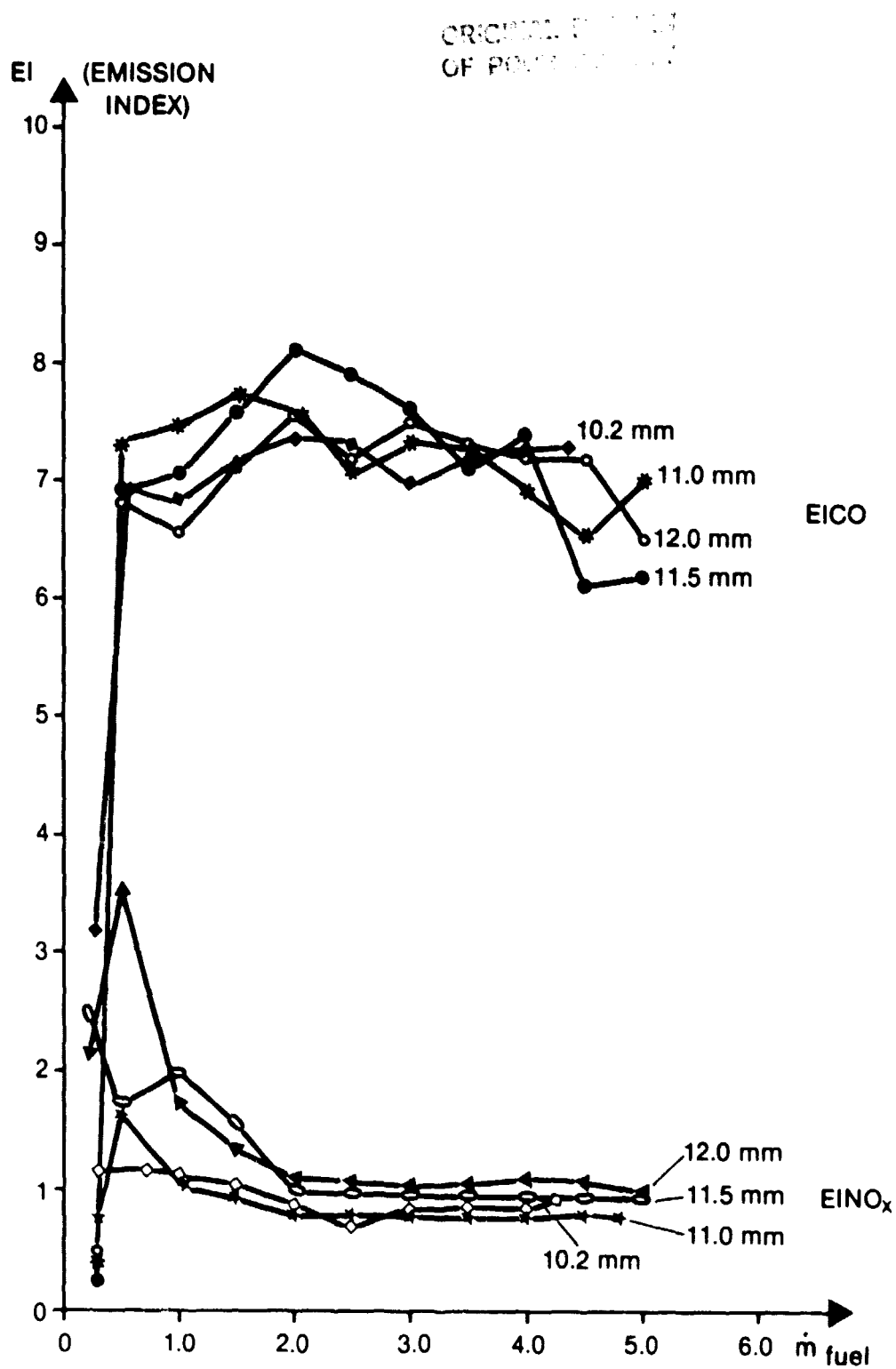


Fig. 4.8:21
Straight guide vanes

CIRCUITRY OF
OF POOR QUALITY

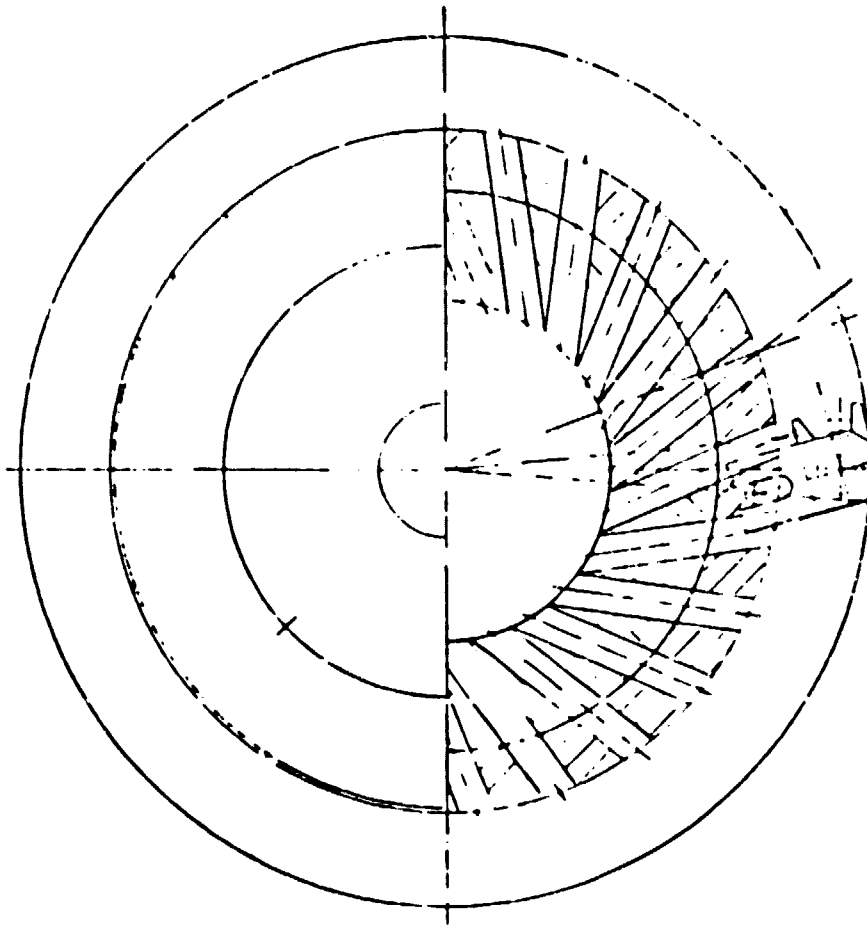
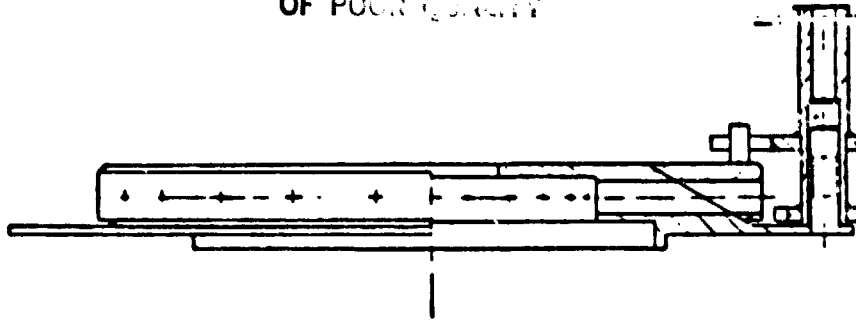


FIG 4.8: 22 BY PASS VALVE

ORIGINAL PAGE IS
OF POOR QUALITY

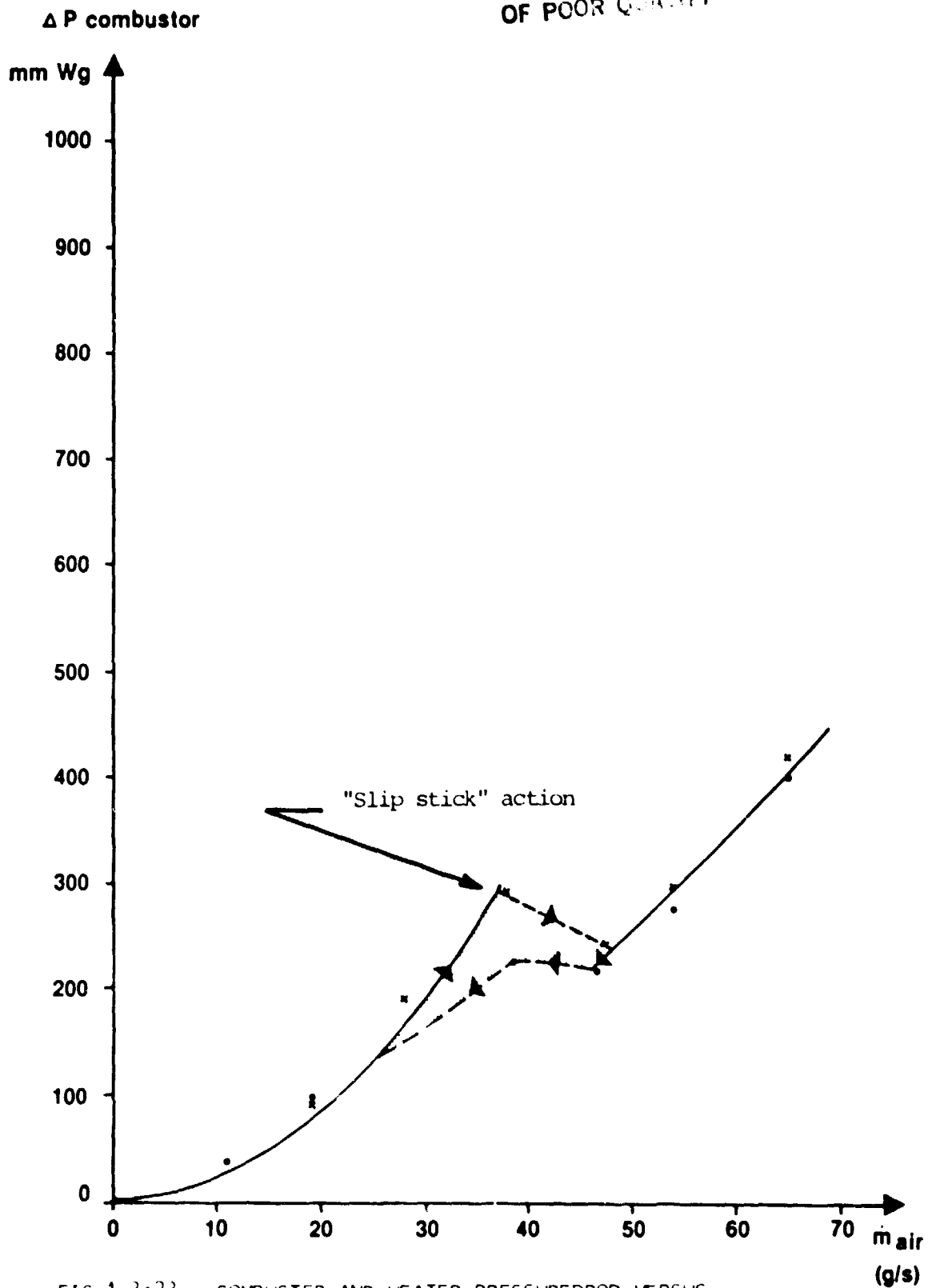


FIG 1.3:23 COMBUSTOR AND HEATER PRESSURE DROP VERSUS
BURNER AIR FLOW WITH AUTOMATIC BYPASS CONTROL

CROSS SECTION
OF PDC VALVE

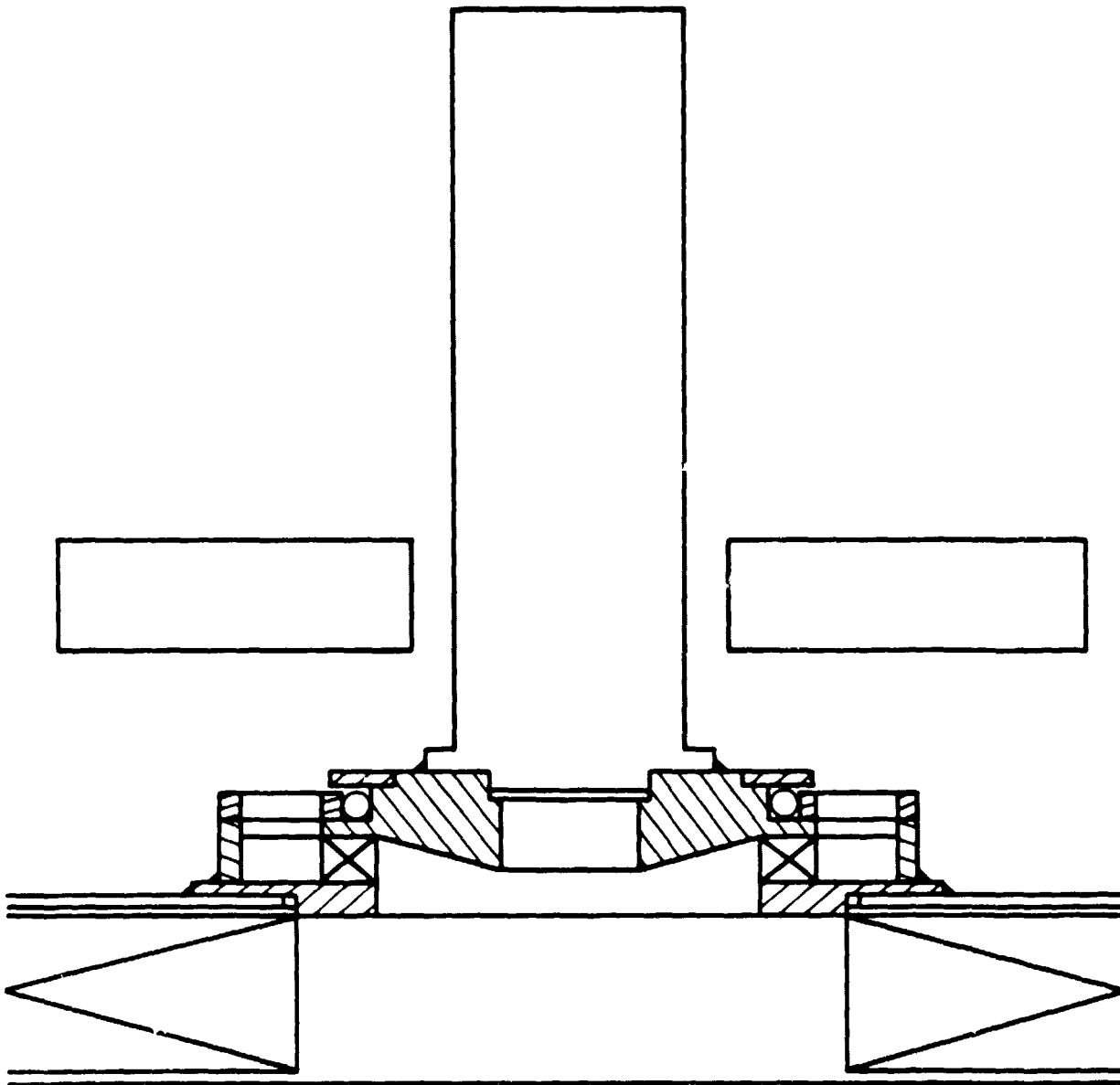


Figure 4.8 : 24 By-pass Valve

Since Design Review 1979 the following has been changed:

- The CGR valve has been removed. The measured % CGR versus air flow is shown in fig 4.9:1.
- Tests have shown that it is possible to use a lower air excess at low loads. The air excess factor (λ) versus fuel flow is shown in fig 4.9:2. The nominal value is used in all calculations.
- The tube temperature is corrected to 720 °C in the calculations and the working gas temperature is set to 680 °C.

All other input data for the calculations are unchanged which means that we have used:

- Atomizer air flow = 1.5 g/s
- Atomizing air temperature = 30 °C
- Air temperature into preheater = 30 °C
- Engine block temperature = 70 °C

The changes result in a higher η_B at low loads. Fig 4.9:3 shows the "new" and "old" η_B , λ and % CGR versus fuel flow. The increase in η_B at low loads is mainly a function of the decreased λ -value. The decrease in η_B at higher loads depends on the higher % CGR in the new data, which gives higher gas flow through the heater. The higher gas flow through the heater gives an increased gas temperature after the heater and thus a decreased η_B .

The exhaust gas temperature increases when the λ -value is decreased, but the heat losses in the exhaust gases is decreased due to less exhaust gas flow, see fig 4.9:4.

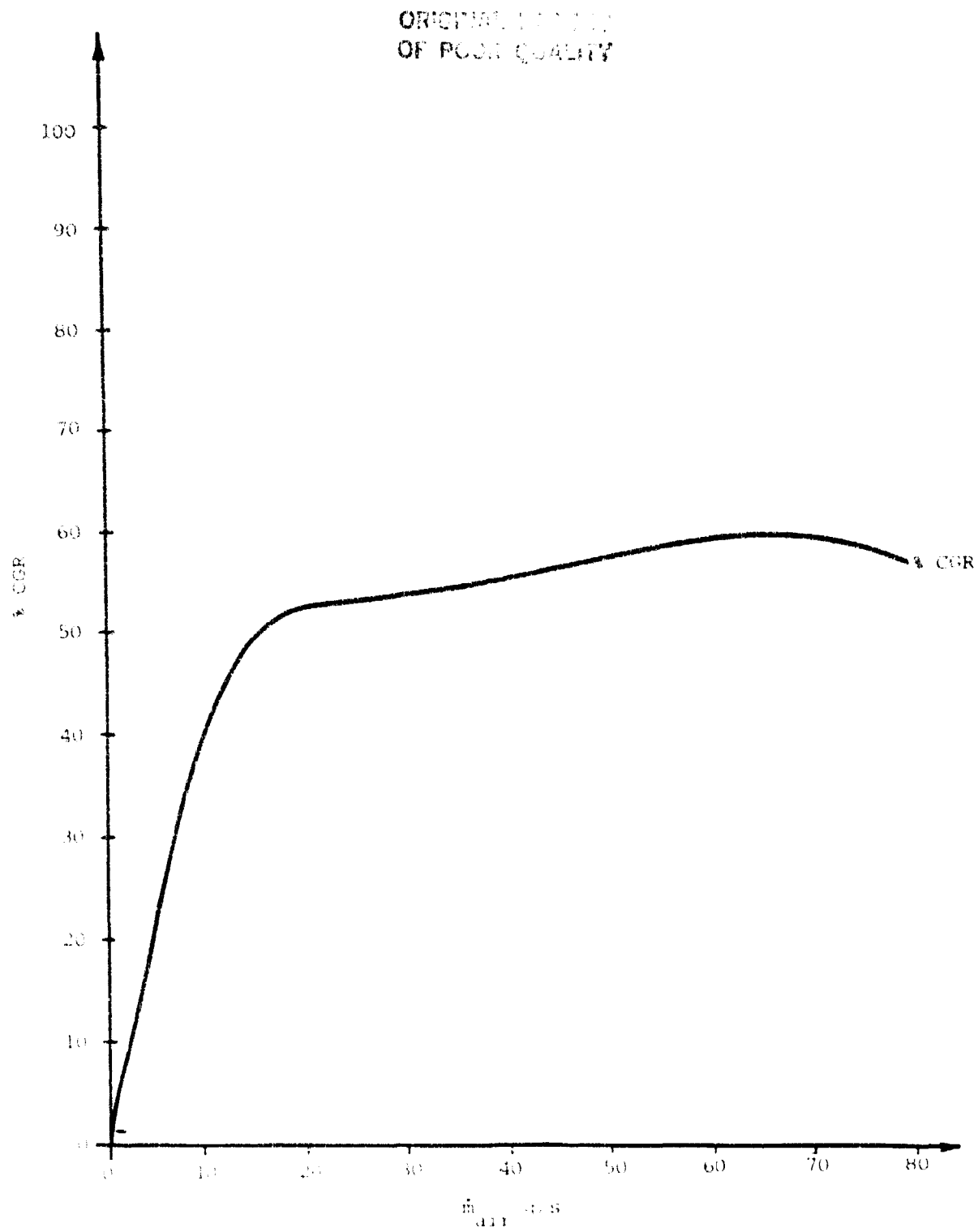


Figure 4.9-1 100% CGR Versus Air Flow

ORIGINAL 12-1-15
OF POCN 6-1-15

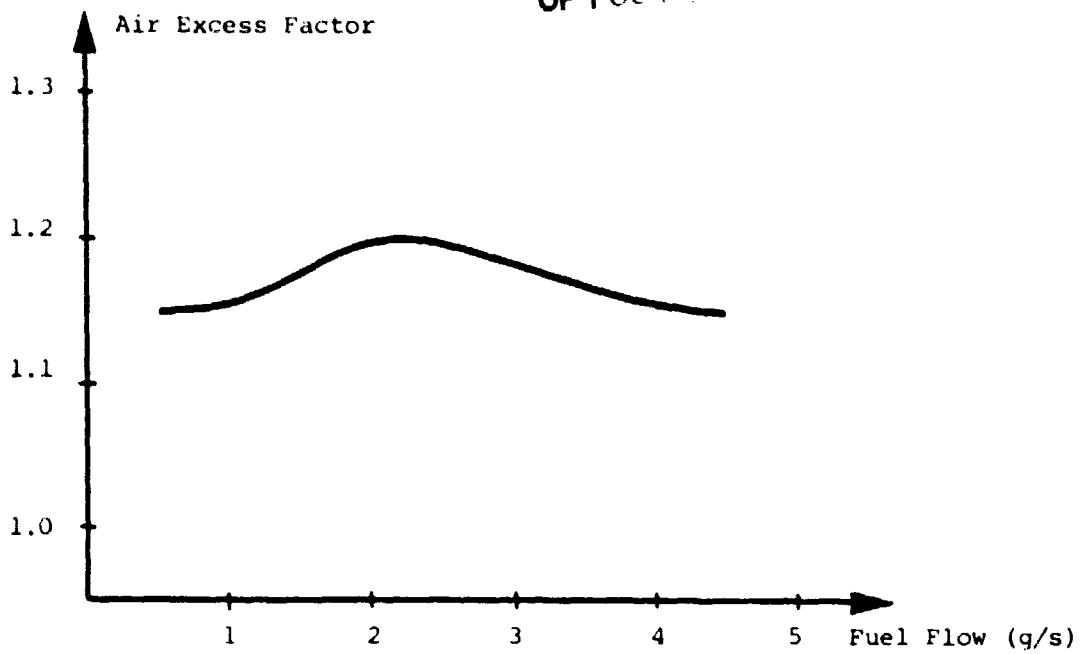


Figure 4.9:2 Air Excess Factor vs Fuel Flow

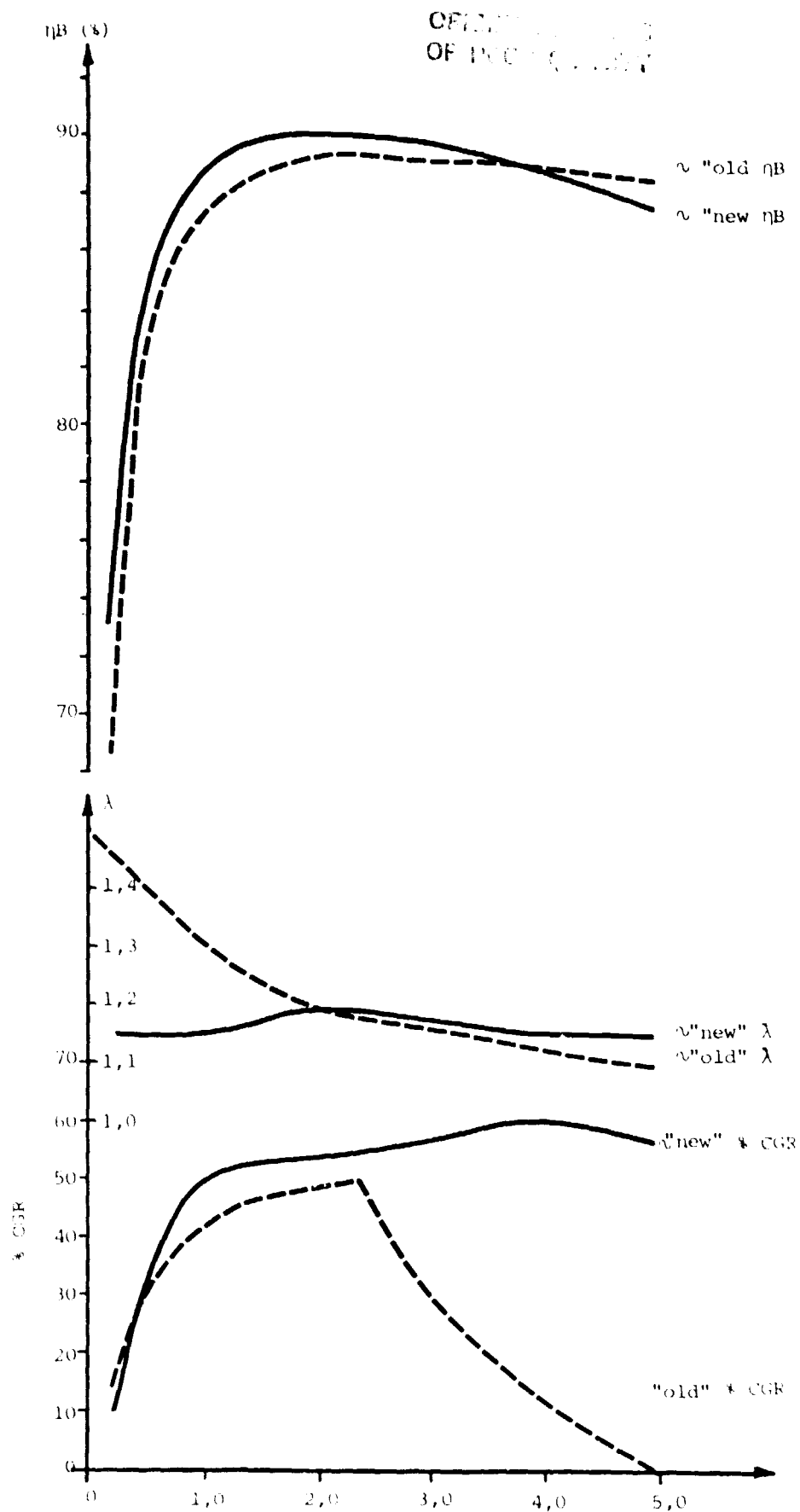


Fig. 4.9:3 η_B , λ and % CGR versus fuel flow for "new" and "old" data

ORIGINAL PAGE IS
OF POOR QUALITY

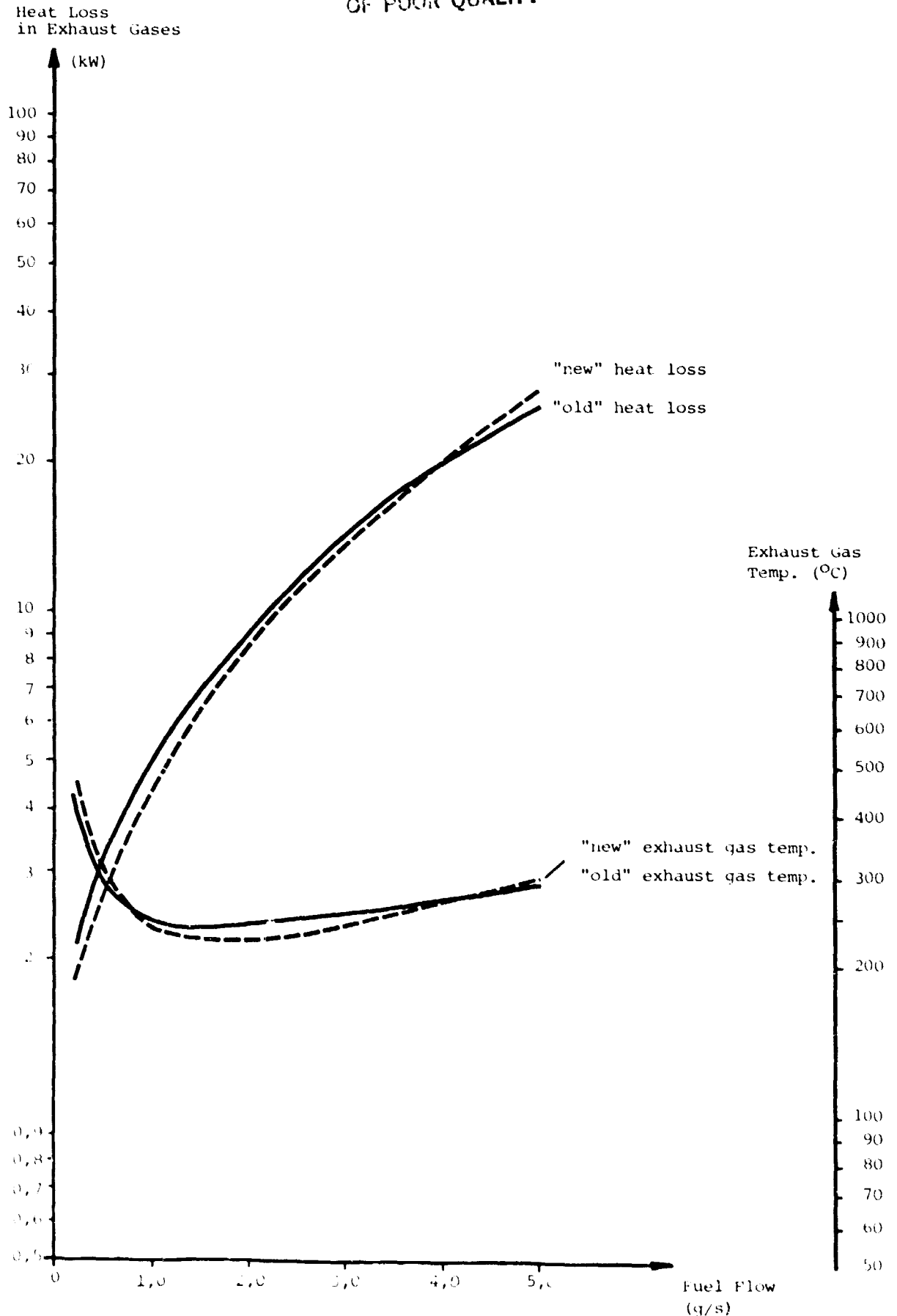


Fig. 4.9.4 Heat Loss in Exhaust Gases and Exhaust Gas Temperature Versus Fuel Flow for Mod I Preheater with "new" and "old" Datas

B.5 Hot Engine System

5. HOT ENGINE SYSTEM

5.1 General description

See drawing.

One regenerator per cylinder was chosen in order to have a compact design. The regenerator housings were moved as close as possible to the cylinders, and with involute shaped heater tubes with a 90 degree span the manifold could be located close to the center of cylinders and regenerators.

The heater tubes give a constant gap width along the tubes and a straight part with surface extensions for second gas passage.

The cylinders and regenerator housings have flanges, separated from the vessels, in their lower ends for connection to the cylinder block.

On each heater head quadrant there will be three adapters for temperature-control measurements.

One is located inside the regenerator housing manifold, in which the closed cycle-gas temperature is measured.

Two adapters are located outside the heater tube, one on the first row and the second one on the rear row.

The regenerator is of the same design as for the P40 engine i.e. fine mesh stainless steel gauze layers, stacked in a thin cylindrical casing.

At the top of the regenerator casing a ring is attached in order to give a correct position of the regenerator in the regenerator-housing.

The gas cooler design is similar to the P40 design i.e. small diameter tubes inserted between circular end-plates, and a cylindrical housing with rubber seal elements to prevent water by-passing the cooler unit.

5.3 Stress Calculations of Heater, Cylinder and Regenerator Housing and Cooler

5.3.1 The Heater

5.3.1.1 General

The heater consists of four quadrants each containing 24 tubes of length 282 mm. The tubes are exposed to a rather severe combination of operating conditions: cycling pressure (max. 15±5 MPa), high temperature, corrosive combustion gases, hydrogen surroundings. The maximum material temperature is 770°C on the front side tube outer surface.

5.3.1.2 Material

The tubes are made of Multimet (N-155) and seam-welded. The following data are valid:

Yield stress (0,2%) $\sigma_y = 240$ MPa at 770°C

Ultimate tensile strength $\sigma_u = 400$ MPa at 770°C

Thermal expansion coefficient $\alpha = 17,3 \cdot 10^{-6}$ °C⁻¹ at 720°C

Young's modulus $E = 150000$ MPa at 720°C

Creep rupture data are given in the figures 5.3:1 and 5.3:2. Fig. 5.3:1 is a Larson - Miller plot for welded Multimet tubes in helium atmosphere and fig. 5.3:2 is a Haigh diagram for combined high cycle fatigue and creep.

5.3.1.3 Design criteria

The heater tubes of Multimet (N155) with 4,5 OD and 3,0 mm ID have been used in several engines at United Stirling in the same environment as for the MD 1, i.e. temperature between 670°C and 770°C and a cycling pressure with a mean value of 15 MPa. The experience from these engines encourages a continued use of this tubing material.

ORIGINAL PAGE IS
OF POOR QUALITY

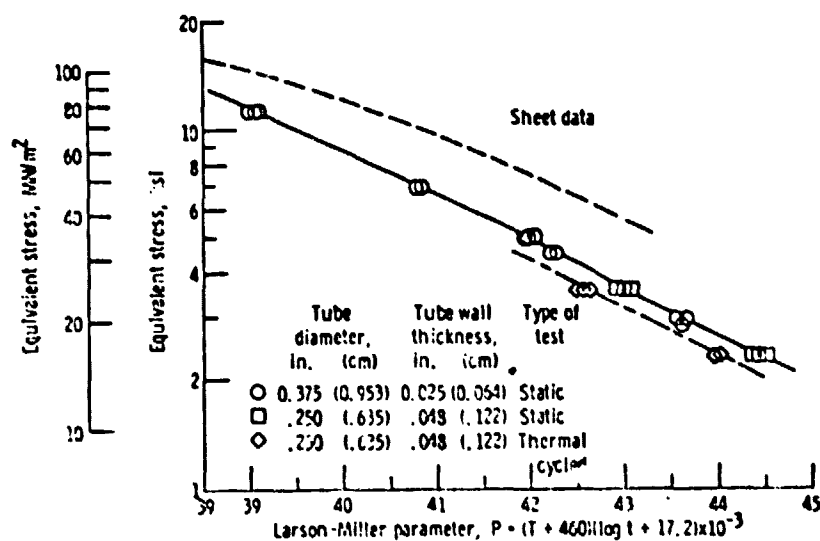


Fig. 5.3:1. Larson-Miller diagram for welded Multimet tubes. NASA Technical Note NASA TN D-5195, "Creep rupture data for welded N-155 tubes."

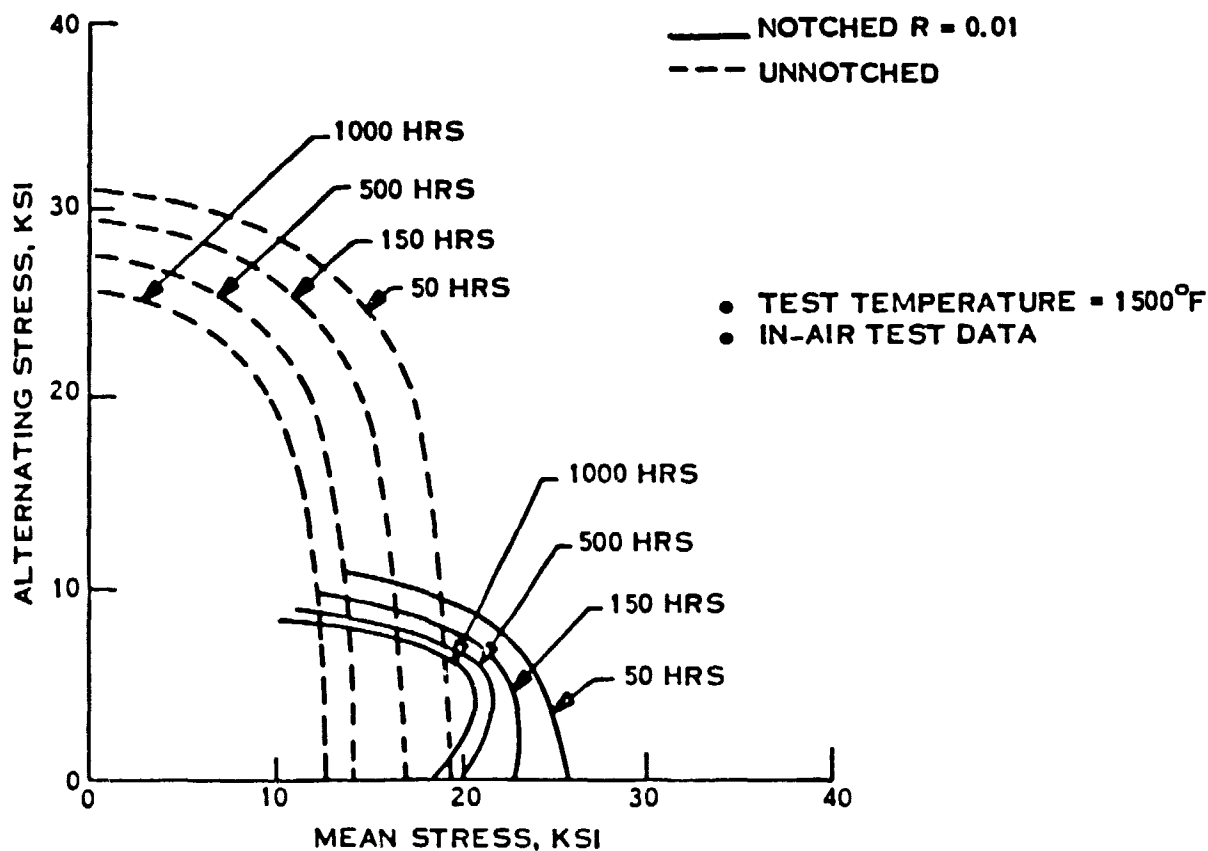


Fig. 5.3:2 Haigh Diagram for Combined Creep and High Cycle Fatigue. NASA CR159391, "Preliminary and Conceptual Design of a Stirling General Purpose Test Engine, Final Report"

Due to the lack of material data for low cycle fatigue, corrosion and hydrogen exposure no precise life time estimations can be made for the heater tubes. The speed of the relaxation of the thermal stresses due to primary and secondary creep is another uncertain factor. In an automotive application the engine is mainly run at part loads and thus at low pressures (around $p_{\text{mean}} = 5 \text{ MPa}$). Final criteria to be used for life time estimations for heater tubes in this application have to be further investigated and correlated with experimental data that not yet exist. For the Mod I engine we are using a conservative model by using the full load conditions ($p_{\text{mean}} = 15 \text{ MPa}$) instead of a complicated load spectra model. This gives us a margin against the effects mentioned above. Considering just the creep process a change of the stress level from 15 MPa to 5 MPa increases the life time between 100 and 1000 times.

The Haigh diagram in fig. 2 is used for the influence of high cycle fatigue. Since the engine operates with an amplitude to mean pressure ratio of about 1/3 the load point is situated at the steep vertical part of the dotted lines. Consequently the mean pressure (15 MPa) can be used in the design against creep and high cycle fatigue rather than the max. pressure (20 MPa).

The Larson-Miller diagram in fig. 5.3:1 is a result from a NASA investigation of welded Multital tubes in helium atmosphere. The investigation shows that the creep strength of welded tubes is only about two-third of that of sheets as given in handbook data. The effective stress used in the diagram is evaluated in the bore due to the secondary creep solution based upon a value of Norton's creep constant equal to 4.5. In our design we use the max. elastic hoop stress (σ_{θ}) which is about 10% larger, giving us another conservative estimation. For this stress we require a factor of safety equal to 1,5 for 4000 h at 770°C, i.e.

$$\sigma_{\theta}(p_{\text{mean}}) \leq \sigma_{\text{CR}}/1.5$$

where σ_{CR} is the rupture stress at 770°C and 4000 hours. Fig. 5.3:1 gives $\sigma_{\text{CR}} = 80 \text{ MPa}$.

In order to avoid initial yielding before the relaxation of the thermal stresses, we require that the maximum effective stress due to the maximum internal pressure and the thermal load is below the yield stress at 770°C, i.e.

$$\sigma_e (P_{\max}, T) \leq \sigma_y$$

As pointed out earlier $\sigma_y = 240 \text{ MPa}$ at 770°C .

5.3.1.4 Analysis

Fig. 5.3:3 shows a cross section of a heater tube. The temperature levels at full load are shown in the figure. From the front to the rear side there is a gradient from about 770°C to 670°C . The radial gradient there between is about 20°C .

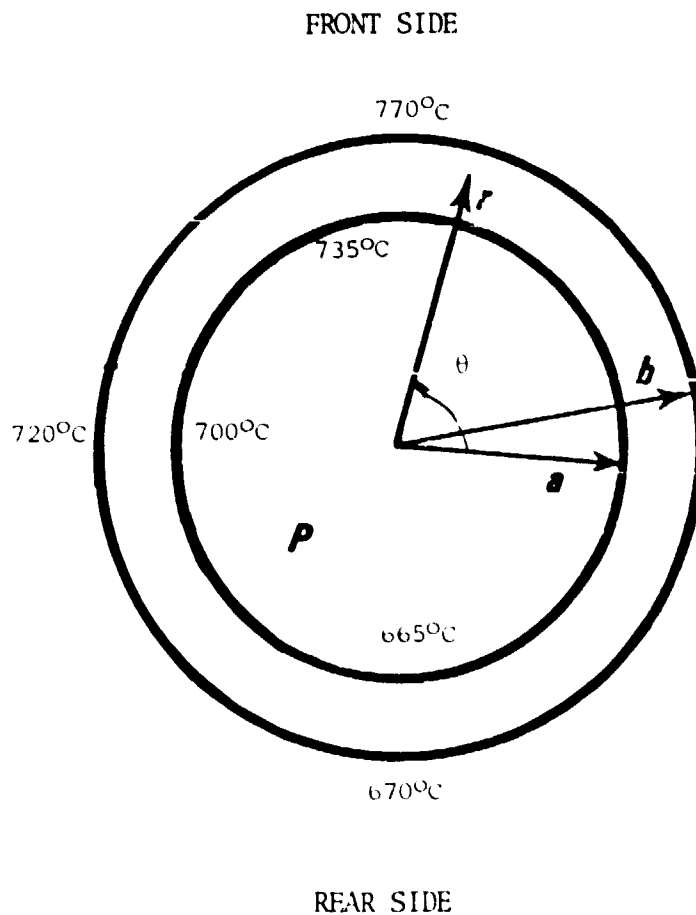


Figure 5.3:3 Cross Section of the Heater Tube With Temperature Levels at Full Load

The elastic stresses in a thick-walled vessel are given by the well-known relations below with notations used in fig. 5.3:3.

$$\sigma_r = \frac{pa^2}{b^2 - a^2} \left(1 - \frac{b^2}{r^2} \right)$$

$$\sigma_\theta = \frac{pa^2}{b^2 - a^2} \left(1 + \frac{b^2}{r^2} \right)$$

$$\sigma_z = \frac{pa^2}{b^2 - a^2}$$

The hoop stress is the largest one with its maximum value at the inside surface of the tube. The classical steady state secondary creep solution under the consideration of plain strain is given below. n is the Norton creep constant.

$$\sigma_r = -p \frac{r^{-2/n} - b^{-2/n}}{a^{-2/n} - b^{-2/n}}$$

$$\sigma_\theta = p \frac{-\left(1 - \frac{2}{n}\right) r^{-2/n} + b^{-2/n}}{a^{-2/n} - b^{-2/n}}$$

$$\sigma_z = p \frac{-\left(1 - \frac{1}{n}\right) r^{-2/n} + b^{-2/n}}{a^{-2/n} - b^{-2/n}}$$

The stress components due to the elastic and relaxed solutions are plotted in the figures 5.3:4 - 5 for the internal pressure equal to 15 MPa. In the creep solution n is assumed equal to 4,5. As can be seen in the figures the hoop stress is the largest one. Initially it has its maximum value in the bore but after the total relaxation it has moved to the outer surface of the tube. In the table below the stress to pressure ratio is given for the hoop stress (σ_θ) and the v. Mises effective stress (σ_e).

ORIGINAL PAGE IS
OF POOR QUALITY

Stresses at the inner and outer surfaces of the heater tube.

Position	Effective stress		Hoop stress	
	elastic	creep	elastic	creep
inside	3,12	2,33	2,60	1,70
outside	1,39	1,95	1,60	2,25

As can be seen in the table the elastic hoop stress is 2,6 p at the bore, i.e. 39 MPa when p = 15 MPa. The factor of safety against creep rupture is then 2 which exceeds our requirement.

The classical temperature solution to the surface temperature given in fig. 5.3:3 can be written.

$$T = A_1 + A_2 \ln \frac{r}{a} + \left(\frac{A_3}{r} + A_4 r \right) \sin \theta$$

A more precise analysis might give trigonometric terms including 2nd order, 3rd order, etc., but such terms will cause no stresses. The classical elastic plain strain solution for the first two just radial dependent terms is given below.

$$\sigma_r = \frac{\alpha E (T_a - T_b)}{2(1-\nu) \ln \frac{b}{a}} \left[- \ln \frac{b}{r} - \frac{a^2}{b^2 - a^2} \left(1 - \frac{b^2}{r^2} \right) \ln \frac{b}{a} \right]$$

$$\sigma_\theta = \frac{\alpha E (T_a - T_b)}{2(1-\nu) \ln \frac{b}{a}} \left[1 - \ln \frac{b}{r} - \frac{a^2}{b^2 - a^2} \left(1 + \frac{b^2}{r^2} \right) \ln \frac{b}{a} \right]$$

$$\sigma_z = \sigma_r + \sigma_\theta$$

ORIGINAL PAGE IS
OF POOR QUALITY

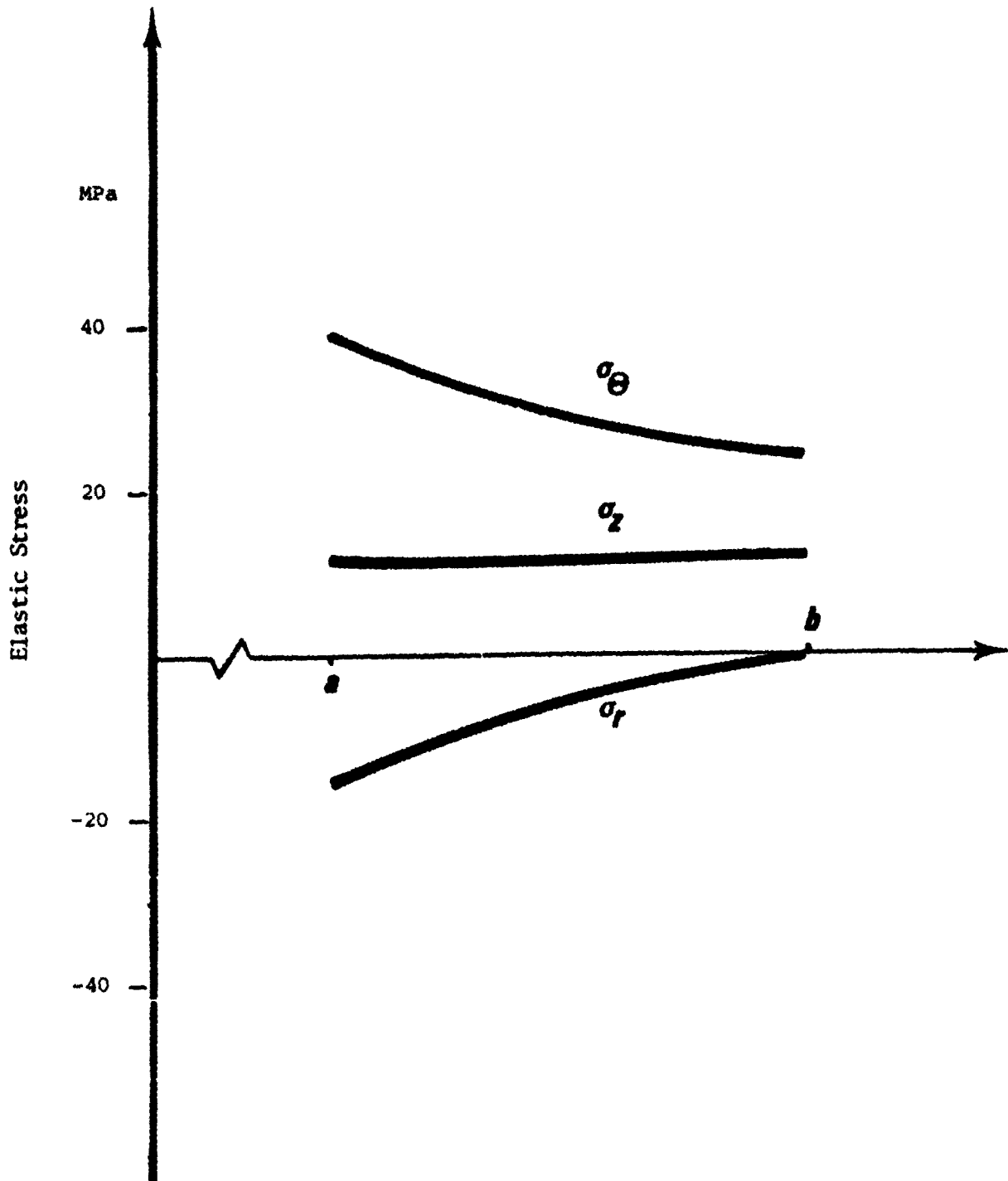


Figure 5.3:4. Elastic stresses due to an internal pressure of 15 MPa.

ORIGINAL PAGE IS
OF POOR QUALITY

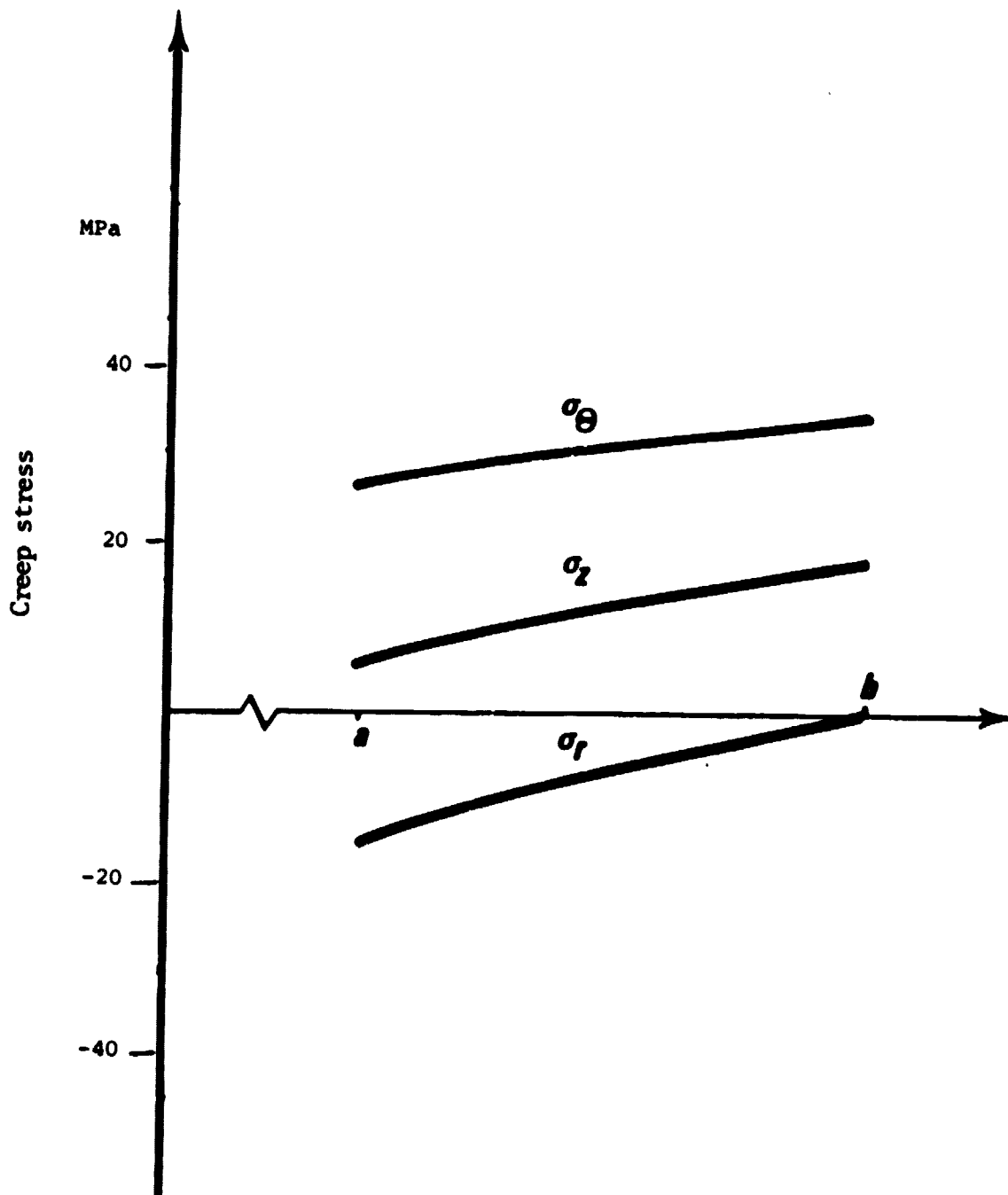


Figure 5.3:5. Creep stresses due to an internal pressure of 15 MPa. $n = 4.5$.

where

- E = Young's modulus
- α = Coefficient of thermal expansion
- ν = Poisson's ratio
- T_a = Tube wall temperature at inner radius
- T_b = Tube wall temperature at outer radius

Insertion of the temperature values given in fig. 5.3:3 gives the stress distribution shown in fig. 5.3:6. With exception of the sign the axial, the hoop and the effective stresses are all the same at the inner and outer surfaces, namely 42 MPa and 32 MPa respectively.

The stress contribution from the $\sin\theta$ -term is

$$\sigma_r = \frac{\alpha E r}{2(1-\nu)} \left(1 - \frac{a^2}{r^2}\right) \left(1 - \frac{b^2}{r^2}\right) B \sin\theta$$

$$\sigma_\theta = \frac{\alpha E r}{2(1-\nu)} \left(3 - \frac{a^2 + b^2}{r^2} - \frac{a^2 b^2}{r^4}\right) B \sin\theta$$

$$T_{r\theta} = \frac{\alpha E r}{2(1-\nu)} \left(1 - \frac{a^2}{r^2}\right) \left(1 - \frac{b^2}{r^2}\right) B \sin\theta$$

$$\sigma_z = \sigma_r + \sigma_\theta$$

$$B = \frac{ab \left(T_a^1 b - T_b^1 a \right)}{(a^2 + b^2)(b^2 - a^2)}$$

ORIGINAL PAGE IS
OF POOR QUALITY

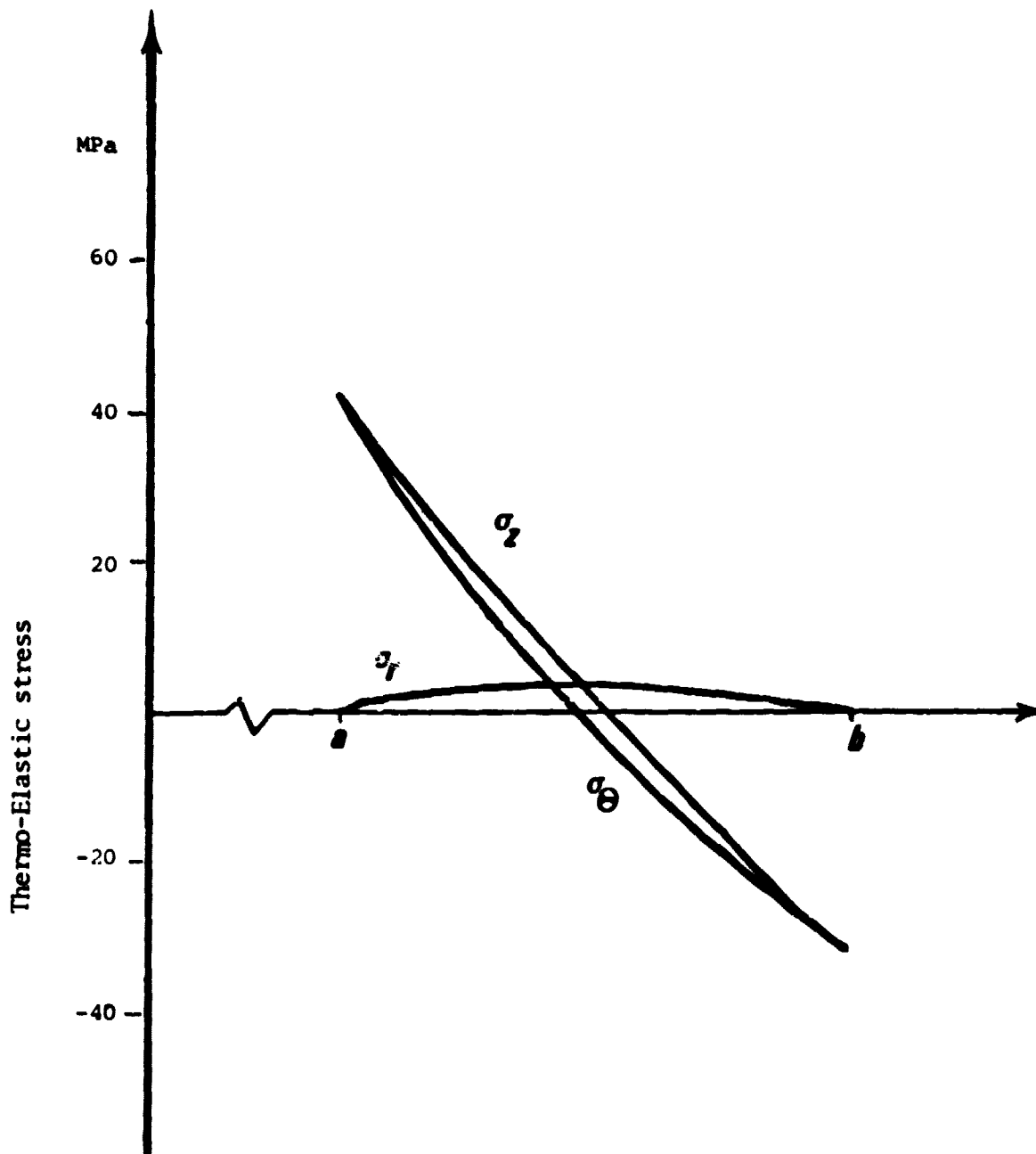


Fig. 5.3:6. Thermo-elastic stresses in the middle between the front and rear sides.

where

$$T_a^1 = 735^\circ - 700^\circ = 35^\circ\text{C}$$

$$T_b^1 = 770^\circ - 720^\circ = 50^\circ$$

The stress contribution from this first harmonic term increases the thermal stress state with just about 10%.

The initial maximum effective stress due to both the maximum pressure of 20 MPa and the total thermal load becomes 102 MPa, i.e. about five times the pressure. This stress level is considerably lower than the yield stress of 240 MPa at 770°C.

In excess of the discussed loadcases additional bending and temperature stresses will be present at the built in ends and at the elbow at the top of the heater. These stresses are assumed to relax rapidly. In the previously built engines we have not experienced any problems at all at these locations. Besides the involute heater is a mechanically soft construction from the thermal expansion point of view.

5.3.2 Regenerator Housing

5.3.2.1 General

The regenerator housing is bolted to the duct plate in a loose flange arrangement. It will be exposed to high temperature loading (about 700°C at the upper part of the housing) and a cyclic internal pressure (about 15 ± 5 MPa). The varying pressure load in combination with the high temperature will result in creep-fatigue interaction phenomena in the top area. A cross section of the housing can be seen in fig.5.3:7.

5.3.2.2 Material

The regenerator housing is investment-cast of a cobalt-base superalloy (HS-31), which has excellent creep strength and corrosion resistance under the current operating conditions. The following material data have been used in the stress analysis.

Yield stress (0.2%) $\sigma_y = 525$ MPa at 20°C
 $\sigma_y = 450$ " " 150°C
 $\sigma_y = 350$ " " 350°C
 $\sigma_y = 290$ " " 500°C
 $\sigma_y = 260$ " " 700°C

Ultimate tensile strength $\sigma_u = 745$ MPa at 20°C
 $\sigma_u = 670$ " " 200°C

Creep rupture stress $\sigma_{CR} = 225$ MPa (after 4000 H at a temperature of 700°C)

Thermal expansion coefficient $\alpha = 14.5 \cdot 10^{-6} (\text{C})^{-1}$

Young's modulus $E = 2 \cdot 10^5$ MPa

From the manufacturers catalogue the following fatigue data are taken.

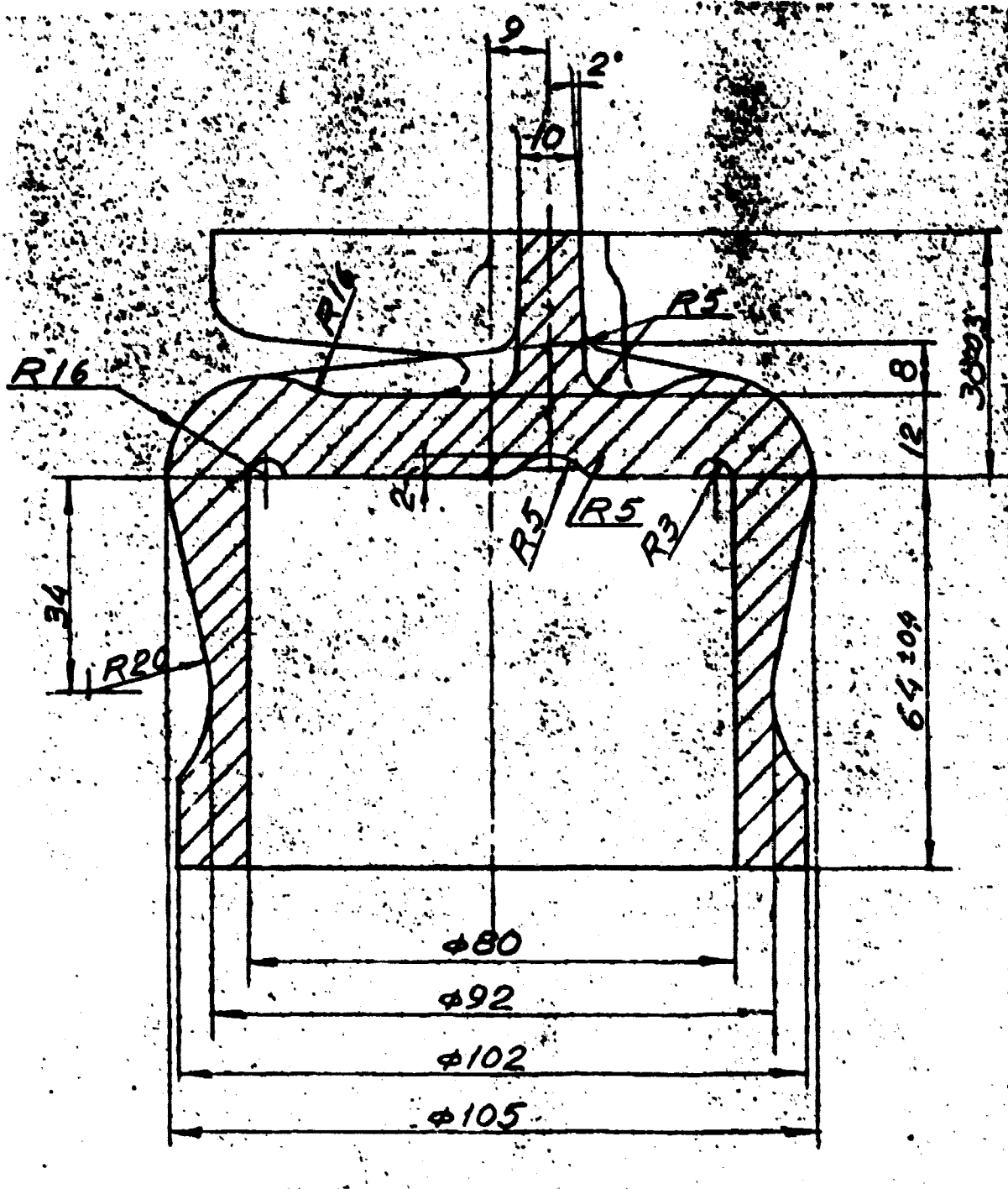
Stress for failure at 10^8 cycles: $\sigma_f = 380$ MPa at 648°C
 " " " " " " $\sigma_f = 321$ MPa at 815°C

The specimens are stressed in alternate bending. Unfortunately no fatigue data are available at lower temperatures. However, there is a german article ("Creep and fatigue behaviour of the X40CoCrNiW 4520 high temperature alloy", by Ernst Keil and George Maier in 'Materialprüf. 10 (1968) No. 4 April) in which a material with a similar composition has been tested. The fatigue test at ambient temperature gave the following relations between the ultimate tensile strength σ_u and the fatigue limit σ_f in two different load conditions.

1. $\sigma_f = \pm 0.45 \cdot \sigma_u$ (mean stress = 0)
2. $\sigma_f = 0.3 (\sigma_u \pm \sigma_u)$ (mean stress = stress amplitude)

By using this relations it is possible to make an approximate Haigh-diagram.

The german article also contained the following Haigh-diagrams, fig. 5.3:8 at elevated temperatures of the tested material. The diagrams can be of interest in discussion of the creep-fatigue behaviour of HS31.



ORIGINAL PAGE IS
OF POOR QUALITY

Fig. 5.3:7. Cross-section of the regenerator housing.

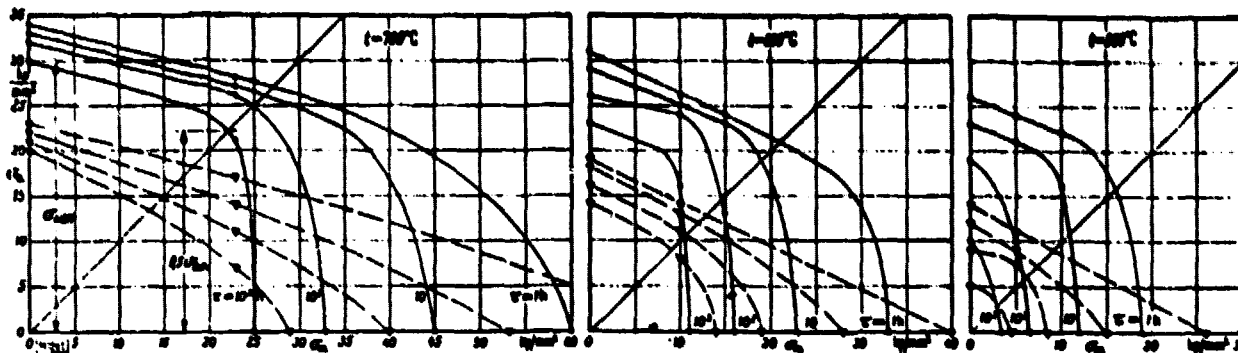


Fig. 5.3:8. Haigh's diagram

Limits of fracture: •—•cylindrical
▼—▼notched

5.3.2.3 Design Criteria

The following stress limit is used to prevent the component from yielding.

$$\sigma_{ea}(p_{max}) \leq \sigma_y / 1.5$$

where σ_{ea} = Average value across the wall thickness of the effective stress according to von Mises yield criterion. The stress value shall be based on a maximal pressure loadcase.

σ_y = Yieldstress of the material at the current temperature

In loadcases where the temperature loading T is combined with the pressure loading P , the following limit is used for the worst case stress.

$$\sigma_{ea}(p, T) \leq \sigma_v$$

Referring to the heater the full load point ($P_{mean} = 15$ MPa) is used for the design against creep rupture, which gives a margin to low cycle fatigue and initial temperature stress. The Haigh diagrams shown earlier motivates the use of the mean pressure as in the case of the heater tubes. Thus, in the hot areas the following stress limit is used to prevent the housing from creep rupture.

$$\sigma_{ea}(p_{mean}) \leq \sigma_{CR} / 1.5$$

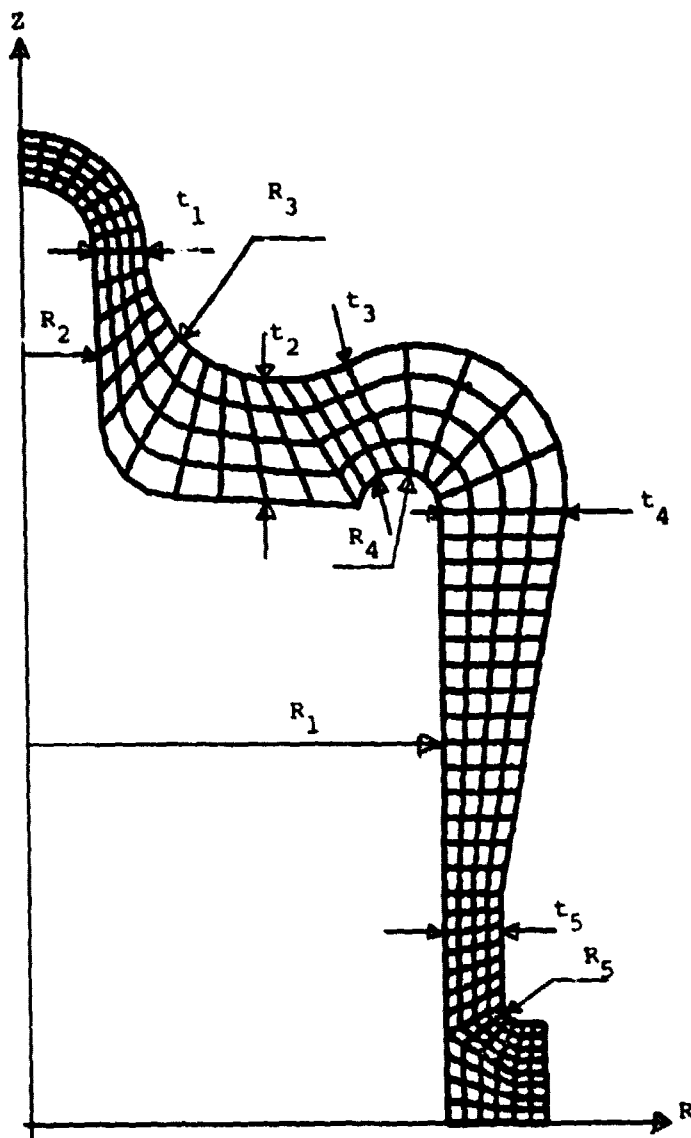
where σ_{CR} = stress level resulting in creep rupture after 4000 h at a temperature of 700°C.

5.3.2.4 Analysis

The regenerator housing has been analyzed using the finite element method. An axi-symmetric finite element model, consisting of 8-nodes isoparametric elements was used, and the mesh and main geometry is shown in figure 5.3:9. The model has been closed in the upper part in order to simulate the manifold connection. This corresponds to an earlier design of the top of the regenerator housing, but the analysis will still be valid for the main part of the housing. The effect on the stress state at the top due to the new design will be discussed later in this section.

The loadcases used in the analysis are defined in figure 5.3:10.

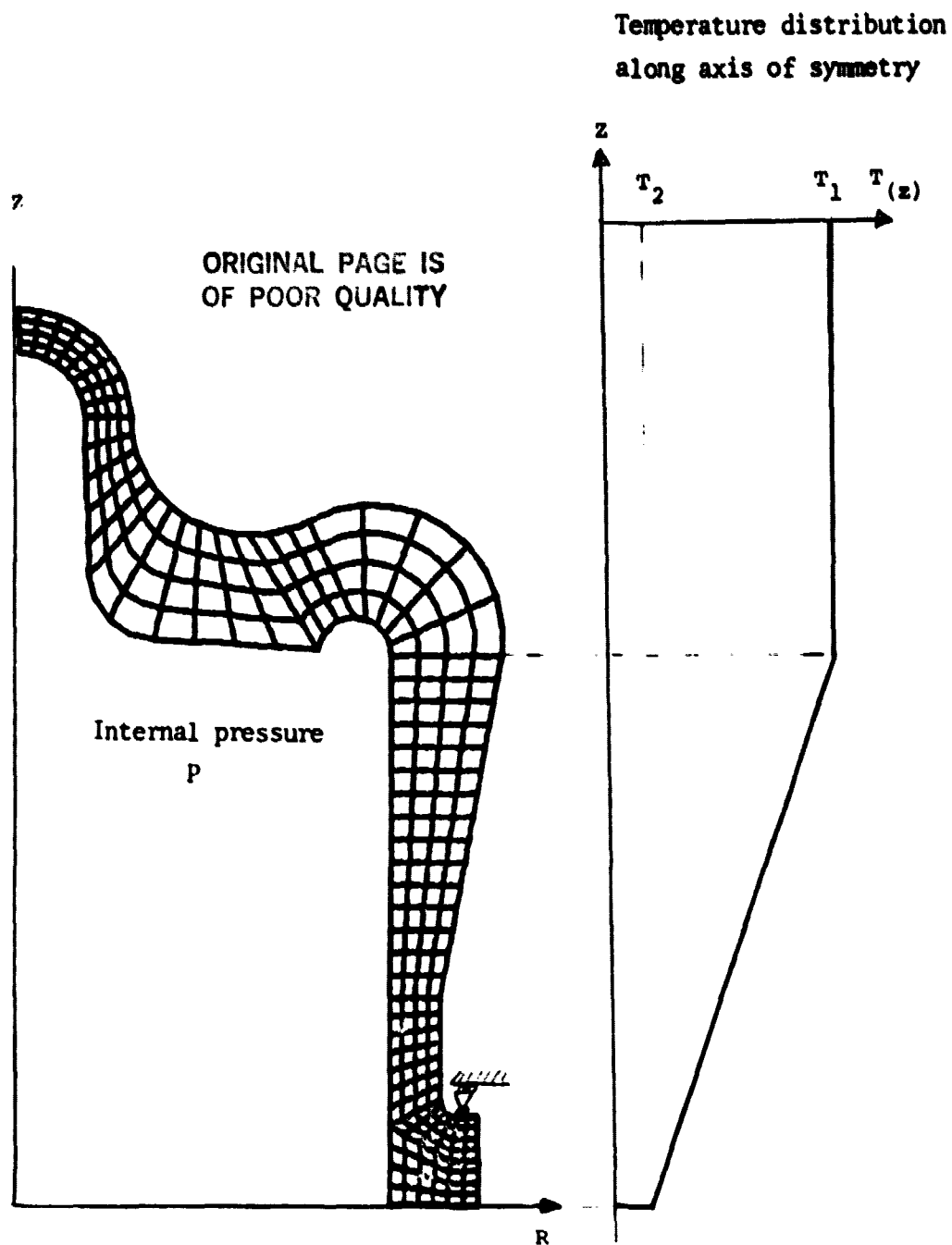
ORIGINAL PAGE IS
OF POOR QUALITY



$t_1 = 5.0 \text{ mm}$
 $t_2 = 11.5 \text{ ''}$
 $t_3 = 11.2 \text{ ''}$
 $t_4 = 12.0 \text{ ''}$
 $t_5 = 5.5 \text{ ''}$

$R_1 = 40.5 \text{ mm}$
 $R_2 = 7.4 \text{ ''}$
 $R_3 = 13.0 \text{ ''}$
 $R_4 = 4.0 \text{ ''}$
 $R_5 = 2.0 \text{ ''}$

Figure 5.3:9. FEM-model and main geometry.



- Loadcases:
1. Temperature load $T_1 = 700^{\circ}\text{C}$, $T_2 = 70^{\circ}\text{C}$
 2. Internal pressure $P = 10 \text{ MPa}$
 3. " " $P = 15 \text{ MPa}$
 4. " " $P = 20 \text{ MPa}$
 5. Temperature load combined with $P = 10 \text{ MPa}$
 6. " " " " $P = 15 \text{ MPa}$
 7. " " " " $P = 20 \text{ MPa}$

Figure 5.3:10. Loadcases used in the analysis.

The average value across the wall thickness of the effective stress according to von Mises (σ_{ea}) have been calculated for section A to J defined in figure 5.3:11. The table shows the temperature in the section, the corresponding yielding stress (σ_y) of the material and the calculated effective stress σ_{ea} for different load cases. The table shows that the maximum value of σ_{ea} in the hot region is 119 MPa in load case 3 (mean pressure $P = 15$ MPa), but the creep rupture stress σ_{CR} is 225 MPa, which gives a safety factor of 1.9 against creep rupture.

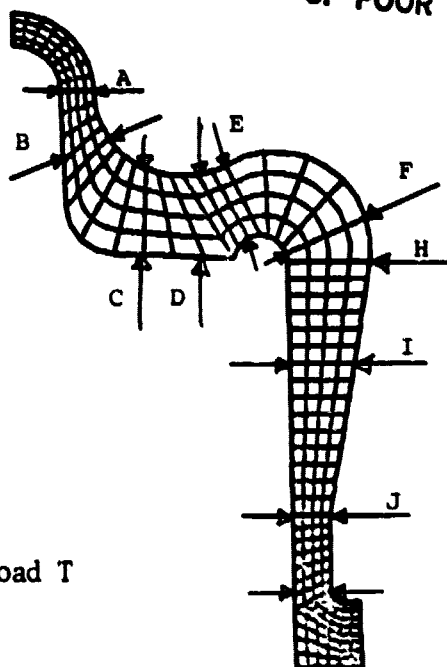
The maximal effective stress in load case 4 (max. pressure $p = 20$ MPa) is 274 MPa and occurs in section J, which gives a safety factor of 1.6 against yielding.

The safety factor against yielding in the worst combination of pressure load and temperature load (case 5 and 7) is 1.3 in section C. However, the safety factors mentioned above are higher because the σ_{ea} -values have been calculated as the average value of the effective stress at the inner and the outer surface, which gives only the correct average value in case of a linear stress distribution over the wall thickness. As can be seen in figure 5.3:12 the stress distribution is not linear, and thus the σ_{ea} -value used is on the safe side.

Figures 5.3:13 and 5.3:14 show the effective stress σ_e along the inner and outer surfaces in load cases 3 and 7. The effective stress in the hot region is 194 MPa in load case 3 (mean pressure $p = 15$ MPa) and 248 MPa in load case 7 (maximal pressure $p = 20$ MPa in combination with temperature load), which means that the peak stresses in the hot region of the MOD I regenerator housing are lower than the corresponding in P40:s regenerator housing.

On the cold side of the regenerator housing a high peak stress value occurs in the radius near the flange (section J), and that point have been analyzed from the fatigue point of view in the following way. The load consists of temperature loading in combination with the cyclic pressure. The effective stress in the point will vary between stress levels

ORIGINAL PAGE IS
OF POOR QUALITY



Load case 1: Temperature load T
3: $p = 15$ MPa
4: $p = 20$ MPa
5: T , $p = 10$ MPa
7: T , $p = 20$ MPa

EFFECTIVE STRESS (MPa)

SECTION	TEMP (°C)	σ_y (MPa)	LOAD CASE				
			1	3	4	5	7
A	700	260	12	35	46	35	58
B			62	95	127	124	187
C			85	86	115	142	200
D			89	48	64	118	148
E			100	55	73	97	104
F			86	119	158	52	108
G	700	260	132	92	122	101	115
H	595	270	143	50	67	123	112
I	355	345	74	143	191	157	249
J	180	435	55	206	274	137	268

Figure 5.3:11. Average effective stress in some sections.

ORIGINAL PAGE IS
OF POOR QUALITY

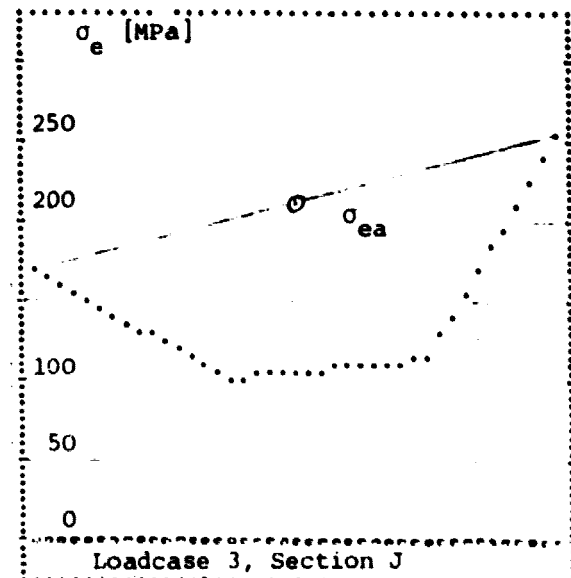
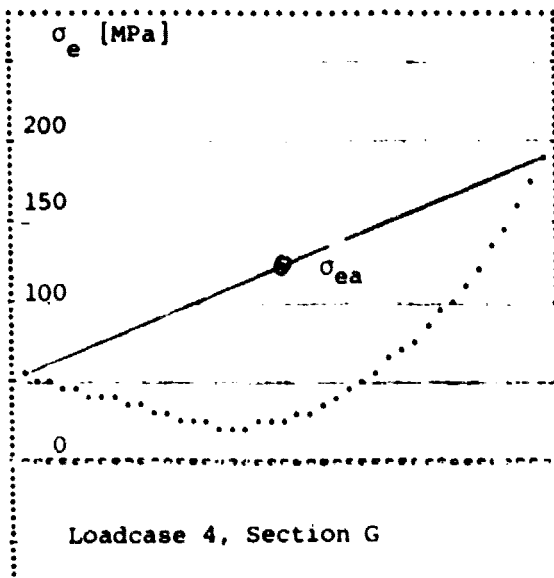
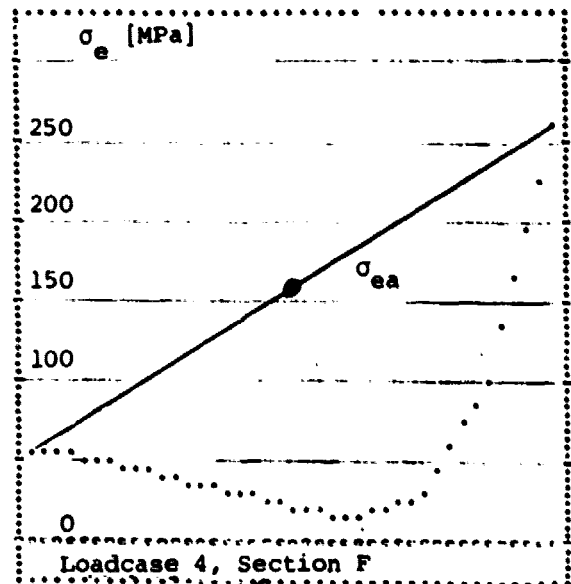
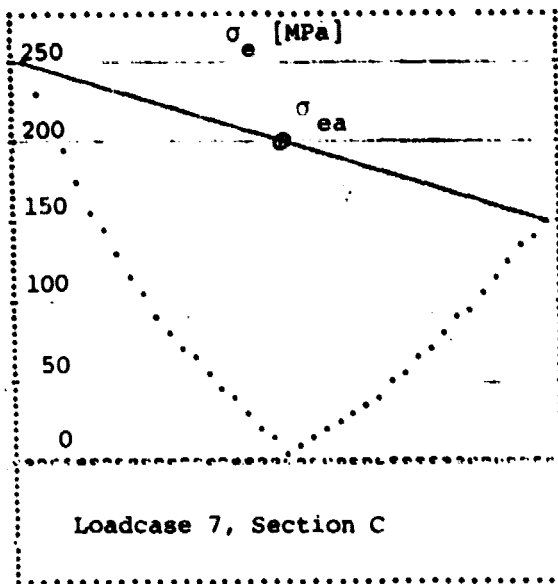
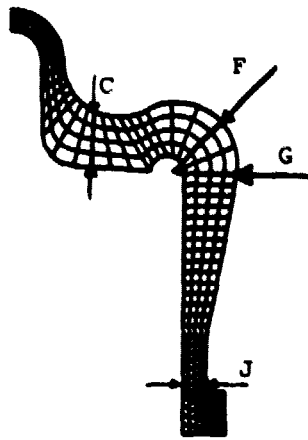


Figure 5.3:12. Effective stress across some sections.

ORIGINAL PAGE IS
OF POOR QUALITY

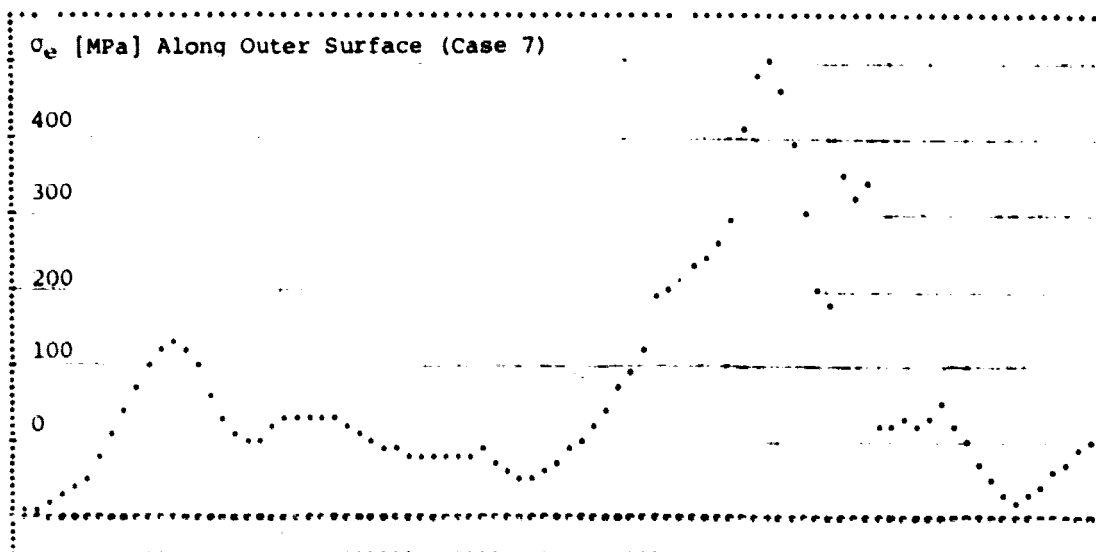
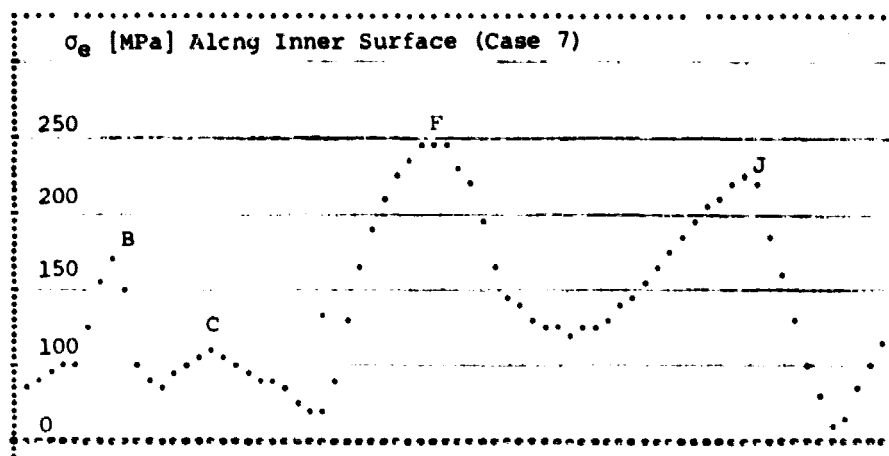
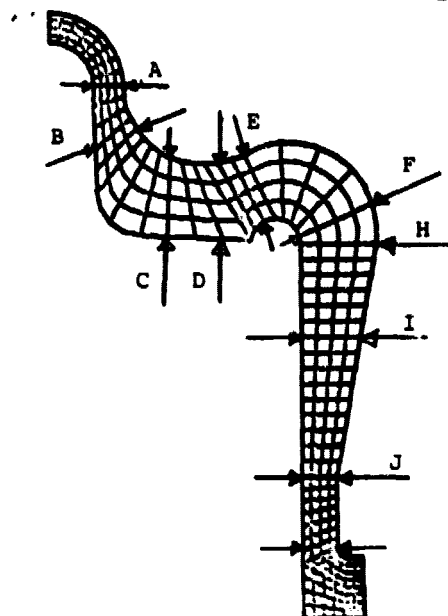


Figure 5.3:13. Effective stress at the surface in load case 3.

ORIGINAL PAGE IS
OF POOR QUALITY

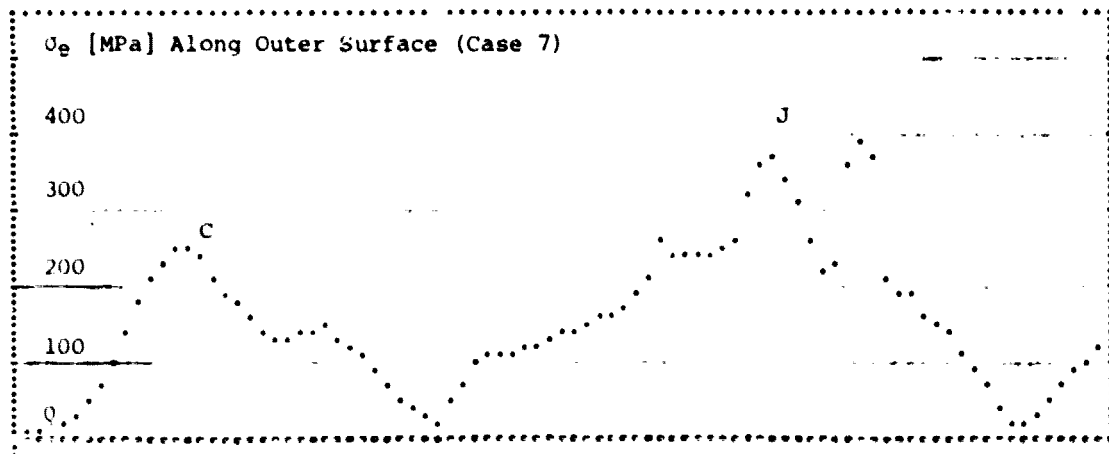
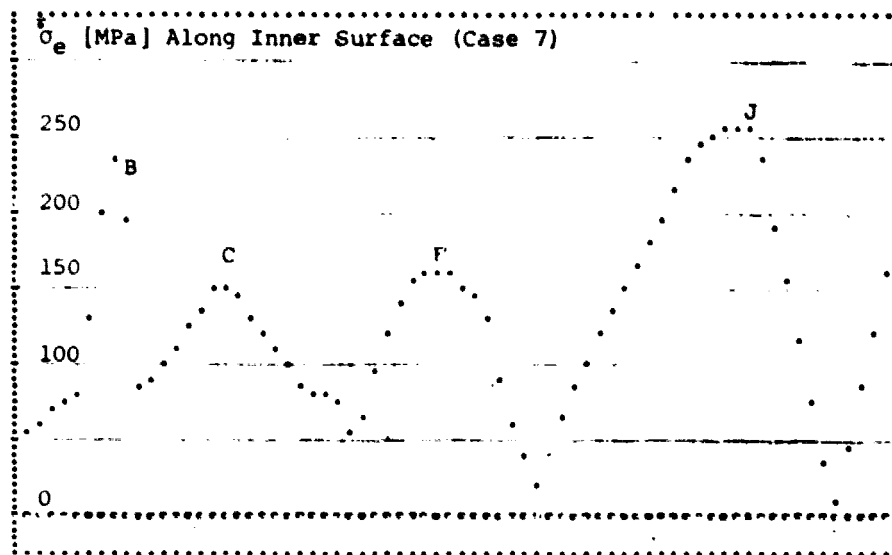
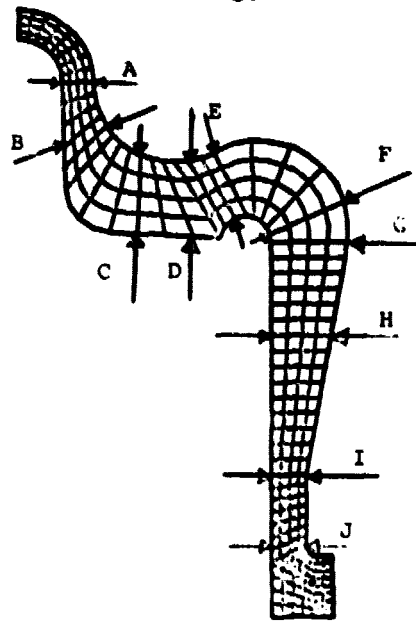


Figure 5.3:14. Effective stress at the surface in load case 7.

corresponding to load cases 5 (temperature load and minimum pressure $p = 10$ MPa) and load case 7 (temperature load and maximum pressure $p = 20$ MPa) with a mean value corresponding to load case 6 (temperature load and mean pressure $p = 15$ MPa). The effective stress in the point will then be $\sigma_e = 270 \text{ MPa} \pm 95 \text{ MPa}$.

The stress concentration factor in the point is 5.2. Assuming a fatigue notch sensitivity of 0.7 results in a fatigue notch factor of 3.9. Taking the notch sensitivity into consideration the working stress must be reduced with the factor $3.9/5.2 = 0.75$ before the comparison with fatigue data. Thus $\sigma_e = (203 \pm 71) \text{ MPa}$ in the interesting point. The temperature is approximately 200°C , and the ultimate tensile strength of the material can be estimated to 670 MPa. Referring to the method described in the material section an approximative Haigh diagram was drawn by taking fatigue limits as fractions of the ultimate tensile strength. The Haigh diagram is shown in fig. 5.3:15 and the point P in the diagram represent the working point. A safety factor against fatigue can be defined as the ratio OQ/OP , which gives the value 1.5.

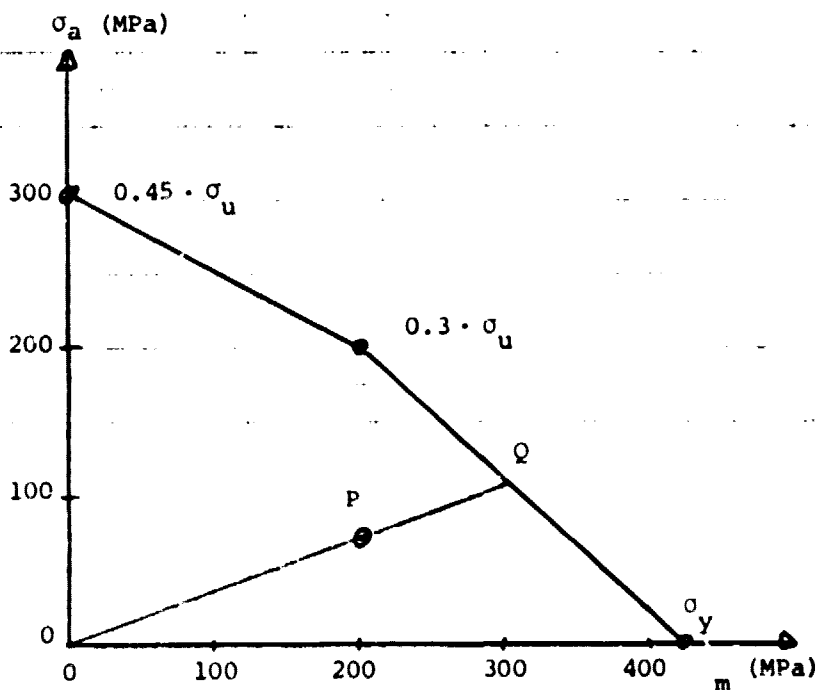


Figure 5.3:15. Approximate Haigh diagram.

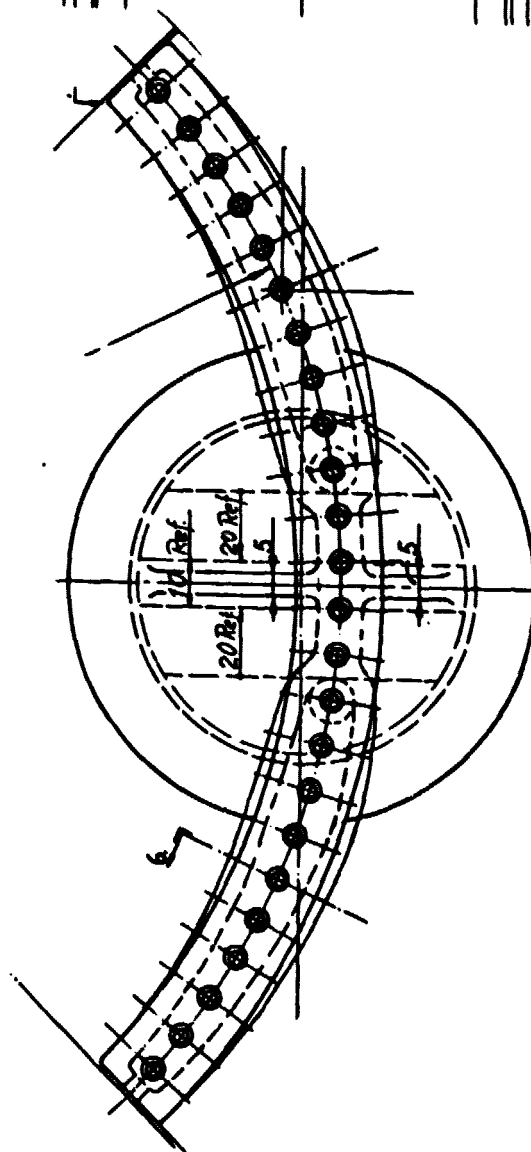
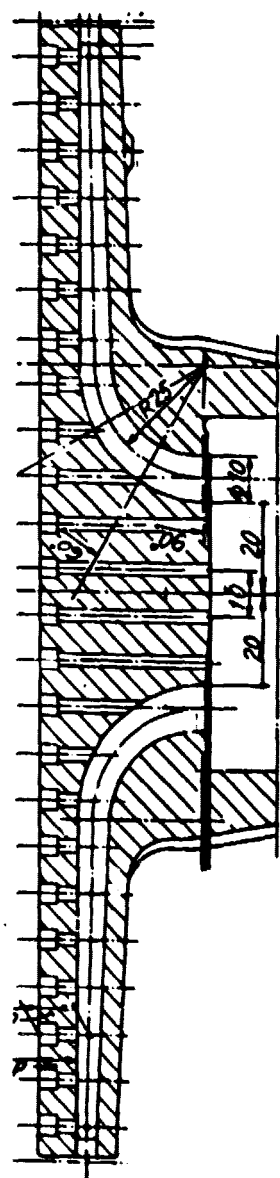
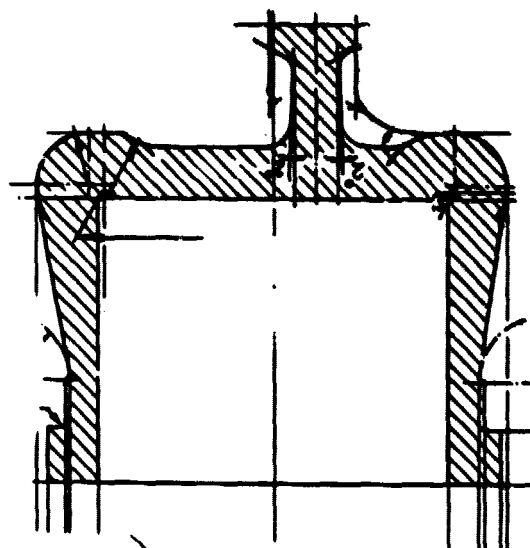
A comparison with the P40 regenerator housing shows that the stresses in the P40 design are higher than the corresponding stresses in MOD 1 regenerator housing.

In order to reduce the dead volume of the regenerator heater connecting space, a new design have been made of the manifold and its connection to the regenerator housing. Cross sections of the manifold and the regenerator housing are shown in figure 5.3:16. Instead of having one central manifold inlet at the top of the regenerator housing as in the earlier design, the main channel in the manifold have been divided into two separate channels discharging into the regenerator housing. From the stress point of view this design is considered at least as good as the first one by the following reasons.

The two main inlets at the top of the regenerator housing are located in areas where the stress level is considerably lower than in the central part, which can be seen in figure 5.3:17. This figure shows the radial variation of the stress components σ_{ϕ} (circumferential direction) and σ_R (radial direction) at the plane top of the regenerator housing for an internal pressure load. The stress values are normalized with respect to the maximum values at the centre (σ_c) and the stress distribution is based on an axi-symmetric finite element analysis made on the regenerator housing of engine P40, which has the same plane upper part if the inlets are not taken into consideration.

The stress distribution differ very little from the corresponding stresses in a circular plate with clamped edges exposed to an uniformly distributed pressure load, which means that the membrane part of the stress state in the plane top of the regenerator housing is very small and thus it is the bending stresses which dominate. Referring to figure 5.3:17, the two main inlets at the top of the regenerator housing are located at a radial position corresponding to $R/R_0 = 0.70$, which means that the hoop stress (σ_{ϕ}) in this point is only about 60% of the corresponding stress at the centre.

As can be seen in figure 5.3: 16, four heater tubes penetrate the top of the regenerator housing directly. However, the manifold forms a pad at the top which makes the central part very stiff with a material thickness of 38 mm.



I- 381

ORIGINAL PAGE IS
OF POOR QUALITY

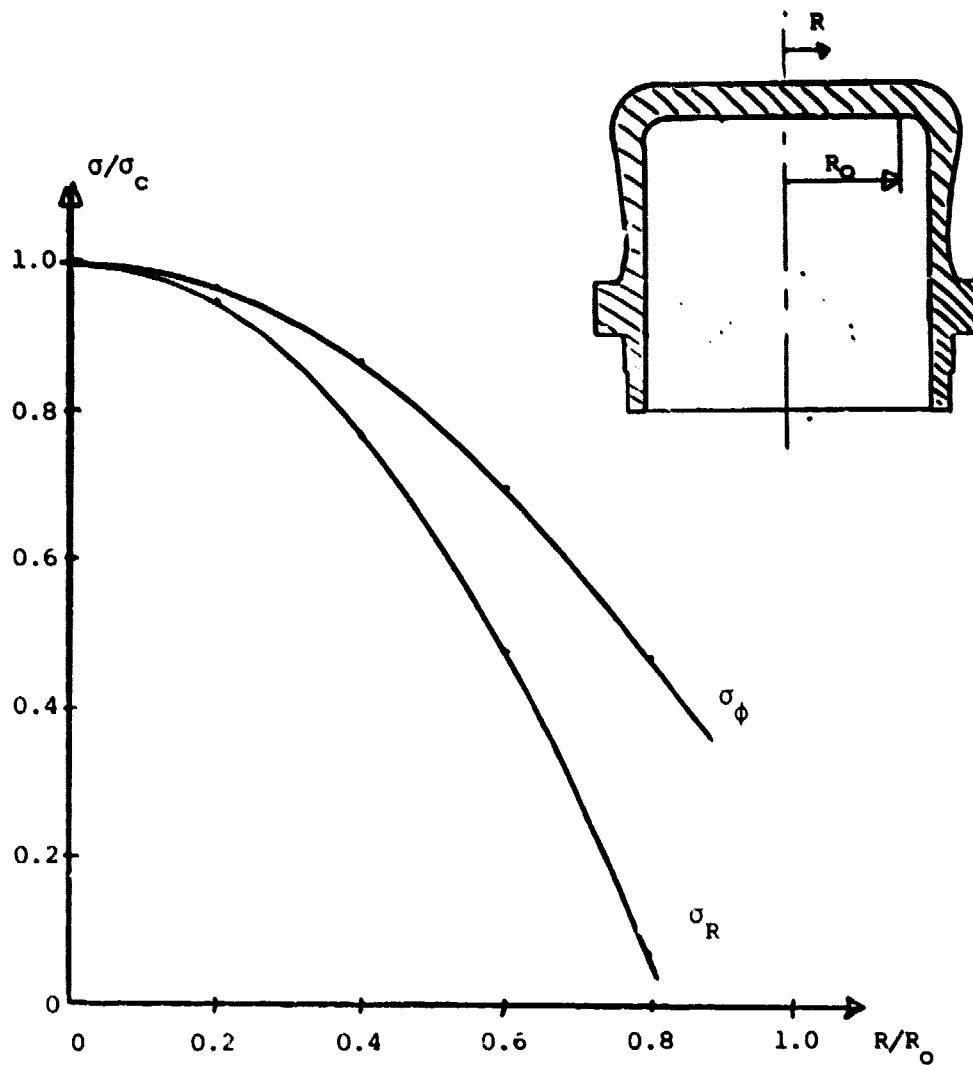


Figure 5.5: 17. Radial hoop stress in the plane top of the regenerator housing.

Internal pressure load. Constant thickness of the plane top and no inlets.

5.3.3 Cylinder Housing

5.3.3.1 General

The cylinder housing is bolted to the crankcase in a loose flange arrangement. It will be exposed to high temperature loading (about 700°C at the top) in combination with a cyclic internal pressure (about 15 ± 5 MPa). Just as in the case of the regenerator housing it is necessary to consider the risk of creep rupture and fatigue. A cross section of the cylinder housing can be seen in figure 5.3:18.

5.3.3.2 Material

The cylinder housing will be investment cast of the cobalt-base superalloy HS-31. In the stress analysis the same material data as for the regenerator housing has been used.

5.3.3.3 Design Criteria

The design criteria used on the cylinder housing will be the same as for the regenerator housing.

ORIGINAL PAGE IS
OF POOR QUALITY

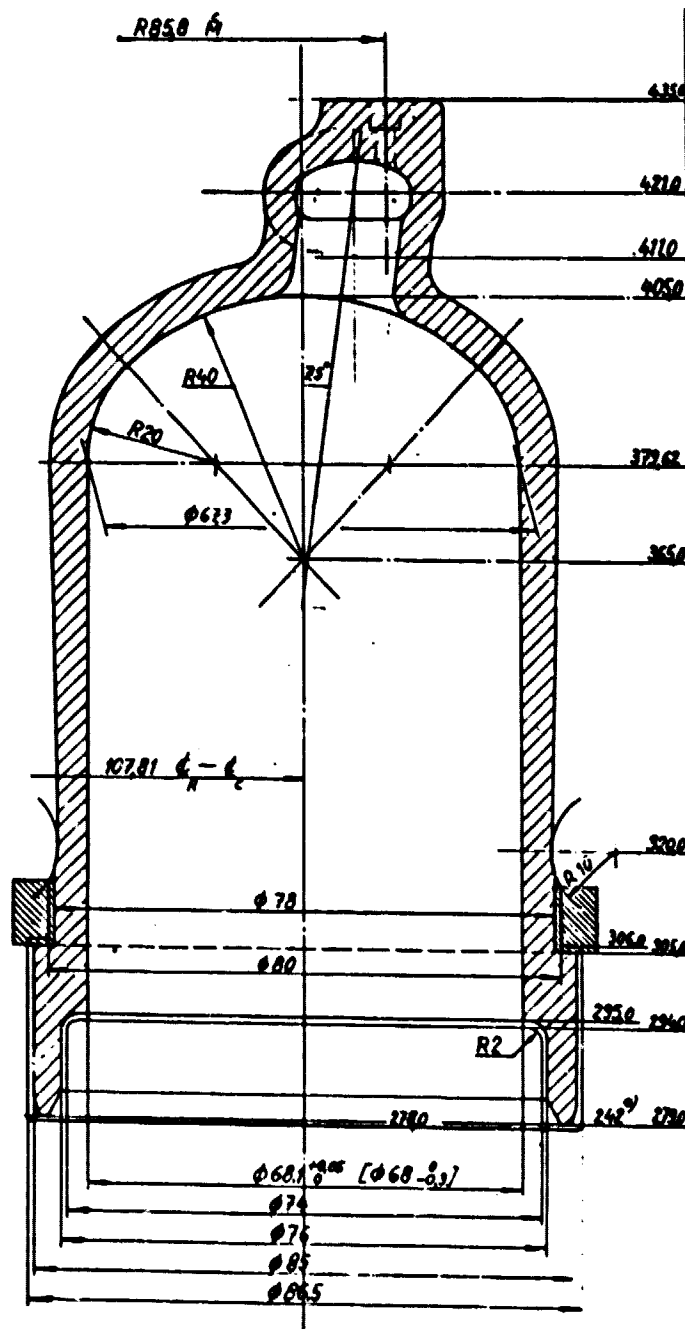


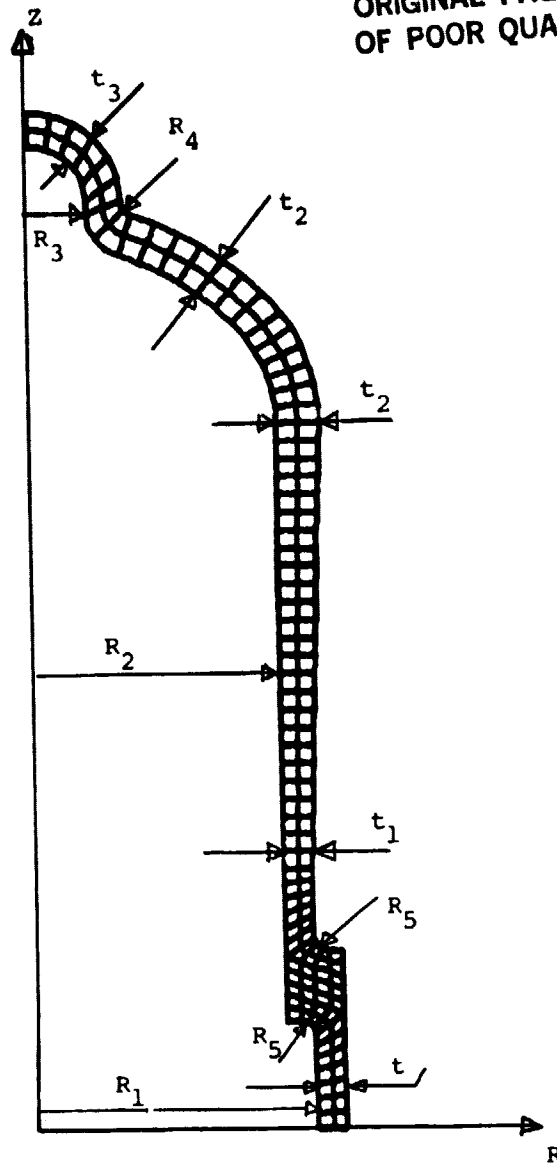
Figure 5.3: 18. Cross section of the cylinder housing.

5.3.3.4 Analysis

The cylinder housing has been analyzed using the finite element method. An axi-symmetric model consisting of 8-nodes isoparametric elements was used, and the mesh and main geometry used in the analysis is shown in figure 5.3: 19. The model has been closed in the upper part in order to simulate the manifold connection. The load cases used in the analysis are defined in figure 5.3: 20.

The average value across the wall thickness of the effective stress (σ_{ea}) have been calculated for section A to E defined in figure 5.3:21. The table shows the temperature in the section, the corresponding yielding stress (σ_y) of the material and the calculated effective stress σ_{ea} for different load cases. In load case 3 (mean pressure $p = 15$ MPa) the maximum value of σ_{ea} is 99 MPa in the hot region (section A). With the creep rupture stress $\sigma_{CR} = 225$ MPa, the safety factor against creep rupture will be 2.3. The maximum effective stress in load case 4 (max. pressure $p = 20$ MPa) is 217 MPa (section E), which gives a safety factor of 2.1 against yielding. The safety factor against yielding in the most severe combination of pressure load and temperature load (case 5 and 7) is 2.0 in section A. The σ_{ea} -values have been calculated in the same way as in the case of the regenerator housing, and consequently the safety factors mentioned above are conservatively estimated. Figures 5.3:22 and 5.3:23 show the effective stress σ_e along the inner and outer surfaces in load case 3 and 7. In the hot upper part of the cylinder housing, the maximal peak stress is 149 MPa in load case 7 (maximal pressure $p = 20$ MPa in combination with temperature load), which is only 2/3 of the maximal peak stress in the hot region of the regenerator housing. On the cold side of the cylinder housing, the maximal peak stress occurs in the radius near the flange, and the effective stress at that point will vary between stress levels corresponding to load case 5 ($p = 10$ MPa and temperature) and 7 ($p = 20$ MPa and temperature) in the following way. $\sigma_e = 145 \text{ MPa} \pm 43 \text{ MPa}$. This can be compared to $\sigma_e = 270 \text{ MPa} \pm 95 \text{ MPa}$, which is the corresponding stress level in the regenerator housing. Consequently the cylinder housing have a higher factor of safety against fatigue than the regenerator housing.

ORIGINAL PAGE IS
OF POOR QUALITY



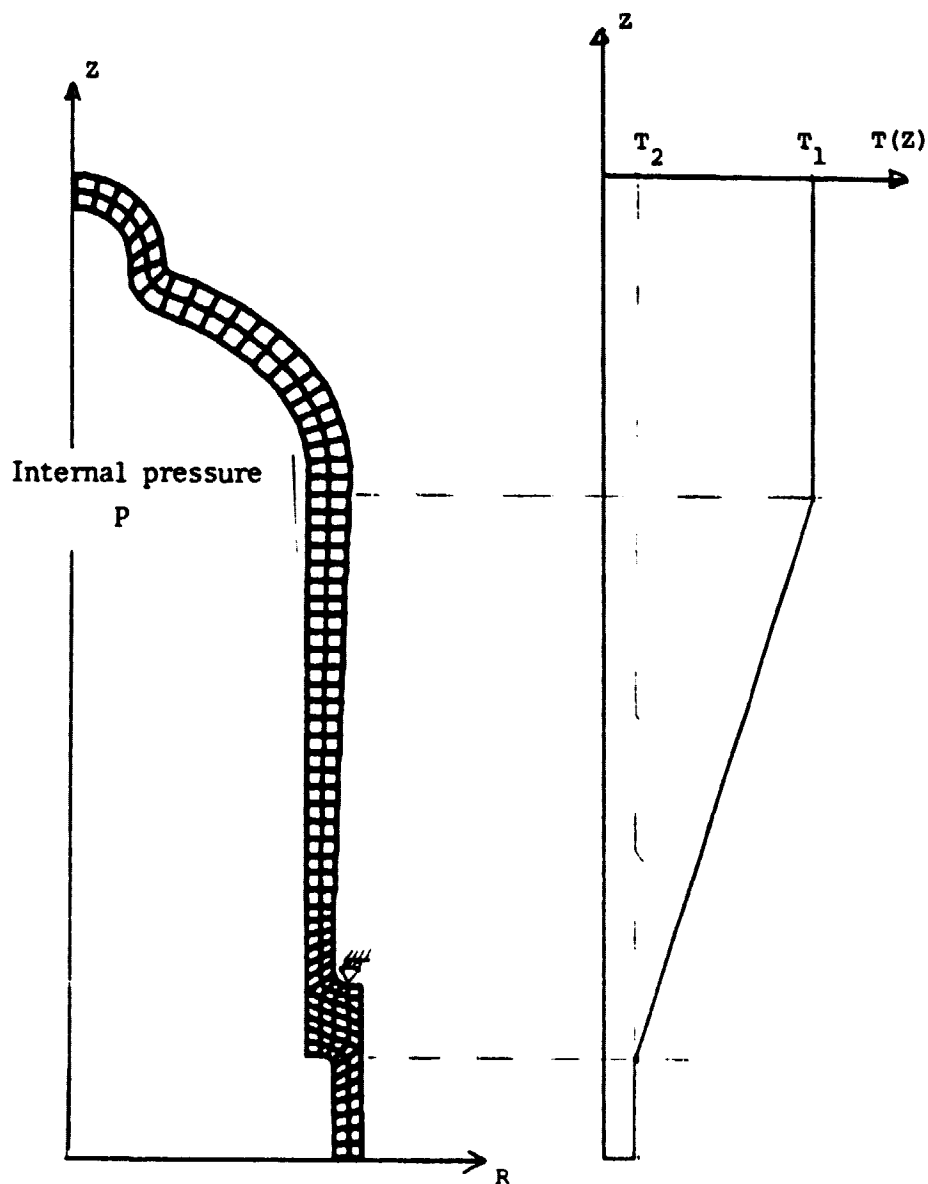
$$\begin{aligned} t_1 &= 4.0 \text{ mm} \\ t_2 &= 6.0 \text{ mm} \\ t_3 &= 5.0 \text{ mm} \end{aligned}$$

$$\begin{aligned} R_1 &= 38.0 \text{ mm} \\ R_2 &= 34.05 \text{ mm} \\ R_3 &= 8.0 \text{ mm} \\ R_4 &= 2.0 \text{ mm} \\ R_5 &= 2.0 \text{ mm} \end{aligned}$$

Figure 5.3: 19. Main geometry used in the analysis.

ORIGINAL PAGE IS
OF POOR QUALITY

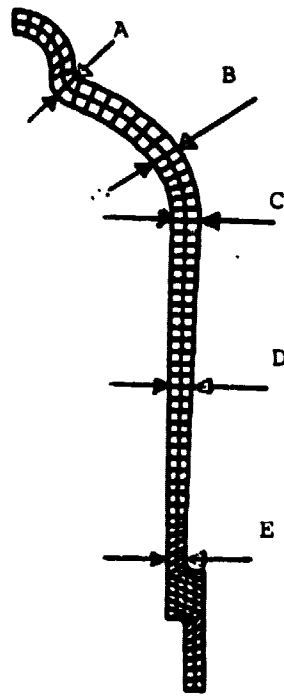
Temperature distribution
along axis of symmetry



- Load case: 1 Temperature load $T_1 = 700^\circ\text{C}$, $T_2 = 70^\circ\text{C}$
 2 Internal pressure $p = 10 \text{ MPa}$
 3 " " $p = 15 \text{ MPa}$
 4 " " $p = 20 \text{ MPa}$
 5 Temperature load combined with $p = 10 \text{ MPa}$
 6 " " " $p = 15 \text{ MPa}$
 7 " " " $p = 20 \text{ MPa}$

Figure 5.3: 20. Load cases used in the analysis.

ORIGINAL PAGE IS
OF POOR QUALITY



- Load case 1 Temperature load T
 3 Pressure load $p = 15 \text{ MPa}$
 4 $p = 20 \text{ MPa}$
 5 $T, p = 10 \text{ MPa}$
 7 $T, p = 20 \text{ MPa}$

SECTION	TEMP (°C)	σ_y (MPa)	LOAD CASE				
			1	3	4	5	7
A	700	260	6	99	132	64	130
B	700	260	30	50	67	33	65
C	700	260	94	53	70	72	69
D	470	300	11	98	131	69	134
E	140	455	105	163	217	107	189

Figure 5.3: 21. Average effective stress in some sections.

ORIGINAL PAGE IS
OF POOR QUALITY

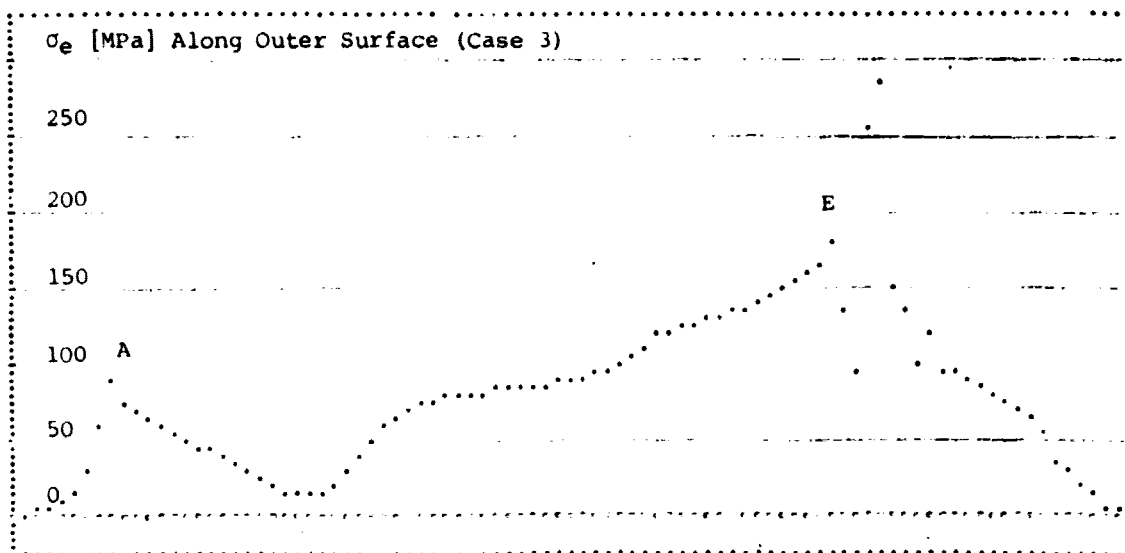
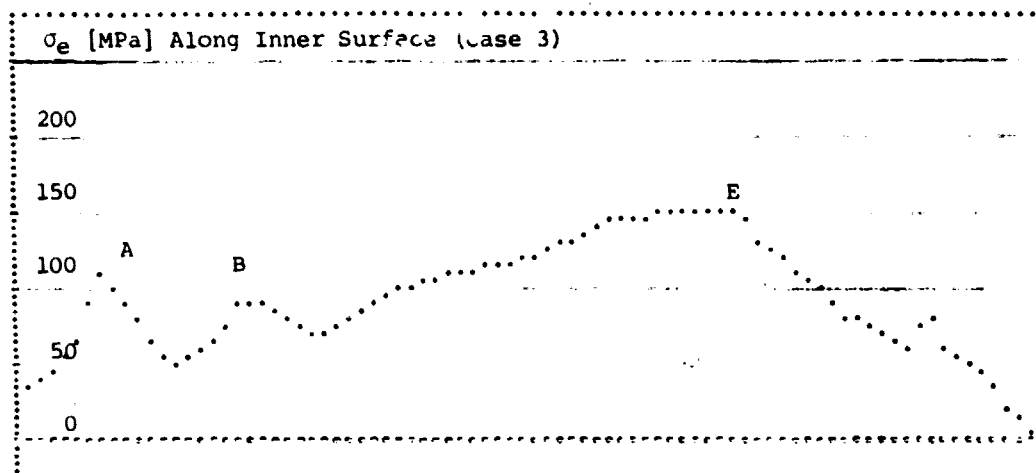
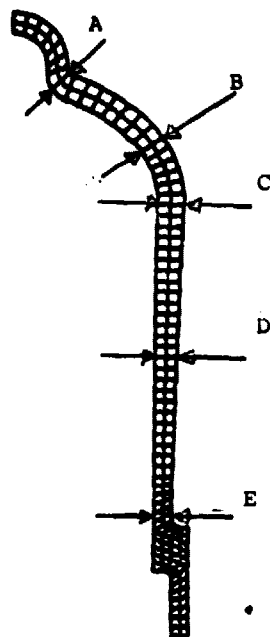


Figure 5.3: 22. Effective stress at the surface in load case 3.

ORIGINAL PAGE IS
OF POOR QUALITY

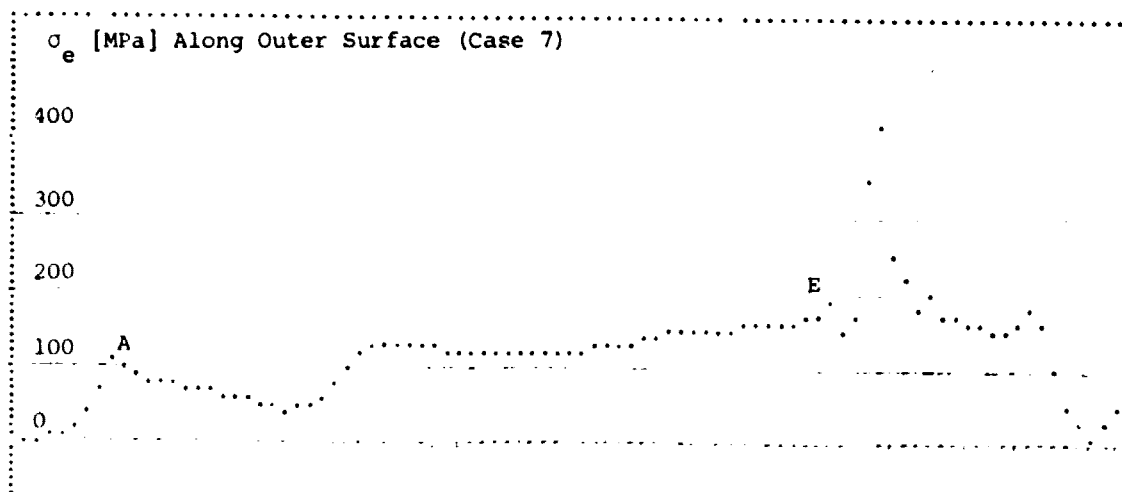
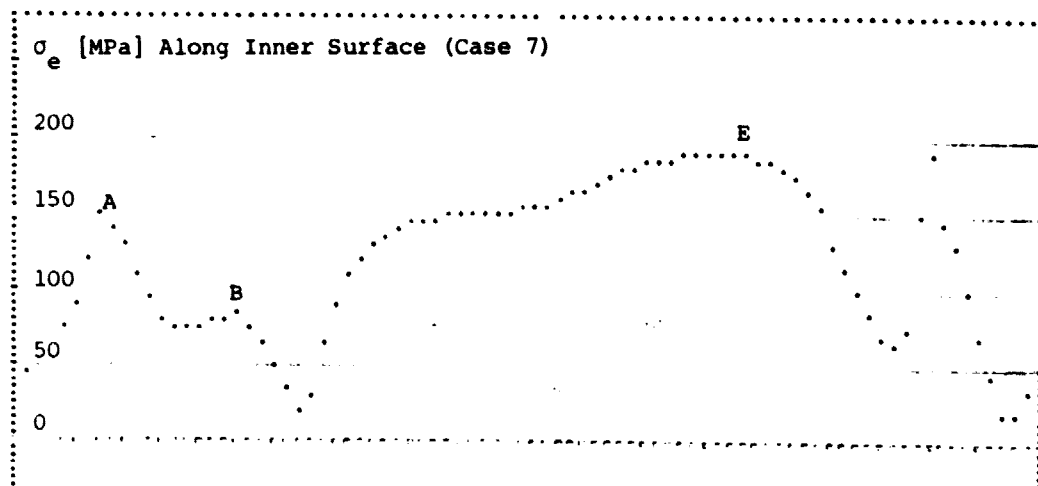
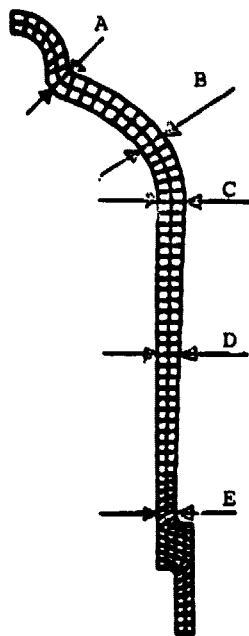


Figure 5.3: Effective stress at the surface in load case 7.

5.3.4 Heater Head Manifolds

5.3.4.1 General

The heater head manifolds are integral parts of the heater heads and they constitute a connection between a heater head and the corresponding heater tubes, which are brazed into the upper part of the manifolds. The heater tubes are connected to the cylinder manifold with a pitch of 5.5 mm and to the regenerator manifold with a pitch of 10 mm, which makes the cylinder manifold to the most critical component from the stress point of view (see figure 5.3: 24). The cylinder manifold and the regenerator manifold will be exposed to the same type of loading, which means high temperature (about 700°C) in combination with the cyclic internal pressure ($p = 15 \pm 5$ MPa).

5.3.4.2 Material

The manifolds are cast together with the heater housings and thus investment cast of a cobalt base superalloy (HS-31).

5.3.4.3 Design Criteria

The lack of applicable information of the high temperature fatigue properties and the degree of stress relaxation that may occur, makes it difficult to define realistic stress limits. The estimation of the risk of creep or fatigue rupture must therefore be based on P40 experience.

5.3.4.4 Analysis

To calculate the stresses in a manifold in an accurate way, it would be necessary to make a finite element analysis using a 3-dim model, due to the very complicated geometry of the manifolds. Such an analysis would be very time consuming and perhaps not cost effective referring to the lack of thermal fatigue property data of the alloy. However, in order to estimate differences in stress levels due to differences in the geometry between the P40 and MOD 1 manifolds, a simple 2-dim finite element analysis was made of typical cross sections of the manifolds, and the main geometry of the models can be seen in figure 5.3: 25.

OF POOR QUALITY

1 2 3 4 5 6 7 8 9 10 11 12

3,

6

190° R25

60°

30°

55

20

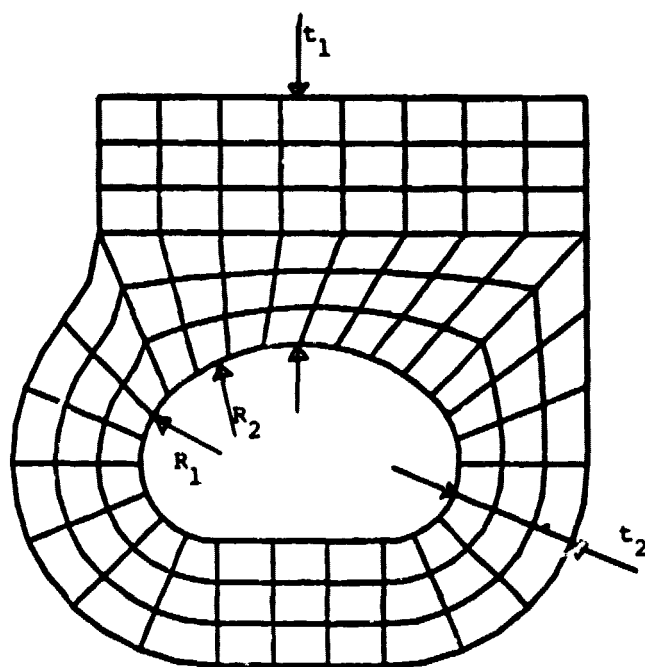
6

50



In the finite element analysis both cross sections were exposed to an internal pressure of 20 MPa, and the effective stress at the inner surface is shown in figure 5.3: 26. The most critical point in the manifolds is at the inner surface at the heater tube inlet. However, considering the hole extension (4 mm diameter in P40 and 3 mm in MOD 1) the average effective stress is 26 MPa in the MOD 1 case and 70 MPa in the P40 case.

Typical MOD 1 manifold cross section



$$R_1 = 3.0 \text{ mm}$$

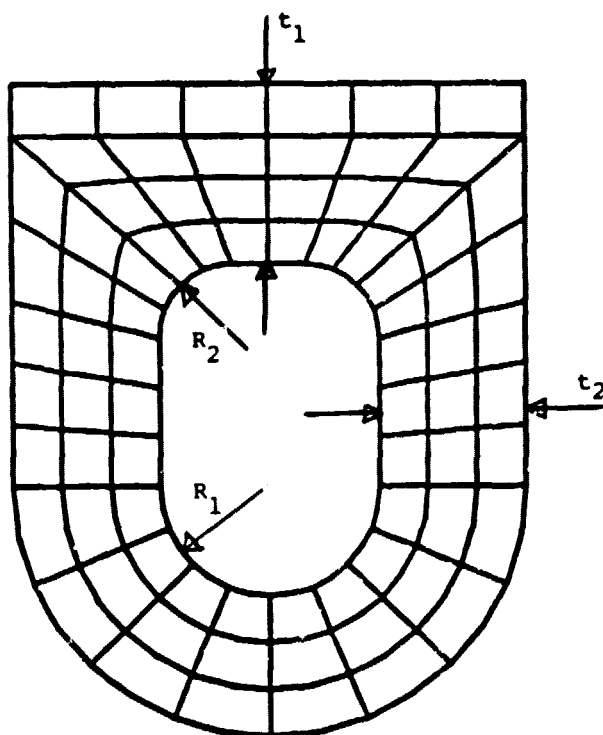
$$R_2 = 7.5 \text{ mm}$$

$$t_1 = 9.5 \text{ mm}$$

$$t_2 = 5.0 \text{ mm}$$

ORIGINAL PAGE IS
OF POOR QUALITY

Typical P40 manifold cross section



$$R_1 = 3.0 \text{ mm}$$

$$R_2 = 2.0 \text{ mm}$$

$$t_1 = 5.0 \text{ mm}$$

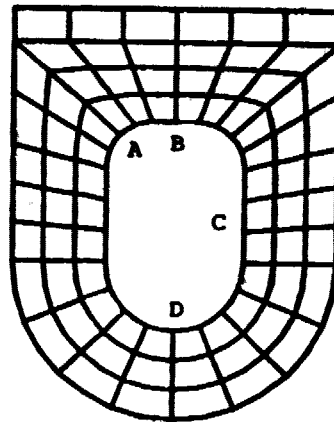
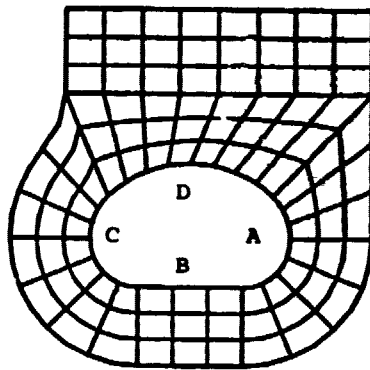
$$t_2 = 4.0 \text{ mm}$$

Figure 5.3:25. Main geometry used in the analysis.

ORIGINAL PAGE IS
OF POOR QUALITY

MOD 1 manifold

P40 manifold



POINT	EFFECTIVE STRESS (MPa)	
	MOD 1	P40
A	99	102
B	30	57
C	106	27
D	20	104

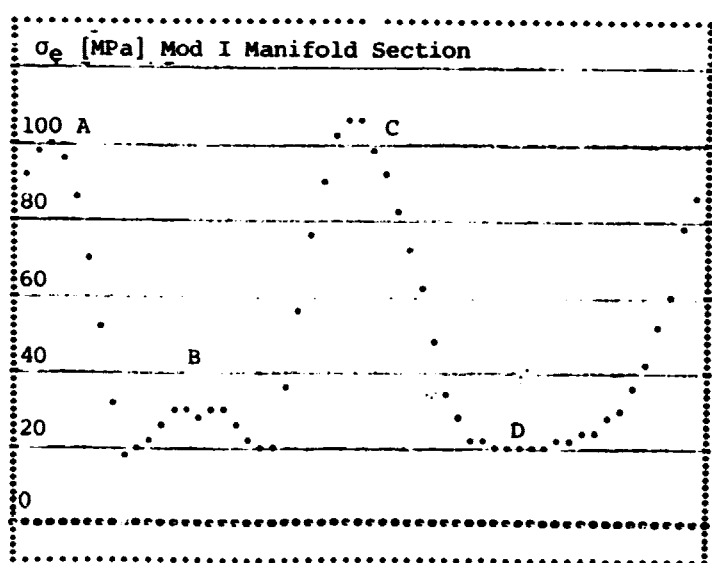


Figure 5.3:26. Effective stress in typical cross sections.

These relative stress levels are based on full area neglecting the holes. The hole pitch is the same in both cases (5.5 mm), but the hole diameter at the inner surface of the manifolds is 3.0 mm in the MOD 1 case and 4.0 mm in the P40 case. This means that the ratio gross area to net area at the inner surface is 3.67 in the P40 case and 2.2 in the MOD 1 case. Considering the reduced area, the effective stress at the inner surface is 57 MPa in the MOD 1 case and 257 MPa in the P40 case. However, the holes are also exposed to the pressure 20 MPa, which gives a stress contribution of 24 MPa in the MOD 1 case and 26 MPa in the P40 case. The new stress level in the MOD 1 case will then be 81 MPa and in the P40 case 283 MPa. These stresses are based on net area and the stress concentrations caused by the holes have not been considered.

Looking at stress concentration factors (according to Peterson) for a uni-axially stressed infinite plate with an infinite row of circular holes, the stress concentration factor is 1.52 in the MOD 1 case and 1.22 in the P40 case. This means that the maximal stress in the MOD 1 manifold is 123 MPa compared to 345 MPa in the P40 case. The comparison is summarized in figure 5.3:27. Without paying too much attention to the absolute stress levels, the comparison shows that the stress level in the MOD I manifold is considerable lower than in the P40 manifold.

Stress level considering:	MOD I Stress (MPa)	P 40 Stress (MPa)	Stress ratio $\sigma(P40) / \sigma(MOD I)$
The hole location at the elliptical section.	26	70	2.7
The reduced area due to the holes.	57	257	4.5
The stress contribution from the pressurized holes.	81	283	3.5
The stress concentration factor of a circular hole	123	345	2.8

Figure 5.3:27. Comparison between MOD I and P40 stress levels.

(-5)

5.3.5 The gas cooler

5.3.5.1 General

The gas cooler is subjected to a compressive load, which is equal to the cycle pressure multiplied by the compressed area inside the outermost O-ring of the gas cooler. The cooler shall resist buckling, yielding and fatigue.

5.3.5.2 Material

The cooler is made of stainless steel SS 2337 (AISI 321) in the tubes and of SS 2343 (AISI 319) in the end plates and the housing. The following data are valid.

SS 2337

Yield stress (0.2%) $\sigma_y = 210 \text{ MPa}$

Ultimate tensile strength $\sigma_u = 510 \text{ MPa}$

Fatigue limit $\sigma_f = 190 \text{ MPa}$

Young's modulus $E = 196000 \text{ MPa}$

SS 2343

Yield stress (0.2%) $\sigma_y = 220 \text{ MPa}$

Ultimate tensile strength $\sigma_u = 490 \text{ MPa}$

Fatigue limit $\sigma_f = 185 \text{ MPa}$

Young's modulus $E = 196\ 000 \text{ MPa}$

5.3.5.3 Design Criteria

Buckling is the most likely failure process for the cooler. The cooler tubes shall resist buckling with normal safety factors, i.e. 2.5 in elastic region and 1.5 in the plastic region. The cooler as a whole shall resist yielding with a safety factor of 1.5.

5.3.5.4 Analysis

The design is based on experience as well as finite element computations. The cooler is very alike that one of the P75 engine and according to finite element computations they have the same strength. The P75-cooler has successfully been fatigue tested.

The cooler consists of two end plates (thickness 6 mm), a cylindrical housing (thickness 4.5 mm) with two water ports and 449 tubes. The tubes have 2 mm OD and 1 mm ID. Three bars with a diameter of 3.5 mm are placed at each water port in order to increase the stiffness in this region.

Consequently the end plates are perforated with 455 holes. See fig. 5.3: 28.

From symmetrical reasons one eighth part of the cooler is analyzed. The end plate and the housing are divided into isoparametric thick shell elements with eight nodes in each element. The mesh is shown in fig. 5.3: 29.

ORIGINAL PAGE IS
OF POOR QUALITY

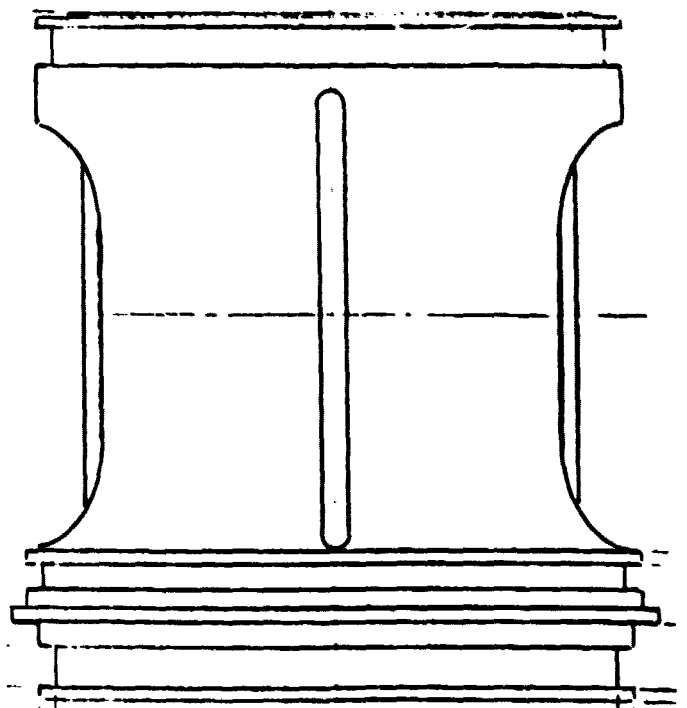
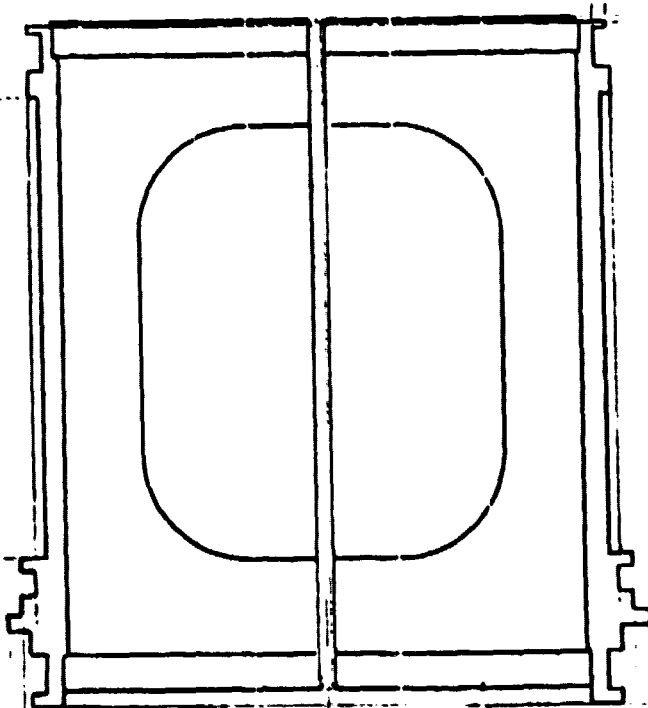
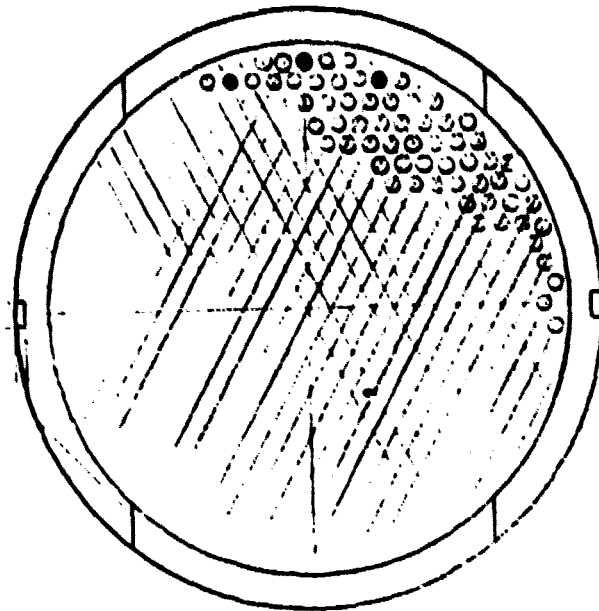


Fig. 5.3: 28. Top view and side view of the gas cooler. The bars at the water ports are marked in the top view.

ORIGINAL PAGE IS
OF POOR QUALITY

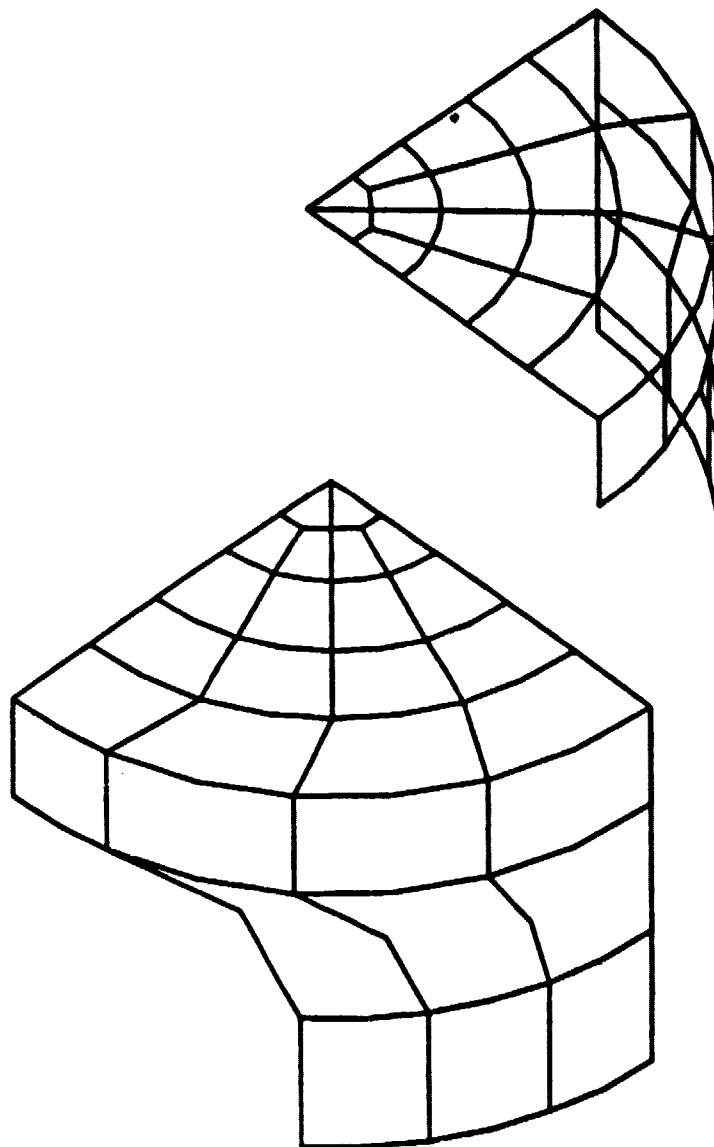
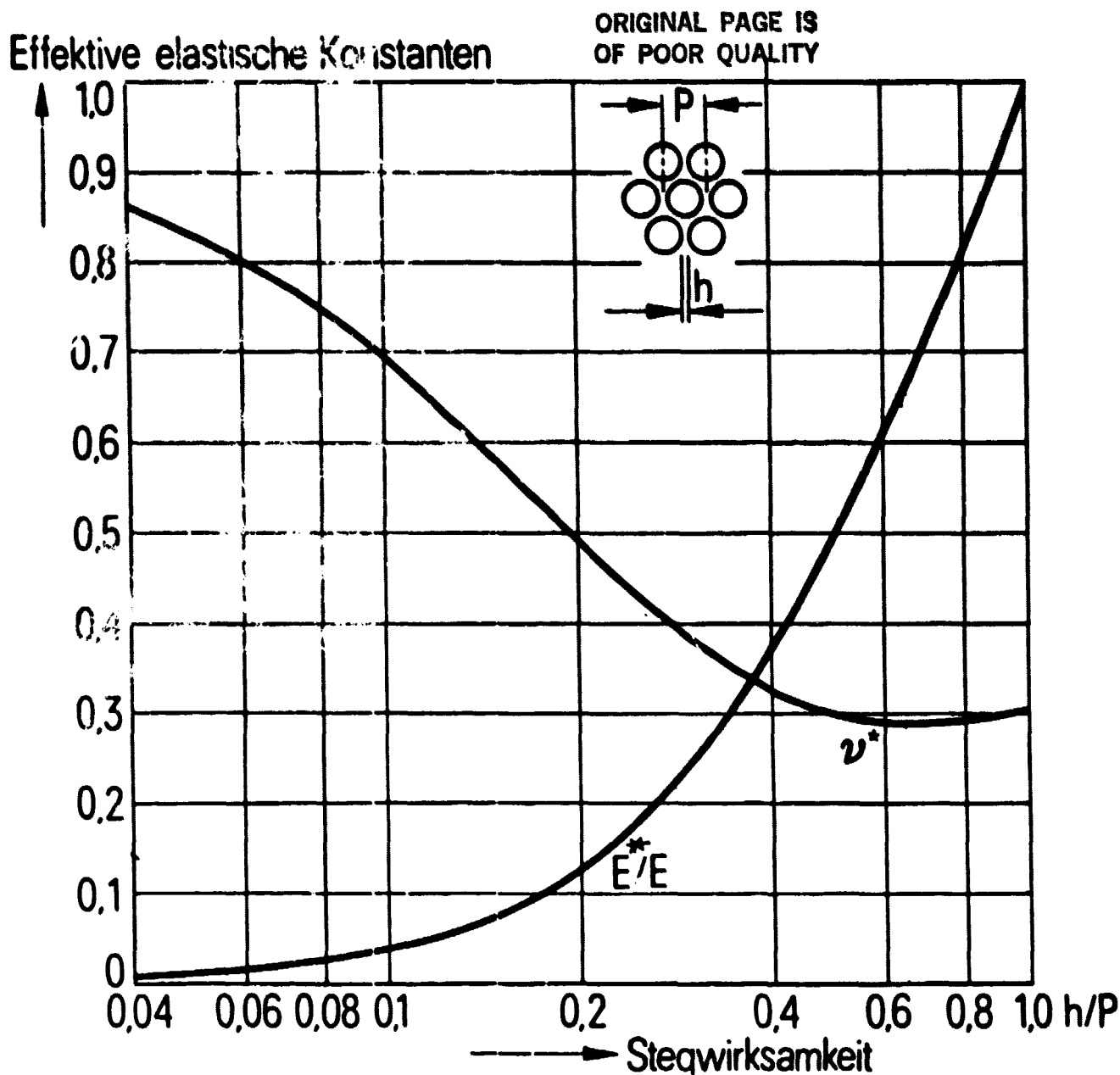


Fig. 5.3:29. The finite element mesh of the gas cooler seen from two different view points.

The total FEM structure has 28 elements and 630 degrees of freedom. In order to simulate the tubes nodal springs are inserted in each node of the end plate, which is not coupled to the housing. At each such node the spring constant is computed according to the distribution of the tubes. Young's modulus of the end plate must be corrected due to the perforation. Such corrections are available from the nuclear power plant industry used for nuclear pressure vessels, see fig. 5.3:30. In this case the correction factor is 0.65.

The computed deflection of the central port of the end plate is $15.1 \mu\text{m}$. On the other hand the largest deflection of the end plate is $19.1 \mu\text{m}$ just above the water port. The largest deflection of the end plate at a tube is $16.5 \mu\text{m}$. The total largest compression of a whole tube will be the double, namely $33 \mu\text{m}$. This can be compared to the compression of a bar with the same cross sectional area as the cooler, which is $24.6 \mu\text{m}$. Thus the cooler is rather evenly compressed.



t - Dicke der perforierten
Platte $t/P \geq 2$

Fig. 5.3:30. Correction diagram for Young's modulus and Poisson's ratio from (Spannungsanalyse der Primärkammer eines Dampferzeugers, IKO Software Service GmbH, Finite element congress 6-7 th November 1972) $P = 2.98 \text{ mm}$, $h = 1.98 \text{ mm}$, $t = 6 \text{ mm}$, $t/P = 2.01$, $h/P = 0.67$.

The maximum tube compression of 33 μm corresponds to an axial stress of - 82 MPa. A recommended reduced length of 60% of the tube length is chosen instead of the theoretical value of 50% (bar with both ends built in). This gives a slenderness ratio of 89. The actual values of the compression stress and the slenderness ratio are shown with dotted lines in the buckling diagram in fig. 5.3:31. As can be seen they intersect below the allowed level of a steel with the yield stress equal to 210 MPa.

The combination of the axial stress and the maximum circumferential stress gives an effective stress (v. Mises) equal to 103 MPa. This gives a safety factor against yielding and fatigue larger than 2.

With the exception of the tubes the largest effective stress occurs at the vertical parts of the water ports. Here the effective stress is 82 MPa. This gives a safety factor against yielding and fatigue larger than 2.5.

ORIGINAL PAGE IS
OF POOR QUALITY

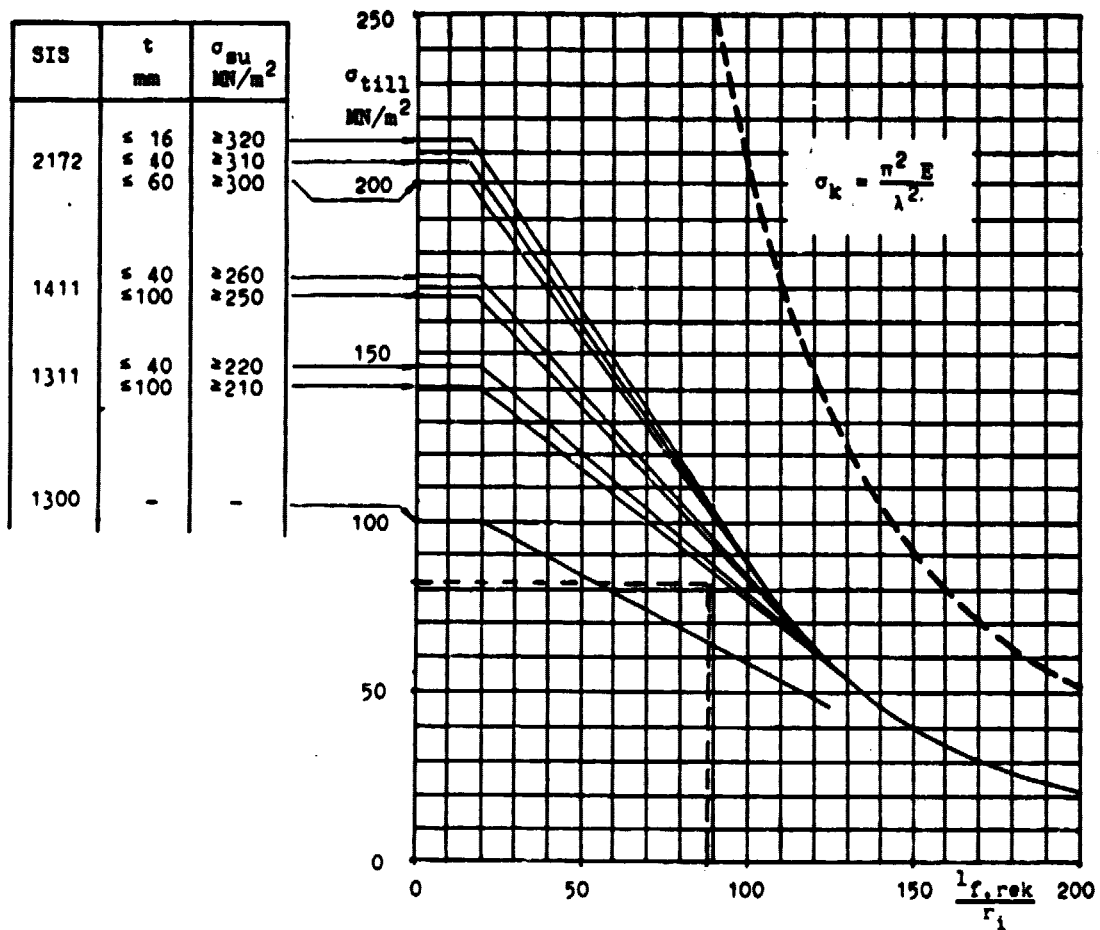


Fig. 5.3:31. Allowed compressive stresses for steel bars as a function of the slenderness ratio. The yield stress in MPa is the parameter of the different curves. The diagram is due to the Swedish Building Construction Norm. The safety factor is 2.5 in the elastic region and 1.5 in the plastic region.

5.4

Heat transfer for heater tubes

The heat transfer number has been calculated for the heater. The efficiency of the heater is very good and the gas temperature after the heater will not exceed the tube temperature more than 55°C at full load.

5.4.1

Definitions

The heat transfer efficiency for the heater is expressed with a value defined as

$$\Lambda = \ln \frac{t_1 - t_w}{t_2 - t_w} \text{ where}$$

t_1 = temperature on fluid before the heat exchanger

t_2 = " " " after " " "

t_w = surface temperature on the heat exchanger

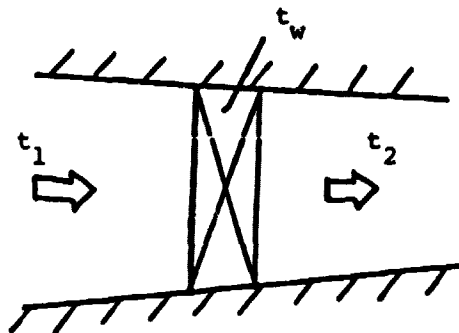


Figure 5.4:1

ORIGINAL PAGE IS
OF POOR QUALITY

ORIGINAL PAGE IS
OF POOR QUALITY

Heat transfer number on the front heater row (see figure 5.4:2)

$$\Lambda_f = \ln \frac{t_{cg1} - t_w}{t_{cg2} - t_w}$$

Heat transfer number on the rear heater row

$$\Lambda_r = \ln \frac{t_{cg2} - t_w}{t_{cg3} - t_w}$$

Total heat transfer number for the heater $\Lambda = \Lambda_f + \Lambda_r =$

$$= \ln \frac{t_{cg1} - t_w}{t_{cg3} - t_w}$$

The thermal efficiency of the heater η_t can be expressed with the Λ -value

$$\eta_t = \frac{t_{cg1} - t_{cg3}}{t_{cg1} - t_w} = 1 - e^{-\Lambda}$$

$$\dot{q}_f / \dot{q}_r$$

$$\dot{q}_f / \dot{q}_r = \frac{t_{cg1} - t_{cg2}}{t_{cg2} - t_{cg3}} \cdot \frac{L_f}{L_r}$$

L = the active tube length
 f = Front Row
 r = Rear Row

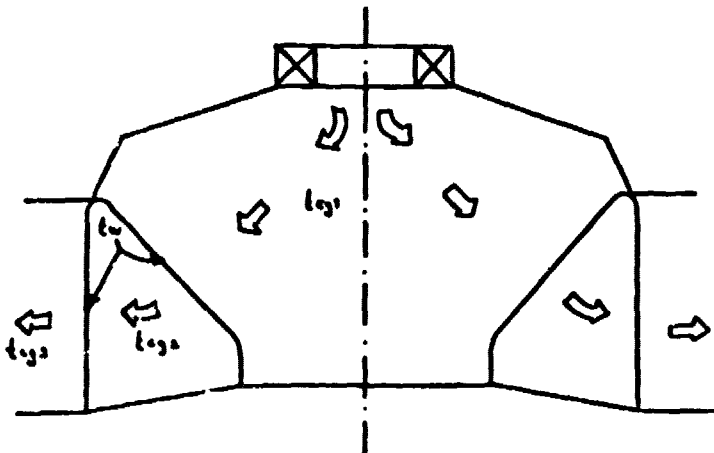


Figure 5.4:2

5.4.2

Results

The calculation is made for the following.

Heater geometry

Total number of tubes: 96.

Front heater row

No surface enlargement.

Active tube length: 150 mm.

Distance between tube centra: 5.62 mm

Rear heater row

Surface enlargement: Plate fins.

Active tube length: 107.5 mm

Distance between tube centra: 10.54 mm.

Length plate fins: 10 mm.

Thickness plate fins: 0.6 mm.

Distance between plate fins: 0.7 mm.

Load

Combustion gas flow: 40,80 and 120 g/s.

Air excess ratio: 1.2.

Flame temperature: 2000°C

Tube temperature: 720°C.

m_{cg}	Λ_f	Λ_r	Λ	\dot{q}_f/\dot{q}_r	t_{cg3}
g/s					°C
40	0.70	4.44	5.14	0.93	727
80	0.50	3.53	4.03	0.61	743
120	0.41	2.76	3.17	0.50	774

Calculated data for the MOD I heater.

5.4.3

Heat transfer test

Test objects will be designed for the two heater rows. A special technique will be used for the cooling of the test objects (at USS called the DMR-technique). A small diameter tube is placed at the centre of the outer tube. The inner tube is cooled by water. Between the tubes is an isolating gaslayer. The low conductivity of the gaslayer makes it possible to have a high heatflux and still keep the outer tube at a high temperature. By changing the composition of the gaslayer it is possible to keep the tube temperature at a constant level throughout the load range.

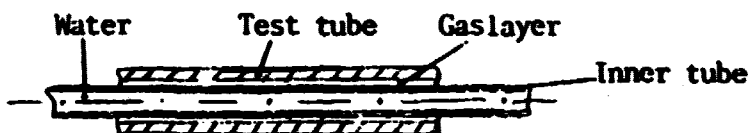


Figure 5.4:3

Test procedure

Gasoline is fired with air in a combustor to which the test objects are mounted. After the test objects the combustion gases are passed to a preheater and/or bypassed the same.

Heat transfer measurements

The test objects are equipped with thermocouples. The combustion gas flow is calculated by measuring the fuel flow and the air excess downstream test objects. Combustion gas temperature downstream test objects is measured with suction pyrometer.

The test objects are cooled by water passing through the inner tube. Water mass flow and temperature increase is measured and the heatflow to the front and rear test object \dot{Q}_F and \dot{Q}_R can be calculated. As the combustion gas flow \dot{m}_{cg} and the combustion gas temperature after the test objects t_{cg3} is also known t_{cg2} and t_{cg1} can be calculated.

With nomenclature from figure 5.4:4

$$\Delta F = \ln \frac{t_{cg1} - t_{wF}}{t_{cg2} - t_{wF}}$$

$$\Delta R = \ln \frac{t_{cg1} - t_{wR}}{t_{cg2} - t_{wR}}$$

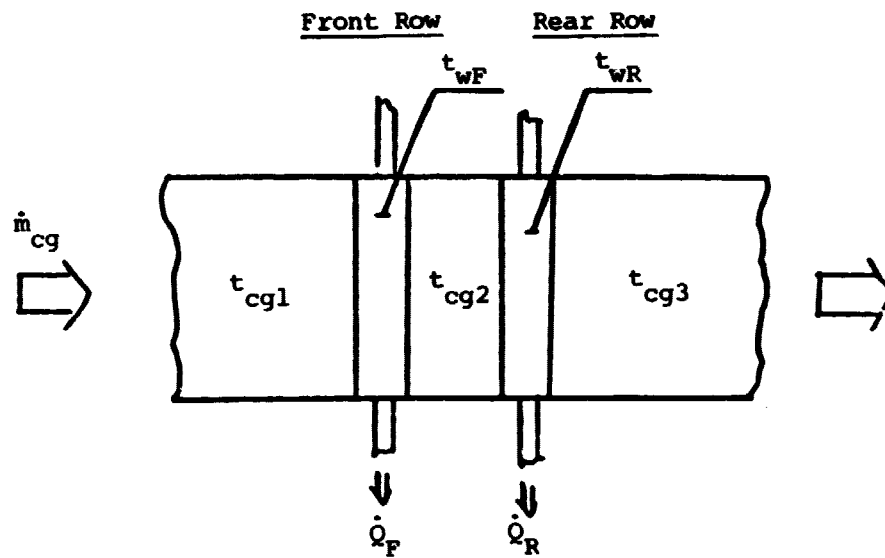


Figure 5.4:4

ORIGINAL PAGE IS
OF POOR QUALITY

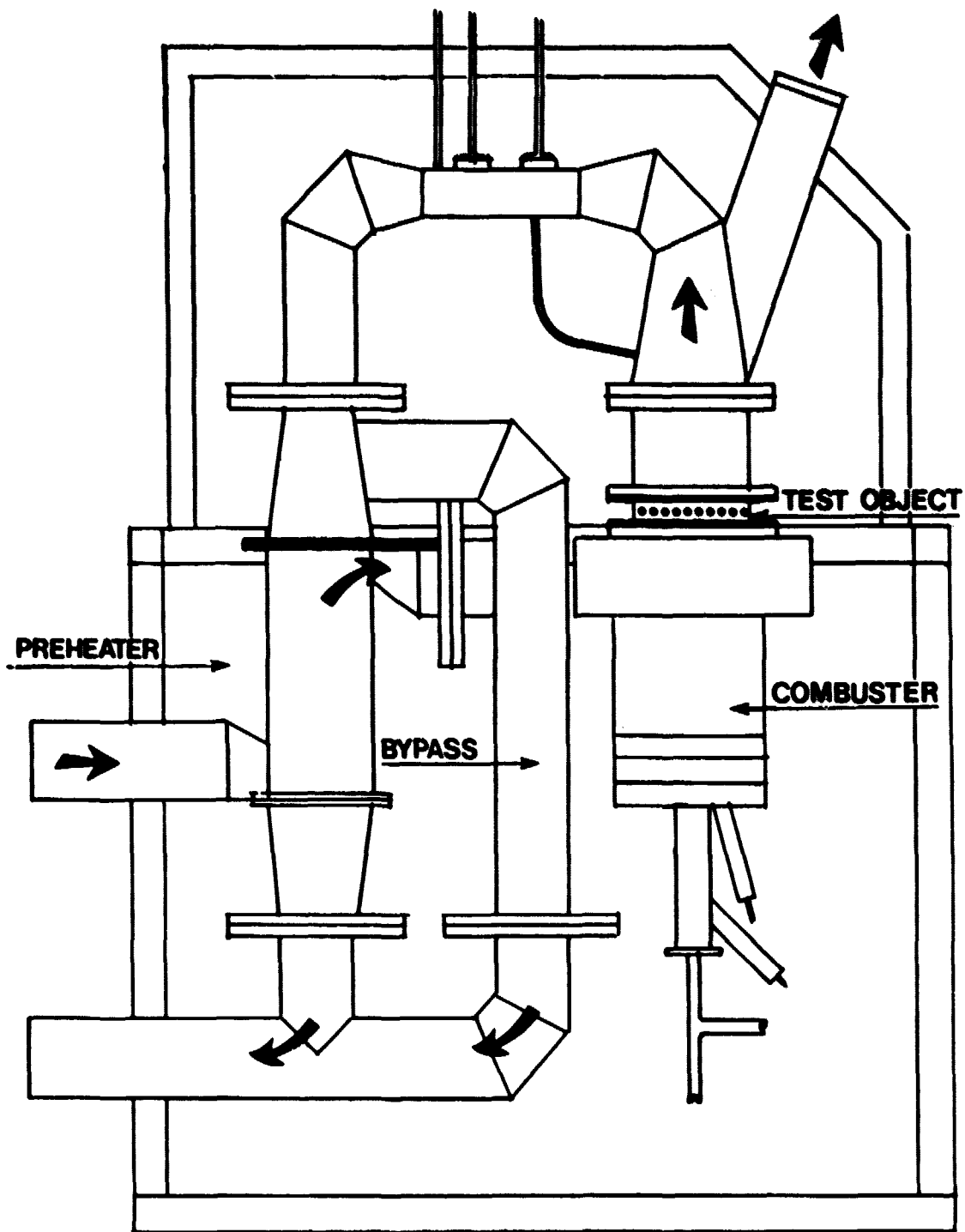


FIG 5.4:5

5.5 Flow distribution tests on cylinder, manifold and regenerator housing

Flow distribution in manifolds above the cylinder and regenerator-housing, see drawing 1-73561.

The heater head is an important component regarding efficiency and life with respect to the Stirling engine. The heater head has been optimized to tube dimensions; tube number and length etc. In the calculations we have considered an equal mass-flow distribution of the hydrogen gas in each tube.

The gas is supplied via the manifolds into the heater tubes from the cylinder into the regenerator housing and vice versa.

The manifolds must have enough volume in order to be sure of proper distribution in the heater-tubes, and the goal is a maximum deviation of $< 10\%$ of mean mass-flow.

The test-object consists of one cylinder- and one regenerator-housing with their manifolds. The two components are connected to each other with heater tubes of the engine length and dimensions.

Water flows from the cylinder housing to the regenerator-housing and vice versa. The pressure drop is measured in a two tubes yielding the mass flow of water. In order to reach as good flow distribution as possible the tests will be performed at the Reynold's number corresponding to the one as resulting with Hydrogen gas in the engine.

Quantitative comparisons between two different manifold configurations (calculated)

The first configuration has one connecting duct towards the centre part of the regenerator housing (drawing 1-S-1281).

The second one has two separate manifolds connecting the outer part of the housing (drawing 2-17037).

The cylinder manifold has nearly the same shape and size in both alternatives (drawing 1-S-1281, 1-17035).

From calculations we have found that as gas flows from regenerator into cylinder (duct B into duct A) there will be insignificant massflow variation in the heater tubes (see calc 1 and 6).

When gas flows from cylinder into regenerator (duct A into duct B) there will be a slight massflow deviation between the two configurations.

The most favoured configuration (1-S-1281) has a deviation between maxflow/minflow of 1.13. The second one 1.17.

In fact the dead volume above the regenerator matrix affects power and efficiency more detrimentally than a small massflow deviation. For this reason we have chosen a manifold according to drawing 2-17037. The difference in volume is about 4 cm³.

CALC. 40 1 ON FLOW DISTR. IN

NO 1 HEATER

SIGN/DATE: EJ/791030 PAGE 10

CALC. OF THE FLOW DISTRIBUTION IN THE HEATER DUE TO THE NOT CONNECTING DUCTS.
 DUCT A = SPACE CYL.-HEATER; DUCT B = SPACE HEATER-REG. FLOW DATA FROM OPT 22-00.
 DUCT GEOMETRY ACCORDING TO DRAWING NO: 1-5-12A1

*****USS*****
 MANIFOLD FLOW DISTR. PROGRAM
 *****MANIF*****

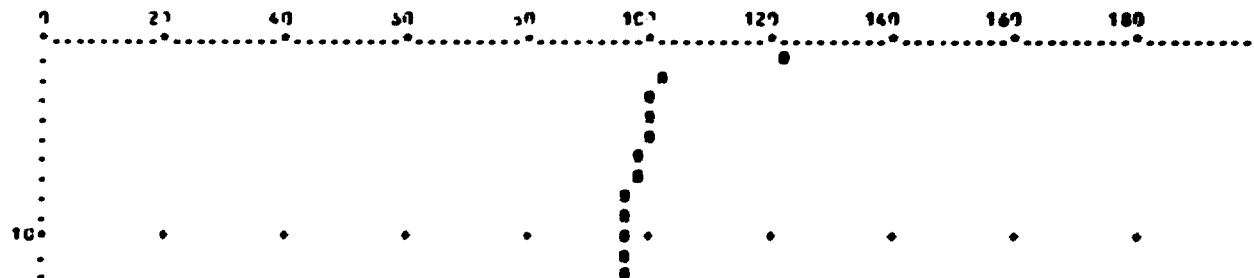
***** FLOW DIRECTION: FROM DUCT 1 INTO DUCT A *****

DUMP OF ALL NON-ZERO ELEMENTS FROM 90/5/1 (1) TO 177/1/1 (400), PAGE 2

104	5.0757E+01	305	5.0872E+06	306	5.0772E+00	307	5.0974E+01	308	5.1050E+03	309	5.1133E+00
110	5.1135E+00	311	5.1154E+00	312	5.1157E+03	351	1.2111E+00	352	1.0155E+00	353	1.0075E+00
154	1.0307E+00	355	9.7243E-01	356	9.4274E-01	357	9.7034E-01	358	9.6354E-01	359	9.6614E-01
360	9.6760E-01	361	9.5837E-01	362	9.5800E-01						

PLOT OF THE VARIABLES. AMOTRA (Y) AMOTON (X)

SCALE: VARIABLE VALUE = $\times 10^{-2}$



I-414

ORIGINAL PAGE IS
 OF POOR QUALITY

CALC. NO 1 UN FLOW DISTR. IN

MOD 1 HEATER

SIGN/DATE: EJ/791030 PAGE 5

CALC. OF THE FLOW DISTRIBUTION IN THE HEATER DUE TO THE HOT CONNECTING DUCTS.
 DUCT A = SPACE CYL.-HEATER; DUCT H = SPACE HEATER-REG. FLOW DATA FROM OPT 22-00.
 DUCT GEOMETRY ACCORDING TO DRAWING NO: 1-S-1291

*****USS*****
 MANIFOLD FLOW DIST. PROGRAM
 *****MANIF0*****

***** F L O W D I R E C T I O N : F R O M D U C T A I N T O D U C T B *****

DUMP OF ALL NON-ZERO ELEMENTS FROM 30/0/1 1) TO 00/5/1 400), PAGE 2

304	5.0117E+00	307	5.1997E+00	308	5.1147E+00	309	5.1272E+00	310	5.1396E+00	311	5.1457E+00
312	5.1466E+00	351	1.2270E+00	352	1.0447E+00	353	1.0333E+00	354	1.0213E+00	355	1.0081E+00
356	9.9871E-01	357	9.7609E-01	358	9.5941E-01	359	9.4497E-01	360	9.3675E-01	361	9.2879E-01
362	9.2767E-01										

PLOT OF THE VARIABLES AMOTRA (1) AMOTRB (2)

SCALE: VARIABLE VALUE = 0.1700 -2



ORIGINAL PAGE IS
 OF POOR QUALITY

CALC. NO 6 ON FLOW DISTR. IN

NO 1 HEATER

SIGN/DATE: EJ/791031 PAGE 10

CALC. OF THE FLOW DISTRIBUTION IN THE HEATER DUE TO THE HOT CONNECTING DUCTS.
 DUCT A = SPACE CYL.-HEATER; DUCT M = SPACE HEATER-WFG. FLOW DATA FROM OPT 22-NO.
 DUCT GEOMETRY ACCORDING TO DRAWING NO: 1-17735, 2-17037

*****USS*****
 MANIFOLD FLOW DIST. PROGRAM
 *****ANIF*****

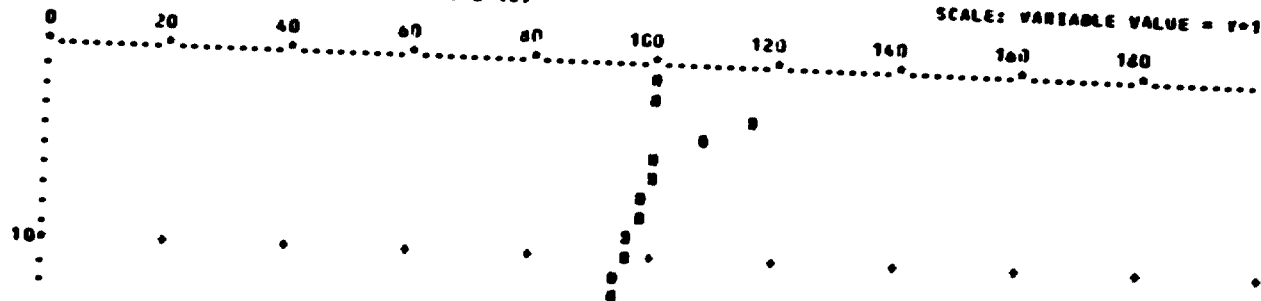
***** F L O W D I R E C T I O N : F R O M D U C T M I N T O D U C T A *****

DUMP OF ALL NON-ZERO ELEMENTS FROM 00/1/1 (1) TO 00/1/1 (400), PAGE 2

304 4.5017E+00	335 5.7021E+00	366 5.0241E+00	397 5.0908E+00	301 5.0982E+00	309 5.1074E+00
310 5.1172E+00	311 5.1254E+00	312 5.1214E+00	351 1.0040E+00	352 9.9417E-01	353 1.1525E+00
354 1.0147E+00	355 9.7353E-01	356 9.9771E-01	357 9.4441E-01	359 9.7066E-01	359 2.6711E-01
360 9.5705E-01	361 9.4844E-01	362 9.4577E-01			

PLOT OF THE VARIABLES AMDTA (X) ANDTAD (Y)

SCALE: VARIABLE VALUE = 1+1000 -2



ORIGINAL PAGE IS
 OF POOR QUALITY

CALC. NO 6 ON FLOW DISTR. IN

NO. 1 HEATER

SIGN/DATE: CJ/793091 PAGE 5

CALC. OF THE FLOW DISTRIBUTION IN THE HEATER DUE TO THE NOT CONNECTING DUCTS.
 DUCT A = SPACE EVL.-HEATER; DUCT B = SPACE HEATER-REF. FLOW DATA FROM OPT 22-00.
 DUCT GEOMETRY ACCORDING TO DRAWING NO: 1-17035, 2-17037

*****USS*****
 MANIFOLD FLOW DIST. PROGRAM
 *****PAUEF*****

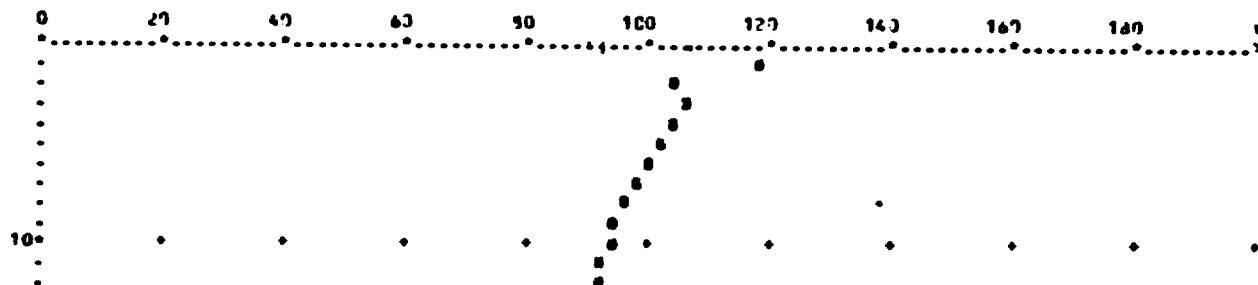
***** F L O W D I R E C T I O N : F R O M D U C T A I N T O D U C T B *****

DUMP OF ALL NON-ZERO ELEMENTS FROM 10/3/(1) TO 20/3/(40), PAGE 2

309	5.1240E+01	310	5.1453E+00	311	5.1553E+00	312	5.1574E+00	351	1.1554E+00	352	1.1319E+00
353	1.0584E+00	354	1.1412E+00	355	1.0174E+00	356	9.9946E-01	357	9.8016E-01	358	9.6364E-01
359	9.4417E-01	360	9.3110E-01	361	9.1747E-01	362	9.1746E-01				

PLOT OF THE VARIABLES AMTRA (1) AMTR2 (2)

SCALE: VARIABLE VALUE = 7.7700 -2



ORIGINAL PAGE IS
 OF POOR QUALITY

5.6 Manufacturing methods

5.6.1 Heater head

The total heater head unit consists of four of a kind of quadrants, consisting of one cylinder and one regenerator joined together by means of a bundle of heater tubes in each quadrant.

The cylinder and regenerator housing and its manifold is precision cast in material Haynes Stellite 31. The heat exchanger unit consists of a total of 96 tubes, 24 in each quadrant of material Multimet (N 155). The tubes are formed in such a way that the front row is made in an involute shape and the second row is bent straight vertical and fitted with fins in stainless material to extend the heat transfer area.

The heater tubes are cut to a length of 282 mm and cold bent in three steps. To achieve dimensions within allowed tolerances for the brazing process the tube ends are cleaned and ground.

The fins for the surface extension area are stamped in a special tool and each fin enclose three heater tubes. The fins are mounted on to the second row of the heater tube which thereafter is nickelplated by means of a chemical process, as a preparation for the brazing joint between the fins and the heater tube.

A recess is arranged for by means of spark erosion in the central tube in the second row for application of a shielding tube in which a thermocouple is to be mounted for the temperature control.

To minimize machining the upper plate of the manifold containing the heater tube passages is precast.

The cylinders are machined internally and at the location at which the cylinder liner is sealed off by means of an O-ring. The only machining made externally is at the sealing face of the flanges and the holes on top of the manifolds into which the heater tubes are mounted.

The regenerator house is machined in the same manner. In one end of the manifold from underneath a hole for the thermocouple shield is drilled. The cylinder and regenerator housing is mounted in a fixture. The heat exchanger tubes are mounted on to the manifold and brazing material type Nicrobraz LM is supplied around the heater tubes.

Tubes to be used as thermocouple shields are mounted on the front end of the second heater tube row and kept in place by means of fine wires.

The brazing sequence occurs in a vacuum oven at a maximum temperature of 1 075°C. (See brazing cycle instructions).

Each heater quadrant is pressure tested with water till a pressure of 30 MPa. Following the pressure test a seal test is made using helium at a pressure of 10 MPa.

Proceeding this a thorough check is performed of all the critical dimensions of the cylinders and regenerator housing.

The heater is then fitted with seal elements to prevent the combustion gas to bypass the heat exchangers.

5.6.1.1 Instructions for brazing of heater with Microbraz LM.

All components shall be dimension checked and assured that all the dimensions are within required tolerances. To achieve an acceptable joint with Microbraz LM the required distance between the mating surfaces shall be between 30 to 80 micro mm.

All components to be joint shall be cleaned in trichloroethane vapor. In case the brazing fixture has not been used in four weeks even those should be cleaned the same way.

Mount the cylinder and regenerator housing on to the brazing fixture as shown on the brazing drawing. Make a check if the green stop off type two on the facing surface against the cylinder and regenerator housing or the bolts are acceptable, if not brush some stop off on the surfaces.

5.6.2 Gas Cooler

The cycle gas cooler is a water cooled fine tube cooler. For the ASH MD 1 design each thermodynamic cycle have 1 cooler unit.

The tube material is stainless steel quality SIS 2337 (AISI 321). The tubes are brazed into holes prepared in top and bottom plate, which in turn is located in the stainless steel SIS 2343 (AISI 316). cooler housing.

The tubes are staggered to optimize the heat transfer on the water side.

The cooler housing main task is to unload the cooler tubes from the force acting on the cooler unit by the pressure difference across the cooler. It furthermore act to distribute the coolant across the tube bundle. The coolant passes the cooler in a type of cross flow. The total amount of coolant flow is 4.6 kg/sec, which is divided in two flow paths each consisting of two cooler units in series. The coolant pressure drop across each cooler is approximately 15kPa at maximum coolant flow rate.

The cooler seals in one end towards the regenerator and in the other against the cold connecting duct. The gas seal consist of O-rings, which are sealing radially in grooves machined in the cooler housing. The water seal is arranged in a similar manner on the cold end side of the cooler housing.

Approximately 20% of the tubing material undergoes a leakage test upon delivery. Thereafter the tubes are cut to length and squashed in one end to ease handling while mounting the tubes while preparing for brazing.

The cooler housings are machined from tube blanks ID/OD = 90/71.

The end plates are manufactured by initial drilling of multiple holes in a stainless steel plate. The plate is then cut and machined to

correct dimensions. All parts are thoroughly degreased and assembled. Cover plates are mounted across the coolant passages. Brazing material is applied and "stop-off" is brushed on to locations onto which brazing material shall not adhere. The brazing is performed one side at the time, and thereafter a gasleakage tested, and then machined to correct dimensions in a lathe, and once more leakage tested.

Onto the cooler housing is then glued two stripess of glykol and water resistant rubber to prevent water by-passing the tube bundle.

5.7

Material selection and rationale

The major components are (see figure 5.7:1):

Heater

Cylinder

Regenerator housing

Tubes

Fins

Sleeves for thermocouples

Regenerator

Cooler

Tubes

Housing

ORIGINAL PAGE IS
OF POOR QUALITY

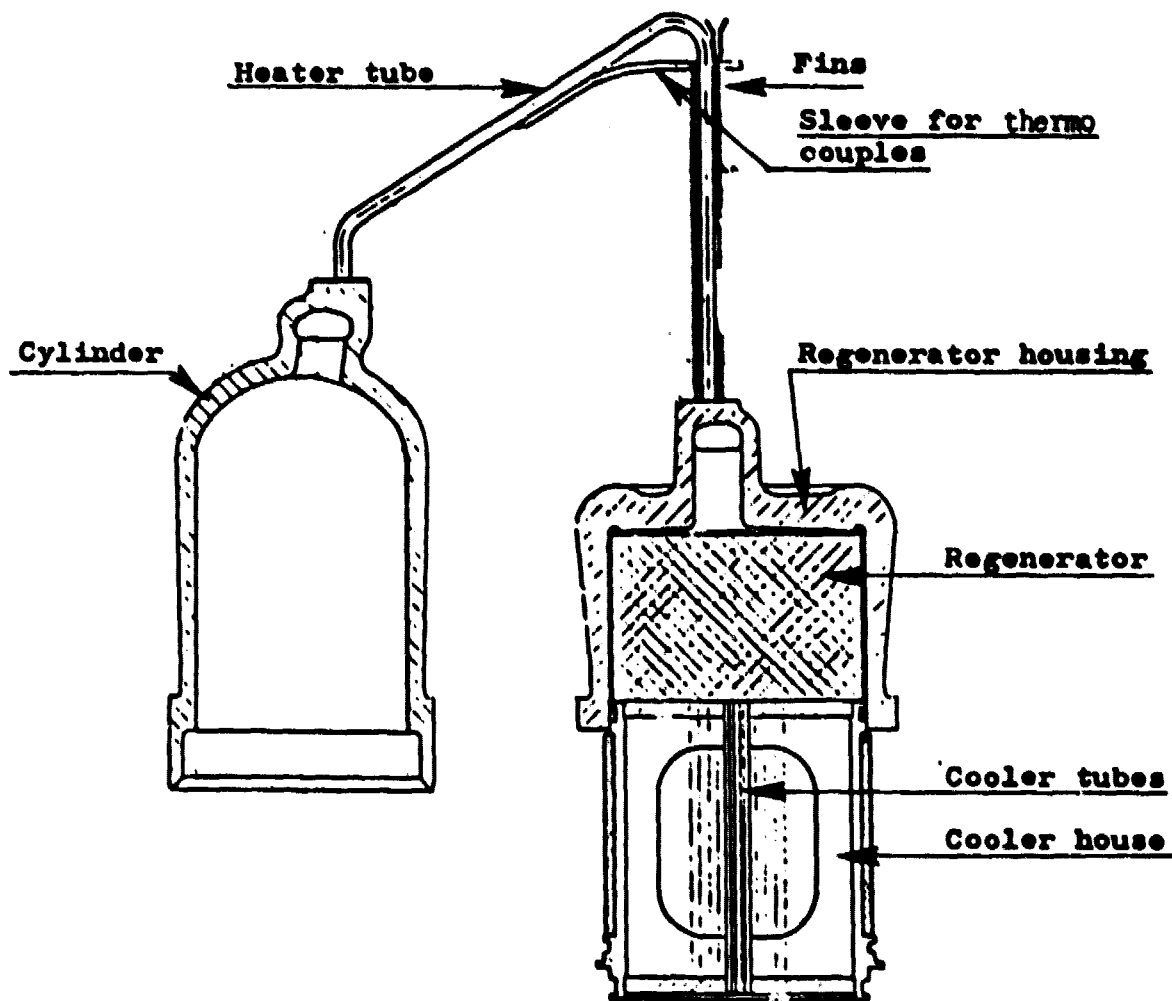


Figure 5.7:1. Cross section of the hot engine system

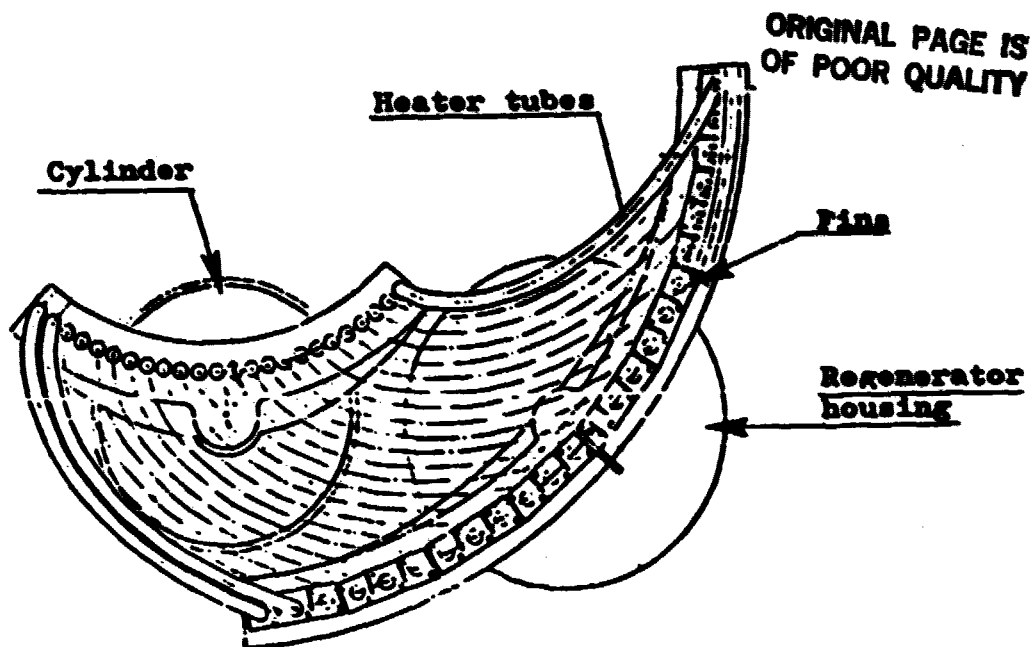


Figure 5.7:2. Top view of the hot engine system

5.7.1 Heater

The heater consists of four heater quadrants which are made up by one cylinder, one regenerator housing, 24 tubes, 3 sleeves for thermocouples and 1 920 fins on the second tube row (see figure 5.7:1 and figure 5.7:2). The heater tubes are exposed to high pressure hydrogen on the inside and combustion gases on the outside. It must also meet stringent requirements regarding low and uniform flow resistance, even temperature distribution, high heat transfer capability and low cost. Since the tubes are brazed to the cylinder and regenerator housing the material should also be easy to braze and it must keep its mechanical properties during the brazing cycle.

The materials chosen has been used in previous engine generations not only by USS but also by Philips and General Motors. They are not the most optimized materials for an automotive application but before considering new materials in the heater an extensive component testing has to be performed.

The cylinder and regenerator housings will be investment cast in Haynes Stellite 31, a Cobalt base alloy with good castability, brazability and high temperature properties (see figure 5.7:3).

The tubes are welded and drawn in Multimet (N155), an iron base alloy with good high temperature properties (see figure 5.7:3), well above the requirements for MOD I. Temperatures less than 800 °C, stresses around 40 N/mm² and a goal for lifetime of 3 500 h. One disadvantage with Multimet is the rather low ductility at 700 to 900 °C (see figure 5.7:4) but if the tubes are not exposed to a rapid overheating, Multimet has shown to be a very good material for the heater tubes.

ORIGINAL PAGE IS
OF POOR QUALITY

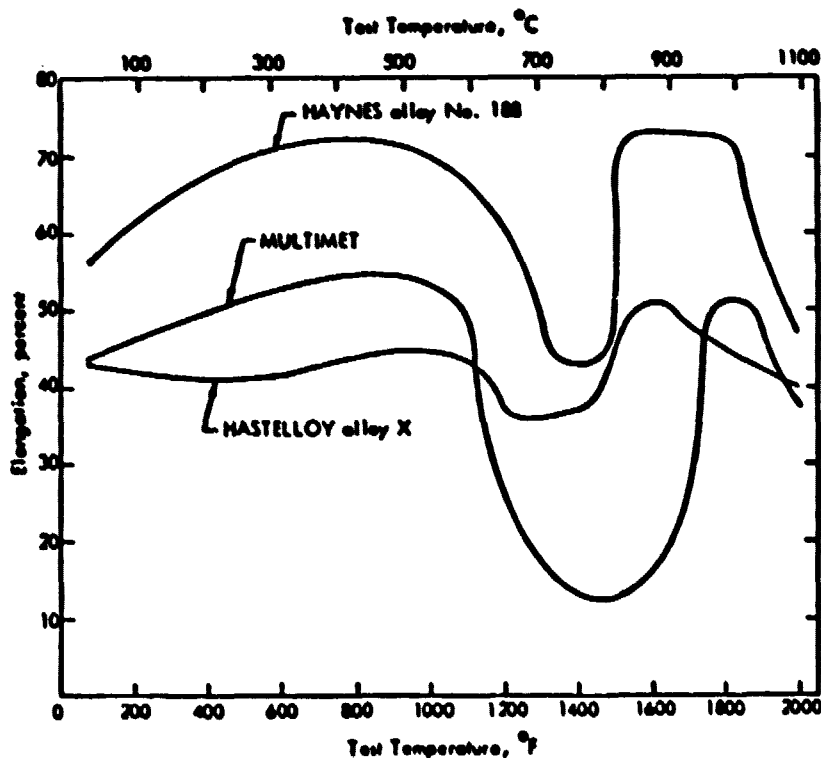


Figure 5.7:4. Comparison of the tensile elongation of Multimet to that of Hastelloy alloy x and Haynes No 188.

STRESS RUPTURE (CATALOG DATA)

ORIGINAL PAGE IS
OF POOR QUALITY

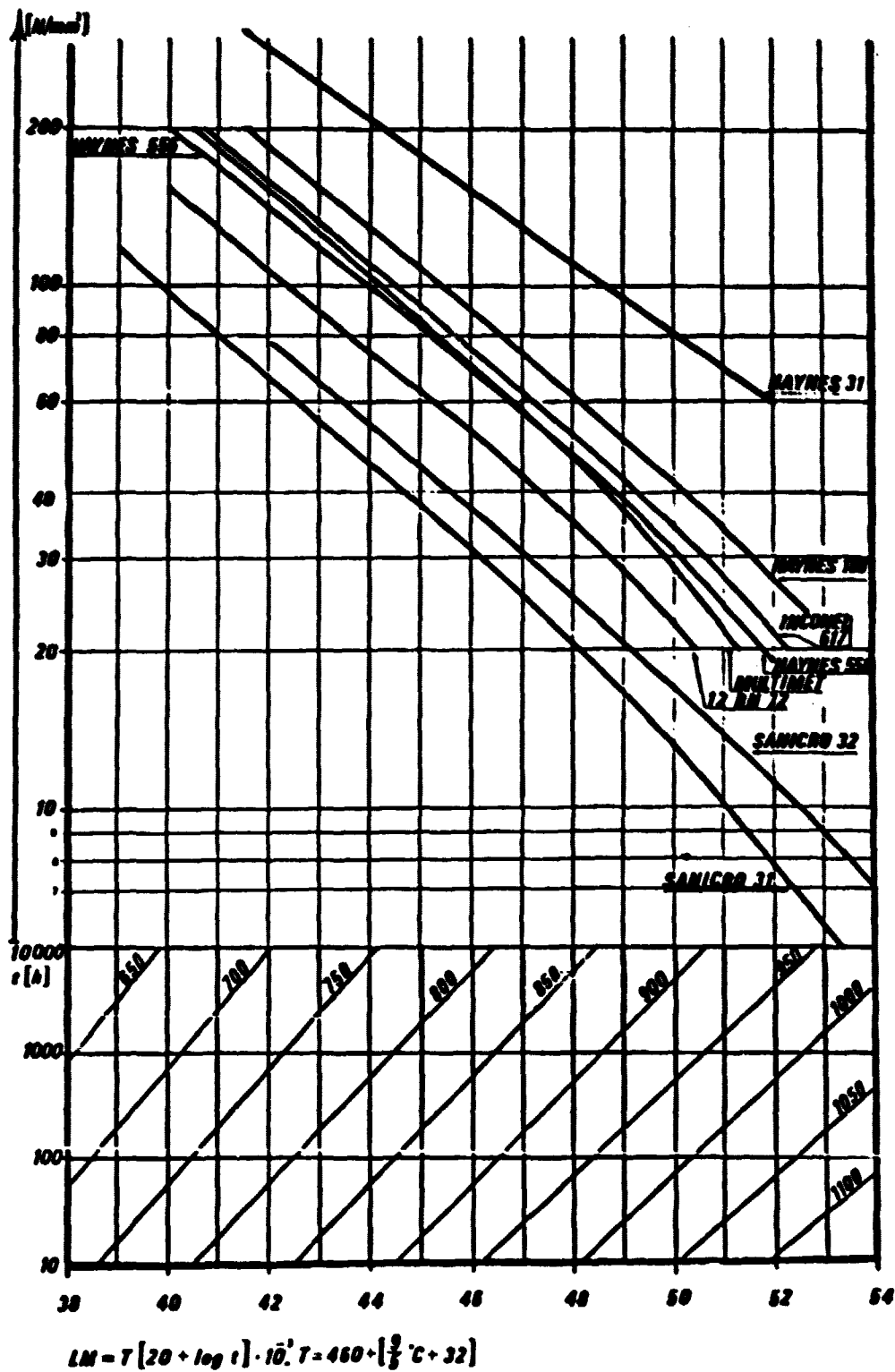


Figure 5.7:3

The fins will be stamped out of 0.6 mm (0.024") thick sheets in AISI 310 S (SS 2361) . After the fins have been stacked on the second tube row, they are plated with electroless nickel which will serve as a filter metal during brazing. The electroless nickel containing about 9 - 12% phosphor which may affect the mechanical properties of the tube material but USS has never had a tube failure on the second tube row where the fins are brazed on.

As material for the sleeves Multimet has been chosen. They are brazed to the heater tube with Microbraz LM as filler metal.

5.7.2 Regenerator

The regenerator is built up of nets. Each net is woven from thick wire. The chosen material is AISI 304 L (SS 2333) an alloy which is easy to draw to this small dimension. AISI 304 L has performed well in our previous engines.

5.7.3 Cooler

The environment for the cooler is high pressure hydrogen on the inside and cooling water on the outside. In operation the hydrogen temperature is approximately 100 °C and the water temperature 50 °C. Antifreezers and/or inhibitors may be added to the water. The stresses under operation are of the order of 80 - 100 N/mm².

For the housing the stainless steel AISI 316 (SS 2343) has been chosen and the tube alloy is the titanium-stabilized AISI 321 (SS 2337) .

The tubes are vacuum brazed to the housing at 1 040 °C using Microbraz 130. The cooling after brazing is accelerated in order to avoid sensitizing. The need to avoid sensitizing is also the main reason to choose a stabilized alloy for the thin-walled tubes.

B.6 Cold Engine System

6. COLD ENGINE SYSTEM

6.1 GENERAL DESCRIPTION

6.1.1 Cylinder Block

In Baseline Engine, the cylinder block - containing the four cylinder barrels and eight cold connecting ducts below gas cooler locations - is a one piece iron casting. It is a complex structure with non-uniform cooling water passages.

In the Mod I design this unit is composed of a cast aluminum water jacket (four instead of eight coolers), four separate nodular cast iron duct plates and separate wet cylinder liners. Piston, piston rod and rod seal systems are to a large extent the same as for Baseline Engine, but improved in various details.

The cylinder and crosshead liners - and thus also the seal cartridge - are spigoted into the duct plates.

All major gas o-ring seals are radially mounted with support rings throughout the design. The use of wet, separate liners and split duct plates provides an improved cooling of the o-ring seals and ease of replacement in case of damage or wear of individual parts.

Better roundness of the liners and less rejection of pressurized coatings is also achieved.

The main bolting connection of the BSE assembly is substantially different from Baseline Engine. The great forces from the enclosed gas pressures are taken up in long waisted studbolts, distributed as symmetrical and as close to the pressure vessels as possible. They are clamping the top flanges, the water jacket, the duct plates and, around the cylinders, also the seal housing flanges. The pressure vessels are loading the flanges when pressurized (via split retainer rings).

6.1.2 Water Jacket

The water jacket contains two mirror-imaged, parallel cooling water circuits and the diagonally placed in- and outlet ports extend from the top face such that air pockets are avoided. Much care has been taken to pro-

vide sufficiently clamped cross-section area around the studbolts penetrating the water jacket without introducing flow restrictions of the water circuits. The water jacket contains holes for the cylinder liners and gas coolers, which are kept in place between the water jacket and the four duct plates. Once these parts are assembled, water and working gas spaces are effectively separated when serviced. The top flange of the water jacket, supported by outside ribs, carries the external heat system.

6.1.3 Cylinder Liners

The wet cylinder liners are spigoted in the duct plates. The seal housing/crosshead liner and the cylinders are in turn spigoted in these liners, resulting in good alignment. Since the liners are not integral with the duct plates they have one o-ring seal on each side of the cold connecting duct. Inside the liner, below the duct entrance, another o-ring seals against the seal housing. The liner finally has a groove and a recess for gas- and water-o-rings respectively in the interface with the cylinder heads. The described gas seal arrangement results in a net force from the cycle gas pressure, that presses the liner downwards. No other locking device is needed and no clamping of the liners causes undesired distortions.

6.1.4 Duct Plates

The duct plates are four separate but identical pieces, which facilitates casting and reduces rejection rates. This also minimizes shear action in the interfaces of adjacent aluminium components due to thermal expansion at operating temperatures. The cylinder studbolts are passing through the duct plates, whereas threads for the regenerator studbolts are contained. The latter bolts may keep the abovementioned cylinder block parts and the gas cycle heat exchangers together to one sub-assembly.

6.1.5

Seal Housings

The four separate seal housings are extended downwards to form cross-head liners. They have large flanges resting on the crankcase top face and are clamped between the cylinder block and the crankcase. There is some free space between these flanges, which allows for adapting the external gas system check-valves and tubes. As a result these need not be disconnected when the upper engine parts are disassembled, for example for servicing piston rod seals etc.

6.1.6

Piston Rod Seal Cartridge

(Experience data are given at the end of section 6.)

The piston rod seal cartridges are contained in the seal housings and covered by a lid centered to the rod. The lid has the cold connecting duct exit to the compressions space profiled into it and also keeps a bushing on top of the cap-seal. Inside the lid and through its bushing there are max.-pressure gas supply passages for the power control. Underneath the cap seal, more than one stroke distance, the springloaded main seal ring is located, centered into a tapered seat. The ring is of the recently developed pumping type. The spring load acts between concentric sleeves, the lower one pressing the seal ring downwards. The seal system interior, sealed against its surroundings, is kept at minimum cycle pressure by means of a check-valve circuit.

For proper cooling of the rod and especially for the seal function, oil is fed to an annular groove in the bottom end of the housing. The oil is delivered from the main lubrication system. A recently suggested alternative is to pump oil through spray nozzles directed to the rod. This is allowed by the present design.

6.1.7

Piston Rod and Crosshead

When installing the seal elements it is important to avoid radial misalignment between rod and seal elements. Assembled the piston rod is guided by the crosshead and the guiding rings glued to the piston. The crosshead is integral with the piston rod. This, due to a shorter gudgeon pin, makes it possible to use a shorter connecting rod than in case of a P40-type separate crosshead.

Another feature, contributing to reduced overall height is the tapered piston bottom into which the seal system lid fits. Piston guidance and clearances are further discussed in Section 3.1.

6.1.8

Pistons and Piston Rings

The piston is attached to the rod by means of pure friction in the coned interface, and secured in place with a locked nut. Special hydraulic tools are used for assembly and disassembly.

All piston rings and guiding rings are located in grooves. These are arranged for the same function as in P40. As pressure difference across the piston reverses during each cycle, the piston rings would move from one side of the grooves to the other, causing uncontrolled leakage and pumping unless minimum cycle pressure is introduced in the space between the rings. Still there is some leakage, increasing this pressure. The increase depends of course on the intermediate space. The piston rings are made to act as check-valves, apart from sealing. As minimum pressure is reached in one cycle the corresponding piston ring opens and the access gas is evacuated from the mentioned space. This space consists of the volume between piston and dome and a minor part of the dome volume. Therefore an o-ring seal is required between the piston and the dome. Reliable function of this seal and of the piston rings calls for a generous dome height to reduce their operating temperature. A high dome also gives acceptable temperatures to the o-ring seal between cylinder liner and cylinder head and to the main bolting connection studs and nuts. The dome height chosen is based on best judgement of all available experiences. The dome is in its bottom part threaded to the piston with a self-locking torque.

6.1.9 The PL-Seal System

The general arrangement of the seal system area was described above. Its build-up is shown in drawing 2-17032.

It is well experienced that the main sealing problem is to prevent oil from entering the working gas cycles. Various combinations of main seal and scraper rings have been tested in the past. In the PL-seal system they are replaced by a single main seal with a tapered extension upwards. See Figure 6.1-1. This part forms an angled gap between the ring and the piston rod. When the rod moves upwards to TDC it unavoidably carries some small amount of oil at its surface roughness. Because of the distance, at least one stroke between the seal ring and the cap seal - this oil does not reach the compression space.

A minor portion of the oil disappears from the rod but the rest follows the rod downwards to BDC and is trapped in the covered gap mentioned above.

The velocity of the piston rod through the seal ring now results in a block-bearing-type oil pressure buildup that pumps oil, fed into the gap, downwards back into the crankcase atmosphere. The result is that "leaking oil" is returned out from the seal system area.

The oil that disappears from the rod to the space in the seal system (below the cap seal) is trapped in the external gas line. The cap seal, acting as an efficient flow restriction, maintains mean pressure in the seal system. The gas line connects the seal system to the compression

space via an oil filter and a check valve. At lower cycle pressures gas flows from the seal system into the compression space leaving any oil content in the filter. The same kind of flow and filtering takes place when gas is pumped from the working cycles for power reduction. These gas flows are, of course, balanced by leakage through the cap-seal, resulting in at least minimum pressure in the seal system.

For proper seal function certain critical dimensions must be kept within close tolerances. To reduce the amount of oil carried along by the rod its sliding part should have minimal surface roughness. Therefore, the rod manufacture includes polishing and super finish. Also very good diameter tolerance, roundness and straightness is required. All these requirements are specified on the piston rod drawing. The manufacturing sequence, listed in Section 6.5, is also specified on the drawing. This includes heat treatment and nitride hardening for high surface hardness to avoid wear or damages, which also would affect sealing negatively.

If the seal element this way slides over a relatively flat rod surface topography, its function may be quite efficient. But for reliable and sufficient function, it is also more essential to achieve a good alignment and concentricity between sliding and guiding parts. Lateral movement of the rod relative to the seal element must be minimized. This is more discussed in section 4.2 of the RESD report (annular regenerator concept). A thorough tolerance study is being

performed as part of the detail design in progress. The principle is to pilot both piston and crosshead guides in one common part, the duct plate, as to specify minimum eccentricity between piston and rod, crosshead and rod. Furthermore, best possible parallelity between horizontal mating surfaces and perpendicularity with diameters must be required.

Another important thing is the proper location of the PL-seal ring can plastically deform into position, this ability should only be accounted for to compensate for successive wear. But it also means that the as-manufactured dimensions of the PL-seal is not that critical since it will adjust to the adjacent parts. An initial adjustment is included in the manufacturing using a coned tool to form its upper tapered part. Further description of the manufacturing of seal system parts is given in section 6.5.

The design of a PL-seal system for Mod I is, of course, due to the encouraging results from running engines with such systems. It seems, from any standpoint, adaptable to the different component arrangement of Mod I and P-40 should give good projections for this engine.

Original P-40 seal systems with scraper rings and oil separator valves showed poor reliability and reproducibility with unacceptable oil leakage into the working cycles after 50-500 hours operation. Best results were rarely above 1000 hours.

To date, P-40 engines equipped with PL-seals have accumulated an order of magnitude longer operation without leakage problems. Best result in one engine is about 4000 hours. The high temperature test engine has accumulated 1500 hours, partly under cyclically power-controlled operating conditions.

Mod I-scaled seal elements have successfully been tested in the P-75 engine and rigs.

The piston rod seal system is United Stirlings new pumping Leningrader (PL) seal which works as follows:

It is well experienced that the main sealing problem is to prevent oil from entering the working gas cycles. Various combinations of main seal and scraper rings have been tested in the past. In the PL-seal system they are replaced by a single main seal with a tapered extension upwards. This part forms an angled gap between the ring and the piston rod. When the rod moves upwards to TDC it unavoidably carries some small amount of oil in its surface roughness. Because of the distance, at least one stroke between the seal ring and the kapseal, this oil does not reach the compression space.

A minor portion of the oil disappears from the rod but the rest follows the rod downwards to BDC and is trapped in the gap mentioned above.

The velocity of the piston rod through the seal ring now results in a block-bearing-type oil pressure buildup that pumps oil, fed into the gap, downwards back into the crankcase atmosphere. The result is that "leaking oil" is returned out from the seal system area.

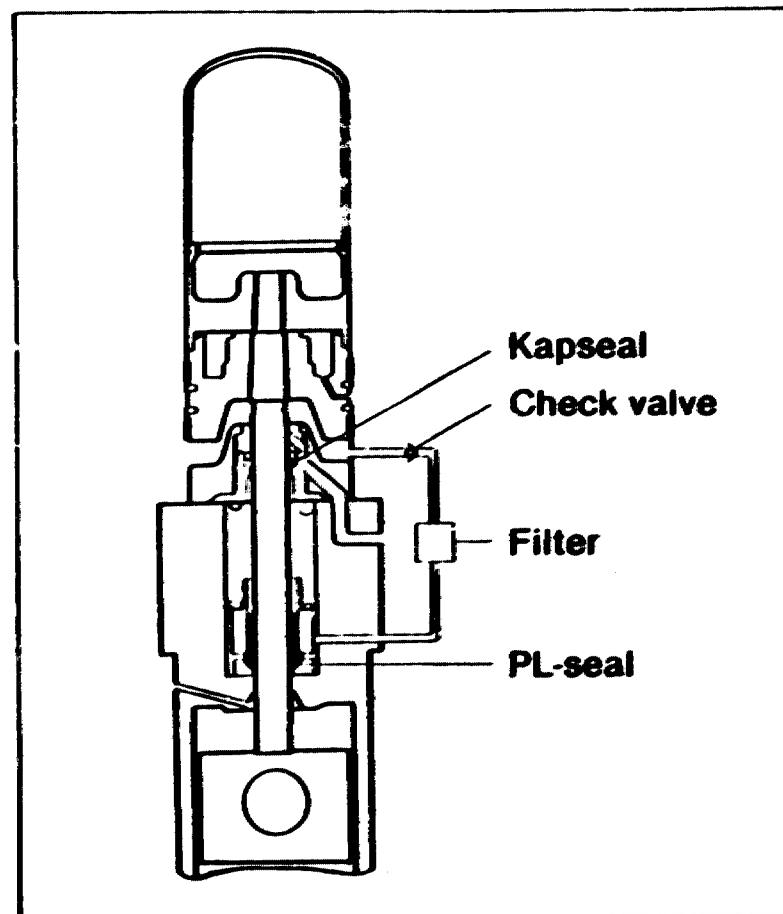


Figure 6.1-1

6.2

Drawings

ASE MOD I, Cold Engine System

- Sub-system Layouts

- Part of BSE Layout
- " " " " (retainer arrangement)
- 2-17032 Piston, Seal, Piston rod, Layout.
- 1-S-1336 Water Jacket, Welded Steel Alt. Prel. Scheme
- 1-17044 Basic Check-valve and Piping Arr. Prel. Layout

- System Details (to be finalized with manufacturer)

- 1-17045 Water Jacket (2 sheets)
- 1-17025 Duct Plate
- 3-17031 Piston rod, Forged Blank

- Supporting Test Object Assemblies

- 2-73544 Main Bolting Test Assembly
- 2-S-1174 Retainer Ring Test Assembly

6.3 Stress calculations of water jacket, cold connecting duct plate, dome, piston, bolts in warm/cold parts

6.3.1 Cold connecting duct plate

6.3.1.1 General

The duct plate contains the cold connecting duct at the compression side of the cycle. It is partly clamped between the water jacket and the crankcase and partly bolted to the regenerator housing. The load consists of the cycle pressure which is 15 ± 5 MPa at full load.

6.3.1.2 Material

The duct plate is cast. The material is SS 0737 corresponding to AISI 100-70-03. The following data are valid:

Yield stress (0.2%) $\sigma_y = 450$ MPa

Ultimate tensile strength $\sigma_u = 700$ MPa

Fatigue limit $\sigma_f = 240$ MPa

Young's modulus $E = 165\ 000$ MPa

6.3.1.3 Design criteria

The duct plate shall be a stiff construction between the crankcase and the water jacket. As a cast component it shall resist yielding with a safety factor of 2. Thus the largest effective stress (v. Mises) shall be lower than 225 MPa. Due to the rough surfaces the fatigue resistance will be mainly based on fatigue tests.

6.3.1.4 Analysis

The tools of the stress analysis have been finite element computations, deflection and strain gauge measurements as well as fatigue testing.

The finite element computations are based on a sketch of the duct plate from an early stage of the design, see fig. 6.3:1. The duct plate is a complicated three dimensional shell structure. The plate is divided into 137 isoparametric thick shell element with 8 nodes in each element. The total finite element mesh is shown from two view points in fig. 6.3:2. It has 437 nodes with totally 2622 degrees of freedom. In the FEM-computation the plate is clamped at the positions of the cylinder and regenerator bolts.

During the progress of the finite element work, the distances between the bolts of the heater head were changed. Besides two different duct plates were designed and manufactured, see Figures 6.3:3 and 6.3:4. Both of these plates have the same height (35 mm) as the analyzed plate in Figure 6.3:1. The plate in Figure 6.3:3 showed only slightly diverges from the first one. The webs on the bottom side have the same thicknesses, 8 mm and 6 mm. On the other hand, the plate in Figure 6.3:4 have quite different shapes of the webs. Besides all of the webs have the same thickness equal to 8 mm and the outer-most trapezoidal webs are larger. For simplicity, the duct plates are called No. 1 (Figure 6.3:1), No. 2 (Figure 6.3:3) and No. 3 (Figure 6.3:4) in the following text.

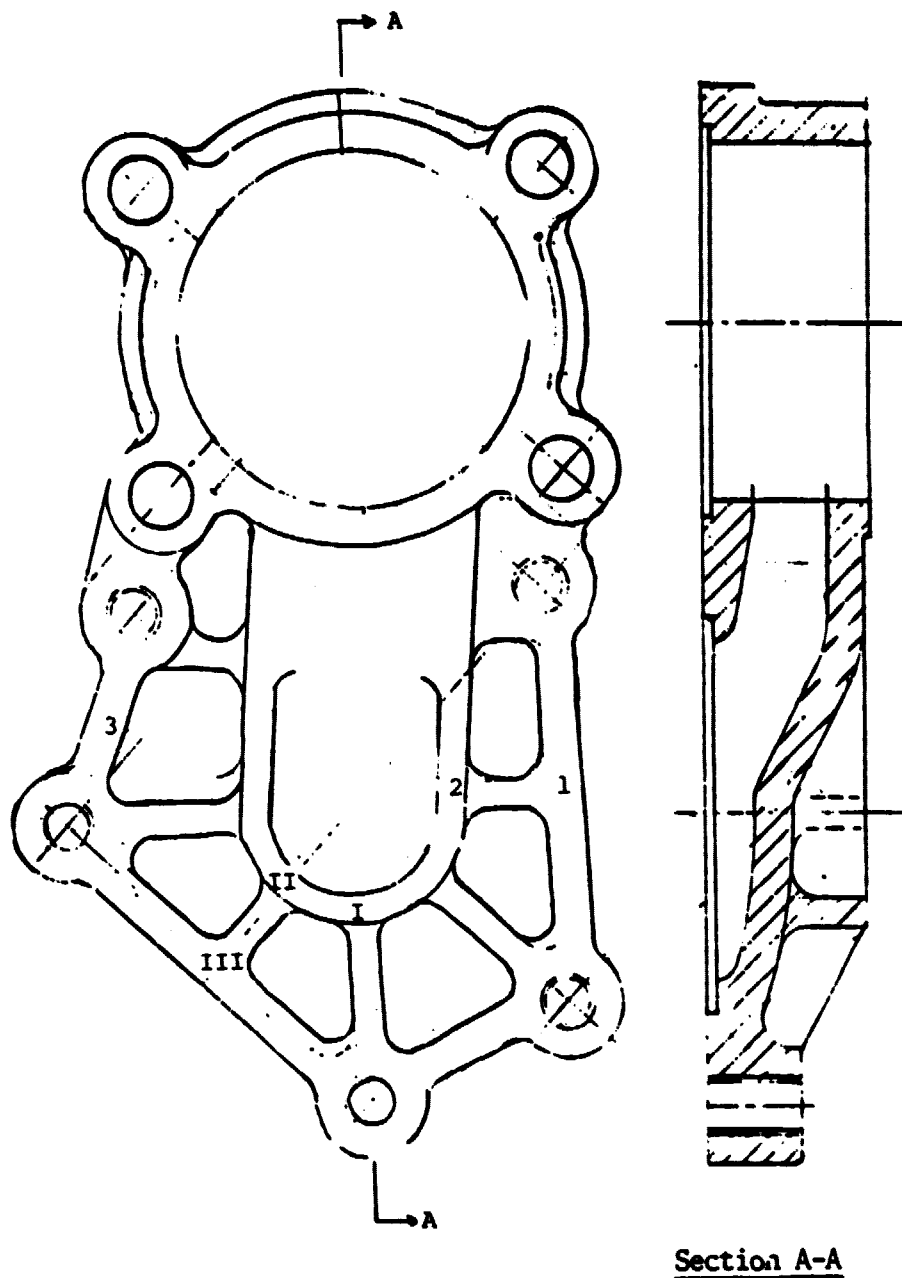
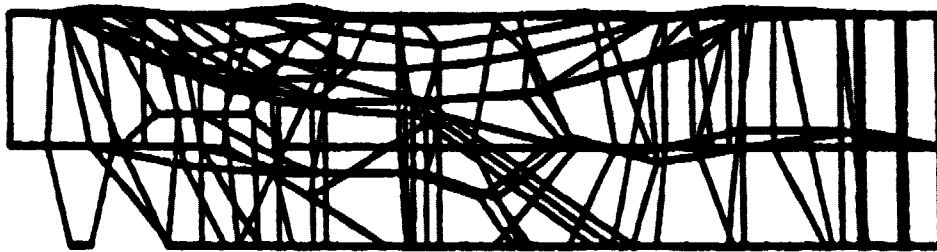


Fig. 6.3:1 Duct Plate Analyzed With the Finite Element Method.
(Plate No. 1). The Figures Refer to Measuring Points
of the Other Duct Plates



ORIGINAL PAGE IS
OF POOR QUALITY

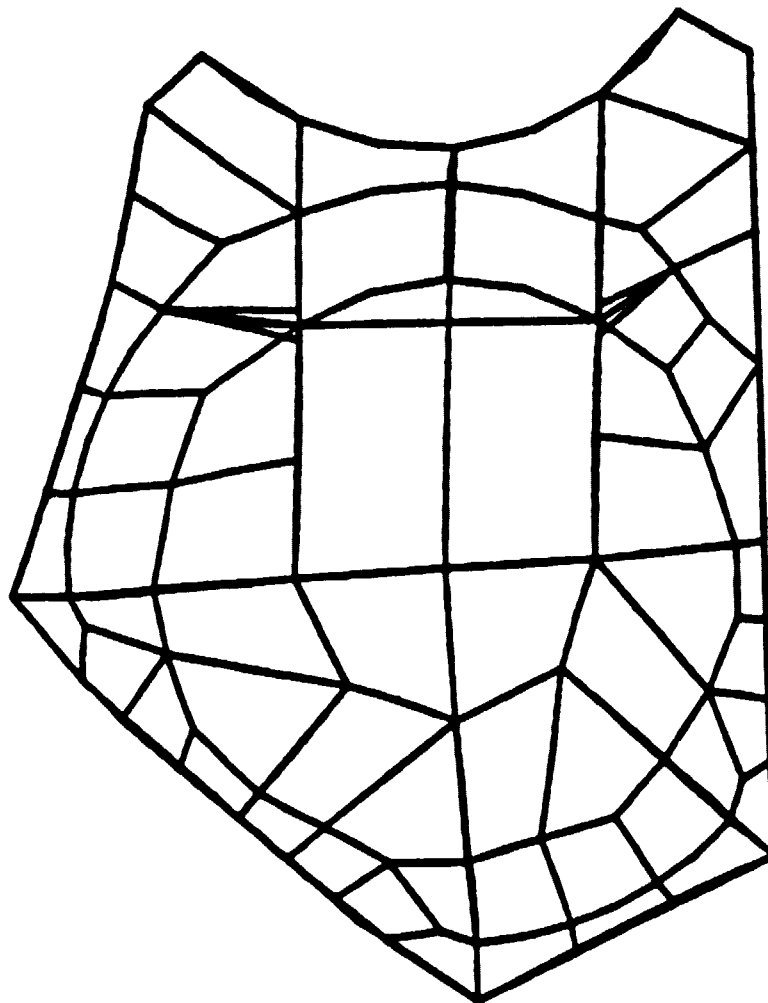


Fig. 6.3:2 The Finite Element Mesh of the Duct Plate Seen
From Two Different View Points

ORIGINAL PAGE IS
OF POOR QUALITY

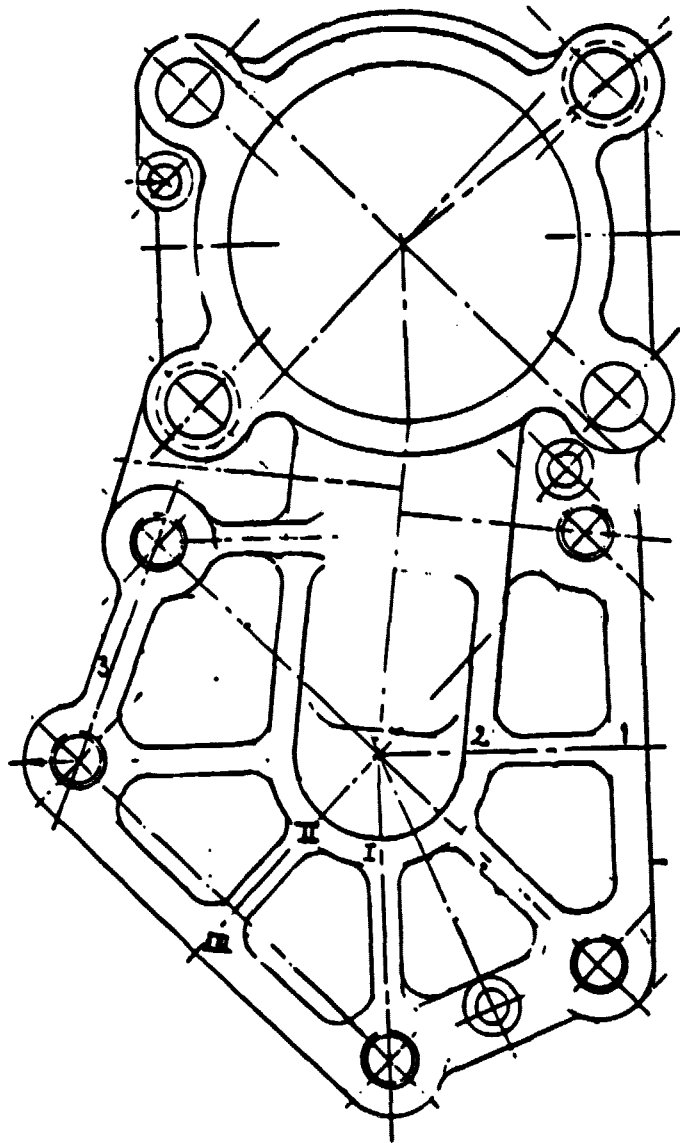


Fig. 6.3:3 Duct Plate No. 2. The Numbers
Refer to Measuring Points

ORIGINAL PAGE IS
OF POOR QUALITY

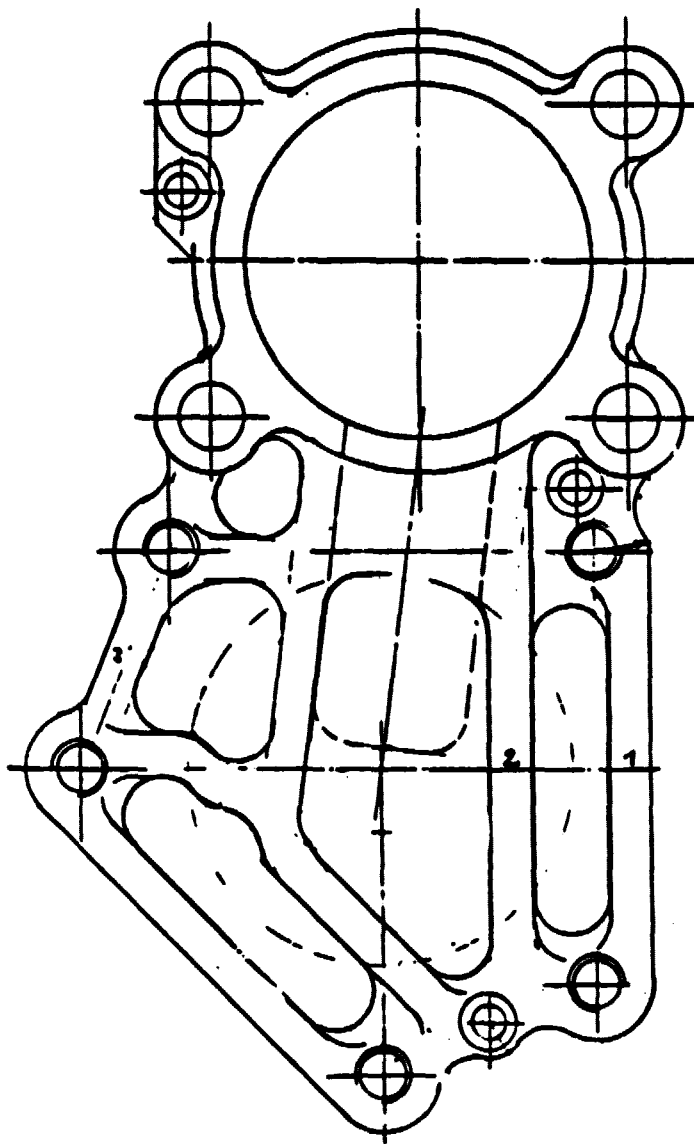


Fig. 6.3:4 Duct Plate No. 3. The Numbers
Refer to Measuring Points

ORIGINAL PAGE IS
OF POOR QUALITY

Deflection measurements have been performed for the plates No. 2 and No. 3. In the table below the measured values are shown together with the computed ones for plate No. 1. The measuring points (1, 2, 3) are shown in the figures 6.3:1, 3 and 4. All values correspond to a pressure of 20 MPa on the duct plate.

Deflection in μm .

Plate Point	No. 1 Computed	No. 2 Measured	No. 3 Measured
1	37	23	14
2	80	69	40
3	5	8	1

When comparing the computed result (plate No. 1) with the measured result (plate No. 2) it should be noted that point 1 lies 20% more apart from the centre in plate 2.

The measurements show that plate No. 3 is about 65% stiffer than plate No. 2. The increased stiffness is mainly achieved by the enlarged webs.

Strain gauge measurements have been performed for the plate No. 2. The strain gauges were placed on the top of the webs and the stresses were computed from the strains under the assumption of an uniaxial stress state at these positions. In the table below the measured values are shown together with the computed ones for plate No. 1. The measuring points (I, II, III) are shown in the figures 6.3:1 and 6.3:3. All values correspond to a pressure of 20 MPa.

ORIGINAL PAGE IS
OF POOR QUALITY

Stresses in the tangential direction of the webs in MPa.

Plate Point	No. 1 computed	No. 2 measured
I	135	116
II	145	124
III	52	68

According to the differences of the plates the computed and measured result are in good agreement.

The computations show that the largest effective stress (v. Mises) in plate No. 1 is 263 MPa. This stress is mainly a bending stress which is obtained at the elbow of the cold connecting duct. This stress exceeds the largest allowed stress of 225 MPa.

Plate No. 3 has been tested due to fatigue. The plate was bolted to the water jacket and dummy housings simulating the heater head and the crank-case. The pressure was 5% higher than the maximum pressure of the engine, i.e. 15.75 ± 5.25 MPa. The test went on 10 million cycles without failure. The test is described in the document from the Swedish National Testing Institute.

Further design work has led to a duct plate according to Figure 6.3:5. This plate has almost the same shape of the webs as plate No. 2. On the other hand, all of the webs have the thickness of 8 mm as plate No. 3. Besides the new duct plate has a height equal to 42 mm instead of 35 mm. Thus, the outer webs have increased in height from 35 mm to 42 mm. At the same time the central webs have increased in height from 17 mm to 19 mm. The thickness of the elbow of the cold connecting duct is changed from 8 mm to 10 mm. Consequently, the new duct plate will be

ORIGINAL PAGE IS
OF POOR QUALITY

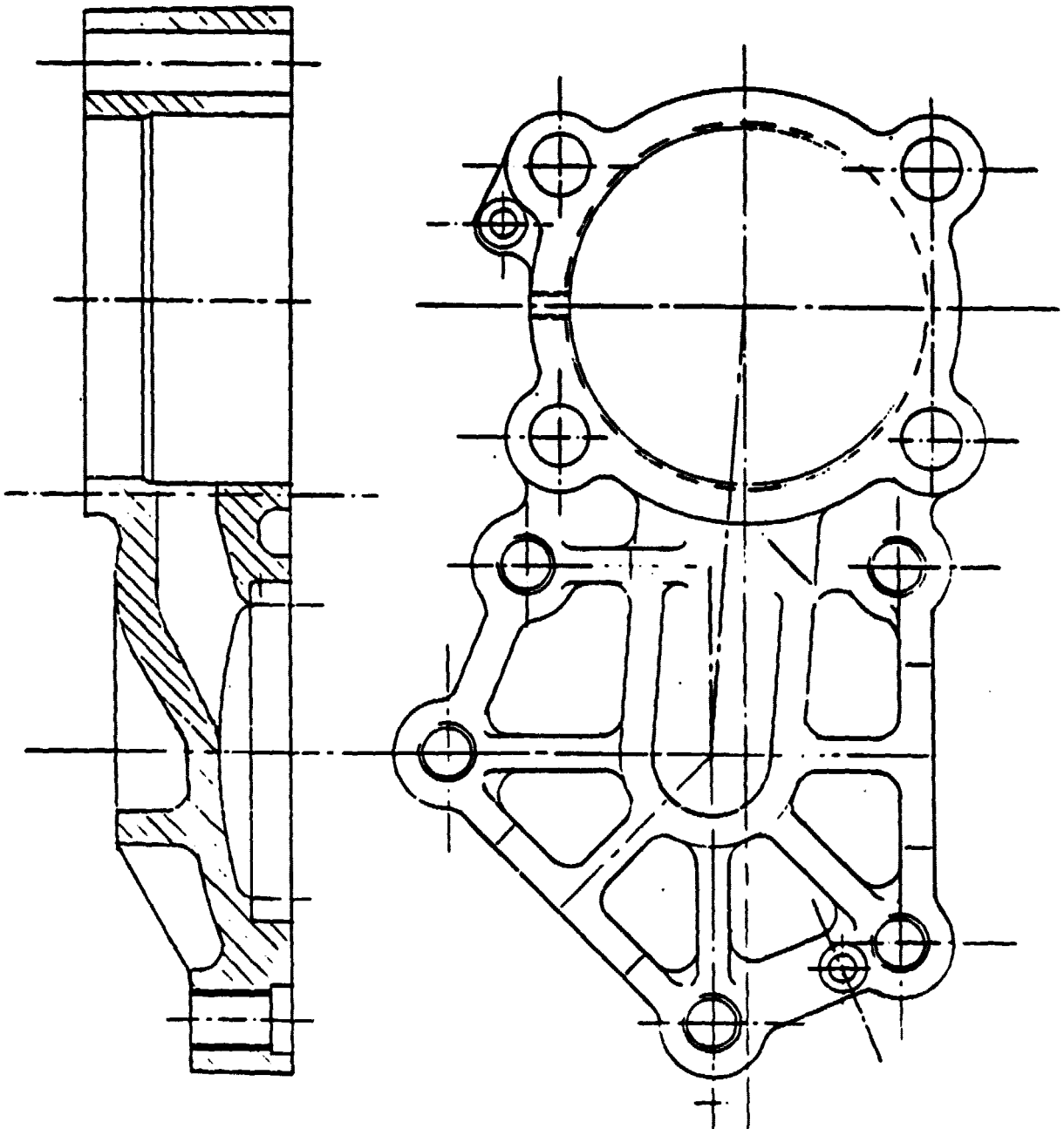


Fig. 6.3:5. Final design of the duct plate.
I-446

considerably stronger than plate No. 1. An extrapolation of the finite element computations indicates that the largest effective stress will be lower than 200 MPa, thus fulfilling the requirements against yielding.

After the manufacturing of the duct plate, the water jacket and the bolts of the heater head, a new fatigue test will be performed.

6.3.2 Piston Rod

6.3.2.1 General

Figure 6.3:6 shows the piston rod, which will be exposed to alternating loads and therefore must be analysed from the fatigue point of view.

6.3.2.2 Material

The piston rod is made of steel (SIS 2940-03) and the following material data have been used in the stress analysis.

Yield stress (0.2%): $\sigma_y = 600 \text{ MPa}$

Ultimate tensile strength $\sigma_u = 850 \text{ MPa}$

Fatigue limit (nitrified):

$\sigma_f = 590 \text{ MPa}$ (bending)

$\sigma_f = 500 \text{ MPa}$ (in tension and compression)

Young's Modulus $E = 2 \cdot 10^5 \text{ MPa}$

6.3.2.3 Design criteria

The piston rod must have a safety factor of 1.5 against yielding and 2.0 against fatigue failure. In addition the piston rod will be fatigue tested.

I-449

6.3.2.4 Analysis

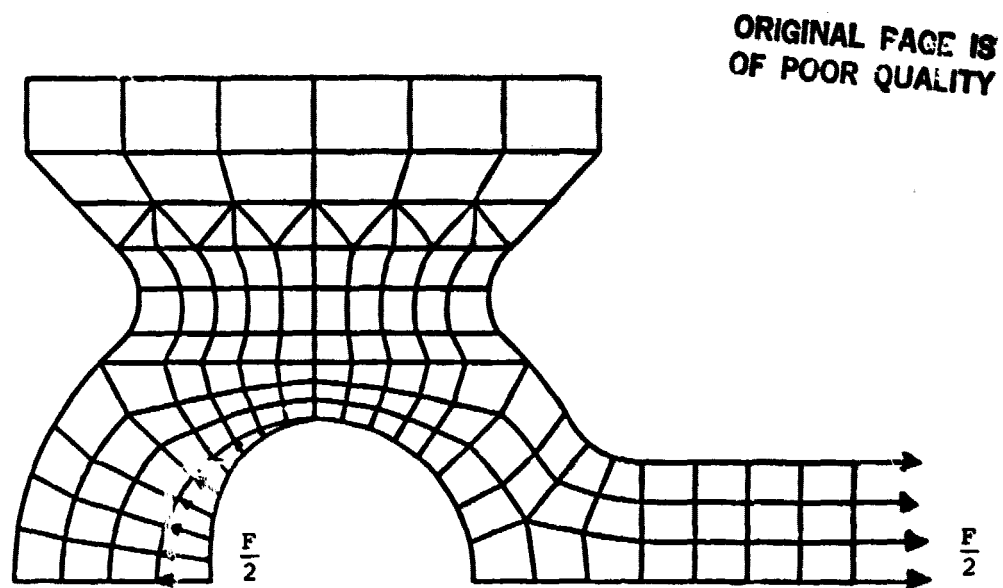
A two dimensional finite element analysis has been performed to calculate the stress state of the piston rod eye. Eight and six node isoparametric plane membrane elements have been used.

Figure 6.3:7 shows the subdivision of the model into finite elements and the applied load. The load alternates between +15300 N and -22950 N, and the load used in the analysis corresponds to an axial force of +15300 N. Figure 6.3:7 shows also the effective stress in some points on the piston rod eye. Figure 6.3:8 shows the principal stress variation in the piston rod eye. Four points of the piston rod have been selected as the most critical in terms of fatigue life, and the points are shown in figure 6.3:9.

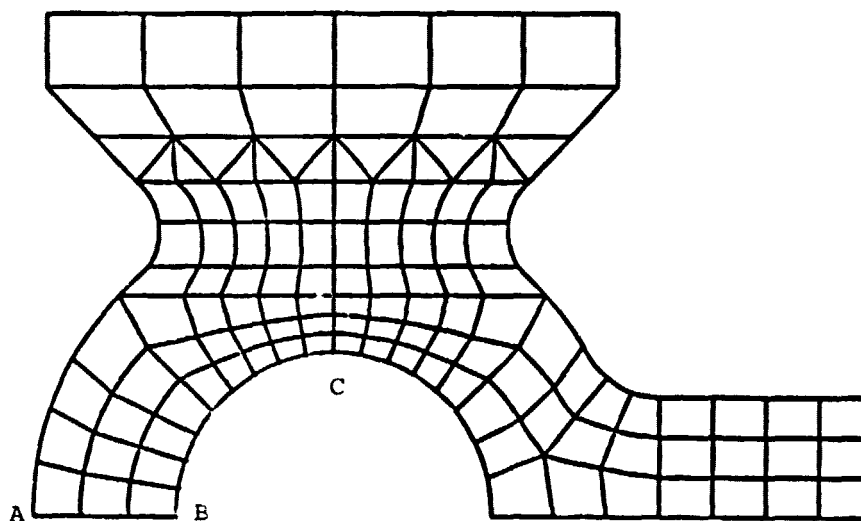
Point 1: Due to manufacturing reasons a hole is drilled at the top of the piston rod eye. This hole has not been considered in the two dimensional finite element analysis, and therefore the stress concentration factor in this point has been separately estimated to 2.02. Using a notch sensitivity factor of 0.85 gives a fatigue notch factor of 1.87. Technological volume dependence have been considered with a factor of 0.9, and the surface influence with a factor of 0.89. Based on these factors a resulting Smith diagram for point 1 is presented in fig.6.3:9. The stress cycle in the point ($\sigma = 71 \text{ MPa} \pm 71 \text{ MPa}$) have been entered in the diagram and the safety factor (f_s) can be estimated to 2.0.

Point 2: In this point the technological volume dependence is considered with the factor 0.9 and the geometrical volume dependence with a factor 0.98. Surface influence is estimated to 0.89. The resulting Smith diagram for point 2 is shown in figure 6.3:9. The stress cycle in the point ($\sigma = 86 \text{ MPa} \pm 86 \text{ MPa}$) can be seen in the diagram and the safety factor is estimated to 3.0.

Point 3: The stress concentration factor in the point has been estimated to 1.45, and with a notch sensitivity factor of 0.9 the fatigue notch factor will be 1.41. Technological volume dependence have been considered with a factor of 0.9, and based on these factors a resulting Smith diagram for point 3 is shown in Figure 6.3:9. The axial force alternates



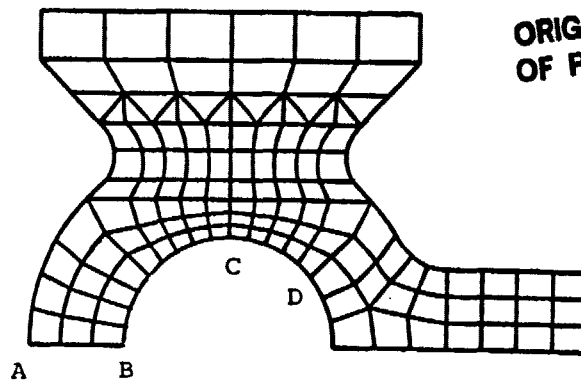
Half model of piston rod eye



Effective stress in point A:	100 MPa
" " " "	B: 83 MPa
" " " "	C: 172 MPa

Figure 6.3:7

ORIGINAL PAGE IS
OF POOR QUALITY



Principal stress variation
across wall thickness
(A \rightarrow B)

Principal stress variation
along inner surface
(B \rightarrow C \rightarrow D)

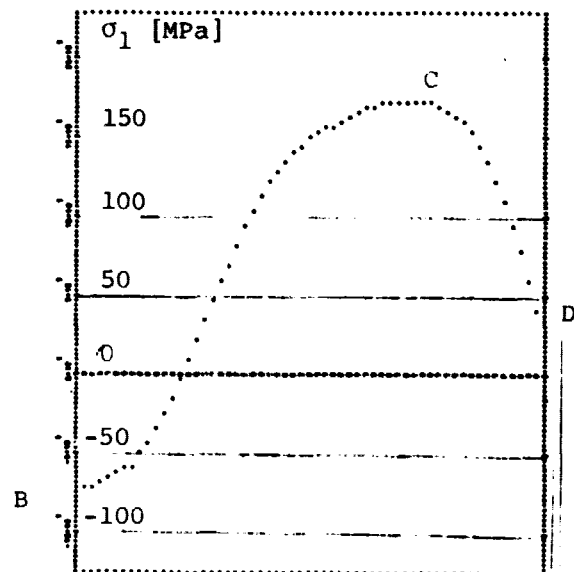
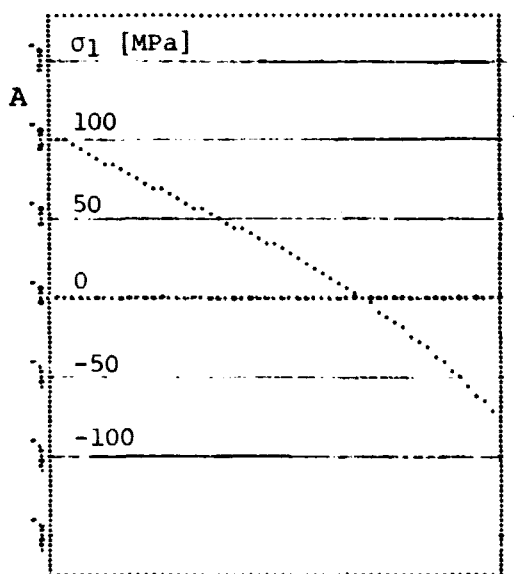
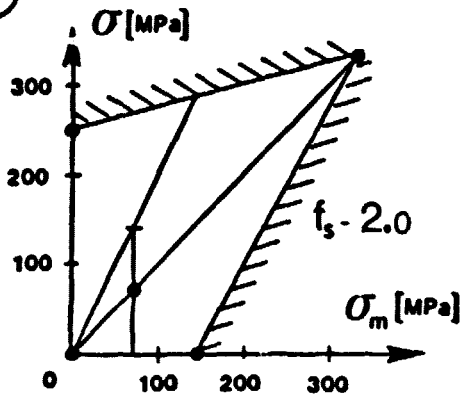


Fig. 6.3:8. Principal stress variation in piston rod eye.

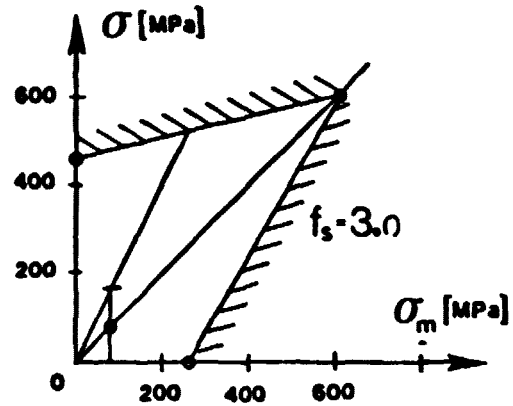
ORIGINAL PAGE IS
OF POOR QUALITY



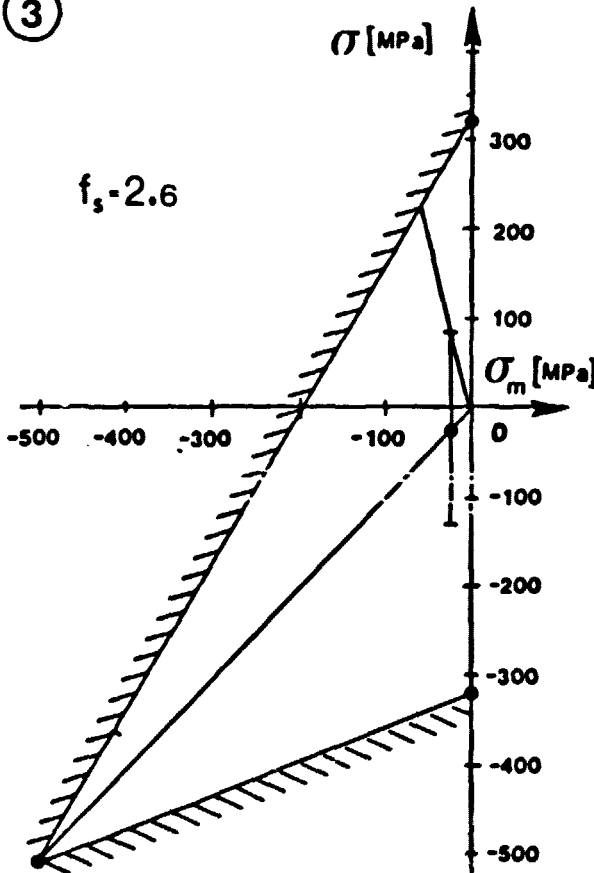
①



②



③



④

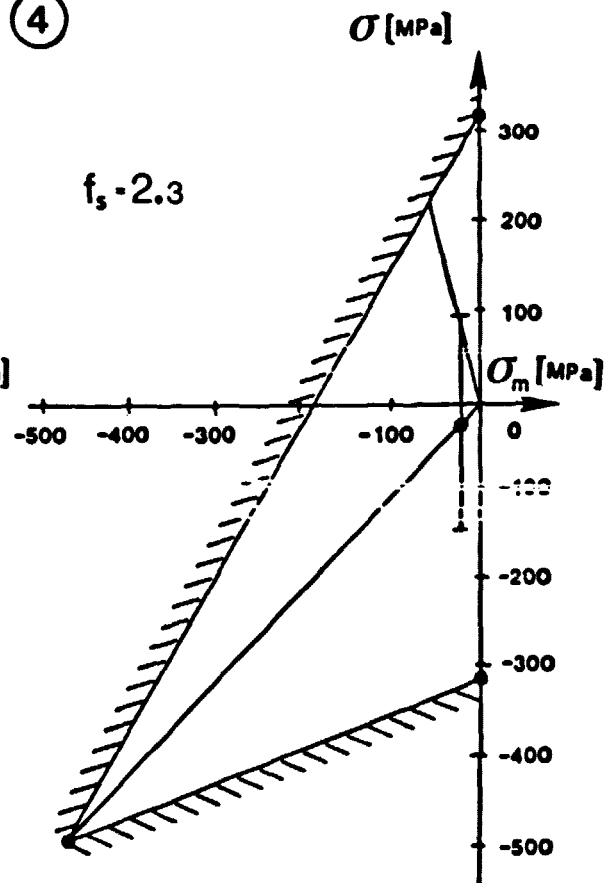


Figure 6.3:9. Smith diagram point 1 - 4.

between +15300 N and -22950 N giving the stress cycle $\sigma = -22 \text{ MPa} \pm 108 \text{ MPa}$, which can be seen in the diagram. In this case the safety factor is estimated to 2.6.

Point 4: The stress concentration factor at the max. supply opening has been estimated to 1.48. Using a notch sensitivity factor of 0.91 gives a fatigue notch factor of 1.44. Surface influence has been considered with a factor 0.89, and the resulting Smith diagram is shown in fig. 6.3:9. The alternating load is the same as in point 3, and the corresponding stress cycle is $\sigma = -24 \text{ MPa} \pm 121 \text{ MPa}$, which has been entered in the daiagram. The safety factor in this case is 2.3.

6.3.3 Piston body

6.3.3.1 General

The piston body is attached to the piston rod in the following way. An axial tapered hole in the body accommodates a mating tapered section of the piston rod. The dome base is threaded on the piston body, which also carries the piston rings. The piston body will be exposed to cyclic pressure loads. Figure 6.3:10 shows the piston body.

6.3.3.2 Material

The piston body is machined from SIS 2541-03, type AISI 4337 alloy steel bar and the following material data properties have been used in the stress analysis.

Yield stress (0.2%) $\sigma_y = 700$ MPa.

Ultimate tensile strength $\sigma_u = 900$ MPa.

Fatigue limit $\sigma_f = \pm 470$ MPa.

6.3.3.3 Design criteria

The piston body must have a safety factor of 1.5 against yielding and must also resist fatigue.

6.3.3.4 Analysis

The piston body has been analyzed using the finite element method.

The axisymmetric model consisting of 8-nodes and 6-nodes isoparametric elements is shown in figure 6.3:11, which also contains the main geometry used in the analysis. The load cases, which have been analyzed are defined in figure 6.3:12.

The effective stress along the upper and lower surface in load cases 1 to 3 is shown in figures 6.3:13 to 6.3:15.

In load case 1 the maximal effective stress at the upper surface occurs in point A. The stress is 222 MPa, which compared to the yieldstress of the material gives a safety factor of 3.2. The maximal effective stress at the lower surface is 252 MPa, which gives a safety factor of 2.8 against

ORIGINAL PAGE IS
OF POOR QUALITY

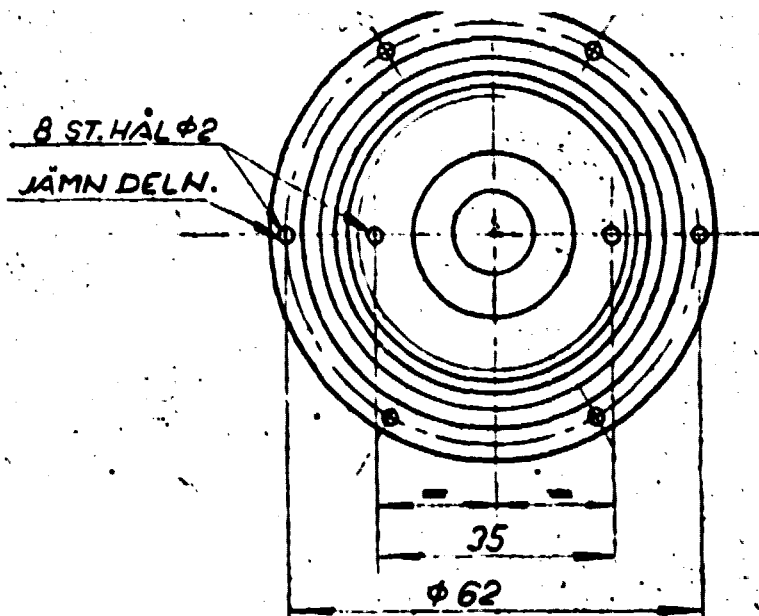
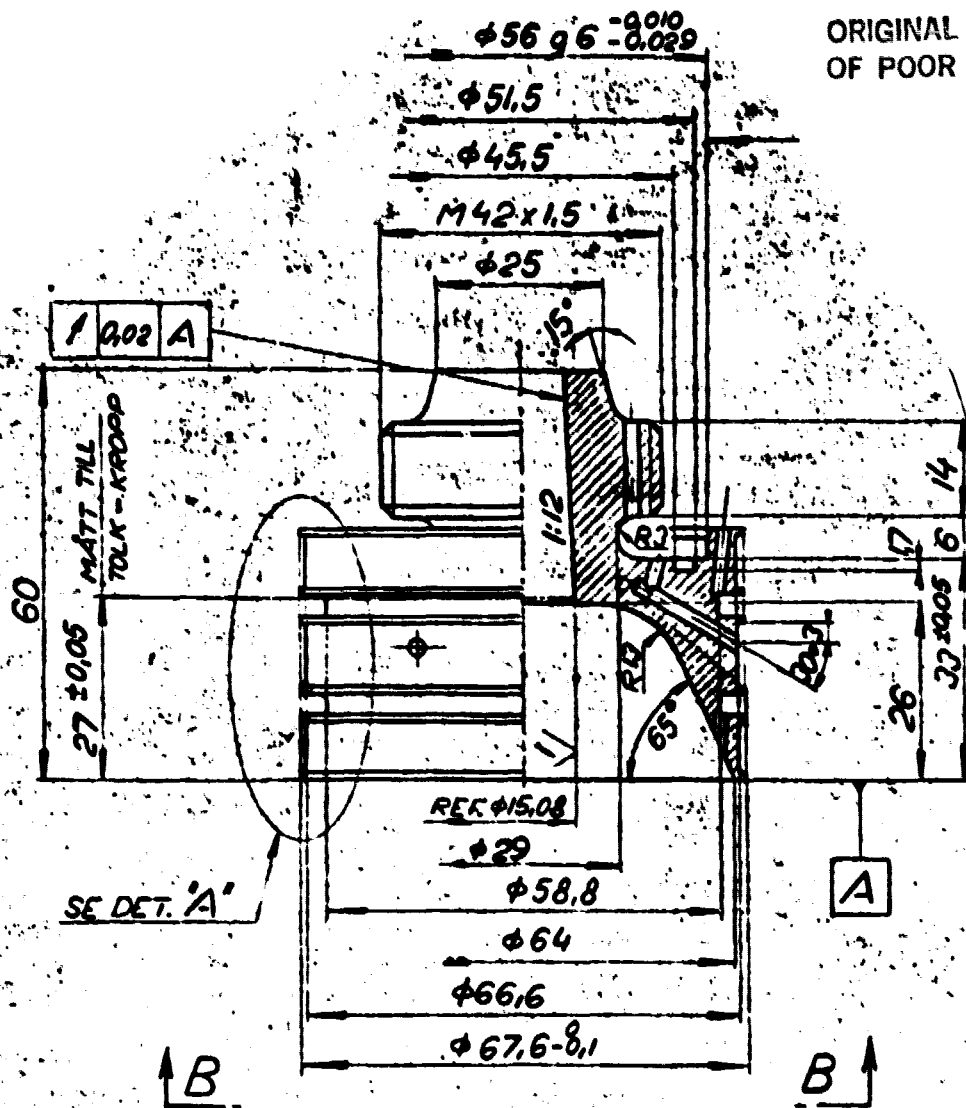


Figure 6.3:10. Piston body.

yielding. In load case 2 the corresponding values are 103 MPa at the upper surface and 313 MPa at the lower surface, which gives a safety factor of 2.2 against yielding.

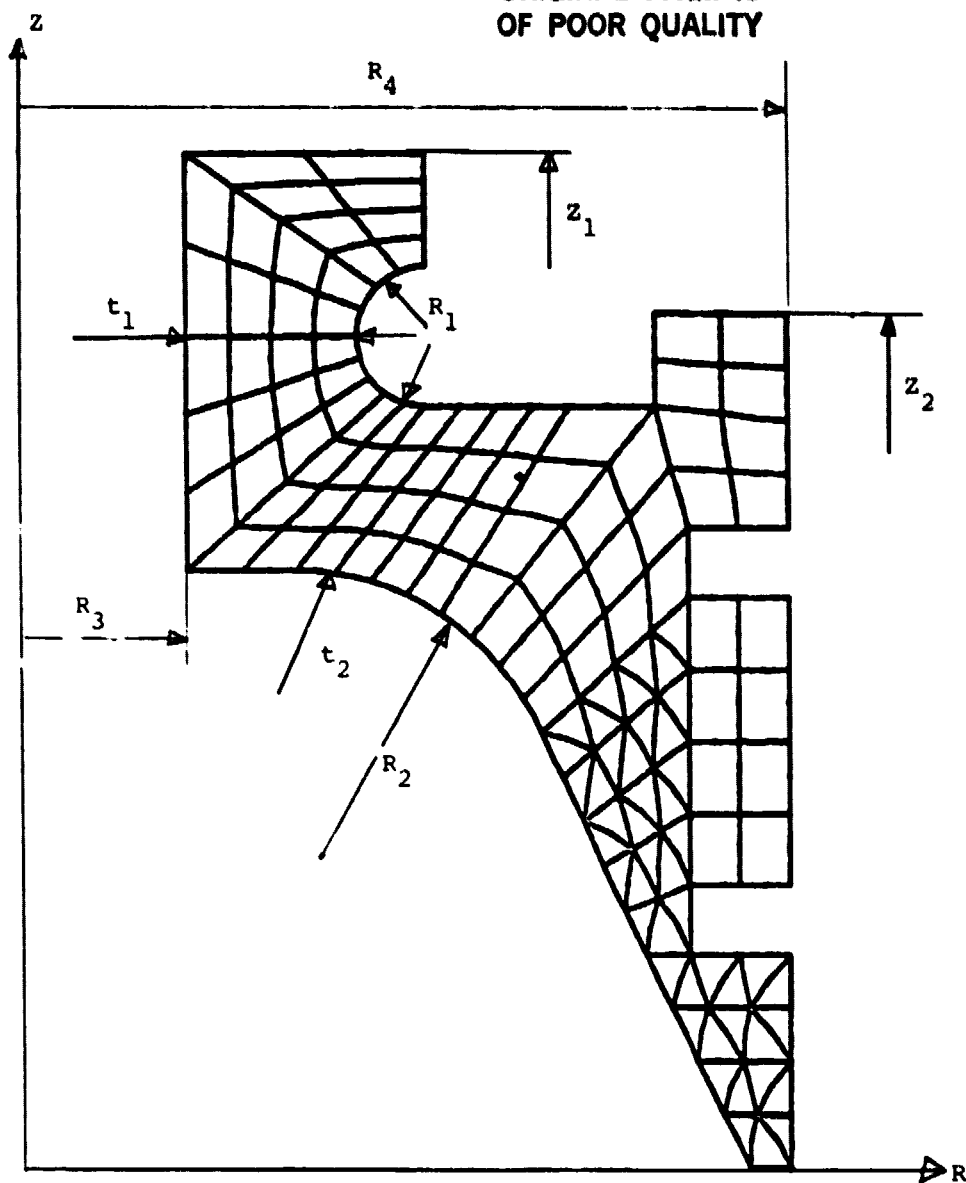
In load case 3 (extreme case) the maximal effective stress is 403 MPa at upper surface and 445 MPa at the lower surface, which means a safety factor of 1.6 against yielding.

Point A at the upper surface has been analyzed from the fatigue point of view. However, an estimation of the fatigue risk, must be based on a normal load condition, which corresponds to load case 1 and load case 2. When the load on the piston body alternates between load case 1 and load case 2, the effective stress in the point will vary in the following way

$$\sigma_e = (137 \pm 119) \text{ MPa.}$$

Assuming a fatigue notch sensitivity of 0.89 and taking volume dependence and surface influence into consideration with a factor of 0.80 gives the resulting Smith diagram shown in figure 6.3:16. The corrected stress cycle have been entered in the diagram and the safety factor (fs) can be estimated to 2.0.

ORIGINAL PAGE IS
OF POOR QUALITY

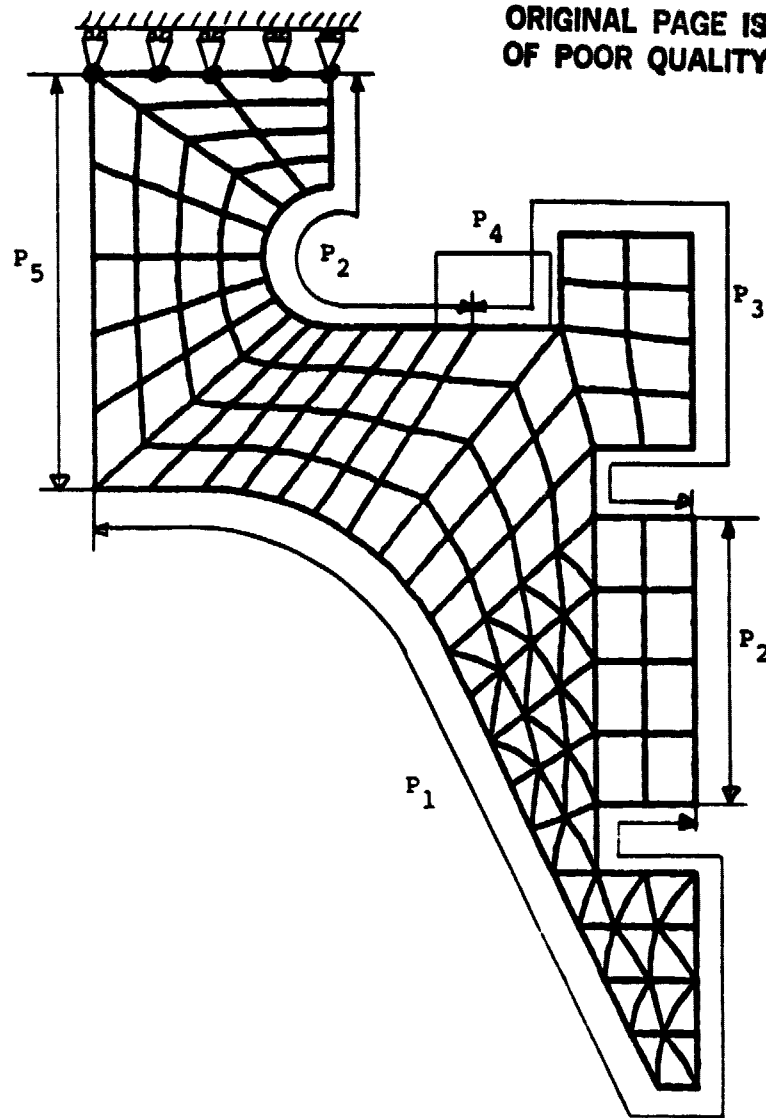


$R_1 = 3.0 \text{ mm}$
 $R_2 = 12 \text{ ''}$
 $R_3 = 7.5 \text{ ''}$
 $R_4 = 33.8 \text{ ''}$

$t_1 = 7.5 \text{ mm}$
 $t_2 = 7.5 \text{ ''}$
 $z_1 = 44.0 \text{ ''}$
 $z_2 = 37.0 \text{ ''}$

Figure 6.3:11. Main geometry used in the analysis.

ORIGINAL PAGE IS
OF POOR QUALITY



Load case 1: $p_1 = 15 \text{ MPa}$

$p_2 = 10 \text{ ''}$

$p_3 = 20 \text{ ''}$

$p_4 = 34.2 \text{ MPa (dome base load)}$

$p_5 = 200 \text{ ''}$

Load case 2: $p_1 = 20 \text{ MPa}$

$p_2 = 10 \text{ ''}$

$p_3 = 15 \text{ ''}$

$p_4 = 23.2 \text{ MPa}$

$p_5 = 200 \text{ ''}$

Load case 3: $p_1 = 20 \text{ MPa}$

(extreme
case)

$p_2 = p_3 = p_4 = 0$

$p_5 = 200 \text{ MPa}$

Figure 6.3:12. Load cases.

ORIGINAL PAGE IS
OF POOR QUALITY

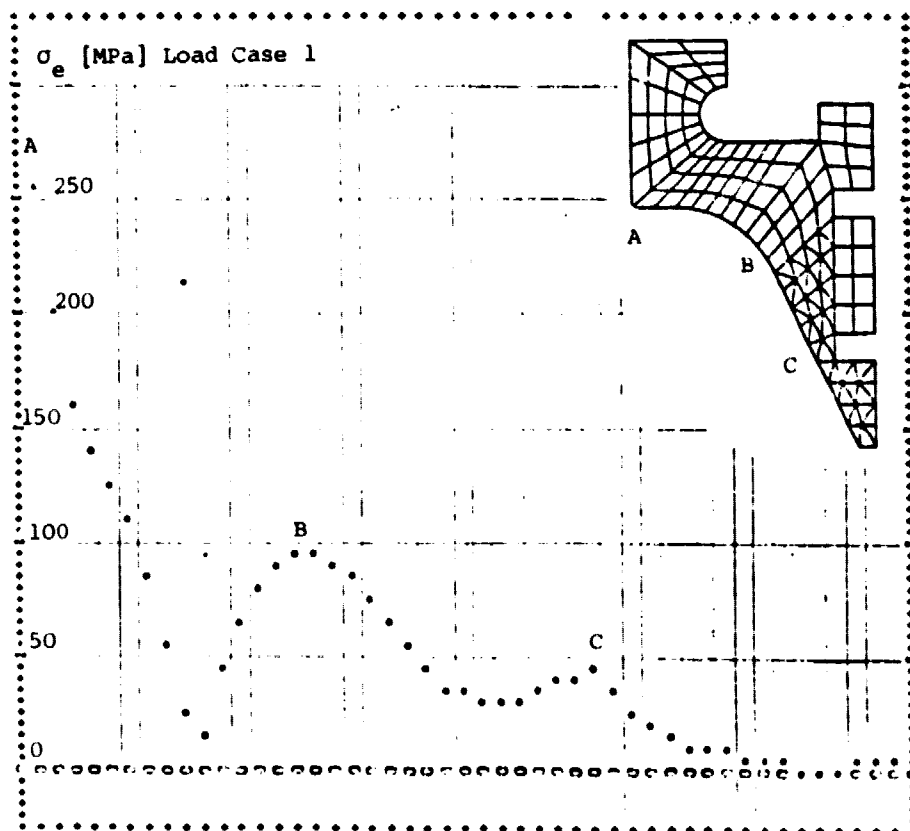
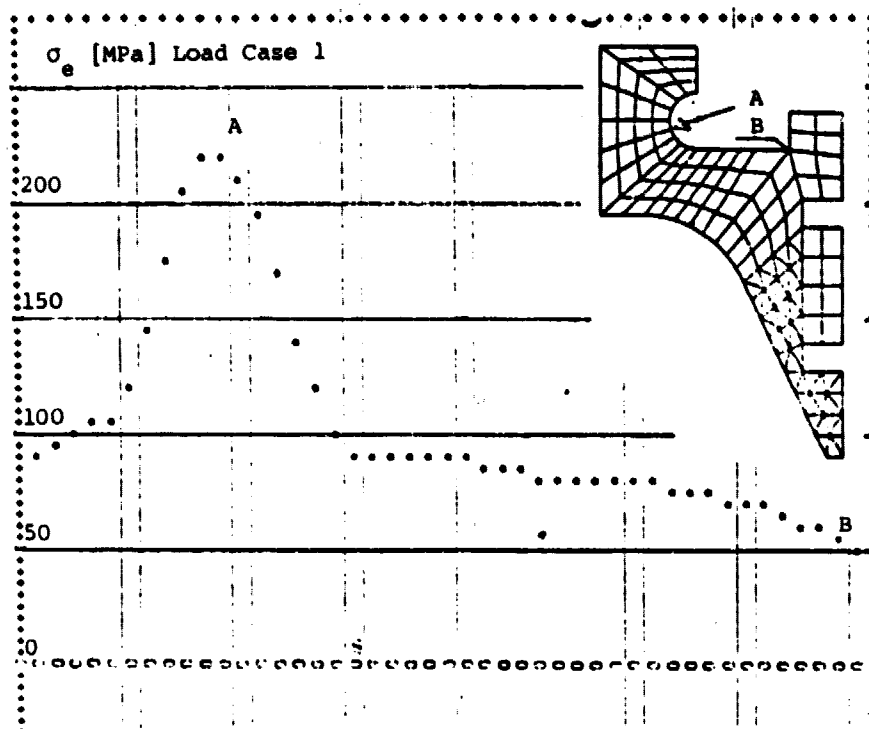


Figure 6.3:13. Effective stress in load case 1.

ORIGINAL PAGE IS
OF POOR QUALITY

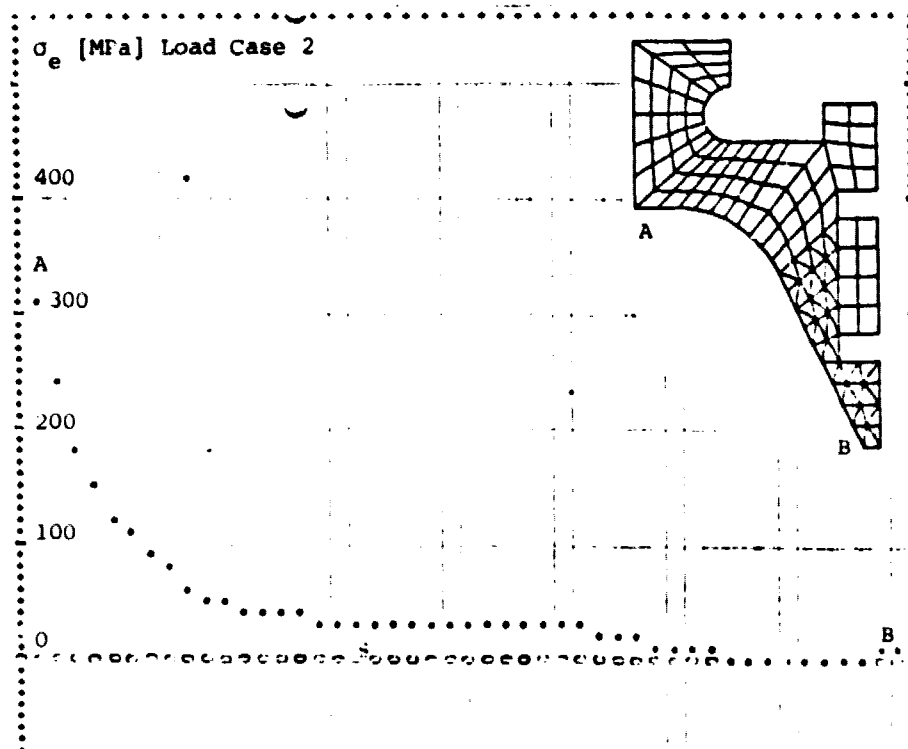
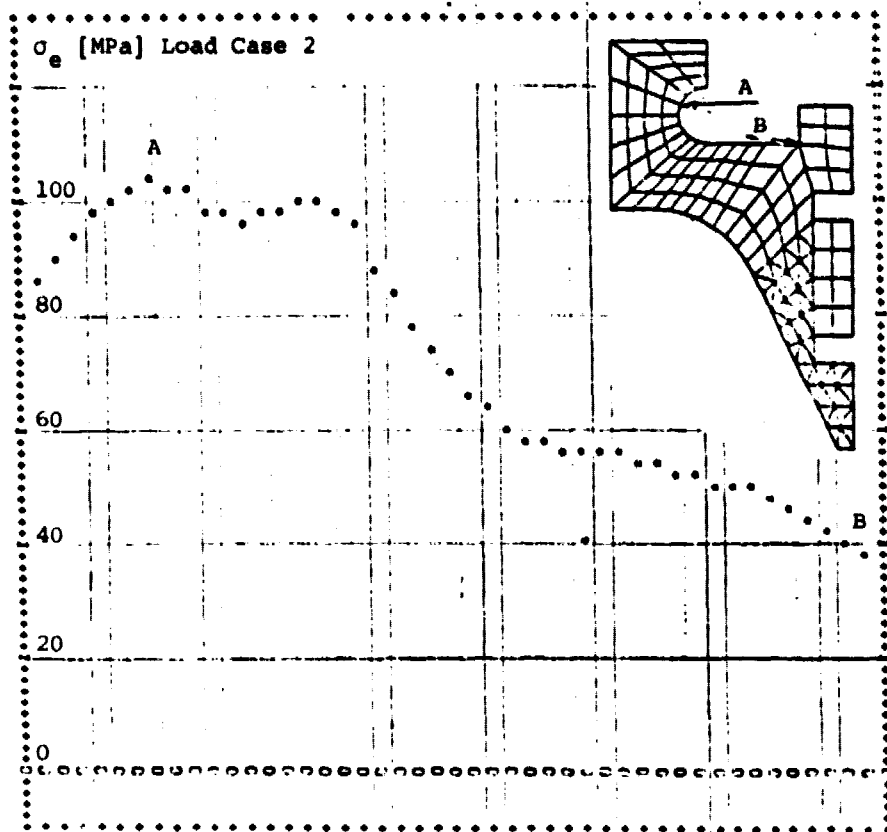
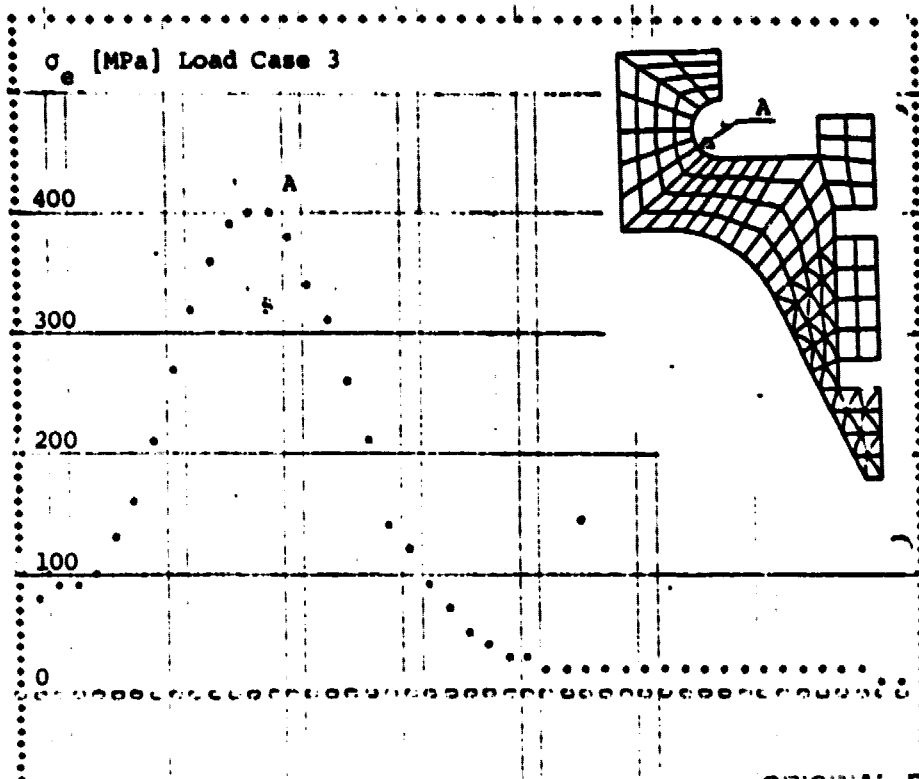


Figure 6.3 : 14. Effective stress in load case 2.



ORIGINAL PAGE IS
OF POOR QUALITY

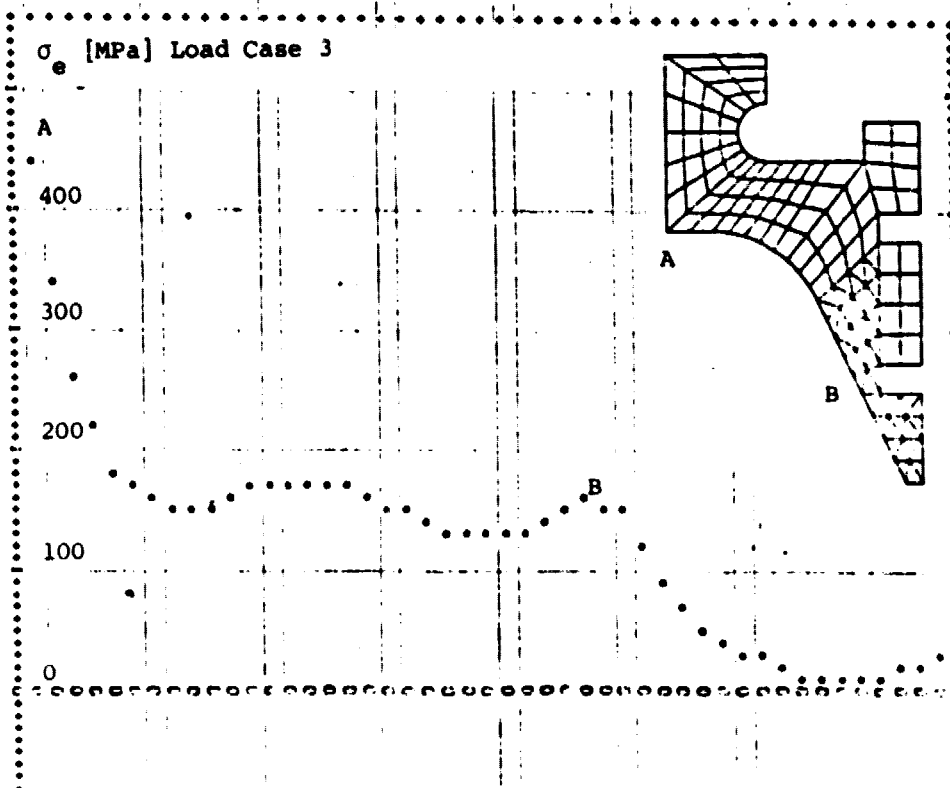
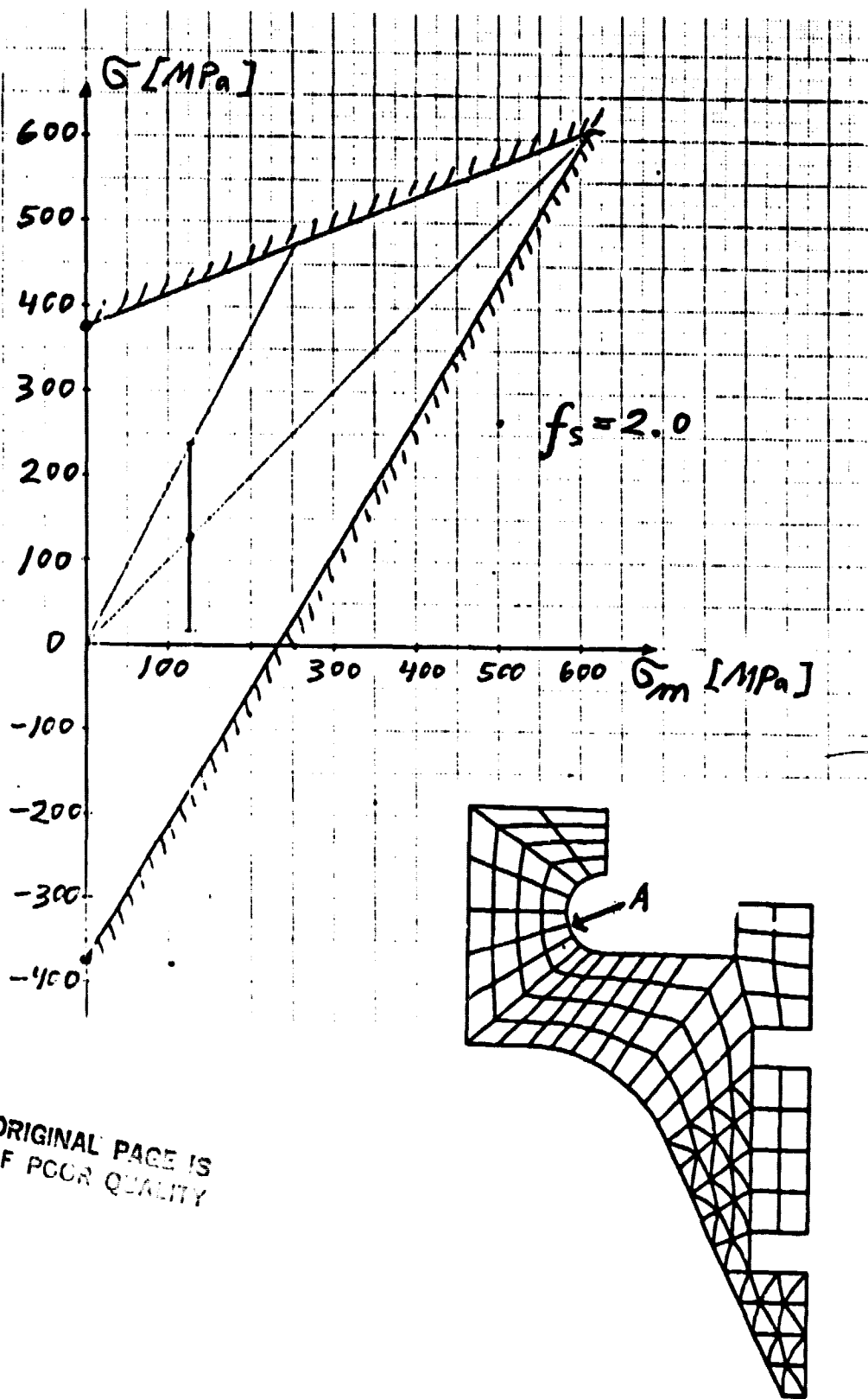


Figure 6.3:15. Effective stress in load case 3.



ORIGINAL PAGE IS
OF POOR QUALITY

Figure 6.3:16. Smith diagram point A.

The surface pressure of the taper between the piston body and the piston rod is determined in order to give a required safety factor of 1.5 against loosening. At the same time the surface pressure must meet the requirement of a safety factor of 1.5 against yielding of the piston body. Otherwise there will be problems in dismounting the piston base from the piston rod. The surface pressure has been chosen to 200 MPa. This corresponds to a demounting force equal to 27000 N. The maximum gas force acting on the piston body is 15300 N, which gives a safety factor against loosening of 1.8. The effective stress in the piston body due to the surface pressure becomes 466 MPa giving a safety factor of 1.5 against yielding.

6.3.4 The dome assembly

6.3.4.1 General

The dome assembly consists of the dome and the dome base, which are welded together. The assembly is subjected to an external pressure by the expansion side. The temperature varies from 700°C on the top to 100°C at the bottom.

6.3.4.2 Material

The dome and the dome base are made of Nimonic 80 A with the following data:

Yield stress (0.2%) σ_y = 660 MPa at 700°C
688 MPa at 650°C
748 MPa at 100°C

Ultimate tensile strength σ_u = 875 MPa at 700°C
964 MPa at 650°C
1200 MPa at 100°C

Young's modulus E = 142000 MPa at 700°C
150000 MPa at 650°C
179000 MPa at 100°C

Thermal expansion coefficient α = $12.7 \cdot 10^{-6} \text{ } ^\circ\text{C}^{-1}$ at 100°C
 $15.5 \cdot 10^{-6} \text{ } ^\circ\text{C}^{-1}$ at 700°C

6.3.4.3 Design criteria

The dome is subjected to an outer pressure from the working gas on the expansion side. Whether or not its interior volume is used as a buffer volume the dome shall resist the outer pressure of 20 MPa under the described temperature conditions (100-700°C). Under these circumstances buckling is the most likely failure process. The dome is designed to resist elastic buckling with a safety factor of 2.5. Normally a lower factor of safety is used for plastic buckling but because of some shatter of the yield stress the dome is also designed against plastic buckling with the same factor of safety.

The dome base shall resist yielding and fatigue.

6.3.4.4 Analysis

The dome assembly is shown in fig. 6.3:17. It is screwed to the piston base and rests on it. The temperature is 700°C at the spherical top and 100°C at the bottom of the base. Along the cylindrical part there is a linear temperature distribution between these values.

The dome base has a conical top which can be closed with a screw thus giving a smaller buffer volume. In this case atmospheric pressure will be present inside the dome. The temperature at the center of the conical top is assumed to be 300°C.

ORIGINAL PAGE IS
OF POOR QUALITY

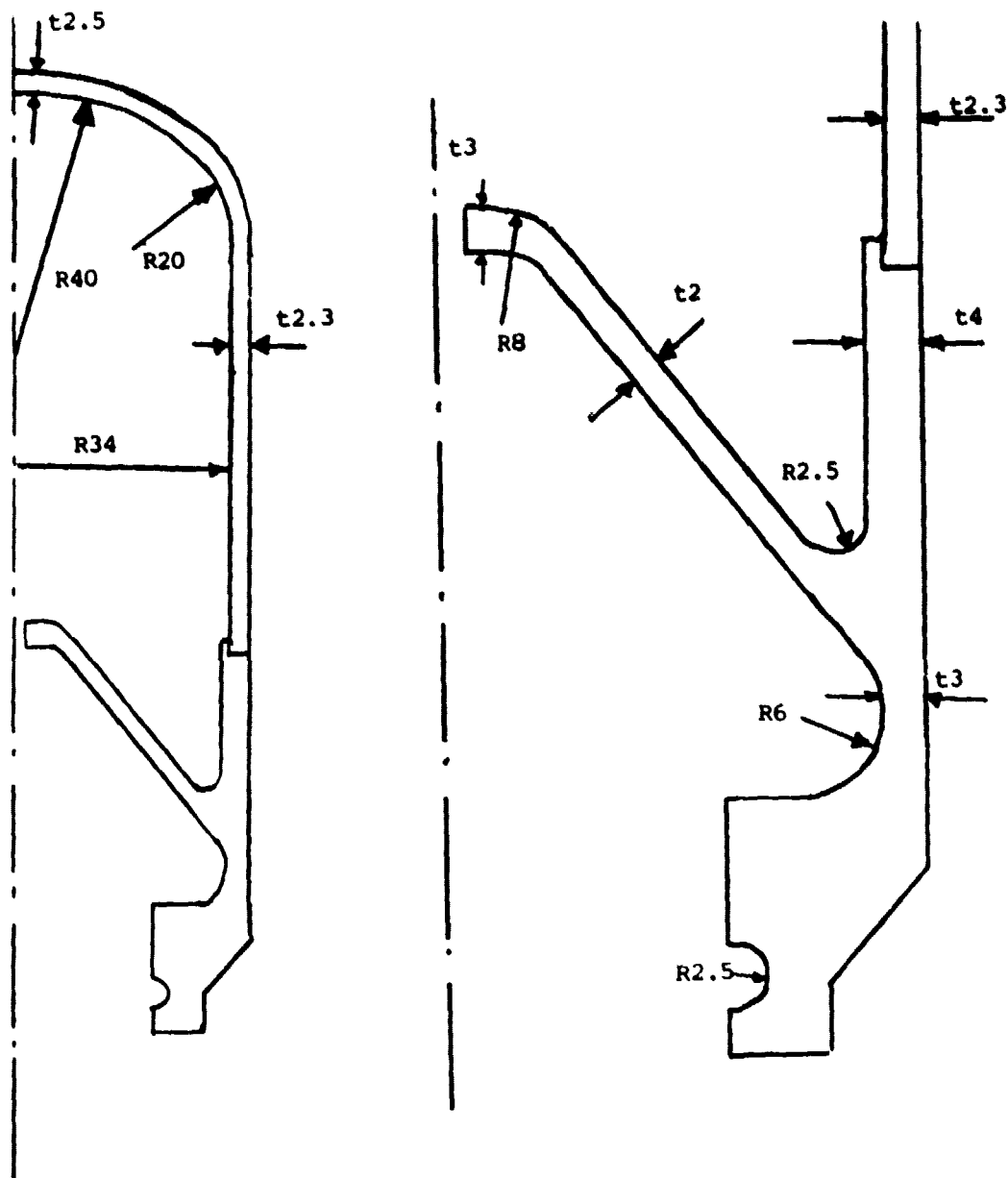


Fig. 6.3:17. The dome assembly. The lower part is shown enlarged to the right.

The classical formulas below are used for the analysis of the elastic buckling (see e.g. Roark & Young; Formulas for stress and strain). The symbols used are:

q = critical external pressure

r = radius of the sphere or the cylinder

t = thickness

ν = Poisson's ratio

E = Young's modulus

n = number of lobes

l = length of the cylindrical tube

I = Thin tube under uniform external pressure.

$$q = 0.365 Et^2/r^2 \quad (r > 10t) \quad (\text{Eq 1})$$

II. Thin tube under uniform external pressure, ends held circular but not otherwise constrained.

$$q = 0.807 Et^{2.5}/lr^{1.5} (1 - \nu^2)^{0.75} \quad (\text{Eq 2})$$

III. Thin tube with closed ends under uniform external pressure, lateral and longitudinal, ends held circular.

$$q = -\frac{Et}{r \left(1 + \frac{k^2}{2}\right)} \left\{ \frac{1}{n^2 (1 + k^{-2})^2} + \frac{n^2 t^2}{12r^2 (1 - \nu^2)} \left[1 + k^2\right]^2 \right\} \quad (\text{Eq 3})$$

where $k = \pi r/nl$

n is chosen to give minimum q .

The following geometrical and material data are valid:

a) The spherical top

$$r = 40 \text{ mm}$$

$$E = 142000 \text{ MPa}$$

b) The cylindrical part

$$r = 34 \text{ mm}$$

$$l = 85 \text{ mm}$$

$$\nu = 0.3$$

$$E = 150000 \text{ MPa}$$

With q equal to 50 MPa the following minimum thicknesses are valid:

a) The spherical top

Eq. 1 gives $t = 1.24$ mm

b) The cylindrical part

Eq. 2 gives $t = 2.12$ mm

Eq. 3 gives $t = 1.98$ mm

In order to ensure a safe design against plastic buckling finite element computations have been performed. The total mesh is shown in the figures 6.3:18 and 6.3:19. Fig. 6.3:18 shows the total mesh, which contains 212 isoparametric axi-symmetric elements with 8 or 6 nodes in each element. Totally there are 1 622 degrees of freedom. To the right in the figure the mesh of the lower part is enlarged. In fig. 6.3:19 the dome and the dome base are shown separately. In the finite element model the surfaces A and B have common nodes, while no contact is present between the surfaces C and D. At the surfaces E and F the displacements in the z -direction are zero. Two loadcases are considered. In both of them the outer pressure is 20 MPa and the upper dome volume has atmospheric pressure. The lower dome volume has atmospheric pressure and minimum cycle pressure (10MPa) resp. in the two cases considered. The thermal load is present in both cases.

In order to get the desired safety factor a thickness of 2.3 mm is chosen in the main part of the dome.

ORIGINAL PAGE IS
OF POOR QUALITY

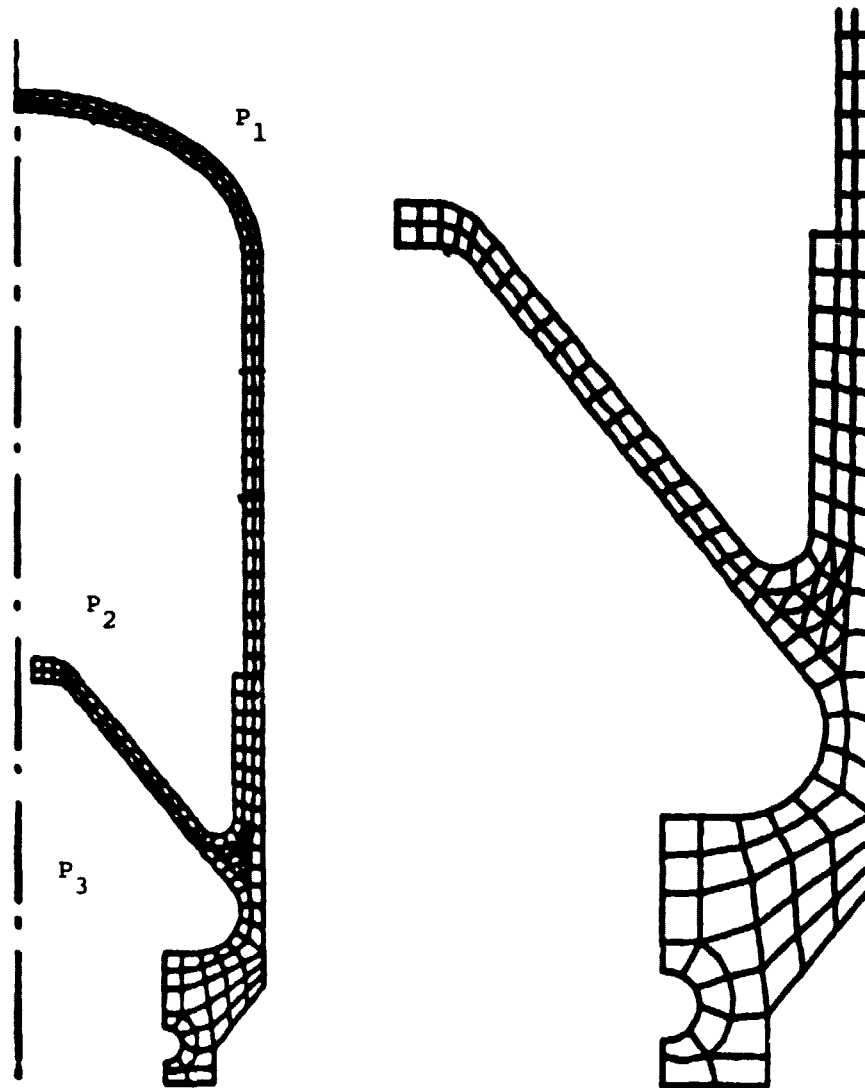


Fig. 6.3:18. Finite element mesh of the dome assembly. The lower part is showed enlarged to the right.

Loadcase 1: $p_1 = 20 \text{ MPa}$, $p_2 = 0 \text{ MPa}$, $p_3 = 0 \text{ MPa}$

Loadcase 2: $p_1 = 20 \text{ MPa}$, $p_2 = 0 \text{ MPa}$, $p_3 = 10 \text{ MPa}$

ORIGINAL PAGE IS
OF POOR QUALITY

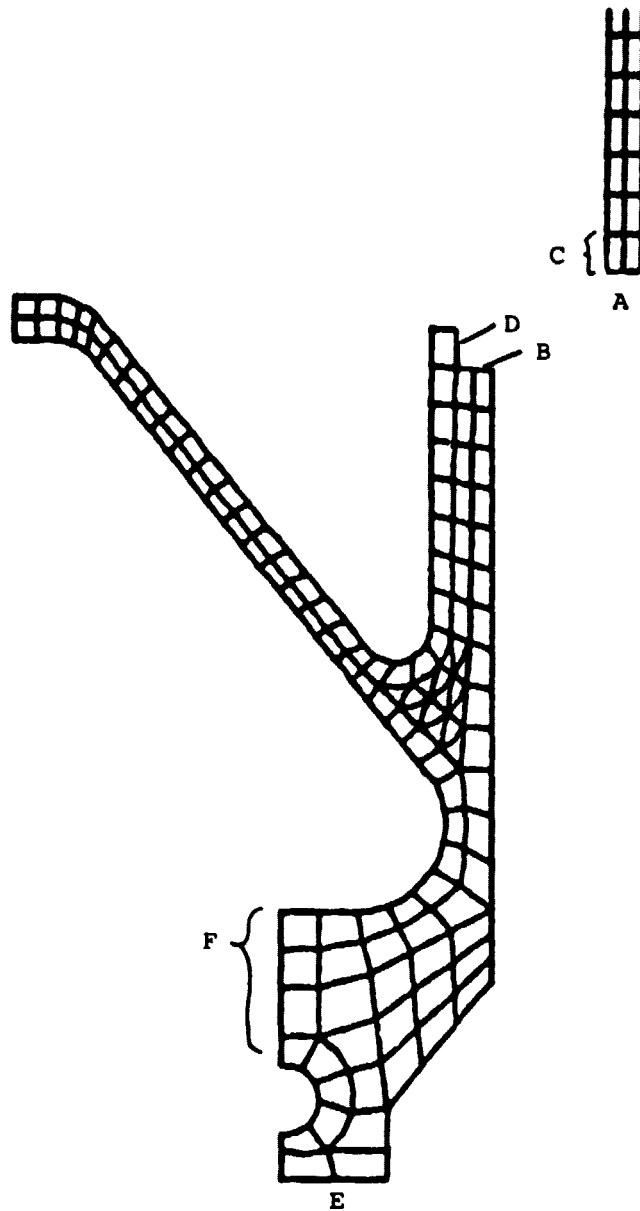


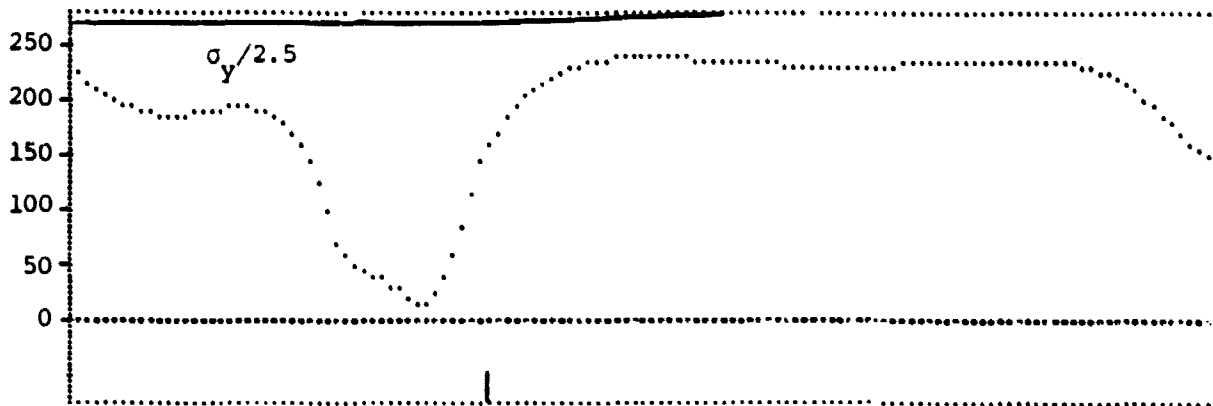
Fig. 6.3:19. Enlarged mesh of the dome base and the lower part of the dome A and B are welded together. C and D are not in contact. E and F are in contact with the piston base.

In figure 6.3:20 the effective stress (v. Mises) for load case 1 is shown along the inner and outer surfaces of the dome. The stress diagram starts with the top and goes on to the dome base. The maximum allowed stress in order to resist plastic buckling with a safety factor of 2.5 is showed in the diagrams. The stress is below the required level in all parts of the dome. Thus a thickness of 2.3 mm fulfils the requirement of a safety factor of 2.5 against elastic as well as plastic buckling.

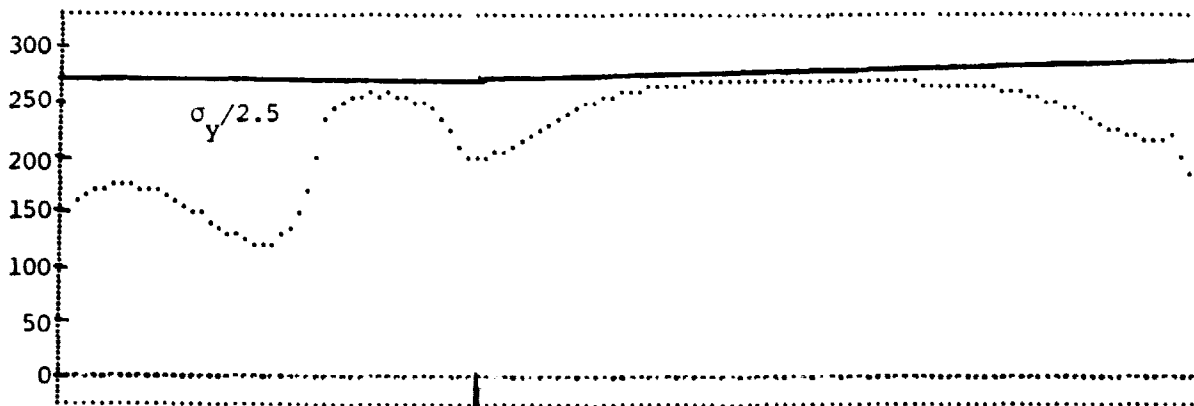
Considering both the load cases the largest effective stress in the dome base is 219 MPa which gives a safety factor against yielding of about 3.

The dome base has mainly just compressive stresses. In combination with the relatively low stress level there will be no fatigue problems.

OUTSIDE STRESSES



INSIDE STRESSES



The spherical part
of the dome

The cylindrical part of
the dome

Fig. 6.3:20. The effective stress for load case 1 at the outer and inner surfaces of the dome shown from top to bottom. The maximum allowed stress $\sigma_y/2.5$ is shown in the diagrams.

6.3.5 Stress Calculations of Water Jacket and Heater Head Bolt Arrangement

6.3.5.1 General

The water jacket encloses the cooling water. It is made of cast aluminum and consists schematically of vertical walls, vertical sleeves around the bolts and two end sheets. It is clamped between the heater head and the duct plate by the heater head bolts. A horizontal section of one fourth of the water jacket is shown in fig. 6.3.21.

The heater head is bolted with long rolled tie-bolts to the crank-case and the duct plate. The bolts of the cylinder housing pass through a loose flange, the water jacket, the duct plate and the seal housing. The regenerator housing bolts just pass a loose flange and the water jacket. Split retainer rings are inserted between the loose flanges and the housings. A schematic picture of the arrangement is shown in fig. 6.3.22.

ORIGINAL PAGE IS
OF POOR QUALITY

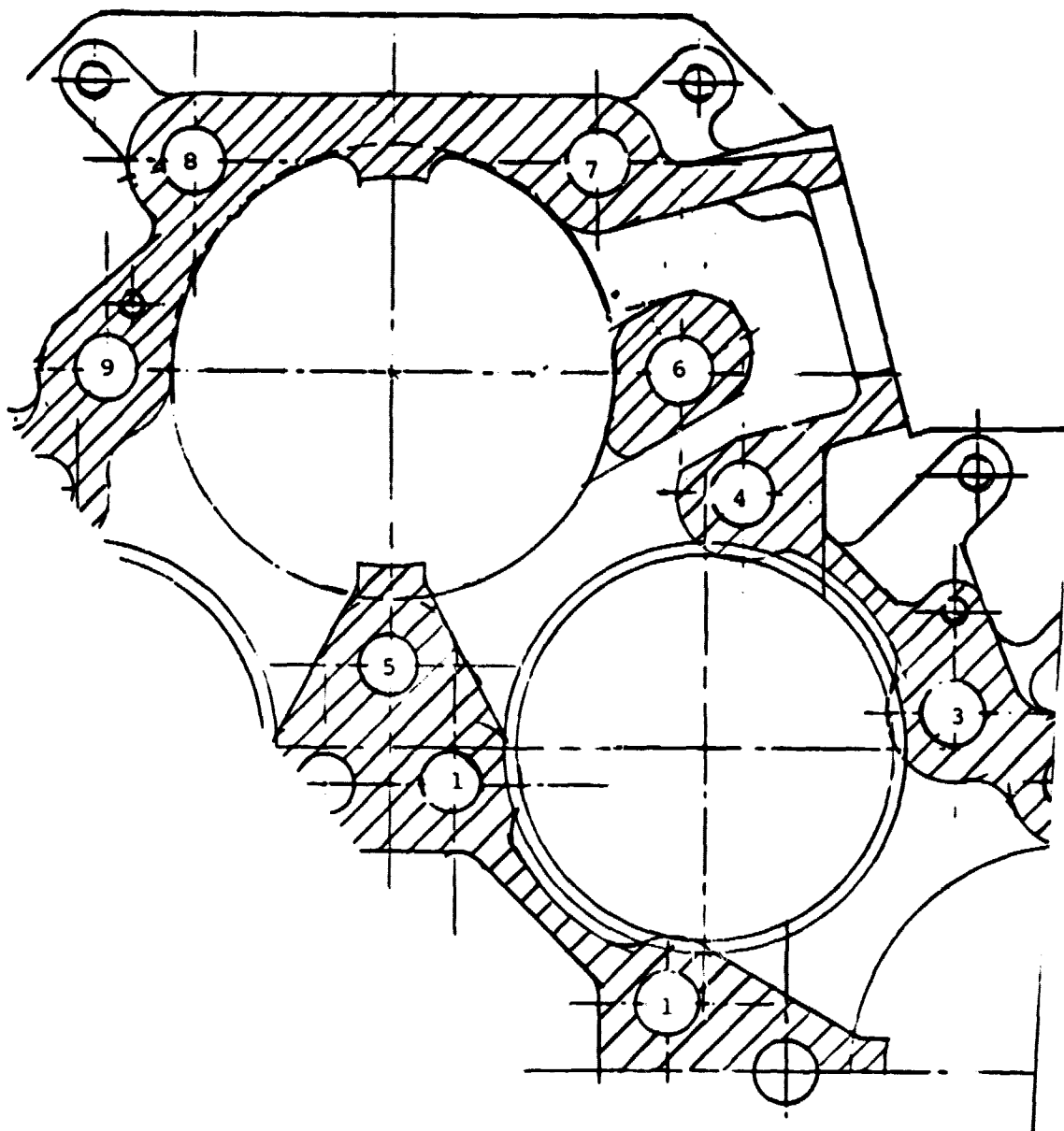


Fig. 6.3.21. One fourth of the water jacket. The locations of the nine bolts of one heater head quadrant is shown with the numbers 1-9.

ORIGINAL PAGE IS
OF POOR QUALITY

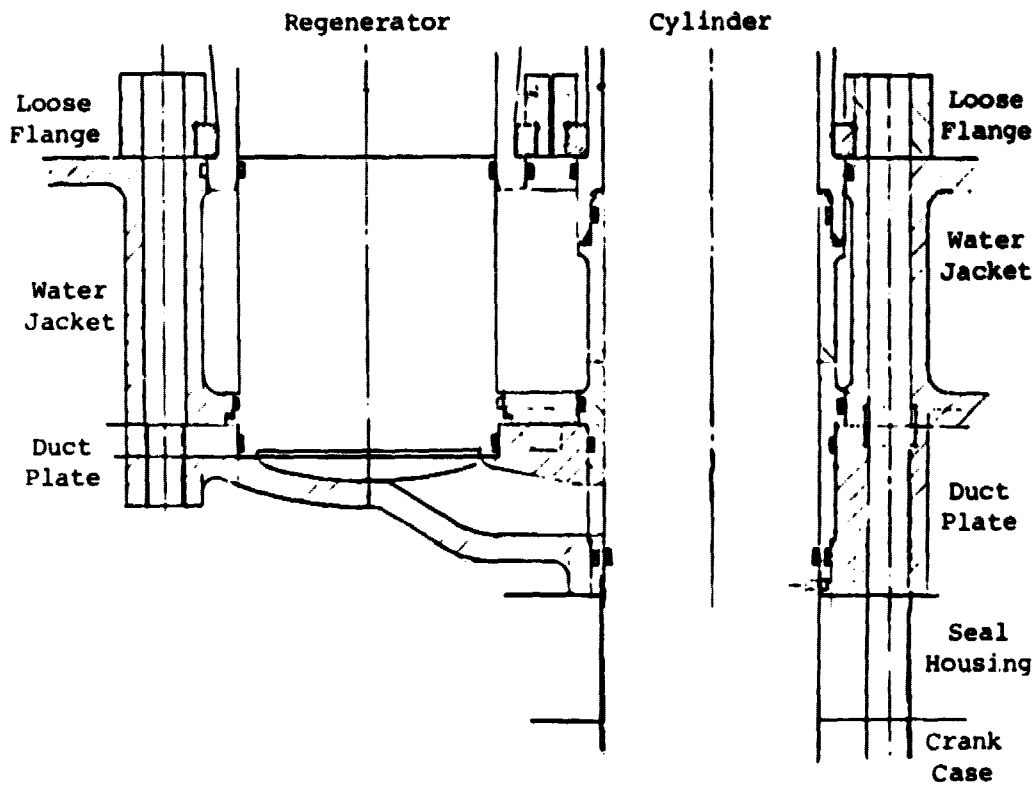


Fig. 6.3:22 Schematic Picture of the Bolt Arrangement of the Heater Head

6.3.5.2 Material

The following data are valid for the water jacket, the bolts and the loose flanges. The data for the duct plate is also given below.

Bolts

M14, Unbrako quality 12.9.

(SS 2225, AISI 4130)

Yield stress (0.2%) $\sigma_y = 1170 \text{ MPa}$.

Ultimate tensile stress $\sigma_u = 1360 \text{ MPa}$.

Young's modulus $E = 206000 \text{ MPa}$.

Coefficient of thermal expansion $\alpha = 11 \cdot 10^{-6} \text{ } ^\circ\text{C}^{-1}$

Loose flanges, split retainer rings.

SS 2541-03 (AISI 4337).

Yield stress (0.2%) $\sigma_y = 700 \text{ MPa}$

Ultimate tensile stress $\sigma_u = 905 \text{ MPa}$

Young's modulus $E = 205000 \text{ MPa}$

Brinell hardness HB = 270

Coefficient of thermal expansion $\alpha = 11 \cdot 10^{-6} \text{ } ^\circ\text{C}^{-1}$

Water jacket, crankcase, seal housing

DIN 1725 Werkstoff 3.2381.61

Al Si10Mg heat treated (cast aluminum)

Yield stress (0.2%) $\sigma_y = 170 \text{ MPa}$

Ultimate tensile stress $\sigma_u = 200 \text{ MPa}$

Young's modulus $E = 66\,400 \text{ MPa}$

Brinell hardness HB = 75

Coefficient of thermal expansion $\alpha = 21 \cdot 10^{-6} \text{ } ^\circ\text{C}^{-1}$

If the seal housing will be machined from bar stock higher values of σ_y , σ_u and HB will be valid.

Duct plate

SS 0737 (AISI 100-70-03)

Yield stress (0.2%) $\sigma_y = 450 \text{ MPa}$

Ultimate tensile stress $\sigma_u = 700 \text{ MPa}$

Young's modulus $E = 165000 \text{ MPa}$

Brinell hardness HB = 229

Coefficient of thermal expansion $\alpha = 11 \cdot 10^{-6} \text{ } ^\circ\text{C}^{-1}$

6.3.5.3 Design criteria

The bolt arrangement is designed to fulfil the requirements of VDI 2230 (Verein Deutscher Ingenieure, "Systematische Berechnung hochbeanspruchter Schraubenverbindungen"). Considering the quality 12.9 these design rules are based on its normal yield stress of 1080 MPa. To get a larger safety we use Unbrako standard 12.9, which has a yield stress equal to 1170 MPa.

6.3.5.4 Testing

A successful fatigue test of the duct plate is described in 6.5. In this test one quadrant of the water jacket was clamped with loose flanges to the duct plate and a thick plate simulating the crankcase, see fig. 6.5.1. In this test M12 10.9 bolts were used with the recommended torque of 79 Nm (no thread lubrication). The water jacket was made of aluminum from bar stocks and sheets by welding and thus stronger than a cast product.

The split retainer rings have been successfully fatigue tested for the cylinder housing of the P75 engine. The contact width has been given the same size in the MOD 1 engine. Since the diameters of the MOD 1 housings are smaller than that one of the P75 cylinder housing the surface pressure will be smaller for the loose flanges of MOD 1.

6.3.5.5 Analysis

The cylinder housing is fastened with 4 symmetrically spaced bolts, while the regenerator housing is fastened with 5 asymmetric spaced bolts. The locations of the bolts for one quadrant are shown in fig. 6.3.21. The bolts 1-4 and the bolts 5-9 belong to the cylinder and regenerator housings respectively. The forces acting on the bolts due to the maximum cycle pressure of 20 MPa are

Bolt 1-4: 22680 N

Bolt 5 : 26405 N

Bolt 6-9: 19800 N

The environment of the bolts is schematically shown in the figures 6.3.23 and 6.3.24. The water jacket has the form of thick tubes around the bolts. This is also valid for the duct plate considering the bolts of the cylinder housing. The tie-bolts have the size M14 and are designed to DIN-norms. They are necked down to a diameter equal to 10 mm, see fig. 6.3.25. The bolts of the cylinder housing are fastened into thread inserts in the crankcase. For all bolts a lubrication with Molycote 1000 will be used between the nuts and the bolts. Thus the coefficient of friction will be about 0.10.

For simplicity the notations shown in fig. 6.3.26 will be used. F_M is the preload and F_A is the applied load. The contribution of the applied load to the bolt load is called F_{SA} . It is derived from the following well-known relation

$$F_{SA} = \phi F_A ; \phi = \frac{1}{\frac{k_c}{k_b} + 1}$$

ORIGINAL PAGE IS
OF POOR QUALITY

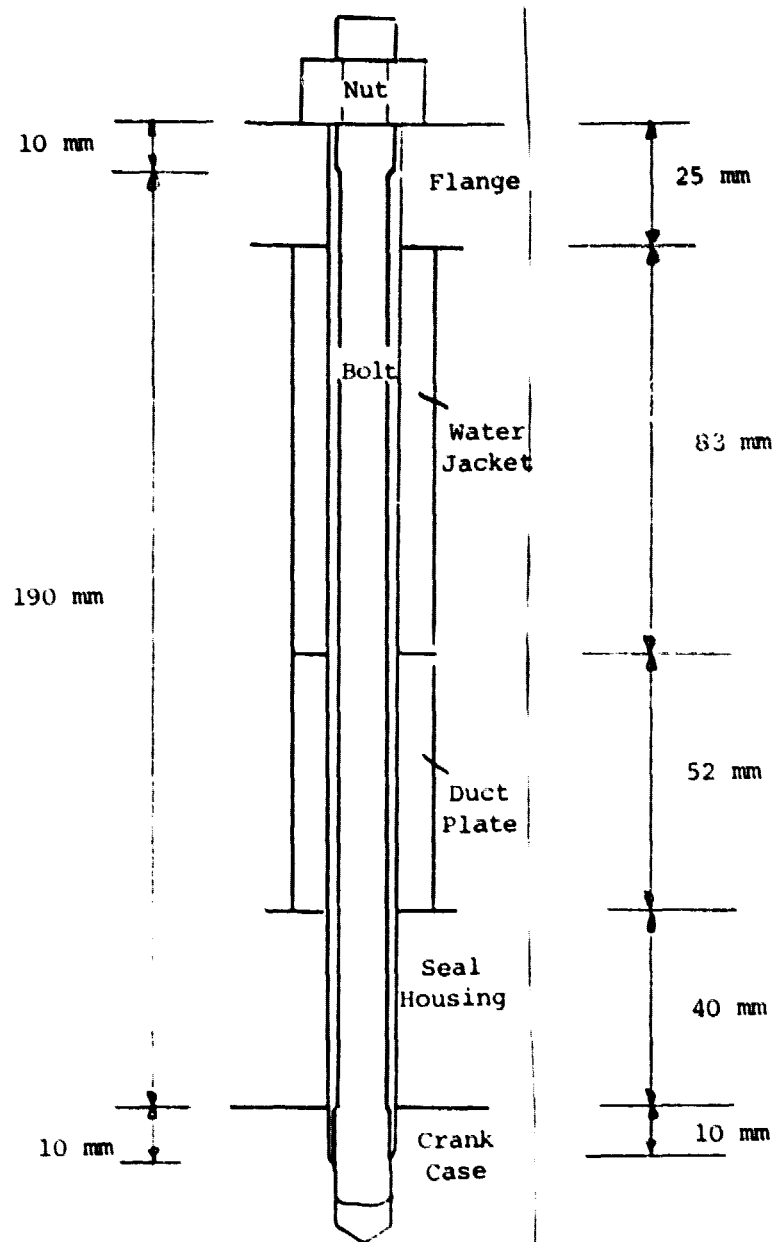


Fig. 6.3.23. Cylinder housing bolt with environment.

ORIGINAL PAGE IS
OF POOR QUALITY

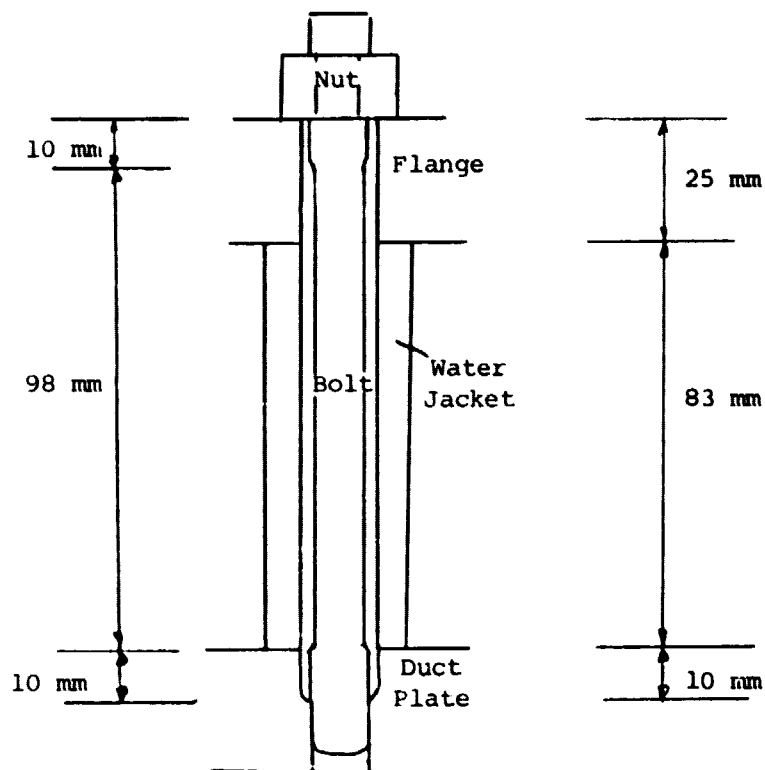


Fig. 6.3.24. Regenerator housing bolt with environment.

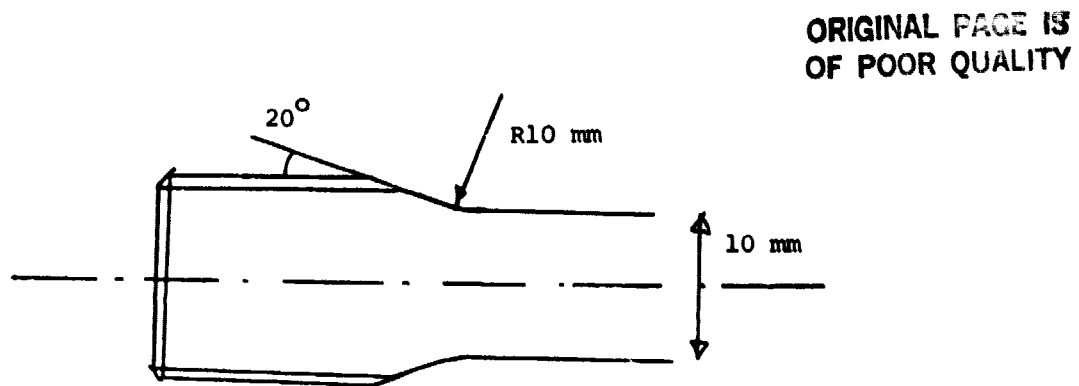


Fig. 6.3:25. Tie-bolt M 14.

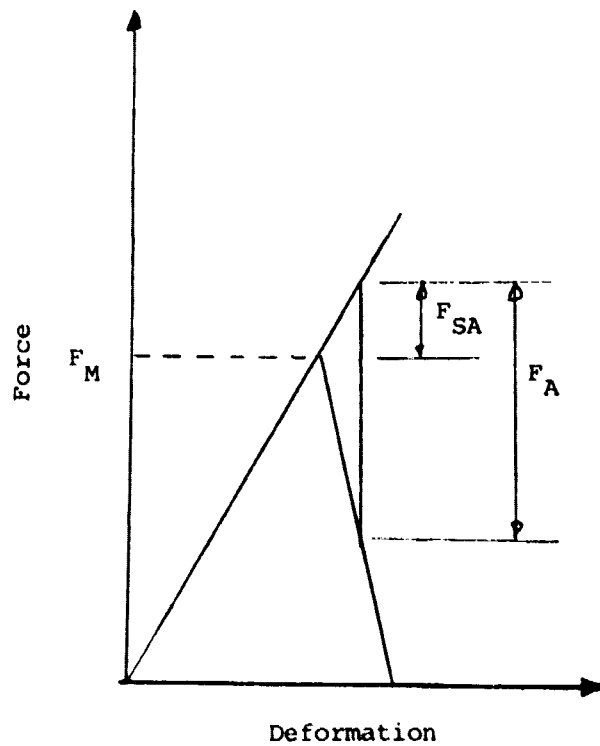


Fig. 6.3.26. Bolt diagram with notations used in the text.

where

k_b = spring rate of the bolt

k_c = spring rate of the bolted material

The values of the forces F_A and F_{SA} are shown in the table below. Since the size of the water jacket sleeves around the bolts are to some extent different for the nine bolts there is a scatter for the factor ϕ . The bolts are arranged in the table due to the size of the applied force.

Bolts	F_A N	ϕ	F_{SA} N
No. 1-4	22680	0,23-0,26	5216-5897
No. 5	26405	0,23	6073
No. 6-9	19800	0,21-0,27	4158-5346

The largest force $F_{SA} = 6073$ N implies a bolt stress equal to 80 MPa. VDI 2230 requires this stress to be below 10% of the yield stress, which is fulfilled.

When computing the lowest preload to maintain clamping the use of a normal torque wrench is taken into consideration. Following VDI 2230 the minimum preload F_M is

Bolt 1-4: 30180 N

Bolt 5 : 34770 N

Bolt 6-9: 27270 N

This can be compared to the recommended preload, which is 60000 N.

The amplitude of the cycle pressure is 5 MPa. The nominal amplitude stress in the threads of the bolts due to this pressure is

Bolt 1-4: 12 MPa

Bolt 5 : 13 MPa

Bolt 6-9: 12 MPa

The maximum allowed amplitude stress is 60 MPa giving a safety against fatigue of about 4.

ORIGINAL PAGE IS
OF POOR QUALITY

Since aluminum has a larger coefficient of thermal expansion than iron a thermal load will be present when the temperature exceeds the ambient. The whole arrangement from the flange at the top to the threads of the bolt at the bottom is assumed to have a temperature increase equal to 100°C , which can be considered as a conservative estimation from the stress point of view. The temperature load can be seen as an increase of the preload. This additional preload is for the bolts as below.

Bolt 1-4: 7790 - 7890 N

Bolt 5 : 8550 N

Bolt 6-9: 8450 - 9485 N

In order to keep the total preload equal to about 60000 N as recommended the torque is chosen equal to 95 Nm, which gives an initial preload equal to 49500 N. Then in combination with the additional thermal load a total preload of about 59000 N is obtained.

In the table below the maximum surface pressure is compared to the allowed levels of the different parts.

Surface pressure

Part	Allowed pressure MPa	Actual pressure MPa
Flange	1250	389
Aluminum material	225	113
Duct plate	1050	113

As can be seen in the table all surface pressures have acceptable margins to the allowed levels.

Considering the water jacket, it is just subjected to a compression load. The maximum compression stress is obtained by the preload. A preload of 60000 N gives a maximum compression stress equal to 95 MPa. This gives a safety against yielding of 1.8.

After the manufacturing of the loose flanges, the split retainer rings, the water jacket, the duct plate and the bolts the whole arrangement will be tested with respect to fatigue. The temperature shall then be kept around 120°C.

6.4 Fatigue test of cylinder-water jacket-duct plate

A fatigue test has been performed in order to validate the new type of cylinder block arrangement compared to the P40 and P75 engines and new components as the duct plate and the loose flanges

The test object is shown in fig. 6.4 a. It corresponds to one quadrant of the engine and consists of

- a) a duct plate, see fig. 6.3:4.
- b) a special water jacket, which is one fourth of the ordinary one.
- c) dummy plates simulating the heater head and crankcase.
- d) a dummy cooler.
- e) loose flanges for the fastening of the heater head.
- f) 9 M12 pin bolts, quality 10.9.

ORIGINAL PAGE IS
OF POOR QUALITY

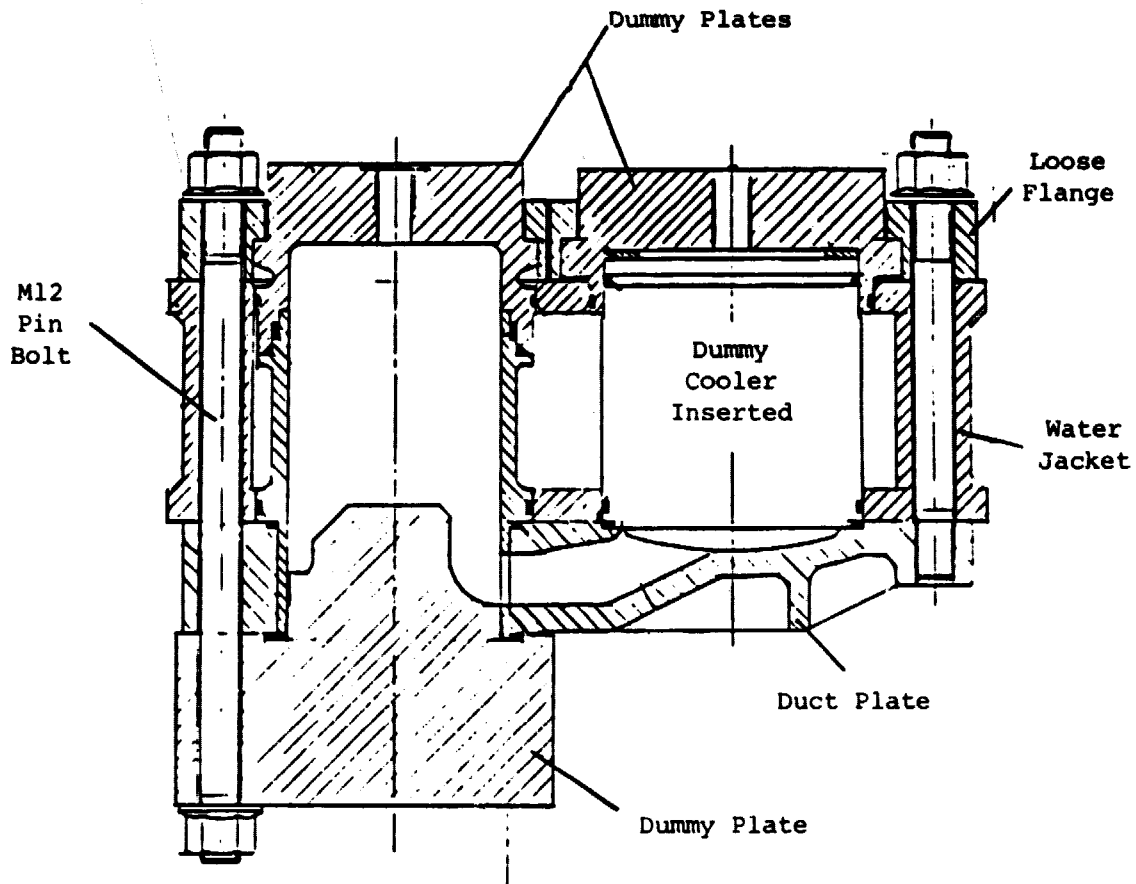


Fig. 6.4:1 Test Object

The object was pressurized with oil with a cycling pressure of 15.75 ± 5.25 MPa, which is 5% above the maximum load level. The temperature was kept constant and equal to 30°C . The test passed successfully 10 million cycles.

The test is verified in the enclosed document from Swedish National Testing Institute.



REPORT NO 7911,555

Customer: KB United Stirling (Sweden) AB & Co

Object: Water jacket and duct plate

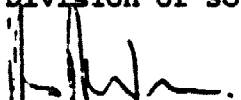
Assignment: Fatigue testing, your order no 3382.

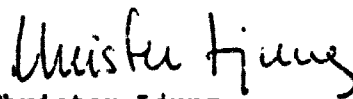
Test procedure: Fatigue testing on water jacket and duct plate for engine MOD 1 has been completed to 10^7 cycles without failure.

The load has been oscillated between 10,5 and 21,0 MPa at a frequency of 34 Hz. The oil temperature was kept below 30°C during the test.

Borås 1979-10-24

SWEDISH NATIONAL TESTING INSTITUTE
Division of Solid Mechanics


Hans Andersson


Christer Ljung

6.5 Fabrication Technique and Material Selection

The cold engine system parts are

Water jacket, cylinder liner

Cold connecting duct plate

Piston dome

Piston, piston rings

Piston rod

Piston rod seal

Bolt connection, heater - crankcase

The fabrication technique and material selection for these parts will be described below.

6.5.1 Water Jacket

The somewhat complicated shape of the water jacket makes casting the most suitable manufacturing method. The water jacket will be sandcast using cores for the internal cavities. After casting, the upper and lower surfaces will be machined levelled and parallel. O-ring grooves and surfaces will be machined and holes for bolts drilled.

The material will be an aluminium alloy G-AlSi10 Mg wa (Werkstoff 3.2381.61 approximately SS 144253-04), a relatively high-strength casting alloy that will be solution-treated ($\approx 500^{\circ}\text{C}$) and aged ($\approx 180^{\circ}\text{C}$). It has a 0.2% yield strength of ≈ 250 MPa.

6.5.2 Cylinder Liner

The engine is designed with exchangeable cylinder liners. The use of unlubricated piston rings demands low friction combined with high wear resistance of the mating surface. The material must also be easily machined since the requirements regarding roundness and diameter tolerances are high. Nodular cast iron, SS 0737, that will be nitrided to approximately HB = 600, has been chosen as the main alternative. Other materials are to be evaluated for a final material selection.

6.5.3 Cold Connecting Duct Plate

The shape of this part makes casting the obvious manufacturing method. After casting the top and bottom surfaces will be machined with high requirements on height and parallelity. O-ring seats will be machined and holes for the bolts drilled.

The main material requirements are strength, stiffness and gas tightness. Nodular cast iron SS 140737-01 has been chosen. It has a modulus of elasticity of 160,000 MPa, a yield strength of approximately 450 MPa and has good casting properties.

6.5.3 Piston Dome

The dome is made from two parts, the upper dome and the dome foot welded together. Both parts will be machined from bar stock and then joined by TIG-welding. (Welding tests are in progress.) The material will be Nimonic 80^A. The main machining and the welding will be done with the material in solution-treated condition. After the welding the domes will be aged and finally machined to required finish.

6.5.5 Piston

The piston will be machined from bar stock. The material is SS 142541-03, a quenched and tempered steel hardened to approximately 300 HB. This is the required hardness for the cone in which the piston is pressed on to the piston rod.

As guiding surface against the cylinder Rulon LD is glued on to the piston and thereafter machined to close tolerances.

6.5.5.1 Piston Rings

The piston rings are machined from bar. The material is Rulon LD.

6.5.6 Piston Rod

The piston rod is made integral with the cross-head. A high tensile strength, high fatigue strength and very high surface hardness (> 1100 RC) is required. A quenched and tempered steel which is possible to nitride harden is therefore chosen, SS 142940-03.

The anticipated manufacturing sequence is as follows:

1. Semi-finished forging
2. Coarse machining
3. Quenching and tempering
4. Straightening
5. Machining
6. Stress relief treatment
7. Straightening
8. Fine machining
9. Nitriding
10. Grinding and polishing to superfinish

6.5.6 Piston Rod Seal

6.5.6.1 Seal Housing

The seal housing is machined from aluminium bar, SS 144212-06, with high requirements on dimensions and surface for the main seal (PL-seal) seat. The main reasons for the material choice for the seal housing are: Much lower hardness than the piston rod and thus no risk for scratch marks, low weight, good thermal conductivity to allow for extracting from the seal area.

In the lower part of the seal housing a cross head liner is fitted. The liner is machined after being mounted into the seal housing. The liner material is nodular cast iron, SS 140737. The combination of SS 142940 in the cross-head and SS 140737 in the liner has been used in other engines with good results.

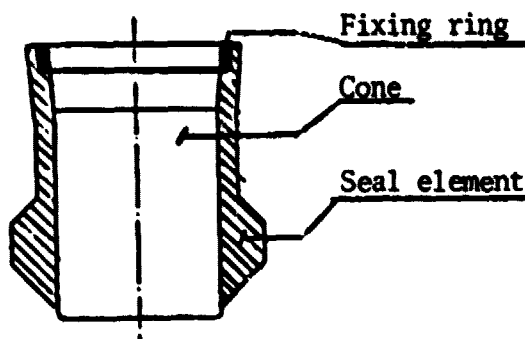
Since the top flange of the housing accommodates the gas system connections with some high stress areas which are difficult to analyze, a fatigue test will be performed and a set of back-up steel housings will be manufactured.

Capseal

Machined from bar. Material Rulon LD.

6.5.7 Main Seal (pumping lenigrader = PL)

The seal element is machined from bar stock and thereafter pressed on to a conical tool in accordance with the figure 6.5:1.



ORIGINAL PAGE IS
OF POOR QUALITY

Figure 6.5:1 Main PL Seal Element

The seal is through heat treated in a furnace in the following way: 280 °C for 1.5 h, thereafter cooling at a rate of 50 °C/h to 80 °C when the furnace is switched off. When room temperature is reached the fixing ring is fitted and the conical tool dismantled.

The PL-seal material is a PTFE filled with 20% carbon powder and 5% graphite. Experienced PL-seal data are given below.

6.5.8 Bolt Connection

6.5.8.1 Bolts

The bolts are manufactured from quenched and tempered steel, SS 142541-03. The threads are rolled. The middle section of the bolts is necked down by grinding in order to dimension the bolts for proper elongation when pre-stressed.

6.5.8.2 Cylinder and Regenerator Housing Flanges.

The cylinders and regenerator housings are bolted to the drive using loose flanges and split retainer rings. The flanges are machined from thick sheet of SS 142225-03, thoroughly levelled on top and bottom faces, the seat for retainer rings machined and bolt holes drilled.

6.5.8.3. Retainer Rings

Machined from bar, hardened and ground. Material SS 142541-03.

Experience Data from Engines Running with PL-Seals

The following endurance tests are made on self-running or motored engines with PL-seals.

ASE-program: P40 4 engine

2 000 rpm, He, $\bar{p} = 4-11$ MPa

Hour counter

0 h Start

1 612 h Inspection: seal housing

oily inside; wear particles,
adhering to the wet surfaces,
cycle dry

2 313 h Switch to H₂

2 803 h Still running

Other USS' engines:

P40 2 engine

800 h with PL-seals, all four seals
exchanged after 200 h. Different
performance and function tests.

P40 3 motored engine

The following runs were made:

514 h varying mean pressure, He

690 h constant " " , no capseal, He

414 h varying " " , He

1 749 h " " " , H₂

444 h " " " , H₂

1 182 h " " " , H₂

619 h " " " , H₂

A report will be issued in a short time.

P40 9 engine

About 2 400 h in total for PL-seals.

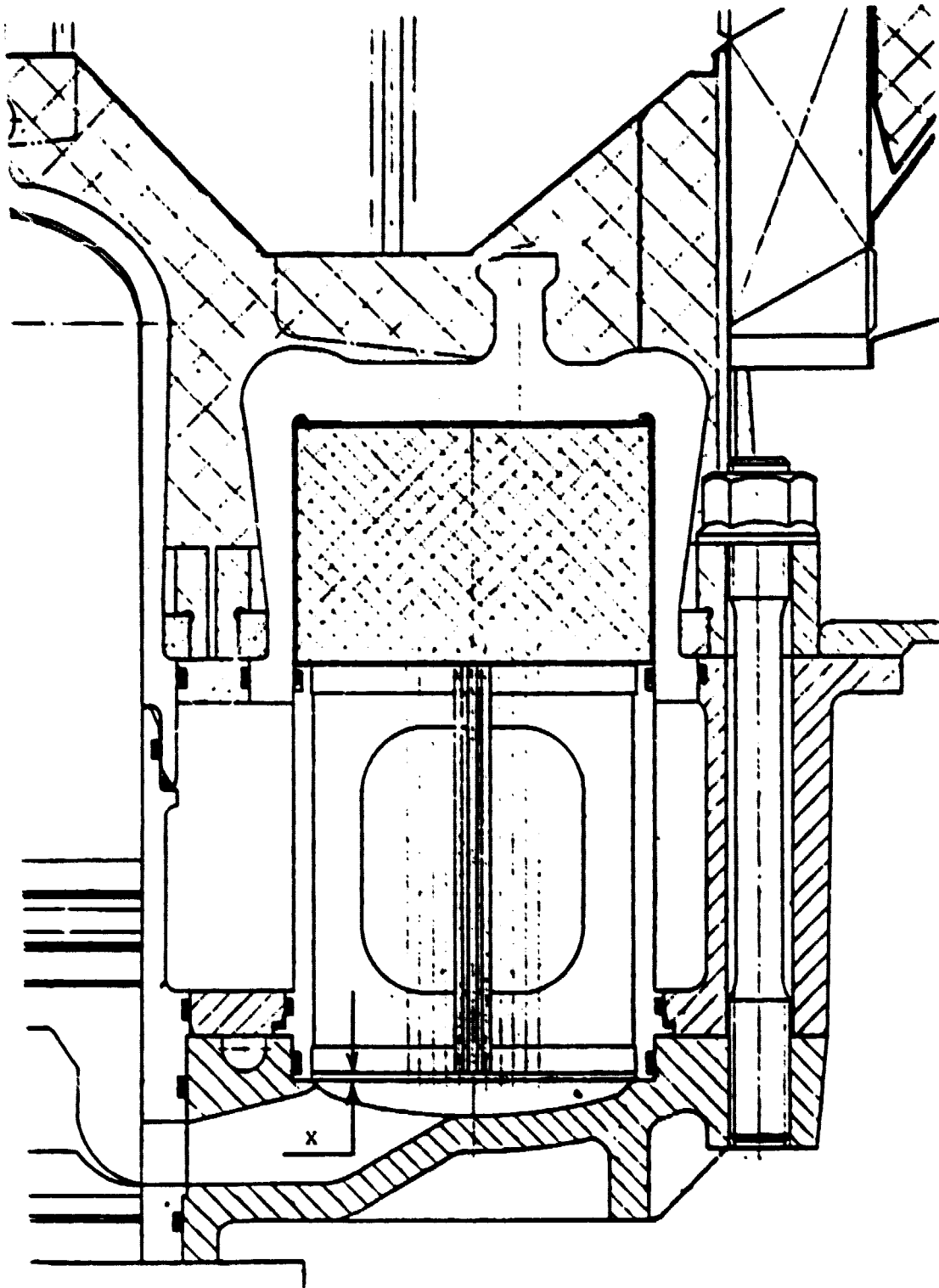
P75 2 motored engine

About 1 000 h in total for PL-seals.

Gas Cooler Flow Test

A gas flow distribution test has been performed for the cooler (P-75 unit) at two different levels in the duct plate. The depth X on the following figure, was varied (0 and 2 mm). Measured pressure drop and mass flow distributions are given in the following graphs, for both flow directions. No significant differences were found between the two X -values.

ORIGINAL PAGE IS
OF POOR QUALITY



B.7 Engine Drive System

PRECEDING PAGE BLANK NOT FILMED

7. ENGINE DRIVE SYSTEM

7.1 General description

The Crankcase assembly has been designed for low weight, low costs, small package size and for high production possibilities. The low weight requirement necessitated that aluminium be used in all major castings, and that care be taken in removing all unnecessary spare volume.

The selected Crankcase/Bedplate arrangement gives a very rigid box construction. Pre-assembled units of the oil pump/filter, water pump, intercasings/gears, and twin links with crankshafts, allow for fast production assembly.

The MOD I design will accept three forms of final drive, all gear (two forms), gear and link, and chain drive. In the event of MOD 2 being an all gear engine only, weight and overall unit length can be reduced marginally.

The engine has been designed primarily for installation in a rear wheel drive passenger car with automatic transmission, but the crankcase has been further strengthened to accept mounting for a transverse engine installation.

7.1.1 Crankshafts

Both crankshafts have been designed as nodular iron castings, giving minimum machining on pins and journals and balance weights, but for initial quantities shafts will be made from solid bar. The basic engine crankshaft form accepts an all gear drive, and a twin link arrangement. When the links are not used, balancing weights will be attached.

The diameter of the big end pin was set by bending stresses across the pin, caused by the wide main bearing centres. The main bearing diameter was governed by the high applied loads of the link drive. The crankshaft of No. 3 and 4 cylinder also contains the hydrogen pump big end pin.

7.1.2 Connecting rods - power and hydrogen pump

Both rods have a forked small end and have been designed as castings in nodular iron, with the split line on the horizontal centre line. This allows a quantity of rods to be cast as a block and then parted, which lends itself to high production.

The shank cross sectional area governs the selection of the material, as we have reduced this area for minimum weight.

7.1.3 Crankcase and bedplate

To gain maximum rigidity and strength for a U-4 type engine, a crankcase and bedplate construction was preferred to the simple low skirt crankcase with bearings caps. This allows the loads applied by the cylinder head studs to be dissipated through the side walls of the crankcase into the bedplate and main bearing studs.

The two parts have been designed for low pressure die casting, although the initial quantities will be sand cast.

7.1.4 Gears

Due to the influence of the drive systems test rig, the rear end of the engine has been designed to accept alternative gear tooth form.

1. 1.25 module (20 DP) straight spur of 33 mm face width.
2. 0.8 module (32 DP) 15 deg helix angle of 40 mm face width.

To minimise the overall length and hence weight, a high strength gear material has been chosen, case hardened and ground teeth.

As the expected power requirement of the water pump is 1 kW, the gear material of the idler and pump has been selected as Tufnol-Carp.

7.1.5 Inter casing

This major casting is mounted on the rear face of the crankcase assembly and supports the A.M.G. automatic transmission starter motor, water pump, and houses the idler gear assembly.

This casting, in aluminum, although containing one loose core, is of simple one piece pattern construction. The idler gear is mounted in an offset spindle allowing a variation of water pump speed by rotating the spindle through 180 degrees, and changing the gear wheel.

The water pump gear area, also contains the oil filler cap.

7.1.6 Water pump assembly

The assembly is spigoted into the front face of the inter casing, and can be easily fitted and removed for speed ratio change in development or maintenance.

The pump body is a simple aluminium casting, with the volute fully cast, which is closed with the fitting of the water intake pipe. The shrouded impeller, in stainless steel, is press fitted onto a central shaft. A gear adaptor flange is fitted to the rear face of the shaft to allow various speed ratios to be fitted.

To reduce overall pump length a single twin-row angular contact bearing has been used to support the impeller shaft.

7.1.7 Oil pump and oil filter

Due to overall engine height packaging limitations the oil pump has been fitted to the front face of the crankcase assembly, driven from crankshaft of No. 1 and 2 cylinder. This allows a low profile sump to be used.

The pump has been manufactured, assembled as a unit and tested by Concentric Pumps Limited. This unit is bolted to the oil filter housing and the assembly is spigoted to the crankcase.

The pump rated at 15 litres per minute, recirculates excess oil into the intake side of the rotor, thereby keeping the oil suction pipe size to a minimum.

Apart from the rotor, all housing are cast in aluminium.

The filter is designed for mounting in a horizontal position, and can be adapted for use with an oil cooler.

The oil pressure relief valve set at 0.4 MPa.

7.1.8 Link drive

The twin links connecting the crankshafts have been designed to transmit full power from one crankshaft to the other, and are mounted inside the crankcase, one each side of the centre main bearing.

To keep rotating weight of the links to a minimum, aluminum has been selected for the link centre section, and S.G. iron for the cap. The imposed stresses inside the link are too high for cast aluminum but forged aluminum is adequate. Prototype links will be hand forged, but dies would be manufactured for production engines.

The assembly will require that the links be fitted to the crankshafts before installing in the crankcase. Due to the position of the link pins, timing of the crankshafts and engine is simplified.

7.1.9 Chain drive

A four strand 7/16" Renold simplex chain (2 strands each side of the centre main bearing) has been designed into the basic engine, however to fit the assembly will require two new crankshafts.

A mounting face, for a double acting adjuster has been allowed in the design of the bedplate, but service life of the chains has been calculated at 900 hours at full engine torque reversed. This should give a chain life at normal running of 2 500 hours.

Assembly will again require that both crankshafts are assembled with the chains before fitting into the crankcase.

Each pair of sprockets has teeth staggered by $1/3$ pitch to keep noise to a minimum.

7.1.10 Supporting tests

An existing P40 United Stirling engine has been adapted as a test unit to accept alternative gear forms, with plain and rolling contact bearings, a twin link drive, a delta plate drive and a chain drive.

The engine conversion, the test rig installation and noise measuring equipment are described.

The test program started in July 1979, is progressing as planned and will be completed by March 1980. To date the noise levels of 4 different gear forms have been measured, mounted in both plain and rolling contact bearings. Gears with very small teeth (0.8 module) give the lowest noise level at speeds below 30 rev/sec, and there is little noise level difference between the plain and ball bearings for these gears. The results obtained are for comparative purposes only and cannot be related to vehicle drive-by levels.

The geared system which couples the twin crankshafts to the output or driven shaft tends to be (subjectively) the predominant noise, as the continuous combustion system and Stirling cycle gives a smoother rate of change of pressure than the internal combustion engine and therefore the Stirling engine generally is comparatively quiet.

The gear noise may be largely caused by the cyclic nature of the input load. Each crankshaft has two crankpins at 90° to each other, and the crankshafts are phased to give equal overall firing intervals. Therefore each crankshaft and gear has a driving and driven period during one revolution.

When fitted with helical gears the crankshafts and drive shaft tend to move axially with respect to each other during a cycle. There is also a separating force between mating gears.

The drive system is then a unique combination of the geometrical relationship of the gears and peculiar cyclic torque input.

Conclusions to be drawn from the results so far obtained may be summarised as:-

1. The operating condition of 6.0 MPa mean gas pressure is representative of all operating conditions. Operation at higher gas pressures affects the overall level of noise and vibration measured, but does not significantly alter the 1/3 octave frequency spectrum shape.
2. At engine speeds up to approx. 30 rev/s, the use of fine-toothed helical gears results in radiated noise levels typically 2 1/2 dBA lower than those produced by any other tested gear system.
3. For speeds between 30 and 45 rev/s, the use of straight cut spur gears gives noise levels approximately 1 1/2 dBA lower than the reference build levels.
4. Inspection of the 1/3 octave noise frequency spectra shows a peak, most likely due to a structural resonance of some form, at a frequency of 630 to 800 Hz. This peak is the controlling factor in the subjective assessment (and the A-weighted overall level) of the radiated noise.
5. Inspection of the noise and vibration signals from the accelerators have not yet been completely analysed.
6. Use of ball bearings at the drive end of the shafts gave no significant overall reduction of either the noise or the vibration levels, although

there were local variations of up to ± 3 dBA depending on engine speed and measuring positions.

7. Very initial link drive tests indicate further noise reductions.

**B.8 Ricardo Consulting Engineerings -
Engine Drive System**

RICARDO CONSULTING ENGINEERS

CLIENT United Stirling
PROJECT ASE Mod 1 Engine
JOB NO. C4813-20
CALCULATION BY DR

SECTION Gears (Water-Pump Driving)
SHEET NO. 1 OF
DATE 7 August 1979
DRAWING KEY NO. 3274-29

OBJECT To design a suitable idler gear in "Tufnol" material with tooth size
0.8 mm.

Assume most severe case is smallest idler shown on scheme 3274-29, with PDC
quoted as 59.787 mm

Rounding PCD up to 60 mm, no teeth, Z is obtained from

$$d = \frac{(Z)(0.8)}{(\cos 18.31)} = 60 \text{ mm} \quad \therefore Z = \frac{(60) \cos 18.31}{0.8} \approx 71.2.$$

Adopt 71 teeth with addendum modification

$$\frac{(71)(0.8)}{\cos 18.31} + 2 \times 0.8 = 60 \quad \therefore x = \frac{60 - 59.829}{1.6}, \approx + 0.107$$

Power to be transmitted is estimated as 1.5 hp,

$$\text{Tangential force (at 5000 rpm, crank)} = \frac{\text{Torque}(12)}{(d)}$$

$$\text{Torque} = \frac{(1.5)}{(2)} \frac{(33,000)}{(\pi) (5,000)} \approx 1.58 \text{ lb-ft} \approx 18.9 \text{ lb-in.}$$

$$d \approx 3.94^\circ (100 \text{ mm crankshaft gear}) \quad \therefore F_t \frac{(18.9)(2)}{3.94} \approx 9.60 \text{ lb, or } 4.35 \text{ kp.}$$

Bending Strength Calculation

Initial assumption for facewidth b = 16 mm

$$W_{F_t} = \frac{(4)(35)}{(16)} (1.0) (1.35) (K_{F_\alpha}) (K_{F_\beta})$$

For K_{F_α} , ϵ_α required. See Blatt 7. $u = \frac{118}{71} = 1.66.$

$$\frac{x_1 + x_2}{z_1 + z_2} = \frac{0.107 + 0.354}{71 + 118} = (2.44) (10^{-3}) \quad \therefore \alpha_{tw} \approx 21.6^\circ.$$

$$Z_v = 71 \sec^3 18.31 = 82.98 \quad \frac{\Sigma x}{\frac{1}{2} \Sigma Z} = (4.88) (10^{-3}) \therefore \alpha_{vw} \approx 20.68^\circ$$

$$\frac{d_{a2}}{d_{b2}} = \frac{101.6}{92.86} = 1.094 \quad \therefore \tan \alpha_{A2} = 0.440$$

$$l = \frac{1}{2} \{ (101.6^2 - 92.86^2)^{\frac{1}{2}} + (61.6^2 - 55.79^2)^{\frac{1}{2}} - 160.0 \sin 21.683^\circ \} \quad \left. \begin{array}{l} (\tan 20.68) (\sec 18.31) \\ = 0.3996 \\ \alpha_{vw} = 21.683 \\ \tan \alpha_{A6} = 2.66 \tan \alpha_{ew} \\ = (1.66) (0.440) \\ = 0.323 \end{array} \right\}$$

$$\frac{d_{a1}}{d_{b1}} = \frac{61.6}{55.787} = 1.1042 \quad \therefore \tan \alpha_{e1} = 0.466$$

$$l = \frac{1}{2} \{ 41.226 + 26.116 - 59.115 \} \dots = 4.114$$

$$\epsilon_a = \frac{71}{2\pi} \cdot (0.466 - 0.323) \approx 1.62 \quad \rho_o = \frac{(\pi) (0.8)}{\cos 18.31} (\cos 21.683) \approx 2.46$$

$$\epsilon_a = \frac{4.114}{2.460} \approx 1.672$$

ORIGINAL PAGE IS
OF POOR QUALITY

Bending Strength Calculation

To find K_{Fa} using DIN 3990 Blatt 4, assume quality grade of "Tufnol" gear is ISO 8.

$$\frac{F_t}{b} = \frac{4.35}{16} = 0.272. \quad \therefore q_L = 1.0.$$

$$L > \frac{1}{\epsilon_a} = \left(\frac{1}{1.672}\right) 0.598 \quad \therefore K_{Fa} = (1.0) (1.672) = 1.672.$$

\therefore Assuming $K_{F\beta} = 1.3$

$$\omega_{Ft} = \frac{4.35}{16} (1.35) (1.672) (1.3) = 0.798.$$

$$\sigma_F = \frac{0.798}{0.8} (Y_F) (Y_\epsilon) (Y_\beta)$$

Y_F from Blatt 2, with $Z = 71$, $\beta = 18.31^\circ$ and $x = 0.107$, ≈ 2.2

$$Y_\epsilon \text{ (from Blatt 3, equation (1)) } Y_\epsilon = \frac{1}{\epsilon_a} = \frac{1}{1.672}.$$

$$Y_\beta = 1 - \frac{18.31}{120} = 0.847.$$

$$\therefore \sigma_F = \left(\frac{0.798}{0.8}\right) \left(\frac{2.2 (0.847)}{1.672}\right) \approx 1.11 \text{ KP/mm}^2.$$

Limiting Bending Strength $\approx 6.0 \text{ KP/mm}^2$

(See DIN 3990 Blatt 9, p. 6)

The "safety factor" for this gear is over 5; the facewidth could therefore safely be halved.

ORIGINAL PAGE IS
OF POOR QUALITY

Surface Strength Calculation

Factored tangential force

$$W_{H_t} = \frac{4.35}{16} (1.0) (1.35) (K_{H_\alpha}) (K_{H_\beta})$$

K_{H_α} from Blatt 4, with $q_L = 1.0$

and $Z_\epsilon = 0.756$, $K_{H_\alpha} \approx 1.75$

K_{H_β} assumed = 1.3. (See figure 11, AGMA 215.01).

$$\therefore W_{H_t} = \left(\frac{4.35}{16}\right) (1.35) (1.75) (1.3) \approx 0.835.$$

$$\sigma_H = \sqrt{\left(\frac{0.835}{60}\right) \left(\frac{\frac{127}{60} + 1}{\frac{127}{60}}\right)} (Z_H) (Z_M) (Z_\epsilon)$$

$$Z_H, \text{ from Blatt 5, with } \frac{x_1 + x_2}{Z_1 + Z_2} = \frac{.107 + .354}{71 + 118} = 0.00244$$

$$Z_H \approx 1.66$$

Z_M , from Blatt 6, is 25.4 approximate.

$$\therefore \sigma_H \approx (.143) (1.66) (25.4) (0.756) \approx 4.54$$

Strength available $\approx 13 \text{ KP/mm}^2$.

"Factor of safety" = 2.86

SUMMARY SHEET

Calculations for Crankshaft Coupling Gears

Module	Number of Teeth	Helix Angle	Pitch Dia.	Facewidth	Safety Factors		Date of Calculation and Page No.
					Bending	Pitting	
m	Z	β	d	b	S_F	S_H	
0.8	118	18.31	99.474	40	1.27	1.5	2/8/79; p. 5 & 6
0.8	125	0	100.0	40	1.1	1.37	2/8/79; p. 7 & 8
1.5	66	0	99.0	40	2.0	1.61	14/8/79; p. 2 & 3
1.5	66	0	99.0	33	1.74	1.48	14/8/79; p. 2 & 3
1.25	80	0	100.0	33	1.52	1.50	14/8/79; p. 4 & 5

1-512

ORIGINAL PROPERTY
OF POOR QUALITY

GEAR SUMMARY SHEET

ALL GEARS

Module 0.8 mm

Helix Angle 18.31° (Axial Pitch 8.0 mm)

Gear	Number of Teeth	Pitch Dia.	Face - width	Material	Safety Factor		Strength Available * from Material		Stress Due to ** Applied Load	
					Bending	Contact	Bending	Contact	Bending	Contact
							(kp/mm ²)		(kp/mm ²)	
Crankshaft Coupling Gear	118	100	40	Carburized Steel, En39	1.23	1.53	45	157	36.5	103
Idler Water Pump Drive	71	60	16	'Tufnol'	5.4	2.86	6	13	1.11	4.54

*From B.I.N. 3990, Blatt 9.

**Calculated by D.I.N. 3390 method.

ORIGINAL PAGE IS
OF POOR QUALITY

RICARDO CONSULTING ENGINEERS

CLIENT United Stirling SECTION Gears (Coupling Crankshafts)
PROJECT ASE Mod 1 SHEET NO. 1 OF
JOB NO. C4814-10 DATE 14 August 1979
CALCULATION BY DR DRAWING KEY NO.

OBJECT To design spur gears to couple crankshafts.

.....
Preferred dimensions initially are:

Facewidth $b = 40$ mm, module 1.5 mm

Pitch diameter $= 99.434$ mm

Number of teeth $= \frac{99.434}{1.5} = 66.29$, say 66

Profile-shift coefficient $= \frac{(99.434 - 66.0)(1.50)}{(1.50)(2)} \approx +0.145$.

If gears without profile-shift are preferred, center distance should be 99.0 mm.

For use of calculation, assume this latter case.

Tangential force $F_t = 450 K_p$ (see Calc, 2 August 1979, sheet 3).

Bending Strength

Factored tangential force

$$W_{F_t} = \frac{450}{40} (K_o)(K_v)(K_{F_\alpha})(K_{F_\beta})$$

K_o assumed $= 1.25$

K_v assumed $= 1.35$ (AGMA 225.01, Fig. 19)

for K_{F_α} , assume accuracy grade is 6; then from Blatt 4

$$q_L \approx 0.595 \quad (q_L \approx 0.565 \text{ with } b = 33 \text{ as schematic}).$$

for contact ratio ϵ_α , $d_a = 99 + [(2)(1.50)] \approx 102.0$

$$d_b = 99 \cos 20^\circ, \approx 93.03$$

$$\therefore \text{length of contact zone, } g = (102.0^2 - 93.03^2)^{1/2} - 99.0 \sin 20^\circ = 7.97$$

ORIGINAL PAGE IS
OF POOR QUALITY

Bending Strength (module 1.5 spur)

$$\text{Base pitch, } p_o = (\pi) (1.50) (\cos 20^\circ) \approx 4.428$$

$$\therefore \epsilon_\alpha \approx \frac{7.966}{4.428}, \approx 1.799 \quad \left(\frac{1}{\epsilon_\alpha} \approx 0.556\right)$$

$$\therefore q_L > \frac{1}{\epsilon_\alpha}, \text{ and } K_{F_\alpha} = q_L \cdot \epsilon_\alpha \approx 1.07 \quad [K_{F_\alpha} = (0.565) (1.799) = 1.02] \\ \text{with } b = 33.$$

$$K_{F_\beta} \text{ assumed} = 1.3 \text{ (AGMA 225.01, figure 16).}$$

$$\therefore W_{F_t} = (11.25) (1.25) (1.35) (1.07) (1.3) \approx 26.4 \\ \approx (13.64) (1.25) (1.35) (1.02) (1.3) \approx 30.5, \text{ for } b = 33.$$

$$\sigma_F = \left(\frac{W_{F_t}}{m}\right) (Y_F) (Y_\epsilon) (Y_\beta)$$

$$Y_F \text{ from Blatt 2,} = 2.28$$

$$Y_\epsilon \text{ from Blatt 3, is } \frac{1}{\epsilon_\alpha}, = 0.556. \text{ and } Y_\beta = 1.0.$$

$$\therefore \sigma_F = \left(\frac{26.4}{1.50}\right) (2.28) (0.556) \approx 22.3 \text{ KP/mm}^2. \\ \left(\frac{30.5}{1.50}\right) (2.28) (0.556) \approx 25.8 \text{ KP/mm}^2. \text{ S.F.} = 1.74 \\ \text{for } b = 33.$$

N.B. with $b = 26$, (min. width for acceptable surface stress,
see sheet 3).

$$W_{F_t} = \left(\frac{450}{26}\right) (1.25) (1.35) (1.07) (1.3) = 40.6.$$

$$\sigma_F = \left(\frac{40.6}{1.50}\right) (2.28) (0.556) = 34.3 \text{ KP/mm}^2.$$

Safety factor, assuming CHS as gear material = $\frac{45}{34.3}, \approx 1.3.$
Acceptable.

Surface Strength (Module 1.5 spur)

Factored tangential force

$$W_{H_t} = (11.25) (K_q) (K_v) (K_{H_\alpha}) (K_{H_\beta})$$

$$K_\beta \text{ assumed} = 1.25,$$

$$K_v \text{ assumed} = 1.4 \text{ (from Figure 12 of AGMA 215.01, Curve \#2)}$$

$$K_{H_\alpha} = 1 + 2 (q_L - 0.5) \left(\frac{1}{Z_{\epsilon^2}} - 1 \right)$$

where $q_L \approx 0.595$ ($q_L = 0.565$, with $b = 33$ (from sheet 1))

and $Z_\epsilon = \sqrt{\frac{4 - \epsilon_\alpha}{3}}$, with $\epsilon_\alpha \approx 1.8$ (from sheet 2)

$$Z_{\epsilon^2} = \frac{4 - 1.8}{3} = 0.733$$

and $K_{H_\alpha} = 1 + (2) (0.095) \left(\frac{1}{0.73} - 1 \right) \approx 1.07$. $1 + (2) (0.065) \left(\frac{1}{0.73} - 1 \right) \approx 1.05$ for $b = 33$.

$$K_{H_\beta} \text{ assumed} = 1.3.$$

$$\therefore W_{H_t} = \frac{(13.64) (1.25) (1.4) (1.05) (1.3)}{(11.25) (1.25) (1.4) (1.07) (1.3)} \approx \frac{32.58 \text{ KP/mm}^2}{27.36 \text{ KP/mm}}$$

or

$$(15.0) (1.25) (1.4) (1.07) (1.3) \approx 36.51, \text{ with } b = 30, \text{ for comparison P-20.}$$

$$\therefore \sigma_H = \sqrt{\left(\frac{27.36}{99}\right)^2} (Z_H) (Z_M) (Z_\epsilon); \sqrt{\left(\frac{32.58}{99}\right)^2} (Z_H) (Z_M) (Z_\epsilon), \text{ for } b = 33$$

$$Z_H \approx 1.765, \text{ from Blatt 5, with } \beta = 0, \frac{x_1 + x_2}{Z_1 + Z_2} = 0$$

$$Z_M \approx 85.7, \text{ from Blatt 6, for steel/steel}$$

$$Z_\epsilon \approx \sqrt{0.733}, \approx 0.856, \text{ see above (in calculation for } K_{H_\alpha} \text{.)}$$

$$(0.811) (1.765) (85.7) (0.856) \approx 105 \text{ KP/mm}^2, \text{ for } b = 33.$$

$$\therefore \sigma_H \approx (0.743) (1.765) (85.7) (0.856) \approx 96.3 \text{ KP/mm}^2.$$

$$(0.859) (1.765) (85.7) (0.856) \approx 111.2 \text{ KP/mm}^2.$$

Using CHS as gear material, surface strength available $\approx 155 \text{ KP/mm}^2$.

$$\therefore \text{Safety factor} = (1.61) \left(\frac{155}{105} \right) = 1.48 \text{ for } b = 33$$

If S.F. 1.3 acceptable, facewidth can be reduced to b.

$$\sqrt{\frac{450}{b} (1.25) (1.4) (1.07) (1.3) \left(\frac{2}{99} \right)} (1.765) (85.7) (0.856) = 155/1.3$$

$$\therefore \sqrt{\frac{22.13}{b}} (129.48) = 119.2 \quad \therefore b \approx 26 \text{ mm.}$$

ORIGINAL PAGE IS
OF POOR QUALITY

Calculation for Spur Gears with A-25 Module

(Preceding calculations show that an adequate safety factor is attainable with facewidth of only 26 mm, using module 1.50. Since the design allows facewidth 33 mm, it appears useful to assess strength of smaller tooth size, which is expected to be quieter in running.)

Assuming $Z = 80$ teeth, $a = 100$ mm.

Bending Strength

Factored tangential force, $W_{F_t} = \left(\frac{450}{33}\right) (K_I) (K_v) (K_{F_\alpha}) (K_{F_\beta})$

Assumed $K_I = 1.25$, $K_v = 1.35$, $K_{F_\beta} = 1.3$

Calculation for K_{F_α} for contact ratio ϵ_α , $d = 100$, $d_a = 102.5$, $d_b = 93.97$.

$$q_\alpha = (102.5^2 - 93.97^2)^{1/2} - 100.0 \sin 20^\circ, \approx 40.94 - 34.20 = 6.74$$

$$\phi_o = (1.25) (\pi) (\cos 20^\circ) = 3.69 \quad \therefore \epsilon_\alpha \approx 1.826; \frac{1}{\epsilon_\alpha} \approx 0.548, = Y_\epsilon$$

Assuming accuracy grade 6, $q_L = 0.555$ (Blatt 4)

$$\therefore q_L > \frac{1}{\epsilon_\alpha}, \quad \therefore K_{F_\alpha} = (0.555) (1.826) \approx 1.013.$$

$$\therefore W_{F_t} \approx (13.64) (1.25) (1.35) (1.01) (1.3) \approx 30.21.$$

$$\sigma_F = \left(\frac{W_{F_t}}{m}\right) (Y_F) (Y_\epsilon) (Y_F) \approx 2.24 \text{ (from Blatt 2)}$$

$$\therefore \sigma_F = \left(\frac{30.21}{1.25}\right) (2.24) (0.548) \approx 29.7 \text{ KP/mm}^2.$$

Assuming carburized En39 as material, and taking strength (bending) at 45 KP/mm²

Safety factor ≈ 1.52

Quite satisfactory

Calculation for Spur Gears with 1.25 Module

Surface Durability

$$\text{Factored tangential force } W_{H_t} = \left(\frac{450}{33}\right) (K_I) (K_V) (K_{H_\alpha}) (K_{H_\beta})$$

$$\text{Assumed } K_I = 1.25, \quad K_V = 1.4, \quad K_{H_\beta} = 1.3.$$

$$K_{H_\alpha} = 1 + 2 (q_L - 0.50) \cdot \left(\frac{1}{Z_e^2} - 1 \right)$$

$$\text{where } q_L \approx 0.555, \quad Z_e = \sqrt{\frac{4 - 1.826}{3}} = 0.851. \quad Z_e^2 = 0.7247.$$

$$\therefore K_{H_\alpha} = 1 + 2 (0.055) (0.3799) \approx 1.04$$

$$\therefore W_{H_t} = (13.64) (1.25) (1.4) (1.04) (1.3) = 32.27.$$

$$\sigma_H = \sqrt{\left(\frac{32.27}{100}\right) (2) (Z_u) (Z_m)}; (Z_e \approx 0.851).$$

$$Z_H, \text{ from Blatt 5, is } 1.765$$

$$Z_M, \text{ from Blatt 6, is } 85.7 \text{ (steel/steel)}$$

$$\therefore \sigma_H = (0.803) (1.765) (85.7) (0.851) = \text{KP/mm}^2 = 103.4$$

Assuming carburized En39 as material and taking allowable surface strength = 155 KP/mm^2

Safety factor = 1.50.

Quite satisfactory.

RICARDO CONSULTING ENGINEERS

CLIENT United Stirling SECTION Bolts, Connecting Rod
PROJECT ASE Mod I Engine SHEET NO. 1 OF
JOB NO. C4814-10 DATE 8 August 1979
CALCULATION BY DR DRAWING KEY NO. 3274-102

OBJECT To check strength of connecting rod big-end bolts relative to working forces and recommend a stretch-figure and a torque load for tightening

Screw thread M9 x 1.25. Tensile stress area = 48 mm^2
Minimum shank diameter = 8.05 mm. Cross section area = 50.9 mm^2
Undercut below bolt head, ϕ 7.85 minimum. Cross section area = 48.4 mm^2
Steel grade 10.9. Stress due to "proof load" = 79.2 kp/mm^2
Assume bolt tensioned to 70% of proof load
Preload = $79.2 \times 48.0 \times 0.70 = 266.1 \text{ kp}$ 6653 Maximum
Total clamping force = 5322 kp 3992 Minimum

Force required to keep joint closed

Bearing shell interference fit

Assume thickness = 1.75 mm (total); 1.5 mm, steel backing compressive stress
 $22. \text{kp/mm}^2$, width 20 mm

Total force required to fit bearing shell in housing bore

$$= 22 \times 1.50 \times 20 \times 2 = 1320 \text{ kp}$$

Total (cylinder pressure - inertia) force acting on connecting rod

$$= 12,523 \text{ N (from sheet 5 of calculation dated 29-3-79, by LT)} \approx 1277 \text{ kp}$$

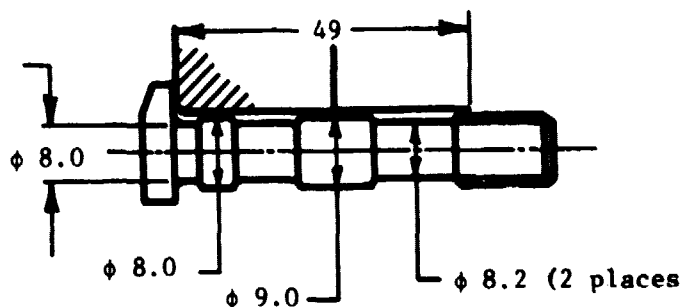
$$\therefore \text{"Cover" factor} = \frac{5322 - 1320}{1277} \approx 3.13.$$

Torque load for tensioning

$$T = \frac{2661 \times 9}{5000} \text{ kp-m} = 4.8 \text{ kpm (47 Nm, 35 lbf-ft)}$$

Elastic extension for bolt tensioning

ORIGINAL PAGE IS
OF POOR QUALITY



Length at	2.0	4.0	16.0 + 12.0	10.0
Diameter	8.0	9.02	8.2	9.0

Servo thread D min.
("Tensile-stress area" = 48 mm²)

Adding flexibilities for shank part of bolt.

$$\Sigma F = \frac{1}{21,000} \cdot \left\{ \frac{2.0}{8.0^2} + \frac{4.0}{9.02^2} + \frac{28.0}{8.2^2} + \frac{10.0}{9.0^2} \right\} \cdot \frac{1}{.785} \approx 0.376 \times 10^{-4}$$

Add further allowances for (i) the deflection of the bolt head, and (ii) relative deflection of screw threads in engagement in nut and bolt.

- (i) Assume deflection is approximately the same as for a further length of shank equal to half the shank diameter.

$$\Delta_F \text{ Head} = \left(\frac{1}{21,000} \right) (9.0^2) (7854) (9.0) \left(\frac{1}{2} \right) \approx 0.0371 \times 10^{-4}$$

- (ii) Assume deflection is approximately the same as an additional length of nonengaged screw thread equal in length to half the minor diameter.

$$\Delta_F \text{ Screw} = \left(\frac{1}{21,000} \right) (7.47) \left(\frac{1}{2} \right) = 0.0371 \times 10^{-4}$$

$$\therefore \text{Total flexibility of whole bolt} \approx (0.376 + 0.034 + 0.037) 10^{-4} \approx 0.447 \times 10^{-4}$$

Stiffness (spring rate) of whole bolt = 2.24×10^4 kp/mm.

Elastic extension of bolt required to induce "proof load" into bolt,

$$\Delta_l = \frac{\text{Proof Load}}{\text{Stiffness}} = \frac{(48) (79.2)}{2.24 \times 10^4} \approx 0.170 \text{ mm.}$$

To provide a safety margin against overstressing of the bolt, specify bolt preload = 0.85 x proof load.

∴ Required elastic extension = 0.144 mm. (\approx 0.0057 in.)

Nominal tightening torque required = $\left(\frac{9}{5}\right)$ (79.2) (48) (.85) = 5.82 kp-m.

Alternatively, bolt stretch to give 70% proof load
(nominal tightening torque 4.7 kp-in.)

$$.0144 \left(\frac{.7}{.85}\right) \approx 0.110 \text{ mm (0.0046 in.)}.$$

ORIGINAL PAGE IS
OF POOR QUALITY

RICARDO CONSULTING ENGINEERS

CLIENT United Stirling
PROJECT ASE Mod 1
JOB NO. C4813-10
CALCULATION BY

SECTION
SHEET NO. 1 OF 1
DATE 22 June 79
DRAWING KEY NO.

OBJECT Traction torque capacity of drive shaft rear end to transmit 20 hp.
.....

Assume hp to range from 10 to 15.

20 hp used for maximum possible

Diameter of joint face = 36 O.D. to 12 I.D.

Bolts - mm6 x grade 12/9 Cap bolts - UNBRAKO

Recommended pretension = 70% of 1.910 per bolt

$$= 4 \times .7 \times 1.910 = 5348 \text{ kg}$$

$$\text{Friction torque} = (0.15) (5348) \left(\frac{18 + 6}{2} \right) / 1,000 = 9.6264 \text{ kpm}$$

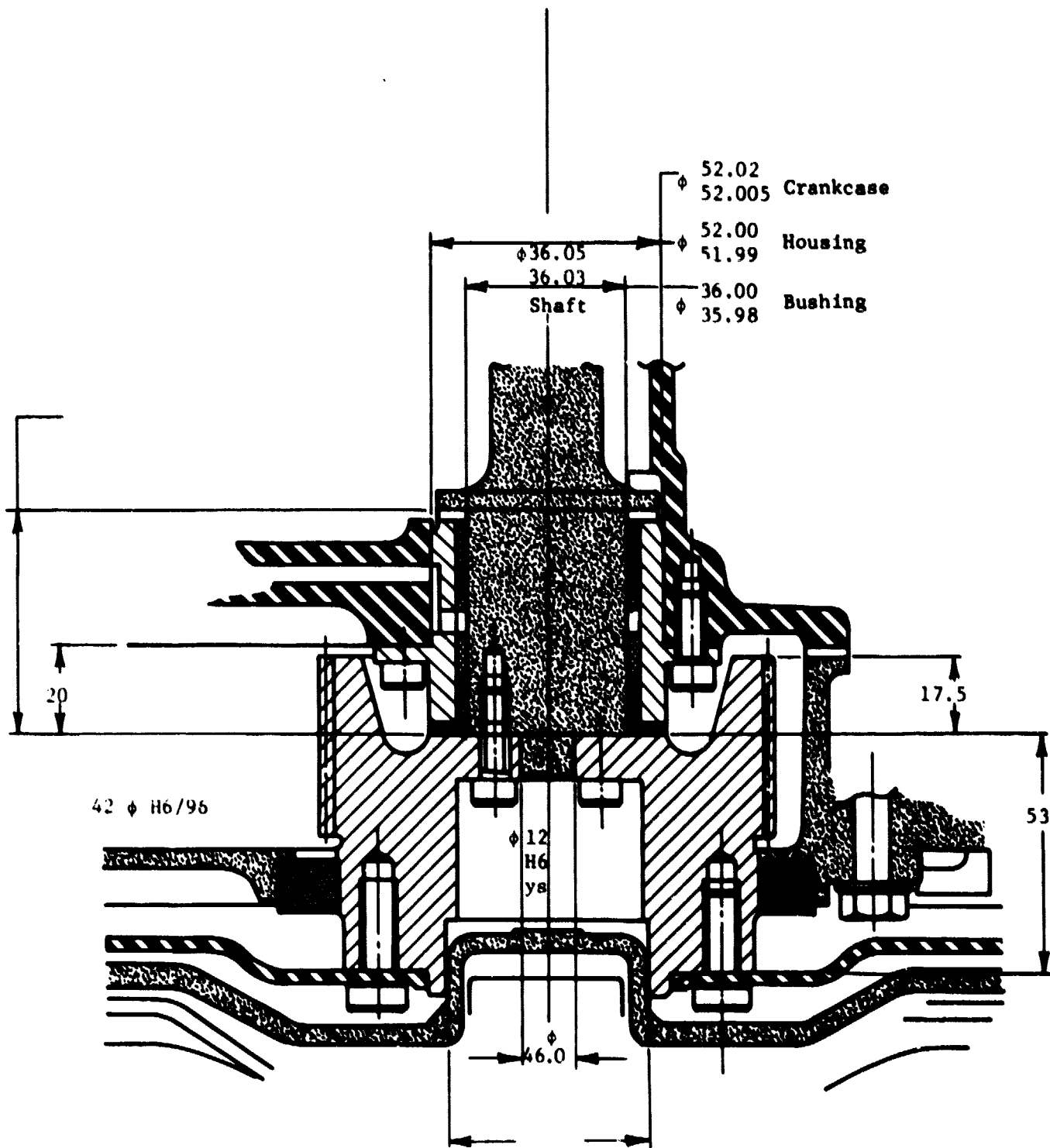
$$\text{Torque applied from 20 hp: } \frac{(20) (33,000)}{(2) (4000)} = 26.26 \text{ lb ft}$$

$$= 36 \text{ kgm}$$

$$= 3.62 \text{ kpm}$$

$$\therefore \text{Cover factor} = 2.66:1$$

ORIGINAL PAGE IS
OF POOR QUALITY



RICARDO CONSULTING ENGINEERS

CLIENT	United Stirling	SECTION	Connecting Rod Shank Stress
PROJECT	MTI/NASA: ASE Mod 1	SHEET NO.	1 OF
JOB NO.		DATE	29-3-79
CALCULATION BY	R. Thorpe	DRAWING KEY NO.	3274

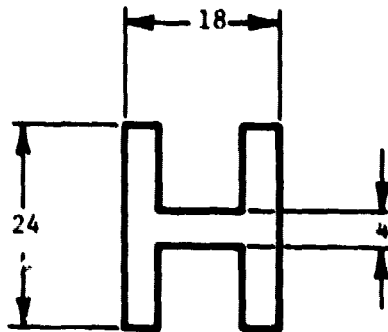
OBJECT To determine shank stress in connecting rod and plot results on a
goodman diagram

68 mm Bore x 34 mm Stroke

Ref Drawing No. 3274/16 and 3274/101.

The shank of the connecting rod is subjected to tensile and compressive stresses due to both inertia and gas forces (ref calculations dated 29-3-79 "Torque Diagram"). The gas loads are independant of speed and exceed the inertia forces at the envisaged over-run speed (5000 rev/min - VCHP) in both senses. As the inertia forces always oppose the gas loads and will be negligible at the lowest operating speed (600 rev/mim) in comparison to the gas loads, they are ignored. The forces are therefore 15424 N tensile and 23346 N compressive.

Con Rod Shank Ref DRG No. 3274/101



Cross Sectional Area

$$csa = (18 \times 24) - (10 \times 20) = \underline{232 \text{ mm}^2}$$

Maximum tensile stress

$$\text{force} = 15424 \text{ N} = 1572 \text{ kg.}$$

$$\sigma = \frac{1572}{232} = \underline{6.777 \text{ kg/mm}^2}.$$

Maximum compressive stress

$$\text{force} = \frac{24000}{232} = \underline{10.545 \text{ kg/mm}^2}.$$

Maximum Stress Range = $10.5 + 6.7 = 17.2 \text{ kgf/mm}^2$

Permissible Stress Range = $11.24 \times 2 = 22.48 \text{ kgf/mm}^2$.

for SNG 37/2.

\therefore reverse factor = $\frac{22.48}{17.2} = \underline{\underline{1.31}}$.

\therefore if the gas forces are increased by 18% the stresses will still be within safe limits.

Goodman Diagram Fatigue Limits.

Material: Nodular iron	SNG 37/2	SNG 42/2
UTS (tonf/in ²)	37	42
UTS (kgf/mm ²)	58.27	66.14
Fatigue limit (Wöhler) (tonf/in ²)	15.7	17.0
Fatigue limit (Wöhler) (kgf/mm ²)	24.72	26.77

Ref: BCIRA Engineering Data on Cast Iron.

Design limit

For a forged steel connecting rod the safe limit for alternating stress is + 25% of the UTS (ref. Designers Viewpoint). For a typical steel, the Wöhler fatigue limit will be + 55% of the UTS. This represents a safety factor of

$$\frac{55}{25} = 2.2.$$

Therefore design limit = $\pm 11.24 \text{ kg/mm}^2$ and $\pm 12.17 \text{ kg/m}$
for SNG 37/2 and SNG 42/2 respectively.

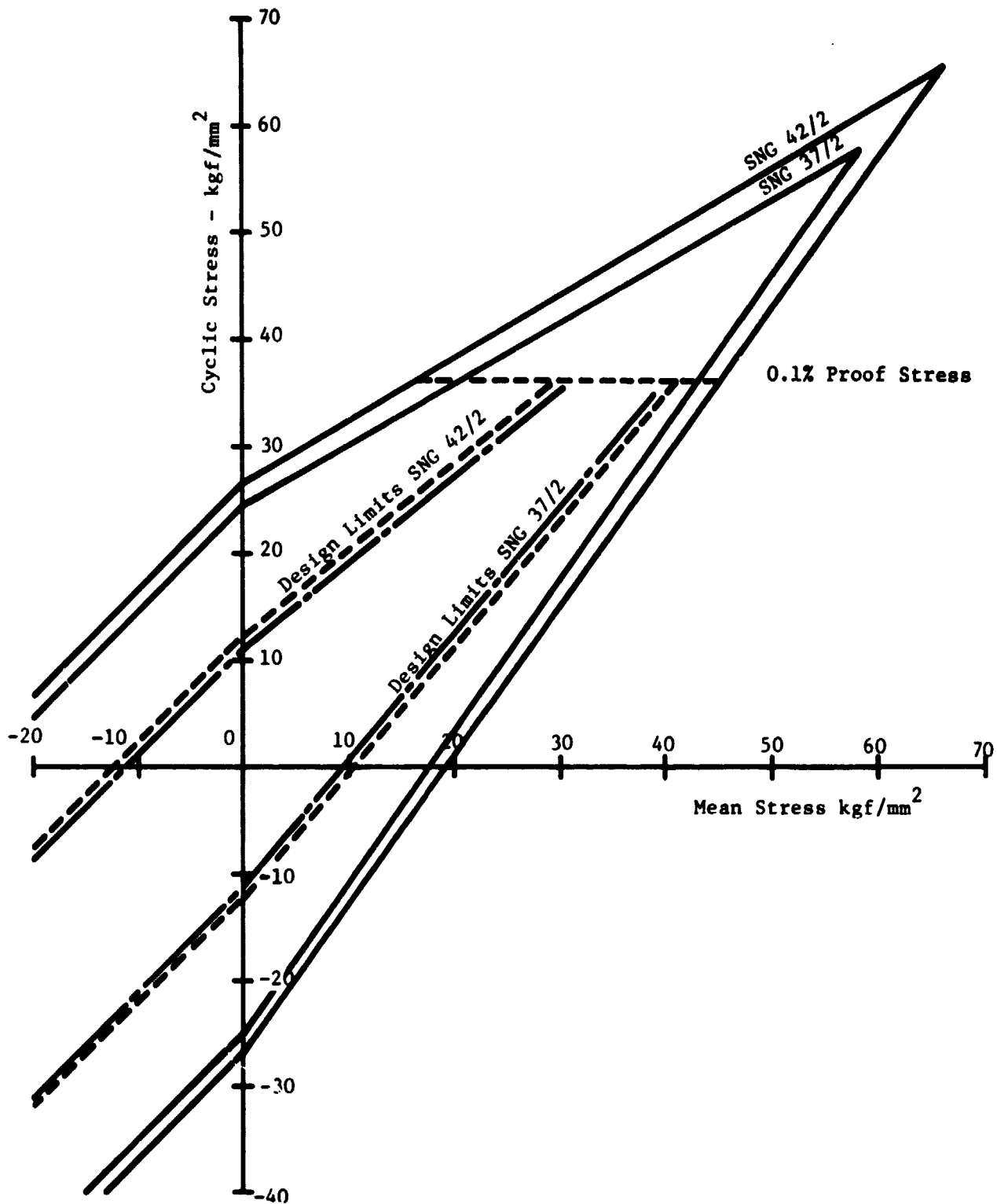
ORIGINAL PAGE 13
OF POOR QUALITY

United Stirling: MTI/NASA Project

ASE Mod I Engine 68 mm Bore x 34 mm Stroke

Goodman Fatigue Diagram for Connecting Rod Shank Stress

Material: Nodular Iron



RICARDO CONSULTING ENGINEERS

CLIENT	United Stirling	SECTION	Connecting Links
PROJECT	MTI/NASA Project	SHEET NO.	1 OF
JOB NO.	C4813-10	DATE	2-4-79
CALCULATION BY	R. Thorpe	DRAWING KEY NO.	

OBJECT To estimate required cross sectional area of links connecting crankshafts (Aluminium or SG Iron)

68 Bore x 34 Stroke

SUMMARY

The crankshafts of the ASE Mod 1 engine are to be coupled by two links mounted on eccentrics on the crankshafts spaced at 90°. The loads in the links have been estimated by scaling the forces in a similar arrangement on the P40 engine. In the present calculations, the instantaneous torques have been calculated for the Mod 1 engine using figures supplied by U.S. for the gas forces and compared with the scaled values for the P40. Excellent correlation between the two torque diagrams exists, and therefore the scaled value of link loads have been accepted without further calculation. The required CSA of the connecting rod shank has been estimated for forged aluminium and for SG iron (SNG 37/2).

These are: 5 cm² Forged Alum BS1472 HF15WP
and 2.44 cm² SG Iron SNG 37/2.

ORIGINAL PAGE IS
OF POOR QUALITY

ORIGINAL PAGE IS
OF POOR QUALITY

Forged Aluminium Data Ref: Hiduminium Technical Data P77-82.

Hiduminium 66 (B.S. 1472 HF15WP).

UTS = $29 \text{ tonf/in}^2 = 45.7 \text{ kgf/mm}^2$ (little change at sump temperature).

.1% proof stress = $25 \text{ tonf/in}^2 = 39.5 \text{ kgf/mm}^2$.

E = $10.7 \times 10^6 \text{ lbf/in}^2$.

Mechanical
Data

Fatigue Strength Semi-Stress Range

10^6	10^7	10^8	cycles
14	11.5	10	20°C
13	10.5	8.5	100°C
11.5	8.5	7.5	150°C
10.5	8.0	6.0	200°C

Sump Temperature
Say 120°C

Fatigue
Data

Goodman Diagram Limits

UTS = $29 \text{ tonf/in}^2 = 45 \text{ kg/mm}^2$

Fatigue Limit = $\pm 75 \text{ tonf/in}^2 = \pm 12 \text{ kg/mm}^2$

Safety Factor = 2.2

Working Stress Limit = $\pm 5.5 \text{ kg/mm}^2$

Reserve Factor = 1.5

Initial Design Stress Range = $\pm 3.6 \text{ kg/mm}^2$

Link Loads (Link No. 2 - worst case).

P-40 x 1.3 = + 14720 x 1.3 - 12870 x 1.3 = + 19140 N - 16730 N

Load Range = 19140 - (- 16730) = 35870 N

Load Semi-Range = $\pm 17935 \text{ N}$

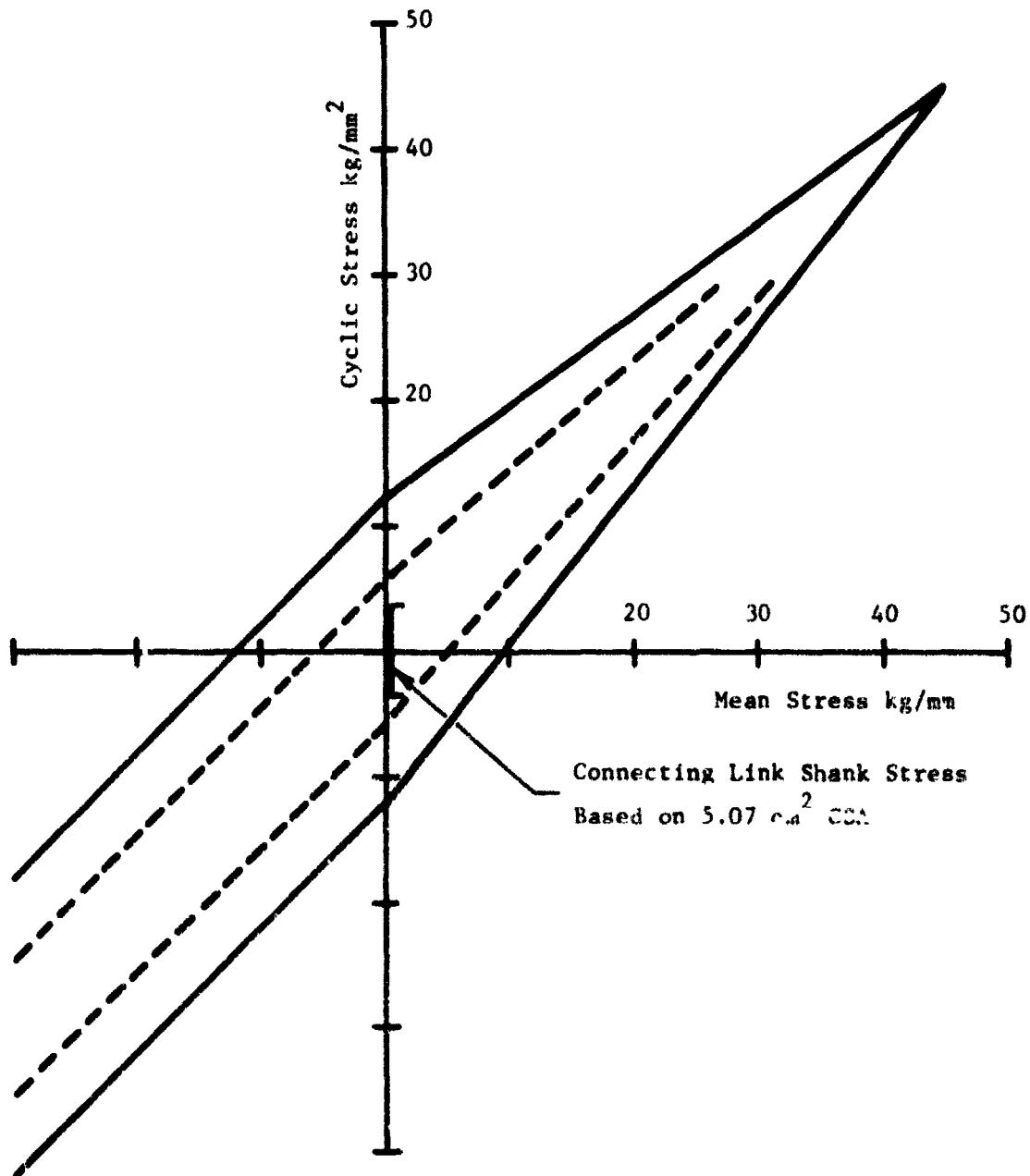
Required Cross Sectional Area = $\frac{17935 \times 10^{-2}}{3.6 \times 9.81} = \underline{\underline{5.07 \text{ cm}^2}}$

United Stirling MTI/NASA Project

ASE Mod 1 Engine 68 mm Bore x 34 mm Stroke

Goodman Fatigue Diagram for Connecting Link Shank Stress

Forged Aluminium: BS 1472 HF15WP



RICARDO CONSULTING ENGINEERS

CLIENT United Stirling
PROJECT ASE Mod I Engine
JOB NO.
CALCULATION BY DR

SECTION Crankshaft/Piston
SHEET NO. 1 OF
DATE 20 July 1979
DRAWING KEY NO. 3274-25

OBJECT Gudgeon pin ovalization.

$$\text{Wall thickness } t = 3 \sqrt{\frac{0.041 D^2 P d^3}{L E \gamma}}$$

D = Piston diameter = $\phi 62 = \phi 2.441$ in.

P = P_{max}

d = gudgeon pin diameter = $\phi 20 = .787$ in.

L = pin length = 36 mm = 1.4173

E = Young's modulus = 30×10^6 lb/in.²

γ = deflection = .0009 in. max.

From U.S.S. computer print out $F_{\text{max}} = 23346$ N.

$F_{\text{max}} = 2379.8$ kgf.

$$\text{Pressure} = \frac{2379.8}{(3.1)^2} = 78.886 \text{ kg/in.}^2 = 1121.4 \text{ psi}$$

$$t^3 = \frac{(.041) (2.441)^2 (1121.4) (.787)^3}{(1.4173) (30) (10^6) \gamma}$$

$$t^3 \gamma = 3.141 \times 10^{-6}$$

For $\gamma = 10009$ in. $\rightarrow t = .152$ in. = 3.85 mm

For 5.00 in. wall $\rightarrow \gamma = .00041$ in.

For 4.50 in. wall $\rightarrow \gamma = .00057$ in.

For 4.00 in. wall $\rightarrow \gamma = .00080$ in.

RICARDO CONSULTING ENGINEERS

CLIENT	United Stirling	Hydrogen Pump
PROJECT	ASE Mod I	SECTION Gudgeon Pin Ovalization
JOB NO.	C4813-15	SHEET NO. 1 OF 1
CALCULATION BY	RSW	DATE 20 July 79
		DRAWING KEY NO. 3271-32

OBJECT To calculate ovalization on gudgeon pin (hydrogen pump)

Using Ricardo formula for wall thickness of pin.

$$t = 3 \frac{(0.041) D^2 p d^3}{L E \gamma}$$

where

D^2 = Piston diameter = 46 mm = 1.811 in.

p = P_{max} - see below

d = gudgeon pin diameter = 15 mm = 0.59 in.

L = gudgeon pin length = 30 mm = 1.181 in.

E = 30×10^6 lb/in.²

γ = 0.0009

Using 60% of P40, max force = $0.6 \times 1556 = 934$ kg.

$$\therefore \text{Pressure} = \frac{(9.34) (4)}{(4.62) (\pi)} = 56.20 \text{ kg/cm}^2$$

$$= 799.34 \text{ lb/in.}^2$$

$$\therefore t = 3 \frac{(0.041) (1.811^2) (799.34) (0.59^3)}{(1.181) (30) (10^6) (0.0009)} = 0.0885 \text{ in.} = 2.25 \text{ mm}$$

say 2.5 mm \therefore Pin = 15 mm O/D, 10 mm I/D.

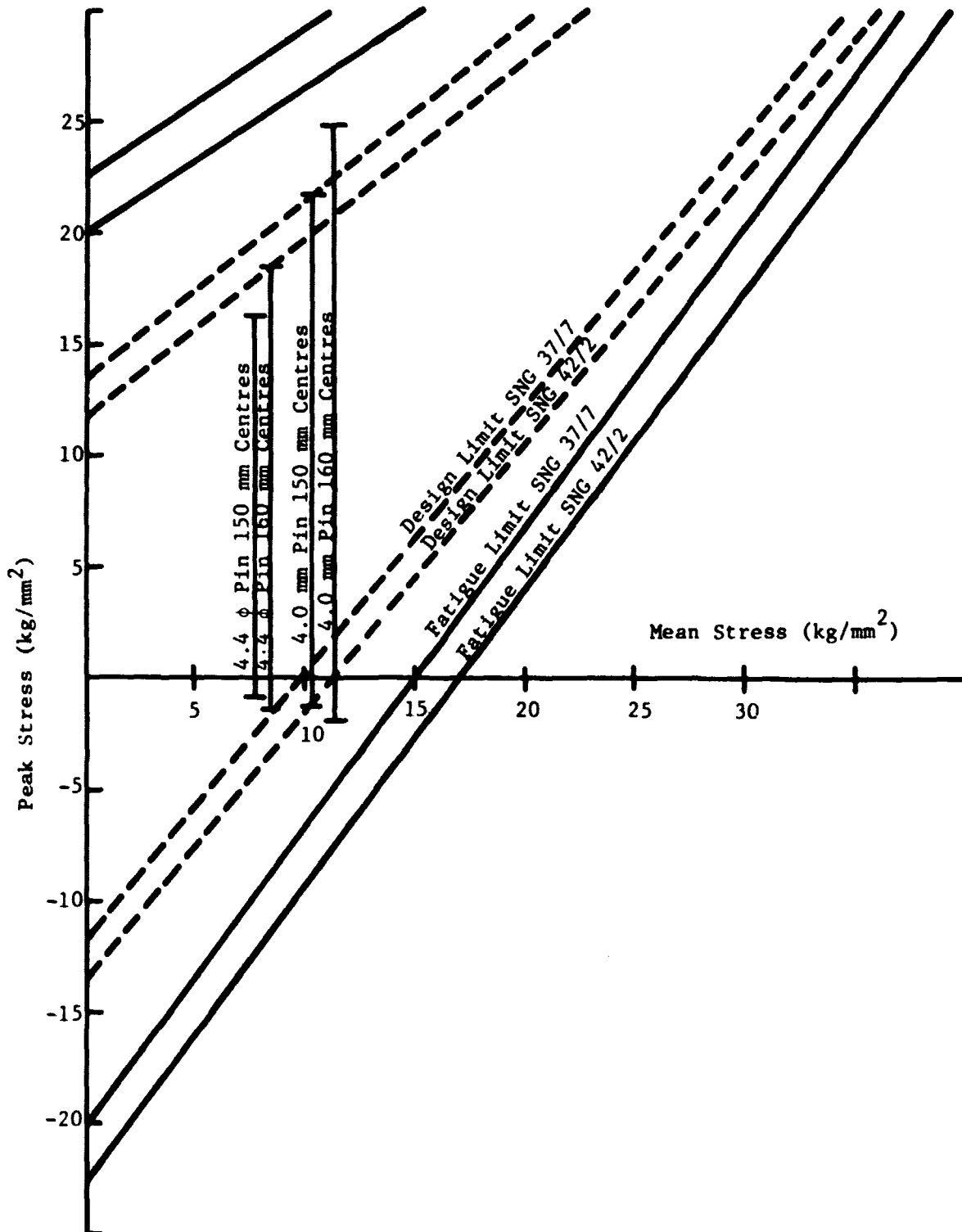
ORIGINAL PAGE IS
OF POOR QUALITY

ORIGINAL PAGE IS
OF POOR QUALITY

United Stirling AP-80 Square-4 Engine

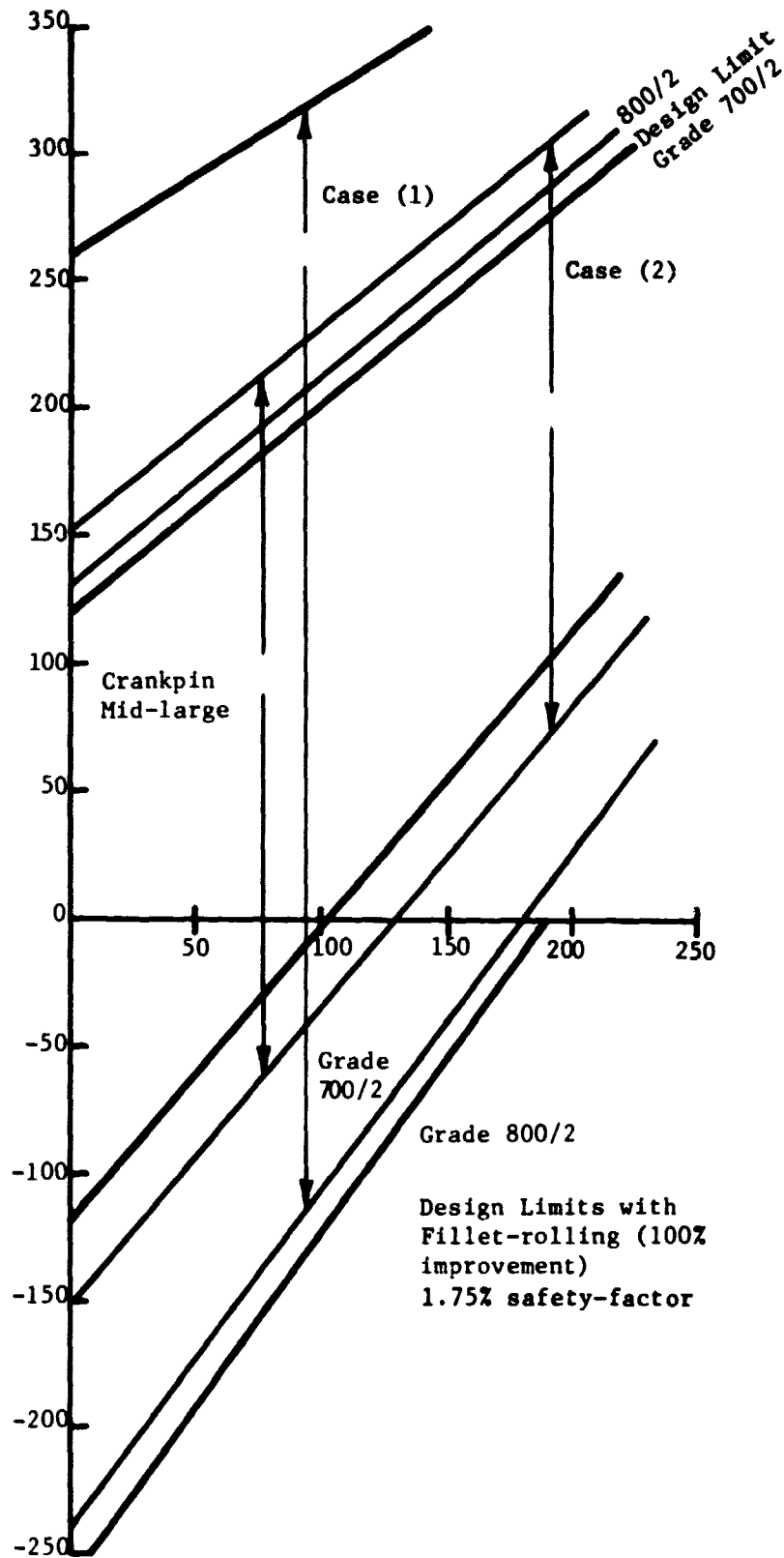
Modified Goodman Diagram Showing Crankpin

Bending Stresses for Alternative Pin Diameters and Cylinder Spacings



United Stirling Mod 1 Engine
(ϕ 68 x 34, with ϕ 42 Crankpin, Scheme 3274-21)
Stresses at Crankpin/Eccentric Pin Junction, (No.1)
(Combined bending and torsion)

N.B. Case(1) Based on Forces Acting at 45° and 135° Crank Rotation;
Case(2) Based on Forces Acting at 45° and 225° Crank Rotation.



RICARDO CONSULTING ENGINEERS

ORIGINAL PAGE IS
OF POOR QUALITY

CLIENT United Stirling

SECTION Main Bearing Bolts

PROJECT ASE Mod I Engine

SHEET NO. 1 OF

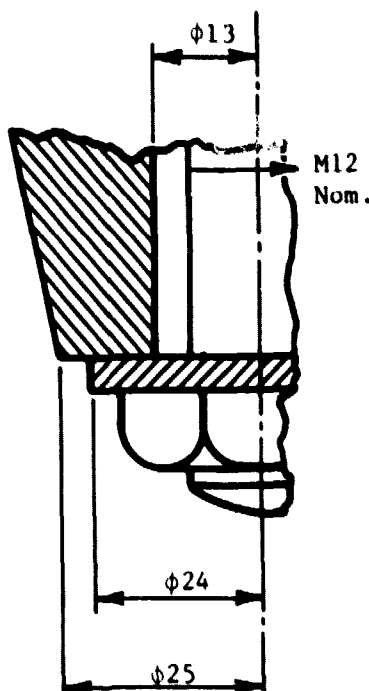
JOB NO. C4813-10

DATE 25 October 1979

CALCULATION BY IDJ

DRAWING KEY NO.

OBJECT To determine whether the main bearing bolt washer will "bed" into
aluminum alloy boss.



Washer area under head = $\frac{17}{4} (24^2 - 13^2) = 319.6 \text{ mm}^2$, for a M12 bolt grade 10.9.
Proof load = 6680 kgf.

70% proof load = 4676 kgf.

This is a stress of $14.63 \text{ kgf/mm}^2 = 143.53 \text{ N/mm}^2$.

For LM21 the limiting surface pressure = 180 N/mm^2 for manual tightening ASE
Mod I crankcase EN 25 TF.

Therefore probably satisfactory although not a large difference in limiting and
actual values. If limiting pressure 120 N/mm^2 then could have problems. PROBLEM -
no exact data on EN 25 TF.

Considering thermal expansion - 84.2% proofload = 5623 kgf gives stress of 172.6 N/mm^2 .

For LM 21 - limiting surface pressure = 180 N/mm^2 .

No figures for LM 25 TF but considering the compressive strength of each material -

LM 21 - 150 N/mm^2

LM 25 TF - 230 N/mm^2

Take limiting surface pressure increasing in proportion to compressive strength.

$$\therefore \text{L.S. Pressure for LM 25 TF} = \frac{230}{150} \times 180 = 276 \text{ N/mm}^2.$$

This is in excess of 172.6 N/mm^2 . The maximum calculated surface pressure (with thermal expansion).

RICARDO CONSULTING ENGINEERS

ORIGINAL PAGE IS
OF POOR QUALITY

CLIENT United Stirling
PROJECT ASE Mod I Engine
JOB NO. C4813-10
CALCULATION BY IDJ

SECTION Main Bearing Bolts
SHEET NO. 1 OF
DATE 26 October 1979
DRAWING KEY NO.

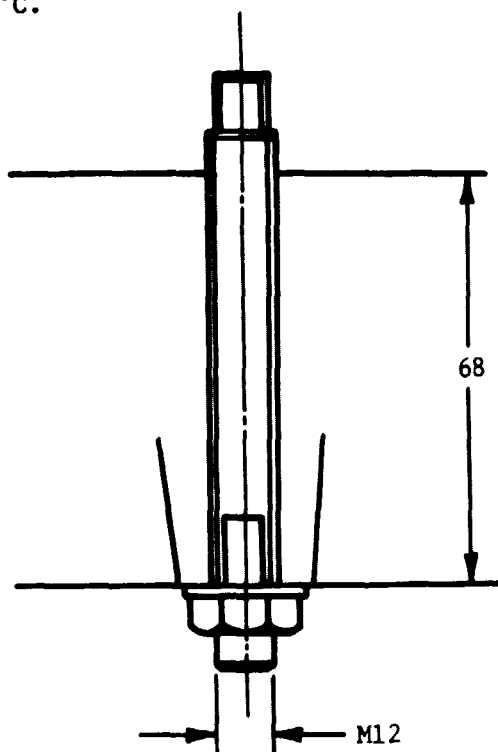
OBJECT To determine the increase in loading of the bolt due to thermal expansion.

At present bolt load is 70% of proofload.

For M12 bolt grade 10.9. Proofload = 6680 kgf.

70% proofload = 4676 kgf.

Take ambient temperature of 10°C and maximum temperature of 80°C, hence temperature increase of 70°C.



Increase in length due to thermal expansion $\delta L = \alpha L t$,

$$\left. \begin{aligned} \delta L_a &= (22.4)(10^{-6})(68)(70) = 0.107 \text{ mm} \\ \delta L_s &= (11.4)(10^{-6})(68)(70) = 0.054 \text{ mm} \end{aligned} \right\} .053 \text{ mm differential expansion}$$

ORIGINAL PAGE IS
OF POOR QUALITY

$$E = \frac{\sigma}{\epsilon} = \frac{F}{A} \cdot \frac{L}{e}$$

$$\therefore F = E \cdot A \cdot \frac{e}{L}$$

Since force in aluminum boss = force in steel bolt then:

$$\frac{E_s A_s e_s}{L} = \frac{E_a A_a e_a}{L}$$

$$\therefore E_s A_s e_s = E_a A_a e_a$$

$$\textcircled{1} \quad \therefore e_a = \frac{E_s A_s}{E_a A_a} \cdot e_s$$

Compressive deflection of boss + elongation of bolt = .053

$$\therefore e_a + e_s = .053$$

$$\textcircled{2} \quad \therefore e_s = .053 - e_a$$

Substitute equation 2 in 1

$$\therefore e_a = \frac{E_s A_s}{E_a A_a} (.053 - e_a)$$

$$\therefore e_a = .053 \frac{E_s A_s}{E_a A_a} - \frac{E_s A_s}{E_a A_a} e_a$$

$$\therefore e_a = .053 \frac{E_s A_s}{E_a A_a} \left/ \left(1 + \frac{E_s A_s}{E_a A_a} \right) \right.$$

$$\frac{E_s}{E_a} = 3 \quad \begin{array}{l} A_s = 113.1 \text{ mm}^2 \\ A_a = 319.6 \text{ mm}^2 \end{array}$$

$$\therefore \frac{E_s \cdot A_s}{E_a \cdot A_a} = 3 \cdot \frac{113.1}{319.6} = .942$$

$$\therefore = \frac{.0499}{1.942} = .026 \text{ mm}$$

$$\therefore e_s = .027 \text{ mm}$$

ORIGINAL PAGE IS
OF POOR QUALITY

$$\text{Since } F = E_s \cdot A_s \cdot \frac{e_s}{L_s}$$

$$\text{Then } F = (21,088)(113.1)\left(\frac{.027}{68}\right) = 947 \text{ kgf.}$$

Additional load in bolt due to thermal effects

$$= 947 \text{ kgf.}$$

$$70\% \text{ proofload (cold)} = 4676 \text{ kgf}$$

$$\text{Additional load (hot)} = \frac{947}{5623} \text{ kgf}$$

$$\text{Proofload} = 6680 \text{ kgf}$$

$$\text{Then } 5623 \text{ kgf is } \underline{84.2\%} \text{ proofload}$$

RICARDO CONSULTING ENGINEERS

CLIENT USSw SECTION Main Bearing Bosses
PROJECT ASE Mod I Engine SHEET NO. 1 OF
JOB NO. C4813-10 DATE 30 October 1979
CALCULATION BY IDJ DRAWING KEY NO.

OBJECT To check that the compressive stress of the main bearing bosses are
within Ricardo design limitations.

Stress under washer at ambient temperature = 14.63 kgf/mm^2
(143.53 N/mm^2)

Stress under washer at 80°C = 17.59 kgf/mm^2
(172.6 N/mm^2)

<u>Material</u>	<u>0.2% Proof Stress</u> <u>(N/mm^2)</u>	<u>Remarks</u>
LM 25 TF	220	> 173
3.2161.01 sin (LM 24 equiv.)	98.1-147.2	< 173
3.2382.05 sin (Ref. 239)	176.6-255.1	\geq 173

The original choice of material LM 25 TF is an excellent choice as regards compressive strength.

Material (Ref. 239) would be satisfactory for use as it exceeds the maximum stress under thermal conditions of 173 N/mm^2 .

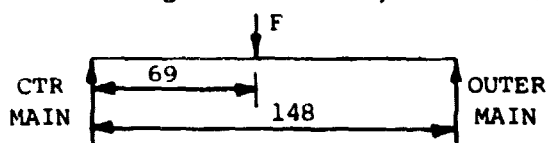
RICARDO CONSULTING ENGINEERS

CLIENT USSw SECTION Crankcase/Bedplate Main Bearing Bolts
PROJECT ASE Mod I Engine SHEET NO. 1 OF
JOB NO. C4813-10 DATE 26 October 1979
CALCULATION BY IDJ DRAWING KEY NO.

OBJECT To determine the main bearing bolt size/grade/torque value, cover factor.

Method 1: Considering gas forces only.

Maximum gas force = 23,400 N = F:



Force at outer main = $\frac{69}{148} \cdot F = 10,909.5 \text{ N} = 5,454.7 \text{ N/bolt.}$

Force at center main $\frac{79}{148} \cdot F = 12,490.5 \text{ N} = 6,245 \text{ N/bolt.}$

Bolt: M12 x 1.75 P - grade 10.9 - proofload 6680 kg.

70% proofload = 4676 kg = preload = 45,872 N.

Crush load Bearing 45 I.D. 49% O.D. 30 wide

Bearing L 10181/2 supplied by Vandervell ϕ 40 I.D. 43.6 O.D. 30 wide

Load on bearing to give .05 maximum "stand up" 4600 N.

To make shell flush - load = P

$$P = E.A. \frac{\delta L}{L}$$

$$\therefore P = (210 \times 10^3)(30 \times 1.6)\left(\frac{0.05}{47}\right) \text{ where } L = \pi r \text{ and } r = \text{mean shell rad.}$$

$$\therefore P = 3413 \text{ N.}$$

\therefore Total crush load = 4600 + 3413 = 8013 N/bolt.

$$\text{Check crush stress} = \frac{8013}{48} = 167 \text{ N/mm}^2 = 17 \text{ kg/mm}^2.$$

ORIGINAL PAGE IS
OF POOR QUALITY

ORIGINAL PAGE IS
OF POOR QUALITY

Cover Factor (C.F.)

$$C.F. = \frac{\text{Available Load/Bolt}}{\text{Dynamic Load/Bolt}}$$

$$C.F. = \frac{\text{Preload} - \text{Crushload}}{\text{Working Load}}$$

$$\therefore C.F. = \frac{45,872 - 8013}{6245} = \underline{6.06} \quad [M12 - \text{grade } 10.9] \\ 70\% \text{ P.L.}$$

C.F. for M10 - grade 10.9 bolt at 70% proofload.

$$C.F. = \frac{(.70)(4590)(9.81) - 8013}{6245} = \underline{3.76} \quad [M10 - \text{grade } 10.9] \\ 70\% \text{ P.L.}$$

C.F. for M12 - grade 8.8 bolt at 70% proofload.

$$C.F. = \frac{(.70)(4910)(9.81) - 8013}{6245} = \underline{4.12} \quad [M12 - \text{grade } 8.8] \\ 70\% \text{ P.L.}$$

Assuming C.F. of 4.0, grade 10.9, M12 bolt - find proofload (P.L.)

$$\therefore 4.0 = \frac{P.L. - 8013}{6245}$$

$$\therefore P.L. = \underline{32,993 \text{ N}} = 3364 \text{ kgf.}$$

Proofload of above bolt = 6680 kgf, hence the 3363 kgf figure is 50.3% of one proofload.

Torque Value

$$\text{Torque} = \frac{WD}{S} \frac{(32,993)(12)}{5 \times 10^3} = \underline{79 \text{ Nm.}}$$

Assume loading on bolt to be 60% of proofload and to be on M12, grade 12.9 bolt.

$$\text{Proofload} = (.6)(6680)(9.81) = \underline{39,319 \text{ N.}}$$

$$C.F. = \frac{39,319 - 8013}{6245} = \underline{5.01}$$

ORIGINAL PAGE IS
OF POOR QUALITY

$$\text{Torque value} = \frac{WD}{S} = \frac{39,319 \times 12}{5 \times 10^2} = 94.4 \text{ Nm} = \underline{94 \text{ Nm.}}$$

$$\text{Stress under 24 O.D. - 13 I.D. washer} = \underline{123 \text{ N/mm}^2}.$$

Method 2: Considering net forces i.e., gas - inertia (relief).

$$\text{At } 30^\circ \text{ ATDC net force} = 19,992 \text{ N} = F.$$

$$\text{Force at center main} = \frac{79}{148} \cdot F = 1,0671 \text{ N.}$$

$$\text{Force/bolt} = \underline{5336 \text{ N.}}$$

$$\text{Hence, C.F.} = \frac{45,872 - 8013}{5336} = \underline{7.1}$$

Note: Method 2 C.F. > Method 1 C.F.

Summar

Main bearing bolt.

Size	: M12
Grade	: 10.9
Cover Factor	: 5
% Proofload	: 60
Torque	: 79 Nm
Stress under Washer:	123 N/mm ²

ORIGINAL PAGE IS
OF POOR QUALITY

RICARDO CONSULTING ENGINEERS

CLIENT United Stirling
PROJECT ASE Mod-1
JOB NO.
CALCULATION BY RE

SECTION Balance
SHEET NO. 1 OF
DATE 8 August 1979
DRAWING KEY NO.

OBJECT Complete Balance of Engine

Calculation of Reciprocating and Rotational Masses of Connecting Rod (con-rod)

Method 1

The con-rod masses at each eye were measured directly from the P40 and P75 rods. The mass is assumed to be $\propto R^2$ * width of eye. The mass of the Mod-1 rod is then estimated by scaling by the method above.

P40 - Big End, 360 g Little End, 148 g

P75 - Big End, 727 g Little End, 300 g

Calculated mass for Mod 1

From P40 - Big End, 717.3 g Little End, 184 g

From P75 - Big End, 520 g Little End, 157 g

The discrepancy is large.

Breakdown into small elements



See Attached Drawing

Note: Weight of con-rod includes bearing shells.

<u>Part</u>	<u>Weight</u>	
1	0.1826 kg	Plus 2 nuts = 0.0024 kg
2	0.0507 kg	Total mass = 0.780 kg
3	0.0650 kg	
4	0.0148 kg	
5	0.1409 kg	
6	0.3155 kg	

ORIGINAL PAGE IS
OF POOR QUALITY

Big end taken as 600 g - Little End, 180 g

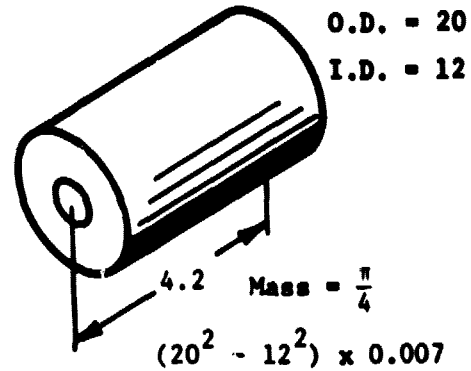
Cross Head and Pin

Pin Mass = 66 g (calc. direct)

P75 Cross Head = 88 g

assume mass \propto (rad of bore)²

$$\text{ASE Mod 1} = \text{Cross Head} = \frac{(68)^2}{(86)^2} (88) = 55 \text{ g}$$



W recip = 1.675 - (from USSw 16 Aug. 79, See DP 79/1189), P.5 item (r)

↑
Weight of Stirling Parts

Weight of Ricardo Parts =
0.246 kg without crosshead
(included in weight of USS
parts; see note below)

W recip =

Note: New cross head form mass included in US recip. weight.

Revised W recip = 1.675 + 0.246 = 1.921 kg

W recip (r) = 3.266 kg-cm

W rot (r)

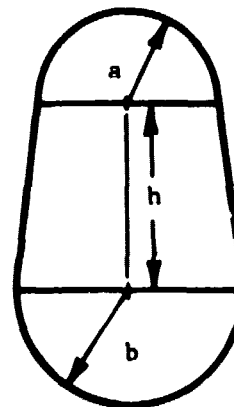
Crank Web (See Attached Diagram)

Slices 1 → 10 model as shape

①	a = 2.6	b = 2.5	h = 0.10
②	a = 2.6	b = 2.5	h = 0.233
③	a = 2.6	b = 2.5	h = 0.366
④	a = 2.6	b = 2.55	h = 0.500
⑤	a = 2.6	b = 2.55	h = 0.6533
⑥	a = 2.6	b = 2.55	h = 0.7666
⑦	a = 2.6	b = 2.55	h = 0.900
⑧	a = 2.6	b = 2.55	h = 1.033
⑨	a = 2.6	b = 2.55	h = 1.166
⑩	a = 2.6	b = 2.55	h = 1.30
⑪	a = 2.6	b = 2.5	h = 1.4

All 0.3 cm Thick

0.5 cm thick



①	$\bar{A}r$ 1.019
②	2.617
③	4.237
④	5.089
⑤	7.108
⑥	8.679
⑦	9.591
⑧	11.548
⑨	13.595
⑩	15.748
⑪	17.414

$$\text{Total } \bar{A}r = \text{of } ① - ⑩ = 79.301$$

$$W_r = (\bar{A}r) (t) (p)$$

$$= (79.301) (0.3) (0.00783)$$

$$= 0.186 \text{ kg-cm}$$

$$W_r \text{ of } ⑪$$

$$= 17.414 \times 0.6 \times 0.00783$$

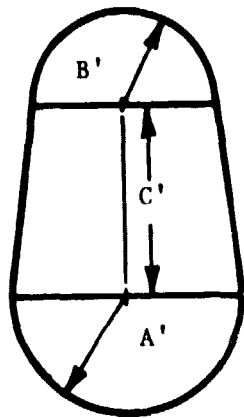
$$= 0.068 \text{ kg-cm}$$

$$W_r \text{ of Crank Web} = 0.254 \text{ kg-cm}$$

$$W_L \text{ of Eccentric Pin} = \pi/4 (5.4)^2 (2.5) (1.5) (0.00783) = 0.6725 \text{ kg-cm}$$

$$W_r \text{ of Crank Pin} = \pi/4 (4.2)^2 (2.7) (1.7) (0.00783) = 0.4979 \text{ kg-cm}$$

Crank/Eccentric Web (Crank 2 Link 2)



$$A' = 3.6 \quad B' = 2.7 \quad C' = 2.3$$

$$\text{Cassie Program } \bar{A}r = 24.25$$

Distance of COG from centre of circle radius

A (F) is AF/A

$$A = \frac{\pi (3.6)^2}{2} + \frac{\pi (2.5)^2}{2} + \frac{2.3}{2} (5.4 + 7.2)$$

$$A = 46.29$$

$$\bar{r} = \frac{24.25}{46.29}$$

$$= 0.5237$$

From the drawing the distance for COG to the centre of rotation is measured to be = 1.2 cm.

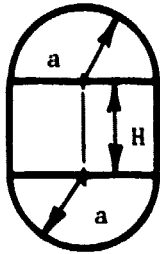
$$W_r \text{ (about centre of crank)} = (46.29) (0.6) (0.00783) (1.2) = 0.261 \text{ kg-cm}$$

Eccentric/Mass Web

Model As:

Where $a = 3.6 \text{ cm}$

$h = 1.5 \text{ cm}$



Cassic Program gives $\bar{A}r = 38.645$

$$W_r = (38.645) (0.6) (0.00783)$$

$$= 0.1815 \text{ kg-cm}$$

Wr values of Link

See drawing attached.

Shank and Top of Link Cap

Volumes

$$\textcircled{1} (0.8) (1.8) (3.3) = 4.752 \text{ cm}^3$$

$$\textcircled{2} \frac{(0.8 + 2.4)}{2} (1.4) (2) (3.3) = 14.784 \text{ cm}^3$$

$$\textcircled{5} \pi (3.8^2 - 2.7^2) (2.4) (0.5) = 26.954 \text{ cm}^3$$

$$\textcircled{3} \pi (1.1^2 - 0.8^2) (3.0) (0.5) = 5.375 \text{ cm}^3$$

$$\textcircled{6} (2.8) (0.5) (1.5) (2 - 18) (\pi) (0.8)^2 = 0.581$$

$$\text{Total Volume} = 52.445 \text{ cm}^3$$

$$\text{Mass} = (52.445) (0.0072)$$

$$= 0.378 \text{ kg (SG Iron)} \quad 0.1416 \text{ kg}$$

Bolts

$$\text{Mass} = (2) \left(\frac{\pi}{4}\right) (1.0)^2 (6.0) = 74 \text{ g}$$

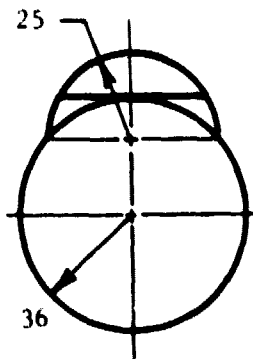
SG Iron Cap

$$\textcircled{4} (3.9^2 - 2.7^2) (\pi) \left(\frac{2.4}{2}\right) = 29.86 \text{ cm}^3 - \frac{\pi (1.0)^2}{4} (1.0) (2) = 28.29 \text{ cm}^3$$

$$\textcircled{3} (2) (1.1^2 - 0.8^2) (\pi) (2.0) (0.5) = 3.58 \text{ cm}^3 \quad \text{Mass of Cap} = 0.229 \text{ kg}$$

$$\text{Total Volume} = 31.87 \text{ cm}^3$$

Crank/Eccentric Web (Crank 1 Eccentric I)



$$\text{Area of Sector} = \frac{(2.5)^2}{2} \left\{ 2.09439 - \sin 2.09439 \right\}$$

$$= 3.8387 \text{ cm}^2$$

$$\text{Distance from centre of circle to COG } (\bar{y}) = \frac{2}{3} \frac{r^3}{\text{area}}$$

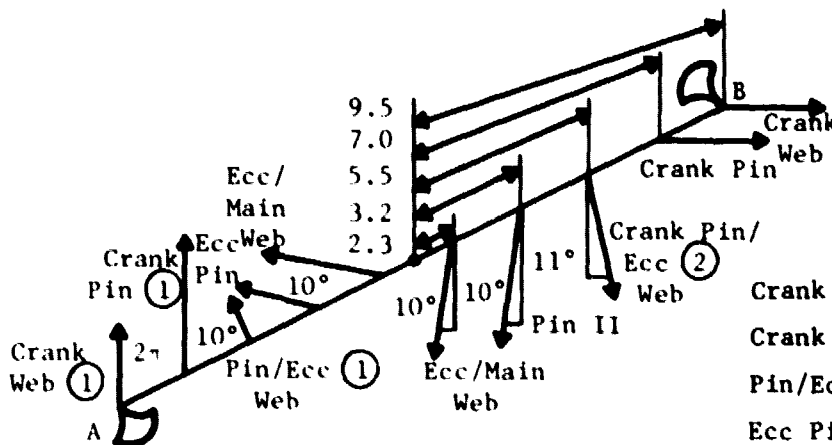
$$\text{Area of large circle} = 40.7 \text{ cm}^2$$

$$\text{Distance of COG from centre of circle} = \frac{3.8}{40.7} (3.7) = 0.35 \text{ cm}$$

By drawing distance from COG = 1.3 cm to centre of rotation

$$W_r = 1.3 \times 44.5 \times 0.6 \times 0.0072 = 0.250 \text{ kg-cm.}$$

Total Wrot x r of Crank (1) and (2)



$$\text{Crank Web } W_r = 0.254$$

$$\text{Crank Pin } W_r + \text{Con-Rod } W_r = 1.52$$

$$\text{Pin/Ecc I Web} = 0.250$$

$$\text{Ecc Pin (1) + Link } W_r = 1.694$$

$$\text{Ecc/Main Web} = 0.182$$

$$\text{Pin (2)/Ecc II Web} = 0.261$$

Take moments about A in horizontal plane clockwise and vertical.

$$\begin{aligned} \text{Moment} = & -(0.25 \times 4.2 \times \cos 27^\circ) + (1.694 \times 5.8 \times \cos 10^\circ) + (0.182 \times 7.3 \times \cos 10^\circ) \\ & - (0.182 \times 11.7 \times \sin 10^\circ) - (8.694 \times 13.2 \sin 10^\circ) - (14.7 \times 0.261 \times \sin 10^\circ) \\ & + (1.52 \times 16.5) + (0.25 \times 19.0) = 140 \text{ kg-cm} \end{aligned}$$

If the counterweight is assumed to act at 10.8 cm from centre of crank

$$W_r (A_1 \text{ hor}) = \frac{14.54}{20.3} = 0.709 \text{ kg-cm}$$

ORIGINAL PAGE IS
OF POOR QUALITY

Moments about A vertically.

$$\begin{aligned} \text{Moment} = & -(2.6) (1.52) - (0.250) (4.2 \sin 27^\circ) - (1.694) (5.8 \sin 10^\circ) - (0.182) \\ & (7.3 \sin 10^\circ) + (0.182) (11.7 \cos 10^\circ) + (1.694) (13.2 \cos 10^\circ) \\ & + (0.261 \cos 11^\circ) = 21.52 \end{aligned}$$

If the counterweight acts at 10.8 cm from centerline

$$W_r(B, \text{vert}) = 1.06 \text{ kg-cm}$$

Take Moments about B - Horizontal Plane

$$\begin{aligned} \text{Moments} = & (1.52) (2.6) - (0.261) (4.2 \sin 11^\circ) + (1.694) (5.8 \sin 10^\circ) + (0.182) \\ & (7.3 \times \sin 10^\circ) + (11.7) (0.182 \times \cos 10^\circ) + (1.694) (13.2 \times \cos 10^\circ) \\ & + (0.250) (14.7 \cos 27^\circ) = 25.10 \end{aligned}$$

If counterweight acts at 10.8 cm from centre line

$$W_r(A, \text{hor}) = \frac{24.27}{20.3} = 1.237 \text{ kg-cm}$$

Take moments about B - Vertically

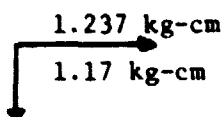
$$\begin{aligned} \text{Moment} = & -(4.2) (0.261 \cos 11^\circ) + (1.694) (5.8 \cos 10^\circ) - (0.182) (7.3 \times \cos 10^\circ) \\ & + (11.7) (0.82 \sin 10^\circ) + (1.694) (13.2 \sin 10^\circ) + (0.250) (14.7 \sin 27^\circ) \\ & + (1.52) (16.5 + 0.254) (19.0) = 23.76 \end{aligned}$$

$$W_r(A, \text{vert}) = \frac{23.62}{20.3} = 1.17 \text{ kg-cm}$$

Wrot x r Summary Crank (1,2)

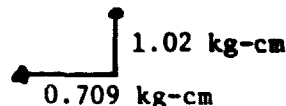
Counterweight A

Adjoining Crank 1



Counterweight B

Adjoining Crank 2



Crank 3 and 4

Crank Pin 3 - Link II Web

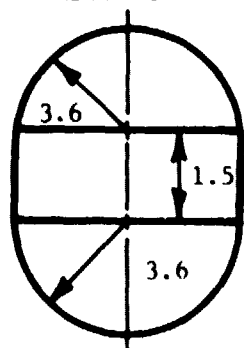
$$W_r = \pi (3.6)^2 (0.6) (1.5) (P) = 0.264 \text{ kg-cm}$$

Similarly C/Pin 4 Link I

$$W_r = 0.264 \text{ kg-cm}$$

Link II/Centre Main Web

Link I/Centre Main Web

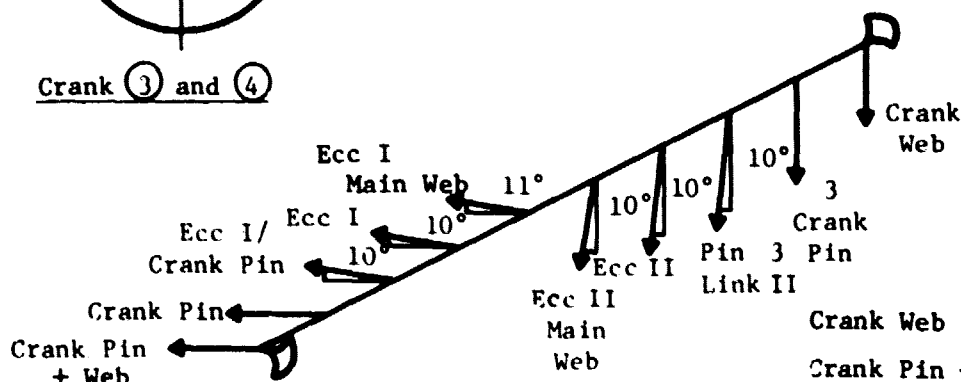


$$\text{Cassie Program} - a = 3.6 \quad b = 3.6 \quad h = 1.5$$

$$\bar{A}_r = 38.65$$

$$W_r = 0.167 \text{ kg-cm}$$

Crank ③ and ④



$$\text{Crank Web} = 0.254$$

$$\text{Crank Pin} + \text{Con-Rod } W_r = 1.52$$

$$\text{Crank Pin/Link Web} = 0.264$$

$$\text{Eccentric} + \text{Link} = 1.694$$

$$\text{Ecc/Main Web} = 0.167$$

Moments about A

Horizontal

$$\begin{aligned} \text{Moment} = & -(1.52) (2.6) - (10.264) (4.2 \cos 10^\circ) - (1.694) (5.8 \times \cos 10^\circ) \\ & - (0.167) (7.3 \times \cos 10^\circ) - (0.167) (11.7 \times \sin 10^\circ) - (1.694) (13.2 \\ & \sin 10^\circ) - (0.264) (14.7 \sin 0^\circ) = 20.8 \end{aligned}$$

If counterweight is assumed to act at 10.8 cm from centre line

$$W_r(B, \text{hor}) = -1.025 \text{ kg-cm}$$

ORIGINAL PAGE IS
OF POOR QUALITY

Vertical

$$\begin{aligned}\text{Moment} = & -(0.264) (4.2 \sin 10^\circ) - (1.694) (5.8 \sin 10^\circ) - (0.167) (7.3 \sin 10^\circ) \\ & + (0.167) (11.7 \cos 10^\circ) + (1.694) (13.2 \cos 10^\circ) + (0.264) (4.7 \cos 10^\circ) \\ & + (1.52) (16.5) + (0.254) (190) = 56 \text{ kg-cm}\end{aligned}$$

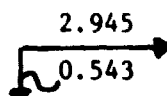
If counterweight acts at 10.8 cm from centre line

$$W_{r(B, \text{vert})} = 2.76 \text{ kg-cm.}$$

Summary of Crank (3,4)

Counterweight A'

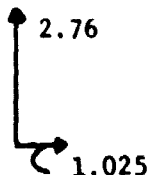
Adjoining Crank (4)



Moments about B

Counterweight B'

Adjoining Crank (3)



Horizontal

$$\begin{aligned}\text{Moment} = & (4.2) (0.264 \sin 10^\circ) (5.8) (1.694 \sin 10^\circ) + (0.167) (7.3 \sin 10^\circ) \\ & + (11.7) (0.167 \cos 10^\circ) + (13.2) (1.694 \cos 10^\circ) + (14.7) (0.264 \cos 10^\circ) \\ & + (1.52) (16.5 + 190) (0.254) = 59.78\end{aligned}$$

Wrot x r = 2.945 kg-cm assume acts at 20.3 cm, etc.

Vertical

$$\begin{aligned}\text{Moment} = & -(2.6) (1.52) - (4.2) (0.264 \cos 10^\circ) - (5.8) (1.694 \cos 10^\circ) \\ & - (0.167) (7.3 \times \cos 10^\circ) + (11.7) (0.167 \sin 10^\circ) + (1.694) (13.2 \\ & \sin 10^\circ) + (0.264) (14.7 \sin 10^\circ) = 11.015 = 0.543 \text{ kg-cm}\end{aligned}$$

Recip Balance

Note: 23rd August 1979 Wrecip = 1.675

For USS parts only see DR 79/1189, p5, item "r"

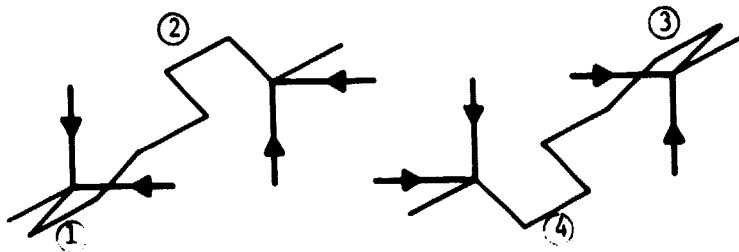
$$\begin{aligned}\text{Wrecip Ricardo parts} & = 0.180 \text{ (con-rod)} \\ & + 0.66 \text{ (pin)} = 0.246 \text{ kg}\end{aligned}$$

ORIGINAL PAGE IS
OF POOR QUALITY

$$W_{\text{recip}} = 1.92 \text{ kg}$$

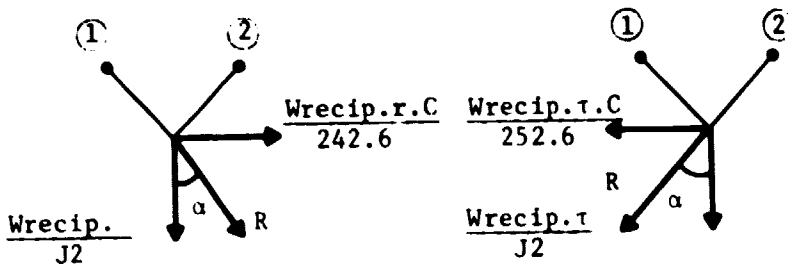
$$W_{\text{recip}} \times \pi = \underline{3.266 \text{ kg} - \text{cm.}}$$

$$\text{Centre line} = \frac{69}{108.5} = 0.636$$



Layout of C/Ws required to
balance recip forces and
couples

Consider Crank ① ②

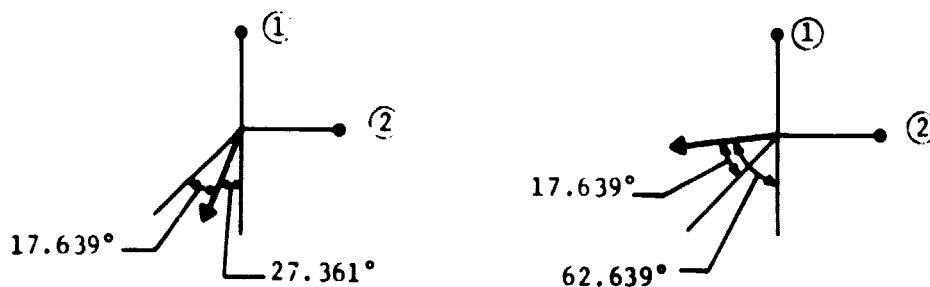


Counter wt at front end

Counter wt at rear

Resultant = 2.308 at 17.639° to the "vertical"

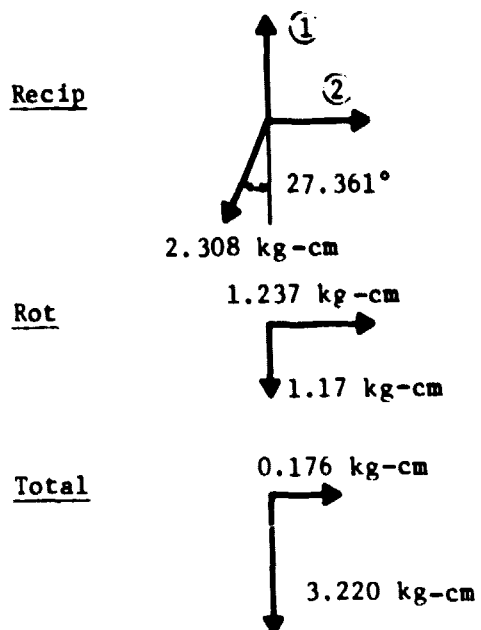
Transforming to Layout Earlier



Total Balance Required

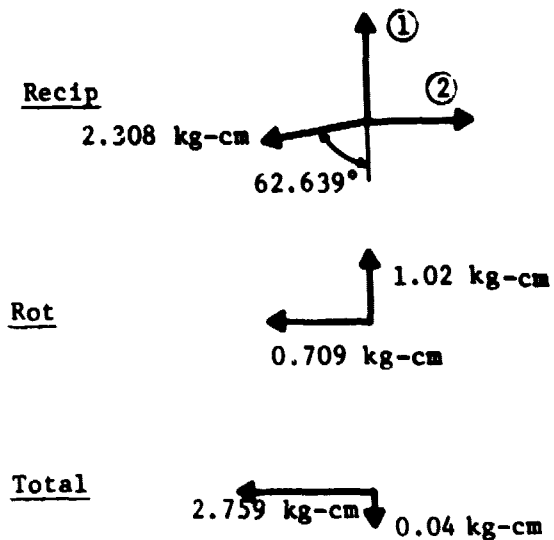
Crank ①②

Front End



Resultant = 3.2246 kg-cm
at 3.133° to "Vertical"

Back End



Resultant = 2.759 kg-cm
at 0.8° to "Horizontal"

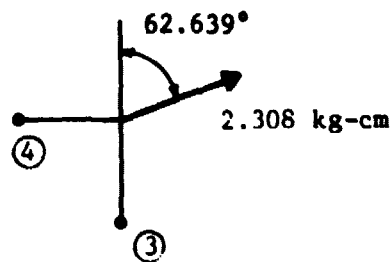
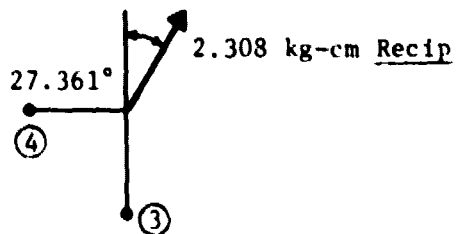
ORIGINAL DRAWING
OF POOR QUALITY

Crank (3) (4)

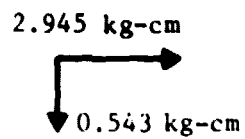
Front End

Back End

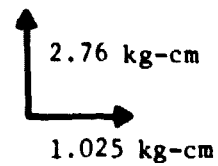
Recip



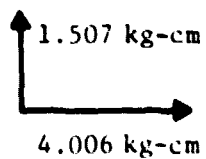
Rot



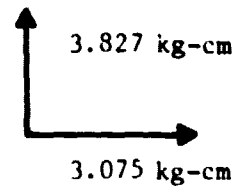
Rot



Total



Total



Resultant = 4.28 kg-cm
at 69.385° to "Vertical"

Resultant = 4.904 kg-cm
at 38.8° to "Vertical"

Annulus

Outside Radius = 6.900, Inside Radius = 2.600, Half Angle = 34.500, Thickness = 4.200, Density = .72000E -3, Offset = 0.000

Mass = 0.744, WR = 3.551, MI = 20.222

Annulus

Outside Radius = 6.900, Inside Radius = 2.600, Half Angle = 29.000, Thickness = 4.200, Density = .72000E -3, Offset = 0.000

Mass = 0.625, WR = 3.039, MI = 16.998

Annulus

Outside Radius = 6.900, Inside Radius = 2.600, Half Angle = 70.000, Thickness = 4.200, Density = .72000E-3, Offset = 0.000

Mass = 1.509, WR = 5.891, MI = 41.030

Circular Chamfer

Outside Radius = 6.900, Inside Radius = 4.700, Half Angle = 34.500, Thickness = 0.800, Density = .72000E -3, Offset = 0.000

Mass = 0.047, WR = 0.292, MI = 1.327

Circular Chamfer

Outside Radius = 6.900, Inside Radius = 4.700, Half Angle = 29.000, Thickness = 0.800, Density = .72000E -3, Offset = 0.000

Mass = 0.040, WR = 0.246, MI = 1.535

Circular Chamfer

Outside Radius = 6.900, Inside Radius = 4.700, Half Angle = 70.000, Thickness = 0.800, Density = .72000E -3, Offset = 0.000

Mass = 0.095, WR = 0.593, MI = 3.706

Total Mass = 3.061

Total WR = 13.61

Total MI = 85.32

ORIGINAL PAGE IS
OF POOR QUALITY

ORIGINAL PAGE IS
OF POOR QUALITY

Mass of counterweights as drawn

See "Shapes" program output

Wr values are annulus Wr's subtract chamfer Wr's

Wr values

Required C/Wt

Crank ① ②

A = 3.259 kg-cm	= 3.225 kg-cm
B = 2.793 kg-cm	= 2.76 kg-cm

Crank ③ ④

A = 5.298 kg-cm	= 4.22 kg-cm
B = 5.298 kg-cm	= 4.91 kg-cm

RICARDO CONSULTING ENGINEERS

ORIGINAL PAGE IS
OF POOR QUALITY

CLIENT USSw
PROJECT ASE Mod I Engine
JOB NO.
CALCULATION BY

SECTION Bearing Loadings
SHEET NO. 1 OF 1
DATE 12 October 1976
DRAWING KEY NO.

OBJECT Gear Reaction Forces

Gear PCR = 62.15 mm

Crank Angle	Torque Crank 1 Nm	Reaction Crank 1 N	20% Pressure L	Torque Crank 2 Nm	Reaction Crank 2 N
0	316	518.3	551.6	139	228.0
10	315	516.6	549.8	138	226.3
20	333	546.2	581.2	125	205.0
30	363	595.4	633.6	101	165.6
40	397	651.1	692.9	76	124.6
50	424	695.4	740.0	56	91.8
60	432	708.6	756.0	46	75.4
70	416	682.3	726.1	54	88.6
80	376	615.1	654.6	85	139.4
90	316	518.3	551.6	137	228.0
100	246	403.5	429.4	207	309.5
110	177	293.6	312.4	279	457.6
120	125	205.0	218.6	339	556.0
130	94	156.7	164.1	380	623.3
140	84	137.8	146.6	395	644.9
150	91	149.3	153.9	387	634.7
160	108	147.1	188.5	362	593.7
170	126	206.4	220.0	334	547.8
180	139	228.0	242.6	316	518.3
190	138	226.3	240.8	315	516.6
200	125	205.2	218.2	331	546.2
210	107	165.3	176.2	363	595.4
220	76	124.6	132.6	397	651.1
230	56	91.8	97.7	404	695.4
240	46	75.4	80.2	432	708.6
250	54	88.6	94.3	416	682.3
260	85	139.4	148.3	395	615.1
270	139	228.0	242.6	316	518.3
280	207	333.5	361.3	246	403.5
290	279	457.6	487.0	179	293.6
300	339	556.0	591.7	125	205.0
310	380	623.3	663.3	94	154.2
320	395	644.9	686.3	84	137.8
330	387	634.7	675.4	91	149.3
340	362	593.7	631.8	108	177.1
350	334	547.8	611.7	126	206.7

RICARDO CONSULTING ENGINEERS

CLIENT USSw

SECTION

PROJECT ASE Mod I Engine

SHEET NO. 1 OF 1

JOB NO.

DATE 29 March 1979

CALCULATION BY R. Thorpe

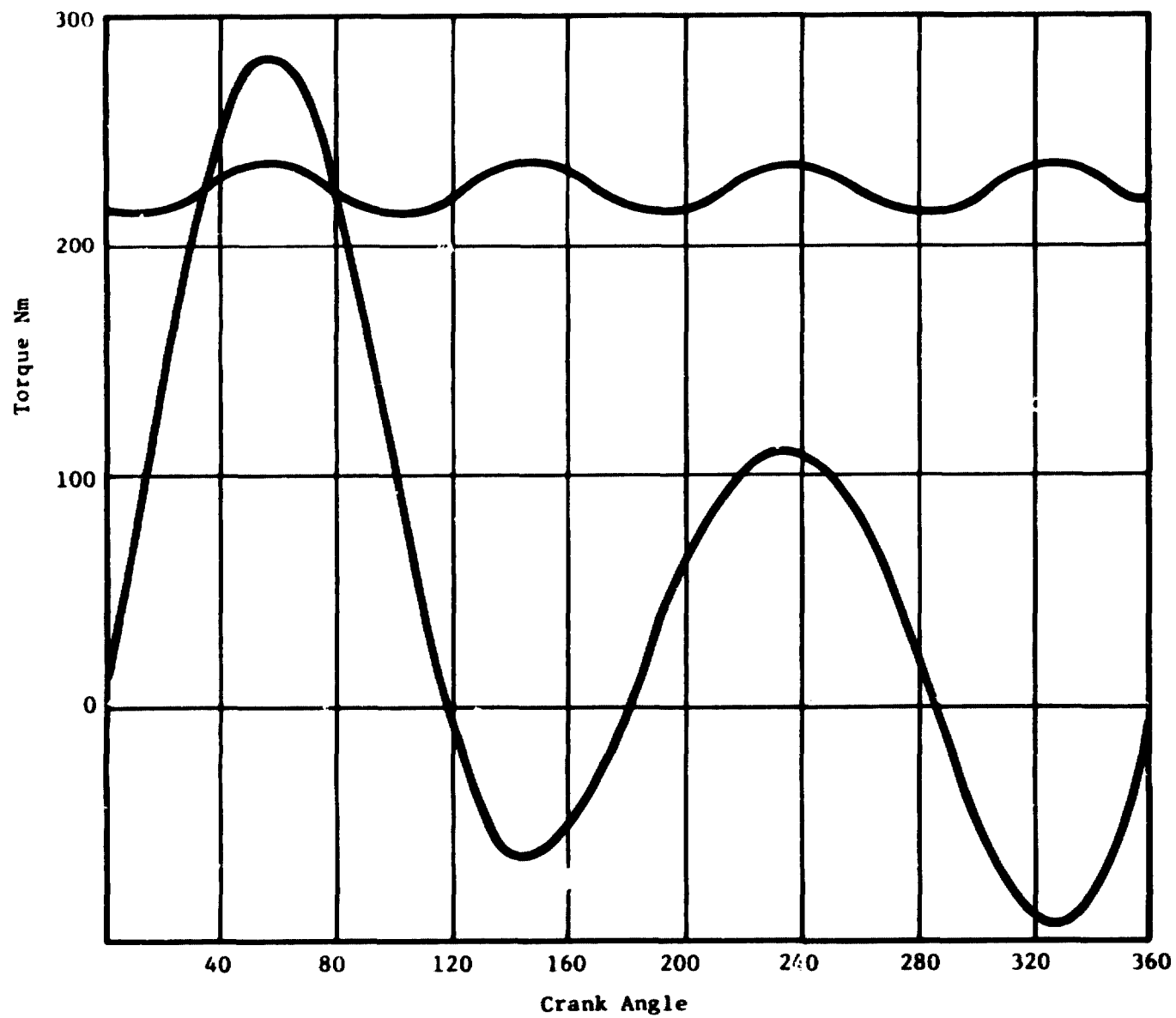
DRAWING KEY NO. 3274

OBJECT Torque Diagram

68 mm Bore x 34 mm Stroke

Summary

United Stirling have supplied a list of gas force ordinates for the revised bore and stroke of the Mod I engine (figure attached). Only the gas forces on this sheet are thought to be correct. The total reciprocating masses of the engine are expected to be 2.1 kg. The crank geometry is shown on Drawing No. 3274/16. The following calculations have been undertaken to assist in connecting rod bolt loads and shank stress calculations.



ORIGINAL PAGE IS
OF POOR QUALITY

ORIGINAL PAGE IS
OF POOR QUALITY

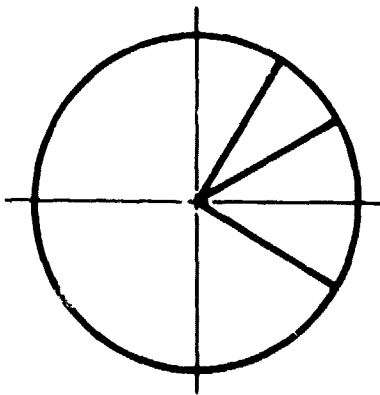
RICARDO CONSULTING ENGINEERS

CLIENT United Stirling
PROJECT Mod I Engine, ϕ 68 x 34
JOB NO. C4843-20
CALCULATION BY DR

SECTION Crankshaft Stresses
SHEET NO. 1 OF
DATE 30 April 1979
DRAWING KEY NO.

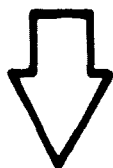
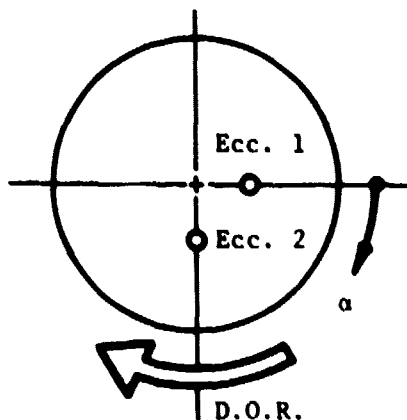
OBJECT To identify most severely stressed part(s) of crankshaft and calculate the maximum stresses for drive arrangement through coupling links.

Forces acting at crankpin and eccentric.

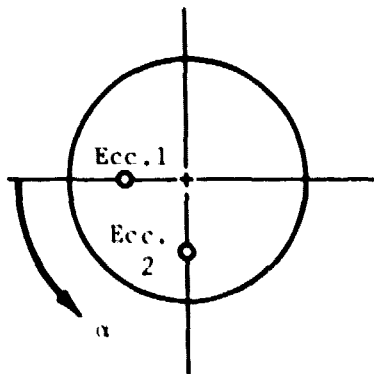


Crank Angle	Gas-Pressure Force on Pin	Coupling-Link Force on Eccentric
0	20462	
30	23346	
60	19200	
90	9050	
120	-2855	

To identify eccentric, the rows referred to as "link 1" and "link 2" in GMF's calculation dated 23 October 1978 (below, left).



View from opposite
end, to make D.O.R.
same as drawing
3219-22 and
3274-17

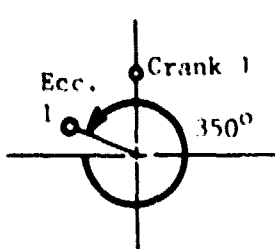
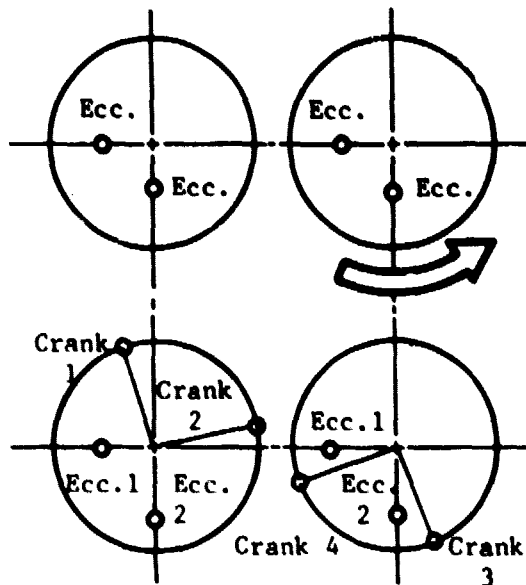


Associating Ecc. 1 with Crank 1
(front crank on Shaft 1-2)
required that Ecc. 1 on shaft
3-4 is also associated with
front crank unit, i.e., crank 4.

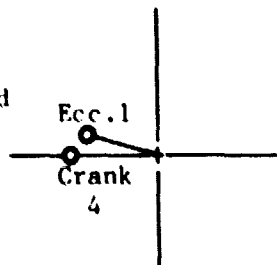
So Ecc. 2 on Shaft 3-4 must
be associated with Crank 3
and arrangement of cranks
and eccentrics is as shown
on drawing 3274-17.

Thus, table on sheet 4 of
calculation, 23 Oct. 1978
could refer to crank unit no. 1.
($\alpha = 350^\circ$ at crank angle $\theta = 90^\circ$)

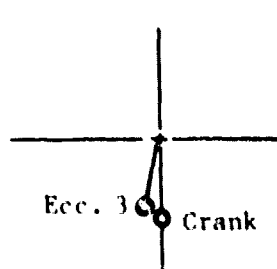
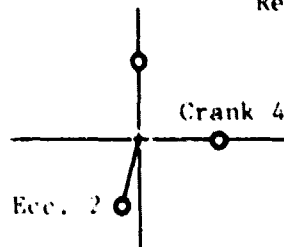
Compare with "View on front end showing
oil holes," from drawing no. 3219-22
(below)



At opp. end
of link,



"Rear" Cranks



Forces acting on crankpins and eccentrics (See notes, sheet 4)

Crank
Angle

(No. 1 Crank)	(1) Pin 1	(2) Ecc 1	(3) Pin 2	(4) Ecc 2	(5) Pin 3	(6) Ecc 3	(7) Pin 4	(8) Ecc 4
0	20462	868	-3739	-4924	-15297	-4924	9051	868
15	22630	-727	151	-8302	-15254	-8302	2980	-727
30	23346	-3791	4330	-10415	-14379	-10415	-2855	-3791
45	22068	-7265	8658	-10376	-12618	-10376	-7765	-7265
60	19200	-9576	12968	-8035	-10214	-8035	-11659	-9576
75	14612	-10272	14345	-4790	-7182	-4790	-14058	-10272

No. 2 TDC

90	9051	-10587	20462	-1867	-3739	-1867	-15297	-10587
105	2980	-11124	22630	973	151	973	-15254	-11124
120	-2855	-11824	23346	4304	4330	4304	-14379	-11824
135	-7765	-11877	22068	8317	8658	8317	-12618	-11877
150	-11659	-9642	19200	11490	12968	11490	-10214	-9642
165	-14058	-5705	14612	12235	14345	12235	-7182	-5705

No. 3 TDC

180	-15297	-1881	9051	10669	20462	10669	-3739	-1881
195	-15254	625	2980	7139	22630	7139	151	625
210	-14379	1567	-2855	4307	23346	4307	4330	1567
225	-12618	2007	-7765	2867	22068	2867	8658	2007
240	-10214	2745	-11659	2303	19200	2303	12968	2745
255	-7182	4154	-14058	1937	14612	1937	14343	4154

No. 4 TDC

270	-3739	4924	-15297	868	9051	868	20462	4924
285	151	4317	-15254	-377	2980	-377	22630	4317
300	4330	2584	-14379	-941	-2855	-941	23346	2584
315	8658	1161	-12618	-812	-7765	-812	22068	1161
330	12968	642	-10214	-766	-11659	-766	49200	642
345	14345	881		-1888				

Forces acting on eccentrics: Base estimate on calculation for P40 engine, 23 October 1978, with maximum torque = 180 Nm, from one crankshaft.

For Mod 1 engine, calculated peak torque from one crankshaft is 225 Nm, approximate, see calculation dated 2-4-79 (R.T.'s calculation for instantaneous torques, link forces).

Also, eccentric throw = 15 mm, Mod 1 engine
10 mm, P40 engine

Force $\propto \frac{\text{Torque}}{\text{Moment}} \text{ Arm}$

$$\begin{aligned}\therefore \text{ for Mod 1, force} &= (\text{force calculated for P40}) \times \frac{225}{180} \times \frac{10}{15} \\ &= (\text{force calculated for P40}) \times \frac{5}{6}.\end{aligned}$$

Coupling links connect eccentric no. 1 to eccentric no. 4, and
eccentric no. 2 to eccentric no. 3.

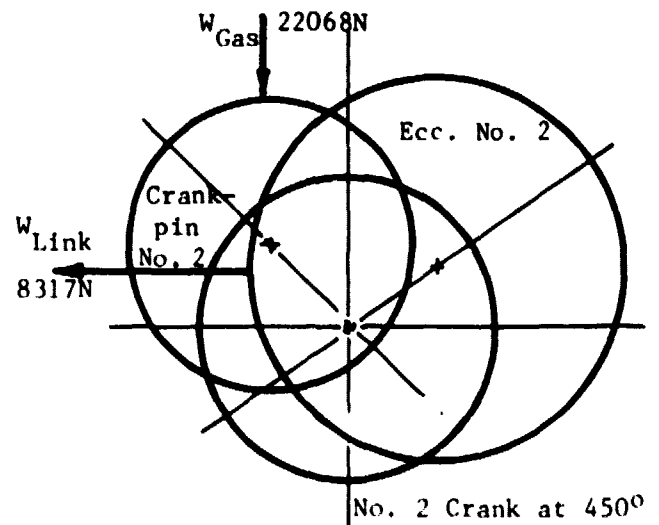
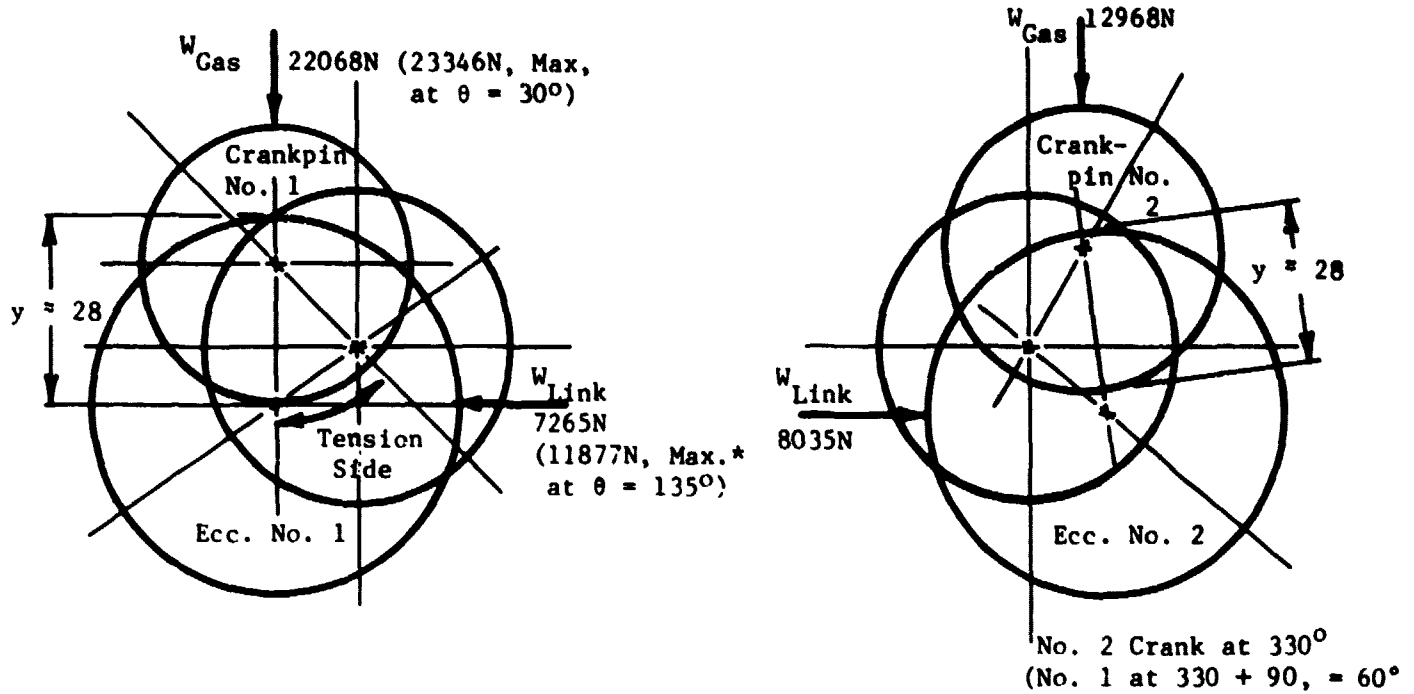
\therefore In the tabulated data, sheet 3, column (8) is the same as column (2),
and column (6) is the same as column (4).

Column (1) is abstracted from data supplied by United Stirling, viz
"Stirling Simulation Program," ref. no. LL/751217 (page 11) (with calculation
dated 29-3-79).

Columns (2), (3), and (4) contain the same forces as column (1), but displaced
by 90°, 180°, and 270°, respectively.

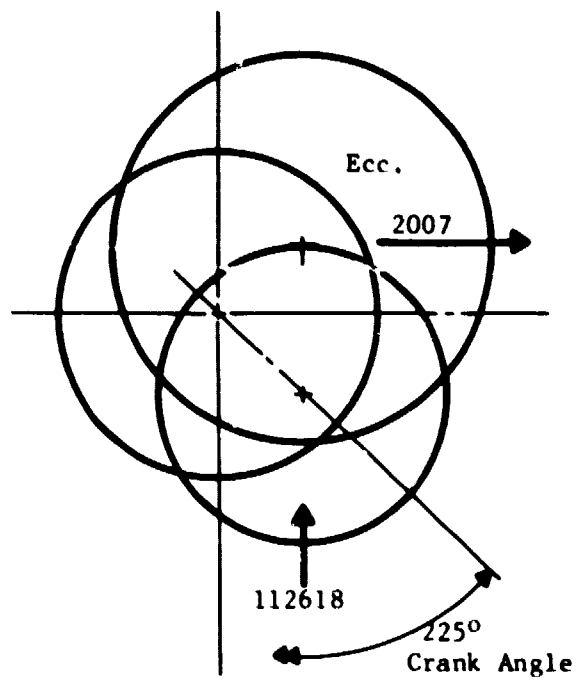
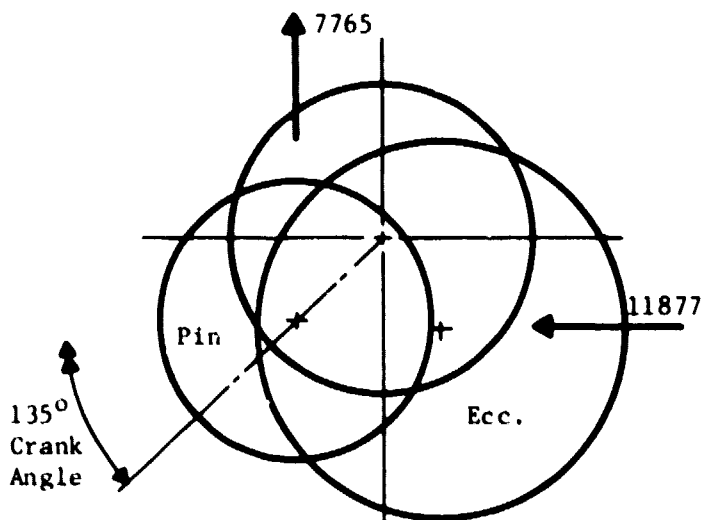
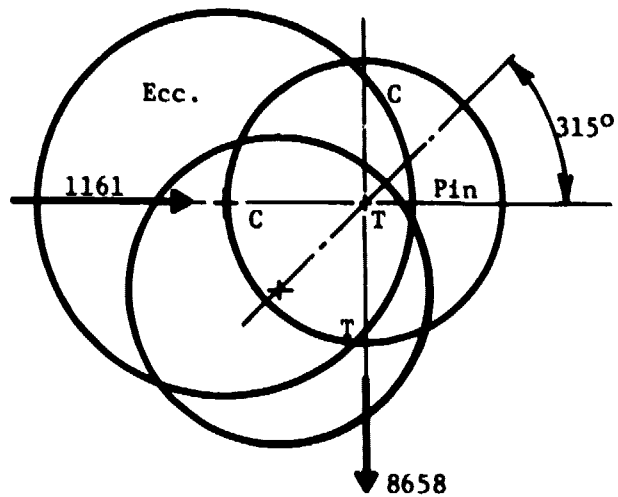
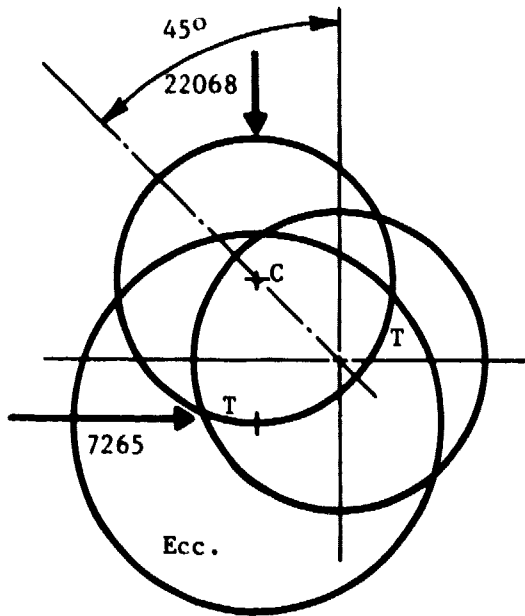
Notation: Positive forces act "downwards," i.e., from cylinder head towards
crankshaft. In coupling links, positive forces are tensile,
negative forces are compressive.

"Worst-Case" Stress Conditions

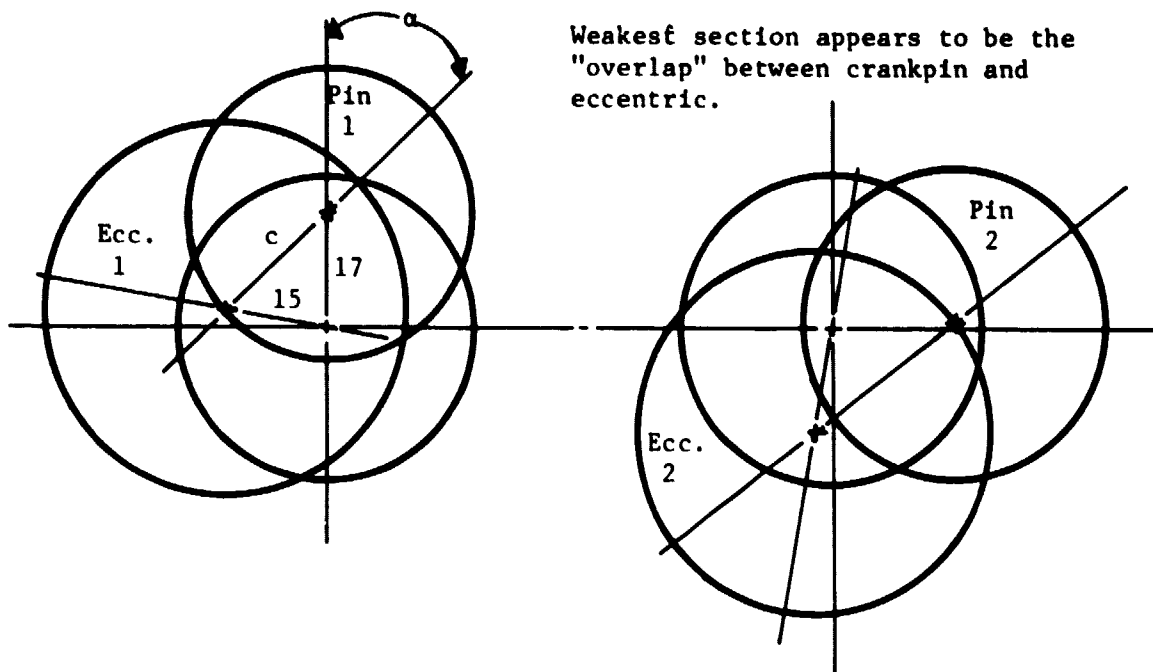


Highest forces, but also highest modulus of resistance to bend of overlap section, in this position.

ORIGINAL PAGE IS
OF POOR QUALITY



Weakest crank units are nos. 1 and 2.



Resolve $||^l$ and \perp^r line of symmetry of pin/eccentric overlap section

$$\text{For angle } \alpha, c^2 = 15^2 + 17^2 - 2 \cdot 15 \cdot 17 \cos 80^\circ \approx 425.44$$

$$c \approx 20.63$$

$$\frac{15}{\sin \alpha} = \frac{20.626}{\sin 80^\circ} \therefore \sin \alpha \approx \frac{15}{20.626} \cdot \sin 80^\circ, \approx .7162$$

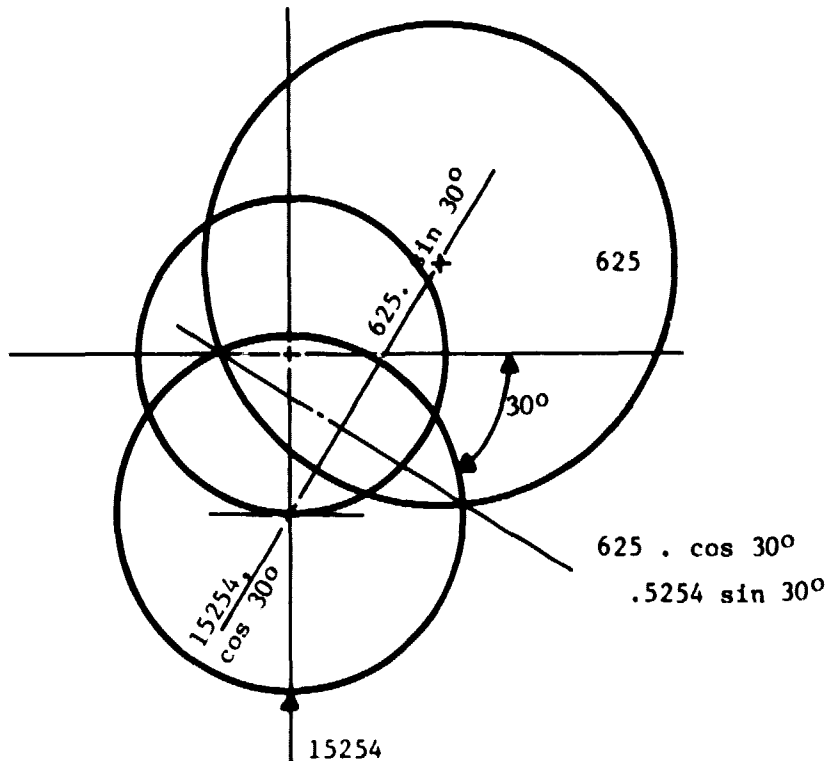
$$\therefore \alpha \approx 45.74^\circ$$

Pin/Eccentric Overlap Section

Smallest depth is in plane at crank angles of 45° and 225° crank 1, where gas loads are near their minimum (45°), and at crank angles 315° and 135° for crank 2, where gas loads are relatively low. (Angle of crank 1 after TDC)

ORIGINAL PAGE IS
OF POOR QUALITY

To identify most severe case for crankshaft stress;



Proposed Procedure ($||^L$ -plane and \perp^R -plane loading refer to plane of cylinder centerline)

Worst extremes of $||^L$ -plane bending, $\theta = 45^\circ$ and $\theta = 135^\circ$

Forces, + 22068 N at pin; -11877 at eccentric.

Extremes of \perp^R -plane bending at same crank angle forces,

Forces, + 7265 N at eccentric, + 7765 N at pin

(both forces produce tension in "corner" of section overlapping journal).

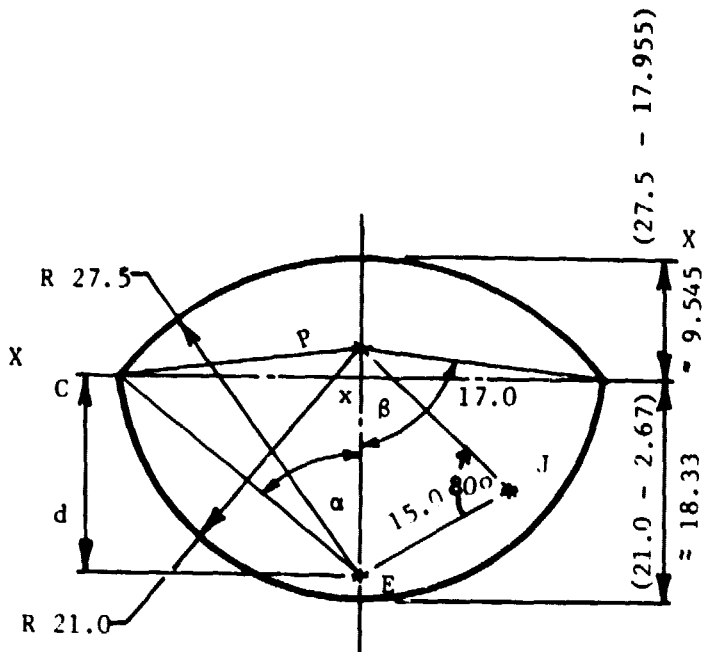
Worst combination of in-plane bending-stress range, $\theta = 45^\circ$ and 225° with \perp^R -plane stress range.

In-plane bending, forces at pin, +22068 N to + 12618 N

\perp^R -plane bending, forces at eccentric, +7265 N to -2007 N

(at same crank angles as $||^L$ -plane forces)

Dimensions of "overlap" section, no. 1 crankpin and no. 1 eccentrics



$$PE^2 = 15.0^2 + 17.0^2 - (2)(15.0)(17.0)$$

$$(\cos 80^\circ)$$

$$\therefore PE \approx 20.626 \text{ mm.}$$

In ΔPCE

$$PE^2 = PC^2 + CE^2 - 2 PC \cdot CE \cdot \cos c$$

$$\text{or } \cos c = \frac{PC^2 + CE^2 - PE^2}{2 PC \cdot CE}$$

$$= \frac{21.0^2 + 27.5^2 - 20.626^2}{(2)(21.0)(27.5)}$$

$$\therefore \cos C = 0.668241, \quad C = 48.07^\circ$$

$$\therefore \frac{20.626}{\sin 48.07^\circ} = \frac{21.0}{\sin \alpha} = \frac{27.5}{\sin \beta}$$

$$\therefore \sin \alpha = \frac{21.0}{20.626} (\sin 48.07^\circ) \approx .757452, \quad \alpha \approx 49.24^\circ, \quad 0.8593 \text{ rad.}$$

(For area under eccentric arc with $R = 27.5$)

$$\sin \beta = \left(\frac{27.5}{20.626} \right) (\sin 48.07^\circ) \approx .991901, \quad \beta \approx 82.70^\circ, \quad 1.4433 \text{ rad.}$$

(For area under crankpin arc, with $R = 21.0$)

$$d = (27.5) (\cos 49.24^\circ) \approx 17.955 \text{ (for area bounded by eccentric arcs)}$$

Corresponding dimension for area bounded by crankpin arc

$$\text{i.e., } P_x = 20.626 - 17.955, \approx 2.671$$

For position of neutral axis

$$\text{Area under crankpin arc} = (21.0^2) (1.4433) - \left(\frac{1}{2} \right) (21.0^2) \sin(2)(1.4433)$$

$$= 21.0^2 (1.4433 - \sin \frac{2.8866}{2}) = 580.88 \text{ mm}^2.$$

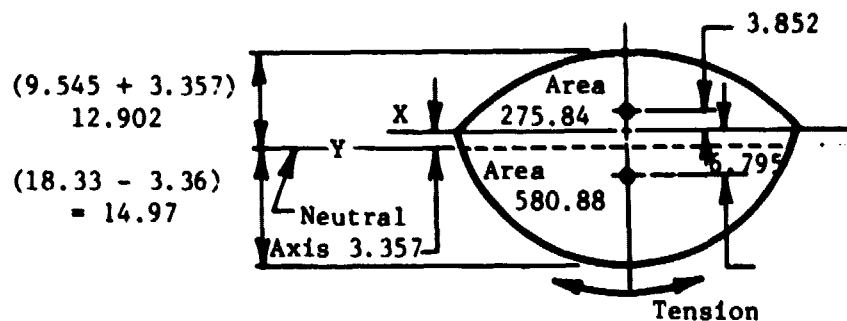
$$\text{C.G. dist.} = \left(\frac{4}{3} \right) (21.0) \left(\frac{\sin^3 1.4433}{2.886 - \sin 2.8866} \right) = 9.466 \text{ (from P)} - P_x (2.671) \\ \approx 6.795 \text{ mm from } x - x.$$

$$\text{Area under eccentric arc} = 27.5^2 (0.8593 - \frac{\sin 1.7186}{2}) \approx 275.84 \text{ mm}^2.$$

$$\text{C.G. dist.} = \left(\frac{4}{3} \right) (27.5) \left(\frac{\sin^3 0.8593}{1.7186 - \sin 1.7186} \right) = 21.84$$

Overlap Section, No. 1 Crankpin/Eccentric

Position of neutral axis



$$\bar{y} = \frac{(580.88)(6.795) - (275.84)(3.882)}{(580.88 + 275.84)} = 3.357$$

Second moment of area about neutral axis y - y

$$I_{yy} = I_{xx} + A(y^2 - x^2).$$

for area 275.84, $I_{xx} = 5893.04 \text{ mm}^4$ (using Casio program)

$$\therefore I_{yy} = 5893.04 + (275.84)(7.239^2 - 3.882^2) \approx 16192.24 \text{ mm}^4$$

for area 580.88, $I_{xx} = 48075.43 \text{ mm}^4$ (using Casio program)

$$\therefore I_{yy} = 48075.43 + (580.88)(3.438^2 - 6.795^2) \approx 28120.94 \text{ mm}^4$$

Total I_{yy} (neutral axis) of overlap section $\approx 44313.18 \text{ mm}^4$

Modulus of resistance to bending

Tension side, $Z = \frac{44313.18}{14.97} \approx 2960.12 \text{ mm}^3$

(Compression side, $Z = \frac{44313.18}{12.90} \approx 3435.12 \text{ mm}^3$)

Approximate check, assuming cross section is an ellipse,

semi axes = 20.8 and 13.95

$$I_{yy} = (0.04909)(27.9^3)(41.6) \approx 44350 \text{ mm}^4$$

$$Z_{yy} = \frac{44350}{13.95} \approx 3180 \text{ mm}^3$$

Overlap Section, Crankpin/Eccentric No. 1

For modulus of resistance to bending in plane of greatest width (i.e., due to coupling-link forces)

Ricardo data sheet gives formula
for I (second moment of area)
with circular sections of equal
radius, R, for the case considered
here, with radius $R_1 = 27.5$,

$$R_2 = 21.0,$$

$$\text{assume } I_{zz} = \frac{27.5^4}{4} \{0.8593 -$$

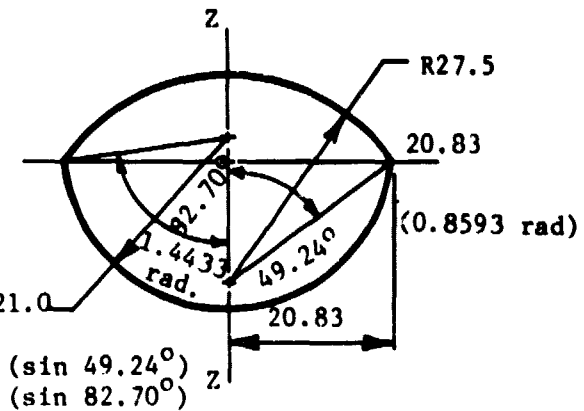
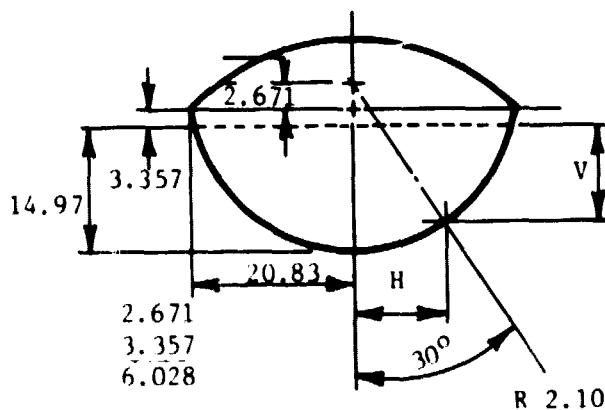
$$(21.0) (\sin 49.24^\circ) \\ (27.5) (\sin 82.70^\circ) \}$$

$$\left(\frac{\sin 3.4372}{4} \right) \left(-\frac{8}{3} \right) (\sin^3 0.8593) (\cos 0.8593) \} = 26370.96 \text{ mm}^4 \text{ for radius } 27.5$$

$$I_{zz} = \frac{21.0^4}{4} \{1.4433 - \frac{\sin 5.7732}{4} - \frac{8}{3} (\sin^3 1.4433) (\cos 1.4433) \} \\ = 60019.75 \text{ mm}^4 \text{ for radius } 21.0$$

$$\text{Total } I_{zz} \text{ for overlap section} = 86390.71 \text{ mm}^4.$$

$$\text{Modulus of resistance to bending} = \frac{86390.71}{20.83} = 4147.79 \text{ mm}^3$$



For intermediate position

subtending angle, say 30° , at

centre of 21.0 R arc,

$$H = (21.0) (\sin 30^\circ) = 10.5 \text{ mm},$$

or, with $\theta = 40^\circ$,

$$H = (21.0) (\sin 40^\circ) = 13.479 \text{ mm}.$$

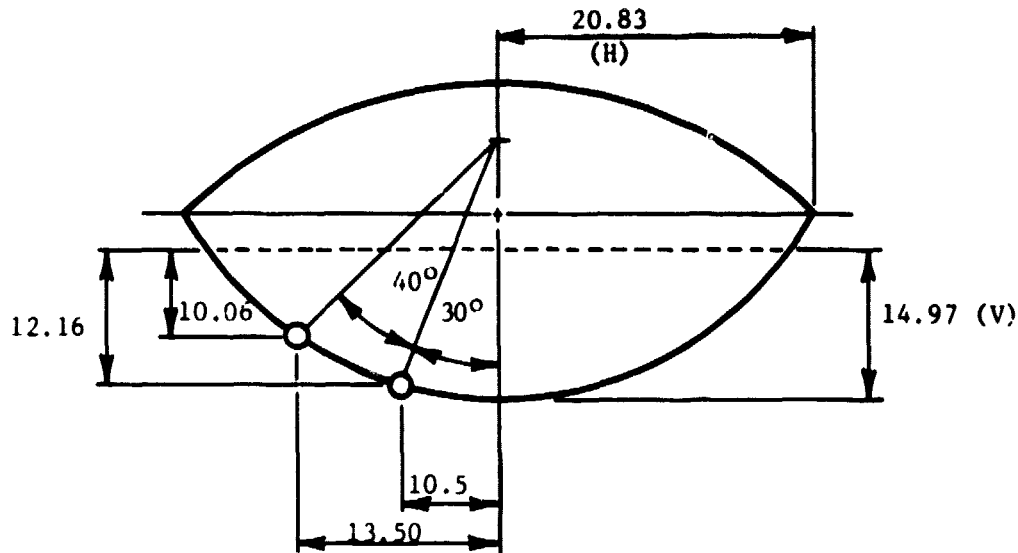
$$V = (21.0 \cos 30^\circ) - (2.671 + 3.357)$$

$$= 12.159 \text{ mm},$$

or, with $\theta = 40^\circ$,

$$V = (21.0 \cos 40^\circ) - 6.028 = 10.059.$$

Crank Angle - Bending Mode



Radius	H Ratios	V Ratios
30°	10.5/20.83, $\approx .504$	12.16/14.97 $\approx .812$
40°	13.50/20.83, $\approx .648$	10.06/14.97 $\approx .672$

Bending moments at crankpin/eccentric junction (No. 1 crankpin, eccentricity)
from attached point, extract from scheme 3274-21, with forces as on sheet 6.

- 1) Forces acting at crank pin, in plane of cylinder center line.

$$R_1 = \frac{(22068)(62)}{133}, \approx 10287 \text{ N} \quad R_2 = \frac{(22068)(71)}{133}, \approx 11781 \text{ N.}$$

$$= 11781 (45) = (530.15)(10^3), \text{ N-mm, (max) force } (W_{\text{gas}}) = 22068 \text{ N} \quad \theta = 45^\circ$$

$$= 6736 (45) = (303.25)(10^3) \text{ N-mm, with force } (W_{\text{gas}}) = 12618 \text{ N} \quad \theta = 225^\circ$$

$$= 4145 (45) = (186.54)(10^3) \text{ N-mm (min) with } W_{\text{gas}} = 7765 \text{ N} \quad \theta = 135^\circ$$

- 2) At right angles to plane of cylinder center line (forces acting at eccentric)

$$M = R_1 (87.5) \text{ and } R_1 = W_{\text{link}} \left(\frac{29.5}{133} \right)$$

$$M = W_{\text{link}} \left(\frac{(29.5)(87.5)}{133} \right) \approx 19.41 W_{\text{link}}$$

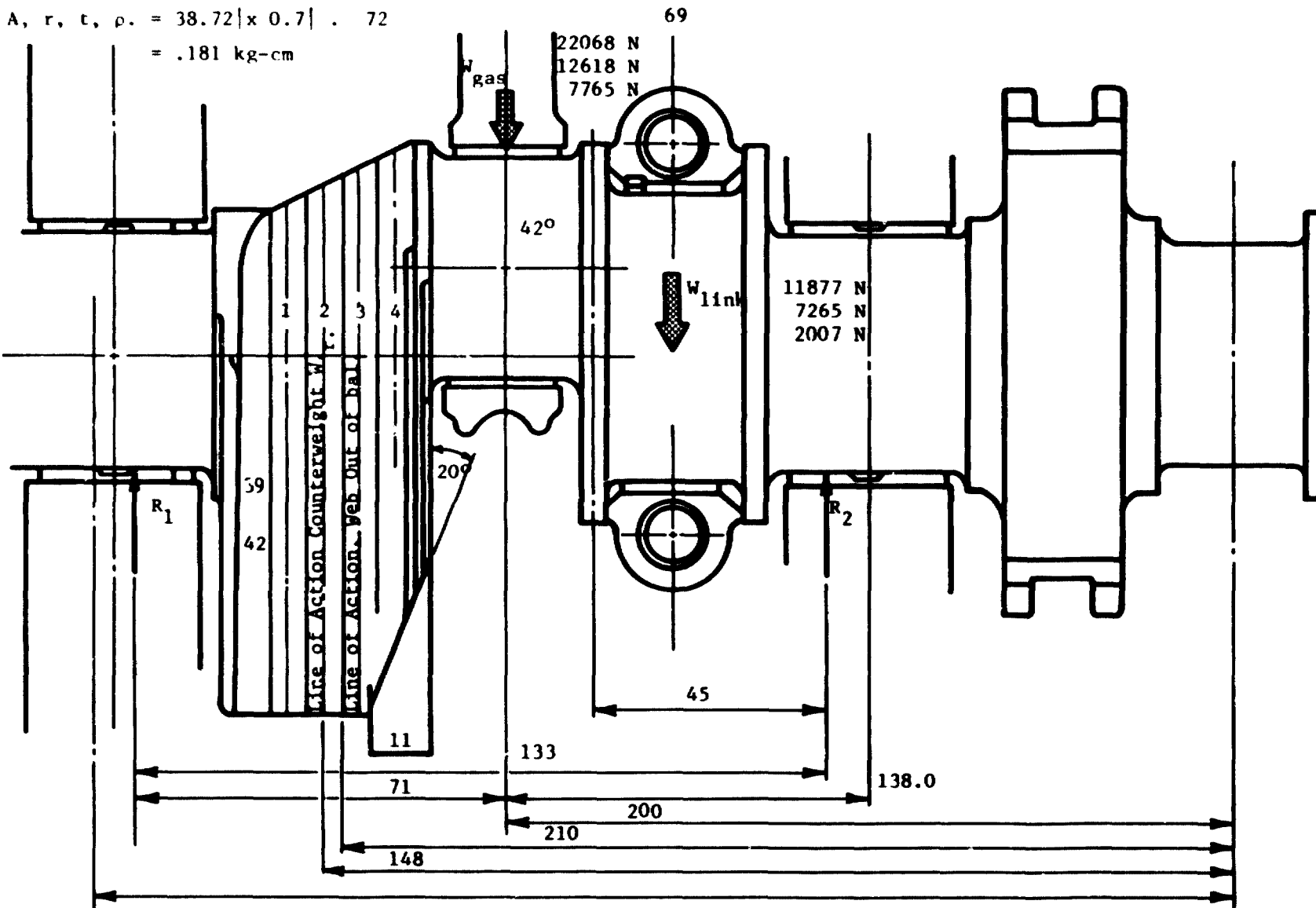
$$M = 230.53 (10^3) \text{ N-mm} \quad \text{with } W_{\text{link}} = 11877 \text{ N.} \quad \theta = 135^\circ$$

$$= 141.01 (10^3) \text{ N-mm} \quad W_{\text{link}} = 7265 \text{ N.} \quad \theta = 45^\circ$$

$$= 38.96 (10^3) \text{ N-mm} \quad W_{\text{link}} = 2007 \text{ N.} \quad \theta = 225^\circ$$

$$W.r = A, r, t, p. = 38.72 | x 0.7 | . 72$$

$$= .181 \text{ kg-cm}$$



1-574

ORIGINAL PAGE IS
OF POOR QUALITY

Copy of dimensional print extract
from 3274-21 322 2 Weight S/Stem
Used in balance calc. 23 April 1979

3274-17 (Extract)

2-Bearing Arrangement

$$R_1 = \frac{58 \times 953 + 189 \times 23127}{247} \approx 17920 \text{ N (Instead of 11034 N, with Bearings)}$$

Banding Stresses Increased by Factor 1.6,
Would Become Excessive for SG Iron

22068 N
12618 N
7765 N

W_{as}

W_{link}
(in plane)

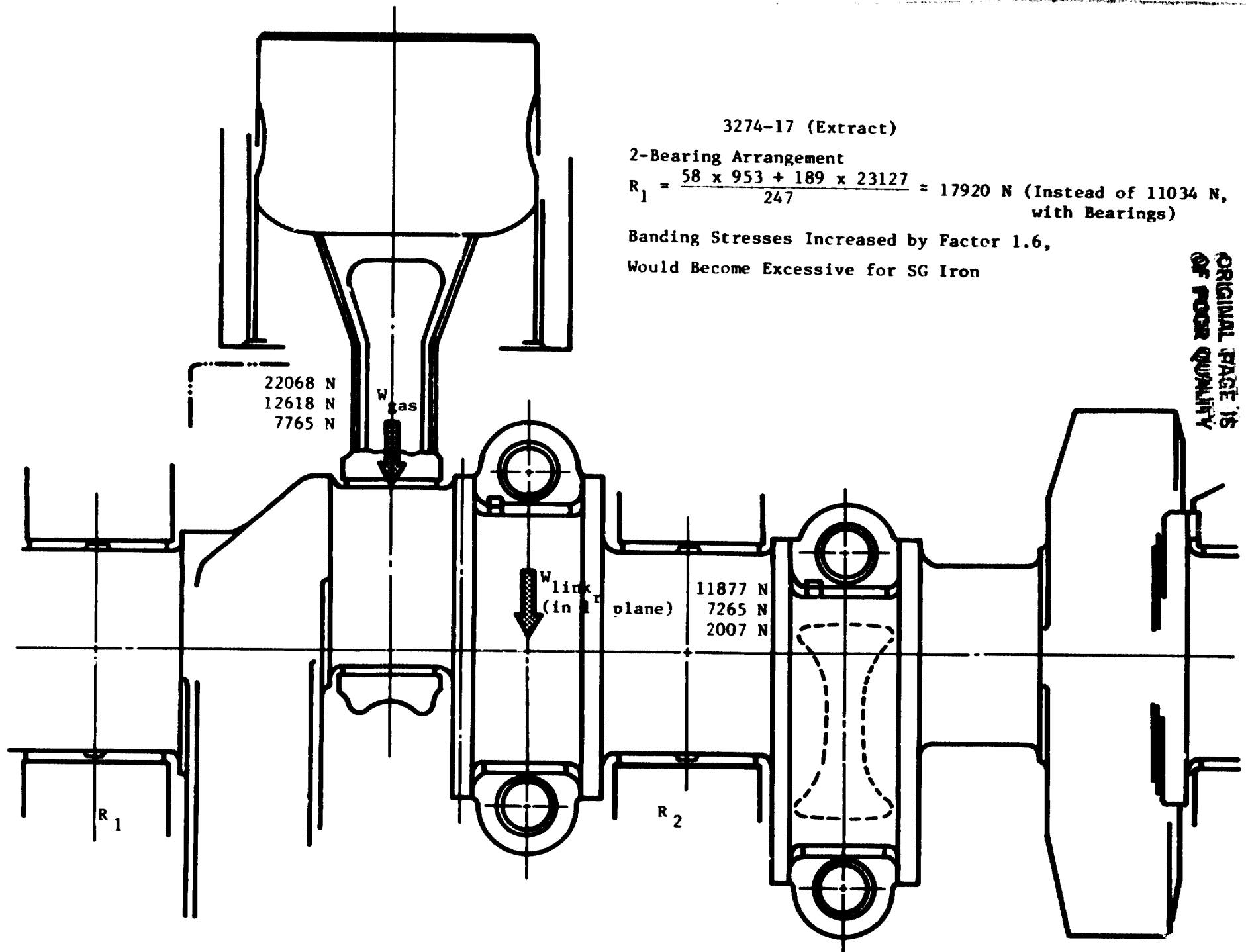
11877 N
7265 N
2007 N

R_1

R_2

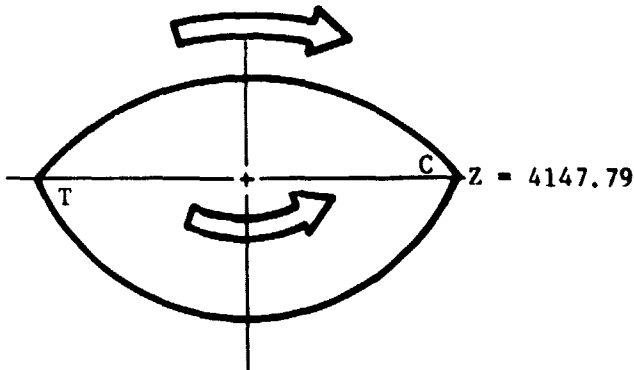
ORIGINAL PAGE IS
OF POOR QUALITY

1-575

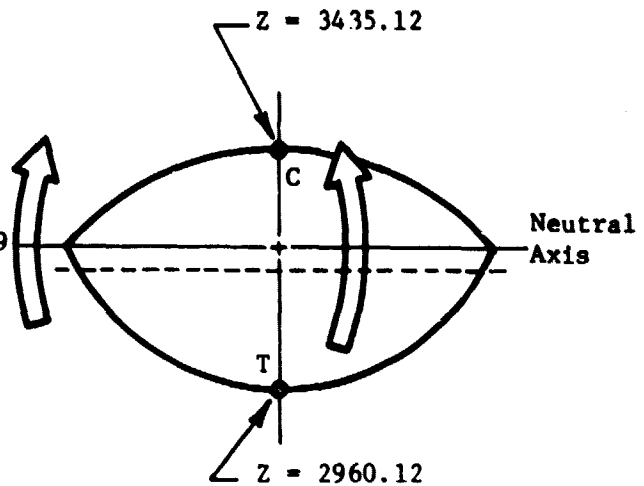


ORIGINAL PAGE IS
OF POOR QUALITY

1) Crank Angle



2) Bending Mode

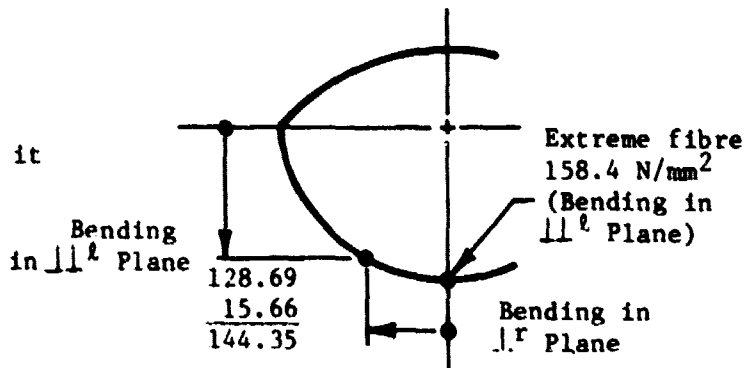


Bending Stress (Nominal)

Crank Angle	Bending Moment	Bending Stresses, N/mm ²		
		Extreme Fibre	Intermed. (1)	Intermed. (2)
Case 1	45°	$\frac{141.01}{4.148}$ ≈ 33.99	33.99 $\left(\frac{10.5}{20.83}\right)$ ≈ 17.13	33.99 $\left(\frac{13.50}{20.83}\right)$ ≈ 22.03
	135°	$\frac{186.53}{4.148}$ ≈ 44.97	22.67	29.15
Case 2	45°	33.99	17.13	22.03
	225°	$\frac{-38.96}{4.148}$ ≈ -9.39	-4.74	-6.10
Bending Mode				
Case 1	45°	$\frac{530.15}{2.960}$ ≈ 179.1	179.1 $\left(\frac{12.16}{14.97}\right)$ ≈ 145.5	179.1 $\left(\frac{10.06}{14.97}\right)$ ≈ 120.4
	135°	$\frac{-230.25}{3.435}$ ≈ 67.11	-54.5	-45.1
Case 2	45°	179.1	145.5	120.4
	225°	$\frac{303.25}{2.960}$ ≈ 102.4	83.2	68.8

Combined Bending Stresses

From the stresses calculated in the table, sheet 11, pg. B.8-69, it can be seen that at positions intermediate between the extreme fibres for bending in the \perp^r plane, the sum of the bending stresses is less than at the external fibre position, for the crank positions considered. It is therefore only necessary to combine the extreme fibre of one bending component with the torsional component.



Torsional Stress

Assume that peak torques from one cylinder are transmitted through the adjacent crank pin/eccentric overlap section.

$$\tau = 315 \text{ Nm, max; } -130 \text{ Nm, min., } \equiv 92.5 \pm 222.5 \text{ Nm.}$$

Assuming that cross-sectional area across which torque acts is an ellipse, with semi axes 20 mm and 13.9 mm.

$$\text{Mean Shear Stress} \approx \frac{2\tau}{(\pi)(20)(13.9)^2} \approx \frac{(92.5)(10^3)}{6069.9} \approx 15.24 \text{ N/mm}^2 \text{ mean.}$$

$$\text{Range of Shear Stress} \approx \frac{\pm 222.5 (10^3)}{6069.9} \approx \pm 36.66 \text{ N/mm}^2$$

Stress Concentration Factor (Bending)

Procedure given by Lowell is adopted as a guide, altogether the value of $\frac{t}{d}$ is outside its range of validity ($\frac{t}{d} = \frac{6}{42}$, $\approx .143$)

$$\alpha_b = A_{bo} \times V_b$$

$$A_{bo} = (1.2) \left(\frac{3}{6} \right) - .455 \approx 1.645$$

$$V_b \approx 1.962 - (2.434)(1.476) + (1.873)(1.476)^2 - (544)(1.476)^3 + (.0615)(1.476)^4 \approx .993.$$

$$\left(\text{with } \frac{b}{d} = \frac{62}{42}, \approx 1.476 \right)$$

$$\text{whence } \alpha_b \approx 1.63.$$

Stress Concentration Factor (Bending)

Alternatively, regarding the crankpin/eccentric overlap region as a shoulder fillet from Peterson's "stress concentration factors," Fig. 78a, p. 104.

$$K_t \approx 1.93$$

Stress Concentration Factor, Torsion

Using the expression

$$\alpha_t = \frac{r}{d} - (.2205 + .1015 \frac{u}{d}) \quad , \quad \text{with } \frac{r}{d} = \frac{3}{42} = .07143$$

$$\alpha_t \approx \frac{1}{(.07143) \cdot 2.879} \quad \text{and } \frac{u}{d} = \frac{27.9}{42} \approx .6635 \quad ,$$

$$\approx 2.14 \quad .$$

For convenience of calculation, and in the absence of more reliably accurate data, make $\alpha_b = \alpha_t = 2.0$.

Equivalent Stress (Combined Tensile and Shear)

Nominal Stresses

Bending, Case 1. $f_{\max} = 179.1$, $f_{\min} = -67.1$ (from sheet 11)

$$\therefore f_{\text{mean}} = 56 \pm 123.1 \text{ N/mm}^2.$$

$$\therefore \text{Equivalent mean stress} \approx \sqrt{56.0^2 + (3) (15.2)^2} \approx 61.9 \text{ N/mm}^2$$

$$\text{Equivalent stress range} \approx \pm \sqrt{123.1^2 + (3) (36.7)^2} \approx \pm 138.5 \text{ N/mm}^2$$

Bending, Case 2. $f_{\max} = 179.1$, $f_{\min} = 102.4$ (from sheet 11)

$$\therefore f_{\text{mean}} = 140.75 \pm 38.35 \text{ N/mm}^2$$

$$\therefore \text{Equivalent mean stress} \approx \sqrt{140.75^2 + (3) (15.2)^2} \approx 143.2 \text{ N/mm}^2$$

$$\text{Equivalent stress range} \approx \pm \sqrt{38.35^2 + (3) (36.7)^2} \approx \pm 74.2 \text{ N/mm}^2$$

Equivalent Stresses (Combined Tensile and Shear)

Calculated Peak Stresses

Assuming stress concentration factor 2, fatigue notch factor (SG iron) ≈ 1.45
(say 1.5)

$$\text{Case 1. } f_{\text{equiv}} \approx (1.5) (61.9 \pm 138.5) = 92.9 \pm 207.8 \text{ N/mm}^2$$

$$\text{Case 2. } f_{\text{equiv}} \approx (1.5) (143.2 \pm 74.2), = 214.8 \pm 111.3 \text{ N/mm}^2$$

For easier comparison with previous crank stress calculations, consider bending alone, case 1, (from page 1)

$$f = (1.5) (48.5 \pm 109.9) = 72.8 \pm 164.9 \quad \begin{aligned} f_{\text{max}} &= 237.7 \text{ N/mm}^2 \\ f_{\text{min}} &= -92.1 \text{ N/mm}^2 \\ f_{\text{range}} &= 329.8 \text{ N/mm}^2 \end{aligned}$$

Stresses in Crankpin

Applied Forces.

Cursory inspection of the piston forces tabulated on sheet 3 shows maximum and minimum loads to be those occurring at 30° crank rotation (gas-only forces). These loads will give max/min stresses which will affect almost the same maximum fibre position.

Link forces are neglected, since the maximum fibre stresses induced by them will affect different regions of the material. The reasoning here is similar to that of sheets 11 and 12.

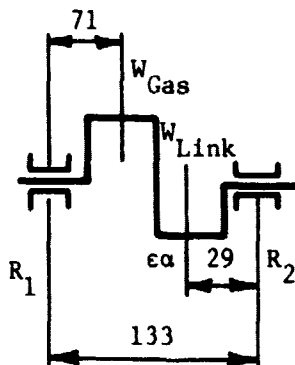
N.B. Note added 17 May 1979. Minimum stress is not at $\theta = 180^\circ$, since crankpin has rotated through 180° as well as load direction.

Minimum stress occurs when gas forces are a minimum and lateral forces from link causes change of signs in stress, viz:

$$\theta \approx 90^\circ. \text{ (Say } \theta = 105^\circ, \text{ where } W_{\text{link}} = 11124 \text{ N).}$$

$$W_{\text{max}} = 23346 \text{ N.} \quad W_{\text{min}} = -11124 \cdot \cos 15^\circ, = -10745 \text{ N.}$$

Bending Moments



$$\begin{aligned} \text{Reaction force } R_1 &= W_{\text{Gas}} \left(\frac{62}{133} \right), \approx \\ &= W_{\text{Link}} \left(\frac{29}{133} \right) \end{aligned}$$

$$\begin{aligned} M &= 71 \cdot R_1, \therefore M_{\text{max}} = W_{\text{Gas}} \left(\frac{62}{133} \right) (71) \\ &= (23346) \left(\frac{62.71}{133} \right) \approx 772.7 (10^3) \end{aligned}$$

$$\begin{aligned} M_{\text{min}} &= W_{\text{Link}} \left(\frac{29.71}{133} \right) = \frac{(-10745) (29.71)}{132}, \\ &\approx -166.3 (10^3) \end{aligned}$$

Nominal Bending Stress (Crankpin Mid-Length)

$$\begin{aligned} f_{b \text{ max}} &= \left(\frac{772.7}{7274} \right) (10^3), \approx 106.2 \text{ N/mm}^2; f_{b \text{ min}} = \left(\frac{-166.3}{7274} \right) (10^3), \approx -22.9 \text{ N/mm}^2. \\ f_{\text{mean}} &= 41.6 \pm 64.5 \text{ N/mm}^2. \end{aligned}$$

Stress Concentration Factors (From Fig. 164, 173 of "Stress Conc. Factors" by Peterson)

$$a = 4.0, d = 42, \frac{a}{d} = .095.$$

$$\begin{aligned} \therefore \text{For bending, } K_t &\approx 2.7, K_f \approx 1.75 \\ \text{For torsion, } K_t &\approx 3.5, K_f \approx 2.0 \end{aligned} \left. \vphantom{\begin{aligned} \therefore \text{For bending, } K_t &\approx 2.7, K_f \approx 1.75 \\ \text{For torsion, } K_t &\approx 3.5, K_f \approx 2.0 \end{aligned}} \right\} \text{SG Iron.}$$

Calculated Peak Stresses

$$\text{Bending } f_b \approx (1.75) (41.6 \pm 64.5) = 72.8 \pm 112.9 \text{ N/mm}^2$$

$$\text{Torsional (Assuming } T_{\text{max}} = 315 \text{ Nm, } T_{\text{min}} = -130 \text{ Nm, } Z_p = \frac{\pi}{16} D^3 \approx 14547 \text{ mm}^3).$$

$$\begin{aligned} f_{s \text{ max}} &= \frac{(2.0) (315000)}{14547}, \approx 43.3 \text{ N/mm}^2, \\ f_{s \text{ min}} &= \frac{(2.0) (-130000)}{14547}, \approx -17.9 \text{ N/mm}^2. \end{aligned} \left. \vphantom{\begin{aligned} f_{s \text{ max}} &= \frac{(2.0) (315000)}{14547}, \approx 43.3 \text{ N/mm}^2, \\ f_{s \text{ min}} &= \frac{(2.0) (-130000)}{14547}, \approx -17.9 \text{ N/mm}^2. \end{aligned}} \right\} f_{\text{mean}} = 12.7 \pm 30.6 \text{ N/mm}^2$$

Combined Stress

$$S_{\text{mean}} = \sqrt{72.8^2 + (3) (12.7)^2} \approx 76.1 \text{ N/mm}^2.$$

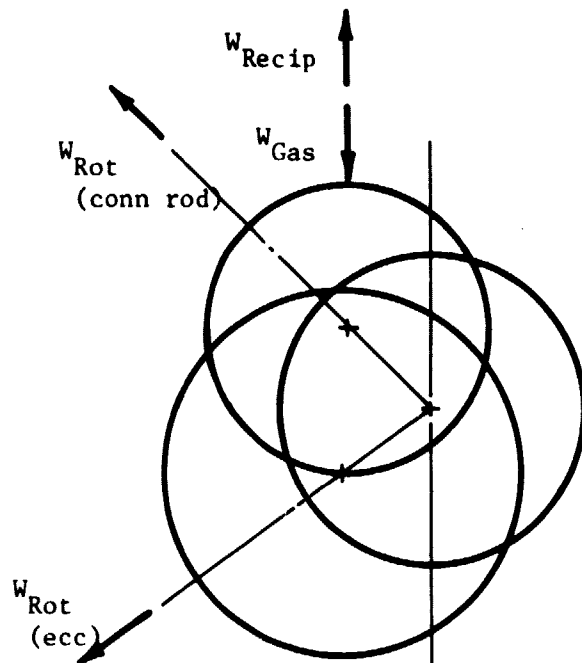
$$S_{\text{range}} = \pm \sqrt{112.9^2 + (3) (30.6)^2} \approx \pm 124.7 \text{ N/mm}^2.$$

$$\begin{aligned} 201.8 \text{ N/mm}^2, &\text{ max} \\ -48.6 \text{ N/mm}^2, &\text{ min} \end{aligned}$$

Crankshaft Bending Stress (Inertia Relief)

In work done previously (sheets 1 to 15), it has been assumed that full cylinder pressure can be developed at speeds which are so low that no appreciable inertia forces are generated.

The (more realistic) assumption is now made that the control system limits the cylinder pressure at speeds lower than 1000 rpm, the same crank positions as on sheets 6 & 7 and again being assumed to represent the most severe stress extremes.



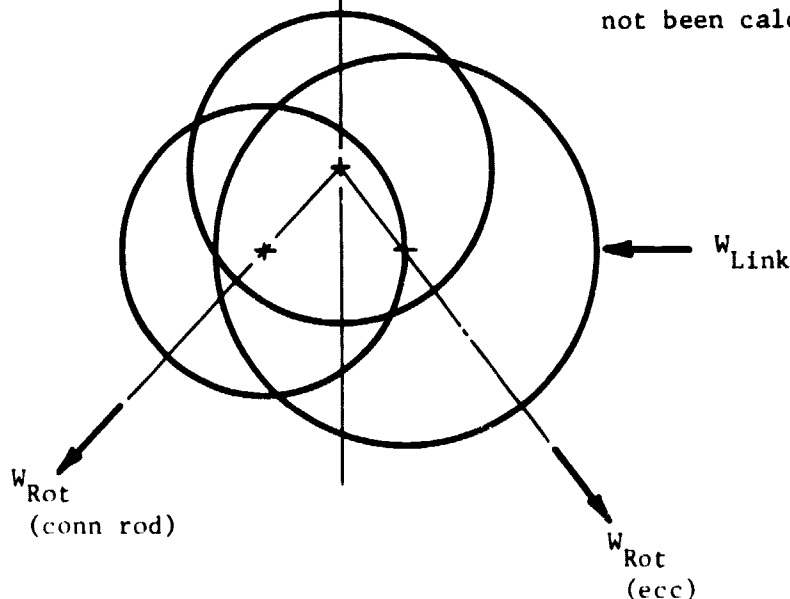
W.r. - Values:

Connecting rod big end	0.91 kg-cm
Coupling link big end	0.98 kg-cm
	(SG Iron)
Reciprocating Parts	3.25 kg-cm
	(from calc. 30 April 1979)

Since the components of W_{Rot} resolved \perp to W_{Gas} are

- i) small compared with W_{Gas} , W_{Recip}
 - ii) act in opposite directions,
- only the effect of W_{Recip} is considered in this approximate calculation.

(N.B. Effect of counterweight is to superimpose a steady bending stress (at constant speed); counterweight has not been calculated for crank 1-2 yet.)



Crankshaft Bending Stress (Inertia Relief)

Inertia force (at 45° crank rotation)

$$F_{\text{Recip}} (45^\circ) = (109.7) (3.75) (\cos 45^\circ) \left(\frac{17}{104}\right) (\cos 90^\circ) \left(\frac{\text{rpm}}{1000}\right)^2 \text{ Newtons}$$
$$\approx (252.1) \frac{\text{rpm}}{1000}^2 \text{ N}, = 252 \text{ N at 1000 rpm}$$

Recalculating sheet 11 onward, with force at crankpin reduced by the amount calculated above:

$$\text{Force at crankpin} \quad 22068 - 252, = 21816 \text{ N.}$$

$$\text{Reactions at supports} \quad R_1 = 21816 \left(\frac{62}{133}\right), \approx 10170 \text{ N.}$$

$$R_2 = 21816 \left(\frac{71}{133}\right), \approx 11646 \text{ N.}$$

Bending moments

$$\text{At crankpin/eccentric overlap, } M = (45) (R_2), \approx 524 (10^3) (\text{maximum}).$$

Minimum M is as calculated previously, sheet 11,

$$\text{i.e., } 230.5 (10^3) \text{ N/mm.}$$

Nominal stresses (with $Z = 2960 \text{ mm}^3$, tension fibres, $\theta = 45^\circ$)

$Z = 3435 \text{ mm}^3$, tension fibres, $\theta = 135^\circ$

$$f_{b \text{ max}} = \frac{524.0}{2.96}, \approx 177 \text{ N/mm}^2.$$

$$f_{b \text{ min}} \approx -67 \text{ N/mm}^2 \quad (\text{see sheet 11})$$

Only the maximum stress is affected by the inclusion of inertia relief and that not to an appreciable extent.

RICARDO CONSULTING ENGINEERS

CLIENT USSW SECTION Cylinder Block/Burner Head
PROJECT ASE Mod I Engine SHEET NO. 1 OF 4
JOB NO. C4813-20 DATE 7 November 1979
CALCULATION BY DR DRAWING KEY NO. _____

OBJECT To examine the bolted joint between burner head and cylinder block

Securing bolts are M14 material strength grade 10.9. Tightening torque specified is 95 N-m.

$$\therefore \text{Pretension} = \frac{(5)(95)}{14} 1000 = 33\,930 \text{ N}$$

Specified proof load (BS 3692) = 9110 kp = 89,370 N

Percentage of proof load developed by tightening torque quoted = 38% approximately.

Differential thermal expansion may need to be taken into account; some of the clamped parts are of aluminum alloy and are at a temperature expected to be well above ambient, in operation.

For maximum operating preload, assume that differential thermal expansion can increase pretension due to initial tightening torque to 70% of proof load (this is considered a maximum safe nominal value bearing in mind the degree of approximation in the torque/tension relationship). Maximum pretension = 62,560 N.

For maximum operating load, assuming maximum "gas-only" force acting at crankspin (from "Stirling Simulation Program LL/751217, page 11") also acts on burner head and is reacted only by the four bolts surrounding the cylinder developing maximum pressure without any support from other bolts, i.e., 23,346 N maximum cylinder-pressure load, shared between 4 bolts.

Total bolt load depends on relative rigidity of bolt and base (see Sheet 2)

RICARDO CONSULTING ENGINEERS

CLIENT USSw

SECTION Cylinder Block/Burner Head

PROJECT ASE Mod I

SHEET NO. 2 OF 4

JOB NO.

DATE 7 November 1979

CALCULATION BY

DRAWING NO.

OBJECT

For proportion of working load supported by bolt assume boss diameter 30 mm

$$E_{\text{alum.}} = 70 \text{ kN/mm}^2.$$

With $E_{\text{steel}} = 210 \text{ kN/mm}^2$, and assuming that effective length of boss $\approx 0.8 \times$ actual length; actual length of boss = length of bolt.

$$R_{bolt} = \frac{210 A_{bolt}}{l} = \frac{32,300}{l}$$

$$R_{\text{boss}} = \frac{70 \text{ A}_{\text{boss}}}{0.8 \ell} = \frac{87.5}{\ell} \cdot 7854 (30.0^2 - 14.5^2) = \frac{47,400}{\ell}$$

Alternating component of load on bolt,

$$F_{alt} = + \frac{23,346}{4} \frac{\frac{32,330}{2}}{\frac{32,330}{2} + \frac{47,400}{2}} = + (5836.5) \frac{32,330}{79,730}$$

$$\therefore F_{alt} = \pm 1744 \text{ N (each bolt)}$$

Total force in bolt = pretension + stress range

(Assumption 1) = 38,660 N, with tightening torque 95 NM

(Assumption 2) = 67,290 N, assuming differential thermal expansion increases pretension to 70% of proof load.

Strength of screw thread in aluminum alloy boss (stripping)

Shear area of thread (using formula from BS 3580)

$$S_n = \pi (1/2 \cdot 14) (13.68 + 2.77) \{ 2.0/2 + 0.577 (13.68 - 2.91) \}$$

$$= 522 \text{ mm}^2 \text{ for } 1 \times \text{diameter } (= 14 \text{ mm}) \text{ length of engagement}$$

(N.B. calculated areas applies to outside dimensions of screw thread insert, where major and effective diameters allowed to be 2.77*mm larger than bolt thread, in each case.

$$\begin{aligned}\text{and, for bolt, } AS_g &= (\pi)(1/2)(14)(12.21) \{2.0/2 + 0.577 (12.50 - 12.21)\} \\ &= 313 \text{ mm}^2.\end{aligned}$$

(Assuming minor diameter of thread insert is same as standard nut.

*See "cross" wire thread inserts data sheet 158)

RICARDO CONSULTING ENGINEERS

CLIENT United Stirling
PROJECT ASE Mod I Engine
JOB NO. C4313-20
CALCULATION BY

SECTION Cylinder Block/Burner Head
SHEET NO. OF
DATE 7 November 1979
DRAWING KEY NO.

OBJECT

Shear Stress in Casting Boss Screw Threads

$$f_s = \frac{38660}{522}, = 74.06 \text{ N/mm}^2 \text{ (Assumption 1)}$$

$$= \frac{67290}{522}, = 128.9 \text{ N/mm}^2 \text{ (Assumption 2)}$$

Ultimate shear stress of heat-treated material assumed

$$= 220 \times .577, = 126.9 \text{ N/mm}^2$$

∴ To carry loads of Assumption 2, length of engagement should be increased to 20 mm (= 1.5 "safety factor").

Check on shear stress in bolt threads. With engaged length $L_c = 20 \text{ mm}$, as recommended above, $AS_s = 313 \times \frac{20}{14} = 447 \text{ mm}^2$.

$$f_s = \frac{38660}{447}, = 86.5 \text{ N/mm}^2 \text{ (Assumption 1)}$$

$$= \frac{67290}{447}, = 150.5 \text{ N/mm}^2 \text{ (Assumption 2)}$$

Compared with ultimate shear stress of stud, $117 \times .577, = 680 \text{ N/mm}^2$, the above stress is safe by a large margin.

Stresses at Junction of Boss with Main Body of Casting

A very approximate calculation assumes that the boss is joined to the rest of the casting by two areas; Area 1) where the barrel jacket wall joins the boss, and the material is in shear, and Area 2) where external pins and barrel jacket join the boss, and the material is in tension.

$$\text{Total area, Area 1) } = 5 \times 45 \times 2 = 450 \text{ mm}^2$$

$$\text{Total area, Area 2) } = 5 \times (15 + 18 + 33) = 330 \text{ mm}^2.$$

Assuming that there is bodily relative displacement δ between the boss and the rest of the casting which affects a thickness of material = 5 mm, in shear, and 8 mm in tension.

$$\text{Shear strain} = \frac{\delta}{5} ; \text{ shear stress } f_s = \frac{\delta}{5} \cdot \frac{2800}{5} = 5600 \delta \text{ mm}^2.$$

RICARDO CONSULTING ENGINEERS**ORIGINAL PAGE IS
OF POOR QUALITY**

CLIENT USSw
PROJECT ASE Mod I Engine
JOB NO.
CALCULATION BY

SECTION Cylinder Block/Burner Head
SHEET NO. 4 OF 4
DATE 7 November 1979
DRAWING KEY NO.

OBJECT

Stress at junction of boss with main body of casting; approximate estimate,
continued.

$$\text{Tensile Strain} = \delta/8; \text{ tensile stress } \sigma_E = \frac{\delta \cdot E}{8}, \quad \frac{\delta \cdot 70000}{8} = \approx 8750 \delta \text{ N/mm}^2$$

∴ Total elastic reaction forces

$$= (5600)(8450) + (8750)(\delta)(8330) = 38,660 (\text{assumption see sheet 2})$$

$$\therefore \delta = 38,660 / 5,407,500 = 7.15 \cdot 10^{-3} \text{ mm.}$$

or assuming differential thermal expansion in excess bolt pretension up to 70% of
proof load, 67,290 N.

$$\text{Deflection, } \delta = 67,290 / 5,402,500 = 12.44 \cdot 10^{-3} \text{ mm (assumption 2).}$$

Stresses

$$\text{Shear, at Section "S", } f_s = 5600 \times 7.15 \cdot 10^{-3} = 40.0 \text{ N/mm}^2$$

(Assumption 1)

$$\text{Tensile, at Section "T", } f = 8750 \times 7.15 \cdot 10^{-3} = 62.6 \text{ N/mm}^2$$

$$\text{Shear, at Section "S" } f_s = 5600 \times 12.44 \cdot 10^{-3} = 69.7 \text{ N/mm}^2$$

$$\text{Tensile, at Section "T" } f = 8750 \times 12.44 \cdot 10^{-3} = 108.9 \text{ N/mm}^2$$

(Assumption 2)

Conclusions

The structure immediately adjacent to the boss appears to have sufficient
strength since the approximately calculated stresses are only about 1/2 x
(ultimate stress for material) for the highest loads considered.

ORIGINAL PAGE IS
OF POOR QUALITY

ENGINEERING DEPARTMENT REPORT

No. 509

LOAD AND LUBRICATION STUDY OF UNITED
STIRLING A.S.E. MOD. 1 ENGINE.

NOVEMBER, 1979

M.R. TAYLOR

CIRCULATION

Mr. R.H. Spikes/R.&D./ Library
Ricardo

C O N T E N T S

	<u>PAGE</u>
Introduction	1
Big-end bearings	2
Main bearing with gear drive	3
Main bearings with connecting links	4
Connecting links	5
Lubrication system	6
Conclusion	7
Appendix I	
Appendix II	

C - 7

INTRODUCTION

We have previously examined a series of square four Stirling Engines for this client. The latest of these studies was our Engineering Report No. 479 which examined the now familiar layout with two crankshafts each driving the single output shaft through gears placed outboard of the No. 3 main bearings. This arrangement is sketched in Appendix I. Also included in that Report was an analysis of a proposed link arrangement whereby two connecting links fitted with plain bearings would be used to connect the shafts only one of which would then be geared to the output shaft.

This study examines the latest version of the engine. In this version the connecting links are placed either side of the centre main bearings. This greatly complicates the analysis because the loads acting through the links are now carried by all six main bearings although the crankshaft layouts are such that the centre main carries three quarters of these loads. Sketch No. 1 in Appendix II illustrates the layout of the engine.

The request for this study was received in a letter dated 20th June. During subsequent discussions it became clear that an intermediate stage of development would be run before the revised design described above. This would have the same top end but would retain the original gear drive mechanism. We were therefore asked in the letter of 28th September to consider this version also so as to provide a standard for comparison with earlier studies. This we have done.

.2.

BIG-END BEARINGS

We began our study at the speed of 3000 rpm, the only speed included in the engine data form, RD1. The earliest calculations were discussed with Ricardo and in consequence an additional low speed of 900 rpm was examined. It is a feature of the Stirling engine that this low speed - full load condition is easily realisable and since this produces the most severe bearing conditions it is important that it be examined.

A full cycle of forces on the piston was supplied from which a bearing load cycle was calculated at both speeds. Appendix I includes a diagram of the 900 rpm cycle which is almost linear because of the very low inertia contribution. At 3000 rpm the cycle would open out and the variation in load direction then provides a less severe environment for the bearing. The maximum bearing pressure found was 29.7 MN/m^2 (4308 psi), occurring at 900 rpm.

The lubrication analysis was performed using a diametral clearance of 0.051 mm (0.002 in.) and an oil viscosity of 7 cP. This viscosity is our standard value used to facilitate comparison between different engines' lubrication conditions. The bearing dimensions used were 42.0 mm (1.654 in.) diameter and 18.49 mm (0.728 in.) minimum effective length. The summary sheet RD31/295 in the Appendix shows the results. As anticipated the lower speed provides the lower minimum oil film thickness. This value of $1.06 \mu\text{m}$ (42 μm) is exactly half that occurring at 3000 rpm. The appropriate journal orbit is in Appendix I.

Taking account of the calculated loads and minimum film thicknesses we recommend VP20 for this bearing.

.3.

MAIN BEARING WITH GEAR DRIVE

During the course of the Stirling Engine studies which we have conducted a computer program has been developed to permit the inclusion of additional forces in the bearing load cycle and calculate the corresponding lubrication conditions. Unfortunately the process is a tedious one including considerable manual effort in data preparation. In view of this it was decided that only the lower speed would be examined for the main bearings as our earlier studies have shown that this provides a more testing bearing condition. This is because the generation of a hydrodynamic oil film is a strongly speed related effect and at the low speed and high load considered here only thin films can be developed.

The bearings are fully grooved and common throughout. A shaft diameter of 45.0 mm (1.772 in.) and a minimum effective length of 28.73 mm (1.131 in.) were assumed. A surface groove width of 4.83 mm (0.190 in.) was used.

The load cycles were calculated first and then the gear forces were added to the two No. 3 mains. A constant gear force equal to the mean reaction force was assumed for simplicity. Since the maximum force is 5.03 kN as compared with the mean of 4.83 kN we do not consider this approximation to be unreasonable. Appendix I shows the resulting load cycles with the direction of the gear reaction force marked.

The Summary Sheet in Appendix I shows the maximum bearing pressures. These are all relatively low and VP19, our aluminium-20% tin material, is the appropriate one for these bearings.

ORIGINAL DESIGN OF POOR QUALITY

.4.

Our lubrication analysis used the same assumptions as before for these bearings, that is a diametral clearance of 0.051 mm (0.002 in.) and an oil viscosity of 7 cP. The results are summarised in Appendix I and show that the worst conditions arise on the two rear (No. 3) mains. The journal orbits show that this is due to the continual net loading on one side of each bearing and the resultant dwelling of the shaft on that side. These orbits are shown in Appendix I along with those for the remaining four main bearings. Oil film thicknesses on these bearings are well above those on the rear mains, their minimum value being 0.89 μm (35 $\mu\text{in.}$) as compared with 0.66 μm (26 $\mu\text{in.}$).

MAIN BEARINGS WITH CONNECTING LINKS

The same calculated load cycles were used as the basis for this version. Here these required the addition of the reaction forces from the connecting links. Because these links are placed either side of the centre main and relatively close to it this bearing has the highest additional forces to be included. The end mains are only affected by one link each with the exception of No. 3 main on crankshaft one. This bearing is adjacent to the gear drive to the output shaft and therefore also carries a gear reaction force. The sketch in Appendix II makes these details of the layout clear. This Appendix also includes the resulting load cycles.

As before we only examined the 900 rpm condition. Once again the maximum bearing pressures mean that VP19 is the appropriate material. In this version the overall maximum of 16.4 MN/m^2 (2373 psi) occurs on the centre main of crankshaft two.

ORIGINAL FILED
OF POOR QUALITY

.5.

The lubrication conditions may be summarised by describing the bearings with substantial additional forces (i.e. the centre mains and the rear main of crankshaft 1) as poor whilst the others are moderate. A clear division between the two types is evident on the Summary Sheet RD31/295 which shows minimum oil film thicknesses in the ranges $0.56 - 0.62 \mu\text{m}$ (22 - 24 $\mu\text{in.}$) and $0.88 - 0.97 \mu\text{m}$ (35 - 38 $\mu\text{in.}$). However these two ranges are similar to those we have seen in previous studies where the division is caused by gear forces being added to the rear mains.

The journal orbits are shown in Appendix II.

CONNECTING LINKS

The load cycles of these bearings were supplied. Because the forces are compressive and tensile along the link the bearings' load cycles are linear.

The bearings are fairly generously dimensioned with a minimum effective length of 16.48 mm (0.649 in.) and a shaft diameter of 54.0 mm (2.126 in.). These provide relatively safe bearing conditions with a maximum bearing pressure of 14.5 MN/m^2 (2104 psi) and a minimum oil film thickness of $1.29 \mu\text{m}$ (51 $\mu\text{in.}$) calculated on the same basis as the other bearings. Our lead based babbitt material VP18 is an appropriate one for this application.

Because these links are being considered as an alternative means of power transmission it is worth examining the consequent power loss so as to provide a basis for comparison. As with all bearing power losses the shaft speed is one of the most important parameters so we have performed the calculation at both 900 and 3000 rpm. Bearing clearance is also important so our assumed range is $25-76 \mu\text{m}$ (0.001 - 0.003 in.) on diameter. Higher values would reduce the power loss

up to the stage where oil churning becomes significant. The losses calculated are 42 - 68W (0.06 - 0.09 BHP) at 900 rpm and 370 - 600W (0.5 - 0.8 BHP) at 3000 rpm. Using the supplied output torque we calculate the engine's output as 70kW (94 BHP) at 3000 rpm so a normal value for the loss in the linkage would be about 0.65%.

LUBRICATION SYSTEM

The data supplied quoted an oil pressure of 4 bar and temperature of 70°C. Whilst this particular version of the engine has yet to run we presume that this temperature is quoted on the basis of previous experience with these engines. If it is realised here with the specified 20W-40 oil then the oil viscosity will be substantially higher than the 7 cP used in the calculation with a corresponding increase in oil film thickness.

We are normally able to make a recommendation for pump capacity on the basis of the oil flow rates calculated from the bearings' average eccentricities. In order to do this here we have estimated values for the average eccentricities at 3000 rpm from the values calculated at 900 rpm. The total calculated flow required for the version with four additional link bearings is 8.6 lpm (1.9 gpm) at 3000 rpm, assuming that all bearings have a diametral clearance of 0.076 mm (0.003 in.).

These calculated flow rates permit us to recommend minimum crankshaft drilling diameters. Because these rates are quite low by automotive standards the appropriate diameter of 2.3 mm (0.091 in.) is well below the diameter we would expect to be necessary for production convenience. A suitable diameter is 4 mm (0.157 in.).

CONCLUSION
OF PDC QUALITY

.7.

CONCLUSION

The connecting rod bearing design appears sound and we anticipate satisfactory performance. VP20 is the appropriate material.

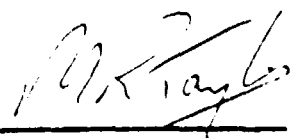
The main bearings as examined in Appendix I with an output gear on each crankshaft have adequate lubrication conditions on the front and centre bearings. Those calculated at the rear are more severe because of the additional forces acting but the low bulk oil temperature anticipated suggests that they will prove adequate in practice. Loads are relatively light and VP19 is the recommended material.

The proposed design using connecting links and one output gear is interesting. The additional forces are here most significant on the centre main and the rear main of crankshaft one and in each case a substantial reduction in minimum oil film thickness results. These values are well below our normal criteria for satisfactory operation but given that this engine has many peculiarities, not least of which is a remarkably low oil temperature, they may prove adequate in this case. The performance of the intermediate version discussed above will provide a useful standard for comparison as these main bearings have only slightly worse calculated oil film thicknesses. The same main bearing design is appropriate.

The connecting links appear to have the safest bearing design in the engine. The loads are sufficiently low for babbitt to be our material recommendation. Oil film thicknesses are excellent.

The Report has included recommendations for drilling diameters. Because oil flow rates are relatively low these are chosen for production convenience.

MRT/SW
2/11/79


M.R. TAYLOR
Product Research

ORIGINAL PAGES
OF POOR QUALITY

APPENDIX I

ENGINE WITH OUTPUT GEAR ON EACH SHAFT.

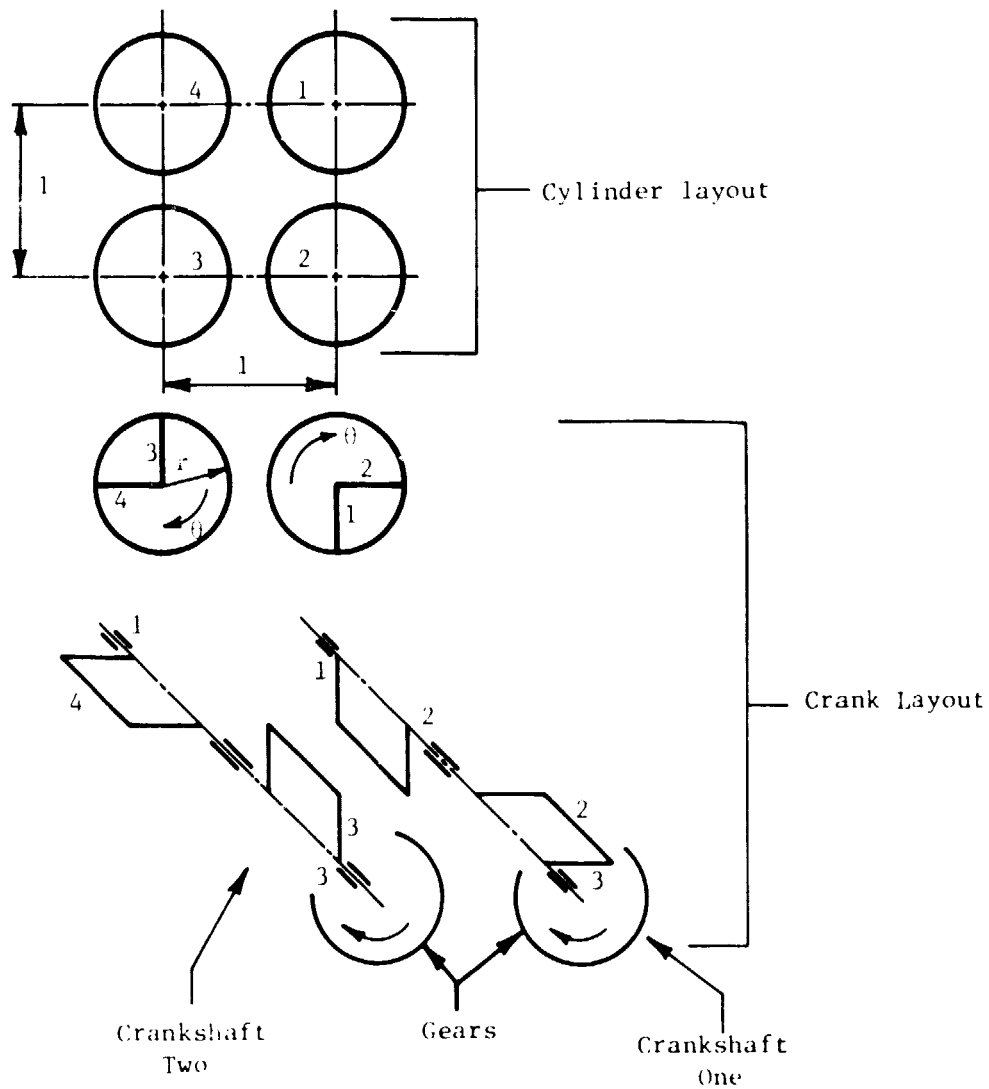
Sketch of engine layout.

Summary sheet RD31/295/1.

Operating load cycles.

Journal orbit diagrams.

ORIGINAL FILE IS
OF POOR QUALITY



Layout Assumed for Version without Link Drive

SUMMARY of LOAD and LUBRICATION STUDY

RECIPROCATING ENGINES

Engine Description		UNITED STIRLING ASE MOD 1 - VERSION WITH OUTPUT GEAR ON EACH SHAFT							
Speed		900		3000					
Bearing Location	Drawing Number	Maximum Bearing Pressure	Minimum Oil Film Thickness	Maximum Bearing Pressure	Minimum Oil Film Thickness	Maximum Bearing Pressure	Minimum Oil Film Thickness	Maximum Bearing Pressure	Minimum Oil Film Thickness
	Vandervell	Lbf/in ²	in x 10 ⁶	Lbf/in ²	in x 10 ⁶	Lbf/in ²	in x 10 ⁶	Lbf/in ²	in x 10 ⁶
	Customer	KN/M ²	M x 10 ⁶	KN/M ²	M x 10 ⁶	KN/M ²	M x 10 ⁶	KN/M ²	M x 10 ⁶
Connecting Rod	42 x 18.49	4308	42	3690	84				
		29702	1.06	25438	2.13				
Number 1 Main	45 x 28.74	1464	44						
	4.8 GROOVE	10093	1.11						
Number 2 Main		2266	35						
		15626	0.89						
Number 3 Main		2050	31						
		14132	0.79						
	ALL DIMS								
	IN MM								
Number 1 Main	45 x 28.74	1162	43						
	4.8 GROOVE	10083	1.09						
Number 2 Main		2266	35						
		15626	0.89						
Number 3 Main		1542	26						
		10629	0.66						
Vandervell Products Limited A MEMBER OF THE GKN GROUP OF COMPANIES			Customer: RICARDO			Drawn by: MRD		Date: OCT 1979 RD 31/295/1	

I-600

M. G. K. N. GROUP

GKN GROUP

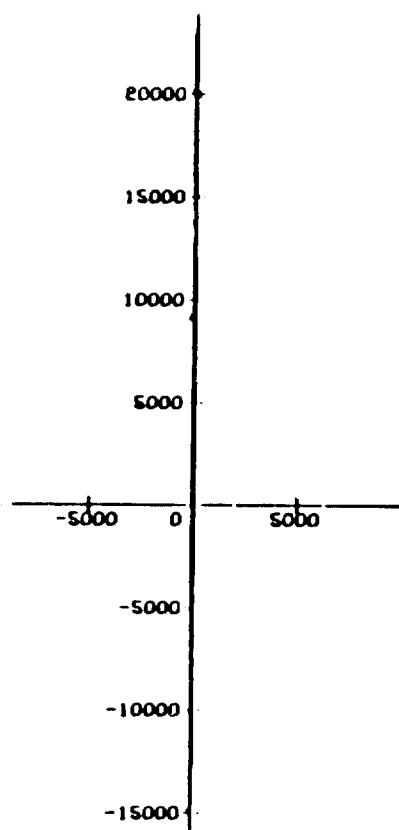
ORIGINAL PAGE 19
OF FOUR OCT 1979

LOAD CYCLE FOR BIG-END BEARINGS

(NEWTONS)

ASE MOD 1 BIG-ENDS

SPEED: 900.RPM



AXES ARE FIXED
RELATIVE TO BEARING

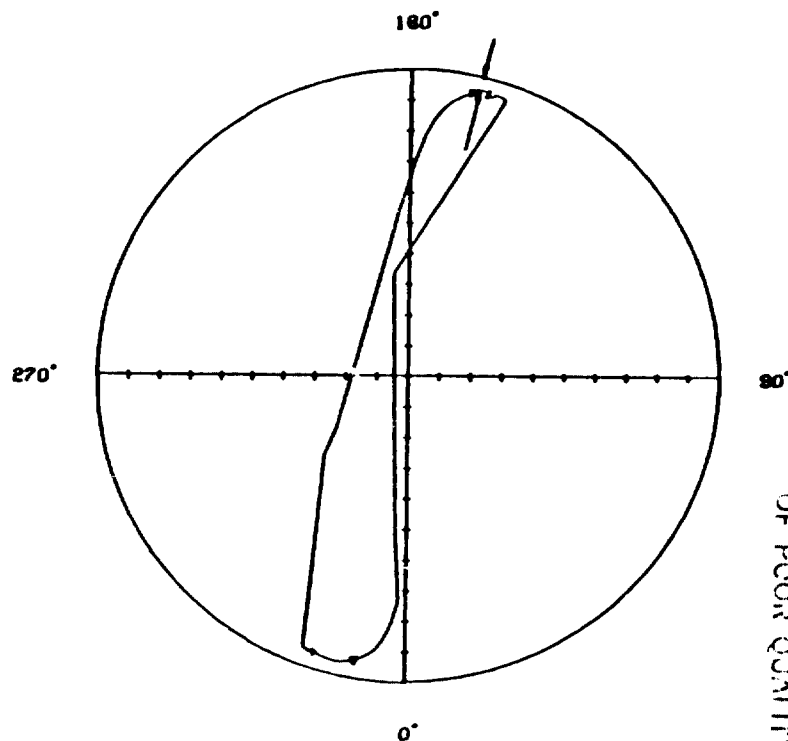
CRANK ANGLE
SHOWN AS FOLLOWS:-

- 0 DEGREES
- ▲ 90 DEGREES
- ▼ 180 DEGREES
- ♦ 270 DEGREES

JOURNAL ORBIT DIAGRAM BIG END BEARINGS

ASE MOD 1 BIG-ENDS

SPEED: 900.RPM



CRANK ANGLE
SHOWN AS FOLLOWS:-

- 0 DEGREES
- ▲ 90 DEGREES
- ▼ 180 DEGREES
- ♦ 270 DEGREES

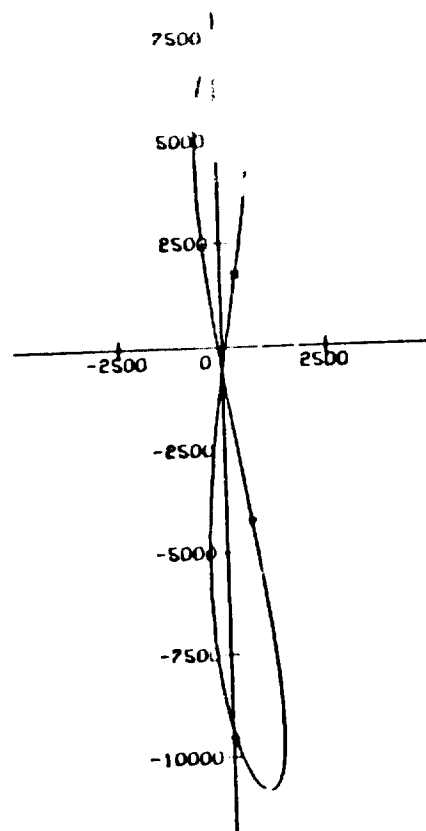
SCALE: 1 DIV. REPRESENTS
2.54 MICRO-METRES
100. MICRO-INCHES

MINIMUM OIL FILM THICKNESS
1.06 MICRO-METRES
42. MICRO-INCHES
SHOWN AT 167 DEGREES
FROM BOTTOM OF BEARING

ORIGINAL PAGE IS
OF POOR QUALITY

LOAD CYCLE FOR MAIN BEARING NO. 1
(NEWTONS)

ASE MOD 1 GEAR DRIVE SPEED: 900 RPM
CRANKSHAFT NO. 1



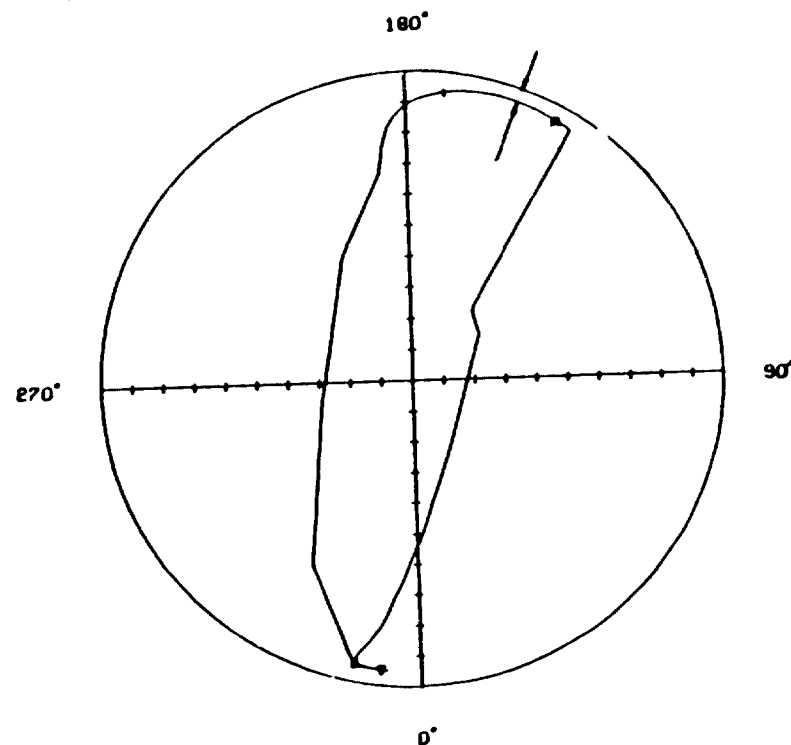
AXES ARE FIXED
RELATIVE TO BEARING

CRANKANGLE
OF MASTER CYLINDER
SHOWN AS FOLLOWS:-

- 0 DEGREES
- ▲ 90 DEGREES
- ▼ 180 DEGREES
- ♦ 270 DEGREES

JOURNAL ORBIT DIAGRAM MAIN BEARING NO. 1

ASE MOD 1 GEAR DRIVE FULLY GROOVED
SPEED: 900 RPM CRANKSHAFT NO. 1



CRANKANGLE
OF MASTER CYLINDER
SHOWN AS FOLLOWS:-

- 0 DEGREES
- ▲ 90 DEGREES
- ▼ 180 DEGREES
- ♦ 270 DEGREES

SCALE: 1 DIV. REPRESENTS
2.54 MICRO-METRES
100. MICRO-INCHES

MINIMUM OIL FILM THICKNESS
1.11 MICRO-METRES
44. MICRO-INCHES
SHOWN AT 158 DEGREES
FROM BOTTOM OF BEARING

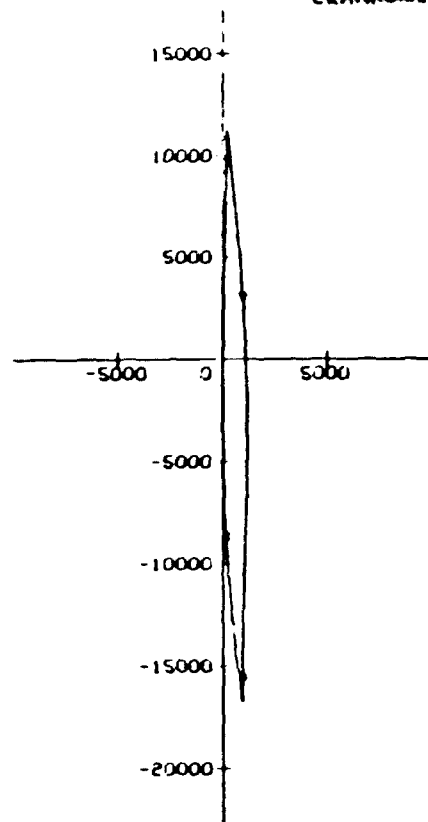
ORIGINAL PHOTO
OF POOR QUALITY

LOAD CYCLE FOR MAIN BEARING NO. 2
(NEWTONS)

ASE MOD 1 GEAR DRIVE

SPEED: 900.RPM

CRANKSHAFT NR 1



AXES ARE FIXED
RELATIVE TO BEARING

CRANK ANGLE
OF MASTER CYLINDER
SHOWN AS FOLLOWS:-

- 0 DEGREES
- ▲ 90 DEGREES
- ▼ 180 DEGREES
- ◆ 270 DEGREES

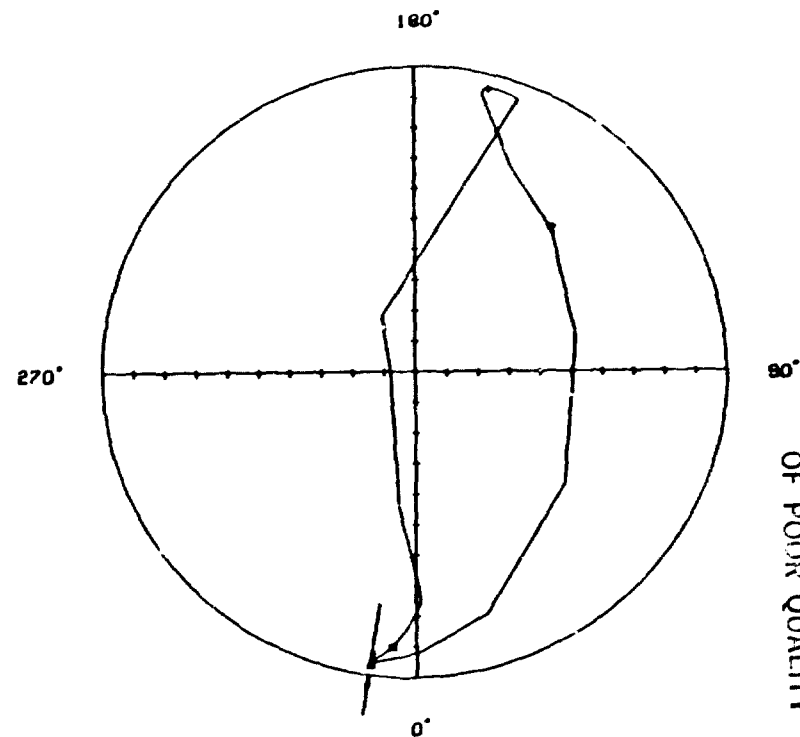
JOURNAL ORBIT DIAGRAM MAIN BEARING NO. 2

ASE MOD 1 GEAR DRIVE

FULLY GROOVED

SPEED: 900.RPM

CRANKSHAFT NR 1



ORIGINAL PHOTO IS
OF POOR QUALITY

CRANK ANGLE
OF MASTER CYLINDER
SHOWN AS FOLLOWS:-

- 0 DEGREES
- ▲ 90 DEGREES
- ▼ 180 DEGREES
- ◆ 270 DEGREES

SCALE: 1 DIV. REPRESENTS
2.54 MICRO-METRES
100. MICRO-INCHES

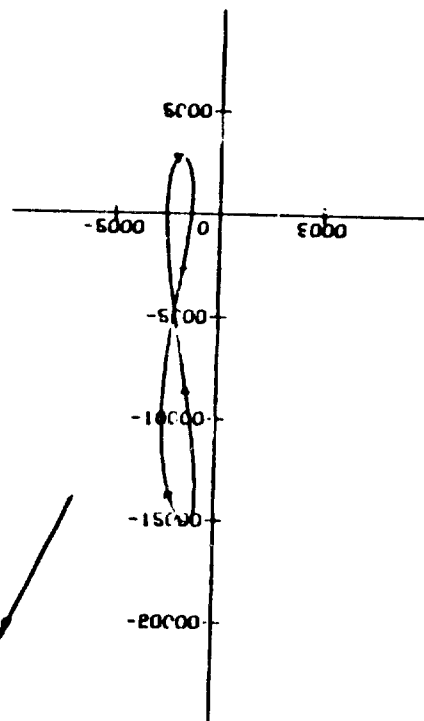
MINIMUM OIL FILM THICKNESS
0.89 MICRO-METRES
35. MICRO-INCHES
SHOWN AT 351.6 DEGREES
FROM BOTTOM OF BEARING

LOAD CYCLE FOR MAIN BEARING NO. 3
(NEWTONS)

ASE MOD 1 GEAR DRIVE

SPEED: 900.RPM

CRANKSHAFT NO. 1



GEAR
REACTION
FORCE

AXES ARE FIXED
RELATIVE TO BEARING

CRANKANGLE
OF MASTER CYLINDER
SHOWN AS FOLLOWS:-

- 0 DEGREES
- ▲ 90 DEGREES
- ▼ 180 DEGREES
- ✦ 270 DEGREES

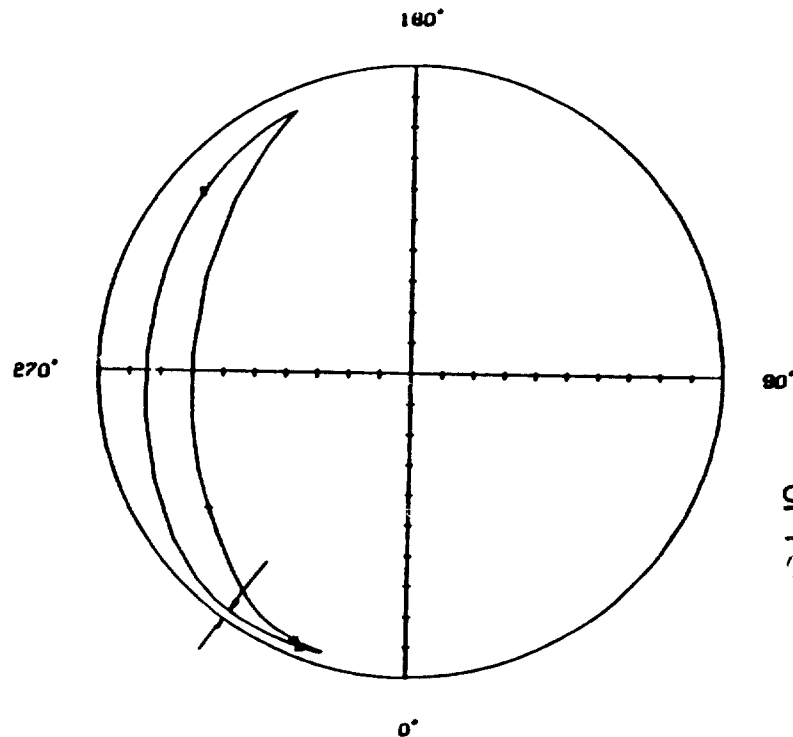
JOURNAL ORBIT DIAGRAM MAIN BEARING NO. 3

ASE MOD 1 GEAR DRIVE

FULLY GROOVED

SPEED: 900.RPM

CRANKSHAFT 1



CRANKANGLE
OF MASTER CYLINDER
SHOWN AS FOLLOWS:-

- 0 DEGREES
- ▲ 90 DEGREES
- ▼ 180 DEGREES
- ✦ 270 DEGREES

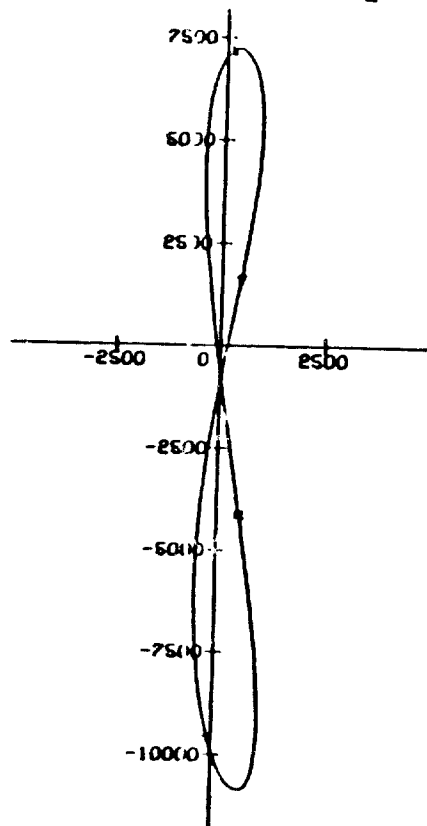
SCALE: ———
1 DIV. REPRESENTS
2.54 MICRO-METRES
100. MICRO-INCHES

MINIMUM OIL FILM THICKNESS
0.79 MICRO-METRES
31. MICRO-INCHES
SHOWN AT 324 DEGREES
FROM BOTTOM OF BEARING

ORIGINAL PAGE IS
OF PHOTO COPY

LOAD CYCLE FOR MAIN BEARING NO. 1 (NEWTONS)

ASE MOD 1 GEAR DRIVE SPEED: 800.RPM
CRANKSHAFT NO.2



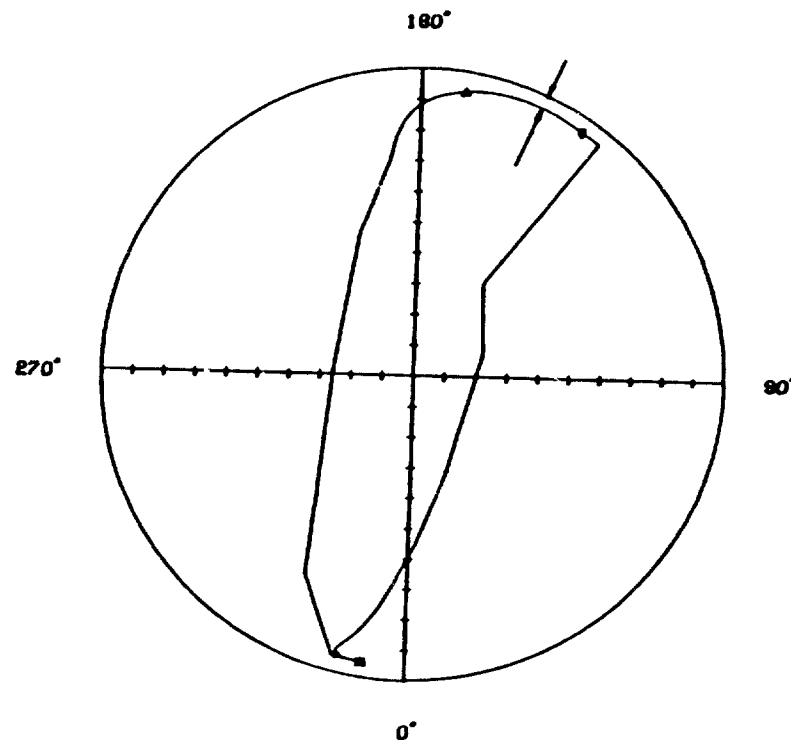
AXES ARE FIXED
RELATIVE TO BEARING

CRANKANGLE
OF MASTER CYLINDER
SHOWN AS FOLLOWS:-

- 0 DEGREES
- ▲ 90 DEGREES
- ▼ 180 DEGREES
- ◆ 270 DEGREES

JOURNAL ORBIT DIAGRAM MAIN BEARING NO. 1

ASE MOD 1 GEAR DRIVE FULLY GROOVED
SPEED: 800.RPM CRANKSHAFT NO. 2



CRANKANGLE
OF MASTER CYLINDER
SHOWN AS FOLLOWS:-

- 0 DEGREES
- ▲ 90 DEGREES
- ▼ 180 DEGREES
- ◆ 270 DEGREES

SCALE: 1 DIV. REPRESENTS
2.54 MICRO-METRES
100. MICRO-INCHES

MINIMUM OIL FILM THICKNESS
1.09 MICRO-METRES
43. MICRO-INCHES
SHOWN AT 156 DEGREES
FROM BOTTOM OF BEARING

QUALITY

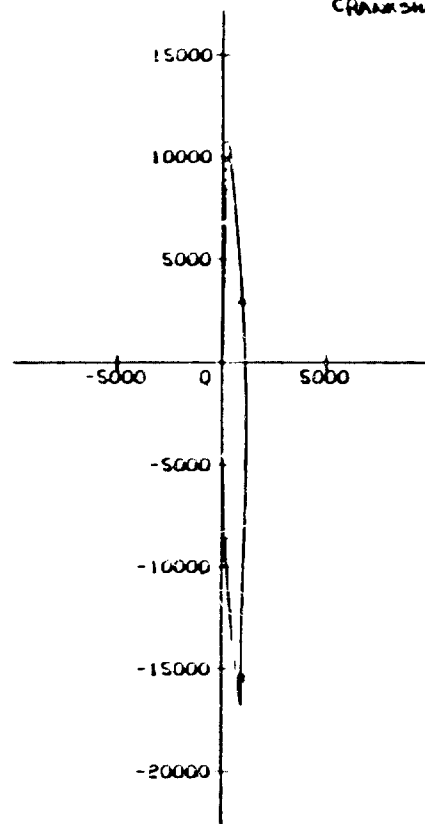
LOAD CYCLE FOR MAIN BEARING NO. 2

(NEWTONS)

ASE MOD 1 GEAR DRIVE

SPEED: 800 RPM

CRANKSHAFT NO. 2



AXES ARE FIXED
RELATIVE TO BEARING

CRANKANGLE
OF MASTER CYLINDER
SHOWN AS FOLLOWS:-

- 0 DEGREES
- ▲ 90 DEGREES
- ▼ 180 DEGREES
- ♦ 270 DEGREES

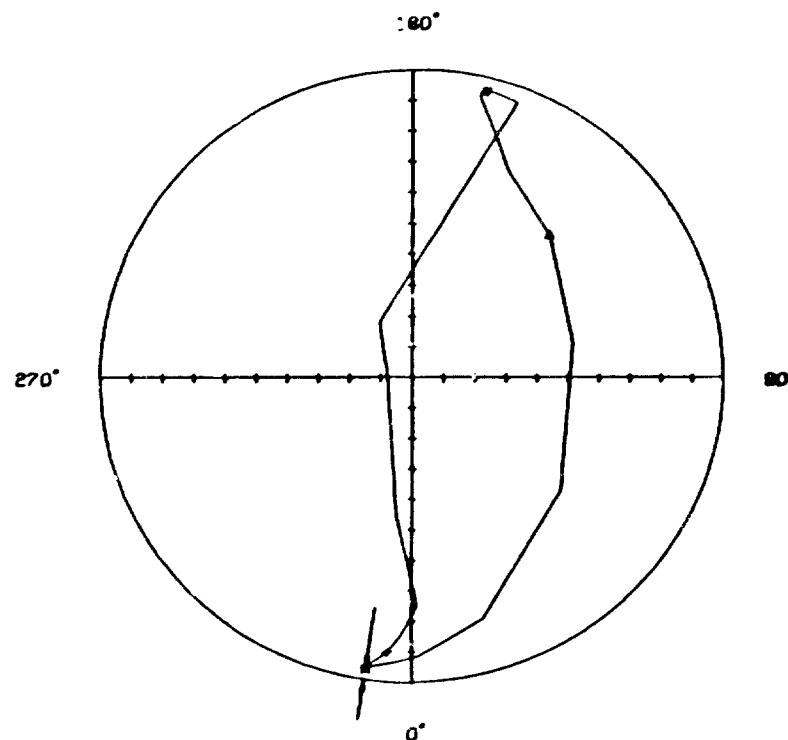
JOURNAL ORBIT DIAGRAM MAIN BEARING NO. 2

ASE MOD 1 GEAR DRIVE

FULLY GROOVED

SPEED: 800 RPM

CRANKSHAFT NO. 2



CRANKANGLE
OF MASTER CYLINDER
SHOWN AS FOLLOWS:-

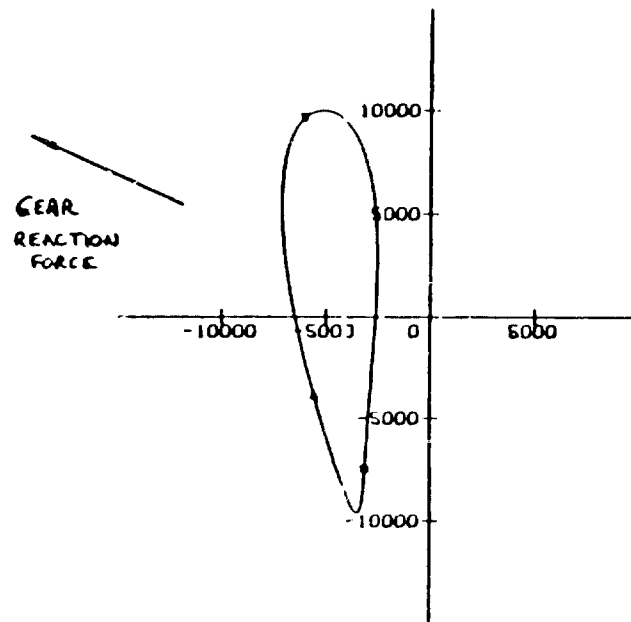
- 0 DEGREES
- ▲ 90 DEGREES
- ▼ 180 DEGREES
- ♦ 270 DEGREES

SCALE: —
1 DIV. REPRESENTS
2.54 MICRO-METRES
100. MICRO-INCHES

MINIMUM OIL FILM THICKNESS
0.89 MICRO-METRES
35. MICRO-INCHES
SHOWN AT 351 DEGREES
FROM BOTTOM OF BEARING

LOAD CYCLE FOR MAIN BEARING NO. 3
(NEWTONS)

ASE MOD 1 GEAR DRIVE SPEED: 900.RPM
CRANKSHAFT NO. 2



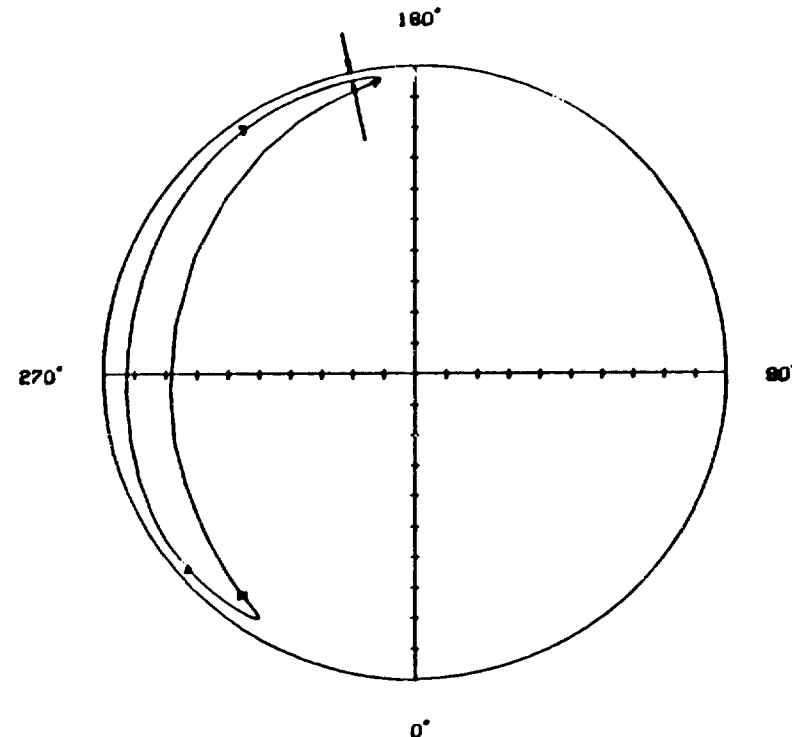
AXES ARE FIXED
RELATIVE TO BEARING

(CRANK ANGLE
OF MASTER CYLINDER
SHOWN AS FOLLOWS:-

- 0 DEGREES
- ▲ 90 DEGREES
- ▼ 180 DEGREES
- ✦ 270 DEGREES

JOURNAL ORBIT DIAGRAM MAIN BEARING NO. 3

ASE MOD 1 GEAR DRIVE FULLY GROOVED
SPEED: 900.RPM CRANKSHAFT NO. 2



CRANK ANGLE
OF MASTER CYLINDER
SHOWN AS FOLLOWS:-

- 0 DEGREES
- ▲ 90 DEGREES
- ▼ 180 DEGREES
- ✦ 270 DEGREES

SCALE: 1 DIV. REPRESENTS
2.54 MICRO-METRES
100. MICRO-INCHES

MINIMUM OIL FILM THICKNESS
0.66 MICRO-METRES
26. MICRO-INCHES
SHOWN AT 192 DEGREES
FROM BOTTOM OF BEARING

ORBITAL PATH IN
OF POOR QUALITY

UNITED STIRLING

30th October 1979

VANDERVELL OIL FILM THICKNESS DATA

BOTH TESTS AT 900 RPM

1. Link and Gear Drive

		Max Pressure	Oil Film	
		mm/mm ² PSI	Micron	M.inch
Conn Rod Bearing		29.7 - 4308	1.06	42
Link Bearing - No.1		14.5 - 2104	1.29	51
	No.2	13.8 - 1998	1.32	52
No.1 Crankshaft - No.1		10.1 - 1462	0.89	35
(No.1 & 2 cyl.) - No.2		15.8 - 2290	0.56	22
*	No.3	14.5 - 2102	0.62	24
No.2 Crankshaft - No.1		10.7 - 1553	0.97	38
(No.3 & 4 cyl) No.2		16.4 - 2375	0.62	24
*	No.3	10.1 - 1477	0.88	35

2. All Gear Drive

Conn Rod Bearings As Above

	No. 1 Crankshaft	No.1	10.1 - 1464	1.11	44
		No.2	15.6 - 2266	0.89	35
*		No.3	14.1 - 2050	0.79	31
	No.2 Crankshaft	- No.1	10.1 - 1462	1.09	43
		No.2	15.6 - 2266	0.89	35
*		No.3	10.6 - 1542	0.66	26

* At Flywheel End.

ORIGINAL FILED
OF POOR QUALITY

A P P E N D I X I I .

ENGINE WITH CONNECTING LINKS.

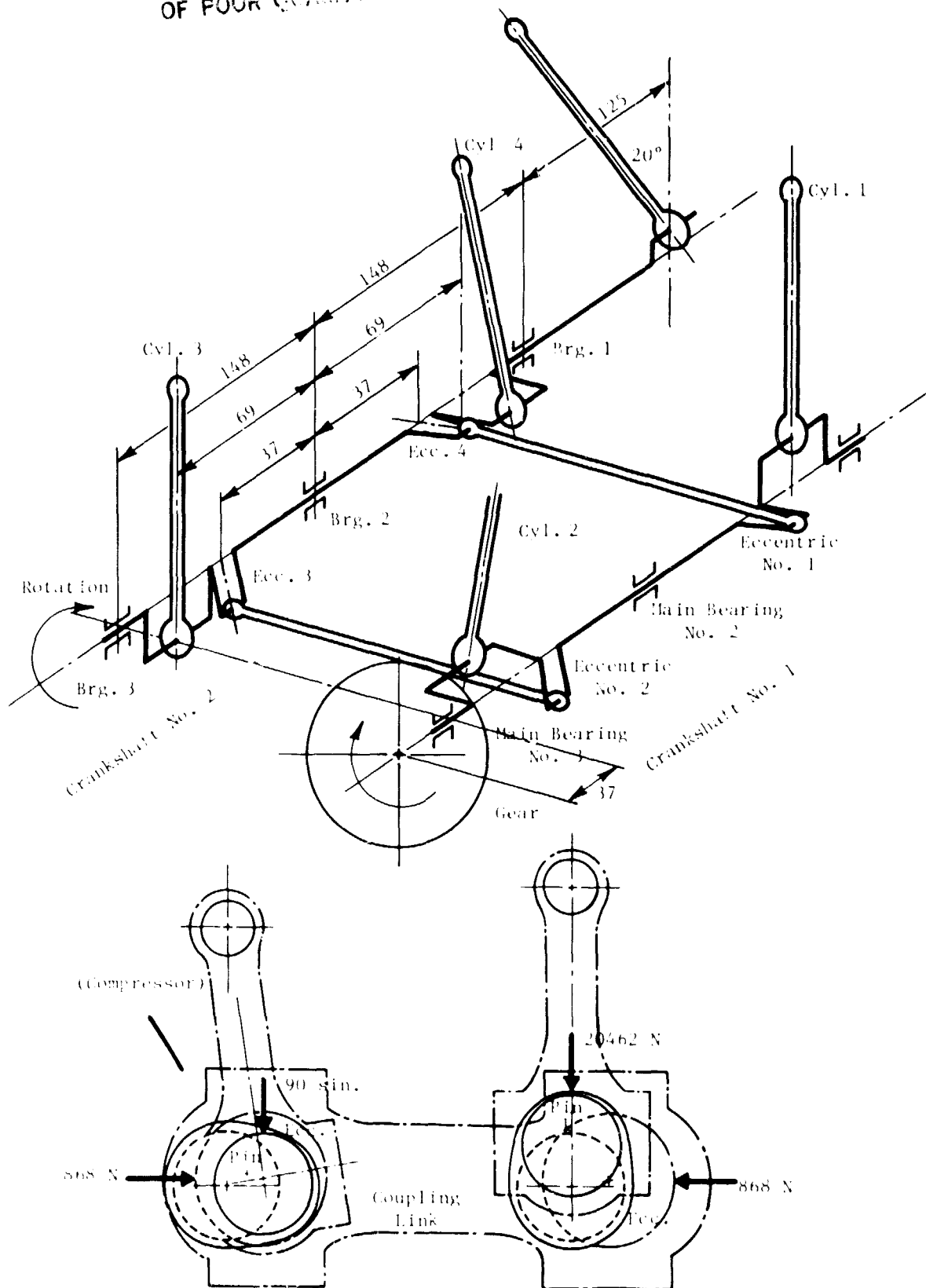
Sketch of engine layout.

Summary sheet RD31/295/2.

Bearing load cycles.

Journal orbit diagrams.

ORIGINAL PAGE IS
OF POOR QUALITY



Example of Forces on Bearings at No. 1 Crank Pin IDC

Section Showing Disposition of Links, Crankpins
and Compressor with Relevant Dimensions

SUMMARY of LOAD and LUBRICATION STUDY RECIPROCATING ENGINES

Engine Description		UNITED STIRLING A.S.E. MOD 1 - VERSION WITH CONNECTING LINKS							
Speed		700		3000					
Bearing Location	Drawing Number	Maximum Bearing Pressure	Minimum Oil Film Thickness	Maximum Bearing Pressure	Minimum Oil Film Thickness	Maximum Bearing Pressure	Minimum Oil Film Thickness	Maximum Bearing Pressure	Minimum Oil Film Thickness
	Vandervell	Lbf/in ²	in x 10 ⁶	Lbf/in ²	in x 10 ⁶	Lbf/in ²	in x 10 ⁶	Lbf/in ²	in x 10 ⁶
	Customer	KN/M ²	M x 10 ⁶	KN/M ²	M x 10 ⁶	KN/M ²	M x 10 ⁶	KN/M ²	M x 10 ⁶
Connecting Rod	42 x 18.49	4308	42	3690	84				
		29702	1.06	25438	2.13				
Number 1 Main	45 x 28.74	1162	35						
	4.8 GROOVE	10079	0.89						
Number 2 Main		2290	22						
		15786	0.56						
Number 3 Main		2102	24						
		14492	0.62						
	ALL DIMS.								
	1:1 MM								
Number 1 Main	45 x 28.74	1553	38						
	4.8 GROOVE	10709	0.97						
Number 2 Main		2373	24						
		16357	0.62						
Number 3 Main		11477	35						
		10180	0.88						
LINK N° 1	54 x 16.48	2104	51	2104	90				
		114510	1.29	114510	2.30				
LINK N° 2		1998	52	1998	100				
		13779	1.32	13779	2.54				
Vandervell Products Limited			Customer: RICARDO			Drawn by: MRE		Date: OCT 79	RD 31/295/
A MEMBER OF THE GKN GROUP OF COMPANIES									

CRANK SHAFT

CRANK SHAFT

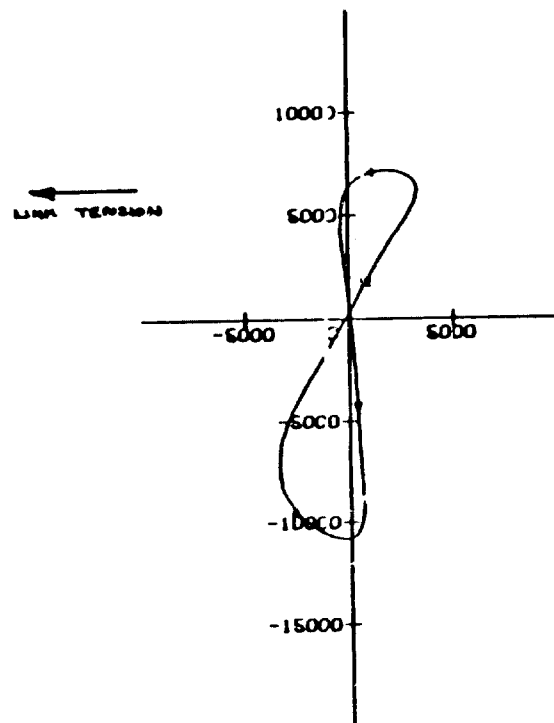
I-611

ORIGINAL FILED IN
OF POOR QUALITY

LOAD CYCLE FOR MAIN BEARING NO. 1
(NEWTONS)

ASE MOD 1 MAINS
CRANKSHAFT 1

SPEED: 800.RPM



AXES ARE FIXED
RELATIVE TO BEARING

CRANK ANGLE
OF MASTER CYLINDER
SHOWN AS FOLLOWS:-

- 0 DEGREES
- ▲ 80 DEGREES
- ▼ 180 DEGREES
- ◆ 270 DEGREES

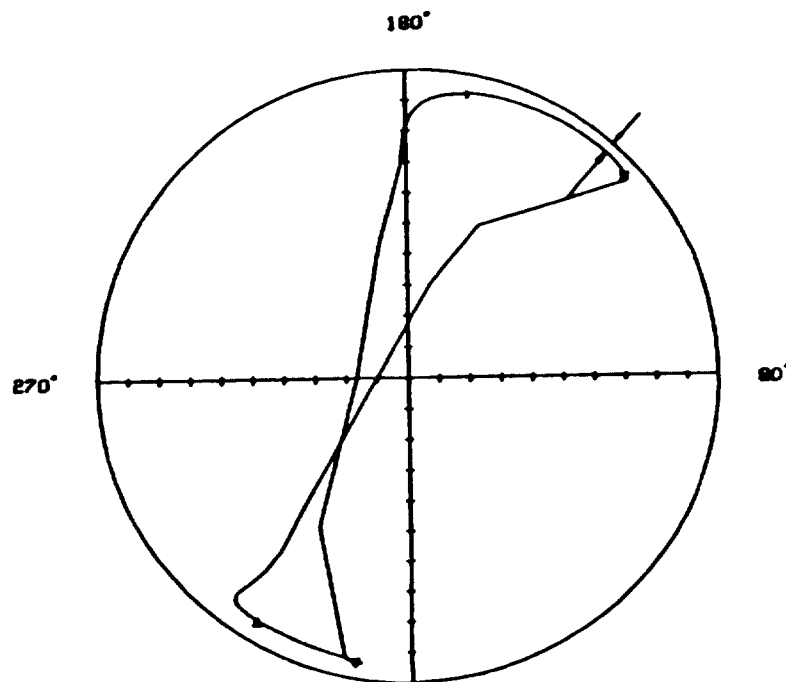
JOURNAL ORBIT DIAGRAM MAIN BEARING NO. 1

ASE MOD 1 MAINS

FULLY GROOVED

SPEED: 800.RPM

CRANKSHAFT 1



CRANK ANGLE
OF MASTER CYLINDER
SHOWN AS FOLLOWS:-

- 0 DEGREES
- ▲ 80 DEGREES
- ▼ 180 DEGREES
- ◆ 270 DEGREES

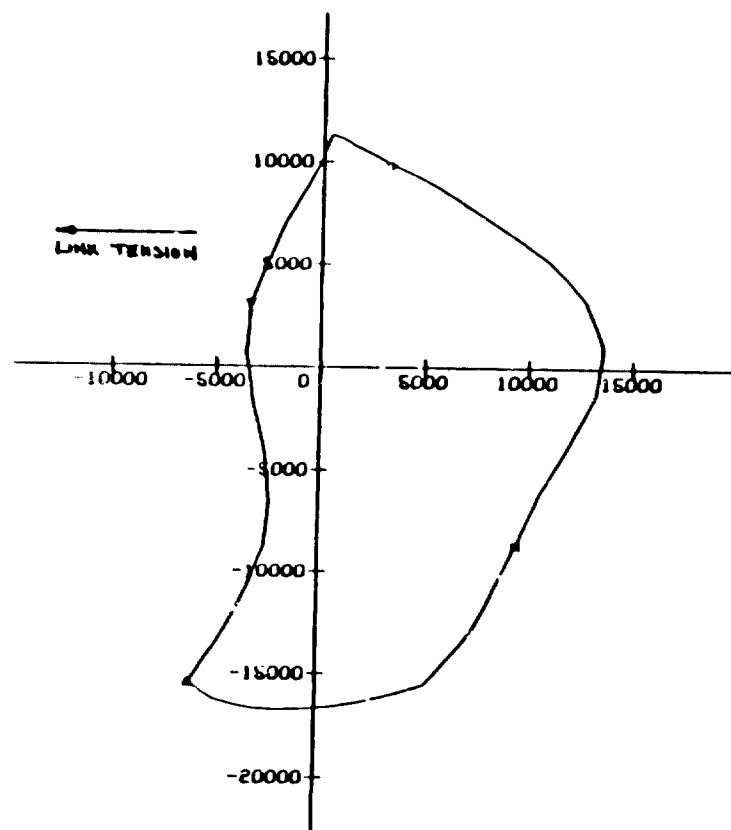
SCALE: 1 DIV. REPRESENTS
2.54 MICRO-METRES
100. MICRO-INCHES

MINIMUM OIL FILM THICKNESS
0.89 MICRO-METRES
35. MICRO-INCHES
SHOWN AT 138 DEGREES
FROM BOTTOM OF BEARING

LOAD CYCLE FOR MAIN BEARING NO. 2
(NEWTONS)

ASE MOD 1 MAINS
CRANKSHAFT 1

SPEED: 800.RPM



AXES ARE FIXED
RELATIVE TO BEARING

CRANKANGLE
OF MASTER CYLINDER
SHOWN AS FOLLOWS:-

- 0 DEGREES
- ▲ 90 DEGREES
- ▼ 180 DEGREES
- ◆ 270 DEGREES

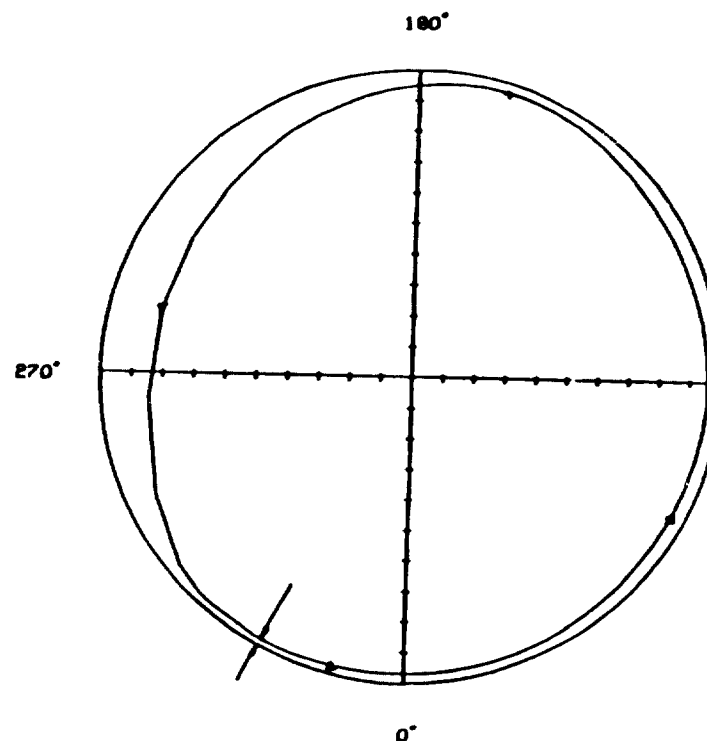
JOURNAL ORBIT DIAGRAM MAIN BEARING NO. 2

ASE MOD 1 MAINS

FULLY GROOVED

SPEED: 800.RPM

CRANKSHAFT 1



CRANKANGLE
OF MASTER CYLINDER
SHOWN AS FOLLOWS:-

- 0 DEGREES
- ▲ 90 DEGREES
- ▼ 180 DEGREES
- ◆ 270 DEGREES

SCALE: ————
1 DIV. REPRESENTS
2.54 MICRO-METRES
100. MICRO-INCHES

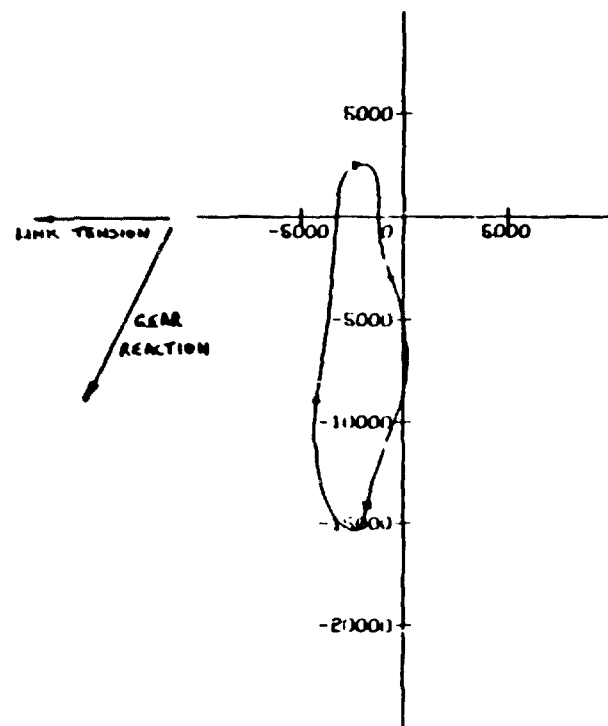
MINIMUM OIL FILM THICKNESS
0.56 MICRO-METRES
22. MICRO-INCHES
SHOWN AT 332 DEGREES
FROM BOTTOM OF BEARING

OF POOR QUALITY

LOAD CYCLE FOR MAIN BEARING NO. 3
(NEWTONS)

ASE MOD 1 MAINS
CRANKSHAFT 1

SPEED: 900.RPM



AXES ARE FIXED
RELATIVE TO BEARING

CRANKANGLE
OF MASTER CYLINDER
SHOWN AS FOLLOWS:-

- 0 DEGREES
- ▲ 90 DEGREES
- ▼ 180 DEGREES
- ♦ 270 DEGREES

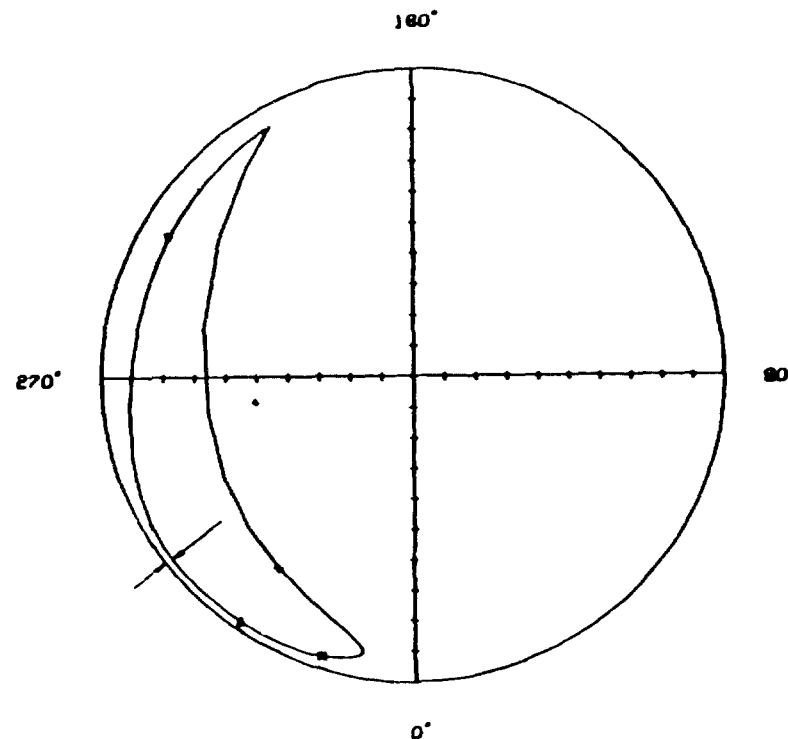
JOURNAL ORBIT DIAGRAM MAIN BEARING NO. 3

ASE MOD 1 MAINS

FULLY GROOVED

SPEED: 900.RPM

CRANKSHAFT 1



CRANKANGLE
OF MASTER CYLINDER
SHOWN AS FOLLOWS:-

- 0 DEGREES
- ▲ 90 DEGREES
- ▼ 180 DEGREES
- ♦ 270 DEGREES

SCALE: 1 DIV. REPRESENTS
2.54 MICRO-METRES
100. MICRO-INCHES

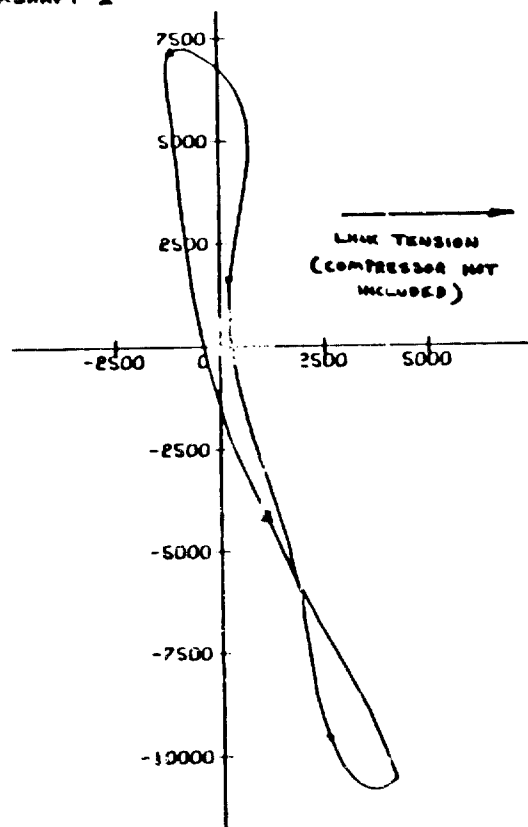
MINIMUM OIL FILM THICKNESS
0.62 MICRO-METRES
24. MICRO-INCHES
SHOWN AT 307 DEGREES
FROM BOTTOM OF BEARING

ORIGINAL PAGE IS
OF POOR QUALITY

LOAD CYCLE FOR MAIN BEARING NO. 1 (NEWTONS)

ASE MOD 1 MAINS
CRANKSHAFT 2

SPEED: 900.RPM



AXES ARE FIXED
RELATIVE TO BEARING

CRANK ANGLE
OF MASTER CYLINDER
SHOWN AS FOLLOWS:-

- 0 DEGREES
- ▲ 90 DEGREES
- ▼ 180 DEGREES
- ◆ 270 DEGREES

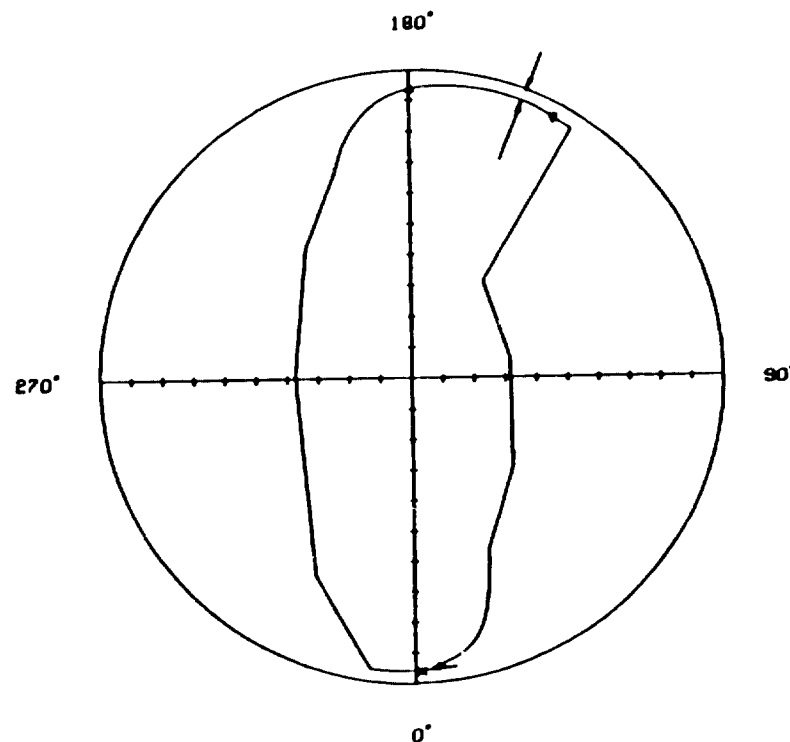
JOURNAL ORBIT DIAGRAM MAIN BEARING NO. 1

ASE MOD 1 MAINS

FULLY GROOVED

SPEED: 900.RPM

CRANKSHAFT 2



CRANK ANGLE
OF MASTER CYLINDER
SHOWN AS FOLLOWS:-

- 0 DEGREES
- ▲ 90 DEGREES
- ▼ 180 DEGREES
- ◆ 270 DEGREES

SCALE: 1 DIV. REPRESENTS
2.54 MICRO-METRES
100. MICRO-INCHES

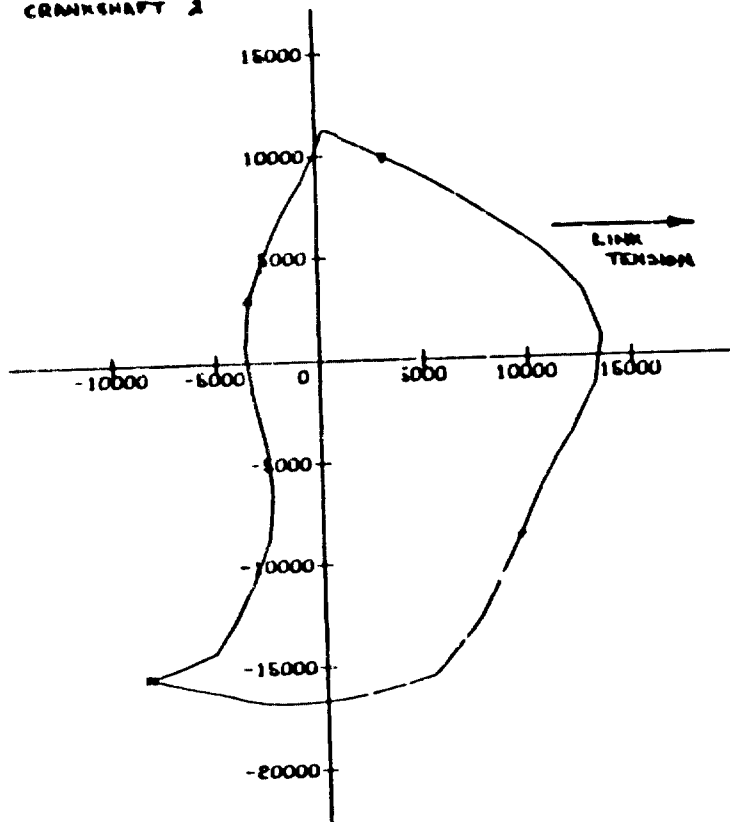
MINIMUM OIL FILM THICKNESS
0.97 MICRO-METRES
38. MICRO-INCHES
SHOWN AT 158 DEGREES
FROM BOTTOM OF BEARING

OF POOR QUALITY

LOAD CYCLE FOR MAIN BEARING NO. 2
(NEWTONS)

ASE NOO 1 MAINS
CRANKSHAFT 2

SPEED: 800.RPM



AXES ARE FIXED
RELATIVE TO BEARING

CRANKANGLE
OF MASTER CYLINDER
SHOWN AS FOLLOWS:-

- 0 DEGREES
- ▲ 90 DEGREES
- ▼ 180 DEGREES
- ◆ 270 DEGREES

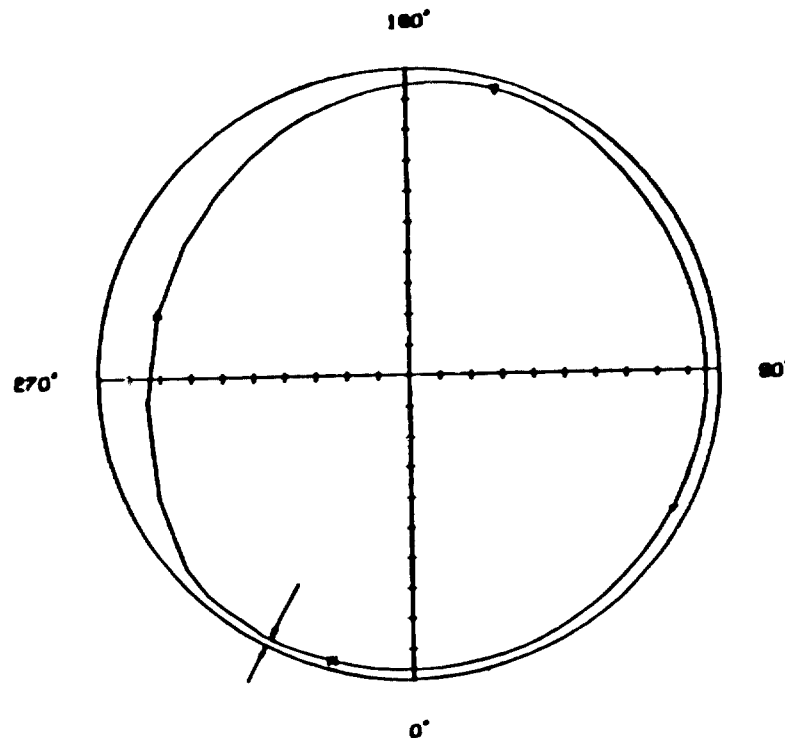
JOURNAL ORBIT DIAGRAM MAIN BEARING NO. 2

ASE NOO 1 MAINS

FULLY GROOVED

SPEED: 800.RPM

CRANKSHAFT 2



CRANKANGLE
OF MASTER CYLINDER
SHOWN AS FOLLOWS:-

- 0 DEGREES
- ▲ 90 DEGREES
- ▼ 180 DEGREES
- ◆ 270 DEGREES

SCALE: 1 DIV. REPRESENTS
2.54 MICRO-METRES
100. MICRO-INCHES

MINIMUM OIL FILM THICKNESS
0.62 MICRO-METRES
24. MICRO-INCHES
SHOWN AT 332 DEGREES
FROM BOTTOM OF BEARING

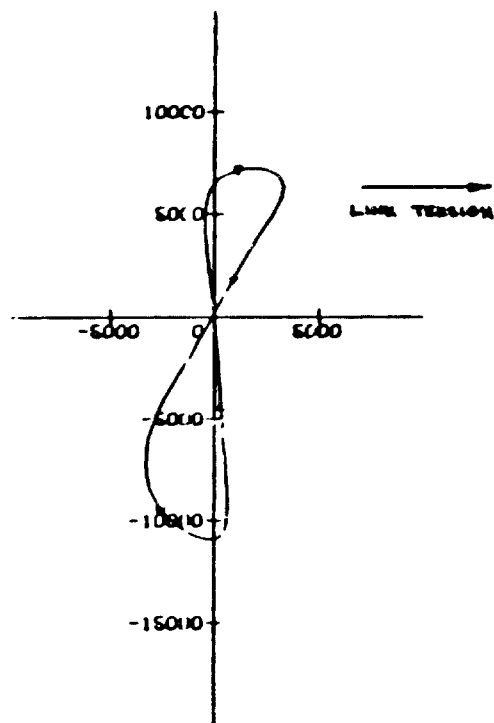
ORIGINAL OF PROOF QUALITY

LOAD CYCLE FOR MAIN BEARING NO. 3
(NEWTONS)

RSE MOD 1 MAINS

SPEED: 800.RPM

CRANKSHAFT 2



AXES ARE FIXED
RELATIVE TO BEARING

CRANK ANGLE
OF MASTER CYLINDER
SHOWN AS FOLLOWS:-

- 0 DEGREES
- ▲ 90 DEGREES
- ▼ 180 DEGREES
- ◆ 270 DEGREES

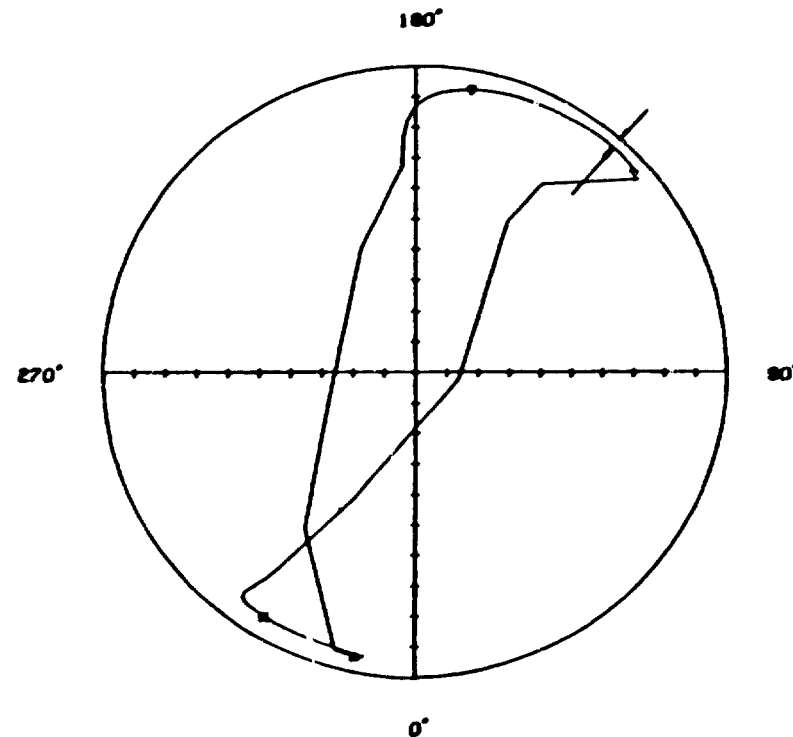
JOURNAL ORBIT DIAGRAM MAIN BEARING NO. 3

RSE MOD 1 MAINS

FULLY GROOVED

SPEED: 800.RPM

CRANKSHAFT 2



CRANK ANGLE
OF MASTER CYLINDER
SHOWN AS FOLLOWS:-

- 0 DEGREES
- ▲ 90 DEGREES
- ▼ 180 DEGREES
- ◆ 270 DEGREES

SCALE: 1 DIV. REPRESENTS
2.54 MICRO-METRES
100. MICRO-INCHES

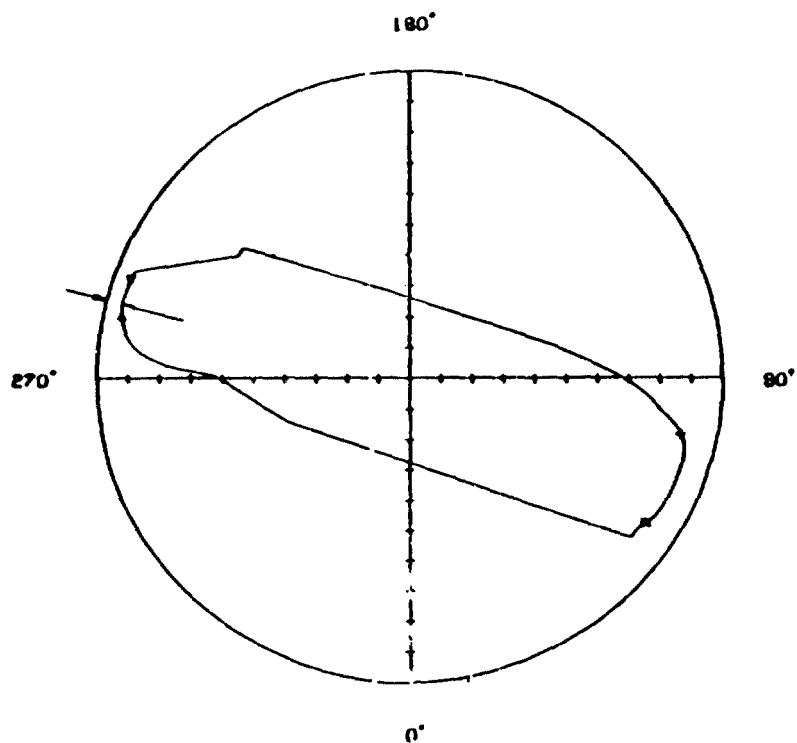
MINIMUM OIL FILM THICKNESS
0.88 MICRO-METRES
35. MICRO-INCHES
SHOWN AT 139. DEGREES
FROM BOTTOM OF BEARING

IS
OF
QUALITY

JOURNAL ORBIT DIAGRAM MAIN BEARING NO. 1

U.S. MOD.1 LINK

SPEED: 800.RPM



CRANK ANGLE
OF MASTER CYLINDER
SHOWN AS FOLLOWS:-

- 0 DEGREES
- ▲ 90 DEGREES
- ▼ 180 DEGREES
- + 270 DEGREES

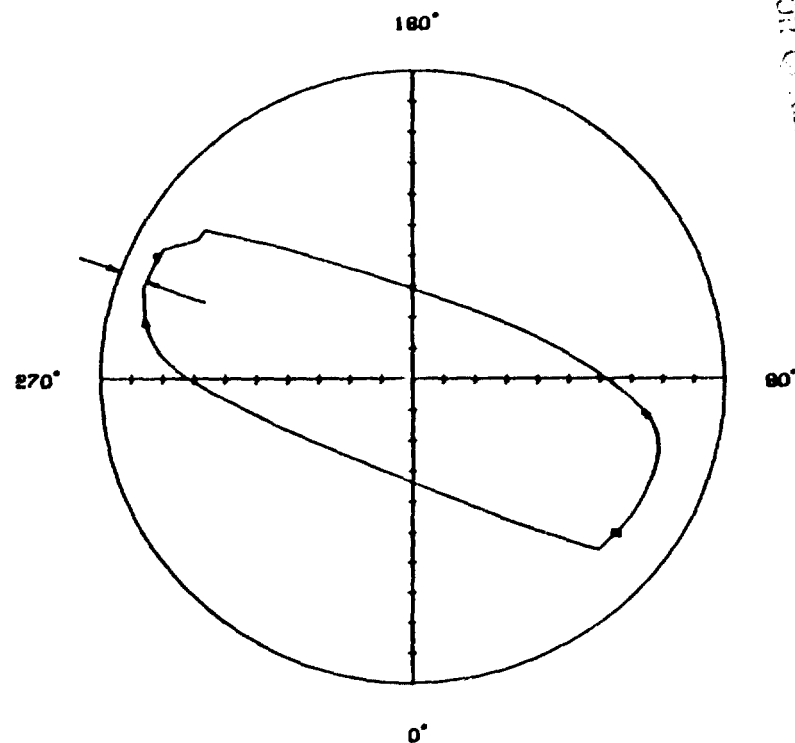
SCALE: ———
1 DIV. REPRESENTS
2.54 MICRO-METRES
100. MICRO-INCHES

MINIMUM OIL FILM THICKNESS
1.29 MICRO-METRES
51. MICRO-INCHES
SHOWN AT 255 DEGREES
FROM BOTTOM OF BEARING

JOURNAL ORBIT DIAGRAM MAIN BEARING NO. 1

U.S. MOD.1 LINK

SPEED: 3000.RPM



CRANK ANGLE
OF MASTER CYLINDER
SHOWN AS FOLLOWS:-

- 0 DEGREES
- ▲ 90 DEGREES
- ▼ 180 DEGREES
- + 270 DEGREES

SCALE: ———
1 DIV. REPRESENTS
2.54 MICRO-METRES
100. MICRO-INCHES

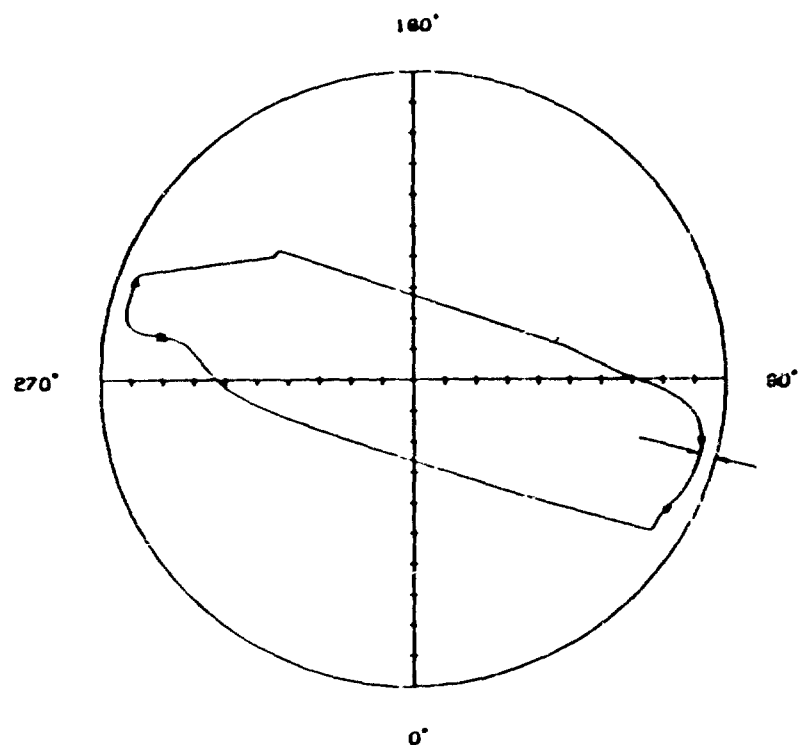
MINIMUM OIL FILM THICKNESS
2.30 MICRO-METRES
90. MICRO-INCHES
SHOWN AT 250 DEGREES
FROM BOTTOM OF BEARING

ORIGINAL PAGE IS
OF FOUR CONTINUED

JOURNAL ORBIT DIAGRAM MAIN BEARING NO. 2

U.S. MOD.1 LINK

SPEED: 900.RPM



CRANKANGLE
OF MASTER CYLINDER
SHOWN AS FOLLOWS:-

- 0 DEGREES
- ▲ 90 DEGREES
- ▼ 180 DEGREES
- + 270 DEGREES

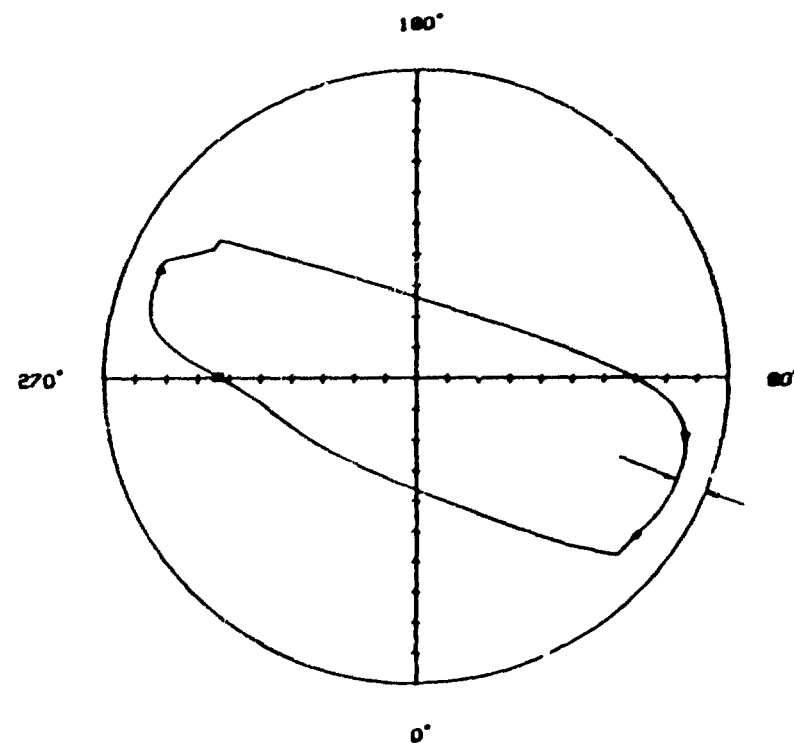
SCALE: ————
1 DIV. REPRESENTS
2.54 MICRO-METRES
100. MICRO-INCHES

MINIMUM OIL FILM THICKNESS
1.32 MICRO-METRES
52. MICRO-INCHES
SHOWN AT 75 DEGREES
FROM BOTTOM OF BEARING

JOURNAL ORBIT DIAGRAM MAIN BEARING NO. 2

U.S. MOD.1 LINK

SPEED: 3000.RPM



CRANKANGLE
OF MASTER CYLINDER
SHOWN AS FOLLOWS:-

- 0 DEGREES
- ▲ 90 DEGREES
- ▼ 180 DEGREES
- + 270 DEGREES

SCALE: ————
1 DIV. REPRESENTS
2.54 MICRO-METRES
100. MICRO-INCHES

MINIMUM OIL FILM THICKNESS
2.54 MICRO-METRES
100. MICRO-INCHES
SHOWN AT 68 DEGREES
FROM BOTTOM OF BEARING

ORIGINAL SOURCE IS
OF POOR QUALITY

RICARDO CONSULTING ENGINEERS

CLIENT United Stirling SECTION Balance
PROJECT ASE Mod I ϕ 68 x 34 SHEET NO. 1 OF
JOB NO. C4813-10 DATE 16 January 1980
CALCULATION BY R. Janczak DRAWING KEY NO. 3274

OBJECT To estimate counterweight sizes for balancer shaft and gears
.....

Introduction

Because of the configuration, the square four engine has primary and secondary balance. There is, however, primary moment unbalance. The moment unbalance affects the engine by producing: 1) rolling and 2) pitching.

To balance the rolling moment, counterweights can be directly added to the crankshaft crankwebs. The pitch moment is balanced with the aid of the balancer shaft. In effect, the balancer shaft balances half the total pitch moment.

When the hydrogen pump compressor is attached to one of the crankshafts, the primary force can be balanced with aid of the balancer shaft. However, a rolling moment is introduced and to counter this, weights must be attached to the crankshaft gears.

To complete the balance on Mod I, counterweights are required for the engine with and without the compressor.

Case 1 For Engine without Compressor (Motoring purposes only)

Required: Balancer shaft counterweights to balance pitching (and yawing) of engine.

$$\text{WR value required on balancer shaft} = \frac{mrc}{\sqrt{2} \ell_1}$$

where mr = recip wr value

c = distance between cylinder centres

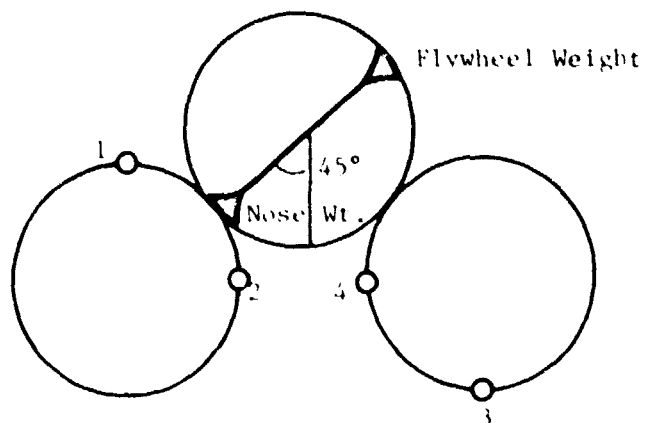
ℓ_1 = distance between counterweights on balance shaft

For power cylinder, Total recip weight = 1.921 kv

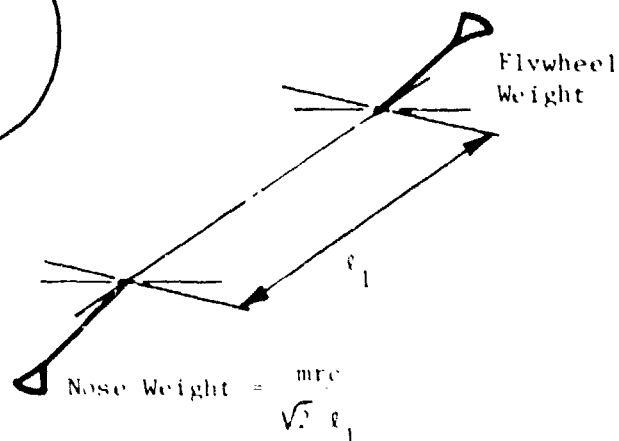
Stroke = 34 mm $r = 1.7$ cm

Wr value for recip = (1.92) (1.7) = 3.266 kg-cm

C distance between cylinder centres = (2) (7.0)cm = 14.0 cm



Looking from Front



Balancer Shaft and Gears

Case 2 For Engine with Compressor

To Balance Primary Recip Force

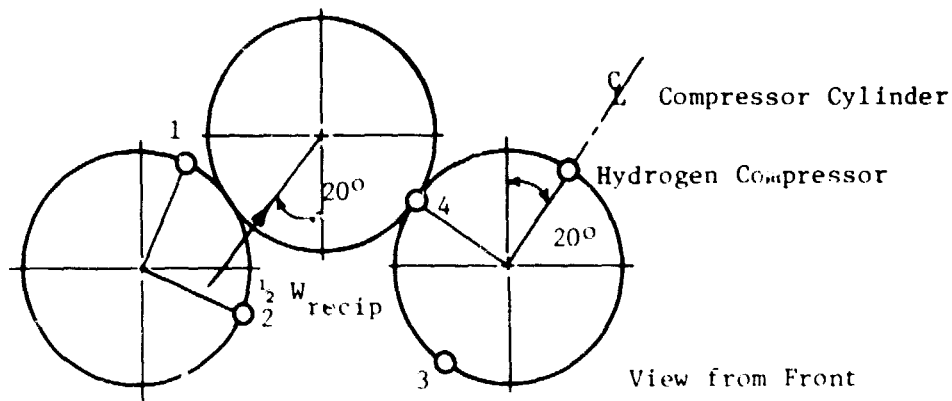
Wr value required on balancer shaft = $\frac{1}{2} W_{\text{recip}}$

For compressor: Total compressor recip weight = 0.36 kg

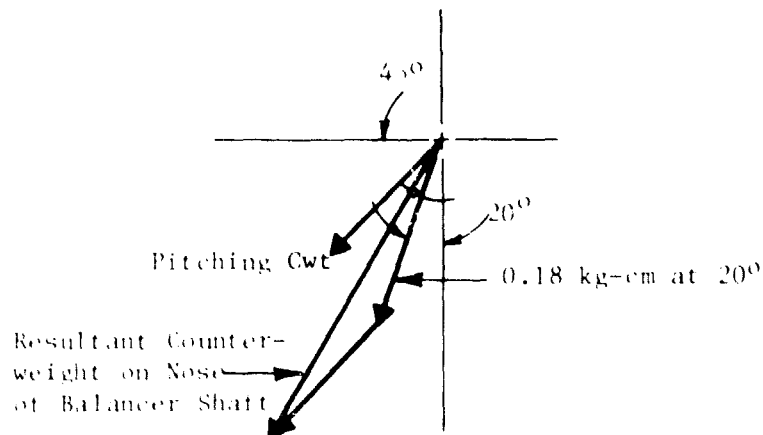
Stroke of compressor = 20 mm $r = 1$ cm

$Wr = (0.36) (1) = 0.36$ kg-cm

$\frac{1}{2} W_{\text{recip}} = 0.18$ kg-cm



This balance weight can be vectorially added to the counterweight already on the front of the balancer shaft.



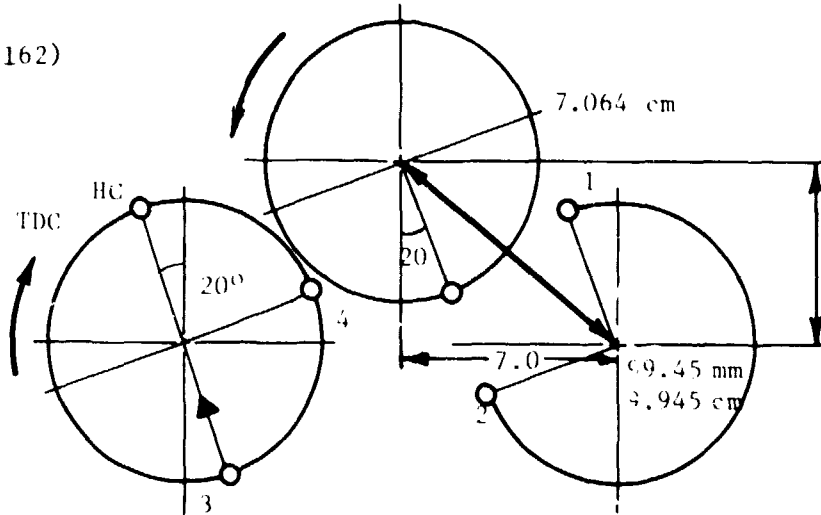
Gear Counterweights

ORIGINAL FIGURES
OF POOR QUALITY

When compressor is at TDC

couple due to inertia force

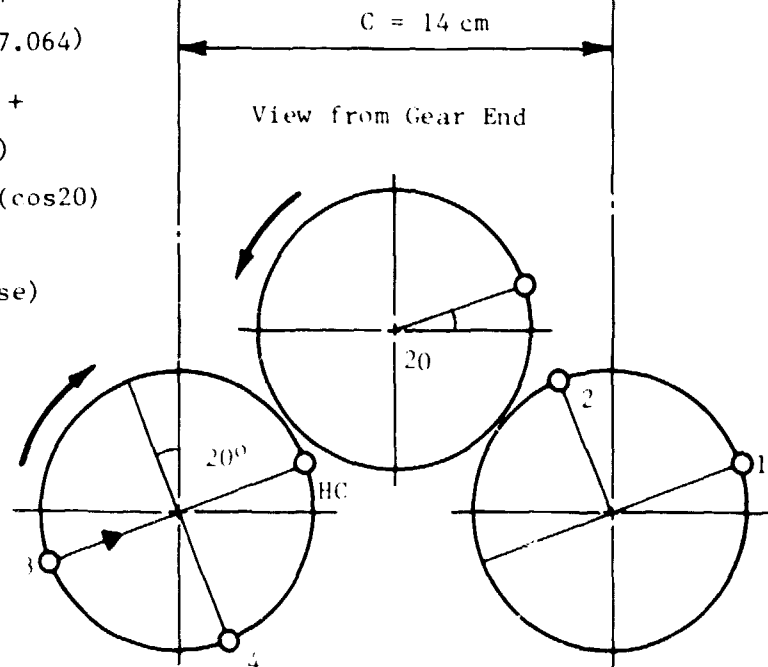
$$\begin{aligned}
 &= (\frac{1}{2} W_{\text{recip}})(\cos 20) (6.9) \\
 &+ (\frac{1}{2} W_{\text{recip}})(\sin 20) (7.162) \\
 &= (0.18) (7) (\cos 20) \\
 &+ (0.18) (7.064) (\sin 20) \\
 &= 1.184 + 0.435 \\
 &= 1.619 \text{ kg-cm}^2 \text{ (clock-} \\
 &\quad \text{wise)}
 \end{aligned}$$



When Pump is at 90° ATDC

Couple due to inertia force

$$\begin{aligned}
 &= -(\frac{1}{2} W_{\text{recip}})(\sin 20) (7) + \\
 &\quad (\frac{1}{2} W_{\text{recip}})(\cos 20) (7.064) \\
 &= -(0.18) (7.0) (\sin 20) + \\
 &\quad (0.18) (7.064) (\cos 20) \\
 &= -(0.425) + (0.18) (7.064) (\cos 20) \\
 &= -0.431 + 1.195 \\
 &= 0.764 \text{ kg-cm}^2 \text{ (clockwise)}
 \end{aligned}$$



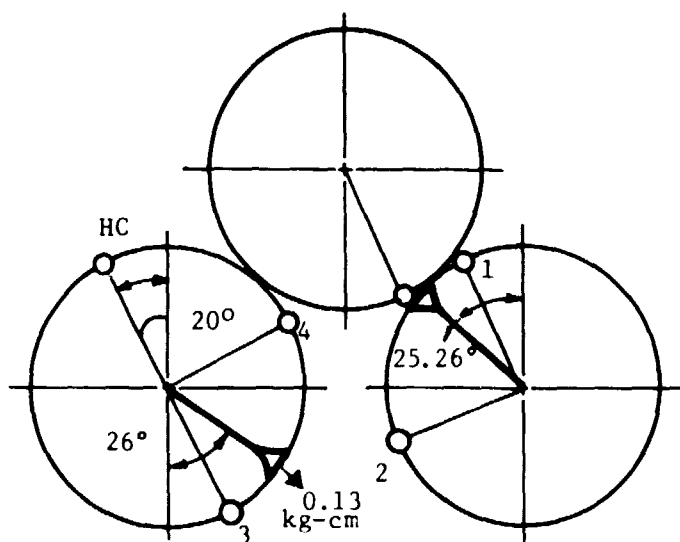
$$\text{Counterweight to balance in-phase moment} = \frac{1.619}{14} = 0.116$$

$$\text{Counterweight to balance } 90^\circ \text{ moment} = \frac{0.764}{14} = 0.055$$

ORIGINAL
OF FOCKE



Resultant - 0.128 kg-cm at 25.26°



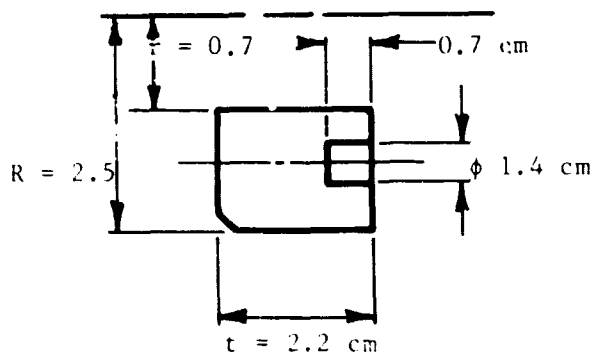
Check

at TDC Couple from balance weights = $13.8 \times 0.13 \times \cos 26$
 $= 1.612 \text{ kg-cm}^2 \text{ (anti-clock)}$

at 90° ATDC Couple from balance weights = $13.8 \times 0.13 \times \sin 26$
 $= 0.786 \text{ kg-cm (anti-clock)}$

Size of Balance Weight (Gear Counter Weights)

Required WR = 0.128 kg-cm



$$W_r = \left(\frac{2}{3}\right) (0.00783) (2.2) (2.5^3 - 0.7^3) \sin \alpha - \left(2 \frac{\pi}{4}\right) (1.4^2) (0.7) (0.00783) (1.6)$$

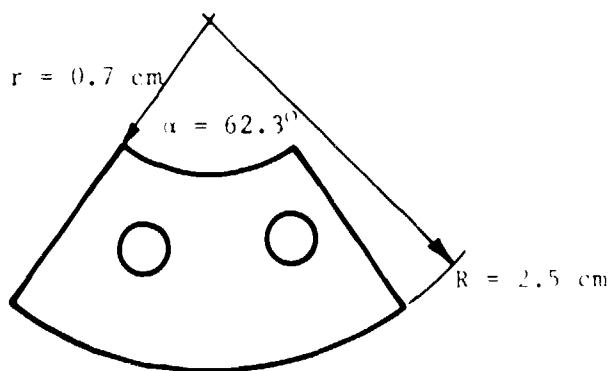
$$= 0.175 \sin \alpha - 0.027$$

$$0.128 = 0.175 \sin \alpha - 0.027$$

$$0.155 = 0.175 \sin \alpha$$

$$\sin \alpha = 0.897$$

$$\alpha = 62.3^\circ$$



Flywheel and Nose Counter Weights

Assume thickness of counter weight = 10 mm

$$= 1 \text{ cm}$$

distance from centerline of engine to centerline counter weight attached to inside of flywheel = $148 + 16 + 58 + 28 - 5 - 5 \text{ mm} = 240 \text{ mm}$

$$\therefore \frac{1}{2} \ell_1 = 24 \text{ cm}$$

$$\therefore \text{WR value required on balancer shaft} = \frac{mrc}{\sqrt{2} \ell_1}$$

$$= \frac{(1.921) (1.7) (14)}{\sqrt{2} (24)} = 1.347 \text{ kg-cm}$$

from flywheel drawing 3274/222

$$r = 12.5 \text{ cm}$$

$$\therefore \text{required mass} = \frac{1.347}{12.5} = 0.108 \text{ kg.}$$

$$\text{Mass} = 0.108 = (A) (t) (0.00783) = (A) (1) (0.00783)$$

$$\text{Required area} = \frac{0.108}{0.00783} = 13.76 \text{ cm}^2$$

$$\text{Use } t = 1.5 \text{ cm} \quad \text{Mass} = 0.108 = (A) (t) 0.00783$$

$$= (A) (1.5) 0.00783$$

$$\therefore A = 9.20 \text{ cm}^2$$

$$\text{using } b = 3 \text{ cm} \quad \therefore L = 3 \text{ cm}$$

Required Wt 3 cm x 3 cm x 1.5 cm

$$\text{Use } 3/8 \text{ in. plate (9.5 mm)} \quad 0.108 = (A) (t) (0.00783)$$

$$A = \frac{0.108}{0.00783 (9.5) (10^{-1})} = 14.5 \text{ cm}^2$$

Use 4.8 x 3 x 0.95 plate.

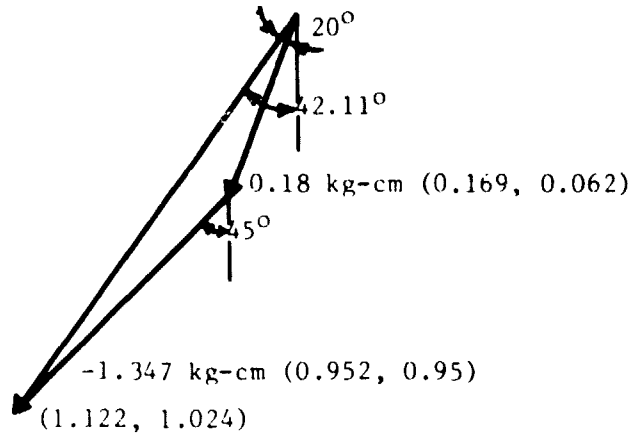
ORIGINAL PAGE IS
OF POOR QUALITY

Nose Counter Weight

WR required for engine without pump = 1.347 kg-cm at 45° (see p. 2)

WR required for compressor = 0.18 kg-cm at 20° (see p. 3)

Resultant WR for Engine with Compressor



Resultant = 1.512 kg-cm
at 42.11°

Summary

Engine without compressor

Flywheel and nose counter weight WR = 1.347 kg-cm

Engine with compressor

Flywheel counter weight WR = 1.347 kg-cm

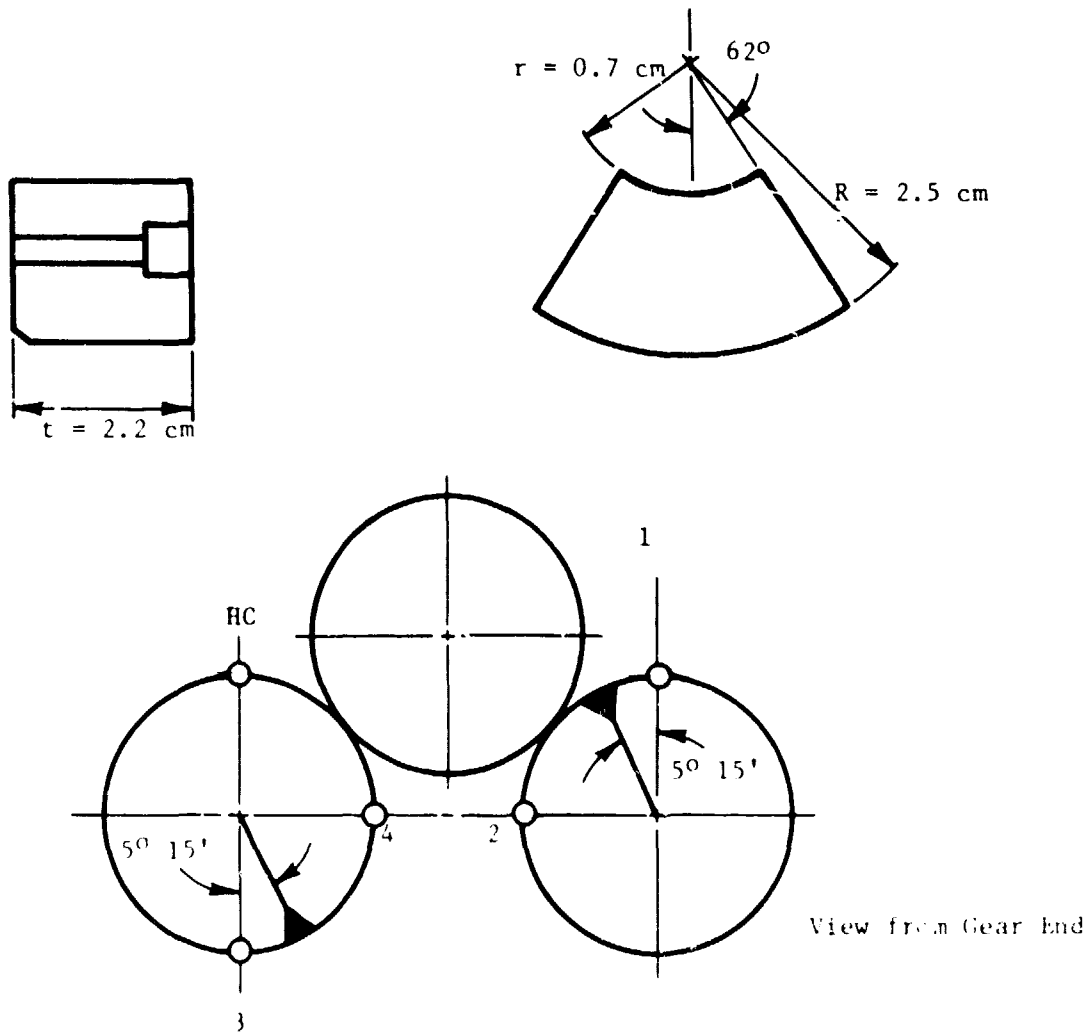
Nose counter weight WR = 1.512 kg-cm

Gear counter weights WR = 0.128 kg-cm

ORIGINAL DESIGN
OF POCA GEAR

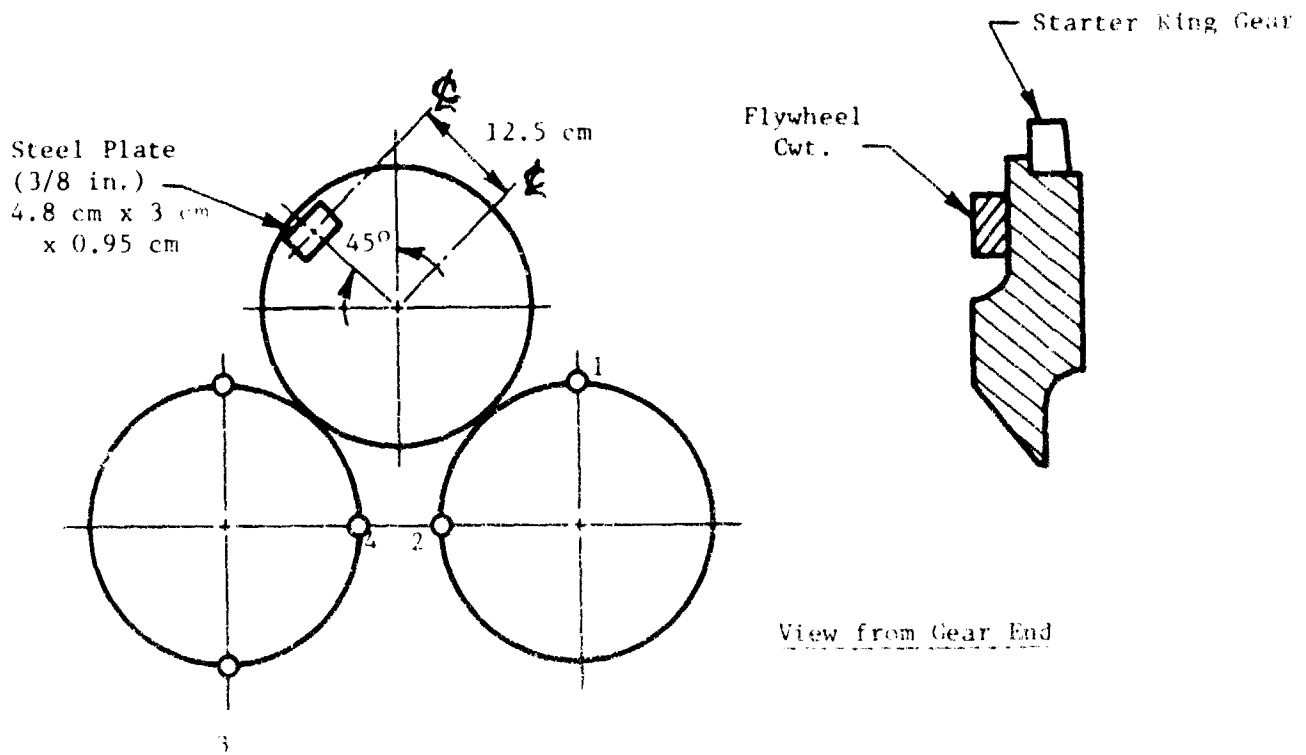
SUMMARY

1) Gear Counter Weights (2 Off)



CHUCKS OF POOR QUALITY

2) Flywheel Balance Weight (1 Off)



RICARDO CONSULTING ENGINEERS

ORIGINAL PAGE IS
OF POOR QUALITY

CLIENT USSW/MLI
PROJECT _____
JOB NO. C48135-100
CALCULATION BY DJI

SECTION Crankshaft
SHEET NO. 1 OF 17
DATE 2/23/81
DRAWING KEY NO. _____

OBJECT Reduced Shank Bolt
Main-Bearing
Bolt m12 x 1.75 4h

Due to high aluminum boss loadings, the shank of the stud is to be decreased.

The load to crush the shell must take into account the diametral dilation in fitting in the case of aluminum.

Diametral crush interference (mean) using 3-61109 circumferential crush, no housing swell $(.038 + .086/2) = .064 + .032 = .096$ for two shells + crush height due to checking load.



$$1/2 \text{ shell stiffness} = \frac{AE}{L} = \frac{30(1.77)206,843}{0.5 \pi (47)}$$

Crush due to check load = 4700 N

$$= \frac{148,771 \text{ N/mm}}{(C_{\text{shell}})}$$

$$= \frac{N}{N} \text{ in.}$$

For mean crush height but circumferential crush = π (diametral crush). Therefore,

$$\text{Diametral interference} = \frac{0.096(2)}{\pi} = 0.061 \text{ mm on diameter.}$$

RICARDO CONSULTING ENGINEERS

CLIENT

PROJECT

JOB NO.

CALCULATION BY

SECTION

SHEET NO. 2 OF 17

DATE

DRAWING KEY NO.

OBJECT Reduced Shank Main Bearing Bolt

Diametral dilation of housing

$$\delta_{HI} = \delta \left\{ \left[uH + \frac{R_3^2 + R_1^2}{R_3^2 - R_1^2} \right] + \frac{FH}{EB} - \left[uB + \frac{R_1^2 + R_2^2}{R_1^2 - R_2^2} \right] \right\}$$

$$uH + \frac{R_3^2 + R_1^2}{R_3^2 - R_1^2} = 0.3 + \left[\frac{45^2 + 24.5^2}{45^2 - 24.5^2} \right] = 2.143$$

Where

R_1 = Housing radius = 24.5

R_2 = Internal radius of bearing = 22.5

R_3 = Effective outer radius = $2(R_1) = 45$

$$uB + \frac{R_1^2 + R_2^2}{R_1^2 - R_2^2} = -0.285 + \frac{24.5^2 + 22.5^2}{24.5^2 - 22.5^2} = 11.486$$

$$\delta_{HI} = 0.061 \left\{ 2.143 + \frac{71.016}{206,843} - (11.486) \right\} = 0.061(0.352) = 0.021$$

RICARDO CONSULTING ENGINEERS

ORIGINAL PAGE IS
OF POOR QUALITY

CLIENT SECTION
PROJECT SHEET NO. 3 OF 17
JOB NO. DATE
CALCULATION BY DRAWING KEY NO.

OBJECT
.....

Therefore,

$$\begin{aligned}\text{Diametral crush shell} &= 0.040 \text{ on diameter} \\ &= 0.040 (\pi) \text{ on circumference} = 0.124 \text{ mm} \\ &= 0.062 \text{ per } 1/2 \text{ shell mm crush}\end{aligned}$$

$$\frac{0.062}{420} \text{ mm} \times \frac{\text{N}}{\text{mm}} = 9236 \text{ N (i.e., } 174 \text{ N/mm}^2; 17.7 \text{ kg/mm}^2).$$

From Vandervell report 509, maximum main bearing load is approximately 17,000 N, at 900 rpm main bearing No. 2; i.e., 8500/6004.

Now, adjust tightening torque to give mean cover of 3.5 hot running.

$$3.5 = \frac{\text{Preload} - \text{Crush Load}}{\text{External Load}_{(\text{Nominal})}}$$

$$3.5 = \frac{P - 9236}{8500}$$

$$3.5 (8500) = P - 9236$$

$$= 38,986 = P$$

Load at present tightening torque = 94 Nm

$$W = 5T$$

$$W = \frac{5T}{d} = 39,167 \text{ N (60\% Proof)}$$

Cover factor at present is 3.52 cold.

Assuming with external load and worst tightening condition proof load can be reached, pressure under face of washer is

$$\frac{6.68 \times 1000 (9.81)}{329.7}$$

RICARDO CONSULTING ENGINEERS

01/01/2013 13:03
ON 7

CLIENT

SECTION

PROJECT

SHEET NO. 4 OF 17

JOB NO.

DATE

CALCULATION BY

DRAWING KEY NO.

OBJECT

where

$$329.7 = \text{cross sectional area of washer } \pi/4 (24^2 - 12.5^2)$$

For example,

$$\text{Pressure under washer} = 198.7 \text{ N/mm}^2 = 12.9 \text{ T/in}^2$$

This is at the minimum proof stress of 13 T/in², and hence, a thick washer of 5 mm is required.

Cover hot with original 94 Nm tightening torque. Stiffness of bearing steel is 193,200 N/mm. Stiffness of abutment is 269,126 N/mm. Stiffness of shell is 148,771.

Differential expansion of bearing is 87 mm at 70°C At

$$87(70) (22 \times 10^{-6} - 12 \times 10^{-6}) = 0.06 \text{ mm}$$

$$\Delta B = \Delta F \frac{C_A}{C_B + C_A} = \frac{269,126}{269,126 + 193,200} = 58(.061) = .036 \text{ mm} = \Delta B$$

Thermal bolt load is mm x N/mm = 6860 N. Total bolt load is hot. Preload is 39,167 (60° proof) + 6860 which equals 46,027 N.

$$\text{Cover Factor}_{\text{Hot}} = \frac{46,027 - 9236}{8500}$$

$$\text{Cover Factor}_{\text{Hot}} = 4.3$$

Design for cover factor_{hot} is approximately 3.5. The hot load required ~ 39,000 N. Say the increase due to thermal load is approximately 6200 N, then shank is : 9.5 mm.

$$\text{Tensile stress area } \frac{\pi}{4} (9.5)^2 = 70.88 \text{ mm}^2$$

RICARDO CONSULTING ENGINEERS

ORIGINAL PAGE IS
OF POOR QUALITY

CLIENT
PROJECT
JOB NO.
CALCULATION BY

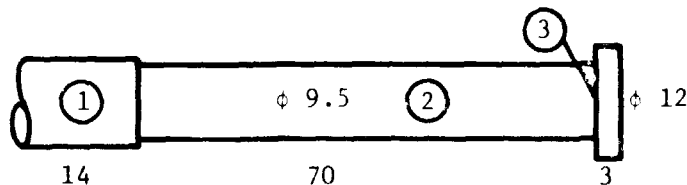
SECTION
SHEET NO. 5 OF 17
DATE
DRAWING KEY NO.

OBJECT

To obtain approximately 33,000 N cold,

$$C_{\text{cold}} = 466 \text{ N/mm}^2$$

Stress under proof load is 777 N/mm^2 (i.e., 60% proof cold). Stiffness of 9.5 ϕ stud.



821004

$$\begin{aligned} \text{Thread C } \textcircled{1} &= \frac{A_{\text{BEB}}}{L_B} = \frac{\pi/4 (10.8)^2 206,843}{14} = 1,353,474 \text{ N/mm} \\ &= 30 \times 10^6 \text{ lb/in.}^2 \end{aligned}$$

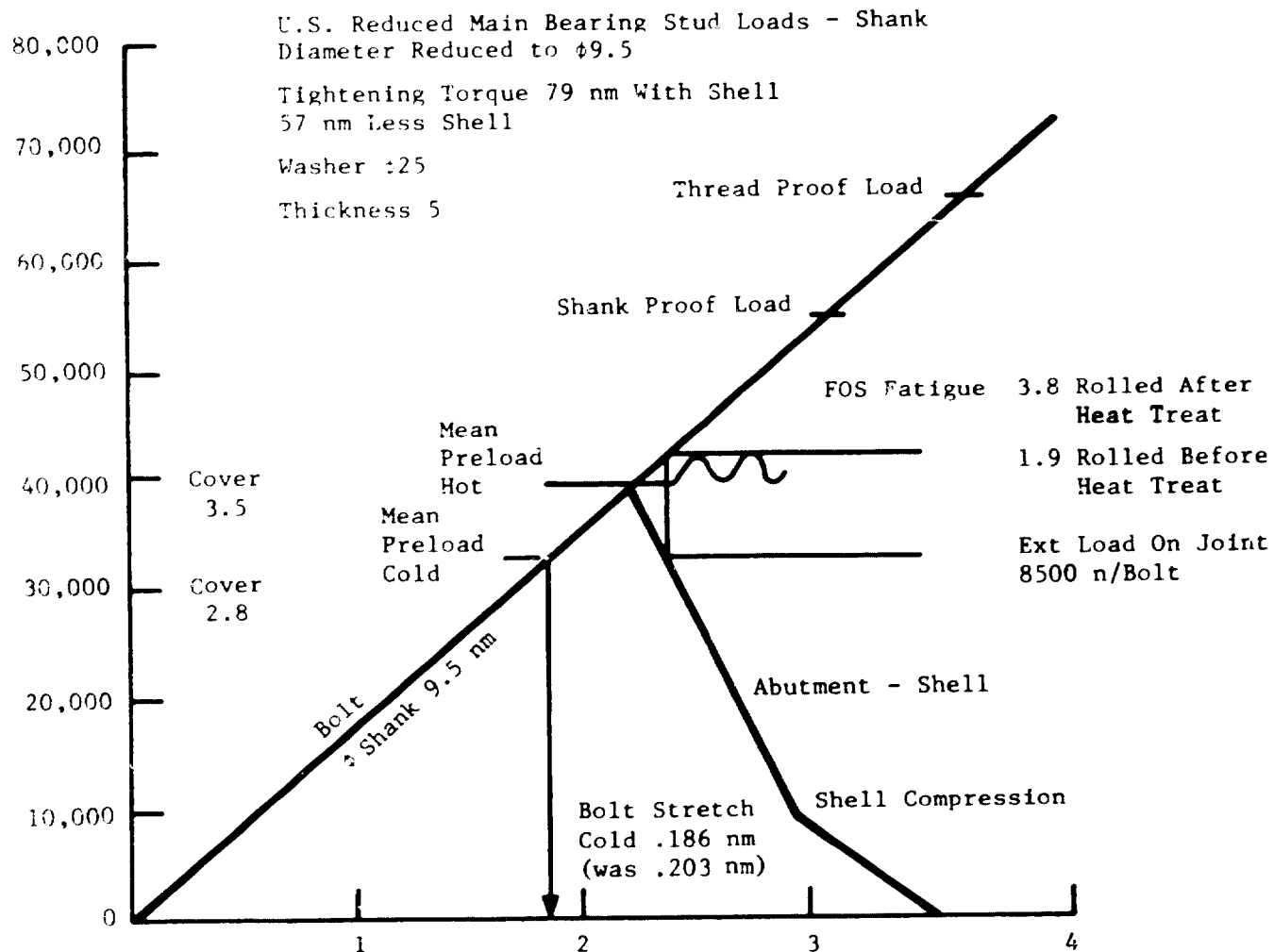
$$\text{Thread C } \textcircled{2} = \frac{\pi/4 (9.5)^2 206,843}{70} = 209,450$$

$$\text{Thread C } \textcircled{3} = \pi/4 (12)^2 (206,843) 1/3 = 7,797,790$$

$$\text{Thread C } \textcircled{B} = \frac{1}{C} + .000 C_B = 177,258 \text{ N/mm (reduced)}$$

$$\begin{aligned} \text{Stretch in bolt cold} &= 33,000/C_B = 0.186 \text{ mm} \\ &= 0.007 \text{ in.} \end{aligned}$$

(Originally .203 mm [.008 in.])



ORIGINAL FILED IN
OF POOR QUALITY

RICARDO CONSULTING ENGINEERS

CLIENT
PROJECT
JOB NO.
CALCULATION BY

SECTION
SHEET NO. 7 OF 17
DATE
DRAWING KEY NO.

OBJECT
.....

Stiffness of abutment is approximately

$$\frac{A_A E_A}{L_A}$$

Taking the effective area under washer (which will be stiffened),

$$E_A = 10.3 \times 10^6 \text{ lb/in}^2 = 71,016 \text{ N/mm}^2$$

$$\pi/4 (24^2 - 12.5^2) = 329.7 \text{ mm}^2$$

$$\frac{329.7 (71,016)}{87} = 269,126 \text{ N/mm}$$

Differential expansion over 87 mm $\Delta t = 70^\circ\text{C} = 0.061 \text{ mm}$.

$$\delta_B = DE \frac{C_A}{C_B + C_A} = \frac{269,126(.061)}{177,258 + 269,126} = .037 \text{ mm}$$

Thermal (bolt) load, mm x N/mm

$$(177,258 \times .037) = 6519 \text{ N}$$

Total bolt load hot

$$33,000 + 6519 = 39,519$$

Cover, hot mean

$$\frac{39,519 - 9236}{8500} = 3.56$$

Cover, cold mean

$$\frac{33,000 - 9236}{8500} = 2.80$$

RICARDO CONSULTING ENGINEERS

ORIGINAL PAGE IS
OF POOR QUALITY

CLIENT SECTION
PROJECT SHEET NO. 8 OF 17
JOB NO. DATE
CALCULATION BY DRAWING KEY NO.

OBJECT
.....

Proof load for thread area is $6.68 \times 1000 \text{ kg}$.

$$\text{Percent Thread Proof Load Hot} = \frac{39,519}{6.68 \times 1000 \times 9.81} = 60\%$$

$$\text{Percent Thread Proof Load Cold} = \frac{33,000}{6.68 \times 1000 \times 9.81} = 50\%$$

$$\text{Percent Shank Proof Load Hot} = \frac{39,519}{777(70.88)} = 72\%$$

$$\text{Percent Shank Proof Load Cold} = \frac{33,000}{777(70.88)} = 60\%$$

Tightening torque:

$$\text{(With Shells)} \quad T = \frac{WD}{S} = \frac{33,000 (12)}{5000} \text{ NM} = 79.2 \text{ NM (58 lb/ft)}$$

$$\text{(Less Shells)} \quad 3300 - 9236 = 23,764 \text{ N}$$

$$\text{(Bolt Load)} \quad T = \frac{23,764 (12)}{5000} = 57 \text{ NM}$$

External load is 8500 N/bolt.

$$F_{Be} = \frac{C_B}{C_A + C_B + C_S}$$

$$(Fe) = \frac{177,258}{177,258 + 269,126 + 148,771}$$

$$F_{Be} = .298 (Fe)$$

Where

$$Fe = \text{external load/bolt} = 8500$$

$$F_{Be} = 2532 \text{ N}$$

RICARDO CONSULTING ENGINEERS

ORIGINAL PAGE IS
OF POOR QUALITY

CLIENT

SECTION

PROJECT

SHEET NO. 9 OF 17

JOB NO.

DATE

CALCULATION BY

DRAWING KEY NO.

OBJECT

Maximum bolt load hot, running =

$$39,519 + 2532 = 42,051 \text{ N}$$

Compression shells .062 mm N/N abutment =

$$\frac{(39,519 - 9236)}{269,126 + 148,771} = .072$$

WASHER

Hot pressure, say, 55,000 N_{max} will increase washer ϕ to 26 ϕ .

$$\text{Area } \pi/4 (26^2 - 12.5^2) = 408 \text{ mm}^2$$

$$\text{Pressure } 135 \text{ N/mm}^2 = 8.7 \text{ T/in.}^2$$

Say,

$$: 25 \pi/4 (25^2 - 12.5^2) = 368 \text{ mm}^2$$

$$\text{Pressure } 150 \text{ N/mm}^2 = 9.7 \text{ T/in.}^2$$

$$\text{Proof strength of material} = 13 \text{ T/in.}^2$$

Thickness of washer to be 5 mm hardened.

RICARDO CONSULTING ENGINEERS

WARNING
OF POOR QUALITY

CLIENT
PROJECT
JOB NO.
CALCULATION BY

SECTION
SHEET NO. 10 OF 17
DATE
DRAWING KEY NO.

OBJECT
.....

Factor of Safety Fatigue

Threads rolled after heat treatment

$$\frac{\sigma_m}{\sigma_{0.2}} = \frac{484}{883} = .55$$

$$\text{Thread area} = \frac{39,519 + 2532/2}{84.3 \text{ mm}}$$

Allowable:

$$\pm \text{ca } 57 \text{ N/mm}^2$$

In thread:

$$\pm \text{ca } = \frac{1266}{84.3} \pm 15$$

Factor of safety = 3.8.

Check Thread Stress (Inch Units)

$$N_{ut} = (TPI) L_e D_{s_{min}} \left[\frac{1}{2r} + .577 (.05 \text{ min} - E_{n_{max}}) \right]$$

L_e = length engagement

$$= \pi \cdot N \cdot L_e \cdot D_s \left[\frac{1}{2r} + .577 D_{s_{min}} - E_{n_{max}} \right]$$

$$= 1.75 \text{ pitch}$$

$$= .571 \text{ threads/mm}$$

$$= (.571)(15)$$

$$D_{s_{min}} = \text{min maj dia} - \text{ext} = 11.830$$

$$E_{n_{max}} = \text{max eff} - \text{nut} = 11.023$$

RICARDO CONSULTING ENGINEERS

ORIGINAL FILED IN
OF PROJECT NO. 17

CLIENT

SECTION

PROJECT

SHEET NO. 11 OF 17

JOB NO.

DATE

CALCULATION BY

DRAWING KEY NO.

OBJECT

$$\begin{aligned} \min^2 = AN &= \pi (.571)(15) 11.83 \left[\frac{1}{2(.571)} \right] + .577 (11.83 - 11.023) \\ &= 427 \text{ mm}^2 \end{aligned}$$

Maximum load, say, proof in threads for initial build

$$6.68 \times 10^3 (9.81)$$

$$\text{Thread stress} = 153.5 \text{ N/mm}^2$$

$$\text{Maximum stud load} \approx 55,000 \text{ N}$$

Thread stress Le 15 mm

$$\frac{55,000}{427} = 129 \text{ N/mm}^2$$

$$\text{Maximum allowable at proof in shear} = 116 \text{ N/mm}^2$$

Length of engagement required is

$$15 \times \frac{129}{116} = 17 \text{ mm}$$

HELICOIL

Check Aluminum Stress

$$\begin{aligned} \text{Nut mm}^2/\text{mm length} &= \pi \frac{.571}{14.273} \left[\frac{1}{2(.571)} + .577 (14.273 - 13.137) \right] \\ &= 39.2 \text{ mm}^2/\text{mm length} \end{aligned}$$

$$Ds_{\min} = 14.273$$

$$Fn_{\max} = 13.137$$

RICARDO CONSULTING ENGINEERS

ORIGINALITY
OF POOR QUALITY

CLIENT
PROJECT
JOB NO.
CALCULATION BY

SECTION
SHEET NO. 12 OF 17
DATE
DRAWING KEY NO.

OBJECT
.....

Original loading, PS of thread is,

$$\frac{6.68 \times 10^3 (9.81)}{l (39.2)} = 116$$

$$l = \frac{6.68 \times 10^3 (9.81)}{39.2(116)} = 14.41 \text{ mm}$$

(say, 14.5 mm)

CONCLUSION

It has been found from the casting that it is possible to obtain a minimum of 19 mm effective thread length by protruding a new longer stud from the tapped hole. (Blind tapped holes have adequate thread length.) This would just be acceptable only with the reduced tightening torque and waisted stud.

Thread stress for 55,000 N load is

$$\frac{55,000}{427(19/15)} = 102 \text{ N/mm}^2$$

Proof load in shear is

$$\frac{1}{\sqrt{3}} (201) = 116 \text{ N/mm}^2$$

Shear stress in thread is 88% proof at $Le = 19 \text{ mm}$.

Also, the stud should not be tightened against the runout in assembly. The stud should be assembled to the crankcase with a very low torque. This feature should be approved for future engines.

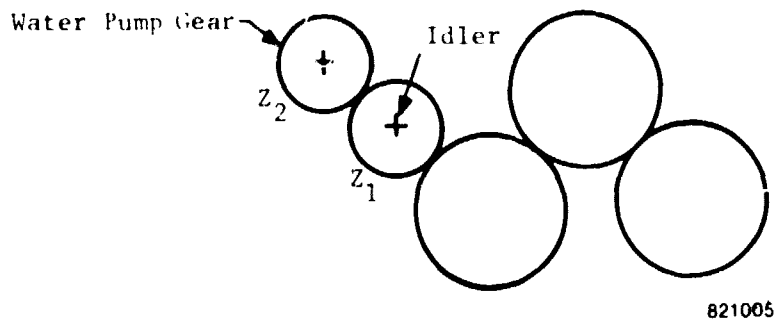
RICARDO CONSULTING ENGINEERS

ORIGINAL PAGE IS
OF POOR QUALITY

CLIENT United Stirling
PROJECT Mod I
JOB NO. C48135-100
CALCULATION BY RNJ
DRAWING KEY NO. 3274

SECTION Gears
SHEET NO. 13 OF 17
DATE 4/6/81
DRAWING KEY NO. 3274

OBJECT Due to gear failures with 0.8 module gears, US have requested an
increase in module - say, 2 module



PROGRAM RESULTS

RCD1	68.328
RCD2	107.668
y/zvm	0.006
ΣX	0.3171
I	1.575
XI	0.244
X2	0.072
DA1	73.282
DA2	111.932
ΔR1	64.307
ΔR2	102.957
L1	801.120
L2	1262.37
SN1	3.498
SN2	3.246

Where,

$$z_1 = 33$$

$$z_2 = 52$$

$$\phi = 15^\circ$$

$$m_n = 2$$

$$a = 88.62 \text{ mm}$$

RCD

$$d_1 = \frac{2 \times 33}{\cos 15} = 68.3282 \text{ mm}$$

$$d_2 = \frac{2 \times 52}{\cos 15} = 107.6687 \text{ mm}$$

Center Distance Modification

$$y = a/m - (d_1 + d_2)/2m = \frac{88.62}{2} - \frac{(68.3282 + 107.6687)}{2 \times 2} = 0.30828$$

RICARDO CONSULTING ENGINEERS

CLIENT
PROJECT
JOB NO.
CALCULATION BY

SECTION
SHEET NO. 14 OF 17
DATE
DRAWING KEY NO.

OBJECT

Mean Virtual (No Teeth)

$$z_{vm} = \frac{1}{2} (33 + 52) / \cos^3 15 + 0.30828 \times \tan^2 15 = 47.18037$$

$$y/z_{vm} = 0.30828 / 47.18037 = 0.006534$$

From Table 2 (PD6457: 1970),

$$x/z_{vm} = 0.0066834$$

$$x = 0.0066834 \times 47.18037 = 0.315327$$

For General Application

$$w_1 = 1/3(1 - 1/u) + x/(1 + u)$$

$$u = 52/33 = 1.5757576$$

Therefore,

$$w_1 = 1/3(1 - 1/1.57576) + 0.315327/(1 + 1.57576)$$

$$w_1 = 0.2442$$

$$w_2 = 0.31527 - 0.2442 = 0.0711$$

Tip Diameters

For nominal tip to root clearance

$$da = d_f + 2r(1 + w_2 + s)$$

$$da_1 = 66.3282 + 2 \times 2(1 + 0.0711 + 0.30828) = 71.277 \text{ mm}$$

$$da_2 = 107.6687 + 2 \times 2(1 + 0.2442 + 0.30828) = 111.925 \text{ mm}$$

RICARDO CONSULTING ENGINEERS

ORIGINAL PAGE IS
OF POOR QUALITY

CLIENT
PROJECT
JOB NO.
CALCULATION BY

SECTION
SHEET NO. 15 OF 17
DATE
DRAWING KEY NO.

OBJECT
.....

Root Diameter

$$df_1 = m_n \frac{z_1}{\cos \beta} - 2 \left(1 + \frac{c}{m} - \infty_1 \right)$$

Assume:

$$c = 0.25 m_n \text{ (i.e., minimum value)}$$

$$df_1 = 2 \frac{33}{\cos 15} - 2 (1 + 0.25 - 0.2442) = 64.3050 \text{ mm}$$

$$df_2 = 2 \frac{52}{\cos 15} - 2 (1 + 0.25 - 0.0711) = 102.9531 \text{ mm}$$

Drive Gears (Application Factor = 1.5)

Gear Program

- 1 Mod 1 - Drive Gears
- 2 48, 48, 2, 15, 40
- 3 3000, 118.2, 82, 82, 7E09
- 4 5, 1.5, 2, 2, 120
- 5 1, 1, 1, 1
- 6 1, 1
- 7 1480, 415, 662
- 8 1480, 415, 662

RICARDO CONSULTING ENGINEERS

OWNED BY
OF PROJECT

CLIENT
PROJECT
JOB NO.
CALCULATION BY

SECTION
SHEET NO. 16 OF 17
DATE
DRAWING KEY NO.

OBJECT
.....

Results

Safety factor contact stress is 1.43. Safety factor root stress is 2.45. If root stress safety factor = 2, what face width is required?

$$b = \frac{2 \times 40}{2.45} = 33 \text{ mm}$$

Therefore,

$$F/b = \frac{118.2 \times 40}{33} = 143.3 \text{ N/mm}$$

$$\text{Helical overlap} = \frac{b \sin \beta}{\pi \sin \alpha} = \frac{40 \sin 15}{\pi \times 2} = 1.65$$

$$\text{Helical overlap} = \frac{33 \sin 15}{\pi \times 2} = 1.36$$

Still fairly high, but ensures good meshing.

SUMMARY

The original analysis using 1,506,836 showed that the drive gears with 0.8 module, 120 teeth, had a 1.1 safety factor for root bending stresses (1.5 application factors applied) and the wear safety factor of 1.4.

By going to a 2-module, 48-tooth gear and using the same face width, the safety factors with a 1.5 application factor should be:

Safety Factor Wear = 1.43

Safety Factor Strength = 2.45

Helical Overlay = 1.65

RICARDO CONSULTING ENGINEERS

CITY OF LOS ANGELES
OFFICE OF PUBLIC WORKS

CLIENT

SECTION

PROJECT

SHEET NO. 17 OF 17

JOB NO.

DATE

CALCULATION BY

DRAWING KEY NO.

OBJECT

.....

If the face width is reduced, say to 33 mm, 16 safety factors become:

Safety Factor Wear = 1.35

Safety Factor Strength = 2.13

Helical Overlay = 1.36.